

Progress on Pellet–Cladding Interaction and Stress Corrosion Cracking

*Experimentation, Modelling and
Methodologies Applied to Support the
Flexible Operation of Nuclear Power Plants*

Report of a Technical Meeting



IAEA

International Atomic Energy Agency

PROGRESS ON PELLETT-CLADDING
INTERACTION AND STRESS
CORROSION CRACKING

The following States are Members of the International Atomic Energy Agency:

AFGHANISTAN	GEORGIA	OMAN
ALBANIA	GERMANY	PAKISTAN
ALGERIA	GHANA	PALAU
ANGOLA	GREECE	PANAMA
ANTIGUA AND BARBUDA	GRENADA	PAPUA NEW GUINEA
ARGENTINA	GUATEMALA	PARAGUAY
ARMENIA	GUYANA	PERU
AUSTRALIA	HAITI	PHILIPPINES
AUSTRIA	HOLY SEE	POLAND
AZERBAIJAN	HONDURAS	PORTUGAL
BAHAMAS	HUNGARY	QATAR
BAHRAIN	ICELAND	REPUBLIC OF MOLDOVA
BANGLADESH	INDIA	ROMANIA
BARBADOS	INDONESIA	RUSSIAN FEDERATION
BELARUS	IRAN, ISLAMIC REPUBLIC OF	RWANDA
BELGIUM	IRAQ	SAINT LUCIA
BELIZE	IRELAND	SAINT VINCENT AND THE GRENADINES
BENIN	ISRAEL	SAMOA
BOLIVIA, PLURINATIONAL STATE OF	ITALY	SAN MARINO
BOSNIA AND HERZEGOVINA	JAMAICA	SAUDI ARABIA
BOTSWANA	JAPAN	SENEGAL
BRAZIL	JORDAN	SERBIA
BRUNEI DARUSSALAM	KAZAKHSTAN	SEYCHELLES
BULGARIA	KENYA	SIERRA LEONE
BURKINA FASO	KOREA, REPUBLIC OF	SINGAPORE
BURUNDI	KUWAIT	SLOVAKIA
CAMBODIA	KYRGYZSTAN	SLOVENIA
CAMEROON	LAO PEOPLE'S DEMOCRATIC REPUBLIC	SOUTH AFRICA
CANADA	LATVIA	SPAIN
CENTRAL AFRICAN REPUBLIC	LEBANON	SRI LANKA
CHAD	LESOTHO	SUDAN
CHILE	LIBERIA	SWEDEN
CHINA	LIBYA	SWITZERLAND
COLOMBIA	LIECHTENSTEIN	SYRIAN ARAB REPUBLIC
COMOROS	LITHUANIA	TAJIKISTAN
CONGO	LUXEMBOURG	THAILAND
COSTA RICA	MADAGASCAR	TOGO
CÔTE D'IVOIRE	MALAWI	TRINIDAD AND TOBAGO
CROATIA	MALAYSIA	TUNISIA
CUBA	MALI	TURKEY
CYPRUS	MALTA	TURKMENISTAN
CZECH REPUBLIC	MARSHALL ISLANDS	UGANDA
DEMOCRATIC REPUBLIC OF THE CONGO	MAURITANIA	UKRAINE
DENMARK	MAURITIUS	UNITED ARAB EMIRATES
DJIBOUTI	MEXICO	UNITED KINGDOM OF GREAT BRITAIN AND NORTHERN IRELAND
DOMINICA	MONACO	UNITED REPUBLIC OF TANZANIA
DOMINICAN REPUBLIC	MONGOLIA	UNITED STATES OF AMERICA
ECUADOR	MONTENEGRO	URUGUAY
EGYPT	MOROCCO	UZBEKISTAN
EL SALVADOR	MOZAMBIQUE	VANUATU
ERITREA	MYANMAR	VENEZUELA, BOLIVARIAN REPUBLIC OF
ESTONIA	NAMIBIA	VIET NAM
ESWATINI	NEPAL	YEMEN
ETHIOPIA	NETHERLANDS	ZAMBIA
FIJI	NEW ZEALAND	ZIMBABWE
FINLAND	NICARAGUA	
FRANCE	NIGER	
GABON	NIGERIA	
	NORTH MACEDONIA	
	NORWAY	

The Agency's Statute was approved on 23 October 1956 by the Conference on the Statute of the IAEA held at United Nations Headquarters, New York; it entered into force on 29 July 1957. The Headquarters of the Agency are situated in Vienna. Its principal objective is "to accelerate and enlarge the contribution of atomic energy to peace, health and prosperity throughout the world".

IAEA-TECDOC-1960

PROGRESS ON PELLET–CLADDING INTERACTION AND STRESS CORROSION CRACKING

EXPERIMENTATION, MODELLING AND METHODOLOGIES
APPLIED TO SUPPORT THE FLEXIBLE OPERATION
OF NUCLEAR POWER PLANTS

REPORT OF A TECHNICAL MEETING

INTERNATIONAL ATOMIC ENERGY AGENCY
VIENNA, 2021

COPYRIGHT NOTICE

All IAEA scientific and technical publications are protected by the terms of the Universal Copyright Convention as adopted in 1952 (Berne) and as revised in 1972 (Paris). The copyright has since been extended by the World Intellectual Property Organization (Geneva) to include electronic and virtual intellectual property. Permission to use whole or parts of texts contained in IAEA publications in printed or electronic form must be obtained and is usually subject to royalty agreements. Proposals for non-commercial reproductions and translations are welcomed and considered on a case-by-case basis. Enquiries should be addressed to the IAEA Publishing Section at:

Marketing and Sales Unit, Publishing Section
International Atomic Energy Agency
Vienna International Centre
PO Box 100
1400 Vienna, Austria
fax: +43 1 26007 22529
tel.: +43 1 2600 22417
email: sales.publications@iaea.org
www.iaea.org/publications

For further information on this publication, please contact:

Nuclear Fuel Cycle and Materials Section
International Atomic Energy Agency
Vienna International Centre
PO Box 100
1400 Vienna, Austria
Email: Official.Mail@iaea.org

© IAEA, 2021
Printed by the IAEA in Austria
June 2021

IAEA Library Cataloguing in Publication Data

Names: International Atomic Energy Agency.
Title: Progress on pellet-cladding interaction and stress corrosion cracking : experimentation, modelling and methodologies applied to support the flexible operation of nuclear power plants / International Atomic Energy Agency.
Description: Vienna : International Atomic Energy Agency, 2021. | Series: IAEA TECDOC series, ISSN 1011-4289 ; no. 1960 | Includes bibliographical references.
Identifiers: IAEAL 21-01418 | ISBN 978-92-0-116521-3 (paperback : alk. paper) | ISBN 978-92-0-116421-6 (pdf)
Subjects: LCSH: Nuclear fuel claddings. | Stress corrosion. | Nuclear power plants. | Nuclear reactors — Cores.

FOREWORD

It is widely recognized that nuclear power has the potential to play a significant role in meeting climate goals by the deadlines established in the Paris Agreement. As the portion of renewable energy in the energy mix grows, the flexible operation of nuclear power plants is increasingly seen as an effective measure to compensate for fluctuations in renewable energy generation due to variable weather conditions. The flexible operation of nuclear power plants usually involves power variations, and the high stress on the fuel cladding upon a power increase, via a strong pellet-cladding interaction (PCI), can result in cladding failure in a corrosive environment (i.e. PCI-stress corrosion cracking or PCI-SCC).

To address this concern, and in line with requests from Member States, the IAEA organized a technical meeting in Aix-en-Provence, France, on 8–11 October 2019, to share information on advanced experiments, modelling, fuel design methodologies and operating guidelines for the flexible operation of nuclear power plants. The meeting was part of a series of international specialist meetings and technical meetings on PCI-SCC phenomena and the effects of power ramping, cycling and load following operation. The meetings were aimed at facilitating the exchange of information on preventing or mitigating PCI-SCC issues. Among the conclusions from these meetings was that PCI-SCC needs to be dealt with together with both reactor system operation and fuel behaviour under power manoeuvring conditions, and that there is a need for a better understanding of some of the basic phenomena of PCI-SCC. To achieve more economical and flexible operating conditions, continued experimental and analytical work is necessary.

The present publication provides a review of progress in PCI-SCC studies in the field of PCI-SCC implementation in reactor core design and operation, experimental investigation of PCI-SCC mechanisms, improvement of PCI-SCC modelling, and optimization of PCI-SCC design methodologies since the early 2000s, based on the presented papers and discussions at the aforementioned technical meeting.

The IAEA thanks the meeting participants for their active involvement and presentations, as well as the members of the technical committee, in particular, V.I. Arimescu (United States of America), T. Forgeron (France), W.-S. Ryu (Republic of Korea), N. Waeckel (France) and J. Zhang (Belgium), for their valuable contributions in organizing the technical meeting and in drafting this publication. Special acknowledgement is given to the CEA Cadarache for hosting the technical meeting and to E. Federici (France) for local coordination of the meeting and for a thorough review of papers presented. The IAEA officer responsible for this publication was K. Sim of the Division of Nuclear Fuel Cycle and Waste Technology.

EDITORIAL NOTE

This publication has been prepared from the original material as submitted by the contributors and has not been edited by the editorial staff of the IAEA. The views expressed remain the responsibility of the contributors and do not necessarily represent the views of the IAEA or its Member States.

Neither the IAEA nor its Member States assume any responsibility for consequences which may arise from the use of this publication. This publication does not address questions of responsibility, legal or otherwise, for acts or omissions on the part of any person.

The use of particular designations of countries or territories does not imply any judgement by the publisher, the IAEA, as to the legal status of such countries or territories, of their authorities and institutions or of the delimitation of their boundaries.

The mention of names of specific companies or products (whether or not indicated as registered) does not imply any intention to infringe proprietary rights, nor should it be construed as an endorsement or recommendation on the part of the IAEA.

The authors are responsible for having obtained the necessary permission for the IAEA to reproduce, translate or use material from sources already protected by copyrights.

The IAEA has no responsibility for the persistence or accuracy of URLs for external or third party Internet web sites referred to in this publication and does not guarantee that any content on such web sites is, or will remain, accurate or appropriate.

CONTENTS

1.	INTRODUCTION	1
1.1.	Background.....	1
1.2.	Objective	1
1.3.	Scope	1
1.4.	Structure	2
2.	OVERVIEW ON FLEXIBLE POWER OPERATION	3
2.1.	Overall status	3
2.2.	Potential fuel failure mechanisms during flexible power operation	4
3.	PCI/SCC PHENOMENA AND REVIEW OF PREVIOUS ACTIVITIES	6
3.1.	PCI/SCC Phenomena.....	6
3.1.1.	Early R&D, PCI mechanism hypothesis	6
3.1.2.	Salient features of the PCI/SCC process	6
3.1.3.	Preventing/mitigating solutions.....	7
3.1.4.	Different PCI/SCC variants and current understanding	8
3.2.	Previous IAEA meetings and International Studies in 1970s –1980s.....	8
3.3.	Recent OECD-NEA Workshop in Lucca, Italy, 2016	9
4.	PCI/SCC RELATED LICENSING CONSIDERATIONS	11
4.1.	IAEA Safety Standards.....	11
4.2.	Licensing application practices with respect to PCI/SCC in some Member States	12
5.	PCI/SCC IMPLEMENTATION IN REACTOR CORE DESIGN AND OPERATION	13
5.1.	Overview	13
5.2.	Reactor operation guidelines	13
5.3.	PCI surveillance and protection system.....	14
5.4.	Impact on reactor core and fuel design.....	14
5.5.	Discussions and recommendations for future work.....	16
6.	EXPERIMENTAL UNDERSTANDING OF PCI/SCC MECHANISMS	18
6.1.	Overview	18
6.2.	In-pile and out-of-the pile tests and analyses.....	18
6.3.	Separate effect tests on unirradiated and irradiated materials.....	19
6.4.	Mitigation by material improvements.....	21
6.5.	Recommendations for future work	22
7.	IMPROVEMENT OF PCI/SCC MODELLING AND SIMULATION	23
7.1.	Overview	23
7.2.	Phenomenological models	23
7.2.1.	Time dependent behaviour of the cladding and pellet material.....	23
7.2.2.	Irradiation effects	24
7.2.3.	Thermochemistry	24
7.2.4.	Cladding SCC failure model	24
7.3.	Computer code developments.....	25
7.3.1.	General features	25

7.3.2.	ALCYONE (CEA, France)	25
7.3.3.	BISON (INL, USA)	26
7.3.4.	DIONISIO 3.0 (CNEA, Argentina).....	26
7.3.5.	OFFBEAT (EPFL, Switzerland).....	26
7.3.6.	START-3A (VNIIM, Russian Federation).....	27
7.4.	Verification, validation and applicable domains	27
7.4.1.	Global experiments (in pile power ramps)	27
7.4.2.	Databases related to PCI/SCC	27
7.4.3.	MIR reactor	27
7.4.4.	Benchmarking	28
7.5.	Uncertainty quantification	28
7.6.	Recommendations for future work	28
8.	OPTIMIZATION OF PCI/SCC DESIGN VERIFICATION METHODOLOGIES.....	29
8.1.	Overview	29
8.2.	Available toolbox to address in-reactor PCI/SCC related issues	29
8.2.1.	Extensive power ramps database covering the critical burnup range.....	29
8.2.2.	Creep and relaxation separate effect tests	29
8.2.3.	SCC out-of-the pile separate effect tests	30
8.2.4.	Advanced modelling	30
8.3.	Improved PCI/SCC core design verification methodologies.....	31
8.4.	Discussion and recommendations for future work	32
9.	CONCLUSIONS	33
	REFERENCES	35
	ANNEX I: A SUMMARY OF I-SCC MECHANISMS	39
	ANNEX II PROCEEDINGS OF THE TECHNICAL MEETING HELD IN AIX-EN-PROVENCE, FRANCE, FROM 8TH TO 11TH OF OCTOBER 2019.....	48
	ABBREVIATIONS	301
	CONTRIBUTORS TO DRAFTING AND REVIEW	303

1. INTRODUCTION

1.1. BACKGROUND

Fuel failure induced by a pellet–cladding interaction (PCI) in water cooled reactors has been considered a chronic issue since it was first observed in the 1960s. With significant efforts to address this issue, for example, through mechanistic understanding of iodine induced stress corrosion cracking (I-SCC) phenomena, and implementation of fuel design improvements and operational restrictions, the PCI induced fuel failure has become an infrequent event. In that respect, the International Atomic Energy Agency (IAEA) has contributed to the understanding of stress corrosion cracking (SCC) of zircaloy cladding through coordination of technical meetings [1–6] and coordinated research projects [7].

As the portion of renewable energy in the energy mix of a State increases, the flexible operation¹ of nuclear power plants increasingly focus as a measure to compensate for variations in the renewable energy generation due to weather conditions.

The flexible operation of nuclear power plants involves power variations and consequently causes high stress on the fuel cladding upon a power increase. This induces strong PCI, which can result in the failure of the fuel cladding in a corrosive environment (PCI/SCC).

Accordingly, the PCI/SCC has become a new concern for the nuclear fuel community. Fuel integrity under an extended reduced power operation (ERPO; also known as extended low power operation or ELPO) is of primary concern.

Traditionally, nuclear power plants have been operated in a ‘baseload’ mode producing their maximum rated power whenever online, although they are known to be capable of flexible operation, for example, changing their power output over time, contributing to power system stability via frequency regulation and operating reserves. Since fuel management in the reactor is optimized for the baseload mode, margins to fuel failure become tightened due to the flexible operation. Therefore, there is a strong need to quantify the margins to ensure fuel reliability under the flexible operating conditions that include load following, frequency control, unexpected grid requirements (e.g. instantaneous return to full power) and ERPO. Based on the quantified margins, operators are able to relax constraints imposed on reactor operation to better accommodate grid requirements.

Such margin assessments need a good understanding of PCI/SCC mechanisms, which can be facilitated by experimental investigation and validated analysis tools (e.g. fuel failure thresholds, fuel performance analysis codes).

1.2. OBJECTIVE

This publication is to provide a review of the state of the art on PCI/SCC technologies and recommendations for future work, based on the presentations and discussions at the technical meeting on “Progress on Pellet-Cladding Interaction and Stress Corrosion Cracking: Experimentation, Modelling and Methodologies Applied to Support the Flexible Operation of Nuclear Power Plants” held in Aix-en-Provence, France, in 8–11 October 2019.

1.3. SCOPE

This publication covers progresses in the following areas:

- PCI/SCC implementation in reactor core design and operation, with a focus on
 - Reactor operation guidelines related to PCI/SCC assessments (e.g. allowable rates of power ramp in different operation scenarios and ERPO duration);
 - PCI surveillance and protection systems;
 - Impact on reactor core and fuel design (e.g. PCI/SCC margin assessments)
- Experimental understanding of PCI/SCC mechanisms, with a focus on
 - In-reactor, out-reactor tests and analyses;

¹ ‘Flexible operation’ is also referred to ‘non-baseload operation’ that includes load following, frequency control and power modulation. Some description on each of these non-baseload operation modes are provided in [8].

- Separate effects tests on fresh or irradiated materials;
 - Mitigation by material improvements;
- Improvement of PCI/SCC modelling and simulation, with a focus on
- Phenomenological models;
 - Computer code developments;
 - Verification and validation, and applicable domains;
 - Uncertainty quantification;
- Optimization of PCI/SCC design verification methodologies.

1.4. STRUCTURE

Section 1 describes the background, objectives and scope of this publication.

Section 2 describes the general features of flexible power operation, and the status and prospects of flexible power operation in some States.

Section 3 provides a summary of up-to-date knowledge on PCI/SCC phenomena and associated major activities previously conducted by the IAEA and other international organizations. This section is intended to form the basis on which the progress of advancing PCI/SCC technologies to support the flexible operation of nuclear power plants is identified.

Session 4 provides PCI/SCC related licensing considerations, extracted from the IAEA Safety Standards and from practices in some Member States.

Sections 5–8 describe a summary of technical meeting results (discussion, papers presented), and identify recommendations for future work on specific subjects.

Section 9 provides overall conclusions made at the technical meeting.

Annex I provides a summary of I-SCC mechanisms, which is a supplementary to Section 3 description on PCI/SCC phenomena.

Annex II contains papers presented at the technical meeting held in Aix-en-Provence, 8–11 October 2019.

2. OVERVIEW ON FLEXIBLE POWER OPERATION

2.1. OVERALL STATUS

Although most operating nuclear power plants have been initially designed to operate at maximum rated power (RP), and operated in a baseload mode, they are also capable of providing variable power output to the grid through some flexible operation mode..

The ideal flexible power operation would be to adapt the power automatically to the grid demand. This operational mode, known as load following, has been implemented in France and Germany in the early 1980s. The typical flexible power operation provided by most nuclear power plants is the frequency control support.

Other forms of flexibility in response to grid occurrences are also possible and are described in [8]. Among them, ERPO is an operation mode that includes a continuous operation at a reduced power level (typically between 20 and 85% RP) for a period of 72 hours at least. During ERPO, the fuel cladding creeps down and, as a result, the radial gap between the pellet and the cladding decreases and can become closed again. The fuel rod is then considered ‘deconditioned’, which is equivalent to ‘conditioned’ at this lower power level. Therefore, at the end of an ERPO, when the reactor core goes back to nominal power, additional tensile stresses are created in the cladding compared to those at nominal power before the ERPO. If an anticipated operational occurrence (AOO) power transient occurs at the same time as the return to nominal power after an ERPO, the cladding will be subject to larger stresses than those that would have occurred during the same AOO transient before the ERPO; this will increase the susceptibility to PCI/SCC. An assessment of the PCI margin is needed at the end of the reference ‘baseload’ conditioning, ERPO (or ELPO) deconditioning, and the subsequent reconditioning phase, as shown in Fig. 1.

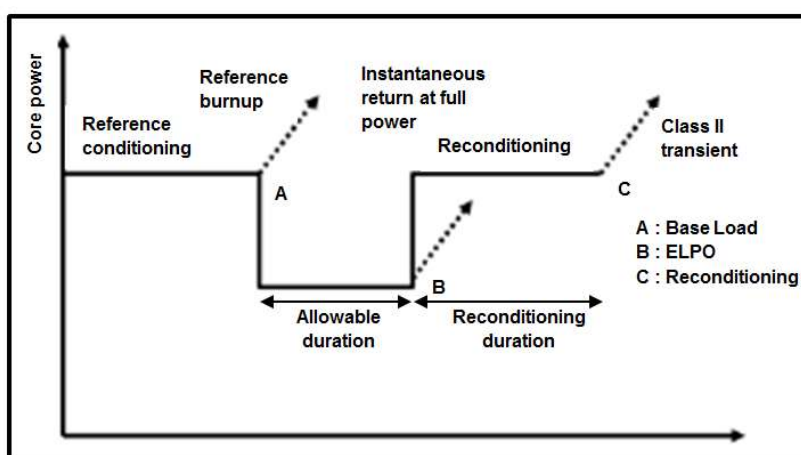


FIG. 1. Operational scenario including ERPO and an AOO event.

The allowable duration (i.e. total number of cumulative days) of ERPO (< 85 % RP) is limited to 4 weeks (28 days) per reload cycle in Belgium (See the paper presented by Zhang, Session I of Annex II). Operation under hot shutdown conditions is not considered if an exceptionally longer ERPO (e.g. duration > 28 days) occurs due to unavailable equipment or extreme climate. In a certain case, a reconditioning at intermediate power level between the full power (P_0) and the rated power (RP) may be needed.

In France, the current electrical energy mix is such that more than ~75% of electricity is generated in Électricité de France’s (EDF’s) nuclear power plants, requiring a high level of flexibility of the fuel cores. Under the circumstance, PCI/SCC phenomena have been studied for more than 30 years in the French nuclear community [9,10]. That is, to address PCI issues in operation, robust ‘PCI design verification methodologies’ have been developed and licensed in France and used to establish operational limits for nuclear power plants experiencing load following operation. Besides, multi-physics investigations, taking account of pellet thermochemistry and oxygen diffusion, are under development for use in identifying the key mechanisms which are activated in the pellet, the pellet-clad gap or on the cladding inner surface during a power transient. These investigations may

suggest innovative solutions while developing PCI/SCC resistant fuel concepts. Such innovative will facilitate to reduce the load following operation constraints (and to simplify PCI/SCC design analyses).

Goldstein and co-author in 1987 [11] reviewed the load following experience in the US light water reactor plants at the time. In summary, it was stated that while not widespread, a number of units had accumulated significant experience and some load following demonstration tests had been performed. The load following experience reviewed referred to daily and weekly load cycles.

In recent years, many operating plants are reconsidering the need to transition to flexible power operations. This is due to increased generation from renewables creating an oversupply resulting in negative electricity prices and localized grid congestion. This condition exists principally during the shoulder months, i.e. in the spring and fall. The operating experience in the United States is manoeuvring the plants between 70 and 100% RP. There is one boiling water reactor (BWR) that has been in flexible operation for over a decade due to hydro, and since 2016 some pressurized water reactors (PWRs) and BWRs have started operating flexibly due to increases in wind power. There are plants in the southern part of the United States that are considering flexible operations due to increasing solar power. The reactor power level is changed only by a licensed reactor operator; the rate of the power change is pre-determined and remains unchanged to ensure the protection of the fuel. Thus, so far, no fuel issues have been reported.

Some North American nuclear power plants have experience with flexible operation on a seasonal basis. Nuclear power plants in Ontario, Canada and in the north western United States are requested to manually reduce power output or extend their outages due to high levels of hydroelectric power generation.

The Electric Power Research Institute (EPRI) has conducted a significant R&D programme to support the flexible operations of nuclear power plants. Besides fuel integrity, EPRI's programme comprehensively deals with various aspects, such as water chemistry, cost-risk evaluation of major components (turbines, moisture separator reheaters and separator pumps) and instrumentation for real-time updates to operators.

It is anticipated that there will be increased pressures for more widespread flexible operation of nuclear power plants due to the increasing growth of renewable generation and the retirement of older fossil plants. However, not all existing nuclear power plants will need to consider flexible operations. The need for flexible operation will depend on local grid conditions, utility fleet economics, and projected future changes in regional generation and transmission.

2.2. POTENTIAL FUEL FAILURE MECHANISMS DURING FLEXIBLE POWER OPERATION

An earlier review, for example, [12] indicated that although there are various failure mechanisms associated with specific fuel designs, only a few of these mechanisms can have major bearing on load following operation. These include:

- Pellet-cladding interaction with stress corrosion cracking (PCI/SCC);
- Fatigue (including corrosion assisted fatigue).

Both failure mechanisms remain operative anytime during the load following operation. Depending on the mode of the load following operation and fuel rod design features, either of the mechanisms or a combination of both may be dominant for fuel failures.

In the United States of America, the cladding performance with respect to fatigue due to power cycling needs to be assessed according to NUREG-800/Standard Review Plan Section 4.2 [13]. The figure of merit used to quantify the fatigue performance is the 'fatigue usage', which is evaluated based on a conservative assumption of number and magnitude of cycles, which covers potential daily load following, as well as other lower frequency cycles and power manoeuvres (especially in BWRs). The fatigue usage calculation is based on previous fatigue experimental data e.g. O'Donnell-Langer's "S-N number of cycles to failure" of a given strain amplitude [14]; a fatigue usage life-fraction is calculated for the spectrum of cycles considered in the analysis. This process stipulated by the US NRC is adopted with some possible adaptations in many other countries.

However, one counter example is the French practice, which does not include the assessment of the additional fuel rod damage by fatigue due to power cycling operations with respect to PCI/SCC. This approach is based on the fact that the French power ramp test database includes fuel rods of various designs which have been irradiated in EDF commercial nuclear power plants. As such, the tested fuel rods experienced extensive load following and frequency control power transients in the nuclear power plants. As a result, the PCI/SCC failure thresholds derived from the database take account of any potential effect of mechanical state (e.g. fatigue damage) that load following

could have had on the fuel rods. This leads a strong support to not calculating fatigue margin, on the top of the extensive verification of excellent fatigue performance during normal operation that includes a large number of cycles in French nuclear power plants.

3. PCI/SCC PHENOMENA AND REVIEW OF PREVIOUS ACTIVITIES

This section provides a summary of up-to-date knowledge on PCI/SCC phenomena and associated important activities, previously conducted by the IAEA and OECD-NEA, to facilitate Member States' implementation of prevention methods. This section is intended to provide the basis on which progress of enhancing PCI/SCC technologies to support the flexible operation of nuclear power plants can be identified. Details of the progress are described in Sections 5 through 8.

3.1. PCI/SCC PHENOMENA

The occurrence of many fuel failures in the 1960s, especially in BWR and CANDU power reactors, triggered a flurry of R&D activities [15] to investigate the causes of those fuel failures and to enhance fuel rod resistance to the still to be identified failure mechanism at that time. The goal was to propose mitigating solutions, which would alleviate, if not prevent fuel rod failures.

A brief overview of PCI R&D and prevention or mitigation solutions is described in the subsequent sections. Annex I contains a supplementary information to support these descriptions, as a summary of the present understanding of SCC mechanisms and related key parameters. These descriptions in this section along with Annex I are intended to form the basis on which recent achievements in enhancing PCI/SCC technology can be reviewed.

3.1.1. Early R&D, PCI mechanism hypothesis

The main outcome of the intensive research programmes in the 1970s and early 1980s was the crystallization of the following theory for fuel rod failures that are possible to occur during power ramps: "Either iodine (I) or cadmium (Cd) is the chemically aggressive fission product that in conjunction with high tensile hoop stress developed in the cladding during a power ramp combines to trigger a SCC process that can result in cladding breach in certain conditions. Because the cladding is mechanically loaded by the pellet-cladding mechanical interaction (PCMI) during a large power increment when the pellet-to-cladding gap is closed, the process was called PCMI-SCC, or simply PCI" [15].

3.1.2. Salient features of the PCI/SCC process

Fuel failures during power ramps in power reactors together with the results of the power ramps performed in material test reactors have revealed that the ramp terminal level (RTL), i.e. ramp terminal linear heat generation rate (LHGR), and the LHGR increment, i.e. the power jump from the initial power level, are the main underlying parameters that affect the PCI/SCC failure threshold. A certain dwell time at the RTL seems another requirement for PCI/SCC; however, the dwell time effect is not clearly unfolded from the data as a critical parameter.

The power ramp rate, i.e. the rate of the LHGR increment, is shown to be a first order parameter. During fast power ramps or during parametric SCC tests where mechanical loading occurs at a high strain rate, the SCC process does not have time to occur and pure overload mechanical failure occurs. When the parametric SCC tests are performed at moderate or low strain rates, the SCC process can take place. Detailed chemical process involved in the SCC process remains to be elucidated. The general consensus is that iodine is the aggressive chemical agent (although Cd was also shown to promote cracks with similar fractography features), but the corrosive mechanism is not clarified between the two proposed hypotheses, namely surface adsorption and weakening of Zr atomic bonds, or diffusion at the crack tip, respectively.

The two main power ramp parameters mentioned above can be clearly correlated to the mechanical and chemical behaviour of the fuel rod during a power ramp. To that end, the maximum (peak) stress achieved during a power ramp is directly proportional to the LHGR increment. The initial LHGR level and the previous power history also play a major role by affecting the pellet-to-cladding gap at the beginning of the power ramp and hence the degree of the pellet-cladding mechanical interaction and hence the magnitude of the peak stress when the RTL is attained. The maximum power level during the power ramp, namely the RTL determines the magnitude of the pellet temperature, which is the main parameter affecting fission gas release. Of course, the fission gas release process is responsible for the release of the SCC aggressive chemical species (presumed iodine) that is assumed simultaneous and proportional with fission gas release.

In the early days, power ramp results from material test reactors and from some power reactors were interpreted by using a correlation of the LHGR increment vs. the initial LHGR level [16, 17].

A power ramp test performed in material test reactors is quickly terminated after a rod failure is suspected by an increase of the coolant activity via online measurements (also by a decrease of the rod elongation when an axial elongation sensor is available). When the material test reactor is shut down right after the fuel failure is recognized, the crack created by PCI/SCC is a pinhole with possible shear lips. On the other hand, power reactors cannot be shut down immediately after the fuel failure is recognized, thus, the initial pinhole crack extends axially and appears as a narrow short axial crack [15].

The other two parameters mentioned above, power ramp rate and dwell time, are related to the kinetics of the SCC process that is divided into three stages for incubation, initiation and propagation. Because the SCC process requires a simultaneous involvement of both mechanical and chemical aspects, either of the two parameters can be considered as a rate controlling depending on the conditions of the power ramp. The mechanical aspect is associated with the strain rate, which is affected by the power ramp rate, and with the time at high stress, which is affected by the dwell time at the RTL. The chemical aspect is associated with the chemical reactions of iodine with Zr and with other gases, which follows a certain dynamic evolution that after a while can lead to the disappearance of the aggressive iodine compound.

The passivating oxide layer at the cladding inner surface can protect the cladding from the SCC process during slow power ramps, by delaying the incubation or initiation phases and requiring higher stresses for the SCC to occur.

It is important to review the parametric experimental studies that were conducted to understand the I-SCC process in view of the above considerations on the mechanical and chemical aspects involved in I-SCC. Specifically, there have been out-of-the pile parametric studies conducted either at a constant stress or at a constant strain rate.

Analysing the two types of tests, namely the constant stress and the constant strain rate, it was revealed that link between the results of the two types of tests is the strain rate, i.e. the lower the strain rate in the constant strain rate test, the lower the stress in the constant stress tests is. This correlation between the constant stress and constant strain rate tests implies that it is not possible to define a unique and generally applicable failure correlation expressed as stress threshold vs. associated time-to-failure and that the strain rate needs to be included.

3.1.3. Preventing/mitigating solutions

To investigate the PCI/SCC phenomenon, separate effect tests were undertaken in a manner to:

- Create stress and chemical environment;
- Simulate the actual mechanical loading situation e.g. mandrel [18] or fuel swelling simulation test [19] experimental setups.

It became evident that the following four factors need to co-exist for an occurrence of the PCI/SCC failure:

- High stress;
- Presence of the right chemical environment;
- Sufficient time;
- A susceptible material.

Therefore, solutions were sought to either prevent or reduce the propensity to PCI/SCC failures, both as new pellet and/or cladding materials that would be less prone to the SCC mechanism, or operating strategies to preclude the critical operational parameters leading to PCI/SCC failures.

The proposed preventing or mitigating solutions were based on the above mentioned PCI/SCC failure theory and by correlating the experimental data. That is, ways to reduce the stress level in the cladding or prevent simultaneous release of the aggressive fission products were investigated. For example, two main ideas gained more attraction for application to BWR fuel, namely, a cladding inner soft liner (called also barrier) made of pure or very low alloying elements' concentration Zr and a 'soft' doped pellet [20].

Eventually the liner concept was adopted in production and it was considered that the PCI/SCC issue was resolved from the engineering point of view, by late 1970s, early 1980s. Other measures were taken as well in operation and fabrication.

Therefore, the main factors contributing to PCI/SCC 'resolution' can be summarized as follows:

- Improved understanding and modelling work resulting from laboratory and power ramp tests;
- Adoption of power plant operational measures to prevent PCI/SCC failures;

- Better control of fuel fabrication variants e.g. fuel dimensional stability against densification;
- Development of cladding with PCI/SCC barriers, notably the sponge Zr liner for BWR fuel rods and graphite coating for CANDU fuel rods, followed by specific liner variants by all vendors.

3.1.4. Different PCI/SCC variants and current understanding

Nevertheless, PCI/SCC failures still occurred and operating guidelines were proposed for fuel with either liner or non-liner cladding. These operating recommendations amount to restrictions on power ascension during the power ramp, depending on irradiation history and burnup of the ramped fuel rods. The implementation of operating guidelines and/or the liner cladding greatly reduced the number of fuel failures by PCI/SCC. However, as mentioned above, spikes of fuel failures still occurred for which all indications were pointing towards a PCI/SCC failure type.

Investigation of some of these failures showed a variant of the PCI/SCC mechanism, in which the stress is generated by the bending of the unsupported arch of cladding over the missing pellet surface (MPS) due to a circumferential chip at pellet end; this MPS assisted PCI/SCC failure mode has been called ‘non-classical PCI’ or PCI-MPS [21]. The solution to this new failure mode consisted in tightening the operating guidelines as a first response, followed by refining manufacturing with tighter specifications for MPS and enhanced pellet inspection plans in order to prevent to the maximum possible level, MPS chips larger than a critical width. The above mentioned actions taken in engineering and manufacturing proved to be effective, as duty related, PCI-MPS failures were very sporadic afterwards.

The research has continued to this day, although at a slower pace, after the engineering solutions mentioned above were implemented in operation. Full understanding of the process is still lacking, in almost all aspects of the SCC process. Early failures and related research indicated that SCC is the main cause of the PCI failures. However, all the details still not yet clarified: e.g. is the aggressive chemical corrosive agent I or Cd (or a combination of corrosive agents)? It was also determined that fuel rod chemistry is a necessary ingredient: e.g. fresh pellets in irradiated cladding did not fail. The other main outcomes of the material test reactors and laboratory studies include:

- Out-of-the pile studies on fresh and irradiated cladding in I and Cd environments showed similar fractographic features;
- Role of stress is very important: Time to failure increases as the stress decreases;
- Very little Iodine concentration can still lead to SCC;
- Cladding texture was determined as an important cladding related parameter from experimental observations, but also surface finish and residual surface stress;
- Pellet stoichiometry is an important factor with beneficial effects if hyperstoichiometric [22].

3.2. PREVIOUS IAEA MEETINGS AND INTERNATIONAL STUDIES IN 1970S –1980S

A series of international specialists’ meetings or technical meetings have been organized by IAEA during the late 1970s and 1980s with emphasis on PCI/SCC [1, 3, 5] and with emphasis on effects on fuel of power ramping, cycling and load following [2, 4, 6]. General conclusions obtained from these meetings included:

- Experimental results obtained in research reactors and models based on them demonstrated that power ramping, cycling and load following could be performed in power reactors under normal operating conditions;
- Extensive experience of power ramping, cycling and load following operations in commercial reactors were available, and indicated clearly that there is no adverse impact on fuel;
- The results yielded by high burnup programmes showed no negative consequence on pellet-clad interaction. This needs to be confirmed and further extended to the higher burnups that utilities are aiming for in the near future;
- There exist some grey area in fully understanding the basic phenomena on PCI/SCC. In order to get even more economical and flexible operating conditions, continuation of experimental work is necessary;
- The PCI/SCC subject should be dealt with in a meeting which will cover both reactor system operation and fuel performance under power cycling and ramping conditions.

The outcomes of the extensive international R&D programmes on PCI/SCC since the 1970s have led to the following achievements:

- An important PCI/SCC database has been established, including ramp tests, separate effects tests and plant data [23–27], to support both mechanistic and statistical data evaluations;
- Appropriate PCI/SCC operational limits or strategy on power changes and power ramp rates [28–31] have been determined and applied to maintain low probability of fuel cladding failures caused by PCI/SCC;
- Various empirical PCI/SCC design limits (technological limits or failure thresholds [32, 33] based on stress or strain energy density) have been determined based on simulation of the ramp tests with fuel rod performance analysis codes;
- Various fuel rod analysis codes and methods [9, 10, 32–39] have been developed for verification of the PCI/SCC design margins or assessment of the PCI/SCC risks;
- Alternative PCI/SCC remedy (or resistant) fuels, such as the liners or doped pellets [40, 41] have been developed (in particular for BWRs);
- Online PCI/SCC monitoring and surveillance systems [42, 43] have been developed and implemented in order to prevent the PCI/SCC failures.

3.3. OECD-NEA WORKSHOP IN LUCCA, ITALY, 2016

The OECD-NEA’s workshop on Pellet-Cladding Interaction (PCI) in Water Cooled Reactors held in Lucca, Italy, 22–24 June 2016 [44] provided an overall review of knowledge and directions for future R&D activities on PCI/SCC. The IAEA’s technical meeting held in Aix-en-provence on 8-11 October 2019 was an extended forum from the OECD-NEA workshop at Lucca, focusing on methodologies applicable to support the flexible operation of nuclear power plants.

Regarding the role of cladding design to prevent PCI/SCC, the workshop drew the following conclusions:

- Liner at the cladding inside surface remains an interesting mitigation option, in particular for BWR fuel rod designs;
- Texture controlled claddings shows improved resistance to PCI/SCC failure;
- Cladding design (i.e. manufacturing process, heat treatment, etc.) and related mechanical properties (i.e. low stress creep and high stress relaxation properties) seem to be more effective than cladding material chemistry with respect to the mitigation of PCI/SCC.

Regarding the role of fuel pellet design on PCI/SCC mitigation, the workshop drew the following conclusions:

- Available power ramp experiments show that UO₂ pellets with additives exhibit improved PCI/SCC resistance. Nevertheless, the actual intrinsic physical mechanisms activated during a power transient, remain unclear or uncertain. Experts claim that additives help trapping the corrosive species within the fuel matrix and therefore delay their action on the cladding inner surface. However, it has been shown, through various experimental programmes, that even very low concentrations of aggressive species in the pellet-clad gap, are sufficient to generate SCC.
- In this perspective, the mitigation role of oxygen, which is released in the pellet-clad gap during the transient, might be important. There is some evidence that additive fuel releases more oxygen in the gap than standard UO₂ fuel, such enabling the formation of a protective oxidized layer and a reduced risk for SCC.

As regards modelling and simulation tools, the workshop drew the conclusion that the conventional 1.5-dimensional (1.5D) and new 3-dimensional (3D) codes remain complementary. That is,

- The 1.5D codes are still used as reference tools for most of the industrial applications (mainly due to calculation time constraints that prevent fuel core designers to use 3D tools to assess core-wide PCI/SCC margins, the number of calculations being very important);
- Although 3D modelling is largely progressing to simulate various specific phenomena in the fuel and cladding during a power maneuvering operation, multi-scale modeling is not ready for as a predictive tool to assess PCI/SCC failure risk.

As for the design verification methodology, the workshop drew the following conclusions:

- The PCI/SCC failure thresholds are based on a series of power ramp tests that accounts for fuel pellets/cladding materials combined with fuel rod design, and a validated 1.5D fuel performance code to analyse the tests. Then, this threshold is used in established methodologies, together with the the same 1.5D fuel performance code to define operational guidelines in nuclear power plants in specific countries;
- This kind of methodologies have been successfully applied to various fuel core designs and management schemes; however, they remain complex and time consuming. Most European licensees expressed a strong interest in developing simpler and faster PCI/SCC risk assessment tools.

4. PCI/SCC RELATED LICENSING CONSIDERATIONS

4.1. IAEA SAFETY STANDARDS

The IAEA Safety Standards, Specific Safety Requirements series No. SSR-2/1 (Rev.1), Safety of Nuclear Power Plants: Design [45] states that “Fuel elements and assemblies for the nuclear power plant shall be designed to maintain their structural integrity, and to withstand satisfactorily the anticipated radiation levels and other conditions in the reactor core, in combination with all the processes of deterioration that could occur in operational states” (Requirement 43).

To meet this safety requirement in terms of PCI/SCC, the recently published IAEA Safety Standards SSG-52 (Specific Safety Guide on Design of the Reactor Core for Nuclear Power Plants [46]) recommends that:

- (Para. 3.48) “Stress corrosion cracking induced by pellet–cladding interaction in the presence of corrosive fission products should be prevented”.
- (Para. 3.61) “The design should ensure that the likelihood of stress corrosion cracking in the fuel cladding is minimized in normal operation and anticipated operational occurrences”.
- (Para. 3.62) “Stress corrosion cracking of the fuel cladding should be prevented by implementing adequate design methods such as those given in the following examples:
 - Reduce tensile stresses in the fuel cladding by restricting rates of power change (allowing for the cladding stresses to relax) or by delaying the time at which the pellet–cladding gap closes (this can be achieved by increasing the initial fill gas pressure in the fuel rod or by optimizing the creep properties of the cladding),
 - Reduce the corrosive effects of the fission products (e.g. iodine, cadmium, caesium) generated by the pellet by using a liner (for boiling water reactors) or a graphite coating (for pressurized heavy water reactors) that is less susceptible to the corrosive effects on the inner surface of the cladding. This liner can also even out local stress concentrations in the cladding,
 - Reduce the availability of corrosive fission products at the pellet–cladding interface by using additive fuels that are able to better retain the corrosive fission gas products within the fuel matrix,
 - Reduce local power peaking factors (and thus changes in local linear heat generation rates) through core design techniques”.
- (Para. 3.63) “The power ramp failure threshold should be established, if applicable, in test reactors by means of power ramp tests for each type of fuel or cladding. The data collected should cover the entire burnup range”.
- (Para. 3.64) “Fuel performance analysis codes can be used to analyse and interpret the data from power ramp tests and to determine a failure threshold. The parameter used to define this threshold is usually the maximum cladding stress but the strain energy density can also be used. These same fuel performance analysis codes can be used to assess risk factors that cause this type of stress corrosion cracking of fuel rods in the reactor core and to define adequate guidelines to avoid it”.
- (Para. 3.153) “The reactor core analysis should verify that the core fuel loading pattern will meet fuel design limits for all applicable plant states”.
- (Para. 3.158) “The effects of operating conditions such as load following, power cycling, reactor startup and refuelling manoeuvring should, whenever specified, be superimposed onto the power level distributions and temperature histories to evaluate the potential effects of thermal cycling on fuel rod thermomechanical responses, such as the buildup of pressure due to fission gas release to the pellet–cladding gap and fuel cladding fatigue”.

These recommendations will provide Member States with guidance to avoid PCI/SCC issues in the reactor core design and operation.

4.2. LICENSING APPLICATION PRACTICES WITH RESPECT TO PCI/SCC IN SOME MEMBER STATES

In most countries, the PCI/SCC risk of failure during normal operation and AOO conditions is not included in the safety analysis report, and therefore its treatment in licensing applications is somewhat different from country to country, with industry self-regulating itself in the case PCI/SCC is not specifically required in licensing. With regards to a tolerable coolant radioactivity level, any nuclear power plant can accommodate a small number of fuel rod failures at one time in the core during operation. Radioactivity limits specified in the operation technical specification document, particularly with regards to ^{131}I concentration level in the primary coolant system, permits plant operation with a limited number of fuel failures.

The current U.S. Nuclear Regulatory Committee (US NRC) does not have specific requirements to prevent PCI/SCC failures; however, the following two limits are applied to prevent fuel failures including those caused by PCI/SCC or PCMI [13] during AOOs or Condition II transient conditions (although it is recognized that the two limits do not fully inhibit PCI/SCC occurrence):

- The uniform strain (elastic and inelastic) in the cladding has to be less than 1%;
- Fuel melting has to be avoided.

US NRC considers that PCI/SCC during AOOs has a low safety impact because PCI/SCC failure has low probability of occurrence during AOOs, owing to the magnitude and duration of the power transient being limited: the maximum power level in an AOO is capped by automatic trip set points and the AOO excursion duration is limited by operator's reasonably quick response time [47].

Practices on PCI/SCC in France, Belgium and Germany are described in the paper presented by Zhang at the technical meeting (see Session I of Annex II), which is summarized below:

- In France, a regulatory requirement exists for the licensee to demonstrate that no fuel failures are caused by PCI/SCC for all the operational states in the reactor core. Operational limits need to be established taking account of load following, extended operation at low power and rates of the power changes. To comply with these requirements, French fuel industry has developed 'analytical PCI verification methodologies' [10, 36].
- Belgium's practice on PCI/SCC is overall similar to US practice, except for submitting to the regulator a PCI technological limit and PCI verification methodology for certain nuclear power plants. Unlike France, there is no need to carry out cyclic PCI verification.
- In Germany, there exists a regulatory requirement [48], which states "The loadings (i.e. increase in power output) resulting from normal operations and AOOs shall be limited such that the integrity of the fuel rod is ensured, and the pertinent PCI criteria shall be derived using experimental results (e.g. ramp tests in test reactors and/or operational experience)". The German industry has developed PCI rules for BWRs and PWRs [28–31] and implemented the automated PCI surveillance and protection system in PWRs [42, 43].

Similar but less restrictive requirements have been followed in other OECD countries like Finland, Sweden, Switzerland and the United Kingdom [49].

5. PCI/SCC IMPLEMENTATION IN REACTOR CORE DESIGN AND OPERATION

5.1. OVERVIEW

The extensive R&D programmes during 1970s–1990s have led to significant achievements in reducing the PCI/SCC failures at the expense of constraints on the core design and operation. Since then, the fuel community has continued conducting R&D programmes to reduce the conservatism embedded in these constraints on the core design and operation, and consequently to allow for relaxation of these constraints without affecting the PCI performance. A number of papers related to this area have been presented, followed by intensive discussions at the technical meeting held in Aix-en-Provence, 8–11 October 2019.

5.2. REACTOR OPERATION GUIDELINES

The PCI phenomenon has been extensively investigated after occurrence of a significant number of PCI/SCC failures in the 1970s. In order to improve nuclear fuel reliability, fuel vendors have introduced ‘fuel operational limits’ imposed on power manoeuvring and rate of power ascension and provided ‘fuel operating guidelines’ to prevent PCI/SCC or PCMI.

The fuel operating guidelines specify prescribed preconditioning, limitations of operating time at reduced power, ramp rates and hold times at the ramped power for different operating modes. Note that start-up conditions after handling of the fuel assemblies could render the fuel more susceptible to PCI/SCC.

These operating guidelines are valid for a specific plant design and a specific fuel design. More PCI/SCC failures have occurred in BWRs mainly due to the frequent use of control blades to compensate for changes in reactivity with burnup and for power variations as needed by load following. This causes significant and localized distortions of the axial power distribution of the nearby fuel rods. Therefore, operating procedures were required for BWRs to impose limits on the rate of power increase at start-up after refuelling or after the exchange of the control rod sequence, as well as for the speed of withdrawal of the control rod in the high power regions when the fuel is not preconditioned.

These operating procedures played an important role in mitigating PCI/SCC failures in BWRs, along with fuel design changes, such as the introduction of the zirconium liner (or barrier) on the clad inner surface and the changing from of 8x8 fuel array to 9x9 and 10x10 fuel, significantly reduced the occurrence of PCI/SCC fuel failures in BWRs. The operating procedures were also implemented in PWRs. However, because the PCI/SCC limits for PWRs practically do not restrict load following operation, there was never an incentive to use cladding with liner in PWR fuel. It has been shown that the doped pellets could further improve the PCI resistance.

The paper presented by Paulin (see Session I of Annex II) described the main aspects of PCI/SCC management and feedback from operation experience of EDF PWRs. It also showed examples of industrial needs regarding manoeuvrability and operation at intermediate power. The main operational constraints related to PCI/SCC at EDF are:

- The potential reduction of manoeuvrability, if the margins between the normal operation conditions (including load following and frequency control) and the thresholds of the alarms are not sufficient;
- The limitation of ERPO durations below the minimal requirements;
- The compatibility with core variability needs.

To ensure the stability of the European electrical grid, which is compromised by the growing part of intermittent renewable sources in some of the countries, it is important to propose innovative PCI/SCC resistant fuel concepts and advanced online monitoring/protections systems.

The paper presented by Arimescu (see Session I of Annex II) provided a review of international power ramp programmes as a basis for BWR operating guidelines. The safe operation of fuel assemblies in BWRs is assured by following the operating guidelines that have been developed over time as a set of rules regarding fuel rod power increases that are permissible during BWR manoeuvres. The basis for the operating guidelines has evolved, from the theoretical point of view, in accordance with the advances in our knowledge of fuel behaviour. Nevertheless, the formulation of the guidelines strongly relies on the experimental body of information acquired from the international power ramp programmes that have been performed in material test reactors, coupled with the experience feedback from fuel operation in power reactors.

Specifically, the paper presented by Arimescu (see Session I of Annex II) provided an outline of the format of the operating guidelines proposed by different organizations and summarized the different safe operating thresholds and assumptions of the guidelines. Then, he reviewed the international power ramp programmes and analysed the results of the international power ramp programmes with respect to fuel rod design vintage as the fuel design and characteristics have evolved over time. The PCI/SCC mitigation at slow ramps is of interest, which is a main component of the operating guidelines. Some remarks were also made in the paper regarding the advanced fuel types currently under development or in the phase of being introduced in operation, from the point of view of enhancing reliability during operation in BWRs.

5.3. PCI SURVEILLANCE AND PROTECTION SYSTEM

Siemens KWU proposed a PCI/SCC surveillance and protection method for plant operation, based on the RSST (power Range, Step, Speed and Time) approach. The RSST method is intended to safely prevent fuel failures after deduction of adequate safety margins [29, 42].

The PCI/SCC operating limits similar to the above concepts have been implemented as the automatic surveillance and protection in the monitoring systems installed in some German PWRs and also adapted in the N4 series of 1400 MW(e) class PWRs (developed by France) and European PWRs (or called EPRs). The paper presented by Daniel and co-authors (see Session I of Annex II) described the Framatome's gliding threshold methodology considered for European PWRs.

5.4. IMPACT ON REACTOR CORE AND FUEL DESIGN

In response to the regulatory requirements, the nuclear fuel industry has addressed PCI/SCC and PCMI issues through improvements in the fuel design, fuel manufacturing, and reactor core design and operation. The risk for PCI/SCC failures has been effectively reduced via modification to both fuel pellet and cladding designs, rigorous quality control of fuel pellets, improved core design and operations, and a combination of any of these.

Although PCI/SCC is not considered as a safety issue in most countries, the fuel vendors and the operators have developed methodologies to verify the PCI/SCC design margins, in order to assure sufficient operational margins to facilitate reactor operation. While the PCI design verification methodologies are efficient to reduce the PCI/SCC risks, a balance is needed between more detailed analysis methods, which may lead to higher margins and a longer calculation time, and simplified methods which are fast but may lead to smaller margins (due to conservative approaches).

The paper presented by Matias and Doncel (see Session I of Annex II) described the ENUSA's PCI design verification methodology to evaluate flexible operation in PWRs, especially the ERPO. The ENUSA's methodology includes the cladding effective (Von Misses) stress, calculated by the fuel rod thermal mechanical analysis code (TREQ), and a technological limit driven on basis of experimental ramp tests. The evaluation is performed for a broad variety of conditioning powers that cover all the real situations in the core. The PCI/SCC margin loss is determined, taking into account the difference between the maximum effective cladding stress during the Condition II transient event after an ERPO and the PCI technological limit. This methodology is used to determine the maximum allowable duration of ERPO immediately after which a return to full power operation is possible.

The paper presented by Daniel and co-authors (see Session I of Annex II) described the Framatome's PCI methodologies that are used to study 'enhanced' manoeuvrability in PWRs. The 'allowable power' methodology is used for a quick assessment of the PCI/SCC margins. The principle of the allowable power methodology consists of quantifying the PCI/SCC margins by comparing limiting Condition II transient power distributions (from the transient neutronic calculation) with the allowable LHGR for each axial node of the core (from the decoupled thermal mechanical calculation). Bounding assumptions for the transient boundary conditions and power ramp simulations induce a greater degree of conservatism, and the 3D calculations for different Condition II transient scenarios lead to considerable computational effort. This methodology has been applied for fuel rod design for each new fuel product to demonstrate an acceptably low risk of PCI/SCC failure. Indeed, the resulting PCI/SCC margins are rather large for the improved fuel products with M5 cladding. During the loading pattern verification, therefore, the PCI/SCC margins are only verified to ensure the fuel reliability.

The paper presented by Sperlich and co-authors (see Session I of Annex II) described German operating conditions and experience on PCI loads in BWR and PWR. German nuclear power plants were explicitly designed

for various flexible operation modes such as primary frequency control, secondary control by plant operator or remote controlled by load dispatcher and classical load following operation mode. In recent years, there has been an increase to demand such flexible operation modes for electricity grid stabilization purpose due to an increase of volatile and heavy renewable energy production. In addition, there have been economically driven considerations in case of low or even negative prices on the spot market. A comparison to baseload cases from BWR and PWR is discussed with respect to PCI relevant loads and operation feedback. These load cases include startup conditions for BWR and PWR, impact of (continuous) load following operation and different control rod operating strategies for BWRs.

The paper presented by Bernard and co-authors (see Session I of Annex II) described the EDF's verification methodology for the flexible operation of nuclear power plants which is used to justify specific operational conditions in French PWRs. In France, the regulator requires the operator (EDF) to demonstrate that no PCI/SCC induced fuel failure would occur during any type of AOOs. Since nuclear energy source is a large fraction of the total energy mix in France, the French nuclear power plants have to be as flexible as possible to accommodate intensive power changes related to frequency control requirements and daily load following. To deal with potential operational events, French nuclear power plants require that the safety demonstration covers ERPO periods as long as (or greater than) 30 days. In order to optimize the long term electricity production at the whole fleet scale, the operator has set up a series of core reload patterns for each fuel management scheme (i.e. one for each nuclear power plant type of the French fleet). PCI/SCC studies at EDF indicated that the PCI/SCC failure would be prevented by two means:

- Adjustment of the reactor protection thresholds;
- Definition of the PCI operational technical specifications.

PCI/SCC analyses were performed for the whole core, considering each operating mode of the reactor. A PCI/SCC failure criterion, called 'technological limit', needs to be determined based on experimental power ramp tests. Two types of design verification methodologies are devoted to PCI/SCC:

- A specific methodology called MIR (renovated PCI method, from the French 'Méthodologie IPG Rénovée'), which was developed in cooperation with FRAMATOME, is based on neutronics (3D kinetics calculations) and thermal mechanical calculations;
- Since the MIR methodology is time consuming and focuses on a single reference fuel reload pattern (one for each type of fuel management scheme), an alternative methodology has been developed recently to deal with variable fuel reload patterns and to reduce the calculations time. The main changes include statics neutronic calculations instead of kinetics calculations and decoupled neutronic and thermal mechanical calculations.

For a same reload pattern, the latter simplifications reduce the computation time but lead to smaller manoeuvrability margins. This approach is well suited to assess the impact of core patterns variability on PCI/SCC margins and to perform sensitivity analysis.

A comparable, simple and quick methodology was proposed by Zhang [50]. A specific loading pattern PCI/PCMI risk assessment (LPPRA) tool has been developed and implemented in the current core design and safety evaluation process. The PCI/PCMI risk is assessed in advance during the loading patterns design process, based on the core neutronic calculation results using the Tractebel's 3D code package. This assessment is based on the simple guidelines and correlations which are either provided directly by the fuel vendors or developed by the operator (Tractebel) using the vendors' fuel design verification results. The PCI/SCC margin is defined as "the difference between the predicted allowable power and the predicted maximum transient power provided by the fuel vendor" [50]. The LPPRA allows quick assessment of the PCI/SCC margin based on the conditioning power and burnup of the fuel rod, which are calculated for the specific loading pattern, without both time consuming neutronic transient calculations and detailed fuel rod thermal mechanical calculations. To enhance the reliability of the assessment tool, the correlations are continuously calibrated and updated on the basis of the fuel vendors' cycle specific PCI design verification results. The correlations have been adapted to cope with the requested plant operational flexibility like extended power modulations [50].

5.5. DISCUSSIONS AND RECOMMENDATIONS FOR FUTURE WORK

It has been shown that significant progress was made for the last decades in reducing the PCI/SCC failures during reactor operation. The IAEA survey on PWR fuel failures worldwide in 1994–2006 is shown in Fig. 2: the fractional failures by PCI/SCC was only 0.1% [51].

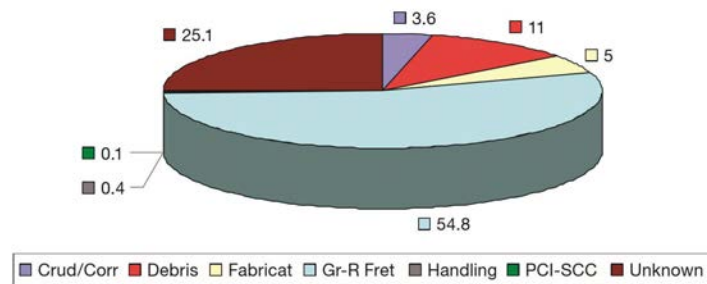


FIG. 2. PWR fuel failure causes worldwide in 1994–2006 [51].

Recent experience revealed that PCI failure may be possible in PWR fuels with defects on the surface of the fuel pellets [52]. The fractional fuel failures by PCI/SCC in PWRs has increased to 5.7% in 2006–2010, as shown in Fig. 3 (left) [52]. Stress concentration at the location of a missing pellet surface (MPS) resulted in ‘non-classical’ PCI/SCC induced cladding failure. To avoid this phenomenon, the size and depth of defects in the pellet are rigorously controlled through manufacturing quality control procedures. Fuel vendors have already adapted the corresponding fuel specifications as well as manufacturing tolerances and/or more stringent inspection procedures. This has greatly reduced the fuel failure by PCI/SCC in 2011–2015 (see Fig. 3 for PWRs and Fig. 4 for BWRs) [52].

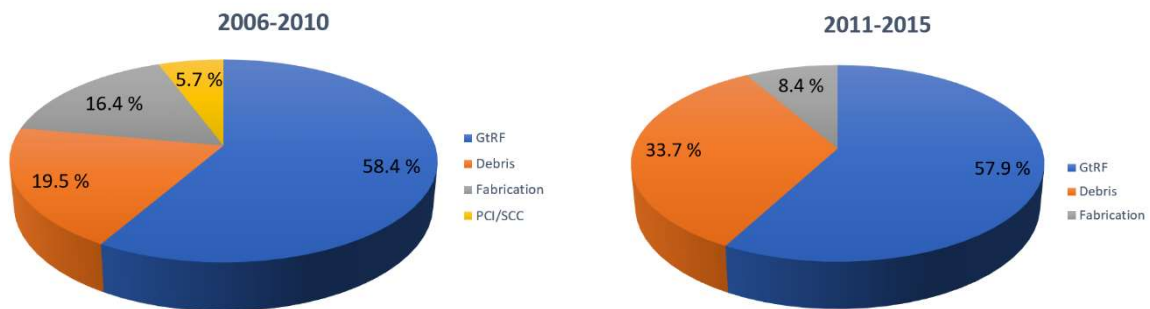


FIG. 3. PWR fuel failure causes worldwide in 2006–2010 (left) and 2011–2015 (right) [52].

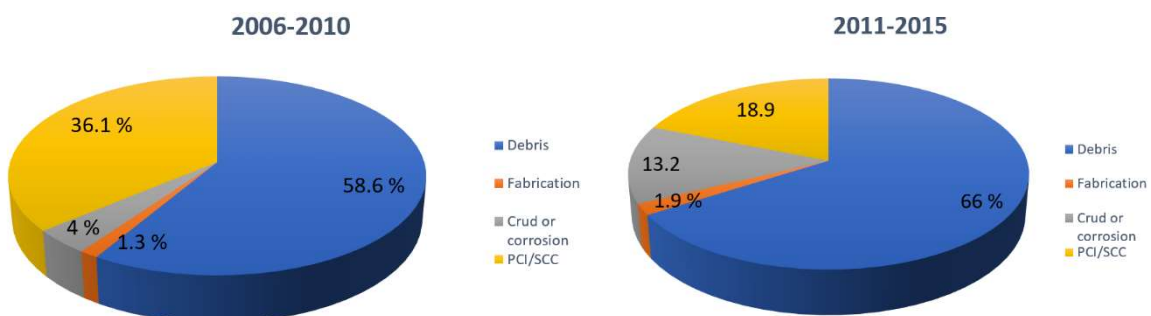


FIG. 4. BWR fuel failure causes worldwide in 2006–2010 (left) and 2011–2015 (right) [52].

No PCI/SCC failures have been observed in EDF nuclear power plants over more than the 1800 reactor years of operation for the whole French power reactor fleet, despite highly flexible power operations and rather fast start up rates (see Paulin, Session I of Annex II). This may be attributed to the rigorous quality control during the fuel

manufacturing process, as well as to the significant constraints imposed to plant operation by the ‘no PCI/SCC related failure requirement’ during any type of AOOs. However, these operating constraints also result in moderate economic losses due to some restrictions in the operational technical specifications (e.g. limited ERPO durations) impacting the nuclear power plant capacity factor.

The current reactor operation guidelines are based on the existing power ramp database that includes various fuel designs and test conditions. Current operational guidelines could be improved by performing ramp tests in more prototypical and comprehensive test conditions. Unfortunately, performing additional ramp tests in the near term is going to be difficult and expensive because of the recent shutdown of two material test reactors that were much utilized power ramp tests (i.e. OSIRIS in 2015 and HBWR in 2018).

A ramp database is very useful to validate fuel performance analysis codes in addition to the PCI/SCC failure thresholds determination. When the fuel rod does not fail, the test protocol is such that the maximum power is maintained during 12 h at least. This high power plateau ‘erases’ most of the information that are essential in validating the models which have been developed to simulate the physical phenomena occurring during the transient phase of the experiment. To address this issue, it is necessary to complement the classical ramp database with some specific ramps without holding time for non-failed rods, in order to ‘freeze’ the state of the fuel rod at the critical time, namely the top of the ramp. The classical ramp test and desired ramp test (with red error) are shown in Fig. 5. These ramps aim at better understanding the key mechanisms at work during the power ramps. The ramp test is, of course, followed by relevant post irradiation examinations (PIEs).

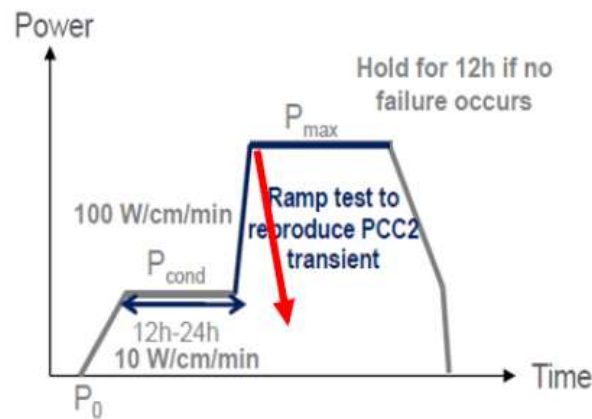


FIG. 5. Concept of ‘understanding’ ramps.

By using the models which have been validated, it becomes possible to more precisely design the test conditions of the next phase of power ramps aiming at determining the PCI/SCC failure limit of the fuel. The current PCI/SCC design verification methodologies also contain considerable conservatisms, mainly due to the use of the deterministic bounding approach (e.g. combination of an AOO at the worst time during the cycle, uncertainties implemented in the worst direction and at the bounding values, etc.).

The current PCI design verification methodologies are also complex and time consuming. They need to be simplified to allow quick assessments of the PCI/SCC margins.

With the introduction of more PCI resistant fuel design (e.g. use of M5 or Optimized ZIRLO claddings with doped pellets) and improved PCI design verification methodologies (see Section 8), it can be possible to better quantify the available PCI/SCC margins and to minimize the operational constraints.

Therefore, the following recommendations can be formulated for further development, as a result of the presentations and discussions with respect to the subject of this section:

- Development of fast running PCI design verification tools and simplified methods (goal is to be less than one week);
- Implementation of cost effective PCI/SCC surveillance in the core monitoring system of existing nuclear power plants;
- Determination of more mechanistic PCI/SCC failure thresholds and reduction of conservatisms in fuel PCI design verification methodologies and related operational technical specifications;
- Relaxation of operating guidelines/rules or operating constrains by PCI/SCC margin quantification using ‘best estimate plus uncertainty’ or risk informed PCI analysis methodologies.

6. EXPERIMENTAL UNDERSTANDING OF PCI/SCC MECHANISMS

6.1. OVERVIEW

This section is intended to review recent experimental studies related to PCI/SCC based on related papers presented at the technical meeting in October 2019. These papers either described the use of the experimental results in I-SCC modelling, or referred to implementation of experimental findings for modelling. To that end, in the introduction remarks, some theoretical aspects of fracture mechanics and fractography elements that have been used in the papers contributed to this session are summarized below:

- The fracture mechanics theory presumes the existence of an incipient crack and identifies the conditions leading to crack propagation. Associated parameters are:
 - Stress intensity ($\text{MPa}\sqrt{\text{m}}$), K (K factor);
 - Fracture toughness or tenacity ($\text{MPa}\sqrt{\text{m}}$), K_{Ic} . This quantity is often written as K_{Ic} to denote Mode I plane strain condition;
 - Moduli (J_{m-2}), G and E .
- The crack propagation thresholds have been derived in two ways:
 - Energy balance, which led to Griffith's fracture stress and related G_c toughness, above which unstable crack growth occurs;
 - Stress calculation at the crack tip, leading to the K_{Ic} stress intensity factor, beyond which the crack propagates rapidly.
- The link between the fracture variables, namely G_c and K_{Ic} , is a linear relationship, whose multiplicative term contains the crack length and a geometrical factor. (A certain crack length is assumed as part of the incubation/initiation stages beyond which fracture mechanics is employed to analyse crack growth.)

The above remark is prefaced by a brief summary of the generally accepted I-SCC stages, including the major factors that can impact the process:

- Incubation
 - I-SCC is not an electrochemical process as the intergranular stress corrosion cracking (or called IGSCC) of structural materials (steels);
- Initiation;
- Propagation
 - texture;
 - stress ratio;
 - hydrides.

In the subsequent sections, some progress on recent experimental studies are described based on related papers presented and discussions at the technical meeting held in Aix-en-Provence, 8–11 October 2019.

6.2. IN-PILE AND OUT-OF-THE PILE TESTS AND ANALYSES

This subtopic was addressed in the papers presented by Novikov and co-authors (see Session II of Annex II) and by Advonina and co-authors (see Session III of Annex II). The main theme of these papers was the impact of the cladding inner surface oxide layer on the PCI/SCC mechanism. To that end, out-of-the pile tests and hot cell PIE data on irradiated fuel rods from in-reactor studies have been combined.

The out-of-the pile tests performed by the authors and reported in the paper were inspired from an earlier study by Mattas and co-authors [53]. The SCC outcome of internally pressurized tubes with and without iodine were used for both unirradiated and irradiated tubes made of Zr1%Nb Russian alloy and compared with similar tests on other Zircaloy-2 and zircaloy-4 alloys. The following possible mechanisms relative to the initiation phase of SCC were considered with respect to the oxide layer on the cladding inner surface:

- (a) Diffusion of iodine through the zirconium oxide layer;
- (b) Chemical interaction of fission products (including iodine and cesium iodide) with ZrO_2 ;
- (c) Mechanical cracking of zirconium oxide and diffusion of iodine along the formed cracks.

Mechanism (a) was concluded as not operational because of very slow iodine diffusion rate through the oxide layer. Mechanism (b) deemed important because it leads to the cracks through the oxide, in addition to the pure mechanical cracking process of mechanism (c). In that sense, cladding irradiated in a material test reactor without fuel pellets lacks the impact of mechanism (b) and therefore studies on such empty cladding tubes irradiated in a material test reactor are not fully relevant for PCI/SCC as they do not contain the initiation phase of SCC. The main conclusions of the studies on Zr-1%Nb and comparison with previous studies for other Zr alloys that were drawn in the paper are:

- The initiation of SCC process in a fuel rod cladding requires overcoming the barrier – ZrO₂ layer on the cladding inner surface;
- The SCC mechanism begins as a result of cracking of the ZrO₂ layer as a combined result of structural changes in zirconium oxide during its growth and the action of high energy particles of fission products and stresses;
- The loss of the protective properties of the oxide layer on the cladding inner surface is the main factor in triggering the stress corrosion mechanism, leading to a drop in SCC threshold stresses with an increase in fuel burnup.

6.3. SEPARATE EFFECT TESTS ON UNIRRADIATED AND IRRADIATED MATERIALS

The paper presented by Hanlon and co-authors (see Session II of Annex II) included summaries of several out-reactor PCI testing campaigns in a variety of environments, which included C-ring compression, tube internal pressurization, mandrel testing, uniaxial tension and fracture mechanics testing. Additionally, new experimental observations of basal plane pseudo-cleavage and twinning near I-SCC cracks were provided in the context of the current literature in an effort to enhance PCI/SCC mechanistic understanding. Based on the review of out-reactor PCI/SCC testing, as well as the compact tension specimen results presented in this study, the following conclusions were reached:

- Observations from both the radial-longitudinal (R-L) and transverse-radial (T-R) specimen suggest that I-SCC cracks tend to follow basal planes and that no pitting occurs under the conditions used in this study;
- Large grains, low iodine partial pressures and low stress intensities allow for high confidence in determining the I-SCC crack path;
- Texture has a dramatic effect on the extent of out of plane cracking, also referred to as ‘tangential cracking’;
- A higher twin density is observed near the I-SCC crack in the R-L specimen than the T-R specimen, likely because more c-axes were aligned with the stress direction in the R-L orientation. Much less twinning was observed away from the crack;
- A need exists to better understand crack initiation, the basal pseudo cleavage growth mechanism, I-SCC crack tip deformation, and the effects of radiation damage on PCI morphology and mechanisms.

The atmosphere of SCC testing apparatus in the Canada Nuclear Laboratories was gaseous iodine, which was controlled separately during the tests. One interesting observation was with respect to surface pits, which have been proposed in the past as pre-requisite crack incubation sites. However, a couple of studies in the past seemed to indicate that surface pitting developed after the SCC cracking occurred and therefore, it was an after-effect and not a cause of SCC. This was summarized as follow:

- The role of pitting on in-service PCI initiation is unclear; at high iodine partial pressures pitting occurs regardless of stress, strain, or temperature, while PCI is also possible at low concentrations without a pre-machined stress riser where no pitting was observed. In the study reported in the paper there was no evidence of pitting, which supports the idea that pitting is not necessary for SCC cracking.

A question was raised regarding the iodine gaseous atmosphere, which was indicated in the test summary table of the paper as iodine pressure in Pa (I partial pressure), while many literature studies report it as surface concentration. It was commented that iodine partial pressure is a more meaningful parameter, considering the set of reactions between iodine and Zr metal surface.

In that respect, previous considerations were evoked, whereby, of the different Zr iodides that can be formed, the tetraiodide, ZrI₄ is the most aggressive gaseous active species. In the past, it was noted that the formation of ZrI₄ requires a certain amount of time and this could be the main (probably not the only one) reason for the observed SCC incubation time. During the compact tension specimen tests with online control of the K stress

intensity factor, an incubation time (time until crack propagation velocity accelerates as measured by the potential drop over the sample) was noticed anytime K was decreased; however, further studies are needed to discriminate between the chemical (e.g. ZrI_4) and mechanical (crack opening/closing effects) factors, which are contributing to the observed incubation times.

One of the findings of the microscopy studies was related to the mechanical behaviour around the crack, namely twinning was observed within a few grains of the crack than away from the crack. Similar observations have been made recently via 3D Electron Back Scattered Diffraction misorientation analysis in a companion study to the one reported in the paper. It was shown that twinning can lead to crack arrest in a grain otherwise well oriented for basal plane cracking. This observation can explain the typical branched appearance of SCC cracks, in that blunting occurs along some propagating directions, because of twinning and the crack branches off in a different direction.

An important contribution of the state-of-the-art microscopy investigation that was reported in the paper was a more comprehensive confirmation of the previously observed feature that SCC transgranular cracking occurs along (or very close to) basal planes. The 3D Electron Back Scattered Diffraction based investigation used in the study reported in the paper, provides far greater statistical significance by analysing a cracked volume containing nearly 1000 grains. Two figures in the paper were used to illustrate this feature: one showed evidence of tangential cracking in a T-R oriented specimen, while another one demonstrated that this cracking is again predominantly along the basal planes, with cracking in nearly every grain occurring along the basal plane. These observations provide conclusive evidence that texture affects the crack direction and morphology.

In the end of the Q&A period, it was suggested to continue the studies with a parametric test matrix, in order to explore the synergies between chemistry and mechanics and to gain more insights into crack incubation and initiation.

The paper presented by Le Boulch and co-authors (see Session II of Annex II) included first the experimental part: The I-SCC behaviour of cold-worked stress-relieved (CWSR) zircaloy-4 was explored by internal pressure tests with both inert and iodine gases. I-SCC susceptibility was explored in the tests on both unirradiated and irradiated cladding tubes. Rates of crack propagation were investigated from tests on pre-cracked tubes. Parametric internal pressure tests on unirradiated CWSR zircaloy-4 samples at different temperatures between 320°C and 380°C indicated an apparent threshold stress below which no I-SCC occurred, in the sense of very long failure times recorded in the internally pressurized tests.

The second part of the paper presented by Le Boulch and co-authors (see Session II of Annex II) presented the theoretical part of the paper, which consisted of a I-SCC model based on a combination of Kachanov's damage law with Miller's stress threshold and which was incorporated in the CAST3M finite element code. The approach presented is of the K_{IC} variant of fracture mechanics and was derived from internal pressure tests on pre-cracked samples.

The experimentally determined stress threshold is about 240 MPa on unirradiated CWSR zircaloy-4. This value is close to the stress threshold of 300 MPa exhibited in [25] on un-irradiated CWSR zircaloy-4. The stress threshold is about 150 MPa on irradiated CWSR zircaloy-4.

The Kachanov's model, used in post-treatment of finite element calculations, was used to model I-SCC initiation. A set of parameters was identified, from inner pressure tests under iodine vapor, for both unirradiated and irradiated CWSR zircaloy-4 and the model properly simulated both I-SCC initiation and I-SCC tenacity ' K_{SCC} ' for irradiated CWSR zircaloy-4. However, I-SCC propagation rates were underestimated with that set of parameters. In order to better evaluate the I-SCC propagation rates, some parameters need to be re-evaluated, or a specific mechanism needs to be added to the modelling of the propagation of I-SCC cracks.

During the paper discussion period, one theme was the duration and physical/chemical mechanisms related to initiation (modelled in the paper by a material damage model) and incubation (not modelled in the paper). In that respect, a link can be made to the ALCYONE paper presented by Sercombe and co-authors (see Session III of Annex II), in which the implementation of the model presented by Le Boulch and co-authors (see Session II of Annex II) was described; part of that implementation was with a model parameter related to crack incubation, namely a certain incubated crack depth. As mentioned in the introductory remarks, any fracture mechanics approach quantifies crack propagation and requires a pre-existing 'incubated' crack – therefore, the modelling requires an assumption about the length of this pre-requisite crack.

The paper presented by Alvarez and co-authors² [54] described the summary of the findings of the extensive programme of mandrel tests:

- The mandrel testing technique accurately simulates the local stress at pellet cracking and local concentration of iodine;
- PIE confirms that fuel cladding tested by means of mandrel testing and in-pile PCI failed rods show similar crack pattern and fracture appearance;
- It is hard to compare the strain to failure in a ramp tests with the strain to failure in mandrel testing, since the mandrel testing measures total strain to failure at test temperature, which has not been measured in R2 or Halden power ramps;
- The residual strain measured at room temperature cannot be compared since the ceramic parts inside the cladding (insert + sleeve) in the mandrel tests are permanently deformed during the tests, while the pellet expansion recedes during cool down during an in-reactor ramp tests;
- Parametric studies confirm that the temperature effect and effect of having a liner can be confirmed qualitatively in the mandrel tests;
- The ability to study the effect of single vs multiple step ramping and the ranking of different cladding types in the mandrel tests is still under examination.

There was a discussion on crack propagation whether fluting requires plastic deformation or iodine causes the crack propagation. Although fluting is often mentioned in connection with SCC fractography, it is not clear the role of iodine in crack propagation; in that respect, a similar ambiguous fluting feature is described in Annex I.

Another aspect of the microscopy investigations of the cracked surfaces is the observation of an inverted sequence of intergranular and intragranular (transgranular) cracking modes in the mandrel test samples, in that the former mode was detected in the latter stages of crack propagation, while the bulk of the literature data (see Appendix I, too) found intergranular cracking to occur at the crack outset and be followed by transgranular cracking along basal planes, mainly. The appearance of transgranular, indicative of large plastic deformation, appearance at the initial part of the crack, was questioned from the perspective of the mandrel test simulating more closely a nonclassical SCC mechanism, similar to the MPS-PCI failures observed in some commercial fuel rod failures. This suggestion was based on the geometry of the zirconia sleeve that has a number of slits at the outer rim, which resemble more a pellet chip (MPS) and are considerably wider than regular pellet cracks.

A paper presented by Nindiyasari and co-authors (see Session II of Annex II) focused on the mechanical aspect of the PCI, namely the frictional contact at an interface between the pellet and the cladding, which creates a shear stress that induces stress concentration in the cladding over opening pellet cracks during a power ramp. Actually, experimentally determined interface properties (interface shear stress) are needed as an input to models of hoop stresses in the cladding during PCMI failures. In this regard, a test fixture was developed for the characterization of pellet-cladding interface properties using the miniature tensile test machine in the hot cell laboratory.

6.4. MITIGATION BY MATERIAL IMPROVEMENTS.

In the paper presented by Jädernäs and co-authors (see Session II of Annex II), it was highlighted at the outset that the Studsvik ramp database points to fuels with additives/dopants having a PCI benefit, but it is unclear why they behave better. Therefore, hot cell PIE studies have been performed in order to gain more insights into doped fuel beneficial PCI mechanisms and the following main findings were summarized (taken from the presentation by Jädernäs):

- (a) “Cs was measured in the Al/Cr and Al/Si additive phases mainly in the center regions of the fuel ($T > 1300^{\circ}\text{C}$) using scanning electron microscope/wavelength dispersive spectroscopy. Iodine was measured in the Al-Si additive phases using transmission electron microscopy”;

² ALVAREZ, A-M., TEJLAND, P., MAGNUSSON, P., “Out-of-Pile Simulations of Iodine Assisted PCI Failure and the Effect of Ramp profiles”, Paper presented at Technical Meeting on Progress on Pellet-Cladding Interaction and Stress Corrosion Cracking: Experimentation, Modelling and Methodologies to Support the Flexible Operation of Nuclear Power Plant, Aix-en-Provence, France, 8-11 October 2019. This paper is not included in the proceedings in Annex II of this publication. However, relevant information can be found in [54].

- (b) “However, out-of-pile experiments (Mandrel testing) suggest very little iodine release is needed to produce PCI cracking (ppm levels of the available inventory)”;
- (c) “Al-Si additive fuel is better at retaining volatile, potentially aggressive, elements within the fuel”;
- (d) “Same comment as above. However, the dynamical behavior may be different and change the chemistry/stress timing. (Not measured, just hypothetical)”;
- (e) “Gd homogenization during the ramp test possibly releases oxygen to the fuel free volume. It could help mitigate PCI”;
- (f) “Cr migrates towards the hot pellet center forming Ba-Cr-Zr and possibly U and O containing precipitates. This could help mitigate PCI by dissociation, releasing oxygen, during high temperature transients. This statement is partly supported by thermodynamic calculations”;
- (g) “Important note: No macroscopic difference between the different fuel types could be observed but this could potentially be due to the relatively low temperature that these rodlets saw in-reactor”.

The above summarized results of the hot cell PIE on doped/additive fuel rods after undergoing a power ramp, point towards a possible PCI beneficial mechanism of cladding inner surface oxidation process, which is enhanced in the case of doped fuel. Compelling evidence of cracks that have been initiated and arrested (blunted crack tip) by oxidation in the cladding of Gd fuel rods was illustrated in the presentation.

A discussion was followed on whether O migration to the cladding inner surface occurs through pellet or through gas phase. Although different views were expressed, the advantage of doped fuels is the same for either O migration process.

Another discussion was on the role played by the cladding inner surface oxide film, whether oxide cracks that exist prior to power ramp promote SCC. The answer in principle to this question is based on the interplay of kinetics of the oxidation and cracking processes, so that enhanced oxygen availability in doped fuels generally promotes the passivation effect of the oxide and hampers to a certain degree the propagation of SCC cracks.

6.5. RECOMMENDATIONS FOR FUTURE WORK

Several papers presented at the technical meeting in October 2019 either confirmed some of the assumptions/hypotheses made in the past or provided some new data on the behaviour of doped/additive fuels, which are in focus lately. Some grey areas that were not clarified or even not touched were pointed out through discussions at the technical meeting. These are listed below as recommendations for further development:

- More experimental study of the incubation/initiation phase is necessary, because the mechanism of chemical attack by iodine (van Arkel or other process) is not known – only a good knowledge of this aspect would allow a proper modelling (refer to assumption adopted in ALCYONE for length of incubated SCC crack);
- The role of oxygen and cladding inside oxide layer requires more experimental studies; in that respect, the chemical interaction between oxygen and CsI or Zr iodides needs to be confirmed experimentally, as currently only thermodynamic calculations are available;
- The mitigating effect of slow ramps deserves more studies in order to fully understand the mitigating factors. The combination of experimental data and code calculations indicated that slow ramp benefit is not only a mechanical factor and that chemistry also plays an important role;
- One aspect that was seldom touched upon in past studies is the cumulative SCC damage in repeated power ramps. This issue is clearly linked to load following, flexible power operations, especially for BWRs in which local power transients occur frequently by control rods manoeuvring. The question is whether a crack that was initiated during a power ramp but did not propagate through the cladding wall is more prone to resume propagation during a subsequent power ramp. In the past, one international power ramp programme looked at the impact of a power ramp on subsequent steady-state normal power operation and concluded no adverse effects occurred, but no reported study of multiple power ramps was published. In lieu of test reactor power ramps, separate effects tests using the most relevant techniques out-of-the pile should investigate this potential cumulative SCC damage.

7. IMPROVEMENT OF PCI/SCC MODELLING AND SIMULATION

7.1. OVERVIEW

The following topics need to be fully addressed and modelled in order that a comprehensive modelling of PCI/SCC is possible:

- Multi-dimensional thermomechanical analysis;
- Irradiation history dependent nonlinear behaviour of the constitutive materials (pellet and claddings under thermal, mechanical and neutron irradiation loadings);
- Pellet-cladding interface behaviour;
- Gaseous swelling and release;
- Corrosive species speciation;
- Cladding stress corrosion cracking behaviour in iodine environment;
- Impact of coupling of physics phenomena such as neutronics and thermalhydraulics.

Although advanced codes such as BISON (see the paper presented by Pastore and co-authors, Session III of Annex II) and ALCYONE (see the paper presented by Sercombe and co-authors, Session III of Annex II) already include many of these features and predict rather well many of the measured parameters obtained from the PIE after ramps (e.g. external increase of diameter, primary and secondary ridges), their capability for accurate prediction of the I-SCC cladding failure in power ramp is not fully satisfactory.

Recommendations on PCI/SCC modelling were outlined at the PCI workshop organized by the OECD-NEA in Lucca in 2016 (see also Section 3.3) as follows:

- Continue the efforts for developing multidimensional and multi-physics approaches;
- Continue the efforts on thermochemistry and modelling for prediction of the availability of corrosive species;
- Address the questions of verification & validation by using benchmarking and on purpose designed separate effect experiments.

Moreover, it was recommended to investigate the approaches for uncertainties evaluation. Synthesis of this section implicitly refers to these recommendations.

7.2. PHENOMENOLOGICAL MODELS

7.2.1. Time dependent behaviour of the cladding and pellet material

A PCI prone situation is driven by the power increase with the associated temperature escalation in the fuel pellet which induces inhomogeneous thermal expansion of the pellets and also generates fission products resulting in corrosive volatile species (SCC) and possible gaseous swelling if the high power is maintained long enough (in addition to the thermal expansion). When the pellet-cladding contact is well established, the strain driven loading induced by the pellet expansion generates local stresses at the inner surface of the cladding. After reaching the terminal power level in the cycling power, the cladding strain remains practically constant and hence the cladding goes into a 'stress relaxation' mode (if the gaseous swelling of the pellet occurring during the terminal power plateau is not too strong).

The elaboration of visco-elastic and visco-plastic constitutive equations for the cladding, which enables to account for response of a complex loading path including some inversions of the stress state, hardening relaxation sequences during the transient and recovery phenomena, has been for a long time the goal of various experimental investigations. It is still the topic under development, which aims at the implementation into fuel codes of more sophisticated new models based on recent experimental results.

The paper presented by Peltonen and co-authors (see Session III of Annex II) described models based on serial or parallel arrangements of classical rheology models (e.g. Kelvin, Maxwell). The development aimed at accounting for primary creep, its recovery in case of load reversal and stress relaxation situations. Several in-pile experiments in the Halden reactor, involving instrumented fuel rod segments subject to specific complex loading paths, were used to evaluate the adequacy of the model. In addition, complex separate effect tests including consecutive stress relaxation sequences were used, as well. The authors underline that this type of modelling is

needed for evaluation of the stress in the cladding under strain controlled loadings, but in the end convey the message that model validation for accurate predictive simulation still represents a challenge.

One must keep in mind that the right form of the constitutive equations for the cladding depends strongly on the availability of various kinds of separate effect tests, which are necessary in order to determine the respective model parameters (especially the internal parameters accounting for history dependent effects). The PIE after integral experiments (in-pile power ramps) gives only the final residual diameter strain profile.

With regards to the role played by the fuel pellet, it is widely acknowledged that thermal expansion and gaseous swelling are the key parameter to account for when analysing PCI. Nevertheless, pellet viscosity together with its cracking behaviour may impact significantly the local stress concentration in the cladding, leading to stress and strain redistributions. The BISON paper presented by Pastore (see Session III of Annex II) showed an example of the benefit brought by the introduction of a softening feature in the pellet model to improve a simulation of some of the international fuel performance experiments (IFPE) datasets.

7.2.2. Irradiation effects

The neutron irradiation induces microstructural evolutions that impact the deformation behaviour of the cladding and the pellet. Cladding irradiation growth, cladding irradiation creep and pellet densification and gaseous swelling are, with thermal expansion, responsible for the conditioning/deconditioning kinetics and magnitude of the fuel rods. As such, these parameters govern the initial thermal mechanical state of the fuel rod prior to the transient (i.e. ‘initial PCI status’). These relevant models are largely incorporated in the fuel performance codes used to simulate PCI.

The recent improvements of PCI/SCC modelling rely on neutronics calculations to estimate the amount of gaseous fission product inventory in the pellet and in the pellet-clad gap. It may also be associated with thermochemistry tools in order to predict the amount of corrosive products which is going to be available at the pellet/cladding interface.

7.2.3. Thermochemistry

Recently developed thermochemistry models showed promising results. They have been implemented to evaluate the availability of corrosive products at the inner surface of the cladding. Several organizations investigated thermochemistry-related phenomena, developed specific models and implemented them in advanced fuel performance codes such as ALCYONE (see the paper presented by Sercombe and co-authors, Session III of Annex II).

The VTT developed stand-alone models featuring thermochemistry capabilities to analyse the radiolysis of CsI. The results show the calculated theoretical concentration of the species including iodine as a function of the stoichiometry (O/U ratio) and the temperature (see the paper presented by Peltonen and co-authors, Session III of Annex II). It is concluded that hydrogen iodide is thermodynamically the most favoured species at low temperature with potential detrimental impact on SCC phenomena.

7.2.4. Cladding SCC failure model

Important progress was presented with the implementation of SCC failure models in advanced multi-dimensional fuel performance codes:

- The influence of temperature on the rate of crack propagation, implemented in ALCYONE (see the paper presented by Sercombe and co-authors, Session III of Annex II);
- The cumulative damage index, implemented in BISON (see the paper presented by Pastore and co-authors, Session III of Annex II) which is envisaged to be applied to PCI (it is implemented in other codes);
- The comprehensive simulation of the I-SCC crack initiation and propagation using finite element method analysis and the Katchanov Katchanov-Miller model (see the paper presented by Le Boulch and co-authors, Session II of Annex II) with promising preliminary results of implementation in ALCYONE 3D code.

Significant efforts have been made to investigate and model the local boundary conditions and the physical parameters leading to I-SCC with the hope of simulating actual ramp tests. Further progress is expected from model upgrades to account for the impact of the concentration of corrosive species (poor or lack thereof) on the SCC model parameter.

7.3. COMPUTER CODE DEVELOPMENTS

7.3.1. General features

At the technical meeting held in Aix-en-provence in October 2019, some general features have been identified which could lead to improvements of the PCI/SCC modelling toward a more predictive simulation of the power ramps. To that end the advanced models presented at the technical meeting have been used to simulate a fuel rod which was submitted to a power transient which occurred after a particular power history, situation that potentially involves a risk of PCI/SCC failure.

7.3.1.1 *Generalization of thermal mechanical multi-dimensional approach*

The PCI/SCC is a local phenomenon initiated in the cladding zone subject to higher stress/strain concentration such as the zone located at pellet-pellet interface, in front of a radial macro crack of the pellet (triple point) or the zone of the cladding affected near the boundary of an MPS. Thus, 3D modelling appears to be well suited to properly simulate the loading condition for PCI/SCC.

Several approaches were presented, based on in-house developed codes, or commercial and open source finite element method software, which have been applied in conjunction with various types of material constitutive equations. However, the generic finite element software simulation of the fuel rod is approximative with respect to pellet behaviour and a relevant 3D modelling approach needs to be associated with the implementation of the relevant models for pellet, cladding and pellet-to-cladding interface.

7.3.1.2 *Pellet-clad interface contact modelling*

The Coulomb friction model with unilateral contact is the more widely used. The friction coefficient is adjusted posteriori in order to give a better agreement with the PIE diameter measurements, because it is not possible to directly evaluate this coefficient. Alternative approaches were presented, such as the introduction of cohesive zone elements (see the paper presented by Scolaro and co-authors, Session III of Annex II), or the penalty model (see the paper presented by Le Boulch and co-authors, Session II of Annex II). The potential advantage or drawback of these approaches remains to be quantified and validated.

Improvements to the following fuel codes have been presented and are summarized below.

7.3.2. ALCYONE (CEA, France)

The status of further developing the ALCYONE code to simulate the fuel behaviour during a power ramp is described in the paper presented by Sercombe and co-authors (see session III of Annex II). This code is considered as the French reference analytical calculational tool enabling a comprehensive modelling of PCI in various transient regimes. The mechanism of the I-SCC is reviewed, and the main features of the 3D mechanical scheme and the boundary conditions are briefly described (symmetry, unilateral contact, and Coulomb friction sliding contact at the pellet-clad interface).

The SCC model as implemented in ALCYONE accounts for the initiation and propagation phases in terms of temperature and stress, assuming that iodine is available in sufficient quantity and that there are pre-existing micro cracks in the internal oxide layer. The model parameters have been derived from laboratory experiments on fresh or irradiated cladding tubes in iodine environment. The SCC model is executed in conjunction with ALCYONE-3D simulation using the calculated local stresses and temperature at the triple point. Model predictions were validated mainly on a set of power ramp experiments in the OSIRIS reactor.

Possible reasons for overpredicting the SCC propagation rate for some power ramp tests were discussed — one of them being identified as the possible lack of corrosive species compared to the laboratory tests. Potential improvement in the ALCYONE code was presented to implement a chemical criterion based on the iodine partial pressure and a threshold giving the probability of initiation flaws under hoop stress using the Weibull theory.

7.3.3. BISON (INL, USA)

The paper presented by Pastore and co-authors (see Session III of Annex II) provided an overview of the BISON fuel performance code and its capability for SCC prediction. Presentation included the recent improvements with a focus on the assessment through IFPE database. The simulated fuel rod experiments are related to PCI and PCMI situations in LWRs. BISON, developed by Idaho National Laboratory, is a modern, fuel performance code using multidimensional finite element method, enabling to simulate several types of fuels and geometries (i.e. LWR fuel rods, tristructural-isotropic (or TRISO) fuel, metallic fuels). Benefits of the recent improvements were evidenced by the simulation of particular experiments, with and without the above-mentioned improvements.

Taking into account the softening effect of fuel cracking on the pellet behaviour (instead of using an elastic approximation), the influence of relocation and recovery, and the gaseous swelling during the transient, significantly improves the prediction of the diameter changes when simulating PCMI fuel rod experiments. The 3D capabilities for MPS impact analysis are illustrated with the impact on local strains and stresses in the cladding and on local temperatures of the gas released during a transient. This 3D MPS model was used to design a dedicated MPS experiment of the Halden reactor project. In the paper presented by Pastore and co-authors (see Session III of Annex II), a detailed discussion on the simulation of the IFA-629.4 power ramp experiment, based on the comparison of measured and predicted axial elongations of the rod, is described with several hypotheses on the pellet behaviour and on the pellet-clad interface friction coefficient. Only qualitative lessons may be derived because PIE results on external diameter profiles are not available. A failure criterion for the cladding based on a cumulative damage index was benchmarked on creep to rupture laboratory tests of internally pressurized tubes with iodine inside the tubes. The cumulative damage index model was then tuned by simulating power ramp experiments of the IFPE database. A probability of failure is assessed from the value of the cumulative damage index.

The multi-dimensional capabilities of BISON for addressing MPS impact was presented also by the paper of Peltonen and co-authors (see Session III of Annex II). A 2D R-Z mechanical scheme was used to evaluate local stresses and temperature on pellet and cladding.

7.3.4. DIONISIO 3.0 (CNEA, Argentina)

A 3-D finite element scheme in which the pellet-clad interface is modelled with the cohesive zone method, has been incorporated in the DIONISIO 3.0 fuel performance code (see the paper presented by Goldberg and Soba, Session III of Annex II). The new 3D method is compared with the unilateral contact approach based on Lagrange multipliers in 2D axisymmetric configurations with contact interfaces (treated examples are: SiC fibre and matrix, flat punch test, heating central mandrel in ceramic tube). The 3D cohesive zone method-based approach allows evaluating the effect of geometrical defects and of relative tangential displacements between the contact surfaces. The authors pointed out the importance of the time step control in the explicit resolution scheme in order to avoid inconsistent interpenetration of the contact surfaces. Beyond the selected test emulating PCI conditions, the simulation of some irradiation results with DIONISIO 3.0 were presented with a satisfactory prediction of the cladding deformation with the ridges due to the bamboo effect.

7.3.5. OFFBEAT (EPFL, Switzerland)

Motivated by the feedback experience of some fuel failures observed in nuclear power plants and by the limited capability of the standard 1.5D fuel performance codes for interpreting complex and multidimensional situations such as PCI, the novel code OFFBEAT (OpenFOAM Fuel Behaviour Analysis Tool) was developed (see the paper presented by Scolaro and co-authors, Session III of Annex II). The approach uses the C++ open source library OpenFOAM, a toolbox for engineering application offering interesting potential for addressing multi-physics and multidimensional problems. OFFBEAT takes into account thermal expansion, densification, relocation and irradiation-induced strains. In particular, the development has been focused on the implementation of history dependent and non-linear material properties, such as plasticity and creep for the zircaloy cladding, with models derived from von Mises theory and from the Limbäck and Anderson model, respectively. The pellet-cladding contact model is based on the penalty method and has been verified against the punch test results. The approach is in an early stage of development (2–3 years) but several examples of application to test cases or

benchmark illustrate the OFFBEAT capability to address MPS and inter-pellet cladding ridges calculation including creep effect. Development perspectives are sketched toward the goal of simulating PCMI scenarios (e.g. fuel cracking model, frictional contact forces). Future plans include the coupling with the TRANSURANUS code to calculate the initial conditions and the coupling with reactor physics Monte Carlo tools for a more accurate transient calculation. The latter is already in an exploratory phase with the coupling between OFFBEAT and the Serpent reactor physics analysis code. The need for validation data specific to multidimensional simulations, including separate effects tests, is underlined. The presentation illustrates the potential of an approach based on open source advanced tools as an alternative to the classical advanced fuel performance codes.

7.3.6. START-3A (VNIIM, Russian Federation)

This Russian fuel performance code was not presented in direct relation with PCI modelling, but a fuel performance code also be used for designing complex experiments carried out in the MIR reactor and devoted to the study on impact of the transient rate on the release of fission products and the gaseous swelling (see the paper authored by Avdonina and co-workers, Session III of Session II).

7.4. VERIFICATION, VALIDATION AND APPLICABLE DOMAINS

7.4.1. Global experiments (in-pile power ramps)

Following the shutdown of the HBWR in Halden in 2018, there is a lack of alternative test reactors with experience in performing power ramp experiments that could immediately fill the gap due to HBWR shut down. Waiting for potential successor facilities to produce new results, the global validation of fuel performance codes relies on the existing data preserved in databases, both publicly available and also in vendor proprietary domain.

7.4.2. Databases related to PCI/SCC

The IAEA and OECD-NEA jointly manage the international experimental database called IFPE. The activities consist mainly in collecting and maintaining in-pile integral tests data involving PCMI or PCI/SCC situations, in specific databases. The OECD-NEA is actively promoting benchmarks of fuel performance codes among the Member States. Recently, the OECD-NEA supported the Halden reactor project initiative aiming at preserving in a database (to be transferred eventually in the NEA databank) all the experimental results of the Halden reactor project over the last 50 years.

The OECD-NEA presented the framework for in-pile fuel and material irradiation experiments (or called FIDES) initiative aiming at launching fuel experiments in the remaining tests facilities (e.g. BR2, CABRI, TREAT, etc.) (see the paper presented by Costa and co-authors, Session III of Annex II). The objective of this project is to make sure that the nuclear community will be able to access experimental capacities on the long term, in particular after the HBWR shutdown.

7.4.3. MIR reactor

A paper presented by Avdonina and co-authors (see Session III of Session II) described an original experiment in the MIR material test reactor focused on the gaseous swelling and gaseous release during a power transient of recent fuel rod design with thinner cladding and large grain UO_2 pellets without central hole. The experimental device with a rotating Hafnium screen that could be moved quickly, allowed performing during the same irradiation sequence a fast power ramp and a slow power ramp on similar fuel rods originating from the same fuel assembly (irradiated to a burnup of 44 $\text{GW}\cdot\text{d}/\text{tU}$). Seven rods were tested, three of them subjected to a fast power ramp ($\sim 25 \text{ kW}/\text{m}/\text{min}$), after a conditioning phase and followed by a slow ramp ($1 \text{ kW}/\text{m}/\text{min}$), while the other ones being subjected only to a slow ramp. One of the rods was refabricated and instrumented with a thermocouple, but the pressurization was compromised by a small leak.

The fuel performance code START-3A was used to analyse the experiment, especially the evaluation of the centreline temperatures (around 200°C at the centreline). The fission gas release was measured for each rod. PIE with diameter measurements and ceramographies were presented.

In terms of cladding diameter increases, no influence of the ramp rate (fast or slow) was observed, with a value of $\sim 1.3\%$ hoop strain being measured for all the rods. In terms of fission gas release, the author indicated

that there was no significant impact of the ramp rate, the differences observed being easily explained by the differences in the times spent at high temperature. The destructive examinations showed the evolution of the microstructure due to the power ramp with a central zone with larger pores but did not exhibit significant differences between the rods subjected to fast and slow ramps, respectively.

7.4.4. Benchmarking

Code benchmarking and shared international data bases were widely promoted as a way to consolidate the validation of fuel performance code for the international community.

The IAEA organized several international benchmarking exercises on different aspects of fuel modelling (e.g. FUMEX II [55], FUMEX-III [56], FUMAC [57]). More recently, the OECD-NEA under the action of its Nuclear Science Committee has launched an international benchmark on PCMI (see the paper presented by Costa and co-authors, Session III of Annex II) with the goal of stimulating the improvement of the nuclear fuel modelling. The status of the PCMI benchmark carried out within the Expert Group on Reactor Fuel Performance was briefly presented. The scope of the benchmark was to compare the predictions of the fuel performance codes, on the one hand through hypothetical cases (purpose to understand the reasons for the differences in results as due to different hypotheses) and on the other hand, by direct comparison with the measurements performed during real experiments. Some results were presented elsewhere [58]. The necessity of updating the interface of the simulation tools with the databases was underlined and the OECD-NEA started a project with this objective (DATIF). The preservation of the Halden experiments with the constitution of a legacy database within the Halden reactor project with the support of OECD-NEA for long term preservation was also mentioned. A second benchmark focused on the methodologies for validation of coupled physics phenomena was also mentioned.

7.5. UNCERTAINTY QUANTIFICATION

The topic of uncertainties is not directly addressed in the current practices as presented above in relation to the improvement of simulation codes by various organizations. Among the many reasons for the difficulty to progress in this direction, it can be cited the experimental approach for direct characterization the PCI/SCC threshold which would require many experiments in the same conditions on similar specimens. The multi-rods loop in the MIR reactor is an example of such a simultaneous transient experiment. The theoretical approach is very involved, with a great number of parameters not directly measurable with complex impact and therefore difficult to reach a conclusion with the described high level of confidence.

7.6. RECOMMENDATIONS FOR FUTURE WORK

The following recommendations can be formulated for further development, as a result of the presentations and discussions with respect to the subject of this section:

- Investigate in priority the phenomena related to promising perspectives (corrosive species characterization and impact on the cladding SCC failure model);
- Promote high performance computing for reference 3D calculations (e.g. work in-progress at Idaho National Laboratory within the consortium for the advanced simulation of light water reactors framework). High power computing could be useful also to deal with time consuming PCI/SCC verification methodologies;
- Develop specific experiments and test conditions in order to confirm that the key parameters, which has been identified with advanced numerical simulations, assuming different hypothesis and value of these key parameters, are relevant;
- Properties that are not accessible through separate effect tests can be derived from computational material science. This approach is often developed independently, based on scientific motivation. The connection via multiscale modelling with application needs to be encouraged;
- Create an expert group for producing a dedicated state-of-the art report and recommendations on the uncertainty analysis and quantification.

8. OPTIMIZATION OF PCI/SCC DESIGN VERIFICATION METHODOLOGIES

8.1. OVERVIEW

As far as load following and ERPO are concerned, the PCI/SCC key features need to be explicitly included in the licensing process for any type of fuel design via regulations by the regulators or industry self-regulation, depending on rules of specific countries.

The application experience has been shown that PCI/SCC design verification methodologies are quite complex and time consuming if all operational cases are to be taken into account. These PCI/SCC methodologies require up-to-date fuel performance codes (to assess fuel dependent PCI/SCC failure thresholds) along with validated neutronic calculation tools (to determine the maximum power transient to be applied locally) in order to determine the resulting margins to failure of each fuel rod in the core, at each axial elevation and at each time step in the fuel reload cycle. This may impose constraints on the design and operation of the reactor core.

To address these various issues, it is important to optimize PCI/SCC methodologies and the overall licensing process.

One option is to use ‘high power computing’ based on fuel rod codes with simplified but physically sound models, which can efficiently take a large number of calculations and thus can make it possible to cover all limiting cases without losing too much margins due to codes’ uncertainties. This option is also amenable to include statistical approaches and uncertainties analyses.

Another option is to use advanced modelling to identify the key phenomena occurring during a PCI/SCC event and develop physics based model to predict PCI/SCC failure. Unfortunately, this objective is difficult to reach in the near future due to the lack of knowledge on the initial state of the fuel rod and the local stress initiating.

In the subsequent sections, the available toolbox, an example of the improved PCI/SCC design verification methodologies and recommendations for future work are described.

8.2. AVAILABLE TOOLBOX TO ADDRESS IN-REACTOR PCI/SCC RELATED ISSUES

8.2.1. Extensive power ramps database covering the critical burnup range

To define a PCI/SCC failure threshold, which is fuel design and pellet/cladding material dependant, a comprehensive experimental power ramp data base is required together with a validated fuel performance code to interpret the ramp test results. A minimum of 10 to 15 ramp tests are typically necessary depending on the degree of novelty of the fuel to be licensed.

Since the shutdown of test reactors, for example, R2 (Studsvik, 2005), SILOE and OSIRIS (CEA, 2018) and HBWR (Halden, 2018), the likelihood of performing a large number of ramp tests is lower than ever. There are opportunities in a few still functioning test reactors, but the number of ramp tests per year is limited. In JHR (Jules Horowitz Reactor), which is still under construction, a specific test rig has been developed (ADELINE ramp test loop) to address this issue. However, JHR is not going to be operational before 2024.

Under these circumstances, the fuel rod code that has been validated on the results of existing in-reactor power ramps can be used to produce supplementary ‘digital ramp test’ data via interpolation of existing irradiation data sets (i.e. the data-driven technology).

8.2.2. Creep and relaxation separate effect tests

Mechanical tests are well suited to determine the cladding properties under relevant test conditions, i.e. strain driven loading prototypical of PCMI and to validate the cladding mechanical models implemented in the fuel performance codes.

The cladding creep law at low stress levels and under irradiation is crucial to better assess the pellet-clad gap closure kinetics prior to the power ramp. Indeed, the pre-ramp gap size has a direct impact on the cladding stress during the power transient, as the gap closes mainly due to pellet thermal expansion being larger than that of the cladding.

The cladding stress relaxation law at high stress level is also important, in order to better assess the stress evolution, in terms of magnitude and kinetics, during the power ramp.

The mechanical properties of the fuel pellet are important as well in order to characterize the initial state of the fuel rod (e.g. gap closure) and the fuel rod behaviour in transient e.g. pellet creep that relaxes the pellet-cladding contact pressure.

As an example, the paper presented by Demyanov and co-authors (see Session IV of Annex II) described the particular behaviour of (U-Gd) O_2 fuel rods, which exhibit an early closure of the pellet-clad gap in the fuel cycle due to less fuel densification than UO_2 fuel. However, this feature was compensated by the lower linear heat rate of the (U-Gd) O_2 fuel rod.

The fuel rod code that has been validated on the results of existing in-reactor power ramps can be used to produce supplementary 'digital ramp test' data on the radial gap closure by taking account of creep and relaxation effects.

8.2.3. SCC out-of-the pile separate effect tests

For decades, researchers have strived to develop out-of-the pile separate effects test rigs capable to simulate the in-pile ramp conditions, such as mandrel tests with controlled atmosphere.

The idea behind these initiatives was to identify the key parameters at work during a PCI/SCC event and, eventually, to reduce the number of costly in-pile power ramp tests to be performed to determine a robust PCI/SCC failure threshold. This approach would allow to study the cladding susceptibility to SCC in terms of various parameters such as corrosive species concentration, oxygen content, cladding stress levels, temperature level, etc. However, it was concluded that none of the various out-of-the pile test devices that have been designed and utilized were able to fully and adequately reproduce the in-pile conditions and behaviour. Nevertheless, the out-of-the pile tests have confirmed some trends and dependencies at a qualitative level, for example, various cladding types have more or less the same susceptibility to SCC if the texture is the same. The PCI/SCC performance of a specific fuel is equally related to its fuel pellet behaviour and to the cladding mechanical properties (i.e. low stress creep and high stress relaxation properties above mentioned), and the out-of-the pile rigs developed have focused on cladding behaviour.

Even if a deterministic SCC model can be derived from these separate effect tests, the model cannot be implemented directly in a 'fuel core design approach' because it requires as input variable the actual local stresses in the cladding (by the fragmented fuel pellets), which cannot be realistically quantified in every single fuel rods of the core because of the still prohibitive computational burden.

In order to quantify the role of corrosive species in the simulation of SCC initiation and propagation in the local zone of the stress concentration, multi-scale modelling is necessary.

8.2.4. Advanced modelling

Advanced multi-scale and/or multi-physics modelling are necessary to identify the key phenomena occurring during a PCI/SCC event (i.e. pellet thermal chemistry, clad SCC models).

The ultimate goal of these advanced tools is to replace in-pile power ramps with digital power ramps. Unfortunately this objective is difficult to reach in the near future, for the reasons mentioned earlier: (1) the initial state of the fuel rod (i.e. cracking pattern of the fuel stack, fuel pellet-clad gap size, fission product diffusion kinetics, etc.) is not precisely known for all pellets of all the fuel rods with the required level of details and (2) the local stress initiating the SCC mechanisms cannot be yet accurately quantified.

Nevertheless, these tools are well suited to assess the additional risk of failure of fuel with surface flaws e.g. fuel rods with pellets exhibiting MPS, as compared to standard fuel containing pellets without any detectable surface flaws. Such an assessment is interesting but utilizing it in operational guidelines requires a realistically accurate estimate of the number and the magnitude of the fuel rods containing flawed pellets in the whole reactor core. It would be too conservative to assume that all the fuel rods of the core exhibit MPS. Such an approach would result in a significant loss of PCI/SCC margin, which would be largely unjustified considering the poor safety significance of the additional risk of failure of a limited number of defective fuels rods. It has been shown that MPS occurrence could be prevented in manufacturing with a high level of confidence.

Advanced modelling tools are also expected to be useful to better explain why certain fuel concepts are more resistant to PCI/SCC than other (e.g. MOX fuel, doped fuel versus standard UO_2). Along this line, deterministic multi-physics tools could help researchers to develop faster new solutions of PCI/SCC free fuel concepts.

The remaining mechanistic features that need to be further investigated to better simulate the phenomena occurring in the fuel pellet, in the pellet-clad gap, at the pellet-clad interface or in the cladding, during normal and AOO conditions, include the following items:

- Quantify the possible SCC beneficial effect of the oxygen potential variations and oxygen thermal diffusion in the fuel and oxygen availability at the pellet-clad interface;
- Quantify the impact of the peripheral fuel stack cracking patterns on the cladding stress;
- Assess the impact of incipient cracks in the inner side corrosion layer on SCC susceptibility;
- Quantify fission products retention in additive fuels in normal and AOO conditions
- Quantify the effect of various dopants on high temperature fuel creep;
- Confirm the best ramp testing protocol enabling the determination of a reliable PCI failure threshold (single ramp test vs stair case ramp test).

8.3. IMPROVED PCI/SCC CORE DESIGN VERIFICATION METHODOLOGIES

As an example of PCI/SCC design verification methodologies evolution, the approaches developed by EDF for flexible operation of nuclear power plants were presented by Bernard and co-authors (see Session I of Annex II). Unlike other countries, French Nuclear Safety Authority requests licensees to demonstrate that fuel would not fail by PCI/SCC during any AOO conditions. Because of the large share of nuclear energy in the French electricity mix, the French nuclear power plants need to be able to operate in flexible operation regime, including frequency control and daily load following. In addition, to deal with potential operational events, the nuclear power plants operators require at least 30 days of ERPO. Finally, in order to optimize the electricity production on the whole fleet scale, EDF sets up various core patterns for each nuclear power plant type.

These specific operational conditions have to be justified with an appropriate approach, based on the following two measures:

- Adjustment of the reactor protection thresholds;
- Definition of the PCI related the operational technical specifications.

To fulfil these conditions, specific PCI/SCC analyses are performed to cover each operating mode of the reactor. The study relates to the full core, yet PCI/SCC failure risk is local. Two types of approaches are devoted to PCI studies. First, a specific methodology called MIR (Renovated PCI Method, from the French ‘Méthodologie IPG Rénovée’) has been developed in cooperation with FRAMATOME (see the paper presented by Daniel and co-authors, Session I of Annex II). This methodology is based on neutronics 3D kinetics calculations and thermal-mechanical calculations. Since the MIR method is computationally demanding, taking a long time and focused on a single reference reload pattern, a new approach has been developed to deal with various core patterns and to reduce the calculation time. The main changes are:

- Static neutronic calculations instead of kinetic calculations;
- Decoupled calculations between neutronic and thermal mechanics.

For a given reload pattern, these simplifications reduce the computation time but lead to smaller manoeuvrability margins. This approach is well suited to assess the impact of core patterns variability on PCI/SCC margins and to perform sensitivity analysis. Similarly, an enhanced methodology ‘allowable power’ methodology has been developed (see the paper presented by Daniel and co-authors, Session I of Annex II).

In some cases, licensees see a benefit in mixing 1D and 3D models to quantify more precisely the available in-core PCI/SCC margins (see the paper presented by Ding and co-authors, Session IV of Annex II). Based on the analysis of the PCI/SCC related mechanisms, 1D models and 3D models are proposed to simulate the overall and the local fuel behaviour respectively, during a power ramp transient. The 3D simulation enables quantifying the critical stress appearing locally in the cladding (e.g. considering specific fuel stack cracking patterns or the presence of MPS). This critical stress is then used in an approach combining 1D calculations with 3D calculations to quantify more precisely (i) the PCI margins available in each fuel rod of a fuel core during an AOO event and (ii) maximum allowable ERPO durations. The authors acknowledge that dealing with a local critical stress is not fully convincing, but it helps showing the PCI/SCC margins trends. They suggest connecting the 1D approach with a core monitoring system and to work on the cladding crack initiation mechanisms.

8.4. DISCUSSION AND RECOMMENDATIONS FOR FUTURE WORK

Advanced investigations and hypothesis, based on pellet thermal chemistry and SCC models (which still need to be confirmed and validated), are not intended to be used directly in an industrial ‘design approach’; in particular, they are not aiming at defining SCC/PCI failure limits.

On the other hand, the thermal mechanical hypothesis used in ‘PCI/SCC design verification methodologies’ (in which full availability of corrosive products is conservatively assumed) does not appear to be called into question by the scenarios based on thermal chemistry hypotheses.

The multi-physics approaches are intended to improve the mechanistic understanding of all the phenomena involved in a PCI/SCC event and to propose innovative solutions to develop PCI/SCC resistant fuels concepts (e.g. doped fuel in which the radial transport of corrosive products is delayed, cladding with inner liner, cladding with improved creep and relaxation properties, etc.) or to anticipate PCI licensing processes of Advanced Technology Fuels (e.g. SiC fuel, uranium-nitride fuel, etc.).

Regarding the design methodologies aiming at defining PCI/SCC related operational limits and PCI risk assessment guidance for flexible operation, licensees have developed a variety of methodologies. These methodologies are more or less comprehensive but rely on similar principles. The trend is to simplify the approaches to reduce the calculation time and improve the coverage level of the variable reload patterns.

9. CONCLUSIONS

Flexible operation and related power changes may impact fuel integrity through effects on the thermal mechanical performance of the fuel rod. As such, PCI/SCC failure risk needs to be assessed by considering additional AOO related to flexible operation.

The safety significance of PCI/SCC failures is not very high in light water reactors because SCC cracks are initially relatively small and hence do not generate prohibitively large radioactivity spikes; in the pressurized water reactor core, SCC primary cracks do not usually degenerate into major degradations of the cladding, while in boiling water reactor core secondary degradation is prevented by power suppression of the defective fuel. The main consequence of a PCI/SCC failure is a radiological pollution of the primary circuit (which is monitored and constrained by the standard radio-chemical limitations of the plant). In this aspect, the consequences of a small number of PCI/SCC failures can be easily managed by the purification system of the nuclear power plant.

For some AOOs that affect the fuel and reactor core with low PCI/SCC margins, however, the number of PCI/SCC failures can be higher, and a significant radiological source-term may be generated. Taking into account such situations, the licensees need to investigate PCI/SCC key features to assess the actual PCI/SCC margins for each fuel rod of the reactor core.

The key features (parameters) to deal with when assessing PCI/SCC failure margins are well identified, i.e.

- Pellet-cladding gap size evolutions;
- Fuel rod conditioning levels;
- Linear heat generation rates (LHGR) and power variations (Δ LHGR);
- Ramp rate;
- Cladding strain;
- Cladding stress and/or strain or energy density, etc.

However, individually, none of these key features (parameters) can quantify the PCI/SCC margins to failure and more elaborated thresholds are needed. For example, LHGR itself is insufficient to properly discriminate failed and non-failed fuel rods within a power ramp database.

Experimental programmes and their analysis have been focused on identifying the key phenomena at work during a power ramp transient, the goal being to characterize the cladding failure risk as accurately as possible to minimize unjustified and costly conservatisms.

Current PCI/SCC related research programmes tend to bridge separate effects tests, mechanistic models and semi-integral experiments. These programmes have been successful in providing valuable outcomes regarding specific phenomena at play during power transients e.g.

- Quantification of enhanced failure risk in presence of missing pellet surfaces;
- Modelling of crack initiation and growth in presence of iodine;
- Quantification of fission products migration in various fuel concepts;
- Identification of cladding creep/relaxation mechanical properties for accurate assessment of the pellet-cladding gap closure evolution;
- Stress relaxation kinetics at ramp terminal level (RTL).

These programmes also include developing new investigation techniques that will help improve our understanding of PCI/SCC phenomena.

For the last decades, there have been a very large number of experimental investigations worldwide and the coordinated development of refined multi-physic models. Nevertheless, it appears that it is still not possible to precisely predict the PCI/SCC failure threshold of a given fuel concept. This is likely due to the complexity of some of the mechanisms involved in the PCI/SCC process e.g. fuel pellet cracking pattern which determine the local stress at the pellet-clad interface. From these aspects, it is obvious that:

- In-pile power ramp databases covering an appropriate burnup range are still necessary;
- PCI/SCC failure threshold (i.e. technological limit) derived from the analysis of this database includes some intrinsic conservatism which is difficult to reduce while designing a whole fuel core.

The nuclear fuel community has made significant efforts to develop and validate multi-scale mechanistic analysis codes as an alternative solution to address the above challenges.

The current PCI/SCC design verification methodologies using such complex multi-scale codes have been successful, whilst they contain considerable conservatism, in particular, due to the use of the deterministic bounding approach (e.g. combination of the AOOs at the worst time in cycle and power ramp, consideration of the uncertainties in the worst direction, etc.). They should be simplified to allow quick assessment of PCI/SCC margins, which pursues better understanding of PCI/SCC mechanisms.

In terms of understanding of SCC mechanisms, it is worthwhile to note that the effect of texture and the role of oxygen and cladding inside oxide layer were confirmed by experimental studies in the technical meeting in 2019. On the other hand, it remains a challenge to explain why some fuel concepts (e.g. MOX fuel or additives fuel) are more PCI/SCC resistant than standard UO₂ fuel, which needs more studies.

As stated, the trend is to simplify the PCI/SCC design verification methodologies to reduce the calculation time and improve their coverage level of the variable reload patterns.

Today, conventional 1.5D and advanced multi-physics 3D codes remain complementary. Since the 3D are too complex to be used for designing a whole fuel core (implying hundreds of thousands of calculations to cover all cases), their outcomes are successfully implemented, in a simplified way, in the 1.5D tools used in the industrial design approaches. The 1.5D codes are basically used for industrial applications because they exhibit calculation times compatible with the large number of calculations requested to design a whole fuel core. PCI/SCC failure prevention risk in normal and AOO conditions is efficiently integrated in operational rules, based on mastered methodologies that include these 1.5D fuel performance codes in combination with the predetermined PCI/SCC technological failure limit.

The current empirical reactor operation guidelines are based on the existing power ramp database with various fuel designs and test conditions. They may be improved by more realistic guidelines based on power ramp database with specific fuel designs and more representative test conditions. With the shutdown of several material test reactors, it seems rather difficult and extremely expensive to perform additional power ramp tests.

With the introduction of more PCI resistant fuel design (e.g. use of M5 or Optimized ZIRLO claddings, and doped pellets) and improved PCI design verification methodologies, it would be possible to better quantify the PCI/SCC margins, such as to allow relaxation of the operating constraints.

Consequently, it is clear that further progress regarding PCI/SCC issues has to involve the determination of a robust and reliable PCI/SCC failure threshold. The evaluation parameter(s) to be used is still a matter of debate and may depend on the fuel concept e.g. stress for zircaloy-4 and ZIRLO/Optimized ZIRLO; strain energy density for M5, damage index for SiC, etc. These parameters are not directly measured but are derived from interpretation of experimental measurements by analytical tools.

To strengthen the analytical capabilities for experimental investigations, the following items need to be implemented:

- In-pile power ramp tests with new fuel designs need to be performed in well-defined test conditions. The LHGR has to be measured as accurately as possible, using redundant systems and accounting for all potential experimental artifacts (e.g. gamma heating, shielding effect, etc.). The initial thermal-mechanical condition of the test fuel rod before the ramp (e.g. gap size, conditioning power) has to be carefully characterized.
- Out-of-the pile separate effect tests are well suited to investigate specific features. Their use in determining a PCI/SCC failure threshold to be incorporated in a fuel performance analysis code needs to be elaborated with local model at a relevant scale.
- Development of 3D models needs to be continued, which is useful to evaluate local effects (e.g. MPS effects) and to confirm the relevance of the simplified models of the 1.5D fuel performance codes.
- In-pile and out-of-the pile separate effect tests can facilitate the validation of advanced multi-physics models. In order to couple thermal mechanical and thermal chemistry features of the fuel, dedicated experiments need to be developed (e.g. to identify the carrier species of the cladding corrosive agent (e.g. Te, Cs or ZrI₄); to assess fission products and oxygen thermal migration during a power transient; to characterize the irradiation creep of the fuel, etc.).
- The uncertainties of codes' prediction need to be accounted for in the PCI/SCC design verification methodologies.

REFERENCES

- [1] INTERNATIONAL ATOMIC ENERGY AGENCY, Proceedings of Specialists' Meeting on Pellet-Cladding Interaction in Water Reactors, Vienna, June 1977, Report No. IWGFPT, IAEA, Vienna (1979).
- [2] INTERNATIONAL ATOMIC ENERGY AGENCY, Proceedings of Specialists' Meeting on Power Ramping and Power Cycling of Water Reactor Fuel and Its Significance to Fuel Behaviour, Arles, France, 14–18 May 1979, Report No. IWGFPT/5, IAEA, Vienna (1980).
- [3] INTERNATIONAL ATOMIC ENERGY AGENCY, Proceedings of Specialists' Meeting on Pellet-Cladding Interaction in Water Reactors, Riso National Laboratory, Denmark, 22–26 September 1980, Report No. IWGFPT/8, IAEA, Vienna (1981).
- [4] INTERNATIONAL ATOMIC ENERGY AGENCY, Proceedings of Specialists' Meeting on Power Ramping and Power Cycling of Water Reactor Fuel and Its Significance to Fuel Behaviour, Petten, 8–9 September 1982, Report No. IWGFPT/14, IAEA, Vienna (1983).
- [5] INTERNATIONAL ATOMIC ENERGY AGENCY, Proceedings of Specialists' Meeting on Pellet-Cladding Interaction in Water Reactors, Seattle. USA, 3–5 October 1983, Report No. IWGFPT/18, IAEA, Vienna (1984).
- [6] INTERNATIONAL ATOMIC ENERGY AGENCY, Proceedings of Technical Committee Meeting on Power Ramping, Cycling and Load Following Behaviour of Water Reactor Fuel, Lyon, France, 18–21 May 1987, Report No. IWGFPT/28, IAEA, Vienna (1988).
- [7] INTERNATIONAL ATOMIC ENERGY AGENCY, Iodine Induced Stress Corrosion Cracking of Zircaloy Fuel Cladding Materials, IAEA-TECDOC-1185, IAEA, Vienna (2000).
- [8] INTERNATIONAL ATOMIC ENERGY AGENCY, Non-Baseload Operation in Nuclear Power Plants: Load Following and Frequency Control Modes of Flexible Operation, Nuclear Energy Series No. NP-T-3.23, IAEA, Vienna (2018).
- [9] BÉGUIN, S., "PCI-Related Constraints on EDF PWRs and Associated Challenges", Seminar Proceedings on in Pellet-Clad Interaction in Water Reactor Fuels, Aix-en-Provence, France, 9-11 March 2004, NEA Series No. NEA-6004, OECD-NEA (2005).
- [10] BARBIÉ, L., TKEITH, T., RAUTENBERG, M., WAECKEL, N., "Safety Requirements for Pellet-Clad Interaction in France – New approach Developed by EDF", Workshop Proceedings on Pellet-Clad Interaction (PCI) in Water-Cooled Reactors, Lucca, Italy, 22-24 June 2016, NEA Working Group on Fuel Safety (WGFS), Report No. NEA/CSNI/R(2018)9, OECD-NEA (2018).
- [11] GOLDSTEIN, L., SHEPPARD, K.D., "A Survey of Load Following Experience in US Light Water Reactors", Power Ramping, Cycling and Load Following Behaviour of Water Reactor Fuels, IWGFPT/28/24, IAEA, Vienna (1988).
- [12] CARTER, T.J., FEHRENBACH, P.J., The Load Following Capability of CANDU Fuel, Atomic Energy of Canada Limited (AECL) Report, AECL-7096, Chalk River, Canada (1983).
- [13] UNITED STATES NUCLEAR REGULATORY COMMISSION, "Fuel System Design", Standard Review Plan for the review of Safety Analysis Reports for Nuclear Power Plants: LWR Edition – Reactor, Section 4.2, Revision 3, NUREG-800 Chapter 4, US NRC (2007).
- [14] O'DONNELL, W.J., LANGER, B.F., Fatigue Design Basis for Zircaloy Components, Nuclear Science and Engineering **20** (1964) 1-12.
- [15] COX, B., Pellet-Clad Interaction (PCI) Failures of Zirconium Alloy Fuel Cladding – A Review, Journal of Nuclear Materials **172** (1989) p249.
- [16] MCDONALD, S.G., et al., "A Statistical Analysis of Pellet-Clad Interaction Failures in Water Reactor Fuel," Proceedings of Specialists' Meeting on Pellet-Cladding Interaction in Water Reactors, Riso National Laboratory, Denmark, 22–26 September 1980, Report No. IWGFPT/8, IAEA, Vienna (1981).
- [17] SIPUSH, P.J., KAISER, R.S., "The Effect of Power Change on the PCI Failure Threshold," Proceedings of Specialists' Meeting on Power Ramping and Power Cycling of Water Reactor Fuel and Its Significance to Fuel Behaviour, Petten, 8–9 September 1982, Report No. IWGFPT/14, IAEA, Vienna (1983).
- [18] NOBREGA, B.N., KING, J.S., WAS, G.S., WISNER, S.B., Improvements in the Design and Analysis of the Segmented Expanding Mandrel Test, Journal of Nuclear Materials **131** (1985) 99-104.
- [19] COLEMAN, C.E., "Simulation of Interaction between Cracked UO₂ Fuel and Zircaloy Cladding," Proceedings of International Conference on Physical Metallurgy of Reactor Fuel Elements, The Metals Society, London, U.K. (1974) pp. 302–307.
- [20] ROWLAND, T.C., DAVIES, J.H., THOMPSON, J.R., ROSENBAUM, H.S., "Statistical Analysis of Power Ramp PCI Test Data", Proceedings of Specialists' Meeting on Pellet-Cladding Interaction in Water Reactors, Seattle. USA, 3–5 October 1983, Report No. IWGFPT/18, IAEA, Vienna (1984).
- [21] POWERS, C. et al, "Hot Cell Examination Results of Non-Classical PCI Failures at La Salle," Paper presented at the International LWR Fuel Performance Meeting, Kyoto, Oct. 2–6, 2005.
- [22] DAVIES, J.H., HOSHI, E.V., ZIMMERMAN, D.L., Ramp Test Behaviour of High O/U Fuel, J Nuclear Mater **270** (1999) 87–95.

- [23] VOGL, W., RUYTER, I., MARKGRAF, J., “The Petten Ramp Test Programme of Kraftwerk Union/Kernforschungsanlage (KWU/KFA) during the Years 1976 to 1981”, Proceedings of Specialists’ Meeting on Power Ramping and Power Cycling of Water Reactor Fuel and Its Significance to Fuel Behaviour, Petten, 8–9 September 1982, Report No. IWGFPT/14, IAEA, Vienna (1983).
- [24] MOGARD, H., KJAER-PEDERSEN, N., A Review of Studsvik’s International Power Ramp Test Projects, STUDEVIK-8S/6, Studsvik, Sweden (1985).
- [25] TSUKUDA, Y., et al., “Performance of Advanced Fuel Materials for High Burnup”, Paper presented at the Int. Conf. Top Fuel, Würzburg, European Nuclear Society (2003).
- [26] NONON Ch., et al., “Differential PCI Behaviour of PWR Fuel Rods under Transient Conditions,” Paper presented at the International Meeting on LWR Fuel Performance, Orlando FL, USA, Sept 19–22, 2004.
- [27] KILLEEN, J., TURNBULL, J. A. et al., “Experimental data on PCI and PCMI within the IFPE Database”, Seminar Proceedings on Pellet-clad Interaction in Water Reactor Fuels, Aix-en-Provence, France, 9–11 March 2004, NEA Report No. 6004, OECD (2005).
- [28] VON JAN, R., WUNDERLICH, F., HOLZER, R., “Power Ramping/Cycling Experience and Operational Recommendations in KWU Power Plants”, Proceedings of Specialists’ Meeting on Power Ramping and Power Cycling of Water Reactor Fuel and Its Significance to Fuel Behaviour, Arles, France, 14–18 May 1979, Report No. IWGFPT/5, IAEA, Vienna (1980).
- [29] VON JAN, R., HERING, W., “Experience and Plans with PCI Protection in KWU LWR Plants”, Proceedings of Specialists’ Meeting on Pellet-Cladding Interaction in Water Reactors, Riso National Laboratory, Denmark, 22–26 September 1980, Report No. IWGFPT/8, IAEA, Vienna (1981).
- [30] VON JAN, R., WUNDERLICH, F., GARTNER, M., Fuel Performance Aspects for Load Following Operation of Light Water Reactors, Kerntechnik 48 [3] (1986).
- [31] VON JAN, R., “Strategy and Experience of PCI Protection and Load Following Operation in KWU LWR Plant”, Proceedings of Technical Committee Meeting on Power Ramping, Cycling and Load Following Behaviour of Water Reactor Fuel, Lyon, France, 18–21 May 1987, Report No. IWGFPT/28, IAEA, Vienna (1988).
- [32] SHEA, J.H., “The Development of an Empirical PCI Criterion for Siemens Fuel to be Loaded into Sizewell B”, Proceedings of a Technical Committee Meeting on Nuclear Fuel Behaviour Modelling at High Burnup and Its Experimental Support, Windermere, United Kingdom, 19–23 June 2000, TECDOC Series No. IAEA-TECDOC-1233, IAEA, Vienna (2000).
- [33] DONCEL, N., MUÑOZ-REJA, C. “PCI Analysis During ERPO with Thermal-Mechanical TREQ Code”, Workshop Proceedings on Pellet-Clad Interaction (PCI) in Water-Cooled Reactors, Lucca, Italy, 22–24 June 2016, NEA Working Group on Fuel Safety (WGFS), Report No. NEA/CSNI/R(2018)9, OECD-NEA (2018).
- [34] JULIEN B., et al., “Performance of Advanced Fuel Product under PCI Conditions”, Paper presented at the International Meeting on LWR Fuel Performance, Orlando FL, USA, Sept 19–22, 2004.
- [35] BILLAUX, M., “Modelling Pellet-Cladding Mechanical Interaction and Application to BWR Manoeuvring”, Paper presented at International Meeting on LWR Fuel Performance, Orlando FL, USA, Sept 19–22, 2004.
- [36] DANIEL, L., ANDRE-POYAUD, G., SCHUH, K.D., SAUTEREAU, A., PAUL, T., ROYERE, C., “AREVA NP’s PCI Methodologies for PWR Enhanced Plant Manoeuvrability”, Workshop Proceedings on Pellet-Clad Interaction (PCI) in Water-Cooled Reactors, Lucca, Italy, 22–24 June 2016, NEA Working Group on Fuel Safety (WGFS), Report No. NEA/CSNI/R(2018)9, OECD-NEA (2018).
- [37] ALESHIN, Y. et al., “The Effect of Pellet and Local Power Variations on PCI Margin,” Paper presented at Top Fuel 2010 Conference, Paper 041, Orlando, Florida, September 26–29, 2010.
- [38] PARAMONOV, D., “PCI Risk Assessment Model,” Proceedings of the 18th International Conference on Nuclear Engineering (ICONE18), May 17–21, 2010, Xi’an, China, ASME (2010).
- [39] SELTBORG, P. et al., “Westinghouse’s PCI Methodology with Operating Guidelines Derived from Enhanced Statistical Treatment of Power Ramp Tests”, paper presented at Top Fuel 2015 Conference, Zurich, Switzerland, 13–17 September 2015.
- [40] DELAFOY, Ch., BLANPAIN, P., et al., “Advanced PWR Fuels for High Burnup Extension and PCI Constraint Elimination”, Proceedings of Technical Meeting on Advanced Fuel Pellet Materials and Designs for Water Cooled Reactors, Brussels, 20-24 October 2003, IAEA-TECDOC-1416, IAEA, Vienna (2003).
- [41] BACKMAN, K., HALLSTADIUS, L., RÖNNBERG, G., “Westinghouse Advanced Doped Pellet – Characteristics and Irradiation Behaviour”, Proceedings of a Technical Meeting on Advanced Fuel Pellet Materials and Designs for Water Cooled Reactors, Villigen, 23–26 November 2009, IAEA-TECDOC-1654, IAEA, Vienna (2010).
- [42] VON JAN, R., HERING, W., “Practical Experience with PCI Protection in KWU LWR Plants”, Proceedings of Specialists’ Meeting on Power Ramping and Power Cycling of Water Reactor Fuel and Its Significance to Fuel Behaviour, Arles, France, 14-18 May 1979, Report No. IWGFPT/5, IAEA, Vienna (1980).
- [43] KUHN, A. and KLAUS, P., Improving Automated Load Flexibility of Nuclear Power Plants with ALFC, VDB Power Tech 5 (2015).

- [44] ORGANISATION FOR ECONOMIC COOPERATION AND DEVELOPMENT (OECD) – NUCLEAR ENERGY AGENCY (NEA), Workshop Proceedings on Pellet-Clad Interaction (PCI) in Water-Cooled Reactors, Lucca, Italy, 22–24 June 2016, NEA Working Group on Fuel Safety (WGFS), Report No. NEA/CSNI/R(2018)9, OECD-NEA (2018).
- [45] INTERNATIONAL ATOMIC ENERGY AGENCY, Safety of Nuclear Power Plant: Design, IAEA Safety Standards, Specific Safety Requirements Series No. SSR-2/1 (Rev.1), IAEA, Vienna (2016).
- [46] INTERNATIONAL ATOMIC ENERGY AGENCY, Design of the Reactor Core for Nuclear Power Plants, IAEA Safety Standards, Specific Safety Guides Series No. SSG-52, IAEA, Vienna (2019).
- [47] UNITED STATES NUCLEAR REGULATORY COMMISSION, “Official Transcript of Proceedings of ACRS Materials”, Metallurgy and Reactor Fuels Subcommittee Meeting, US NRC, 3 March 2009.
- [48] NUCLEAR SAFETY STANDARDS COMMISSION (KTA), Design of Reactor Cores of Pressurized Water and Boiling Water Reactors; Part 3: Mechanical and Thermal Design, KTA Safety Standard, 3101.3 (2015).
- [49] ORGANISATION FOR ECONOMIC COOPERATION AND DEVELOPMENT (OECD) – NUCLEAR ENERGY AGENCY (NEA), Fuel Safety Criteria in NEA Member Countries – Compilation of Responses Received from Member Countries, Report No. NEA/CSNI/R(2003)10, OECD-NEA, Paris (2003).
- [50] ZHANG, J., DETHIOUX, A., UMIDOVA, Z., DRIEU, T., SCHNEIDESCH, C., “Development and Applications of a Loading Pattern PCI Risk Assessment Tool for Flexible Core Design”, Workshop Proceedings on Pellet-Clad Interaction (PCI) in Water-Cooled Reactors, NEA Working Group on Fuel Safety (WGFS), Lucca, Italy, 22-24 June 2016, Report No. NEA/CSNI/R(2018)9, OECD-NEA (2018).
- [51] INTERNATIONAL ATOMIC ENERGY AGENCY, Review of Fuel Failures in Water Cooled Reactors, Nuclear Energy Series No. NF-T-2.1, IAEA, Vienna (2010).
- [52] INTERNATIONAL ATOMIC ENERGY AGENCY, Review of Fuel Failures in Water Cooled Reactors (2006-2015), Nuclear Energy Series No. NF-T-2.5, IAEA, Vienna (2019).
- [53] MATTAS, R.F., YAGGEE, F.L. NEIMARK, L.A., “Effect of Zirconium Oxide on the Stress-Corrosion Susceptibility of Irradiated Zircaloy Cladding”, Proceedings of the Fifth International Conference on Zirconium in Nuclear Industry – Boston, USA, August 4–7, 1980, ASTM-STP 754 (1980) p158.
- [54] ALVAREZ, A-M., JÄDERNÄS, D., SCIP III - Task 2.1: Mandrel Tests, STUDSVIK/N-19/126, SCIP III-262 (to be published).
- [55] INTERNATIONAL ATOMIC ENERGY AGENCY, Fuel Modelling at Extended Burnup (FUMEX-II), IAEA-TECDOC-1687, IAEA, Vienna (2012).
- [56] INTERNATIONAL ATOMIC ENERGY AGENCY, Improvement of Computer Codes Used for Fuel Behaviour Simulation (FUMEX-III), IAEA-TECDOC-1697, IAEA, Vienna (2013).
- [57] INTERNATIONAL ATOMIC ENERGY AGENCY, Fuel Modelling in Accident Conditions (FUMAC) - Final Report of a Coordinated Research Project, IAEA TECDOC-1889, IAEA, Vienna (2019).
- [58] DOSTÁL, M., ROSSITER, G., DETHIOUX, A., ZHANG, J., et al. "OECD/NEA Benchmark on Pellet-Clad Mechanical Interaction Modelling with Fuel Performance Codes: Impact of Number of Radial Pellet Cracks and Pellet-Clad Friction Coefficient," ENS Trans. Top Fuel 2018, Prague, Czech Republic, 30 September – 4 October 2018.

ANNEX I: A SUMMARY OF I-SCC MECHANISMS

The stress corrosion cracking (SCC) of zircaloy cladding has been studied for a long time since late 1960s, and thus a number of theories and parameters have been proposed for use in the mechanistic understanding of the SCC behaviour of zirconium alloys. Some are consistent and supplementary to each other whilst some are inconsistent and contradictory to each other. Since this publication is intended to deal with the up-to-date evolution of understanding the SCC behaviour of Zr cladding, it is necessary to define first a basis on which an incremental progress in the technology area can be evaluated. For this purpose, a review of the state of the art understanding of the SCC behaviour of Zr alloys has been extracted from the IAEA-TECDOC-1185 publication [I-1] and summarized in this Annex. Thus, a significant part of this Annex is reproduced from the IAEA-TECDOC-1185 publication [I-1].

I-1. I-SCC MECHANISMS OF ZIRCONIUM ALLOYS

Pellet-cladding interaction failures of zircaloy clad UO_2 fuel were first discovered during the testing of high powered fuel at General Electric Vallecitos in 1963 [I-2], and research showing that stress corrosion cracking by iodine was a probable explanation was published by Hermann Rosenbaum in 1965 [I-3, I-4]. For a number of years after that PCI failures were infrequent and were observed in a few loop tests where significant uprating of fuel occurred. It became evident that an epidemic of failures was starting when on-load refuelling in the CANDU-prototype reactors NPD and Douglas Point started in 1969, and the situation became serious with the start-up of Pickering-1 (the first CANDU full-scale plant) in 1971. As a result of this a crash programme to develop a cure was instituted by the Atomic Energy of Canada Limited, and the graphite coating was tested and adopted for all new fuel by the end of 1972 [I-5].

Similarly, the early occurrence of boiling water reactor (BWR) fuel failures led to the development of another type of solution: a thin inner liner of low oxygen, soft pure zirconium was metallurgically bonded to the bulk of the cladding. The aim of this solution was to reduce the initiation rate of inner cracks by having a soft material and to reduce the stress level by improvement of the sliding of the UO_2 fragments on the inner surface of the cladding. This solution was indeed implemented and currently almost all the fuel assemblies delivered for BWR reloads are provided with "liner fuel" [I-6]. The improvement in reducing the failure rate is evident as it allowed the attainment of a failure rate below 10^{-5} [I-7].

In addition, although PCI type failures are rarely if ever reported in pressurized water reactor (PWR) fuel during normal operation, new safety requirements include consideration of this possibility. This led to extensive R&D work in this area. Its aim was to acquire a better understanding of the mechanisms involved in this failure mode and to develop new fuel cladding with improved resistance to I-SCC under some accident conditions [I-8, I-9]. The same requirements led to comparable R&D work performed on Zr-1-%Nb Russian cladding alloy [I-10 – I-13].

Among the conditions controlling the fuel cladding behaviour, several parameters have been observed to have major contributions.

- The maximum power is often considered as a criterion for failure. Starting at a high power at beginning of life, in the presence of a large initial gap and fresh fission product free fuel, the maximum power sustainable reduces to reach a stable value above a burn up of about 20 $\text{GW}\cdot\text{d}/\text{t}$. The answer to the question of whether or not this failure limit may increase again at high burnup is still pending [I-8];
- A closer analysis of the conditions causing PCI failures allowed the introduction of other factors. Among these the power increase between the stable conditions before the power ramp and the maximum power reached. The process responsible for failure requires a consideration of the dynamic thermal mechanical equilibrium between cladding and pellet. Indeed, the stress state in the cladding during the transient is controlled by the contact conditions between pellet and cladding. This is termed 'conditioning' and focuses on the fact that the stress state of the cladding is relevant to the PCI failure mechanisms;
- The third factor is linked with the power change rate. Several experiments have been performed with very slow power changes. Maximum power levels well above the standard values were obtained without failure. Detailed thermal mechanical analysis were able to show that during slow power ramping the cladding and the pellet will creep, reducing the stress state of the former [I-14].

All these observations are in agreement with a mechanism based on stress corrosion, where stresses are induced by thermal mechanical interaction between pellet and cladding due to thermal expansion and the corrosive species being a fission product.

Various reviews have led to the conclusion that a compound of iodine should be the chemical species involved. Indeed, it has a relatively high fission yield, is known, as is any halogen, to react with the IV B elements and experimental I-SCC has similar fracture surfaces to the those obtained during PCI test failures. However, it remains unclear whether iodine itself, or some compound resulting from reaction with zirconium, is the actual active species.

I-1.1. Relation between pellet-cladding interaction (PCI) and iodine-induced stress corrosion cracking (I-SCC)

The first question requiring an answer relates to the exact chemical species involved in the I-SCC during PCI failure. It is well known [I-15] that iodine has a significant fission yield (^{127}I and ^{129}I , considered as stable sum to 1.25% in thermal reactors), but it is exceeded by Caesium (the 133, 135 and 137 isotopes have a total yield of more than 18.5%). Thus, it is expected that any iodine released will be trapped by a larger amount of caesium. Nevertheless, the highly radiolytic environment in the gap, due to fission product recoils, continuously generates radical species like iodine atoms or ions, that will be able to react with any material instead of remaining trapped on other chemical compounds. Computations performed initially for breeder fuel and later extended to water reactor fuel have proven the possibility of a raise in the iodine partial pressure to 3×10^{-10} atm., high enough to induce an I-SCC phenomenon [I-16]. Experiments using gamma irradiation in order to induce radiolysis lead to the same conclusions [I-17]. Thus, the question of the availability of iodine is no longer valid and I-SCC is clearly a mechanism of high importance with respect to PCI failures.

The state of our understanding of PCI cracking in connection with I-SCC, can be summarized as follows:

- There was a degree of certainty that the culprit was iodine or an iodine compound and not a caesium/cadmium mixture, based on detailed fractography of the fuel failures [I-18];
- It had been established that, provided the fuel remained in a high power position for no more than half an hour, the probability of failures was small. Much higher failure frequencies occurred if the residence time at high power was between a half and two to three hours, and all the failures that were likely to occur had happened during this period [I-19];
- This apparent ‘incubation period’ was also observed in laboratory testing and was thought to be a real phenomenon associated with the SCC cracking process [I-20];
- The graphite coating was shown to both lubricate the UO₂/zircaloy interface and to absorb the iodine in the form of a carbon stabilized zirconium iodide complex [I-21]. There remain some doubts about the precise chemical form in which the effect of the iodine is neutralized in the presence of a graphite coating;
- The observation of very rapid fuel failures (<1 minute) in some Swedish ramp tests cast doubt on the actual cause of the ‘incubation period’ [I-22], although ‘pre-soaking’ the fuel before ramping appeared to be necessary in order to obtain the very rapid failures;
- Tests in the laboratory using a cam-driven stressing system that could apply loads for very brief (<10 seconds) periods showed that it was necessary to allow the chemistry within the fuel cladding to come to equilibrium for about 30 minutes before it was possible to initiate a crack by a single <10 s stress pulse. It was clear from this work that getting the chemistry right was the essential feature of the ‘incubation period’, and that I₂ vapour was not the key aggressive species [I-23];
- Unfortunately, funding to pursue these chemical studies to establish the form of the key species (e.g. ZrI₄, ZrI₃ or others) was never forthcoming.

I-1.2. Three-stages of I-SCC

It is possible to distinguish three distinct stages in the cracking process. The experimental conditions and the mechanisms operating during each of these stages will be discussed under the following headings:

- The incubation period;
- Crack initiation;
- Crack propagation through the tube wall.

I-1.2.1. The incubation period

Whatever the method used for studying iodine-induced SCC of zircalloys, there appears to be an initial period when no crack-like features can be found in the highly stressed regions of smooth specimens. The length of the incubation period varies with the test method and the testing conditions, but is always there, even for pre-cracked specimens, although it may be short in this instance.

The evidence obtained at Chalk River [I-23] suggested that I_2 vapour was not the most aggressive species and that chemical changes occurred in the environment (during the incubation period) without which a crack could not be initiated upon loading the specimen. The species being produced chemically during this period were never identified, so there is no advantage to speculation on what they might be. The more aggressive nature of ZrI_4 as the active species is still not enough to demonstrate that this is the key species. It appears that 'incubation times' are still observed when adding ZrI_4 to the system, so further chemical modification of this species may be occurring during this period. The possibility that the process may be autocatalytic, with some minor alloying element or impurity as the catalyst cannot be eliminated on current evidence.

A possible explanation of the incubation time may be linked with the time necessary for the chemical environment to react with the protective oxide layer always present on any Zr alloy sample and to weaken it. After this chemical reaction the SCC process will occur by interaction between the iodine bearing environment and the base metal. In this respect, the possibility of cracking fuel rod cladding during very short power transients [I-22] can be explained by the local absence of any oxide layer on the inner wall of the cladding, due to dissolution of the oxide layer in the base metal, during any pre-conditioning treatment. It should be noted that the fractography of the cracks initiated during very short power ramp transients has never been published.

I-1.2.2. Crack initiation

If the specimen has been equilibrated at temperature in a static iodine environment (without external stresses) for long enough (20-30 minutes) then a short (<10 s) stress pulse to beyond the yield stress can initiate cracks in an initially smooth specimen. These cracks were found to be completely trans-granular in nature and were often only one or two grains deep [I-23, I-24]. It appeared that the number of these initiation sites could be related to the frequency of basal poles in the circumferential direction [I-24].

The number of such initiation sites, for any one batch of cladding, was greatly increased (by a factor >10), however, by the presence of trace impurities of organic iodides [I-25]. Thus, it is clear that not all suitably oriented basal planes crack in the absence of these agents. Since the density of basal poles increases rapidly for all batches as one moves from the circumferential towards the radial direction, it may be that the effect of the organic iodides is merely to reduce the normal stress necessary to obtain pseudo-cleavage. Thus, for a given set of experimental conditions, a much larger number of basal planes would see a resolved stress high enough to cause pseudo-cleavage. Since we have only a speculative understanding of the mechanism of pseudo-cleavage, it is not possible to be more rigorous about the above effects.

In other types of test, intergranular initiation can be quite common. The extent of intergranular cracking is greater in statically loaded tests; with thick walled cladding rather than the 0.4 mm wall thickness CANDU cladding; and particularly for iodine solutions in organic solvents some of which give almost completely intergranular features [I-26]. Both inter-granular initiation and propagation are thought to result from removal of material from the grain boundaries - specimens lose weight during cracking. In iodine vapour the mechanism is thought to be a version of the van Arkel process [I-20], whereas in organic solutions grain boundary dissolution (not necessarily electrochemical since the solutions are usually non-electrolytes) is thought to be the mechanism [I-26, I-27]. Crack initiation at fractured hydrides is relatively uncommon and was peculiar to one or two batches of early CANDU cladding [I-28], and to tests at elevated temperature with excessive moisture in the container (e.g. initial in-reactor tests in CsI) [I-29].

I-1.2.3. Initiation mechanisms

Due to the limited number of slip systems activated in Zr alloys (prismatic and to a limited extent pyramidal), the strain compatibility from grain to grain during straining (the Taylor problem) is of high concern. Indeed, the five independent slip systems are not available in zirconium alloys. Therefore, some experimenters have tried to correlate the occurrence of crack initiation at a grain boundary with the crystallographic orientations of the two adjacent grains. Kubo [I-30] found that a crack may occur when dislocations pile-up at a grain boundary, while the grain on the other side has no easy slip system for relaxing the stresses induced by this family of dislocations. In addition, he found that large Fe-bearing precipitates enhanced the formation of an intergranular crack.

Detailed experiments performed in CEA Grenoble [I-31] aimed at finding a quantitative relation between grain to grain misorientation and intergranular crack nucleation. It was found that, in Zry-4, the density of intergranular cracks increased with local strain. Examination of the locations of the incipient intergranular cracks after slow tensile tests in iodine vapour at 350°C led to the conclusion that the major parameter controlling the position of the crack was not the grain to grain misorientation, but the orientation of the grain boundary plane with respect to the maximum tensile stress orientation: the more normal to the tensile stresses, the higher the probability for a crack to nucleate at this grain boundary.

In laboratory tests performed in iodine vapour on non-irradiated materials, and in methanol/I₂ solutions on irradiated materials, close to the free surface, the intergranular crack grows to a depth of not more than 100 µm. By analysis of the depth of these cracks, an average intergranular crack growth rate can be calculated. It increases from 5 nm/sec at 300 MPa to 20 nm/sec at 400 MPa [I-32]. The transition between the intergranular cracking mode and the pseudo-cleavage mode occurs when the stress intensity factor at the crack tip exceeds a critical value for trans-granular SCC to proceed.

Similar work has been undertaken in the case of the Russian Zr-1% Nb alloy [I-12, I-13]. A careful examination of the inner surfaces of the cladding allowed the characterization of the intergranular cracks: a minimum plastic strain was required for the formation of the intergranular cracks. Similarly, to the zircalloys, an increase in number of cracks with strain was found and their orientation density was higher when they were perpendicular to the tensile stresses. Cross sections permitted the description of the shape in depth of the intergranular cracks. It was found that increasing the stress level above the critical value for initiation did not change the mean crack length. The surface density was increased mostly due to the nucleation of new small size micro-cracks. Surface crack widening occurred faster than its increase in depth.

During irradiation, the fission fragments recoil from the original nucleus with energies in the range of 60-80 MeV. Due to their masses and to the density of the fuel and of the cladding, the typical ranges for these ions are between 6 and 8 µm. Thus, the inner cladding surface is slowly doped with the fission products throughout their ranges. The computation of the amount of fission products within the cladding gives a value of about 5% foreign atoms at the inner surface, declining to zero at a depth corresponding to the fission product range [I-33]. Most of these are deposited in the oxide formed on this surface which can be from 1-2 µm up to 10 µm as a function of the burn up. The extensive damage induced by these recoils (well above 100 dpa), as well as the chemical doping corresponding to it, has been considered as a possible cause for the formation of a brittle surface layer that could ease the initiation step of the I-SCC process. Several experimenters have analyzed in detail the consequences of such a surface irradiation on the susceptibility to I-SCC. Using different ions for the irradiation of the inner surface of Zr alloys plates or cladding, it was found that no significant cracking can be induced by this process [I-34]. The reason may be due either to the limited impact of the rather low level of the implanted iodine (about 120 ppm for two PWR cycles), or to the iodine having a very low diffusion coefficient in Zr [I-23, I-35], so that it cannot reach the grain boundaries [I-33].

I-1.2.4. Crack propagation through the tube wall

It is generally agreed that the cracks at the initiation sites grow until the stress intensity at the crack tip exceeds a critical value named $K_{I,SCC}$. After then, a faster crack propagation process takes over. The trans-granular pseudo-cleavage process occurs only on (or very close to) basal planes [I-36]. If very few of these planes lie in the crack propagation plane, then a large number of uncracked grains will be left behind the propagating crack front. These residual webs then fail either by ductile tearing on the prism planes (to give the characteristic fluting features), or by the slower intergranular corrosion process. Fluting is generally restricted to residual webs that are only one (or a few) grains thick [I-37]. If the trans-granular cracking is widely dispersed and the residual webs represent a large fraction of the crack area, then high stresses will be needed to fail the specimen and a mainly normal ductile fracture will occur by void nucleation and growth.

The mechanism of the trans-granular pseudo-cleavage process is not well understood. By elimination, it has been suggested that an adsorption-induced reduction in bond-strength at the crack tip is operating. A computation of the surface energy and its modification due to iodine adsorption shows a much higher reduction of basal plane surface energy, compared to other planes. Thus, the pseudo-cleavage may be enhanced by the lowering of the surface energy of the <c> planes, making a favourable energy balance for crack propagation on these planes [I-38]. Other possible mechanisms can be eliminated since no electrochemical processes are possible in iodine vapour; cracking occurs in a hydrogen free system and when all internal hydrogen must be in solution (and hydride cracking is distinguishable fractographically) [I-39].

The shapes of the velocity versus stress intensity curves that are obtained using different experimental techniques and conditions can be very different and, if the velocity does not fall rapidly at low K_I , this can cause difficulties in establishing K_{I-SCC} . Measured values for K_{I-SCC} seem to differ significantly for results obtained on sheet and tubing, the latter usually giving significantly lower values (3 – 6 MPa·m^{-1/2}) whereas the former often give values of 10–15 MPa·m^{-1/2}. It has been shown that these differences can be explained by the specimen texture and/or state of stress [I-40].

Using fatigue pre-cracking of cladding tubes, it was possible to measure the I-SCC crack growth rate of cladding tubes under iodine vapour between 300 and 400 °C [I-40 – I-42]. In the case of Zry-4, crack growth rates and K_{I-SCC} values have been measured and gave a minimum stress intensity factor for crack growth of 3.5 MPa·m^{-1/2}, depending of material conditions, and an average crack growth rate of about 1 µm/sec at K_I values corresponding to the plateau of the da/dt- K_I curves [I-43]. Similar experiments on Russian Zr-1% Nb cladding gave good I-SCC resistance, probably due to the weak recrystallized state of the Zr matrix at 350°C: $K_{I-SCC} = 4.8$ MPa·m^{-1/2}, crack growth rate at plateau = 3.9x10⁻⁴ mm/sec.

I-1.3. Tubing degradation after wall penetration

Once a PCI crack has penetrated the tubing wall then the subsequent degradation of the tubing depends upon the test conditions. Fuel failed in service in a water cooled reactor will flood with water immediately after penetration of the wall occurs, stopping the PCI cracking process. Thus, the initial penetration of the outer wall may be very short (1–2 mm) and oxidation of the crack surfaces often effectively plugs the crack so that only a limited volume of water enters the fuel pin. Therefore, primary PCI failures usually show secondary hydriding degradation quickly at some point well removed from the initial PCI crack, provided the fuel-clad gap is closed. The secondary hydriding will then be the most obvious feature of the failed pin. The primary PCI failure may not grow any further but will develop "rabbit ears" by ductile deformation at the ends of the arrested crack. It will appear as an "X-mark" on the outer cladding surface.

I-1.4. Effects of irradiation

Whether the susceptibility of tubing to iodine-induced SCC can be related to the tube texture appears to depend on the method of testing. When using split-ring tests with a fixed deflection no clear correlation of susceptibility and texture was evident [I-20], whereas for pressurised tube tests [I-44] and compressed tube tests [I-23], a relationship between texture and susceptibility does appear to be present. Once the tubing is irradiated, however, all batches of tubing appear to become susceptible to cracking, and this susceptibility develops at irradiation doses lower than those necessary for a saturation of the irradiation induced changes in mechanical properties. No clearly established mechanism for this effect has been established, but it obviously cannot just be related to the increased ability to sustain a high stress intensity at the crack tip without blunting, since it occurs before major irradiation hardening of the matrix is evident [I-45]. Dislocation channelling in irradiated cladding was suggested as a possible explanation, but no unequivocal evidence for this was found.

There is no evidence for any changes in crack velocity during irradiation, but specimens tested after irradiation by the pressurised tube technique show reduced times to failure. This does not necessarily imply an increased crack velocity but may be explained by the irradiation induced hardening of the zirconium matrix.

Testing performed on pre-irradiated materials usually shows a higher resistance to I-SCC for the pre-irradiated case, when expressed in terms of time to failure in an iodine environment. This seems to be clearly an effect of the irradiation hardening induced by the <a> dislocation loops. Indeed, the lifetime at a given stress under iodine is much longer for pre-irradiated alloys, than for unirradiated ones; but the reductions in life, compared to the tests performed on un-irradiated materials, are similar for irradiated and unirradiated alloys. For zircaloy-4 the reduction in K_{I-SCC} was really significant, dropping from 3.2 to 1.5 MPa·m^{-1/2} [I-46].

In BOR-60, the Zr-1% Nb alloy were irradiated at a temperature of 325–345 °C, up to a fluence of 0.45 to 0.90x10²² n/cm². The stress corrosion testing (in the time to failure mode) was performed both with and without iodine for up to 40 hours over a stress range of 200 to 520 MPa. The analysis of the results indicated the following points:

- The rupture mode, as revealed by fractography, is the same for unirradiated and irradiated material;
- Compared to unirradiated material, the reduction of time to failure due to iodine is higher for irradiated material;
- Under iodine, the life time of irradiated materials is higher compared to unirradiated ones.

I-2. SUMMARY OF THE RESULTS OF THE CRP ON I-SCC OF ZIRCONIUM ALLOYS

This section is summarized the results performed during the Coordinated Research Project (CRP) on Stress Corrosion Cracking of Zirconium Alloy Fuel Cladding during 1994-1999 [I-1]. The purpose of this CRP was to provide basic data on I-SCC using a matrix of different temperature and iodine levels. The major variables influencing SCC in Zr alloys are metallurgical state (including composition, orientation, thermo-mechanical treatment, texture and cold work), environment (composition, concentration and temperature) and stress. It was not feasible to investigate the effects of all these variables within the scope and timescale of the programme. The test programme was thus focused on determining the dependency of SCC propagation rate on temperature, iodine concentration and stress within the range of available materials. The following summarizes the results from the CRP in terms of the main experimental variables.

I-2.1. Effect of temperature

The test matrix included tests at three temperatures: 300, 350 and 400°C. The results from the laboratories do not show a clear, consistent effect of temperature on the threshold stress intensity factor or the crack propagation rate in the Stage II region. The three laboratories found K_{I-SCC} to decrease with increasing temperature. And the results also showed the Stage II crack propagation rate to increase with temperature. Scatter in a laboratory results masked any temperature effect in their tests. Temperature would be expected to influence SCC due to its effect on the mechanical properties of the material and on the diffusion rate of iodine. This would be expected to produce a reduction in K_{I-SCC} and increase in Stage II crack propagation rate as found in most of these tests.

I-2.2. Effect of material condition

Five materials were tested from two manufacturers. These were recrystallised zircaloy-2 (Zry-2) and zircaloy-4 (Zry-4) and stress-relief annealed Zry-4. By determining X-ray pole figures, each was shown to have a similar texture, so any effect on I-SCC would be expected to arise due to the effect on the mechanical properties and grain shape of the different heat treatments. The results from the two laboratories were consistent with this, with both finding a higher K_{I-SCC} for recrystallised materials compared to the stress relief annealed zircaloy. The other two laboratories were inconclusive in this respect.

I-2.3. Effect of iodine partial pressure

Iodine pressure was studied in the range 100 to 10 000 Pa I_2 . The two laboratories found no effect of iodine pressure on K_{I-SCC} . A laboratory on stress relieved Zry-4 and another laboratory on recrystallised Zry-2 indicated an increase in Stage II crack growth rate with increasing iodine concentration. These results are consistent with literature observations of a threshold iodine concentration and with crack propagation being diffusion controlled, so that a higher external iodine concentration will produce more rapid diffusion of iodine to the crack tip and hence higher crack propagation rates. This latter effect has also been shown to saturate once sufficient iodine is present. The supervisory group believe that the iodine replenishment rate in the test chambers varied markedly between laboratories, so that the true iodine concentrations in each test were unlikely to be consistent between laboratories.

I-2.4. Effect of texture

The CRP was extended in order to capitalise on the improvements in test facilities and experimental technique of the laboratories, both from the advice provided to them by the supervisory group, and from their increased experience in performing the tests. All previous tests in the CRP were performed on specimens in the T-L orientation, so the additional series of tests were to generate crack growth data in the opposite, L-T orientation. From texture considerations, SCC was expected to be more difficult in the L-T specimens, producing a higher K_{I-SCC} . This was found to be the case by the two laboratories. For another laboratory, in the L-T oriented specimens, the velocity increased gradually without achieving the plateau region with similar behaviour as for creep until rupture occurred. Thus, K_{I-SCC} of the L-T specimens couldn't be drawn.

I-2.5. Fractography

One important aspect of any experimental programme on iodine SCC of zirconium alloys is the fractography of the crack surfaces produced. The features to be expected are by now well known, and the extent to which they are observed can be very helpful in understanding the test results. The features that would be expected are:

- Trans-granular pseudo-cleavage on the basal planes of suitably oriented zirconium grains;

- Prismatic slip on the planes of the zirconium hexagonal prism surfaces, giving rise to the very characteristic feature termed "fluting" because of the similarity of its appearance to that of a fluted pillar;
- Intergranular separation along the grain boundaries to reveal the characteristic grain shape of the metal;
- Some ductile tearing of residual webs in the fracture surface.

By the end of the CRP most laboratories were obtaining good fractographs showing the above features. One interesting general observation was the infrequency of fluting in these tests. The fracture surfaces obtained were a mixture of trans-granular cleavage facets and grain boundary surfaces, with few fluting features, or their complete absence. Since the textures of these sheets were such that there should have been many grains in the crack propagation plane oriented for prismatic slip, rather than basal cleavage, the absence of fluting suggests that intergranular separation proved to be easier than prismatic slip as a crack propagation mechanism for the material used in this programme.

REFERENCES TO ANNEX 1

- [I-1] INTERNATIONAL ATOMIC ENERGY AGENCY, Iodine Induced Stress Corrosion Cracking of Zircaloy Fuel Cladding Materials, IAEA-TECDOC-1185, IAEA, Vienna (2000).
- [I-2] LYONS, M.F., COPLIN, D.H, JONES, G.G., High Performance UO₂ Fuel Program., US Report GEAP 3770-10 (1994).
- [I-3] ROSENBAUM, H.S., DAVIES, J.S., PON, J.Q., US Report GEQP-5100-5 (1966).
- [I-4] ROSENBAUM, H.S., ELECTROCHEM. Tech. 4 (1966) pp153.
- [I-5] COX, B., Pellet-Cladding Interaction (PCI) Failures of Zirconium Alloy Fuel Cladding - a Review, J. Nuclear Mater. **172** (1990) 249-292.
- [I-6] WILLIAMS, C.D., et al., "Zircaloy 2 Lined Zirconium Barrier Fuel Cladding", Zirconium in Nuclear Industry (proc. 11th Int. Symp. Garmisch-Partenkirchen), ASTM STP **1295** (1996) 676-694.
- [I-7] HARBOTTLE, J.E., et al., "The Behaviour of Defective BWR Barrier Cladding, Non-Barrier Fuel", (proc. Int. Top. Mtg on LWR Fuel Performance, West Palm Beach, 1994), American Nuclear Society (1994) 391-397.
- [I-8] JOSEPH, J., ATABEK R., TROTABAS, ML, "The CEA-Fragema Ramp Test Programme For The Study of the Effect of Power Cycling on PCI at High Burn-Up", Proceedings of Specialists' Meeting on Power Ramping and Power Cycling of Water Reactor Fuel and Its Significance to Fuel Behaviour, Petten, 8-9 September 1982, Report No. IWGFPT/14, IAEA, Vienna (1983).
- [I-9] CAILLOT, L., LINET, B., LEMAIGNAN, C., "Pellet Clad Interaction in PWR Fuel: Analytical Irradiation Experiment, Finite Element Modelling", Proceedings of SMIRT-12 (1993) 69-74.
- [I-10] NOVIKOV, V.V., et al., "Study of Crack Initiation, Propagation Mechanism on SCC of Zr-1%Nb VVER Fuels", proceedings. Int. Conf. on Radiation Material Science, Alushta, USSR (1990) 158-164.
- [I-11] NOVIKOV, V.V., "Mechanism of Fuel Cladding Failure in PCI", proceedings of Tech. Committee Mtg on Fuel Failure in Normal Operation of Water Reactors, Experience, Mechanisms, Management, IAEA-TECDOC-709, IAEA, Vienna (1992) pp255.
- [I-12] GORYACHEV, S.B., et al., Iodine Induced SCC Of Zr Alloys at Constant Strain Rate, J. Nuclear Mater. **199** (1992) 50-60.
- [I-13] BIBILASHVILI, Y.K., et al., Propagation of Stress Corrosion Cracks in Zr-1%Nb Claddings, J. Nuclear Mater. **224** (1995) 307-310.
- [I-14] PORROT, E., CHARLES, M., LEFEBVRE, F, LEMAIGNAN, C., "Mechanisms of Cladding Deformation, Fission Gas Release During Power Transients at High Burnup.", Paper presented at LWR Fuel Performance, Williamsburg, Va., 1988.
- [I-15] MATZKE, H., Oxygen Potential in the RIM Region of High Burnup UO₂ Fuel., J. Nuclear Mater. **208** (1994) 18-26.
- [I-16] KONASHI, K., et al., Radiation Effect on the Chemical State of Fission Product Iodine, J. Nuclear Mater. **248** (1997) 220-225.
- [I-17] BIBILASHVILI, Y.K., et al., "Studies of Radiation-Thermal Decomposition of Caesium Iodide, Stress Corrosion Cracking of VVER Fuel Clads in Gamma-Irradiation", Fuel Internal Chemistry, Fission Product Behaviour, IWGFPT/25, IAEA, Vienna (1985) pp167.
- [I-18] COX, B., SURETTE, B.A., WOOD, J.C., "Pellet-Clad Interaction Failures: Stress Corrosion Cracking by Iodine or Metal Vapour Embrittlement by Cesium/Cadmium Vapours", Proceedings on Environmental Degradation of Materials in Aggressive Environments, Blacksburg, VA (1981) 293-302.
- [I-19] PENN, W.J., LO, R.K., WOOD, J.C., Nuclear Technol. **34** (1977) 249-268.
- [I-20] WOOD, J.C., J. Nuclear Mater. **45** (1972) 105-122.
- [I-21] WOOD, J.C., SURETTE, B.A., AITCHISON, I., J. Nuclear Mater. **88** (1980) 81-94.
- [I-22] MOGARD, H., HOWE, D., GROUNES, M., "The international Trans-Ramp II Fuel Project - A study of the effects of rapid power ramping on the PCI resistance of PWR Fuel.", Proceedings of LWR-Fuel Performance, Williamsburg, VA, American Nuclear Society (1988) 232-244.
- [I-23] COX, B., HADDAD, R., "Recent Studies of Crack Initiation During Stress Corrosion Cracking of Zirconium Alloys", Proceedings of 7th Int. Symposium on Zr in Nuclear Industry, Strasbourg, ASTM STP **939** (1987) 717-733.
- [I-24] COX, B., HADDAD, R., J. c Mater. **138** (1986) 81-88.
- [I-25] COX, B., HADDAD, R., J. Nuclear Mater. **137** (1986) 115 -123.
- [I-26] COX, B., "Stress Corrosion Cracking in Iodine Containing Environment", Proc. 2nd Int. Symposium on Zr in Nuclear Industry, Portland, ASTM STP **551** (1974) 419-434.
- [I-27] COX, B., Corrosion **33** (1977) 79-84.
- [I-28] COX, B., "Hydride Cracks as Initiators for Stress Corrosion Cracking of Zircaloy.", Proc. 4th Int. Conf. on Zr in Nuclear Industry, Stratford upon Avon, ASTM-STP **681** (1979) 306-321.
- [I-29] COX, B., SURETTE, B.A., WOOD, J.C., J. Nuclear Mater. **138** (1986) 89-98.
- [I-30] KUBO, T., WAKASHIMA, Y., AMANO, K., NAGAI, M., Effects of Crystallographic Orientation on Plastic Deformation, SCC Initiation in Zirconium Alloys, J. Nuclear Mater. **132** (1985) 1-9.

- [I-31] JACQUES, P., LEFEBVRE, F., LEMAIGNAN, C., J. Nuclear Mater. **264** (1999) 239-256
- [I-32] SCHUSTER, I., LEMAIGNAN, C.5 JOSEPH, J., Testing, Modelling the Influence of Irradiation on Iodine-Induced Stress Corrosion Cracking of Zircaloy-4, Nuclear Eng., Design **156** (1995) 343-349.
- [I-33] FREGONESE, M., LEFEBVRE, F., LEMAIGNAN, C., MAGNIN, T., Influence of Recoil-Implanted, Thermally Released Iodine on I-SCC of Zircaloy-4 in PCI Conditions: Chemical Aspects, J. Nuclear Mater. **265** (1999) 245-254.
- [I-34] SCHUSTER, I., LEMAIGNAN, C., Embrittlement Induced, by Fission Recoils, of the Inner Surface of PWR Fuel Cladding - A Simulation Using Heavy Ions, J. Nuclear Mater. **151** (1988) 108-111.
- [I-35] GLADKOV, V.P., et al, Iodine Diffusion in Alpha-Phase of Zr-1%Nb Alloy, Atomnaya Energiya **75** [2] (1993) 97-103.
- [I-36] HADDAD, R., DORADO, A.O., "Grain-to-Grain Study of the Mechanisms of Crack Propagation During Iodine Stress Corrosion Cracking of Zircaloy-4.", Proc. 10th Int. Symp. on Zirconium in Nuclear Industry, Baltimore, ASTM STP **1245** (1994) 559-575.
- [I-37] AITCHISON, I., COX, B., Corrosion **28** (1972) 83-87.
- [I-38] HWANG, S.K., HAN, H.T., "Anisotropic Surface Energy Reduction of Zr by Chemisorption", J. Nuclear Mater. **161** (1989) 175-181.
- [I-39] COX, B., "Environmentally Induced Cracking of Zirconium Alloys - A Review", J. Nuclear Mater. **170** (1990) 1-23.
- [I-40] KNORR, D., PELLOUX, R.M., Effect of Texture, Microstructure on The Propagation of Iodine Stress Corrosion Cracks in Zircaloy, Metal. Trans. A **13** (1982) 73-83.
- [I-41] SCHUSTER, I., LEMAIGNAN, C., "Influence of Texture on Iodine-Induced Stress Corrosion Cracking of Zircaloy-4 Tubes", J. Nuclear Mater. **189** (1992) 157-166.
- [I-42] BRUNISHOLZ, L., LEMAIGNAN, C., "Iodine Induced Stress Corrosion Cracking of Zircaloy Fuel Cladding: Initiation, Growth", Proc. 7th Int. Symp. On Zr in Nuclear Industry, Strasbourg, ASTM STP **939** (1987) 700-716.
- [I-43] SCHUSTER, I., LEMAIGNAN, C., "Link Between Stress Corrosion, Corrosion-Fatigue Behaviour of Zircaloy in an Iodine Environment", Proc. 8th Int. Symp. on Zirconium in the Nuclear Industry (1989) 535-547.
- [I-44] MATTAS, R.F., YAGGEE, F.L., NEILNARK, L.A., "Effect of Zirconium Oxide on the Stress Corrosion Susceptibility of Irradiated Zircaloy Cladding", Proc. 5th Int. Symp. on Zirconium in the Nuclear Industry, Boston, ASTM STP **754** (1982) 158-170.
- [I-45] NELSON, H.G., WACHOB, H., Proceedings of Conf. on the Environment Sensitive Fracture of Engineering Materials, Chicago, AIMMPE, Warrendale, PA (1977) pp314.
- [I-46] SCHUSTER, I., LEMAIGNAN, C., JOSEPH J., "Influence of Irradiation on Iodine Induced Stress Corrosion Cracking Behaviour of Zircaloy-4.", Proceedings of SMIRT-12 (1993) 45-50.

**ANNEX II PROCEEDINGS OF THE TECHNICAL MEETING HELD IN AIX-EN-PROVENCE,
FRANCE, FROM 8TH TO 11TH OF OCTOBER 2019**

IMPLEMENTATION OF PCI/SCC IN CORE DESIGN AND OPERATION (Session I)

Impact of PCI/SCC on Reactor Core Design and Safety Evaluation	53
<i>J. Zhang</i>	
PCI Methodology to Evaluate PWR Flexible Operation	68
<i>R. Matias, N. Doncel</i>	
Framatome's PCI Methodologies for PWR Enhanced Plant Maneuverability	75
<i>L. Daniel, C. Royere, G. Andre-Poyaud, K-D. Schuh, A. Sautereau, T. Paul</i>	
PCI/SCC Loads in BWR and PWR: German Operating Conditions and Experience.....	87
<i>M. Sperlich, F. Frömel, K-D. Schuh, T. Salnikova</i>	
Safety Requirements For Pellet-Clad Interaction In France – New Approach Developed By EDF	103
<i>A. Bernard, J. Zeghdoui, L. Barbié, T. Keith, M. Rautenberg, N. Waeckel</i>	
Flexible Operation for Full Service to the Grid: Feedback from EDF Experience	114
<i>P. Paulin</i>	
Review of International Power Ramp Programs as a Basis for BWR Operating Guidelines.....	129
<i>V.I. Arimescu</i>	
Nuclear Fuel Operational Experience at Kozloduy NPP	136
<i>D. Hristov, K. Kamenov</i>	
Thermo-Mechanical Analysis of FBR Fuel Pin Behaviour	149
<i>A.K. Deo, A.J. Gaikwad, S.C. Ravichandar</i>	

UNDERSTANDING PCI/SCC MECHANISMS (Session II)

Fracture Mechanics I-SCC Testing and Review of Out-Reactor PCI Behaviour	165
<i>S.M. Hanlon, M. Topping, M.R. Daymond, C. Gillen, P. Frankel</i>	
Experimental Characterization and Modelling of I-SCC of Zirconium Alloy in an Iodine Vapor Environment.....	178
<i>D. Le Boulch, M. Bono, E. Federici, N. Mozzani, L. Barbie, B. Baurens, V. Chabretou</i>	
Ramp Testing and Microstructural/Chemical Evolution of Advanced Pellet Nuclear Fuel Related to PCI	192
<i>D. Jädernäs, A. Puranen, J.Karlsso, J. Pakarinen</i>	
Hot Cell Setup for Pellet Cladding Interface Investigation.....	196
<i>F. Nindiyasari, M. Kolluri, S. Van Til, R. Hania, T. Bakker, A. de Jong</i>	
Damage to the Cladding of the Fuel Elements in the Water-Water Power Reactor under PCI/SCC.....	204
<i>V. Novikov</i>	

IMPROVING PCI/SCC MODELLING AND SIMULATION (Session III)

3D Modelling of PCI-SCC in ALCYONE Fuel Performance Code	213
<i>J. Sercombe, D. Le Boulch, P. Konarski, C. Riglet-Martial, J. Julien, C. Introini</i>	
Multi-Dimensional Creep Analysis Using the Novel OFFBEAT Fuel Performance Code	226
<i>A. Scolaro, C. Fiorina, I. Clifford, A. Pautz</i>	
Three-Dimensional PCI Modelling in DIONISIO 3.0	236
<i>E. Goldberg, A. Soba</i>	
Development and Assessment of the BISON Fuel Performance Code for PCMI and PCI Analysis	245
<i>G. Pastore, R.L. Williamson, B.W. Spencer, A. Casagrande, J.D.Hales, Y.R. Rashid, W. Liu</i>	

Simulating of the Fuel Rod Behaviour under Fast Power Ramp Conditions in START-3A Fuel Performance Code	256
<i>E.A. Avdonina, A.V. Krupkin, V.I. Kuznetsov, B.I. Nesterov, V.V. Novikov, A.I. Dolgov, A.G. Eshcherkin, A.L. Izhutov, V.A. Ovchinnikov</i>	
Recent Development of PCI Modelling at VTT	262
<i>J. Peltonen, H. Loukusa, V. Tulkki</i>	
PCMI Benchmarks and the NEA Framework for In-Pile Fuel and Material Testing	271
<i>D. Costa, J-F. Martin, M. Fleming, I. Hill, T. Ivanova</i>	

OPTIMIZING PCI/SCC DESIGN METHODOLOGY AND LICENSING (Session IV)

Regulatory Approaches to Justify the Strength and Operability of WWER Reactors Fuel Elements	281
<i>V.S. Rubtsov</i>	
Lessons Learned from Safety Analyses Including a Design Criterion for Cladding Hoop Stress	287
<i>K. Kulacsy</i>	
A PCI Margin Analysis Framework Based on Combined 1-D and 3-D Fuel Rod Modelling Method.....	291
<i>Y. Ding, X. Wei, L. Zhu</i>	
U-Gd Fuel Size Change Modelling in START-3A Fuel Performance Code	292
<i>P.G. Demyanov, V.V. Novikov, V.I. Kuznetsov, A.S. Eremenko, E.A. Zvir, V.A. Zhitelev, T. Tverberg</i>	

IMPLEMENTATION OF PCI/SCC IN CORE DESIGN AND OPERATION

(Session I)

Chairpersons

J. ZHANG

Belgium

E. FEDERICI

France

IMPACT OF PCI/SCC ON REACTOR CORE DESIGN AND SAFETY EVALUATION

J. ZHANG
Tractebel (ENGIE),
Brussels, Belgium
Email: jinzhao.zhang@tractebel.engie.com

Abstract

This review paper summarizes the perspectives of flexible power operations in Belgium, the pellet-clad interaction (PCI) assisted by stress corrosion cracking (SCC) phenomena and the previous international R&D activities, the PCI/SCC design bases and licensing requirements, the impacts of PCI/SCC on the reactor operation procedures/guidelines, reload core & fuel design and safety evaluation, as well as the expectations from this IAEA technical meeting on PCI/SCC.

1. INTRODUCTION

During plant operation or under Condition II transients, the fuel rod could be failed due to pellet-clad interaction (PCI) assisted by stress corrosion cracking (SCC) [1]. This PCI/SCC failure is a combination of complicated effect of high stresses in the cladding due to power ramps, aggressive fission product environment (e.g. iodine, cadmium, caesium), and locally highly strained or stressed regions at cladding defects [2]. It is different from the pellet-clad mechanical interaction (PCMI) failure due to power ramps and pellet cracks or missing pellet surfaces (MPS) [3, 4], or due to cladding embrittlement by in-reactor hydriding at high burnup levels under very rapid power transients (e.g. design base accidents such as reactivity initiated accidents or RIAs) [5].

The IAEA Safety Standard on the Design of the Reactor Core, SSG-52 recommends that “the design should prevent fuel failures due to PCMI and PCI/SCC in normal operation and anticipated operational occurrences” [6]. For this purpose, various PCI related design limits have been determined by the fuel vendors based on the ramp tests, various codes and methods have been developed for verification of the PCI margins (or evaluation of the PCI risks), appropriate operational limits have been determined and applied by the utilities on power changes and power ramp rates. It has been shown that the PCI/SCC failure risk has been effectively and significantly reduced by improvements in fuel design, manufacturing, core design and operation [7, 8].

In recent years, however, large scale deployment of intermittent renewable energy sources worldwide has introduced significant and irregular variations in the power supply, and it has become increasingly difficult to it manage electricity supply and demand. Therefore, as requested by the grid operators, the utilities have to operate some of their nuclear power plants (NPPs) in a flexible power operation (FPO) mode, such as daily load following, frequency control, extended power modulations (EPMs), or extended reduced power operation (ERPO) [9, 10]. The FPOs have significant impacts or constraints on the core operation and fuel performance, core design and safety evaluation process, mainly due to the PCI/SCC concerns [10]. For example, in Belgium, in order to ensure the reliability of the fuel during FPOs, the core design and safety evaluation process has been improved on the verification of the PCI/SCC aspects, either by verification of the Condition II transient power limit or by verification of specific PCI margin [11, 12].

This review paper summarizes the perspectives of FPOs in Belgium (§2), the PCI/SCC phenomena and the previous international R&D activities (§3), the PCI/SCC design bases and licensing requirements (§4), the impacts of PCI/SCC on the reactor operation procedures/guidelines, reload core design and safety evaluation (§5), as well as the expectations from this IAEA technical meeting (§6).

2. PERSPECTIVES OF FLEXIBLE POWER OPERATION IN BELGIUM

In Belgium, the nuclear power plants have been initially designed to operate at full power, as they were supposed at the construction time (1970s – 1980s) to provide a base load power capacity. However, they are capable of providing some flexible services to the grid [11].

The ideal FPO would be to adapt the power automatically to the grid demand. This operational mode, known as load following, has been implemented in France [14] and Germany [15] plants, but excluded explicitly in the original safety case and is therefore not considered as an FPO option for the Belgian NPPs [11].

The first FPO provided by the Belgian NPPs is the frequency control support [11]. The power plants will adapt their power output to stabilize the frequency of the grid. In most Belgian power plants this is performed by

derating the power plant to 97.5% RTP. This allows the power plant to increase the power to sustain the grid when the frequency becomes too low. For example, at Doel 4 and Tihange 3, an asymmetric system of frequency control has been installed. These plants operate at 100% RTP all the time and will decrease their electrical power when required by the grid. Therefore, they only provide FPO service in case the frequency of the grid becomes too high.

The feasibility of power modulations has been studied for the Belgian NPPs [11]. It was considered that power modulations would only be acceptable if they were controlled by the operators in the control room and well prepared. In this case the power change pattern (power level, duration and power ramps) is defined and fixed before performing the power change. This allows the operator to prepare and check the status of the plant before performing the power manoeuvre. A power modulation is requested by the grid dispatch at least 2 hours in advance and is manually executed by the NPP operator. The operator can decide not to perform the requested power modulation if, for example, this could have a negative impact on nuclear safety.

The first step was the application of limited modulations (< 6 per cycle). In this case the power would only be reduced up to 75% RTP and for a very limited time up to 6 hours. The frequency of occurrence was limited to only several times a year. However, this limited flexibility was considered insufficient to give an answer to the future needs of the grid. Therefore, extended power modulations (EMPs) have been proposed, as illustrated in Fig. 1.

The EMPs would request reducing the power from 100% RTP down to 75 or 50% RTP, maintaining at lower power up to 72 hours before reaching again full power and stabilizing full power for at least 72 hours before the next power modulation. The frequency of EMPs was limited to 30 times per fuel cycle (Belgian NPPs have cycle lengths of 12 and 18 months). To reduce the PCI risk, the power change rate is limited to lower than 1% RTP/min (rather than the commonly recommended rate of 5% RTP/min), and a power modulation will be allowed only when the nominal boron concentration of the cycle is well above 200 ppm and no leaking fuel rods have been identified in the core.

The extended reduced power operation (ERPO or ELPO) is defined as operation at a reduced power level P_0 less than or equal to maximum available power during the ‘natural’ cycle and the stretch-out (typically 20 – 85% RTP) during at least a continuous period of 72 hours. In Belgium, to prevent PCI problems and most particularly to cover unknown phenomena, the number of cumulative total days of ERPO (< 85% RTP) is limited to 4 weeks per cycle, stretch-out included. The operation in hot shutdown conditions is not considered as ERPO [13]. Specific justifications or demonstrations should be made if exceptionally longer ERPO (e.g. duration > 28 days) occur due to unavailable equipment or extreme climate, and in certain cases, a reconditioning at intermediate power level between P_0 and RTP may be needed.

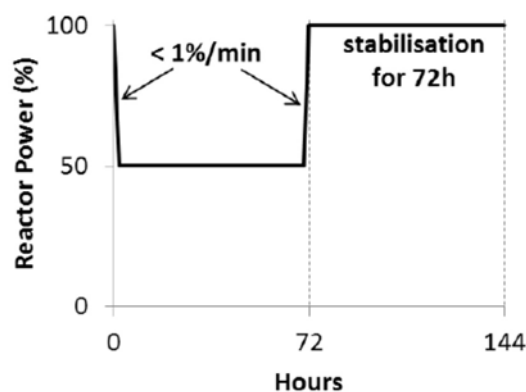


FIG.1. Extended power modulation (EPM) (reproduced courtesy of Flachet and Zhang, et al. [11]).

3. THE PCI/SCC PHENOMENA AND THE PREVIOUS INTERNATIONAL R&D ACTIVITIES

3.1. The PCI/SCC phenomena

The fuel loaded in an NPP has a circumferential gap between the surface of the fuel pellets and the inner surface of the cladding tube at cold state. On the first power increase following reactor start-up, this gap is gradually reduced due to the pellet thermal expansion and cladding creep. Due to the radial temperature gradient, the fuel pellets fragment into cracks, and the gap is further reduced as the pellet fragments relocate outwards radially. As

irradiation continues, cladding creeps down, the gap closes, and the pellet fragments move closer. This gap closure occurs roughly in the range of 10–20 GW·d/tU for most claddings. Any increase in power at any stage after the gap closure can lead to the expansion of the pellets due to thermal expansion and fission product swelling. The cladding expands outward due to elastic deformation and subsequently plastic strain and creep. This phenomenon is usually termed pellet-clad mechanical interaction (PCMI).

If the pellet temperature is sufficiently high, corrosive fission products (e.g. iodine) are released, brittle cracks may be initiated at the inner surface by irradiation-assisted stress corrosion cracking (SCC) if the cladding hoop stress becomes sufficiently large. If the large hoop stress is maintained, the PCI cracks would grow outwards and the cladding may eventually fail. This failure is usually referred to as PCI/SCC, or simply PCI [2].

It is thus clear that four conditions must occur simultaneously to induce a PCI failure (as shown in Fig. 2): a high tensile stress induced by the power ramp, aggressive fission products released if the fuel pellet temperature becomes large enough during the power ramp, the existence of a sensitive material with cracks, and a sufficient time for the cracks to develop.

During extended reduced power operation (ERPO), for example, the thermal contraction of the fuel pellets causes re-opening the pellet-cladding gap or the gaps between the pellet fragments after a power reduction. If the reduced power operation is maintained long enough, the fuel cladding will creep down and close the gaps again. The fuel element is then considered as re-conditioned at this lower power level. When the reactor core goes back to full power later on, tensile stresses will appear in the cladding. Those residual stresses will increase the susceptibility to PCI/SCC.

It is therefore important to understand the PCI/SCC mechanisms, to develop codes and method to assess the PCI/SCC risks, and to provide operating guidelines and improved fuel design to prevent the PCI/SCC risks.

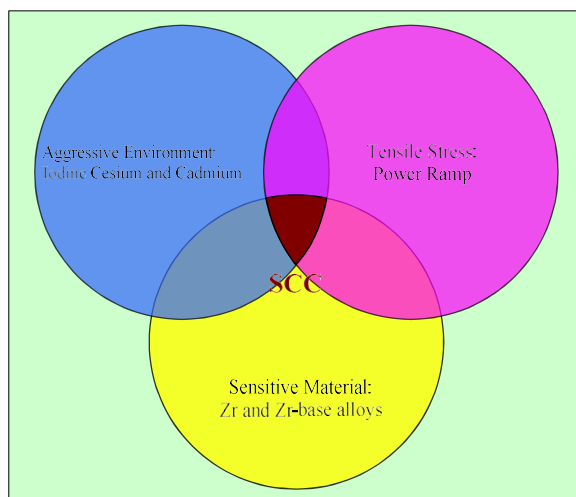


FIG.2. Schematic view of the sufficient conditions for PCI/SCC (reproduced courtesy of ANT International [2]).

3.2. Outcomes of the previous international R&D activities on PCI/SCC

A series of international specialist or technical meetings have been held by IAEA during late 1970s and 1980s on the PCI [16–18], power ramping, cycling and load following [19–21], followed by specific technical meetings during 1990s and 2000s on fuel behaviour testing and modelling [22,23], fuel chemistry and failures analyses [24–26], and advanced fuel design [27, 28].

It was concluded at the last IAEA Technical Committee Meeting in Lyon, France, on 18-21 May 1987 [21], that:

- “Experimental results obtained in research reactors and models based on them have demonstrated that power ramping, cycling and load following could be performed in power reactors under normal operating conditions”;
- “Over the last few years, a large number of such operations have been performed in commercial power plants so that at present extensive experience is available. It shows clearly that there is no adverse impact on fuel”;

- “The results yielded by high burnup programmes showed no negative consequence on pellet-clad interaction. This will have to be confirmed and further extended to the higher burn-ups that utilities are aiming for in the near future”;
- “However, some of the basic phenomena are not completely understood or linked and in order to get even more economical and flexible operating conditions, continuation of experimental work is felt to be necessary, especially on the items mentioned in the recommendations for each session”;
- “No other specific meeting on this subject is recommended in the future. The subject should be rather dealt with either in a future topical meeting on fuel behaviour or in a more general meeting which will cover both reactor system operation and fuel behaviour under cycling and ramping conditions”.

Recently, two international seminars on PCI have been held by OECD/NEA in 2004 [29] and 2016 [30]. The most recent OECD-NEA workshop in Lucca, Italy, 22–24 June 2016 [30] arrived at the following conclusions:

- “Liner fuel remains of interest to fuel designers”;
- “Texture controlled cladding shows improved resistance to (SCC-)PCI failure”;
- “Cladding design seems to be more effective than cladding material (alloy) with respect to the mitigation of the SCC driven by PC(M)I”;
- “Available experiments and analyses on pellet additive effects do not fully explain all aspects of the potential PCI benefits”;
- “There is some evidence that additives trap aggressive species in the fuel. However, it has been shown through multiple experimental programmes that very low concentrations of aggressive species are sufficient to drive PCI”;
- “The role of oxygen liberation seems important. There is some evidence that additives release oxygen to the gap and that this serves to oxidise and protect cladding ID cracks”;
- “The 1.5D (fuel rod) codes still form the basis of industrial applications as a result of run time constraints. Although 3D modelling is largely progressing to address specific phenomena that are mandatory for PCI, multi-scale modelling is not yet used as a predictive tool to evaluate the PCI failure risk”;
- “PCI risk prevention is efficiently integrated in operational rules based on mastered methodologies that include these 1.5D fuel-performance codes in combination with technological limits. However, although they have proven to be practicable for the design, evaluation methods remain complex and time consuming. Operators expressed their strong interest in simpler and faster PCI risk assessment tools”.

In summary, the outcomes of the extensive international R&D programmes on PCI since 1970s have led to the following achievements:

- An important PCI database has been established, including ramp tests, separate effects tests and plant data [31–35], to support both mechanistic and statistical data evaluations;
- Appropriate PCI operational limits or strategy on power changes and power ramp rates [36–39] have been determined and applied to maintain low probability of fuel cladding failures caused by PCI;
- Various empirical PCI design limits (technological limits or failure thresholds) [40–43], based on stress or strain energy density, have been determined based on simulation of the ramp tests with fuel rod codes;
- Various fuel rod codes and methods [40–49] have been developed for verification of the PCI design margins or assessment of the PCI risks;
- Alternative PCI remedy (or resistant) fuels, such as the liners or doped pellets [50, 51], have been developed (in particular for BWRs);
- Online PCI monitoring and surveillance systems [52, 53] has been developed and implemented in order to prevent the PCI failures.

As a consequence, the fuel failures due to PCI/SCC has been significantly reduced, in particular for PWR. Figure 3 shows PWR fuel failure causes worldwide in 1994 – 2006, and the percentage of fuel failures due to PCI/SCC is only 0.1% [7].

However, recent experience shows that PCI failure may be possible in PWR fuels with defects on the fuel pellet surfaces [3, 4], and that the percentage of fuel failures due to PCI/SCC for PWR has been increased to 5.7% for 2006-2010, as shown in Fig. 4 (left) [8]. This unconventional PCI failure is caused by the localized stress concentration at the location of a missing pellet surface (MPS). Fuel vendors have adapted the fuel specifications for the pellet manufacturing tolerances on the size and depth of the defects and applied more stringent fuel pellet

quality inspection procedures and/or devices. This has greatly reduced the fuel failure due to PCI/SCC in 2011 – 2015 (see Fig. 4 right) [8].

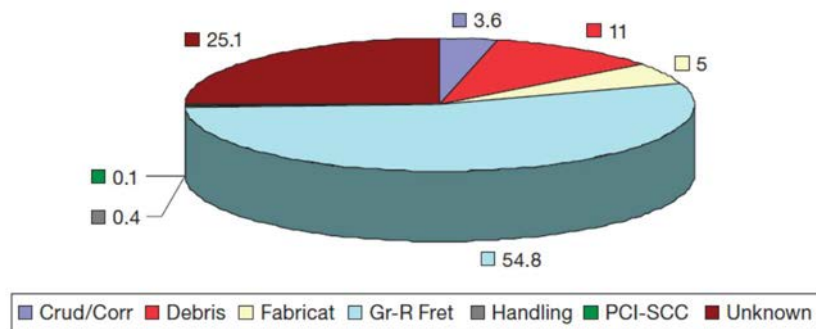


FIG. 3. PWR fuel failure causes worldwide in 1994–2006 (reproduced courtesy of the IAEA [7]).

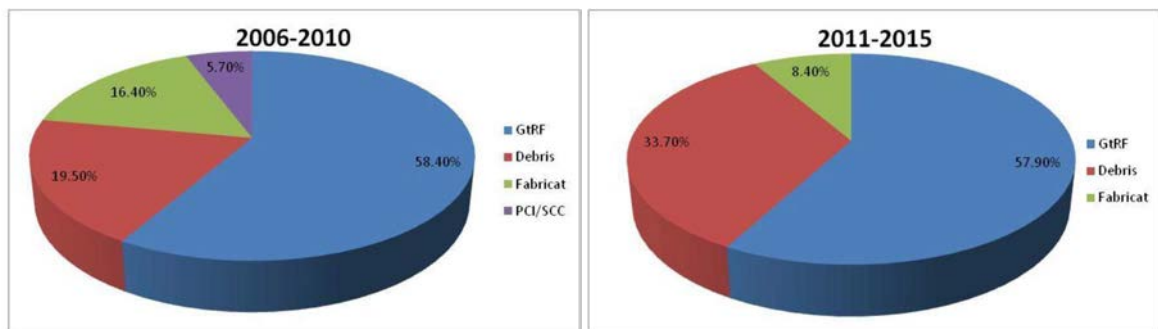


FIG.4. PWR fuel failure causes worldwide in 2006–2010 (left) and 2011–2015 (right) (reproduced courtesy of the IAEA [8]).

Note that the recent perspectives on FPOs attracted again the interests of international R&D activities in PCI [9, 10].

4. THE PCI DESIGN BASIS AND LICENSING REQUIREMENTS

Regarding to the PCI/SCC prevention in core and fuel design and operation, the recently revised IAEA safety standard SSG-52 on design of the reactor core [6] recommends that:

- (Para. 3.48) “Stress corrosion cracking induced by pellet–cladding interaction in the presence of corrosive fission products should be prevented”;
- (Para. 3.61) “The design should ensure that the likelihood of stress corrosion cracking in the fuel cladding is minimized in normal operation and anticipated operational occurrences”;
- (Para. 3.62) “Stress corrosion cracking of the fuel cladding should be prevented by implementing adequate design methods such as those given in the following examples:
 - Reduce tensile stresses in the fuel cladding by restricting rates of power change (allowing for the cladding stresses to relax) or by delaying the time at which the pellet–cladding gap closes (this can be achieved by increasing the initial fill gas pressure in the fuel rod or by optimizing the creep properties of the cladding),
 - Reduce the corrosive effects of the fission products (e.g. iodine, cadmium, caesium) generated by the pellet by using a liner (for boiling water reactors) or a graphite coating (for pressurized heavy water reactors) that is less susceptible to the corrosive effects on the inner surface of the cladding. This liner can also even out local stress concentrations in the cladding,

- Reduce the availability of corrosive fission products at the pellet–cladding interface by using additive fuels that are able to better retain the corrosive fission gas products within the fuel matrix,
 - Reduce local power peaking factors (and thus changes in local linear heat generation rates) through core design techniques”.
- (Para. 3.63) “The power-ramp failure threshold should be established, if applicable, in test reactors by means of power ramp tests for each type of fuel or cladding. The data collected should cover the entire burnup range”;
- (Para. 3.64) “Fuel performance analysis codes can be used to analyse and interpret the data from power-ramp tests and to determine a failure threshold. The parameter used to define this threshold is usually the maximum cladding stress, but the strain energy density can also be used. These same fuel performance analysis codes can be used to assess risk factors that cause this type of stress corrosion cracking of fuel rods in the reactor core and to define adequate guidelines to avoid it”;
- (Para. 3.153) “The reactor core analysis should verify that the core fuel loading pattern will meet fuel design limits for all applicable plant states”;
- (Para. 3.158) “The effects of operating conditions such as load following, power cycling, reactor startup and refuelling manoeuvring should, whenever specified, be superimposed onto the power level distributions and temperature histories to evaluate the potential effects of thermal cycling on fuel rod thermomechanical responses, such as the buildup of pressure due to fission gas release to the pellet–cladding gap and fuel cladding fatigue”.

However, PCI is not considered as a safety issue in all countries, and the requirements are quite different [55, 56]. Indeed, each NPP design and the OTS limits (particularly the primary coolant system I-131 concentration level) will allow plant operation with a limited number of fuel failures including PCI.

The current US NRC regulation does not put any specific requirements for fuel failures induced by PCI, but two design criteria under Anticipated Operational Occurrences (AOOs) or Condition II transients can be considered as relevant to PCI/PCMI failures [57]:

- The uniform strain (elastic and inelastic) in the cladding should be less than 1%;
- Fuel melting should be avoided.

It has been observed by some members of the advisory committee on reactor safeguards (ACRS) that although respecting this strain limit may preclude some PCI and PCMI failures, it will neither preclude the PCI/SCC failures that occur at low strains nor the highly localized strain-driven failures introduced by MPS on the outer fuel diameter. The ACRS members recommended that "reliance on the PCMI cladding strain criteria to protect fuel from PCI fuel from stress corrosion failures during AOOs should be discontinued. New criteria appropriate to the PCI stress corrosion mechanism should be developed based on peak nodal powers, hold times, and cladding strains that can be produced during AOOs."

However, the US NRC staff considers that PCI/SCC has low safety significance, and PCI/SCC failure has low probability of occurrence, because the magnitude and duration of the power excursion are limited: the maximum power level must remain below automatic trip set points, and the duration below timing for reasonable Operator response [60]. Later in 2014 [61], the US NRC staff screened Chapter 15 AOOs for PCI susceptibility and selected potential AOOs, considering the “limiting combination of initial conditions and assumptions to either delay or avoid reactor trip(s) or maximize the over-shoot of the trip setpoint (to maximize power).” The staff also provided FRAPCON-3.4 fuel performance analyses of the inadvertent opening of turbine admission valve transients. The staff asserted that 250 MPa represented a PCI threshold below which PCI failures would not occur on PWR fuel. This threshold was derived from the staff’s preliminary analysis of the SCIP data. The staff concluded that the “due to design features and operating restrictions, PWRs are not susceptible to PCI/SCC cladding failure during normal operation. This conclusion is backed by operating experience” [61].

Finally, the ACRS decided in 2013 that the PCI/SCC is not an immediate concern, and there is no need to require specific evaluation of PCI/SCC for PWRs during AOOs. Nevertheless, the US nuclear industry has taken initiatives to reduce the PCI risk by applying administrative measures according to PCI Operating and Manoeuvring Rules (PCIOMR) for BWRs, and enhancing the PCI risk assessment for PWRs, in order to improve the fuel reliability [47–49, 62].

In France, since the load follow operation was implemented in nearly all French NPPs in the 1980s, the French nuclear safety authority (ASN) requires EDF to demonstrate that PCI/SCC will not lead to fuel rod failures

even under condition II transients [56]. These requirements led to the definition of the so-called PCI technological limit based on the power ramp tests at different burnup levels, and the development of analytical PCI design verification methods based on detailed neutronic transient calculations and thermal mechanical calculations, in co-operation between EDF and the Fuel Vendors [45, 46].

In Germany, the recent revision of the safety standards KTA-3101.3 [63] requires that the loadings (i.e. increase in power output) resulting from nominal operation and AOOs shall be limited such that the tightness of the fuel rod is ensured, and the pertinent PCI criteria shall be derived using experimental results (e.g. ramp tests in test reactors and/or operational experience). The industry (e.g. former Siemens-KWU and Framatome) has developed PCI operating and manoeuvring rules for BWRs and PWRs [36–39] and implemented the automated PCI surveillance and protection system in PWRs, based on the maximum local LHGR for the core upper and the core lower half [52, 53].

Similar but less restricting requirements have been followed in other OECD countries like Finland, Sweden, Switzerland and the United Kingdom [56].

The Belgian reactor safety regulations followed generally the US NRC rules. However, during major plant modification projects (e.g. power uprate and steam generator replacement) or fuel design changes, the similar PCI technological limit and verification methodology by fuel vendors as in France and Germany (e.g. the former Siemens-KWU, AREVA, or Framatome) were accepted for applications to certain Belgian NPPs with their fuels [56], although the Belgian NPPs are not in load follow operation. On the contrary to France practice, there is no requirement to perform cycle specific PCI verification.

5. THE IMPACT OF PCI ON REACTOR OPERATION PROCEDURES/GUIDELINES

The following mitigation solutions are described in [7] to prevent PCI failures during plant operation:

- “Restricting flexible operation early in the fuel cycle until the fuel has been properly conditioned in accordance with fuel vendor guidance”;
- “Following periods of extended low power operations, ensuring proper fuel reconditioning during power ascension (e.g. accommodated power increase or power level holding periods). Fuel reconditioning promotes cladding stress relaxation and has been shown to improve PCI resistance”;
- “Plant manoeuvring guidelines, including power levels and ramp rate restrictions, have proven to be effective”;
- “In some cases, analytical models, based on stress modelling and validated against in-pile ramp tests, have been utilized to predict cladding stress (or strain energy density) prior to the planned power manoeuvring. The predicted stress/strain energy is then compared to an empirically based PCI failure threshold to assess the plant evolution in terms of PCI induced cladding failure risk, demonstrating that the planned plant evolution will not result in cladding failure”;
- “Plant TSs may need to be updated to reflect the established fuel conditioning guidelines or safety limits to prevent PCI induced cladding failure (e.g. power ramp limitations or analytical limits on cladding stress) and to include power manoeuvring during flexible operation, which becomes a normal plant transient. In particular, during periods of extended low power operations, it is possible to decondition fuel that has previously been conditioned, thus leading to restrictions for flexible operating and manoeuvring conditions”;
- “Cyclic LHGR variations below the conditioned LHGR profile must not lead to cladding strain or PCI failures. A transient overshoot beyond the conditioned LHGR can potentially lead to transient fission gas release and additional cladding stress due to PCI. It is therefore sufficient to restrict the transient overshoot to a permissible limit”.

In order to improve nuclear fuel reliability, fuel vendors have introduced empirical fuel operational limits on power manoeuvring and rate of power ascension and provided operating guidelines to prevent PCI/SCC or PCMI.

Siemens KWU derived operational recommendations from extensive ramp experiments and plant operating experience [36]. Those recommendations have been widely adapted by other vendors and applied in most of the operating NPPs. They may need to be verified and validated for any particular fuel design and using updated data and tools.

In addition, a PCI surveillance and protection method for plant operation was proposed, based on the RSST (power Range, Step, Speed, and Time) approach by translating their critical values into maximum or acceptable values to prevent PCI failures, after consideration of adequate safety margins [37,52]. The PCI operating limits

similar to the above concepts have been implemented as automatic PCI surveillance and protection in the monitoring systems in Germany PWRs [39,53] and later on adapted for the French N4 plants and European PWR (EPR) (shown as the gliding PCI threshold methodology [45]).

In summary, the fuel operating guidelines/rules or automatic surveillance and protection systems, together with the fuel design improvements, have been beneficial for mitigating the PCI/SCC failures in both BWRs and PWRs. However, they also bring negative impacts on the NPP operational performance by restrictions on the maximum power, power ramp rates, operation time and burnup [54]. It should be also noted that the above measures may not preclude the PCI failures for other fuel designs.

6. THE PCI IMPACT ON REACTOR CORE & FUEL DESIGN AND SAFETY EVALUATION

In response to the regulatory and operational excellence requirements, the industry has addressed PCI/PCMI through improvements in core and fuel design, manufacturing, and operation. Fuel design approaches to prevent failures due to PCI have focused on both pellet and cladding. Modifications to both the pellet and the cladding design, tighten the fuel pellet quality inspection, as well as improving core design and operating have proven effective at reducing PCI risks.

In Belgium, the PCI/PCMI aspect is treated for the reference safety analysis during major plant modifications, or the reload fuel compatibility and safety evaluation during the introduction of new fuel design [13].

In order to prevent any PCMI problems with the fuel, the linear heat generation rate (LHGR) in Condition II conditions has been limited [13]. The calculated Condition II transient power level must remain below the level which results in predicted fuel failure calculated using conservative analytical models along with conservative assumptions and initial conditions. This is ensured by preventing fuel centre melting and hence fuel expansion during the phase change which might rupture the fuel cladding. To preclude centre melting, a lower centreline fuel melting temperature limit has to be considered. This fuel melting temperature reduction takes into account the decrease of the melting temperature with the exposure, the fabrication tolerances, the model uncertainties, and an additional safety margin has to be applied on this value. This safety margin applied to the peak linear power used for the overpower protection system setpoints provides provision to avoid fuel rod damage (due to excessive clad stress, clad strain, internal pressure...) occurring at linear powers lower than the limit. The Condition II transient rod power limit is obtained by scaling upwards the Condition I rod bounding power history (BPH) limit so that by meeting the BPH the transient rod power limit is also assured to be met. A verification is performed for each reload cycle to confirm that the Condition I rod bounding power history limit is indeed met for all fuel rods in the core and thus indirectly the transient rod power limit is also confirmed to be met.

In addition, for certain plants with Framatome fuels, the Belgian TSO accepted generic design verification of a PCI failure criterion, using a qualified fuel rod code based on the PCI technological limit and considering Condition II transients based on a reference equilibrium cycle. The currently accepted PCI/SCC limits are either based on a critical Hoop stress limit (the formerly Siemens-KWU approach for improved Zr-4 cladding) or a critical strain energy density limit (CSED, the formerly AREVA or Framatome approach for M5 cladding). The method for the assessment of the PCI margins for the reference equilibrium cycle should be established in the fuel rod design methodology report, which should be licensed before applications. One example of such approved methodology is the Framatome's "allowable power methodology" [45], as illustrated in Fig. 5. The methodology has been first developed for Doel 3, and then applied to other NPPs with Framatome fuels.

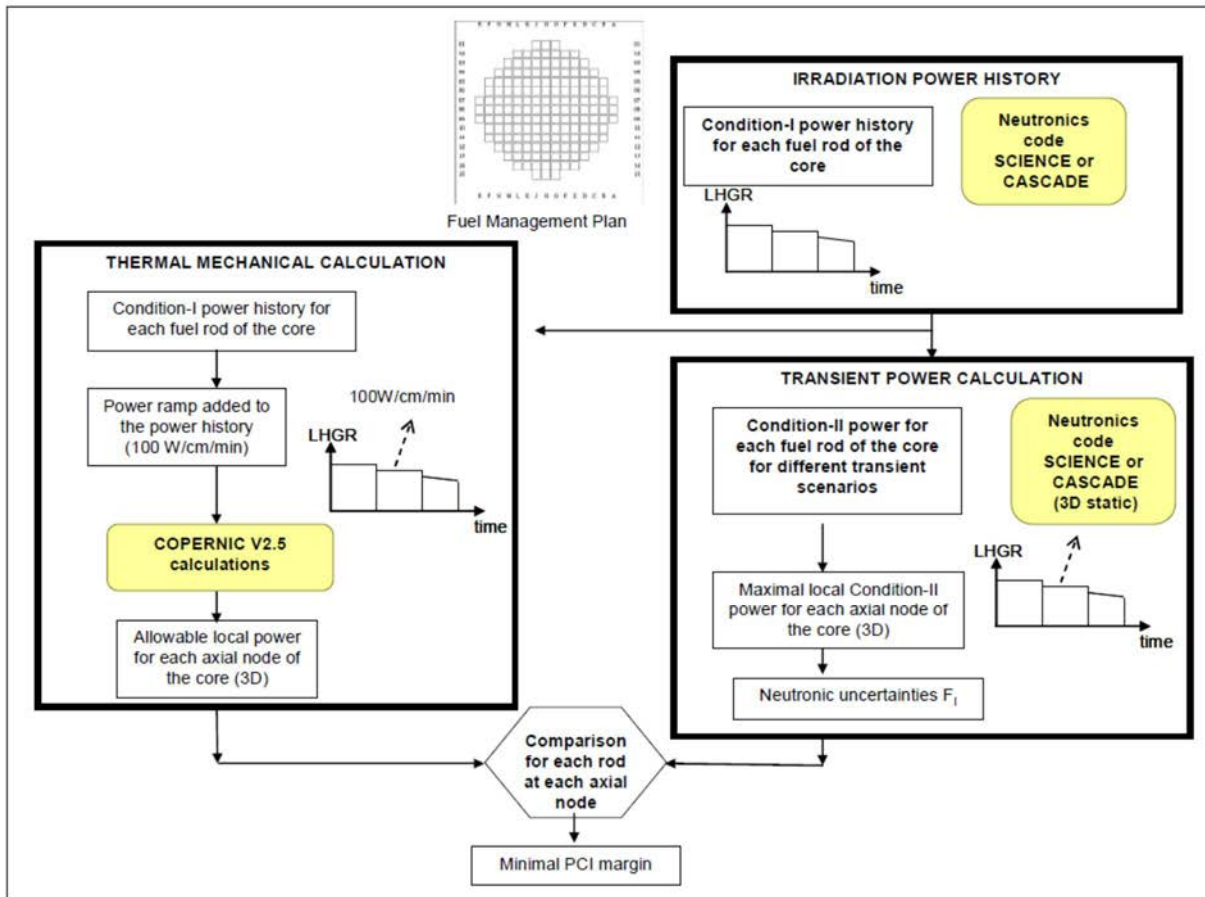


FIG.5. Schematic view of the Framatome's allowable power methodology (reproduced courtesy of Daniel and Andre-Poyaud, et al. [45]).

The essential principle of the 'allowable power' methodology consists in quantifying the PCI margins by comparing limiting Condition II transient power distributions (from the transient neutronic calculation) with the allowable LHGR for each axial node of the core (from the decoupled thermal mechanical calculation). Bounding assumptions for the transient boundary conditions and power ramp simulations induce a greater degree of conservatism, and the 3D calculations for different Condition II transient scenarios lead to considerable computational effort. This methodology has been applied for fuel rod design for each new fuel product to demonstrate an acceptably low risk of PCI failure. Indeed, the resulting PCI margins are rather large for the improved fuel products with M5 cladding. During the loading pattern verification, therefore, the PCI margins are only verified to ensure the fuel reliability.

In order to perform the extended power modulations (EPMs) in certain nuclear power units in Belgium without implementing hardware modifications, the impact on the fuel design has been verified by the Fuel Vendors. Post irradiation examinations revealed that no additional effect was observed on fission gas release or on changes in fuel microstructure due to power cycling and modulation conditions. In addition, operating experience showed that load following operation and power cycling does not have a significant impact on the fuel performance. Therefore, from the fuel rod design point of view, the related thermal-mechanical parameters are not impacted by EPMs. The limited impacts on the cladding stress and strain, or the PCI margins are quantified or verified by the Fuel Vendors.

For example, for the target plants with, the Fuel Vendor first verified that the nuclear design inputs to the fuel rod design reports are not affected by extended power modulations, with exception of the local power changes during Condition II overpower transients. Therefore, Condition II local power transient limits were regenerated conservatively as input for fuel rod thermal mechanical design verification. Using the licensed fuel rod design codes and methods, and the updated neutronic transient inputs, the impacted cladding stress and strain were shown

to remain within the design limits. For other target plants with Framatome fuels, the Fuel Vendor has quantified the impacts on the PCI margins, which are in general more than compensated by the available PCI margins for the reference equilibrium cycle. It is thus concluded that all existing fuels loaded in the Belgian plants allow up to 30 power modulations per fuel cycle [11].

The fuel design verification process for each loading pattern is adapted to cope with the requested plant operational flexibility like extended power modulations. Since the PCI margins in the reference fuel design verification based on an equilibrium cycle are significant with the improved fuel designs, a cycle specific PCI verification is not requested. Moreover, the impacts of the EPMs on the PCI margins remain limited [11], a simplified PCI verification is justified [12].

Therefore, a specific loading pattern PCI/PCMI risk assessment (LPPRA) tool has been developed and implemented it in the current core design and safety evaluation process [12]. The PCI/PCMI risk have been assessed in advance during the loading patterns design process based on the core neutronic calculation results using the Tractebel's LWP 3D code package. This assessment is based on the simple guidelines and correlations which are either provided directly by the Fuel Vendors or developed by Tractebel using the vendors' fuel design verification results. The PCI margin was defined as the difference between the predicted allowable power and the predicted maximum transient power:

$$PCI_{margin} = P_{all} - P_{tran} = k_1 f_1(P_{in}, BU) - [P_{in} + k_2 \cdot f_2(P_{in}, BU) + k_3] \quad (1)$$

where

$P_{all} = k_1 f_1(P_{in}, BU)$ = Maximal allowable rod power before clad failure during power ramp

$P_{tran} = P_{in} + \Delta P$ = Maximum transient rod power during power ramp due to Condition II transients

with

P_{in} = Transient initial rod power = Condition I conditioning rod power,

$\Delta P = P_{in} + k_2 \cdot f_2(P_{in}, BU) + k_3$ = Power variation during power ramp due to Condition II transients

BU = Rod burnup,

$f_1(P_{in}, BU)$ = correlation based on the fuel vendor's allowable power data,

$f_2(P_{in}, BU)$ = correlation based on the fuel vendor's maximum transient power data,

k_1, k_2, k_3 = calibration constants.

The LPPRA allows quick assessment of the PCI margin based on the Condition I conditioning rod power and rod burnup calculated for the specific loading pattern, without time consuming neutronic transient calculations and detailed fuel rod thermal mechanical calculations. To enhance the reliability of the assessment tool, the correlations are continuously calibrated and updated on the basis of the Fuel Vendors' cycle specific PCI verification results. In particular, the correlations has been adapted to cope with the requested plant operational flexibility like extended power modulations [12].

Finally, generic PCI margin assessment methodologies for justification of the exceptional extended reduced power operation (ERPO) [43, 45] have been developed, which required the approval of the Belgian TSO.

In France, load following mode was implemented in EDF's NPPs in 1980s. French Safety Authorities required to include PCI/SCC in the fuel core design analysis for both normal operations and AOOs conditions in 1984. Specific PCI design methodology was developed between 1984-1994, and the first complete PCI design analysis was implemented in 1994 [42, 46].

Currently, the PCI/SCC risk management for EDF's NPPs is based on three levels [42, 46, 54]:

- The surveillance system: determination of the surveillance (or alarms) set-points on the monitoring parameters (normal operation domain ($\Delta I, P$) and/or linear power margins, temperature regulation and power regulation banks positions), which are adapted to operation and compatible with PCI constraints;
- The protection system (scram or reactor trip): determination of the OPDT setpoints and/or rest functions or high linear power thresholds on the Digital Integrated Protection System (SPIN) to stop the transients before PCI cladding failure, in case of AOOs (Condition II transients);

- The Operational Technical Specifications (OTS): monitoring the PCI "credit" or K factor, based on the operating conditions (i.e. global core power profile versus time), to ensure that the current thermo-mechanical state of the fuel rods is compatible with safety analysis studies.

Specific PCI/SCC analyses were performed for each operating mode of the reactor, in order to determine the set-points/thresholds and/or reset functions. Two types of methodology were developed: a specific methodology called MIR (or RPM - Renovated PCI Method) based on 3D kinetics calculations and thermal-mechanical calculations, and a new static (PCI with variability) approach based on statics neutronics calculations and decoupled thermal-mechanics calculations. The former allows more realistically determine the set-points/thresholds and/or reset functions for the reference in-core fuel management and fuel design, while the latter allows quick verification of specific loading pattern [46].

7. CONCLUSIONS AND PERSPECTIVES

The PCI/SCC is a very complex multi-physics phenomenon, which has been extensively studied in previous international R&D projects during 1970s – 1980s. It was concluded that the knowledge was sufficient, and no more specific IAEA meetings on PCI/SCC were held after 1987. The R&D has continued since 1990s, but in a much slow pace. However, the recent trends in flexible power operations of the nuclear power plants attracted new interests of R&D in this field.

The recently revised IAEA safety standard SSG-52 on design of the reactor core recommended detailed measures regarding to the PCI/SCC prevention in core and fuel design and operation. However, the requirements on PCI/SCC are quite different in different countries.

The fuel operating guidelines/rules or automatic surveillance and protection, together with the fuel design improvements for BWRs (linear, fuel configuration) have satisfactorily resolved the PCI/SCC problem at the expense of restricted operational performance (i.e. maximum power, power ramping and burnup) that limit potential revenue in operation. However, the implementation of these measures does not preclude the reoccurrence of PCI failures following other design changes in the future.

The PCI/SCC failures for PWRs were rare, except for the significant increase of PCMI failures with defects on the surface of the fuel pellets (MPS) during 2006-2010, which were resolved by improved inspection of the fuel pellets during the PWR fuel manufacturing. It is expected that the implementation of the doped pellets would further improve the PCI design or operating margins.

PWR PCI fuel design verification methodologies have been developed by various fuel vendors and utilities, which were very complicated and time consuming for the verification. A balance is needed between more detailed analysis methods which lead to higher margins and calculation time, and simplified methods which are fast but lead to small margins.

There seem remain the following open questions:

- Is PCI-SCC a real issue if more realistic multi-physics and multi-scale approach can be used to simulate the neutronic transients and more mechanistic failure threshold can be established?
- Are there any simple and reliable engineering approaches to facilitate flexible core design and operation, while ensuring adequate design margins?

It is expected that this IAEA technical meeting will provide some answers to these questions. In particular, it is expected this IAEA technical meeting will adopt a top-down approach, that is, focus on the impacts on reactor operation (operating margins and constraints, procedures, best practice guidelines), the improvements in reload core and fuel design methodologies and the licensing process.

In particular, it is expected this IAEA technical meeting will lead to a state-of-the-art review of the existing knowledge/experiments on fuel behaviour during power modulations and/or load follows, covering the following subjects:

- Fission gas release during power transient / reduced power operation / power cycling.
- Clad strain during an irradiation sequence consisting of a power transient / reduced power operation / power cycling.
- The rate of fuel deconditioning / reconditioning as a function of prior conditioning time and power.
- Maximum time (or number of power cycling) at reduced low power (deconditioning) and minimum time at higher power (reconditioning).

- PCI/PCMI failure thresholds, impacts of cladding materials and operating histories.

It is also expected that a state-of-the-art review of the codes and methods development for PCI analysis during power modulations and/or load follows can be made, covering:

- Improvement of the mechanical models (relocation, gas swelling, creep, relaxation...)
- Development of 2D/3D modelling (FEA for cladding/pellet, modelling of bonding...)
- Definition of relevant parameter(s) to characterize the PCMI/PCI risk (global failure threshold): LHGR, stress, strain, SED, and/or any other damage parameter ...
- Practical method for power histories and condition II transient power generation
- Treatment of uncertainties

ACKNOWLEDGEMENT

The author is grateful to the IAEA for providing this opportunity as a consultant to make a review of the previous international R&D activities on PCI/SCC, in particular its impacts on the reactor core and fuel design, safety evaluation and operation.

REFERENCES

- [1] COX, B., Pellet-Clad Interaction (PCI) Failures of Zirconium Alloy Fuel Cladding – A Review, *Journal of Nuclear Materials* **172** (1990) 249–292.
- [2] ADAMSON, R. et al., Pellet-Cladding Interaction (PCI and PCMI), ZIRAT-11 Special Topic Report, ANT International, Sweden, October (2006).
- [3] POWERS, C. et al., “Hot Cell Examinations Results of Non-Classical PCI Failures”, Proceedings of the Water Reactor Fuel Performance Meeting, Kyoto, Japan (2005).
- [4] LEE, J.S. et al., “The Mechanical Behaviour of Pellet-Cladding with the Missing Chip under PCMI Loadings during Power Ramp”, Proceedings of the 2007 International LWR Fuel Performance Meeting, San Francisco, California, Paper 1022 (2007).
- [5] VITANZA, C., CONDE LOPEZ, J.M., “PCMI Implications for High Burn-Up Light Water Reactor Fuel in Reactivity-Initiated Accidents”, Paper presented in Pellet-clad Interaction in Water Reactor Fuels, Aix-en-Provence, France, 9-11 March 2004, NEA-6004, OECD/NEA (2005).
- [6] INTERNATIONAL ATOMIC ENERGY AGENCY, Design of the Reactor Core for Nuclear Power Plants, Safety Standards Series, Specific Safety Guide SSG-52, IAEA, Vienna (2019).
- [7] INTERNATIONAL ATOMIC ENERGY AGENCY, Review of Fuel Failures in Water Cooled Reactors, Nuclear Energy Series No. NF-T-2.1, IAEA, Vienna (2010).
- [8] INTERNATIONAL ATOMIC ENERGY AGENCY, Review of Fuel Failures in Water Cooled Reactors (2006–2015): An Update of IAEA Nuclear Energy Series No. NF-T-2.1, Nuclear Energy Series No. NF-T-2.5, IAEA, Vienna (2019).
- [9] ORGANIZATION FOR ECONOMIC CO-OPERATION AND DEVELOPMENT/NUCLEAR ENERGY AGENCY, Technical and Economic Aspects of Load-following with Nuclear Power Plants, OECD/NEA (2011).
- [10] INTERNATIONAL ATOMIC ENERGY AGENCY, Non-Base Load Operation in Nuclear Power Plants: Load Following and Frequency Control Modes of Flexible Operation, Nuclear Energy Series No. NP-T-3.23, IAEA, Vienna (2018).
- [11] FLACHET, F., ZHANG, J., VAN PARYS, R., VANTROYEN, D., SCHNEIDESCH, C.R., "Core and Fuel Feasibility Study for Improved Flexibility on the Belgian Nuclear Power Plants," Proceedings of WRFPM 2014, Paper No. 100136, Sendai, Japan (2014).
- [12] ZHANG, J., DETHIOUX, A., UMIDOVA, Z., DRIEU, T., SCHNEIDESCH, C., “Development and Applications of a Loading Pattern PCI Risk Assessment Tool for Flexible Core Design,” Pellet-Clad Interaction (PCI) in Water-Cooled Reactors: Paper presented at Workshop of NEA Working Group on Fuel Safety (WGFS), Lucca, Italy, 22-24 June 2016; NEA/CSNI/R(2018)9, OECD (2018).
- [13] HOLLASKY, N., “In-core Fuel Management in Belgium: Licensing Aspects”, Proc. Advances in Nuclear Fuel Management III (ANFM 2003), Hilton Head Island, South Carolina, USA (2003).
- [14] DUMONT, A., BOURNAY, P., “Load Follow and Frequency Control Operating Experience of FRAGEM A Fuel in EDF Reactors,” Proc. IAEA Technical Committee Meeting on Power Ramping, Cycling and Load Following Behaviour of Water Reactor Fuel, IAEA-TC-624/25, Lyon, France, 18-21 May 1987, IAEA, 1988.
- [15] LUDWIG, H. et al., Load Cycling Capabilities of German Nuclear Power Plants (NPP), *International Journal for Nuclear Power* **55** [8] (2010).
- [16] INTERNATIONAL ATOMIC ENERGY AGENCY, Specialists' Meeting on Pellet-Cladding Interaction in Water Reactors, Vienna, June 1977, IWGFPT, IAEA, Vienna (1979).

- [17] INTERNATIONAL ATOMIC ENERGY AGENCY, Specialists' Meeting on Pellet-Cladding Interaction in Water Reactors, Riso National Laboratory, Denmark, 22-26 September 1980, IWGFPT/8, IAEA, Vienna (1981).
- [18] INTERNATIONAL ATOMIC ENERGY AGENCY, Specialists' Meeting on Pellet-Cladding Interaction in Water Reactors, Seattle. USA. 3-5 October 1983, IWGFPT/18, IAEA, Vienna (1984).
- [19] INTERNATIONAL ATOMIC ENERGY AGENCY, Specialists' Meeting on Power Ramping and Power Cycling of Water Reactor Fuel and Its Significance to Fuel Behaviour, Arles, France, 14-18 May 1979, IWGFPT/5, IAEA, Vienna (1980).
- [20] INTERNATIONAL ATOMIC ENERGY AGENCY, Specialists' Meeting on Power Ramping and Power Cycling Of Water Reactor Fuel and Its Significance to Fuel Behaviour, JRC, Petten, 8-9 September 1982, IWGFPT/14, IAEA, Vienna (1983).
- [21] INTERNATIONAL ATOMIC ENERGY AGENCY, Technical Committee Meeting on Power Ramping, Cycling and Load Following Behaviour of Water Reactor Fuel, Lyon, France, 18-21 May 1987, IWGFPT/28, IAEA, Vienna (1988).
- [22] INTERNATIONAL ATOMIC ENERGY AGENCY, Water Reactor Fuel Element Computer Modelling in Steady State, Transient and Accident Conditions, Proceedings of A Technical Committee Meeting Organized by The International Atomic Energy Agency and Held in Preston. 18-22 September 1988, IWGFPT/32, IAEA, Vienna (1989).
- [23] INTERNATIONAL ATOMIC ENERGY AGENCY, Nuclear Fuel Behaviour Modelling at High Burnup and Its Experimental Support, Proceedings of a Technical Committee Meeting held in Windermere, United Kingdom, 19-23 June 2000, TECDOC-1233, IAEA, Vienna (2000).
- [24] INTERNATIONAL ATOMIC ENERGY AGENCY, Fuel Failure in Normal Operation of Water Reactors: Experience, Mechanisms and Management, Proceedings of a Technical Committee Meeting held in Dimitrovgrad, Russian Federation, 26-29 May 1992, TECDOC-709, IAEA, Vienna (1993).
- [25] INTERNATIONAL ATOMIC ENERGY AGENCY, Fuel Chemistry and Pellet Clad Interaction related to High Burnup Fuel, Proceedings of the technical committee, held in Nyköping, September 1998, TECDOC-1179, IAEA, Vienna (2000).
- [26] INTERNATIONAL ATOMIC ENERGY AGENCY, Fuel Failure in Water Reactors: Causes and Mitigation, Proceedings of a Technical Meeting held in Bratislava, Slovakia, 17-21 June 2002, TECDOC-1345, IAEA, Vienna (2003).
- [27] INTERNATIONAL ATOMIC ENERGY AGENCY, Advanced Fuel Pellet Materials and Designs for Water Cooled Reactors, Proceedings of a Technical Committee Meeting held in Brussels, 20-24 October 2003, TECDOC-1416, IAEA, Vienna (2003).
- [28] INTERNATIONAL ATOMIC ENERGY AGENCY, Advanced Fuel Pellet Materials and Designs for Water Cooled Reactors, Proceedings of a Technical Committee Meeting held in Villigen, 23–26 November 2009, TECDOC-1654, IAEA, Vienna (2010).
- [29] ORGANIZATION FOR ECONOMIC CO-OPERATION AND DEVELOPMENT/NUCLEAR ENERGY AGENCY, Pellet-Clad Interaction in Water Reactor Fuels, Seminar Proceedings, Aix-en-Provence, France, 9-11 March 2004, NEA-6004, OECD/NEA, Paris (2005).
- [30] ORGANIZATION FOR ECONOMIC CO-OPERATION AND DEVELOPMENT/NUCLEAR ENERGY AGENCY, Pellet-Clad Interaction (PCI) in Water-Cooled Reactors: Workshop Proceedings, NEA Working Group on Fuel Safety (WGFS), Lucca, Italy, 22-24 June 2016, NEA/CSNI/R(2018)9, OECD/NEA, Paris (2018).
- [31] VOGL, W., RUYTER, I., MARKGRAF, J., “The Petten Ramp Test Programme of Kraftwerk Union/Kernforschungsanlage (KWU/KFA) during the Years 1976 to 1981”, IAEA Specialists' Meeting on Power Ramping and Cycling Behaviour of Water Reactor Fuel, JRC, Petten, 8-9 September 1982, IWGFPT/14, IAEA, Vienna (1983).
- [32] MOGARD, H., KJAER-PEDERSEN, N., A Review of Studsvik's International Power Ramp Test Projects, STUDEVIK-8S/6, Studsvik Report, Sweden (1985).
- [33] TSUKUDA, Y., et al., “Performance of Advanced Fuel Materials for High Burnup”, Int. Conf. TopFuel, Würzburg, ENS (2003).
- [34] NONON Ch., et al, “Differential PCI Behaviour of PWR Fuel Rods Under Transient Conditions”, Proc Intl Meeting on LWR Fuel Performance, Orlando, FL, Sept 19-22, 2004.
- [35] KILLEEN, J., TURNBULL, J. A. et al, “Experimental Data on PCI and PCMI within the IFPE Database”, Seminar Proceedings on Pellet-clad Interaction in Water Reactor Fuels, Aix-en-Provence, France, 9-11 March 2004, NEA-6004, OECD/NEA, Paris (2005).
- [36] VON JAN, R., WUNDERLICH, F., HOLZER, R., “Power Ramping/Cycling Experience and Operational Recommendations in KWU Power Plants,” Specialists' Meeting on Power Ramping and Power Cycling Of Water Reactor Fuel and Its Significance to Fuel Behaviour, Arles, France, 14-18 May 1979, IWGFPT/5, IAEA, Vienna (1980).
- [37] VON JAN, R., HERING, W., “Experience and Plans with PCI Protection in KWU LWR Plants,” Specialists' Meeting on Pellet-Cladding Interaction in Water Reactors, Riso National Laboratory, Denmark, 22-26 September 1980, IWGFPT/8, IAEA, Vienna (1981).

- [38] VON JAN, R., WUNDERLICH, F., GARTNER, M., “Fuel Performance Aspects for Load Following Operation of Light Water Reactors,” *Kerntechnik*, **48**[3] (1986).
- [39] VON JAN, R., “Strategy and Experience of PCI Protection and Load Following Operation in KWU LWR Plant”, Proc. IAEA Tech. Comm. Mtg on Power Ramping, Cycling and Load Following Behaviour of Water Reactor Fuel, Lyon, 1987, IAEA-IWGFPT/28, IAEA, Vienna (1988).
- [40] SHEA, J.H., “The Development of an Empirical PCI Criterion for Siemens Fuel to be Loaded into Sizewell B”, Proceedings of a Technical Committee meeting on Nuclear Fuel Behaviour Modelling at High Burnup and Its Experimental Support, Windermere, United Kingdom, 19–23 June 2000, IAEA-TECDOC-1233, IAEA, Vienna (2000).
- [41] JULIEN B., et al., “Performance of Advanced Fuel Product under PCI Conditions”, Proc Intl Meeting on LWR Fuel Performance, Orlando FL (2004).
- [42] BÉGUIN, S., “PCI-Related Constraints on EDF PWRs and Associated Challenges”, Seminar Proceedings on Pellet-clad Interaction in Water Reactor Fuels, Aix-en-Provence, France, 9-11 March 2004, NEA-6004, OECD/NEA, Paris (2005).
- [43] DONCEL, N., MUÑOZ-REJA, C. “PCI Analysis during ERPO with Thermal-Mechanical TREQ Code”, Workshop Proceedings on Pellet-Clad Interaction (PCI) in Water-Cooled Reactors, Lucca, Italy, 22-24 June 2016, NEA/CSNI/R(2018)9, OECD/NEA, Paris (2018).
- [44] BILLAUX, M., “Modelling Pellet-Cladding Mechanical Interaction and Application to BWR Manoeuvring”, Proc Intl Meeting on LWR Fuel Performance, Orlando FL (2004).
- [45] DANIEL, L., ANDRE-POYAUD, G., SCHUH, K.D., SAUTEREAU, A., PAUL, T., ROYERE, C., “AREVA NP's PCI Methodologies for PWR Enhanced Plant Manoeuvrability”, Workshop Proceedings on Pellet-Clad Interaction (PCI) in Water-Cooled Reactors, Lucca, Italy, 22-24 June 2016, NEA/CSNI/R(2018)9, OECD/NEA, Paris (2018).
- [46] BARBIÉ, L., TKEITH, T., RAUTENBERG, M., WAECKEL, N., “Safety Requirements for Pellet-Clad Interaction in France – New approach Developed by EDF,” Workshop Proceedings on Pellet-Clad Interaction (PCI) in Water-Cooled Reactors, Lucca, Italy, 22-24 June 2016, NEA/CSNI/R(2018)9, OECD/NEA, Paris (2018).
- [47] ALESHIN, Y. et al., “The Effect of Pellet and Local Power Variations on PCI Margin,” Top Fuel 2010, Paper 041, Orlando, Florida (2010).
- [48] PARAMONOV, D., “PCI Risk Assessment Model”, Proceedings of the 18th International Conference on Nuclear Engineering (ICONE18), 17-21 May 2010, Xi'an, China, ASME (2010).
- [49] SELTBORG, P. et al., “Westinghouse’s PCI Methodology with Operating Guidelines Derived from Enhanced Statistical Treatment Of Power Ramp Tests,” Proceedings of Topfuel 2015 Conference, Zurich, Switzerland (2015).
- [50] DELAFOY, Ch., BLANPAIN, P., et al., “Advanced PWR Fuels for High Burnup Extension and PCI Constraint Elimination”, Proceedings of a Technical Committee Meeting on Advanced Fuel Pellet Materials and Designs for Water Cooled Reactors, Brussels, 20-24 October 2003, TECDOC-1416, IAEA, Vienna (2003).
- [51] BACKMAN, K., HALLSTADIUS, L., RÖNNBERG, G., “Westinghouse Advanced Doped Pellet - Characteristics and Irradiation Behaviour”, Proceedings of a Technical Committee Meeting on Advanced Fuel Pellet Materials and Designs for Water Cooled Reactors, Villigen, 23–26 November 2009, TECDOC-1654, IAEA, Vienna (2010).
- [52] VON JAN, R., HERING, W., “Practical Experience with PCI Protection in KWU LWR Plants”, Specialists' Meeting on Power Ramping and Power Cycling Of Water Reactor Fuel and Its Significance to Fuel Behaviour, Arles, France, 14-18 May 1979, IWGFPT/5, IAEA, Vienna (1980).
- [53] KUHN, A., KLAUS, P., Improving Automated Load Flexibility of Nuclear Power Plants with ALFC, *VDB Power Tech* **5** (2015).
- [54] PAULIN, Ph., “Operational Constraints Related to SCC-PCI,” Workshop Proceedings on Pellet-Clad Interaction (PCI) in Water-Cooled Reactors, Lucca, Italy, 22-24 June 2016, NEA/CSNI/R(2018)9, OECD/NEA, Paris (2018).
- [55] ORGANIZATION FOR ECONOMIC CO-OPERATION AND DEVELOPMENT/NUCLEAR ENERGY AGENCY, Nuclear Fuel Safety Criteria Technical Review, ISBN 978-92-64-99178-1, OECD/NEA, Paris (2012).
- [56] ORGANIZATION FOR ECONOMIC CO-OPERATION AND DEVELOPMENT/NUCLEAR ENERGY AGENCY, Fuel Safety Criteria in NEA Member Countries - Compilation of Responses Received from Member Countries, NEA/CSNI/R(2003)10, OECD/NEA, Paris (2003).
- [57] U.S. NUCLEAR REGULATORY COMMISSION, Fuel System Design, Standard Review Plan Section 4.2, NUREG-0800, Rev.2 (1981) & Rev.3 US NRC (2007).
- [58] ARMIJO J. S., ABDULLAHI, Z., “Pellet Cladding Interaction Fuel Failures during Anticipated Operational Occurrences in Boiling Water Reactors,” White Paper for US NRC, June 21, 2009.
- [59] ARMIJO J. S., ABDULLAHI, Z., “Pellet Cladding Interaction Fuel Failures during Anticipated Operational Occurrences in Pressurized Water Reactors,” White Paper for US NRC, Feb. 28, 2014.
- [60] U.S. NUCLEAR REGULATORY COMMISSION, Official Transcript of Proceedings of ACRS Materials, Metallurgy and Reactor Fuels Subcommittee Meeting, March 3, 2009.
- [61] U.S. NUCLEAR REGULATORY COMMISSION, Official Transcript of Proceedings of ACRS Materials, Metallurgy and Reactor Fuels Subcommittee Meeting, June 17, 2013 (Adams access number ML13182A649).

- [62] DAUM, R., PYTEL, M., YAGNIK, S., "Guidance and Risk Assessment for Mitigating Duty-related Fuel Failures", Workshop Proceedings on Pellet-Clad Interaction (PCI) in Water-Cooled Reactors, Lucca, Italy, 22-24 June 2016, NEA/CSNI/R(2018)9, OECD/NEA, Paris (2018).
- [63] KTA, Design of Reactor Cores of Pressurized Water and Boiling Water Reactors; Part 3: Mechanical and Thermal Design, Safety Standards of the Nuclear Safety Standards Commission (KTA), 3101.3 (2015-11), 2015.
- [64] POTTS, G.A., PROEBSTLE, R.A., "Recent GE BWR Fuel Experience", Proc. Int. Top. Mtg on Light Water Reactor Fuel Performance, West Palm Beach, 1994, ANS, LaGrange Park, IL (1994).
- [65] MOON, H., "Advanced Core Design Using MICROBURN-B2 BWR Core Simulator, Proc. Am. Nucl. Soc. Topl. Mtg on Advances in Nuclear Fuel Management II, 1997, Myrtle Beach, South Carolina (1997).
- [66] ALAPOUR, A., et al., "Robust PCI Monitoring During PWR Operation at Southern Nuclear," Proceedings of 2010 LWR Fuel Performance/TopFuel/WRFPM, Orlando, Florida (2010).
- [67] KIM, Y-D. "PCI Analysis a Vendor recommended fuel Preconditioning Guideline for PWR Fuel Rods in Korea", Paper presented at 2013 LWR Fuel Performance Meeting, 15-19 September 2013.

PCI METHODOLOGY TO EVALUATE PWR FLEXIBLE OPERATION

R. MATÍAS, N. DONCEL

Fuel Technology - ENUSA Industrias Avanzadas SA, SME,

Madrid, Spain

Email: rdm@enusa.es

Abstract

Flexible operation (i.e. operation at reduced power, load following or frequency control) is a need for nuclear power plants to adapt competitively to the new demands of the electrical system, mainly due to the growing importance of renewable energy. Flexible operation affects the design of the fuel rod with many factors, among which are the changes in the distribution of linear power density, the primary water chemistry programme or a possible increase in the time that the fuel stay in the core. Therefore, the development of methodologies capable of studying the effects associated with this form of operation is required. ENUSA has studied the effects of operational flexibility in the design of the fuel rod and has developed a methodology to study the risk of PCI (pellet-cladding interaction) focused on the extended reduced power operation (ERPO). The methodology is based on an effective stress threshold, called 'PCI technological limit', to discriminate between failed and intact fuel rods. For the determination of this limit, power ramp tests conducted on 17x17 PWR fuel rods, where pellets with confirmed quality are loaded in the advanced materials cladding, have been analyzed using a thermal mechanical fuel performance analysis code (TREQ). For each ramp test, the cladding stress is calculated, and the 'PCI technological limit' is defined as the minimum stress below which no PCI failures exist. The available PCI design margin is determined between baseload operation maximum stress during the Condition II transient and the 'PCI technological limit'. To evaluate the effect of an ERPO, a margin loss related to the stress increase due to ERPO conditions is calculated. A wide set of constant power histories (conditioning powers), covering the thermal mechanical state of the rods in the core, is simulated with TREQ code. The goal is obtaining the peak effective stress during the Condition II transient event after an ERPO. The comparison between the design margin and the margin loss is analyzed for each constant power history for the critical burnup range of a PCI failure. If margin loss is higher than the available margin, the duration of the ERPO is not acceptable. ENUSA has developed this methodology to study the allowable ERPO duration which is both robust and reliable without requiring large time-consuming calculations.

1. INTRODUCTION

Electrical power systems require a perfect coordination between generation and demand, which implies that electricity generation by each of the power suppliers needs to be managed to match electrical demand. Due to the significant growth of renewable energy, there is an increasing need in the nuclear power plants to improve the plant manoeuvrability to follow the variable demand of the grid applying load follow operations [1] as the extended reduced power operation (ERPO) in which the plant operates below nominal power for a prolonged period of time. This operation flexibility implies power variations that can impose high stresses in nuclear fuel cladding.

At the beginning of the operation, the cladding is in a uniform compressive stress state until the gap between with the pellet and the cladding is closed. When the gap closure occurs, the contact pressure between the pellet and the cladding causes the cladding to go from compressive stress to increasing tensile stress until a balance between cladding creep and fuel expansion due to swelling is reached. In this situation, local power increases can impose additional tensile stress that can induce pellet-cladding interaction (PCI) if the pellet-cladding gap is small or it is closed and there is fission products such as iodine acting as an aggressive environment during the power ramp along with a sensitive material.

PCI failures are more frequent in boiling water reactors (BWRs) since power changes are more usually controlled by control rods movements in this type of reactors. In pressurized water reactors (PWRs), boron concentration is decreasing throughout the cycle to compensate reactivity reduction due to burnup. This causes the number of power ramps during operation and PCI failures less common than in BWRs less. However, depending on the gap pellet-cladding state there are reactor power increases such as a Condition II transient event (anticipated operational occurrence) which could cause PCI failures on a PWR, although it is not clear all the dependences [2].

During an ERPO event, the return to full power after having operated at reduced power is especially critical due to the state of the pellet-cladding gap at that moment. ENUSA has developed a specific methodology to evaluate the PCI risk under ERPO conditions in order to provide margins for flexible operation [4].

2. METHODOLOGY FOR PCI ANALYSIS DURING ERPO

A yield stress-based criterion is used to prevent PCI failures for the operational states including normal operations and transient II conditions. Additionally, restrictions on the rate of power increase are also imposed to power manoeuvres after refuelling or prolonged periods at reduced power. These limitations were successful in preventing PCI cladding failures. Nevertheless, some experiences confirmed that cladding failure occurred in some high energy cores caused by increased local hoop stress (due to pellet cracks or imperfections) in combination with a critical fission product concentration.

Although fuel vendors incorporated improved manufacturing process to reduce the incidence of pellet defects and cladding has evolved to materials with a higher capacity of stress relaxation, there is a trend in the industry toward the use of additional experimental limits based on the behaviour of commercially irradiated rods subjected, later on, to power ramp tests. The use of this kind of limits constitutes an additional barrier to PCI failures, especially in non-base operating conditions as returns to power after long periods at reduced power, load follows or power modulations. This kind of limits is especially useful to ensure fuel integrity during flexible operation [2].

Following this trend, ENUSA has developed a methodology for the calculation of PCI in ERPO conditions consisting of comparing the maximum Von Mises stress that the cladding can reach during an ERPO operation with the limit stress obtained from the power ramp tests. In this way, the risk to PCI can be assessed or the maximum number of days allowed to operate at reduced power can be calculated (Fig.1).

TREQ code has been used for the simulations. TREQ is a fuel performance analysis code used for the design of fuel rods for PWR reactor and to provide input for other codes used in the accident analyses [3]. TREQ code is used to calculate fuel rods thermal-mechanical behaviour under normal operating conditions including transient events. The code resolves thermal-mechanical and fission gas models that are developed based on theoretical models and experimental or in-pile data for Zirconium alloy cladding rods with uranium and gadolinia doped pellets. TREQ compromises between computationally intensive microscopic modelling and practical engineering correlation approach, so it does not require large computational times.

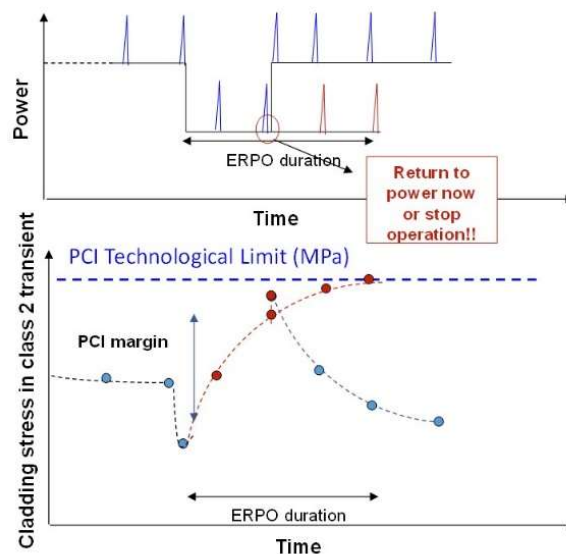


FIG.1. Evolution of cladding stress after Condition II transients during ERPO.

2.1. PCI technological limit

'PCI technological limit' (TL) is defined as the equivalent stress value calculated in the cladding below which there is not any rod failure due to PCI mechanism. It is calculated simulating power ramp tests (PRT) performed in experimental reactors using TREQ code.

ENUSA and Spanish nuclear industries has been engaged since the 1990s in several irradiation and PIE programmes [5, 6] to get a critical size database on ramp test. These efforts have produced large amount of valuable information on in-reactor performance of fuel materials representing current and potential future fuel designs. Among these programmes, the Segmented Fuel Rod Program (SFRP) conducted in a Spanish PWR 3 loop plant

has been the main data contributor to the final database on ramp tests. The SFRP comprised the design and manufacturing of specific rods composed by seven shorter (segmented) rods welded together for operation. These segmented rods were later on separated in the hot cells for characterization and ramp testing. The main aspect of this project is that these rodlets did not need to be re-fabricated before they were ramped in R2 Studsvik reactor. Therefore, internal pressure and fission gas composition remained as in the final base irradiation state.

For the development of the PCI TL, a number of the PRT from about 40 rodlets of the available database have been selected. These rodlets have different characteristics: cladding material, fuel pellet grain sizes, power irradiation history in the reactor (rod average power and burnup). The PRT have also some differences on its definition in terms of terminal power, ramp rate or ΔP . The main features of a Power Ramp Test are shown in Fig. 2:

- Rod tested is conditioned to the power in which this rod operated in its last.
- Then, a power ramp is applied to the rod. Power ramp rates and end powers pretend to simulate Condition II transient events.
- After the ramp, the power is maintained at the end power value for a while, to check if the rod fails or not.

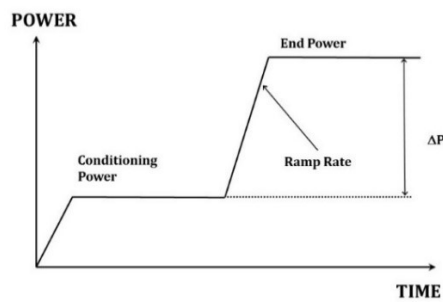


FIG. 2. Generic Ramp Test.

Figure 3 shows the data available for the calculation of this PCI (TL). As it can be observed, the number of non-failed rods is larger than the failed ones, but what is more important is that there is a non-negligible number of failed rods due to PCI phenomenon. These failed rods are the critical ones for the determination of a technological limit related to PCI.

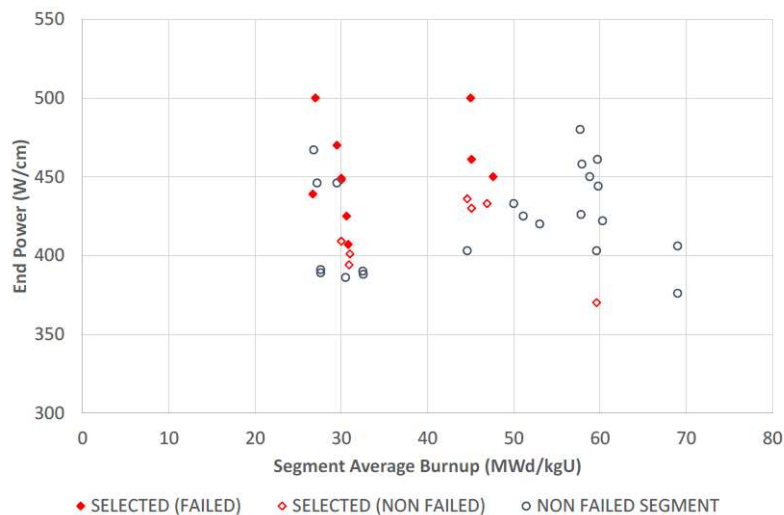


FIG.3. Ramp tests experiments since 1997.

From the total database, the following rods were selected for the determination of the PCI (TL):

- All failed rods (F);
- Non-failed rods (NF), with similar characteristics than failed rods in terms of terminal power and ΔP , were chosen to get quite similar results. This is the only way to determine a fine technological limit able to discern between failed and intact rods;
- Additional rods were also selected in order to define a clear border between F and NF rods and to bound the operative burnup range.

Each one of the selected ramped rods have been simulated with TREQ code using the fuel rod as-built characterization information, the specific base irradiation conditions during in-reactor operation and, later on, the ramp test conducted in the Studsvik R2 experimental reactor. The maximum effective cladding stress value (Von Mises) predicted during the simulation is obtained for each of the selected rodlets. Finally, PCI TL is defined as the equivalent stress value below which there is not any rod failure due to PCI mechanism, as shown in Fig. 4.

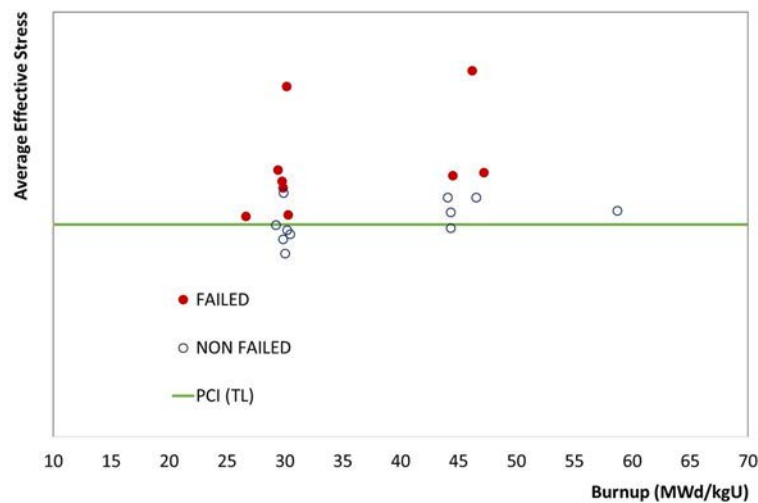


FIG. 4. PCI Technological limit with TREQ code.

2.2. Thermal-mechanical evaluation of ERPO

The methodology to evaluate the effect of an ERPO is based on calculate the margin loss on PCI risk related to the stress increase during the operation at reduced power (Fig. 5).

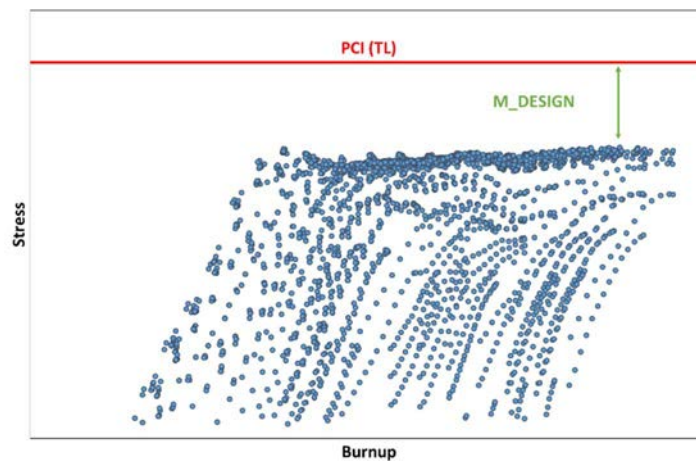


FIG. 5. PCI design margin definition.

Operation at reduced power with the control rods inserted an appropriate amount could affect the core characteristics, such as the power and burnup distributions and peaking factors. An evaluation was made of the impact of this operation on the nuclear inputs used in TREQ for the fuel rod design (power burndown history limit,

fast fluence limits, axial power distributions, radial power profiles and transient rod power limits). ERPO periods were simulated at different moments of the cycle with a two-group 3D NEM-based neutron diffusion theory code. The results show that the core strategy is able to effectively control the core axial power distribution during the ERPO manoeuvre and following the return to full power and subsequent full power operation. The only significant nuclear parameter impacted immediately following return to full power is the planar radial peaking factor.

Therefore, the limited impact of the ERPO operation on the core axial and radial global and local power distributions it is judged that the nuclear inputs for fuel rod design remain valid for the evaluated ERPO. Only the Class II transient limits have to be recalculated due to the changes on the planar radial peaking factor.

Furthermore, the applicability of the thermal-mechanical and fission gas models to the conditions associated to the ERPO operation has been verified with test on commercial reactors or experimental reactors as Halden. No additional effects were observed on fission gas release or on changes in fuel microstructure due to this kind of operation.

The next step on the methodology is to determine the PCI margin on baseload operation for the current cycle. All rods on the core are evaluated with TREQ code to obtain the maximum effective stress at Condition II transient. This value is compared to the PCI TL to calculate the design margin. Figure 6 shows an example of this situation.

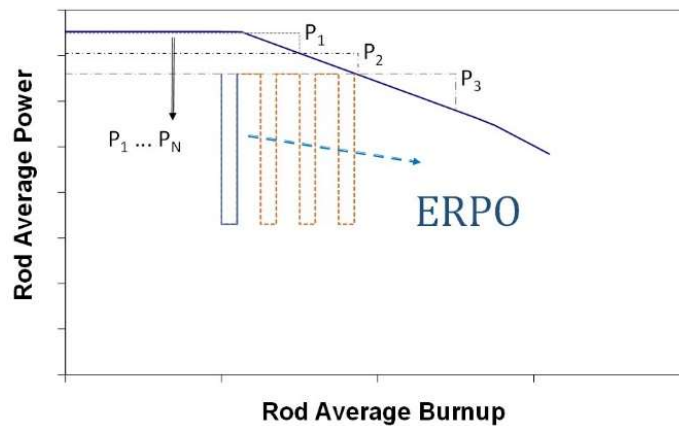


FIG. 6. Schematic ERPO simulation.

The thermal-mechanical evaluation of the ERPO operation is based on analytical cases aimed to capture the thermal-mechanical state of every rod in the core before the ERPO. Any possible power history in the core can be represented in a simplified way by its conditioning power, that consists on maintaining the rod average power constant for a sufficient period of time. This assumption allows to evaluate the ERPO regardless the instant where the ERPO begins by evaluating a broad variety of constant powers (P_1 to P_N) that cover all the real situations in the core. The selected burnup is typically within 20 to 50 MW·d/kgU average rod burnup that is the range where the pellet to cladding gap should be closed and where the PCI risk is greater. Figure 6 represents these powers.

For all these powers (P_1 to P_N), two different cases are studied (Fig. 7):

- ERPO case: Conditioning power up to the chosen burnup, instantaneous power decrease during the ERPO specified duration, instantaneous power increase up to the initial power and, finally, a Condition II transient event.
- BASE case: Constant power up to the rod average burnup when the ERPO ends and a Condition II transient event.

For both cases, the maximum effective stress reached during the Condition II transient is calculated and compare to the PCI TL:

$$M_{BASE} = \sigma_{PCI} (TL) - \sigma_{eff}$$

$$M_{ERPO} = \sigma_{PCI} (TL) - \sigma_{eff}$$

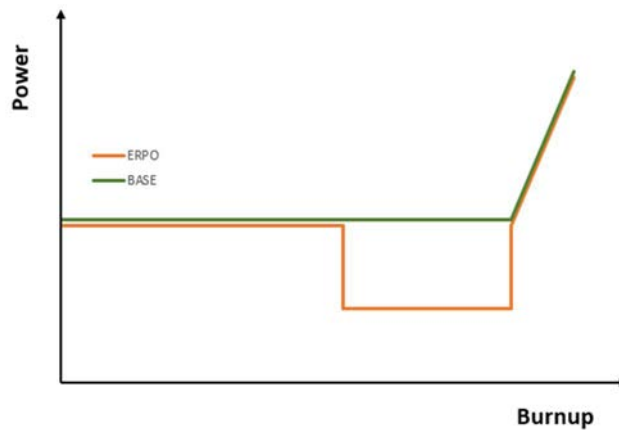


FIG. 7. Power scheme for BASE and ERPO cases.

The margin loss is defined as the difference between these two values and represents the increase of risk to have a PCI failure during an ERPO. Finally, margin available in an ERPO without PCI failure is calculated as the difference between the margin loss and the design margin. If the margin loss due to an ERPO event is lower than the design margin, the analyzed ERPO duration is acceptable, while if the margin loss is higher than the design margin, the analyzed ERPO duration is rejected and the process is repeated until an acceptable ERPO duration is found.

Figure 8 represents an analysis with a target ERPO duration (black lines) that exceed the design margin and a second ERPO duration (green lines) that do not exceed the limit and, therefore, is admissible.

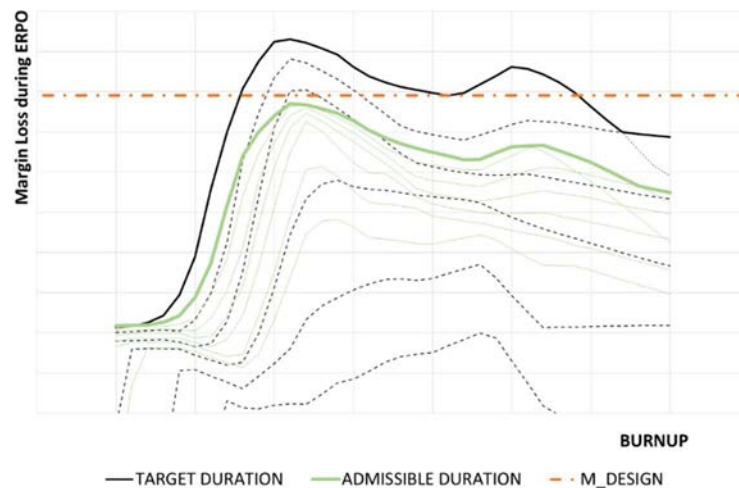


FIG. 8. PCI Margin Loss during ERPO.

3. CONCLUSIONS

The increasing importance of renewable energy on the grid is leading the nuclear power plants to operate in flexible modes to be able to follow the variable demand. Extended Reduced Power Operation may have implications for PCI margins for PWR, so the assessment of the risk of PCI failure is an important challenge to accommodate to this new situation in the electrical power system.

ENUSA has developed a technological limit based on experimental ramp tests database as well as an associated methodology to apply this limit to assess the PCI risk on an ERPO event. An ERPO event has been comprehensively modelled, including nuclear manoeuvre and thermal mechanical impact, showing reasonable results. This methodology is both robust and reliable without requiring large time-consuming calculations.

ACKNOWLEDGMENTS

The Segmented fuel rod program was cosponsored by ENUSA, ANAV, ENDESA and MHI. The demonstration case was performed in collaboration with Tractebel/Electrabel. The authors are grateful to these organizations for their cooperation.

REFERENCES

- [1] INTERNATIONAL ATOMIC ENERGY AGENCY, Non-baseload Operation in Nuclear Power Plants: Load Following and Frequency Control Modes of Flexible Operation, IAEA Nuclear Energy series NP-T-3.23, IAEA, Vienna (2018).
- [2] ALESHIN, Y. et al; "The Effect of Pellet and Local Power Variations on PCI Margin", Proceedings of Top Fuel, Orlando, Florida (2010).
- [3] PASTOR, I. et al.; "TREQ – Fuel Rod Performance Code for demanding PWR plants", Proceedings of the 17th International Conference on Nuclear Engineering ICONE17, Brussels, Belgium (2009).
- [4] DONCEL, N. et al., "PCI Methodology to Evaluate PWR Flexible Operation", Proceedings of WRFPM, September Korea (2017).
- [5] UCHIDA, H. et al., "Segmented Fuel Irradiation Program Investigation on Advanced Materials", Proceedings of TOPFUEL '99, Avignon, France (1999).
- [6] SERNA, J.J. et al; "Experimental observations on fuel pellet performance at high burnup", Proceedings of the 2005 Water Reactor Fuel Performance Meeting, Kyoto, Japan (2005).

FRAMATOME'S PCI METHODOLOGIES FOR PWR ENHANCED PLANT MANEUVERABILITY

L. DANIEL, G. ANDRE-POYAUD, A. SAUTEREAU
Framatome, Lyon – FRANCE
Email: lucile.daniel@framatome.com

Ch. ROYERE
Framatome, Paris La Défense – FRANCE

K.-D. SCHUH, T. PAUL
Framatome GmbH, Erlangen – GERMANY

Abstract

Enhanced plant manoeuvrability is being targeted by a growing number of PWR utilities. Such operating modes have an unfavourable impact on PCI margins and may require specific PCI-analyses. For that purpose, Framatome has developed a portfolio of innovative PCI methodologies with a bottom line based on thermal-mechanics computations during class-II transients. The margin to rod failure is given by the comparison of the cladding Strain Energy Density to a threshold previously assessed on representative experimental power ramp tests. Through its portfolio benefiting of the strong points of the MIR methodology and the alternative ‘allowable power methodology’, Framatome supports utilities for a more flexible nuclear energy production.

1. INTRODUCTION

Since the early stage of PWR development, pellet-to-clad Interaction (PCI) has been recognized as the critical failure mechanism of fuel rods. However, in the mid 1990s, new operating modes such as Load Follow were introduced in France for PWRs, providing an impulse for the development of advanced approaches [1] to replace the so called ‘(P,ΔP) guidelines’ which dealt with the fuel rod linear heat generation rate (LHGR) and its changes during a class-II transient.

Framatome has thus developed the MIR methodology in the early 2000s and the alternative “allowable power methodology” [2].

Nowadays, as the production of nuclear energy has to be more flexible, Framatome capitalizes on the strong points of both approaches to expand its PCI methodologies portfolio. Following the description of this portfolio, this paper describes how utilities benefit from Framatome support for enhanced flexibility purposes.

2. DESCRIPTION OF FRAMATOME'S PCI METHODOLOGIES

2.1. PCI phenomenology and associated thermal mechanical approach

During a class-II transient, the large increase of local power in the fuel induces substantial pellet expansion and stretching of the cladding. The cladding stresses are gradually relaxed by thermal creep. This mechanical loading takes place in presence of an aggressive chemical environment due to the fission products released by the fuel during the power transient (mainly iodine). The global mechanical-chemical phenomenon is referred to ‘pellet/cladding interaction assisted by stress corrosion cracking’ (PCI/SCC, named currently PCI). A comprehensive CEA-EDF-Framatome ramp test programme has been performed to determine a mechanical parameter discriminating failed and non-failed M5_{Framatome} rods [3]. This mechanical parameter is referred to as the strain energy density (SED) and is calculated with the COPERNIC code [4]. The boundary between failed and intact rods is referred as ‘critical strain energy density’ (CSED).

The SED is a combination of the strain and the stress in the cladding during the transient and it reflects the quantity of mechanical energy stored in the cladding per volume unit during a power transient:

$$SED = \int_A^B \sigma_{\theta\theta} d\varepsilon_{\theta\theta} \text{ (in MPa or J/cm}^3\text{) during the transient (from A to B)} \quad (1)$$

where:

$\sigma_{\theta\theta}$: tangential stress (clad inner skin),
 $\varepsilon_{\theta\theta}$: total tangential strain (clad inner skin).

In a PCI analysis, the transient evolution of the SED is computed with conservative assumptions and the SED is compared to the CSED to determine PCI margins. Values below the CSED ensure absence of failure risk.

PCI margins are strongly dependent on the thermal-mechanical state before the class-II transient: reduction of power as ELPO has a deleterious impact on the PCI behaviour, whereas the reconditioning at full power for a certain period of time allows to progressively recover the reference conditioned state thanks to stress relaxation.

2.2. Introduction of Framatome's PCI methodologies portfolio

Framatome's PCI methodologies for PWR reactors aim at excluding PCI induced rod failure during class-II transients. They are based on neutronic calculations and thermal-mechanical modelling and mainly differ on:

- The level of sophistication of the neutronic calculations,
- The way thermal-mechanics and neutronic calculations are linked.

The considered class-II transients are those that induce a local increase of LHGR resulting in PCI failure risk:

- Excessive load increase,
- Uncontrolled rod bank withdrawal at power,
- Rod drop,
- Uncontrolled boron dilution.

2.3. The MIR methodology

The MIR methodology ('Méthodologie IPG Rénovée' in French meaning 'upgraded PCI methodology') is the most accurate to estimate the PCI failure risk during class-II accidental transients and, for this reason, constitutes the reference one.

The first step consists in calculating the power evolution of each fuel rod of the core from its first irradiation up to the time of class-II transient occurrence with the 3D kinetic core neutronic code SMART of the SCIENCE code package [5, 6].

In a second step, class-II transients are simulated using coupled calculations between SMART and the system code MANTA modelling the nuclear steam supply system (NSSS) with I&C, protection and safety systems [7]. These simulations provide the time evolutions of both LHGR at each point of the core and maximum linear power over the core calculated by the protection system.

The thermal-mechanical code COPERNIC calculates the evolution of the Strain Energy Density of an $M5_{\text{Framatome}}$ fuel rod during the transient based on the evolution of LHGR. The PCI margin is evaluated by comparing the SED to the CSED (see Figs 1 and 2). In case of failure, the linear power value calculated by the protection system modelled in MANTA at the time of the failure is used to design the high linear power reactor trip threshold.

A great number of class-II transients are simulated from class-I situations obtained by xenon oscillations to cover all of the (Relative power, ΔI) operating domain; different burnup steps in the cycle are also examined.

- First, reactor trip threshold is estimated to avoid PCI failure in case of base load operating mode only.
- Then, PCI calculations are performed during an ELPO; in order to maintain a positive PCI margin, despite this more penalizing operating mode, high linear power reactor trip threshold is adjusted (decreased) to accommodate wished ELPO duration.
- Finally, during "Reconditioning stage" following the ELPO, the power is set back to the nominal and thanks to stress relaxation in the cladding, PCI margins are progressively restored until saturation.

The PCI margins assessment in base load, ELPO and reconditioning (see Fig. 3) allows to define Operating Technical Specifications (OTS) for the reference core for the manoeuvrability of the plant.

Thanks to its high level of sophistication the MIR methodology allows justifying a broad manoeuvrability of the plant.

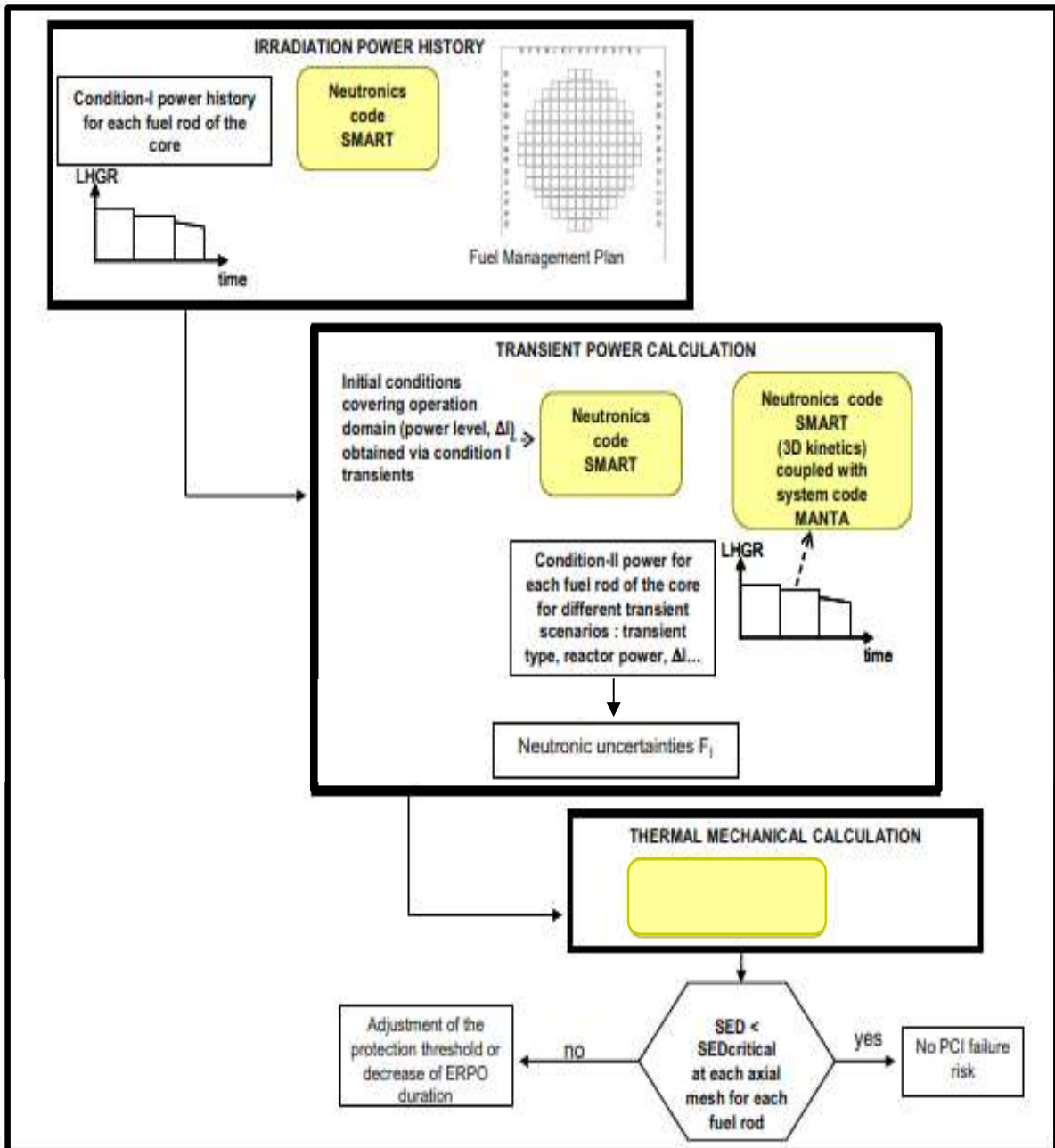


FIG. 1. Flowchart of the MIR methodology.

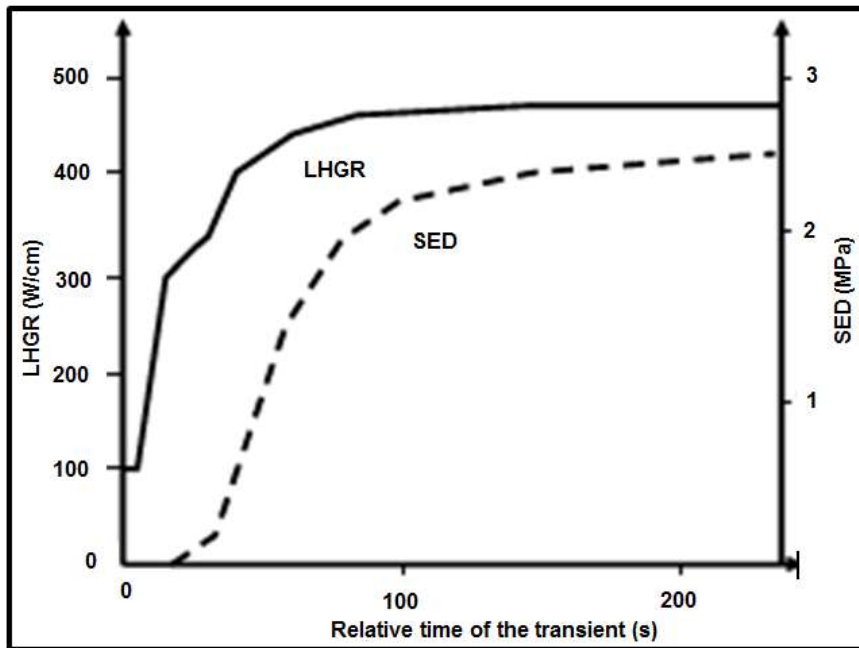


FIG. 2. Example of a class-II transient.

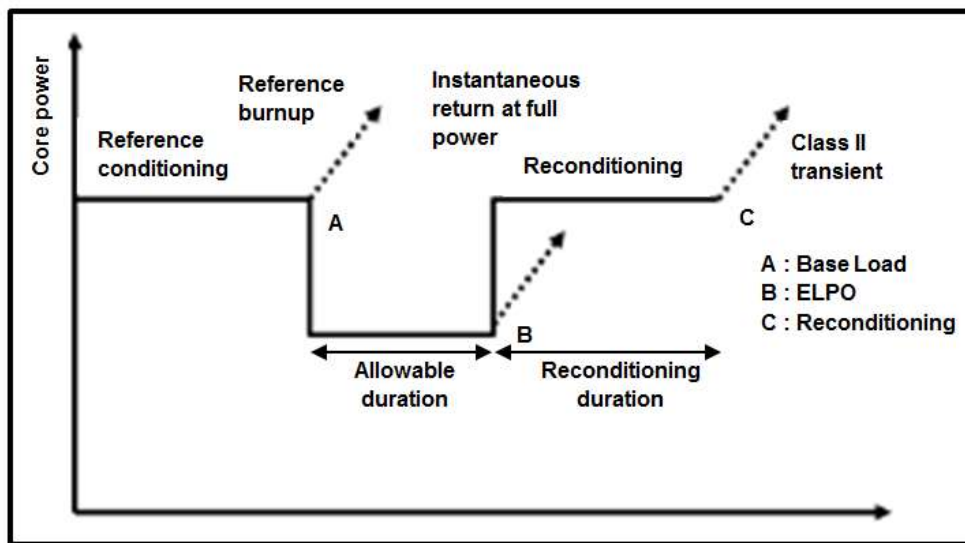


FIG. 3. Calculation stages of a PCI study with the MIR methodology.

2.4. The allowable power methodology

Framatome has also designed an alternative 4-stage approach based on the concept of allowable power. By decoupling the neutronic calculations of class-II situations and the thermal-mechanics calculations and considering bounding assumptions for the transient boundary conditions and power ramp simulations, the allowable power methodology is an effective tool for performing cycle specific PCI analysis in a limited period of time.

The essential principle of the methodology consists in quantifying the PCI risk by comparing limiting transient power distributions with the allowable LHGR as described below (see Fig. 4):

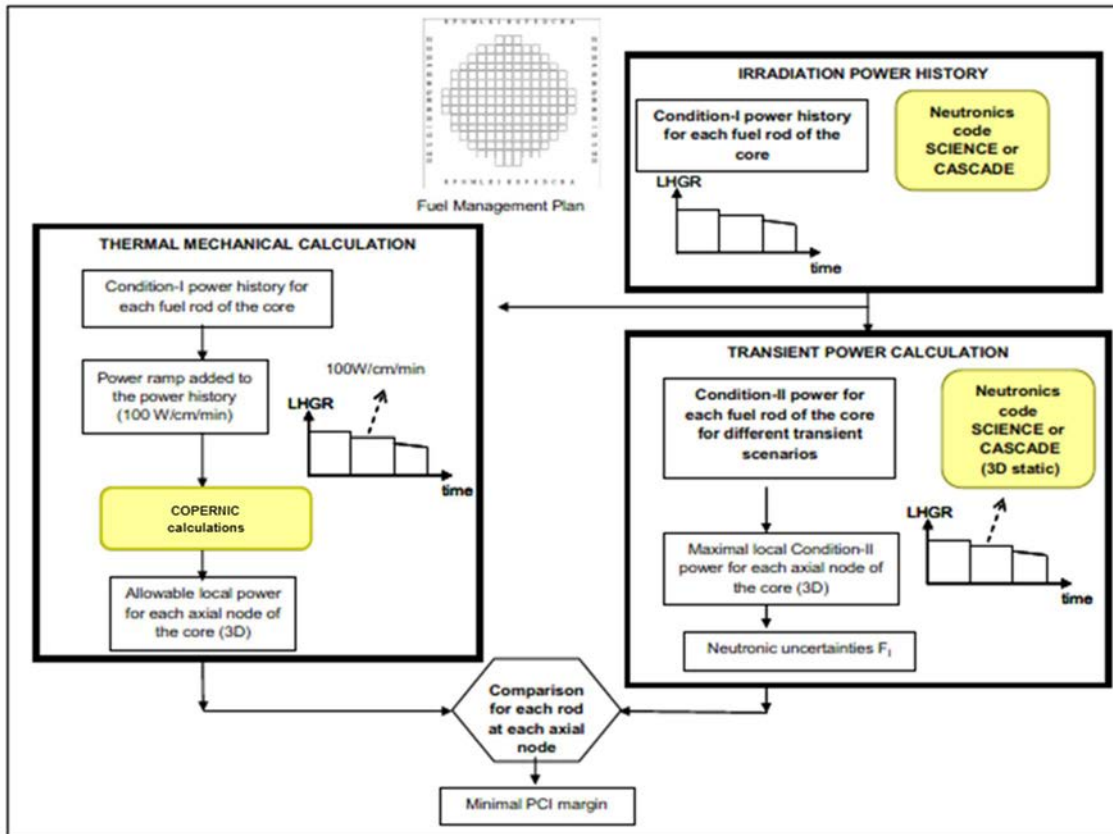


FIG. 4. Flowchart of the allowable power methodology.

- Stage 1: Class-I local (rod by rod) power histories based on the complete irradiation cycle in the plant are provided from a neutronic 3D depletion calculation of the relevant cycles.
- Stage 2: Fuel Rod Design Calculations - allowable linear heat generation rate ($P_{allowable}$). The fuel rod PCI behaviour in initial and transient condition is calculated with the fuel rod performance code COPERNIC. The class-II conditions are simulated for each fuel rod by a power ramp using a prototypical power variation rate of 100 W/cm/min independently of the actual incident kinetics. During these simulated power ramps performed for each fuel rod and axial node, the SED values are traced locally up to the CSED to define the corresponding allowable LHGR ($P_{allowable}$).
- Stage 3: Neutronic Calculations – Class-II transient power simulation. Limiting class-II power distributions are determined by neutronic simulations, based on 3D static calculations performed with SMART or CASCADE [8]. Hypotheses are taken in order to obtain a bounding static simulation of class-II states. Most limiting 3D power distributions are retained (occurring typically at the end of the transient), and the maximal class-II power P_{cl2}^{unc} is then determined for each axial node considering relevant neutronic uncertainties.
- Stage 4: Calculation of PCI Margin. For all fuel rods and for all axial nodes, a local PCI margin is determined as a difference of the maximum power with respect to the allowable power, i.e. $M_{PCI}^{local} = P_{allowable} - P_{cl2}^{unc}$. The global PCI margin is considered as the minimum of these local margins during the cycle.

2.5. Coupling of MIR and allowable power methodologies

To cover extended flexible operations (so-called flexibility cycles), MIR methodology and allowable power approach can be coupled through the following steps (see Fig. 5).

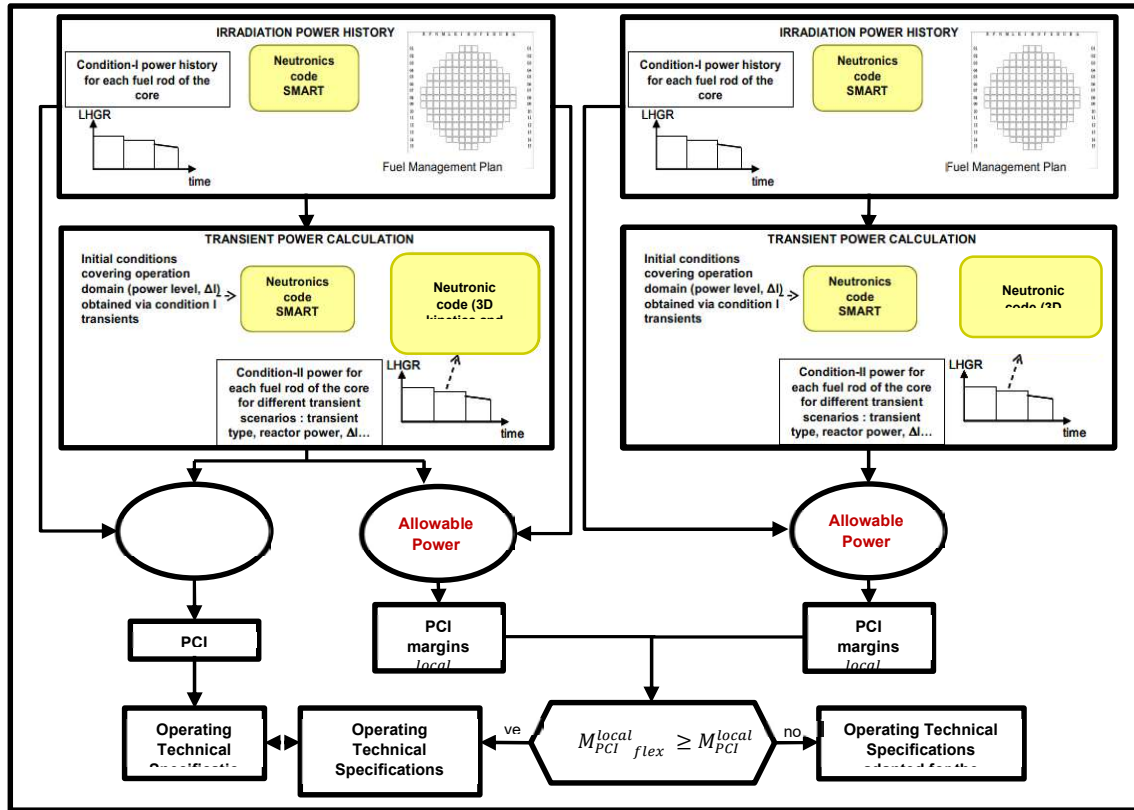


FIG. 5. Flowchart of the coupled approach.

2.6. The gliding threshold methodology

Specifically retained for the EPR reactors, this methodology uses the linear power density from 72 measurements and the limitation function for the linear power density in the reactor control surveillance and limitation (RCSL) system. This limitation function constitutes a PCI gliding threshold for each half of the core, that follows the measured peak power density through the deconditioning rate (DR) and the increase rate (IR) in order to maintain a limited variation of LPD (overshoot allowance or OA). This PCI gliding threshold is bounded by a minimal and two maximal values (Min PCI limit, Max PCI limits for upper and lower half core) (see Fig. 6). When the peak power density exceeds the gliding PCI limit, staggered actions are initiated up to a Partial Trip (PT), whose purpose is to achieve a fast power reduction when reaching a limitation function threshold.

- Step 1: Calculation of PCI margins on the reference core.
 - With MIR methodology for Base Load, ELPO and reconditioning for translation in OTS
 - With allowable power methodology to associate PCI margins $M_{PCI}^{local equ}$ to the OTS defined with MIR methodology.
- Step 2: Calculation of PCI margins with allowable power methodology for flexibility cycles.

The PCI margins for the flexibility cycles $M_{PCI}^{local flex}$ are then evaluated and compared to the PCI margins $M_{PCI}^{local equ}$ of the equilibrium cycle:

- If $M_{PCI}^{local flex} \geq M_{PCI}^{local equ}$ for each configuration analyzed, then the OTS are valid for the studied cycle
- If $M_{PCI}^{local flex} < M_{PCI}^{local equ}$, then specific OTS are defined for the studied cycle.

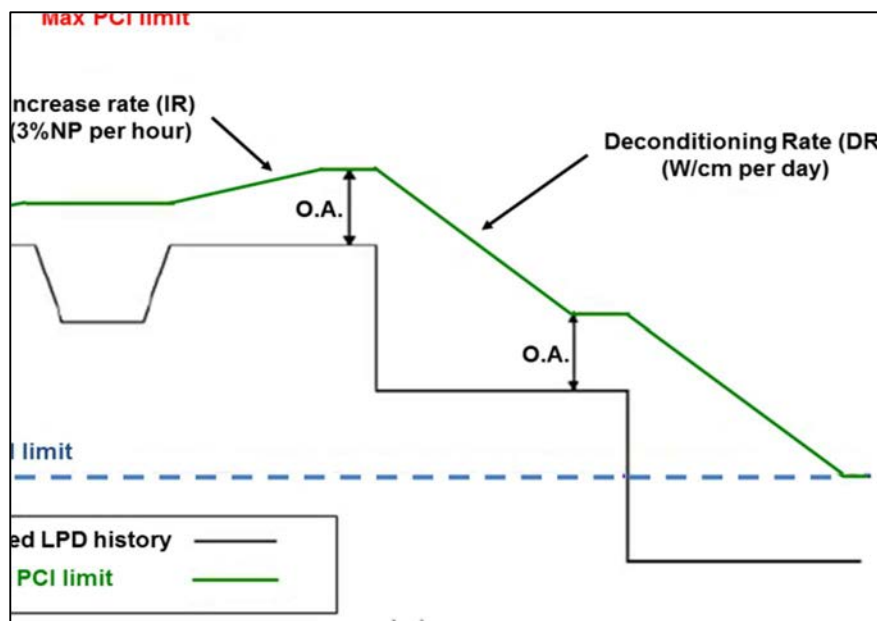


FIG. 6. Example of gliding PCI threshold.

A large manoeuvrability is proposed to the operators as the OTS defined for the equilibrium cycle are extended to flexibility cycles with limited computational efforts.

The Min PCI limit, the OA and the DR are specific to the considered fuel management whereas the IR is based on experience feedback on the current practice of power manoeuvring. The Max PCI limits are determined in consistency with “High Linear Power Density” limitation channel to ensure that both limitation channels have the same range of applicability.

The overall methodology is based on 3D calculations and includes the following four main steps (see Fig. 7):

- Generation of fuel rod conditioning power histories;
- Determination of the parameters of the PCI limitation function based on thermal-mechanical calculations;
- Simulation of class II-transients to construct the corresponding 3D linear power distributions;
- Verification of the performance of the limitation function through PCI margins evaluations.

With a limited computational cost, the Limitation Function provides operators an extended flexibility as it covers several operating modes such as fixed ELPO and flexibility cycles.

2.7. Developments on-going to value the core monitoring system

To meet the increasing need for manoeuvrability, Framatome is currently developing a methodology allowing to reduce bounding conservatisms by making the most of a Core Monitoring System (CMS). This approach is relying on a five-step process:

- Step 1. Definition of the PCI protection thresholds: Based on the reference core, this study is performed with the MIR methodology.
- Step 2. Evaluation on-line of allowable powers based on the local powers at any point of the core provided by the CMS. The maximal local power is more precisely estimated than with the protection systems. Using allowable power methodology and with constant progress of computational tools, this evaluation can be done quickly and on a frequent basis.
- Step 3. Neutronic Calculations – Class-II transient power simulation: This simulation of class-II transients is fully consistent with the step 3 of the allowable power methodology: limiting class-II power distributions are determined by neutronic simulations based on 3D static calculations. The maximal variations of power during transients are evaluated at any point of the core.

- Step 4. Determination on-line of limiting powers for each rod and axial node by assessing the difference between the allowable power calculated on-line and the maximal variations of power during transients.
- Step 5. Evaluation of ELPO duration and potential relaxation of PCI protection thresholds: By comparing the Limit Powers to the maximal Local Power estimated by the CMS, ELPO durations are evaluated. If the ELPO durations are longer than the conservative values covering ranges of burnups and power levels determined with the MIR methodology on the reference core, the customer has the opportunity to choose operation at low power for an extended period of time or to raise the PCI protection thresholds hence increasing the reactor manoeuvrability.

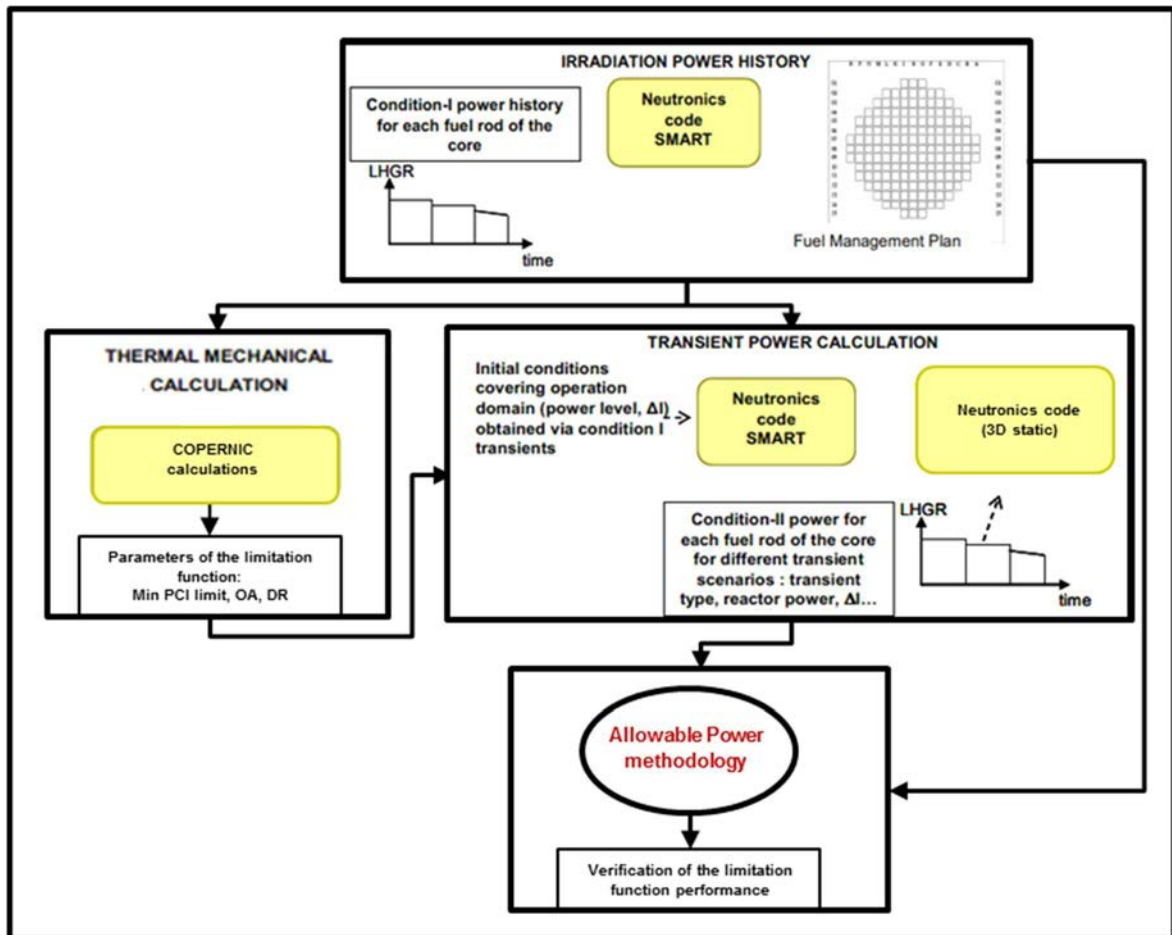


FIG. 7. Flowchart of the determination of the limitation function parameters.

3. APPLICATIONS

3.1. Description of enhanced plant manoeuvrability conditions

Flexible plant operation is targeted by a growing number of utilities and, as variations from a “conditioned” thermal-mechanical equilibrium state are unfavourable for the PCI risk, studies have to account for enhanced manoeuvrability. The two main operating modes associated to enhanced manoeuvrability are Modulations of Power (MP) and ELPO (see Figs 8 and 9). ELPO and MP can also be combined without overlapping:

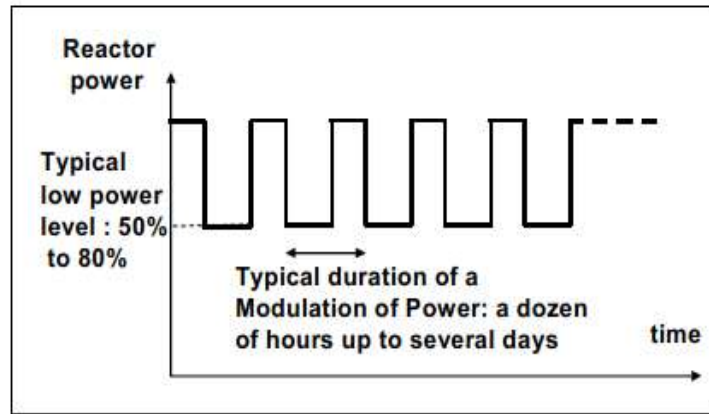


FIG. 8. Schematic drawing of modulation of power.

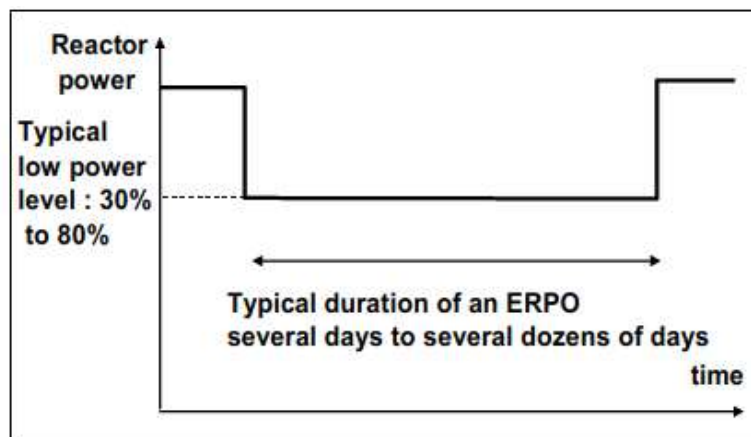


FIG. 9. Schematic drawing of ELPO.

- Modulations of Power: Their aim is adjusting the produced energy to the anticipated demand, which fluctuates during the day and during the week. With alternative deconditioning and reconditioning stages with specific kinetics, the global impact of such operating mode is a decrease of the PCI margin. The assessment of the impact of MP can be achieved by an explicit modelling of the power oscillations during the PCI analysis for a given cycle (typically the case of a study performed with the allowable power methodology). Or in case of the MIR methodology, through a bounding impact first determined - thanks to parametric analysis - and then applied on the PCI margins obtained during normal operation.
- ELPO: Utilities might have to operate at reduced power either for grid or for technical reasons. Typical orders of magnitudes range for durations between a couple of days to several dozens of days or, in exceptional cases to several months. For all cases of ELPO, the deconditioning is explicitly modelled, and the PCI margins are assessed at the end of the ERPO. The calculations take into account also the return at full power.

3.2. Application of the MIR methodology

The ELPO study with the MIR methodology allows justifying allowable durations ranging between several dozens of days to one hundred or more days for some low power levels at several instants during the cycle. Figure 10 shows an example of PCI margin decreasing along with the ERPO duration; the maximum authorized duration is defined as the time of null margin.

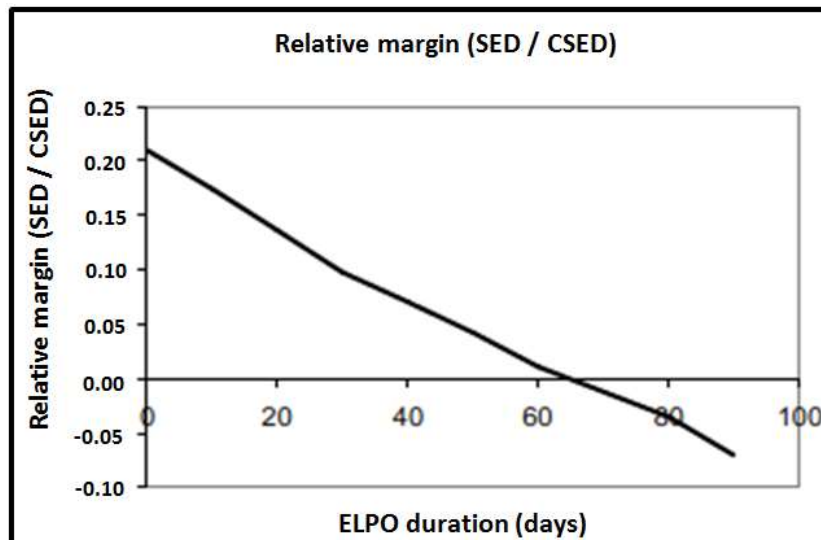


FIG. 10. PCI margin evolution during an ELPO – Search of the allowable duration.

The reconditioning study, after the ELPO analysis, specifies the kinetics of the fuel reconditioning and defines the durations when the PCI margins are restored. The evolution of the PCI margins during the ELPO and reconditioning phase are translated in mathematical functions, which represent the kinetics of deconditioning and reconditioning. These functions are followed on-site through a PCI parameter, depending on the ELPO level and duration and on the reconditioning duration as well: it decreases during an ELPO, and increases during the reconditioning stage (see Fig. 11) and shall always remain positive.

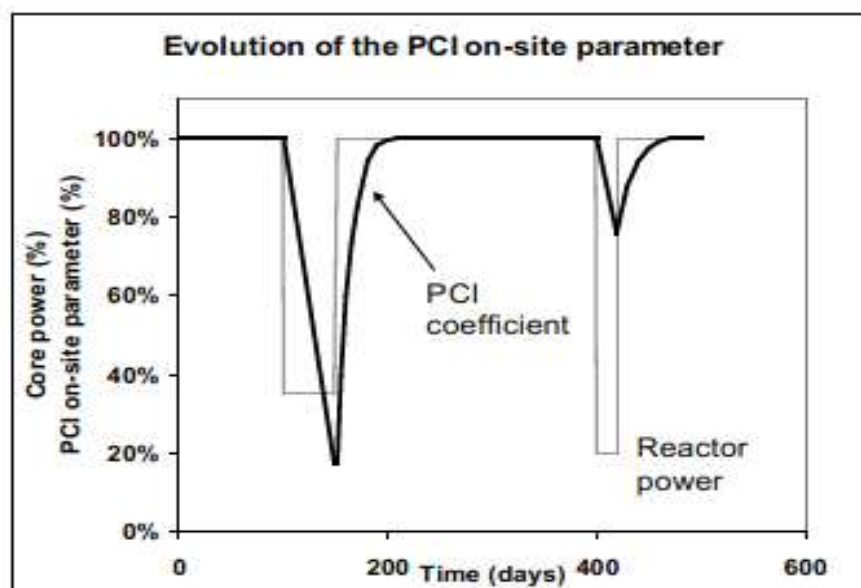


FIG. 11. Example of on-site monitoring of the PCI parameter.

3.3. Application of the allowable power methodology

Initially deployed on plants operating in base load mode, this method bears the capability to deal with short ELPO and Modulations of Power.

The impact of Modulations of Power (between 50% and 100% core power) on the PCI margin is shown in Fig. 12, the reference being the base load operation. To assess such impact, a base load case and a case with Modulations of Power have been performed at a given burnup; the impact being obtained by subtracting minimal PCI margin (from all the rods in the core) obtained with MP from base load margin. The upper part of the plot shows the evolution of the core average impact (normalized with respect to impact after 30 modulations).

The figure clearly demonstrates:

- a saturation effect of the deconditioning process along with the number of power modulations (effective after about 30 modulations),
- a reconditioning process if the sequence of Modulations of Power is followed by a return to full base load operation. A reconditioned state is reached after a certain period of time.

The allowed ELPO duration (of the order of 20 to 50 days, if justified with the Allowable Power methodology) depends on the cycle operation (loading pattern and power history) and the combination of Modulations and ELPO shall be taken into account when assessing the net margin. Therefore, studies for a specific reactor are in any case needed to confirm the possibility of ELPO.

As the allowable power is suited to justify ELPO duration the order of 20 to 50 days and Modulations of Power, this methodology provides an excellent tool to access the PCI risk without restraining plant manoeuvrability with reduced engineering efforts.

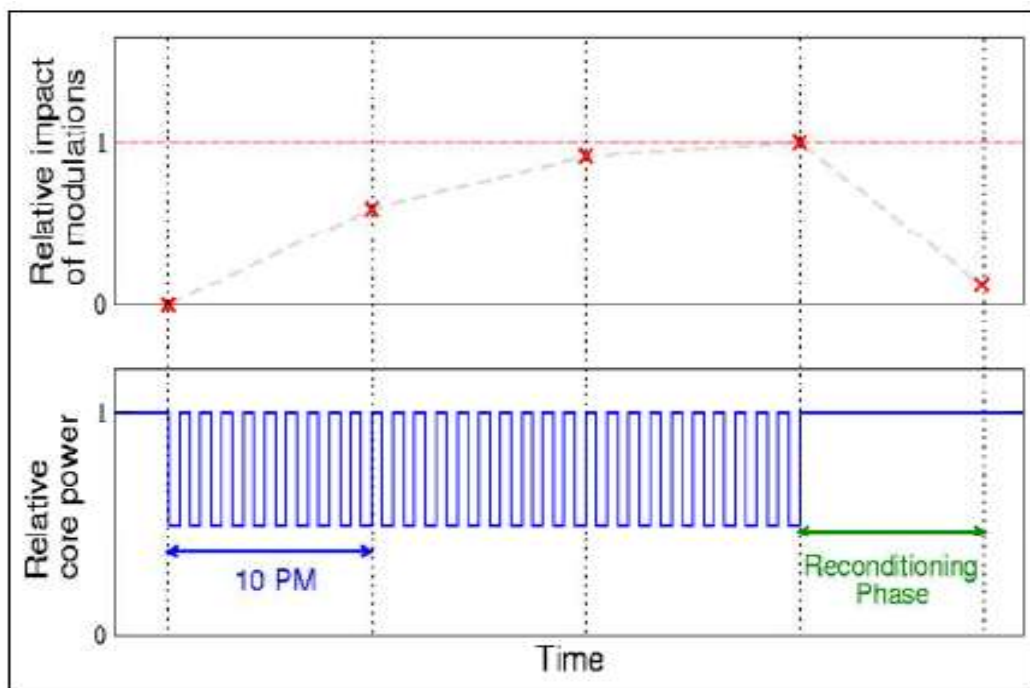


FIG. 12. Relative impact of modulations of power on the average core PCI margin.

4. CONCLUSIONS

Broad use of flexible operation may require specific PCI analysis and for that purpose Framatome has developed a set of innovative methodologies addressing PCI risk in PWRs. They are based on a common thermal-mechanical approach supported by a series of experimental ramp tests and on assessments by the fuel rod code COPERNIC.

Based on two primary methodologies, the MIR methodology and the allowable power Methodology, Framatome has developed a set of approaches to support utilities for a more flexible nuclear energy production. Finally, these methodologies have also potential for evolution by optimizing the computational cost and by

benefiting of the new generation of codes, ARCADIA code system for neutronic / thermalhydraulics [9] and GALILEO for thermal mechanics [10].

NOMENCLATURE

CMS:	Core Monitoring System
CSED:	Critical Strain Energy Density
DR:	Deconditioning rate
ELPO:	Extended Low Power Operation
I&C:	Instrumentation and Control
IR:	Increase rate
LHGR:	Linear Heat Generation Rate
LPD:	Linear Power Density
Max PCI limits:	Maximal PCI limits (upper half core and lower half core)
Min PCI limit:	Minimal PCI limit
MIR:	Méthode IPG Rénovée
MP:	Modulations of Power
NSSS:	Nuclear Steam Supply System
OA:	Overshoot Allowance
OTS:	Operating Technical Specifications
PCI/SCC:	Pellet-Cladding Interaction assisted by Stress Corrosion Cracking
PT:	Partial Trip
RCSL:	Reactor Control Surveillance and Limitation System
SED:	Strain Energy Density

ARCADIA, COPERNIC, GALILEO and M5_{Framatome} are trademarks or registered trademarks of Framatome or its affiliates, in the USA or other countries.

REFERENCES

- [1] BÉGUIN, S., “PCI-Related Constraints on EDF PWRs and Associated Challenges”, Proc. PCI in Water Reactor Fuels, Aix-en-Provence, France, 9-11 March 2004.
- [2] BILLAUX, M., “Modelling Pellet-Cladding Mechanical Interaction and Application to BWR Manoeuvring”, Proc Intl Meeting on LWR Fuel Performance, Orlando FL, USA, Sept 19-22, 2004.
- [3] NONON Ch. et al, “Differential PCI Behaviour of PWR Fuel Rods under Transient Conditions “, Proc Intl Meeting on LWR Fuel Performance, Orlando FL, USA, Sept 19-22, 2004.
- [4] JULIEN, B. et al, “Performance of Advanced Fuel Product under PCI Conditions”, Proc Intl Meeting on LWR Fuel Performance, Orlando FL, USA, Sept 19-22, 2004.
- [5] VALLÉE, A., FRANCILLON, G., et al., “SCIENCE: A New Reactor Physics Codes Package Approach”, Proc 1992 Topical Meeting on Advances in Reactor Physics, Charleston.
- [6] GIRIEUD, P., “SCIENCE: The New FRAMATOME 3D Nuclear Code Package for Safety Analysis”. Proc of the ENC’94 Meeting. Lyon, France. October 1994.
- [7] GANDRILLE, J.-L., HAULBERT, A., PETETROT, J.-F., “MANTA a Modular Advanced Neutronic and Thermalhydraulic Analysis Code”. ICONE 8. April 2-6, 2000, Baltimore, MD USA.
- [8] Van de VELDE et al., “An Integrated Software System for Core Design and Safety Analysis – CASCADE-3D” TopFuel’99 Int. Topical Meeting, Avignon, Sept. 13–15, 1999.
- [9] SENEAL, J. et al., “Recent Developments in ARCADIA, Framatome’s Advanced Core Physics Methods for LWRs”, Proc 2019 TopFuel, Seattle WA, USA, Sept. 22-27, 2019.
- [10] QI, Y. et al, “Qualification of Framatome Fuel Performance Code - GALILEO”, Proc 2019 TopFuel, Seattle WA, USA, Sept. 22-27, 2019.

PCI/SCC LOADS IN BWR AND PWR: GERMAN OPERATING CONDITIONS AND EXPERIENCE

M. SPERLICH, F. FRÖMEL, K.-D. SCHUH, T. SALNIKOVA
Framatome GmbH,
Erlangen, Germany
Email: martin.sperlich@framatome.com

Abstract

Nuclear power plants (NPP) in Germany are explicitly designed for various flexible operation modes such as primary frequency control, secondary control by plant operator or remote controlled by load dispatcher and classical load-follow operation mode. Recently there has been an increase in demand of such flexible operation modes for electricity grid stabilization purpose due to an increase of volatile and heavy renewable energy production. In addition, there have been economically driven considerations in case of low or even negative prices on the spot market. The following paper gives an overview on the Framatome's experience regarding load changes during various flexible operation modes in German NPPs. A comparison to base load cases from BWR and PWR is discussed with respect to PCI/SCC relevant loads and operation feedback. These load cases include start-up conditions for BWR and PWR, impact of (continuous) load-follow operation and different control rod operating strategies for BWRs.

1. INTRODUCTION: FLEXIBLE OPERATION MODES FOR LWRS, REACTIVITY AND POWER CONTROL

Fuel rod cladding consisting of Zr alloys can exhibit a stress corrosion cracking (SCC) failure mode named pellet cladding interaction (PCI). The basis of this failure mode is the influence of aggressive fission products on the cladding internal surface, when stresses due to the interaction between an expanding ceramic pellet and the metallic Zr-based cladding occur. This failure mode typically occurs in combination with the pellet-cladding gap closure during the irradiation of the fuel rod and fast power increase causing a significant thermal expansion of the pellet and considerable stress levels in the cladding.

In flexible operation modes as load-follow operation a series of contact and non-contact conditions between pellet and cladding can occur due to highly varying reactor power. These conditions are supposed to imply stresses in the cladding, which have been seen as potential source of PCI failures in the past.

Starting with the classical view on flexible operation, there are three closely linked types of reactor operation, generally addressed as primary and secondary control and load-follow operation (including tertiary control). Primary control acts within seconds and is used for frequency stabilization as well as secondary control within minutes. Classical control for load-follow operation is in the order of hours or days. Primary and secondary control is used for stabilizing the high voltage grids with fast response times, while load-follow operation mode is typically used to cover planned variations in the power demand. This may include high demand at day times and lower at night, power reduction on weekends as the industrial demands are lower or reduction for public holidays as Christmas. Other constraints as tidal related constraints at coastal locations or river water temperature restrictions can be seen as further influences. A newer source for flexible operation requirements for conventional NPPs is the continually increasing amount of volatile renewable energy produced by solar and wind power sources influencing the power production independent from the demand. Solar and wind power sources are more or less non-dispatchable. Thereby, tertiary control is the special case of the short response load-follow operation mode (time of response less than 15 minutes).

Taking into account the duration periods of the three control modes, a pre-ranking on the influence on PCI relevant conditions can be made. Primary and secondary control is based on fast power changes with short duration (holding times). These conditions typically have a limited influence on fuel deconditioning and lead to low stress levels for return to higher power levels. The longer time periods of load-follow operation in with hours or days on low power have a higher impact on the basic stress levels. Especially, an Extended Low Power Operation (ELPO) mode for time periods in the order of weeks or months is seen as an important factor for fuel deconditioning and high stress levels upon return to full power.

The German nuclear power plants have been designed already in the 1980s for enhanced flexible operation. Although, till 2007 mainly base-load operation has been performed, more and more flexible operation modes are used recently including load-follow operation, primary, secondary and tertiary control. But also, environmental demands due to tidal influence or river water thermal limits.

In addition to these external flexible operation requirements this paper is taking into account a slightly broader view by influences of reactor operation itself. This includes especially the boiling water reactors (BWR) with higher flexibility for cycle lengths, fuel shuffling limits during outages or different operating strategies.

1.1. Reactivity control

There are some basic design differences between the reactivity control in PWRs and BWRs. Neglecting the continuous influence of burnable absorber rods, the variable PWR reactivity control is based on control rod operation for short term and boron concentration for long term power adaptations. For BWRs, the reactivity control by boron injection cannot be used, but the recirculation pumps can effectively regulate the core power via the coolant flow rate in addition to the control rods (arranged within control blade cross between four fuel assemblies). Regarding PCI, which is a local phenomenon on the pellet length scale, boron and flow rate control are global, core related modes of reactivity control with high influence in terms of rated reactor thermal power, but limited impact on the local pellet level. On the other hand, control rod influence has a high impact on the local power level with pronounced axial gradients in the fuel in vicinity to the control rod tips.

In the German PWRs a small number of control rods are grouped into control rod groups called D-bank. These “driving” control rods are directly used for fast reactor power control with no or very limited impact on the axial core power shape. All other control rods are grouped in the L-bank (“non-driving” control rods) and can be operated independently of the D-bank. Variations of the axial core power shape during the cycle are typically small for PWRs.

In BWRs the control rods are grouped by default with typically four control rods in one group homologue in each of the reactor quadrants. Contrary to PWRs, pronounced core wide axial power peaks are given in a BWR. At beginning of cycle, the axial power peak will typically be in the lower core half, while the control rods in BWRs are inserted from the bottom of the core. Here, some shallow insertion of a few control rod groups from the bottom can be used for slight adaptations of the reactor axial power shape. This is not possible anymore at end of cycle, when the axial power peak is shifted to the upper core half. However, flow rate adaptation using the recirculation pumps can be used for power adaptation without influencing the axial power shape significantly in a broader range of rated thermal reactor power depending on the limitations by the licensed coolant flow window.

1.2. Pressurized water reactors

Primary control in the German pressurized water reactors (PWR) is based on an automatic support to the 50.0 Hz power grid frequency stabilization within seconds response time. Here, the turbine controller gets an input from the power grid frequency and acts in response to deviations from the 50.0 Hz frequency. Typical values are in the order of 2-10% of reactor power.

Secondary control is currently performed remote controlled by load dispatcher. Within maximum of five minutes typical power gradients in the order of 30 MW(e)/min are applied by remotely setting of the turbine controller set point.

Finally, load-follow operation incl. tertiary control utilizes power ranges between 30-40% (minimum power load) and 100% of rated reactor power (with the same power gradients as for secondary control) and is ordered by the load dispatcher per telephone communication more than an hour in advance. Tertiary control can be performed in combination with primary and secondary control.

More details on the German PWR operation with respect to flexible operating modes can be found in [1] (Annex I) as well as in [2]. Reference [3] gives an overview on the carried-out core control optimizations and the reached flexible capabilities in German PWRs. Possible adaptations of German measures towards enhanced flexibility to other types of NPPs are summarized in [2]. Thereby it is important to mention, that the modernization of the reactor control started with the aim to achieve maximal flexibility, also with respect to the core loading.

See also [4] for additional information on power cycling capacity of the German PWRs.

1.3. Boiling water reactors

BWRs are capable of load-follow operation within their coolant flow window in addition to using local control rod groups. Besides this type of flexibility, modern European BWR operation often takes into account different cycle lengths varying from about half year cycle length up to about 1.5 years in consecutive operation

cycles. This operation can be seen as flexible operation compared to the usual annual or biennial fixed cycle lengths.

Further differences between the operation of the BWRs are given in control rod manoeuvring strategies.

Mono-sequence operation in the German (and Northern Europe) BWRs utilizes fine motion (or screw drive) control rod drives. Here, a single control rod step is in the order of 2.5cm for the German BWRs (and 0.5% or 1.8cm for the Northern European BWRs). Mono-sequence operation consists of one or several control rod groups fully inserted during the cycle and withdrawn at full power, when the reactivity from burnable absorber burnup is already released. This type of operation is typically used in conjunction with controlled cell core (CCC) type fuel loading, where already some years burned fuel (typically third annual cycle) is loaded into the controlled cells in order to limit the maximum power levels. However, modern neutronic designs can lead to high local power levels even for this medium burned fuel (about 30-40 MW·d/kgU) with local power levels up to 400 W/cm.

Contrary to the mono-sequence type operation, some plants are applying sequence-exchange operation. In this type of operation, the controlled cells are exchanged during the cycle by reducing the reactor power (with control rod insertion and coolant flow reduction) down to approximately 60-80%, exchange of controlled cells and return to full power with the coolant flow. For the final control rod withdrawal called all-rods-out (ARO) manoeuvre, the same scheme is used.

This type of operation is typically performed for notch drive control rod drives with a single withdrawal step in the order of nearly 15 cm (consistent with the core simulator axial resolution). Control rod retraction for this comparably big step is usually restricted to conditions of reduced reactor power, i.e. prior reactor power reduction by reduced coolant flow rate, control rod withdrawal operation and subsequent return to full power, or only single withdrawal steps. This prevents high localized power increase from fully controlled to nearly fully uncontrolled conditions with the risk of inducing PCI-relevant loads. For some regulation this also prevents exceeding thermal reactor load limits even for the short time periods until the adaption of coolant flow rates would regulate the core power.

For reactors operating in biennial cycles, the fuel assemblies on the sequence-exchange controlled cells are of the full range from low to high burnup fuel (one up to three biennial operating cycles). For typical annual insertion cycles some more flexibility is given, and some plants choose to use fuel assemblies in their second to fourth annual cycle for the sequence-exchanged controlled cells.

Some German BWRs use a hybrid type of control rod operation with sequence-exchange during the cycle and stepwise control rod withdrawal at rated thermal reactor power at the final control rod withdrawal phase. Here, various cycles burned fuel can be operated on the controlled cells extending up to fuel assemblies operated in their sixth annual cycle.

Based on the operational characteristic of sequence-exchange operation with local power levels varying between 50 W/cm up to more than 300 W/cm it can be interpreted as a proto-type of load-follow operation. Hence, experience for load-follow operation with longer time at low power is available from various BWRs. Furthermore, the mono-sequence type of operation with low power operation in the order of 50-70 W/cm for more than 300 days is even longer than usual low power operation periods.

2. EXPERIENCE WITH FLEXIBLE REACTOR OPERATION

The German power plant operators have been demonstrating advanced, safe and reliable flexible operation of various types.

2.1. Short periods of reduced power operation in BWRs

The existing operating experience includes power reduction in times of low demand for short time frames, e.g. power reductions during Christmas times, weekends, and nights, which have been performed in both, PWRs and BWRs. For the short time period of reduced power during Christmas a small impact can be seen (Fig. 1) for the axial power distribution upon return to full power in the BWRs. Slightly higher local power levels than expected from operation without power reduction are reached. This local overshoot is in the order of 40 W/cm and well within acceptable regions without a risk of causing PCI failures.

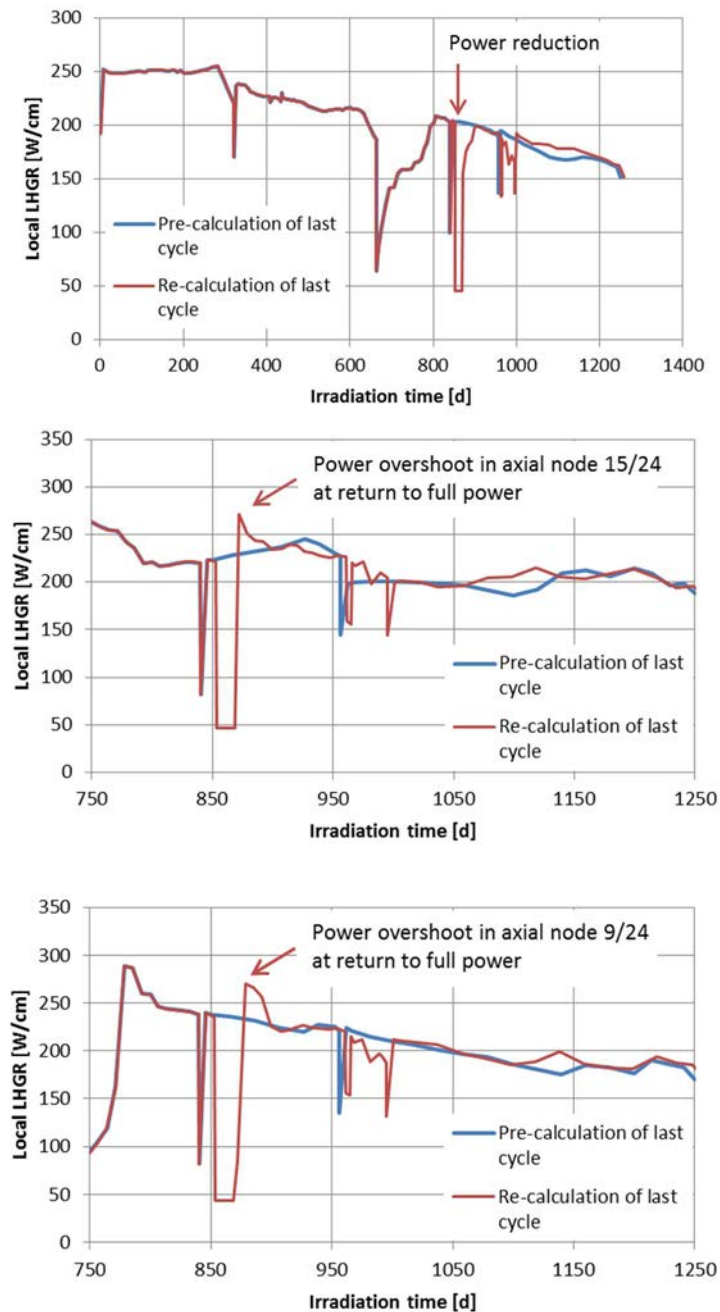


FIG. 1. Comparison of planned operation without and with short power reduction during Christmas in a German BWR for a fuel assembly in controlled cell during power reduction, top: fuel rod average power level, middle: local power overshoot at axial node 15/24, bottom: local power overshoot at axial node 9/24 (node 24 is the topmost node in the core).

2.2. Flexibility on cycle length in BWRs with mono-sequence operation

The influence of flexibility with regard to different cycle lengths in a German BWR can be seen in Fig. 2. The figure shows the operating domain of the maximum power levels after control rod withdrawal operation. Cycle N in green shows a rather short cycle with a cycle length of 263 EFPD (Effective Full Power Days), while the consecutive cycle N+1 in red has been planned with a cycle length of 433 EFPD. Both cycles have been operated in mono-sequence control rod operation. However, the number of deep inserted control rod groups differs from eight controlled cell in cycle N to eleven in cycle N+1. Both cycles applied partly inserted control rod groups (about two third insertion length) and some shallow rod operation at begin of cycle (up to about one third insertion length).

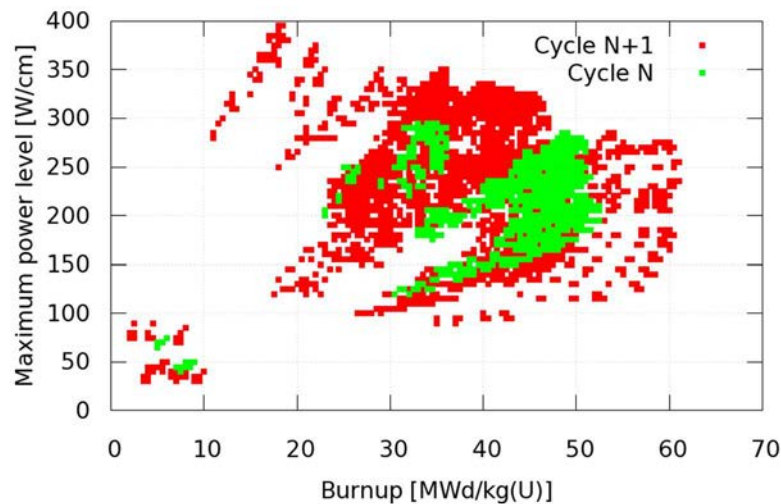


FIG. 2. Example of a German BWR operating domain for maximum power levels after control rod withdrawal operation in mono-sequence operation, green: cycle with 262 equivalent full power days (EFPD) cycle length, red: consecutive cycle with 433 EFPD.

Furthermore, the extent of power increase for the control rod withdrawal operation is substantially higher for the longer cycle. One reason for this observation is related to fuel assemblies with increased reactivity loaded into the core to provide the expected longer cycle length. This effect applies especially to fuel assemblies located in cells with control rod withdrawal at mid cycle. For the final deep inserted control rod group, the power peak has already been shifted to the upper core half. In addition, for controlled periods of more than 300 days, the Pu breeding in the upper core half is rather high, especially in the fuel rods next to the control rod corners. The breeding effect is usually wanted and supported by the spectral shift. Both effects lead to a pronounced power peak in the upper quarter of the fuel rods at control rod withdrawal operation. They may add up to local linear heat generation rates of more than 400 W/cm at burnups around 30 MW·d/kg(U). Starting from fuel conditioned at linear heat generation rates (LHGR) of 50–100 W/cm, such high power increase steps are guided by PCI operating rules to avoid PCI failures. This impact should be taken into account, when designing longer cycles in mono-sequence operation modes.

2.3. Extensive load-follow operation in PWRs

An example of extensive load-follow operation is given in Fig. 3 for a German PWR. Here, the power levels varied between about 45% of rated thermal power and nearly full power for more than three months. Afterwards, an ELPO was performed for about 2.5 months with power levels slightly above 30% of rated thermal reactor power. Finally, near the end of cycle a return to slightly above 85% of rated thermal power was performed, however, with a limited ramp rate due to the long ELPO period.

Figure 3 shows a short sample cycle containing different features of load-follow operation types. However, this PWR was operated in extensive load-follow operation already during the years before, but without long ELPO periods. The consecutive short cycle to the one in Fig. 3 was operated at ELPO during most of the cycle including small load-follow variations at reduced power. At the end of cycle, the reactor returned to about 80% of rated power. Finally, the next (and last cycle) has been operated at full power again. This extensive experience with load-follow operation shows that such operation even with power increase back to full power after long ELPO periods is possible without a single fuel rod failure. A good overview for load-follow operation in Germany for consecutive years is given in e.g. [5–8].

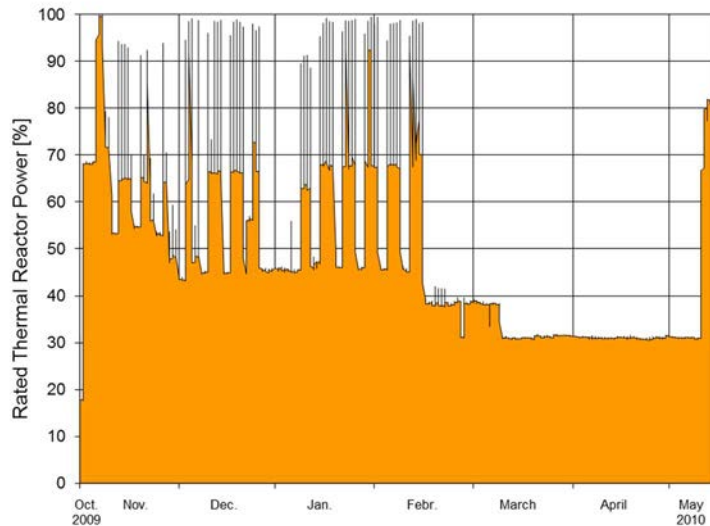


FIG. 3. Example of extensive load-follow operation in a German PWR from October 2009 to May 2010.

3. PCI RELEVANT LOADS

3.1. Load-follow operation in a PWR

Based on the experience from PWR load-follow operation, typical load schemes as day-night or weekly load-follow have been modelled with high timely resolution for recalculation of the mechanical loads. The thermal reactor power for this continuous load-follow operation is shown in Fig. 4. The corresponding local LHGR (Local Linear Heat Generation Rate) in dependency of the time and axial height (power history) of selected first and second annual operating cycle fuel rods is shown in Fig. 5. The second cycle fuel rod includes one cycle of normal baseload operation in lower timely resolution, before the load-follow operation is applied in the second cycle.

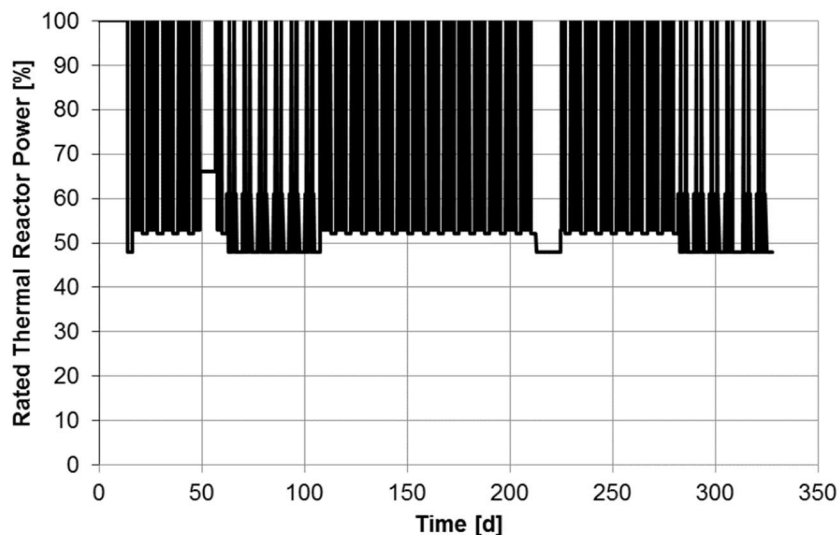


FIG. 4. Thermal reactor power from a simulation of load-follow operation in one cycle of a German PWR applying typical reduced power operation from real operating observations.

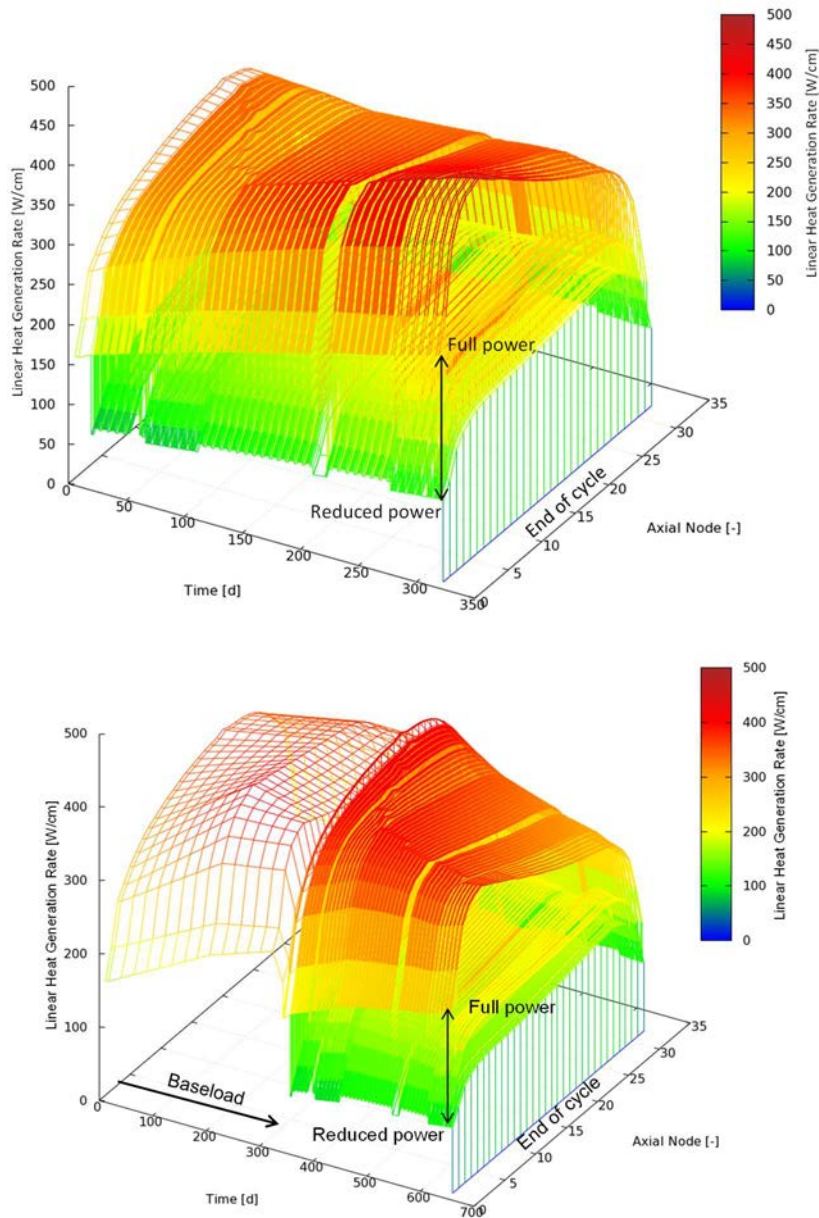


FIG. 5. Local LHGR from a simulation of load-follow operation applying typical reduced power operation from real operating observations for a fuel rod in a German PWR, top: one annual operating cycle and bottom two annual operating cycles.

Best estimate fuel rod design calculations using the steady-state fuel rod performance code CARO-E have been performed for the two fuel rods. CARO-E is used for licensing purposes in Germany and numerous other countries. Initial data and irradiation behaviour according to the power histories have been used for a new coupled mechanical simulation for the cladding mechanical response. No further influence by pellet creep or other possible pellet relaxation processes have been applied in the mechanical simulation. Hence, the simulated cladding response is based on the rigid ceramic pellet assumption, however, the steady-state calculations of the fuel rod performance code take into account pellet strain contributions from thermal loads as well as irradiation effects. The mechanical simulation applies a thin-wall approximation for the cladding stress and strain response to the coolant and fuel rod internal pressures as well as the pellet contact loads in combination with a visco-plastic creep model. In this simulation, a stress-relieved Zry-4 cladding type has been applied.

The resulting strain loads for the pellet and cladding are shown in Fig.6 and Fig.7 for the one cycle and two cycle fuel rod, respectively. For the first cycle fuel rod, clearly no interaction between the pellet and the cladding can be seen. Hence, the load-follow operation has a limited effect on this rod. However, the second cycle fuel rod shows at least some interaction in the full power phases near the end of cycle. This effect is visible in the cladding

total strain response in Fig. 7(bottom) and is fully elastic. The calculated stress response on the pellet-cladding contact is shown in Fig. 8 and shows very low values of tensile stress in a very limited number of axial calculation nodes.

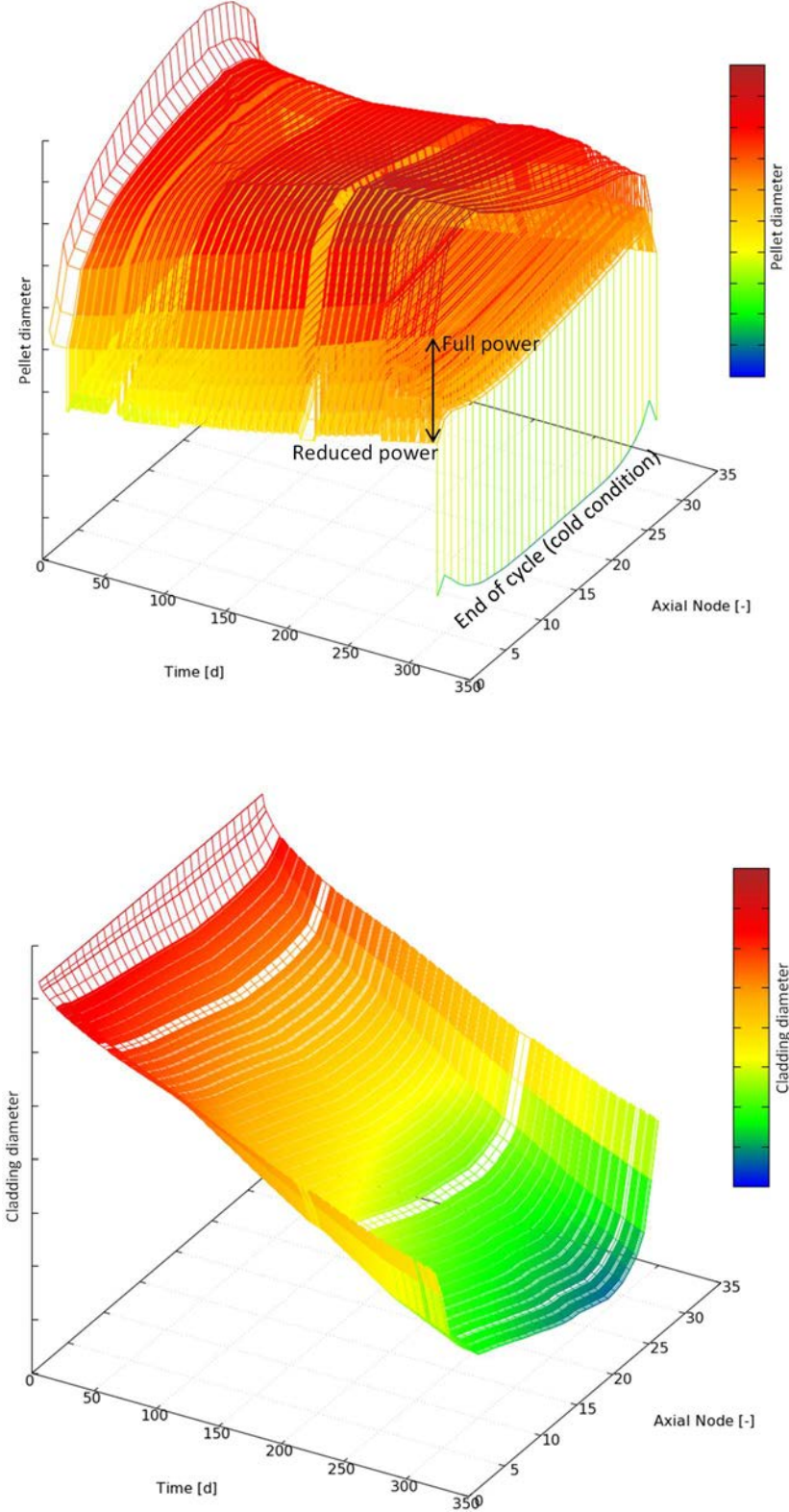


FIG. 6. Pellet (top) and cladding (bottom) total strain response of the one annual cycle fuel rod in load-follow operation of a German PWR: the cladding shows no sign of significant influence by the load-follow operation in the first cycle.

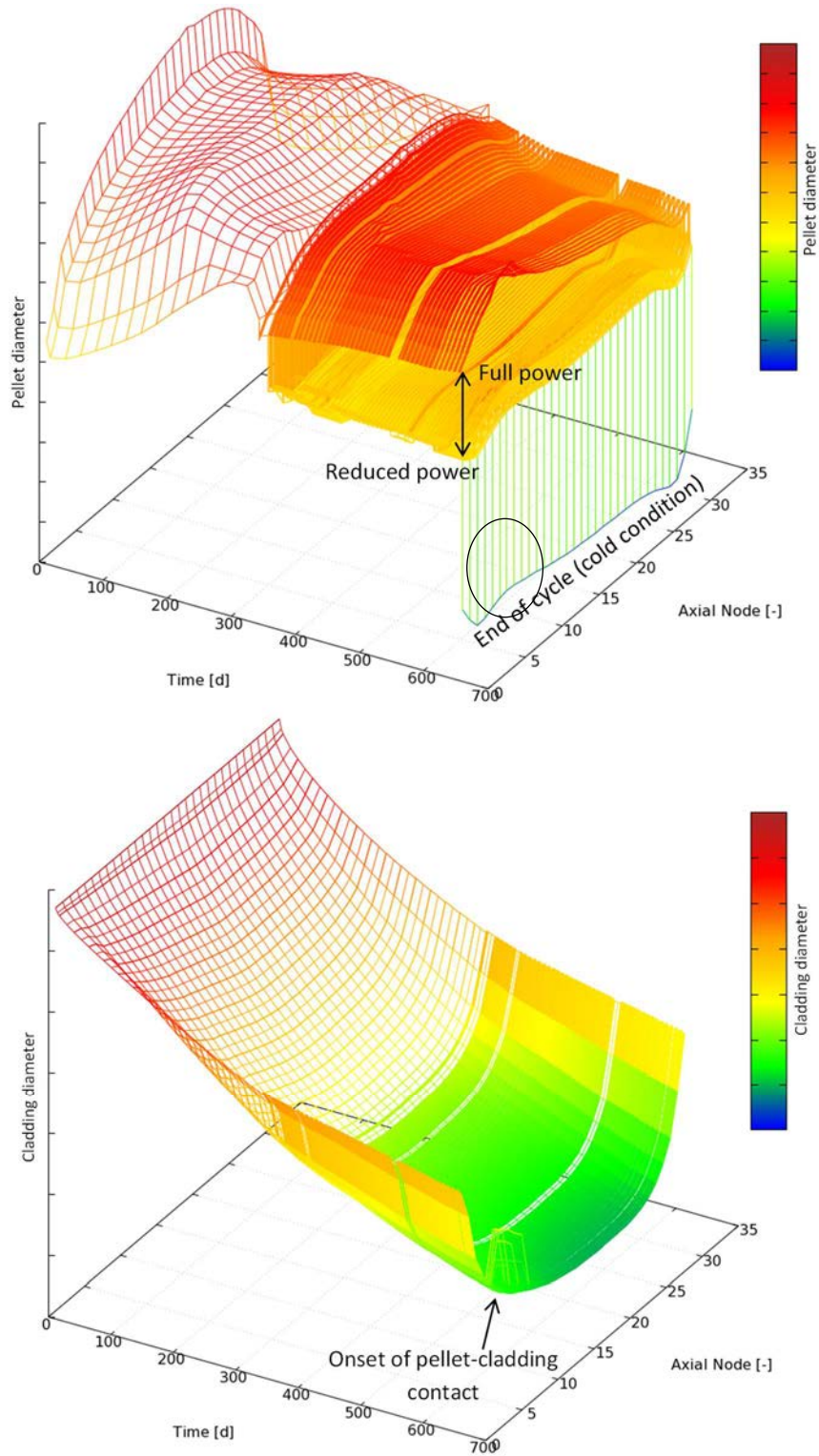


FIG. 7. Pellet (top) and cladding (bottom) total strain response of the two annual cycles fuel rod in load-follow operation of a German PWR: the cladding shows first contact with the pellet only near the end of the second cycle coincident with the bottom peaked power profile.

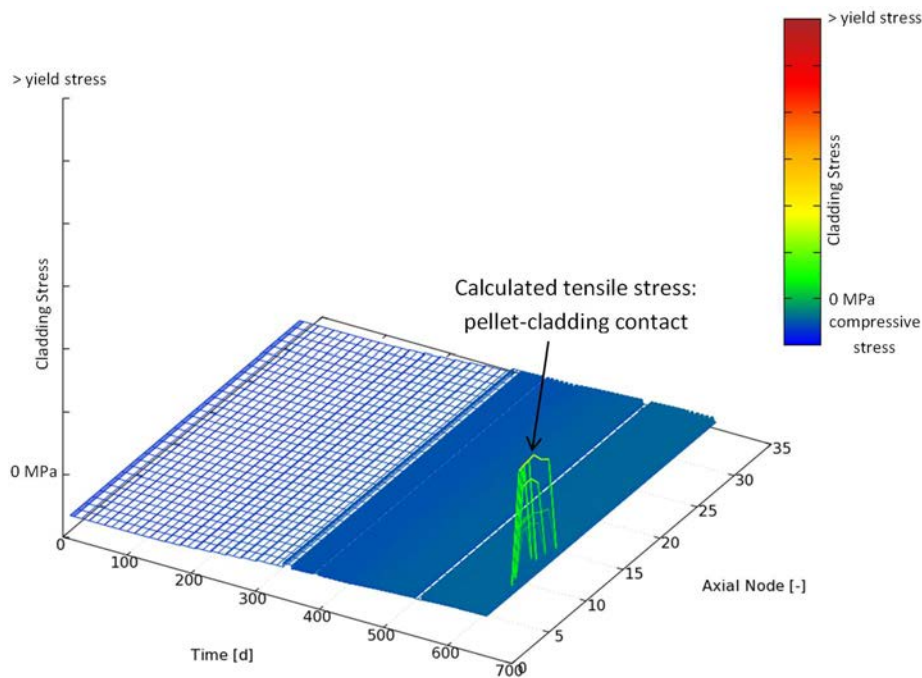


FIG. 8. Cladding stress response of the two annual cycles fuel rod in load-follow operation of a German PWR for best estimate calculation.

A variation of the second cycle fuel rod calculations with reduced initial gap size has been performed and is shown in Fig. 9. In this calculation, the first cycle is again operated without significant pellet-cladding contact. In the second cycle an increase of the stress as a response to the higher power level at reactor start-up after the fuel shuffling can be seen. This is a typical effect of fuel assembly shuffling and can be pronounced for fuel rods directed to the core boundary during operation in the low leakage ring in the first cycle and shuffled into more central core positions for the second cycle. For some loading patterns this may induce PCI-relevant stress levels for fast ramp rates at reactor start-up. However, the calculated stress levels in this example are well within an acceptable range.

During the load-follow operation, additional nodes at the top and bottom of the fuel rod show pellet-cladding contact and stress built-up during full power periods is calculated (Fig.9). However, the calculated stress levels reach an equilibrium state not exceeding the stress levels at second cycle reactor start-up.

Figure 10 shows the cladding total strain (top) and cladding creep strain (bottom) response. The influence of the power cycling of the load-follow operation on the cladding deformation can be seen in the cladding total strain. The maximum cladding total strain is increasing during the second cycle, although, the stress response is not (compare Fig. 9 and Fig. 10 (top)). This can be explained by the cladding creep process shown in Fig. 10 (bottom), which shows the permanent cladding deformation. This creep process basically consists of a continuous slow irradiation induced creep and a thermally stress-activated creep, which is pronounced on higher stress levels. In conclusion, the creep process limits the maximum stress levels to a limited equilibrium condition, which is well within an acceptable range.

Note, that the pellet strain takes into account all relevant effects: thermal strains depending on the LHGR as well as irradiation effects on the UO_2 fuel matrix as decreasing thermal conductivity during burnup and fuel swelling (the latter counteracted at begin of operation by the fuel densification).

Further stress increase due to power increase in case of anticipated operational occurrences is still limited for the German PWRs. Note, that the maximum local power levels in the core are already approaching 450 W/cm and the reactor control system effectively limits the power levels with passive and active measures in case of too high power levels for German PWRs. Passive measures include preventing further control rod withdrawal, when the first power limit is reached. Active measures are actively inserting control rods to reduce power levels on the second power limit and may also initiate a SCRAM in case of transient conditions or even higher power levels.

Here, the reactor control system monitors the maximum LHGR in the upper and lower core half based on the feedback of the in-core neutron flux detectors with high spatial resolution.

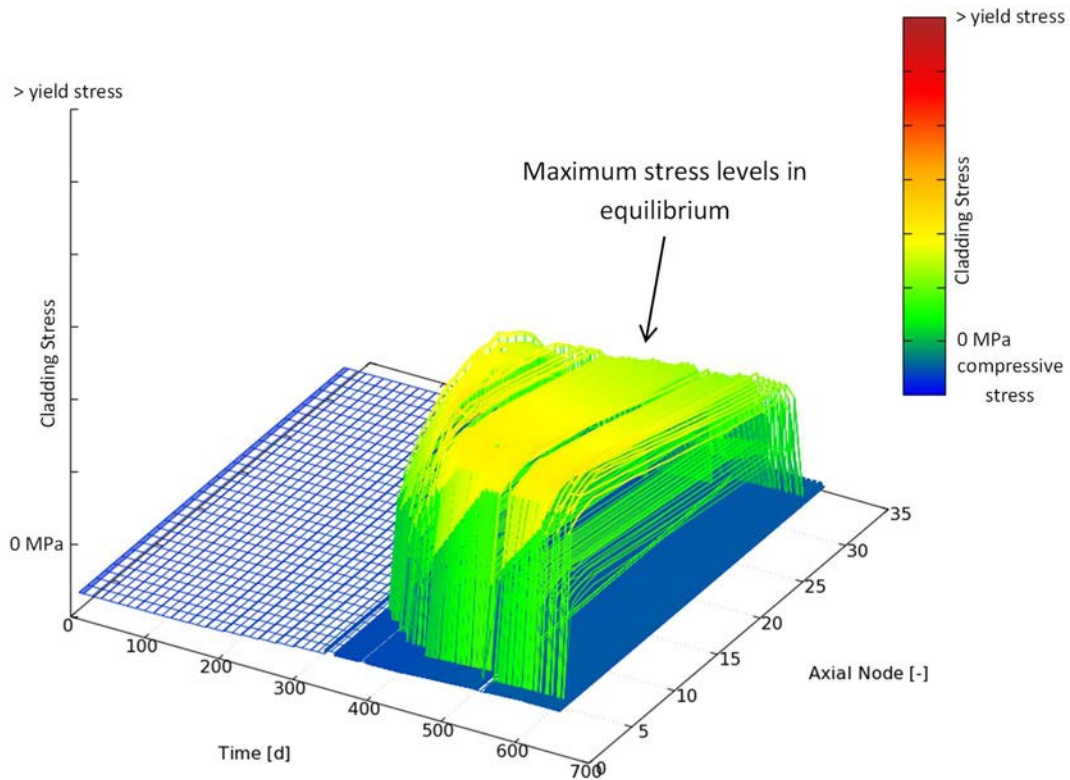


FIG. 9. Cladding stress response of the two annual cycles fuel rod in load-follow operation of a German PWR, calculated with reduced initial gap size to illustrate cladding response in closed gap conditions.

In conclusion, load-follow operations with frequent power cycling is self-limiting with respect to the stress levels. This is not the case for long ELPO durations with significant conditioning of the fuel to low power levels. Here, the maximum stress levels depend on the duration of the ELPO and the ramp rate on return to full power. Furthermore, anticipated operational occurrences during ELPO periods may have to be taken into account, which are reactor design dependent and may impose a need for further restrictions on ELPO duration.

3.2. Base load operation in a BWR with high operating flexibility of the fuel assemblies

For German BWRs, some PCI-related experience has been gained in the past. For fuel rods examined in hot-cell examinations, missing pellet surfaces (MPS) by ceramic chips were observed. Such MPS are known to increase the inner cladding surface stress levels at the chips' position during PCI-relevant loads.

PCI-related fuel rod defects in German BWRs from the past two decades have only been observed for fuel assemblies in their fourth or fifth annual operating cycle at local burnups in the range of about 40-65 MW·d/kg(U). Although, fuel assemblies with less than four annual cycles have been operated on controlled cells in mono-sequence operation in high numbers, no PCI-related defects have been observed for those. About 90% of the PCI-related defect fuel rods have been located in the first outer row of the fuel assemblies, directly adjacent to the control rods.

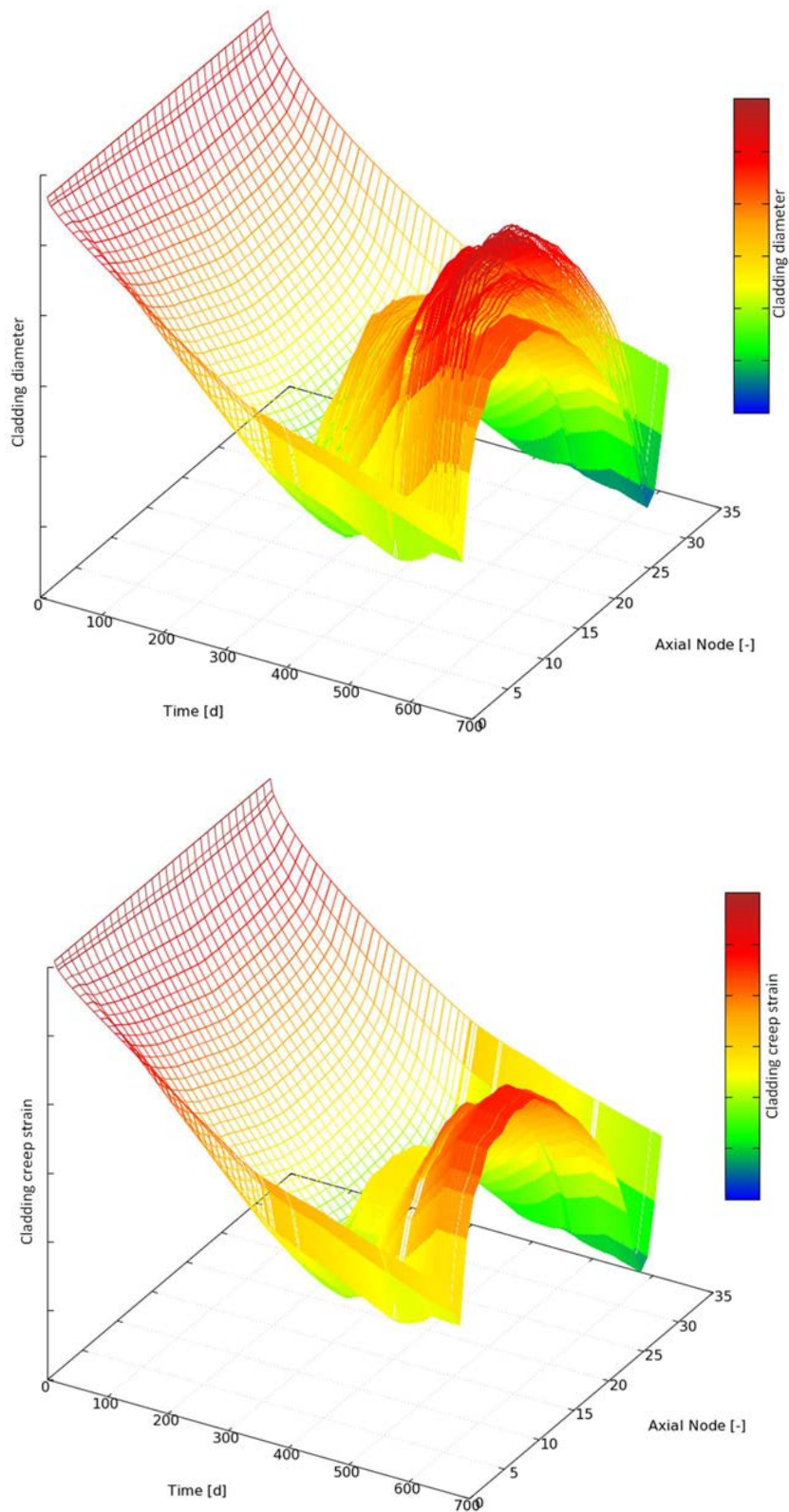


FIG. 10. Cladding total strain (top) and permanent creep strain response (bottom) of the two annual cycles fuel rod in load-follow operation of a German PWR, calculated with reduced initial gap size to illustrate cladding response in closed gap conditions on load-follow operation.

The power history of one fuel rod, located directly in the control rod corner and exhibiting MPS-assisted PCI-failure (confirmed in hot-cell examinations) is shown in Fig. 11. This fuel rod was operated for five operating cycles before pellet design modifications and manufacturing improvements were established to improve pellet

quality by reduction of MPS. During the first two cycles, low power periods occurred as the fuel assembly was placed in controlled cells with sequence-exchange influence. At the beginning of the fifth cycle, the fuel assembly was operated uncontrolled and at approximately one third of the cycle a sequence-exchange put it into controlled conditions. Near the end of cycle, the control rods were withdrawn stepwise at 100% reactor power with typical holding times between subsequent control rod withdrawal steps required by PCI guidelines. During this manoeuvre radiology indicated a fuel rod defect and the control rod withdrawal was stopped. The fuel rod average burnup was about 52 MW·d/kg(U).

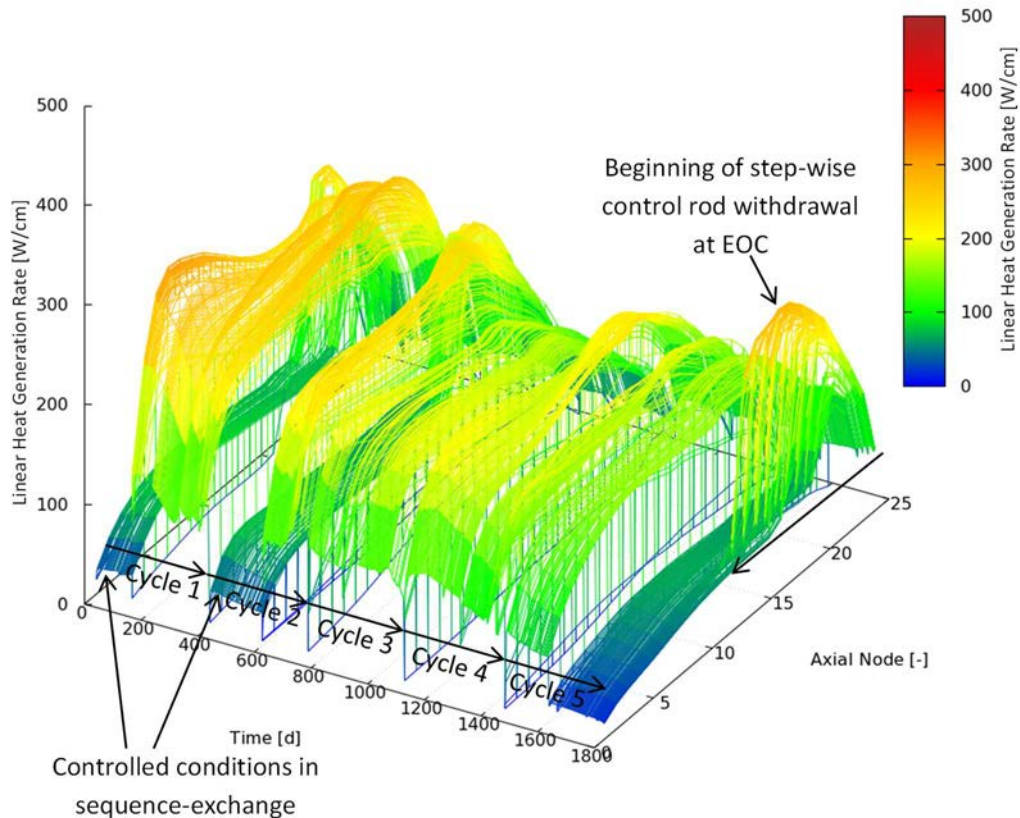


FIG. 11. Power history of a five operating cycles non-linear fuel rod from a German BWR with sequence-exchange operation in its first and second operating cycle and final step-wise control rod withdrawal at full power at EOC (2.5 cm withdrawal length per step).

The same type of calculations as for the PWR load-follow case that was discussed above has been applied considering the re-crystallized non-linear Zry-2 cladding material constitutive laws of the fuel rod. The pellet total strain response according to the calculations is shown in Fig. 12. The increase of the local pellet strain is visibly coherent with the power increase during control rod withdrawal. The calculated stress levels are approaching the yield stress as can be seen in Fig. 13. However, due to the conservative approach using the rigid pellet assumption, the maximum stress levels are supposed to be overestimated in the calculations. This view is supported by hot-cell examination, where some dish filling has been observed indicating that the rigid pellet assumption is too conservative for such load conditions. However, the failure position has been identified at the top of the calculation node directly below the one with the highest calculated stress level.

Another observation from Fig. 13 is that nearly no hard pellet-cladding contact occurs during the first four cycles under these load conditions. Especially, the sequence-exchange operation had no impact on the compressive cladding stress state due to the external coolant overpressure compared to the fuel rod internal pressure. As this type of operation is very similar to an ELPO condition, no influence is expected by typical load-follow operation or ELPO conditions at least in the first four annual operating cycles at comparable power levels. Furthermore, PCI-related loads may occur at the fourth and fifth insertion cycle only, consistent to the observation.

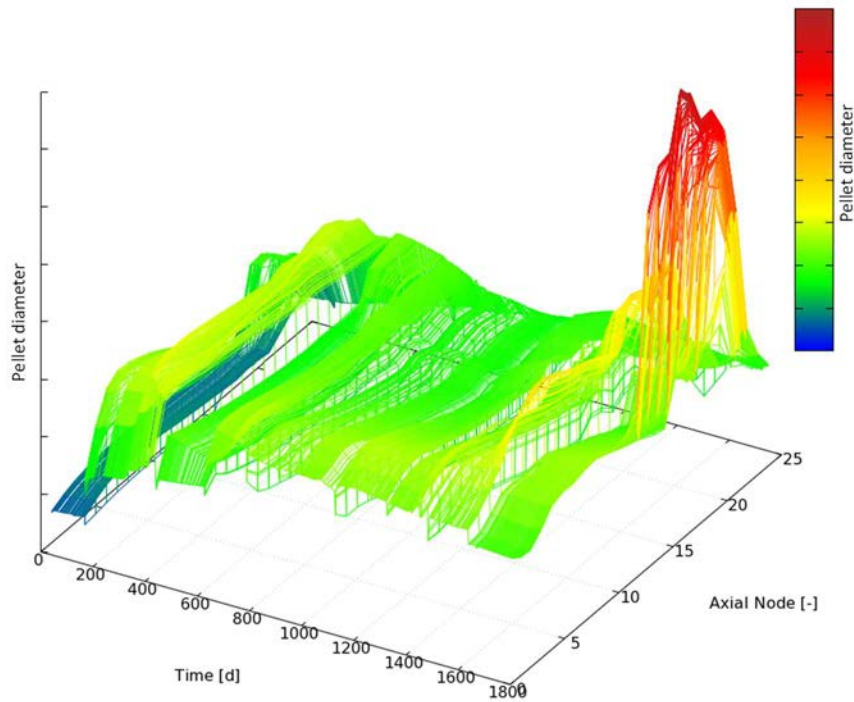


FIG. 12. Pellet total strain response of a five operating cycles non-linear fuel rod from a German BWR with sequence-exchange operation in its first and second operating cycle and final step-wise control rod withdrawal at full power at EOC (2.5 cm withdrawal length per step).

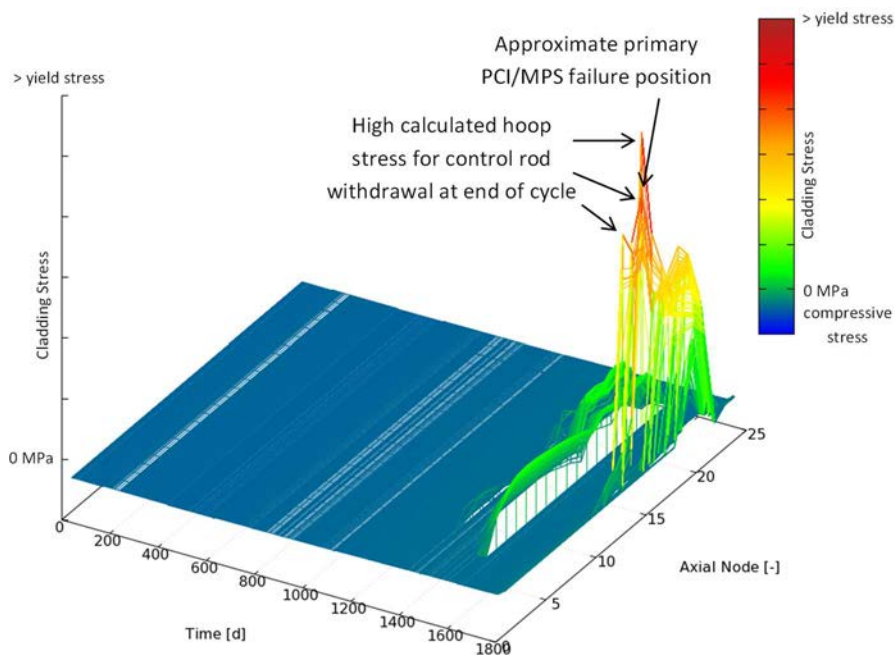


FIG. 13. Cladding stress response of a five operating cycles non-linear fuel rod from a German BWR with sequence-exchange operation in its first and second operating cycle and final step-wise control rod withdrawal at full power at EOC (2.5 cm withdrawal length per step).

In Northern European BWRs, the power levels reach LHGRs in the order of 450 W/cm at begin of life and may still reach 400 W/cm for control rod withdrawal operations in their third annual operating cycle. These power levels are considerably higher than the shown experience in Fig. 11 and may lead to high cladding stress already

in the third operating cycle during control rod withdrawal. PCI operating and manoeuvring rules are applied to restrict ramp rates and subsequent control rod withdrawal steps by holding times to reduce the stresses in the cladding and prevent PCI failures.

4. DISCUSSION

4.1. Flexible operation in PWRs

Extensive operation experience for operation with day-night and weekly load-follow as well as with low power periods during other low power demand times is available. Analyses show self-limiting stress conditions for the full power periods for such operation with low power durations for several hours up to some days. No risk for PCI-related fuel rod failures are seen for such conditions even for several consecutive cycles, which is supported by the operating experience. Fuel shuffling during outages can cause significant stress increase during reactor start-up leading to higher stresses especially in high duty plants.

Longer durations of ELPO may considerably increase the stress levels and would need a limitation in terms of allowed ramp rates upon return to full power or a limitation in the duration. Furthermore, different reactor designs or regulatory constraints may require more detailed analyses.

4.2. Flexible operation in BWRs

Typical load-follow operation in BWRs is basically less demanding with respect to PCI-related loads than the conditions during typical control rod withdrawal operations at 100% reactor power plants with fine motion control rod drives. Consequently, the usual manoeuvres seen in every cycle are the more limiting load cases compared to typical load-follow operation. However, continuous sequence-exchange operation for a lot of BWRs worldwide provides broad basis for PCI-free operation in conditions similar to load-follow operation.

Some influence of flexibility regarding the burnup states of fuel assemblies in controlled cells (i.e. number of operating cycles) is given. Especially fuel assemblies with burnups above 40 MW·d/kg(U) show an onset of gap closure at low power levels and tends to reach considerably increased stress levels even for moderate power increase during control rod withdrawal operation at 100% reactor power (e.g. as given in Fig.11). For core loading concepts as scatter loading, where fuel assemblies of different operating cycles may be in the same controlled cell, this can lead to high potential PCI-relevant loads of the higher burnup fuel. Less flexible loading concepts like the controlled cell core (CCC) with predefined medium burnup fuel assemblies of the same number of operating cycle may have some advantage with regard to lower power levels compared to fresher fuel but can still reach high power levels for modern fuel assembly designs with potential PCI-relevant loads.

A high impact is seen from the cycle length (cf. Fig. 2). Considerable power increase for the control rod withdrawal operations in mono-sequence conditions are to be expected for longer cycles. However, one German BWR has been operated with 1.5 year cycles in mono-sequence operation for more than a decade without any PCI failures observed.

From a more general point of view, different control rod operating strategies as sequence-exchange or mono-sequence operation (the latter restricted to BWRs using fine motion drives) have both some disadvantages. The sequence-exchange strategy exhibits short time frames of reduced power operation for the sequence-exchange. The mono-sequence type operation tends to higher local power levels with increased PCI loads, most likely based on the Pu built-up during controlled conditions and shift of the power peak to the top part of the reactor towards the end of cycles. Contrary, the role of long time (e.g. more than 300 days for typical annual mono-sequence cycles) on low power leading to some conditioning on these low power levels seems to be of less importance for the BWRs up to their fourth annual operating cycle. The onset of pellet-cladding contact is established somewhat later in life even for full power (see stress levels in Fig. 13 and compare for power history in Fig. 11). Hence, both types of control rod strategies have some continuous conditioning of the fuel to lower power levels.

5. CONCLUSIONS

In conclusion, usual design cases from base-load operation tend to show higher PCI relevant cladding loads than continuous load-follow operation. The only exception are long durations of ELPO conditions, where high PCI loads can be achieved. This is valid for both, BWRs and PWRs.

Flexibility in core loading concepts or control rod manoeuvre strategies in BWRs show an impact for increased PCI-relevant loads depending on the details. A general trend for an increase of loads of control rod withdrawal in mono-sequence operation with increasing cycle lengths is seen. The influence of differences in scatter or CCC loading concepts depend on the details and cannot be generally answered. Sequence-exchange reduces the maximum loads for final stepwise control rod withdrawal in fine motion drives compared to mono-sequence operation.

ACKNOWLEDGEMENT

Data provided by courtesy of Rheinisch-Westfälische Elektrizitätswerke (RWE) und Energie Baden-Württemberg Kernkraft (EnKK).

REFERENCES

- [1] INTERNATIONAL ATOMIC ENERGY AGENCY, Non-BaseLoad Operation In Nuclear Power Plants: Load Following And Frequency Control Modes Of Flexible Operation, IAEA Nuclear Energy Series No. NP-T-3.23, IAEA, Vienna (2019).
- [2] SALNIKOVA, T., MOROKHOVSKYI, V., RUDOLPH, J., Transfer of Concepts for Flexible Operation to Different Plant Types, AMNT 2017, Berlin, May 2017.
- [3] KUHN, A., KLAUS, P., Improving Automated Load Flexibility of NPPs with ALFC VGB, Power Tech. 5 (2016).
- [4] LUDWIG, H., SALNIKOVA, T., WAAS, U., Int. J. Nucl. Power 55 [8/9] (2010).
- [5] Kernkraftwerke in Deutschland Betriebsergebnisse für 2007, atw – Internationale Zeitschrift für Kernenergie (2008).
- [6] Kernkraftwerke in Deutschland Betriebsergebnisse für 2008, atw – Internationale Zeitschrift für Kernenergie (2009).
- [7] Kernkraftwerke in Deutschland Betriebsergebnisse für 2009, atw – Internationale Zeitschrift für Kernenergie (2010).
- [8] Kernkraftwerke in Deutschland Betriebsergebnisse für 2010, atw – Internationale Zeitschrift für Kernenergie (2011).

SAFETY REQUIREMENTS FOR PELLET-CLAD INTERACTION IN FRANCE — NEW APPROACH DEVELOPED BY EDF

A. BERNARD, J. ZEGHDAOUI, L. BARBIÉ, T. KEITH,
M. RAUTENBERG, N. WAECKEL
EDF,
Lyon, France
Email: aurelien.bernard@edf.fr

Abstract

The French Nuclear Safety Authority requires EDF to demonstrate that no fuel will fail by SCC-PCI (stress corrosion cracking – pellet-clad interaction) during any AOO (anticipated operational occurrence). Because of the large part of nuclear energy in the French energetic mix, the French nuclear power plants (NPPs) have to be capable of doing flexible operations, particularly including frequency control and daily load following. In addition, to deal with potential operational events, the NPPs operators require at least 30 days of ELPO (extended low power operation). Finally, in order to optimize the long term electricity production on the whole fleet scale, EDF sets up various core patterns for each NPP type. These specific operational conditions have to be justified with an appropriate approach. PCI studies prevent the SCC-PCI failure by two means:

- Adjustment of the reactor protection thresholds;
- Definition of the PCI Operating Technical Specifications.

It is interesting to mention that, despite these specific operational conditions and rather fast start-up rates, no SCC-PCI failures have been observed in EDF NPPs over more than 1600 reactor-years of experience. This good result is likely due to the EDF's SCC-PCI design approach which includes specific constraints on the manufacturing process and on the operational conditions. To fulfil these safety requirements, specific SCC-PCI analyses, presented in this paper, are performed and cover each operating mode of the reactor. The studies relate to the whole core, as SCC-PCI failure risk is local. A SCC-PCI failure criterion, called Technological Limit, must be defined, based on experimental ramp tests. Two types of approach are devoted to SCC-PCI studies. First, a specific methodology called MIR (Renovated PCI method) had been developed in cooperation with FRAMATOME. This methodology is based on neutronics (3D kinetics calculations) and thermal mechanical calculations. Since the MIR method is time consuming and focused on a single reference reload pattern, a new approach has been developed to deal with various core patterns and to reduce the calculations time. The main changes are:

- Statics neutronics calculations instead of kinetics calculations;
- Decoupled calculations between neutronics and thermal mechanics.

For a same reload pattern, these simplifications reduce the computation time but lead to smaller manoeuvrability margins. This approach is well suited to assess the impact of core patterns variability on SCC-PCI margins and to perform sensitivity analysis.

1. INTRODUCTION

French nuclear power plant (NPP) fleet includes 58 standardized pressurized water reactors (PWRs) owned by EDF, which generates 60 to 75% of the annual electric production. French NPP fleet should comply with the demand of the grid, which leads to a significant plant manoeuvrability operation such as frequency control, daily load follow, extended low power operations (ELPO).

Load follow operation in French NPPs in the 1980s was subjected to requirements from the French Nuclear Safety Authority. One of the regulatory requirements was to maintain the integrity of the fuel rod against pellet-clad interaction (PCI) failure during anticipated operational occurrences (AOOs), i.e. PCC-2 events. Since then in France, safety requirements have been extended to cover no fuel failure by PCI during normal operations as well as during PCC-2.

This paper is intended to present the PCI from the aspects of French utility. First, the paper gives an overview of the PCI failure criterion developed for EDF PWRs. The paper provides with the specific methodology developed by EDF and FRAMATOME, which accounts for the PCI risk in the operational states. The paper provides and discusses the new static approach that is currently investigated to fulfil the recent Nuclear Safety Authority requirements (impact of the fuel loading pattern variability).

2. SCC-PCI FAILURE CRITERION – TECHNOLOGICAL LIMIT

PCI failures caused mainly by stress corrosion cracking (SCC) of the Zr alloy is usually observed as a millimetre size axial crack. The PCI failure results in the contamination of the coolant by fission products.

The goal of this paragraph is to present the approach used in France to assess the PCC-2 PCI performances of a fuel product. This assessment is based on a mechanical criterion, the so-called Technological Limit, derived from the analysis of an experimental database including several failed and non-failed power ramps. This analysis is based on post-irradiation examinations (PIEs) interpretations and on ramp simulations with a fuel performance code.

2.1. Experimental procedure

Samples are obtained from rods irradiated in commercial PWRs. Samples can be of two kinds:

- A rodlet refabricated from a standard rod span, and pressurized at the pressure of this rod after irradiation;
- A segment removed from a segmented rod.

Tests consist in power ramps performed in a material testing reactor (MTR). A particular care is given to limit the variation of the experimental parameters, in order to compare each power ramp on a steady basis. The main parameters that are controlled during the ramps are summarized in Table 1. As shown in this table, the tolerance on several parameters, such as temperature and power rate, are very narrow. It enables a rationalization of the modelling rules during the simulation step and makes the comparison of the ramp results easier. Furthermore, regarding cladding temperature (which has a significant impact on clad creep-relaxation properties); 342°C corresponds to the state of nucleate boiling of water at 150 bars. Thus, by ensuring a forced convection regime with nucleate boiling at the clad surface, the operator can control the outer clad temperature very precisely and uniformly along the axial and radial directions.

On the other hand, parameters like water chemistry or neutron flux, are not mentioned in Table 1 as power ramps are short-term experiments for which clad corrosion and irradiation creep do not play a significant role.

To cover the full ranges of operational burnups, maximum powers or conditioning powers, a minimum of 10 to 15 power ramps (according to the number of failed ramps) is needed for each fuel type.

TABLE 1. MAIN INPUT PARAMETERS FOR SCC-PCI POWER RAMP USED IN THE FRENCH APPROACH

Parameter	Required value
Burn-up of Rodlet	25 GWd/tU – 55 GWd/tU
Conditioning power	150 W/cm – 250 W/cm during more than 12 h
Maximum power	350 W/cm – 550 W/cm
Power rate between conditioning and max. power	100 W/cm/min
Holding time at maximum power	In case of failure: no hold time. If no failure: 12 h
Pressure	145 – 155 bars
Outer clad temperature	For P>300 W/cm: 342°C

2.2. Post-irradiation examinations and code calibration

PIEs are performed on ramped rodlets for two main reasons:

- To confirm the validity of the ramp by checking that there was no experimental artefact and, in the case of failed ramps, by identifying evidences of I-SCC;
- To provide experimental data for use in calibrating calculation models incorporated in the fuel performance analysis code.

This implies that visual inspection, eddy current testing profilometry measurements and inner pressure measurements by puncture are systematically done on ramped rodlets. Optionally, additional examinations (ceramography, gamma scanning, neutron radiography, metallography, etc.) can also be carried out.

The fuel performance analysis code used to derive the technological limit from the ramp test data has to be the same as the one used to perform the safety case analysis based on this Technological Limit. Thus, this code has to be qualified for both normal operations simulation (to simulate the irradiation of the fuel rod prior to ramp testing) and PCC-2 transients (to simulate the power ramp test). The two fuel performance analysis codes approved by the French regulators for such studies are CYRANO3 [1], developed by EDF, and COPERNIC [2], developed by FRAMATOME. Beyond the usual experimental data which are used to calibrate and validate the calculation tool for normal operations, specific experimental results have to be taken gathered to validate the code in transient (i.e. thermal creep law, for each cladding material, has to be assessed after the interpretation of hardening-relaxation tests).

The validation of a fuel performance code in PCC-2 conditions is done through a comparison of simulation with two sets of experimental values:

- Post-ramp diameter increases, obtained from post-ramp profilometries;
- Ramp-induced fission gas release, obtained after rodlet puncturing.

2.3. SCC-PCI Technological Limits of the fuel products used in French PWRs

The following fuel products are used on French PWRs:

- M5, zircaloy-4, ZIRLO and Optimized ZIRLO claddings;
- UO₂, MOX and UO₂-Gd₂O₃ fuel pellets;
- Enriched natural Uranium and re-enriched reprocessed Uranium.

Power ramps performed on MOX fuel have shown that SCC PCI performances of MOX fuel are significantly higher than those of UO₂ fuels. Regarding gadolinium fuel rods, neutronic studies show UO₂-Gd₂O₃ rods are bounded by UO₂ fuels during the entire irradiation in a commercial reactor.

As a result, SCC-PCI studies on UO₂ fuel are sufficient to cover all the other fuel products that might be present in the reactor cores (e.g. MOX fuel or UO₂-Gd₂O₃ fuel).

From the UO₂ EDF power ramps database, a Technological Limit can be determined for each fuel product, from an analysis of the simulation results. An example of such analysis is shown on Fig. 1. zircaloy-4, ZIRLO and Optimized ZIRLO are analyzed together because experimental results showed that:

- The sensitivity to the SCC-PCI risk can be expressed with the same mechanical parameter (the hoop stress) for these three alloys;
- The improvement of ZIRLO and Opt. ZIRLO SCC-PCI performances compared to those of zircaloy-4 is not valued in the SCC-PCI studies.

Therefore, for zircaloy-4, ZIRLO and Optimized ZIRLO, a single Technological Limit value, expressed as an inner clad hoop stress, is considered.

For M5, a saturation of the computed hoop stress has been observed for power levels below the lowest power leading to failure. That is why the hoop stress alone cannot be used as a discriminating parameter for failure prediction in the case of M5 cladding. Instead, strain energy density (SED) has been chosen as the discriminating parameter.

3. RENOVATED SCC-PCI METHOD (MÉTHODE IPG RÉNOVÉE - MIR)

3.1. General information about the MIR approach

An analysis of the risk of clad failure by SCC-PCI must guarantee the integrity of the fuel rod during any anticipated operational occurrences (AOOs) by checking the adjustment of the reactor protection thresholds.

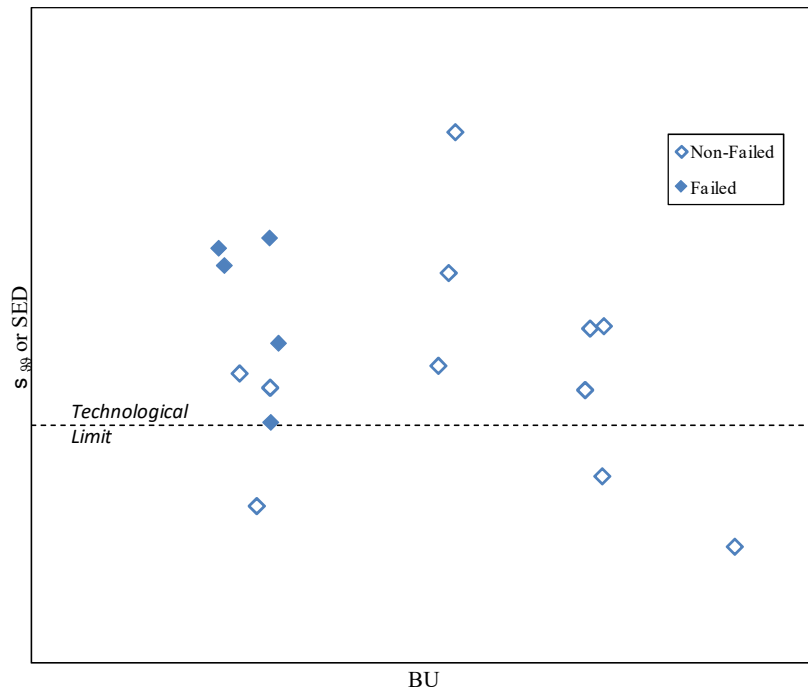


FIG. 1. Technological Limit assessment from ramp simulation results of a given cladding.

Indeed, any transient of power likely to lead to failures of rods must be stopped by a SCRAM before the first failure occurs on one rod. This is why EDF and FRAMATOME have developed fuel performance codes and analysis methods of the risk of clad failure by SCC-PCI, for all the fuel rods of the core, during any PCC-2.

The study is divided into five parts, detailed in the continuation of this paragraph:

- (a) Generation of conditioning power histories.
- (b) Simulation of the initial conditions of the PCC-2.
- (c) Simulation of the PCC-2 transients.
- (d) Thermomechanical evaluation of PCI risk for base load operation, frequency control and load follow, ELPO de-conditioning or return to full power after ELPO re-conditioning, which allows defining PCI operating technical specifications (OTSs).
- (e) Modification of the reactor protection thresholds (not presented here).

Comparing with other PCC-2 PCI methodologies used abroad, this kind of study requires more human and computing resources. Only a generic study on a prototypical reference core reload pattern is carried out. The objective is:

- To define the protection thresholds for PCC-2 operations;
- To limit the manoeuvrability of the plant in PCC-1 operations (ELPO, load follow, etc.) at a level that can guarantee the absence of PCI failure if a PCC-2 event occurs.

Because of their complexity, MIR studies cannot be duplicated rapidly when the impact of a change of the input data (evolution of the fuel management for example) has to be quantified.

Within the frame of the SCC-PCI methodology review, the French Authority of Nuclear Safety asked EDF to complement the demonstration to include the potential impact of core reload pattern variability on the outcomes of the analysis. As a result, EDF developed a new methodology to address this request. In this context, a variation of the fuel loading pattern refers to any deviation from the reference loading pattern, in term of number and/or type of fuel assemblies.

3.2. Generation of conditioning power histories

For the thermomechanical analysis, the power history of each rod at the beginning of the AOO is needed. The local thermomechanical state of the rod depends on its history. It is thus necessary to follow each rod from its new fuel loading into the core until the beginning of the transient. It enables to take into account the cycles which precede that from which the transients are analyzed.

The power histories associated to each rod are generated under various conditions:

- Base load operation at full power;
- Extended Low Power Operation (ELPO) with inserted RCCA;
- ELPO with extracted RCCA.

3.3. Simulation of the initial conditions of the transients

The PCC-2 transients are initiated from a conditioning state obtained after normal operations simulation. The initial conditions are selected so as to maximize the local power increase.

For each transient, the initial conditions are characterized by the burn-up, the power level, the power axial distribution, the Xenon axial distribution, the position of the regulation groups, the Boron concentration. These assumptions can vary depending on the transient under investigation.

3.4. Simulation of the PCC-2 transients

The behaviour of the whole core is simulated by taking into account the regulation and the protection systems. The neutronic behaviour of the core is modelled kinetically. The fine kinematic power distribution in the entire core as a function of time is also provided with an uncertainty factor.

The transient simulations include simulations from the initial states described in the previous paragraph at several moments in the irradiation cycle till transients.

The conventional PCC-2 power transients considered to be restrictive for the SCC-PCI failure risk (i.e. leading to fastest and strongest local power increase) are:

- Excessive increase in secondary system flow;
- Uncontrolled bank withdrawal at power;
- Control rod drop.

The initial thermo-hydraulic parameters are taken at their nominal value without uncertainty. The regulations are taken into account only if they have unfavourable consequences. The limitation systems are not taken into account.

3.5. Thermomechanical evaluation of SCC-PCI failure risk

The clad failure risk during the PCC-2 transient is estimated by comparing the evaluation parameter calculated by a fuel behaviour analysis code with the Technological Limit (see Section 2).

The fuel code used for this study has to be the same as the one used to determine the Technological Limit. It has to be licensed by the Safety Authorities.

The evaluation of the clad failure risk consists in explicit thermomechanical calculations: the evolutions of stress or SED in the clad are calculated according to the applied local power history. The PCI margin of a rod is defined as the difference between the maximum simulated stress (or SED) and the Technological Limit. Minimal PCI margins are assessed in every fuel rod for various operational states (base load operation, ELPO, return to base load operation after ELPO, frequency control and load follow).

3.5.1. Base load operation

The study consists in the sequence of an irradiation under base load operation followed by a PCC-2 transient. Each mesh of each rod shows specific pre-transient thermomechanical characteristics evolving with the burn-up.

3.5.2. ELPO and reconditioning

During an ELPO, the fuel rod is subjected to ‘deconditioning’ due to the gap closure between the fuel pellet and the clad at a prolonged low power operation. For given situations, this type of operation should be restricted so that SCC-PCI margin exists. An increase of power after an ELPO also leads to a ‘reconditioning’. The ELPO analysis should account for the limiting PCC-2 transients that occur at various different times during an ELPO. It should also include the limiting PCC-2 transient that occurs after returning to the nominal power (from 1 to 100 days). Deconditioning and reconditioning, and associated evolution of PCI-SCC margins are illustrated in Fig. 2.

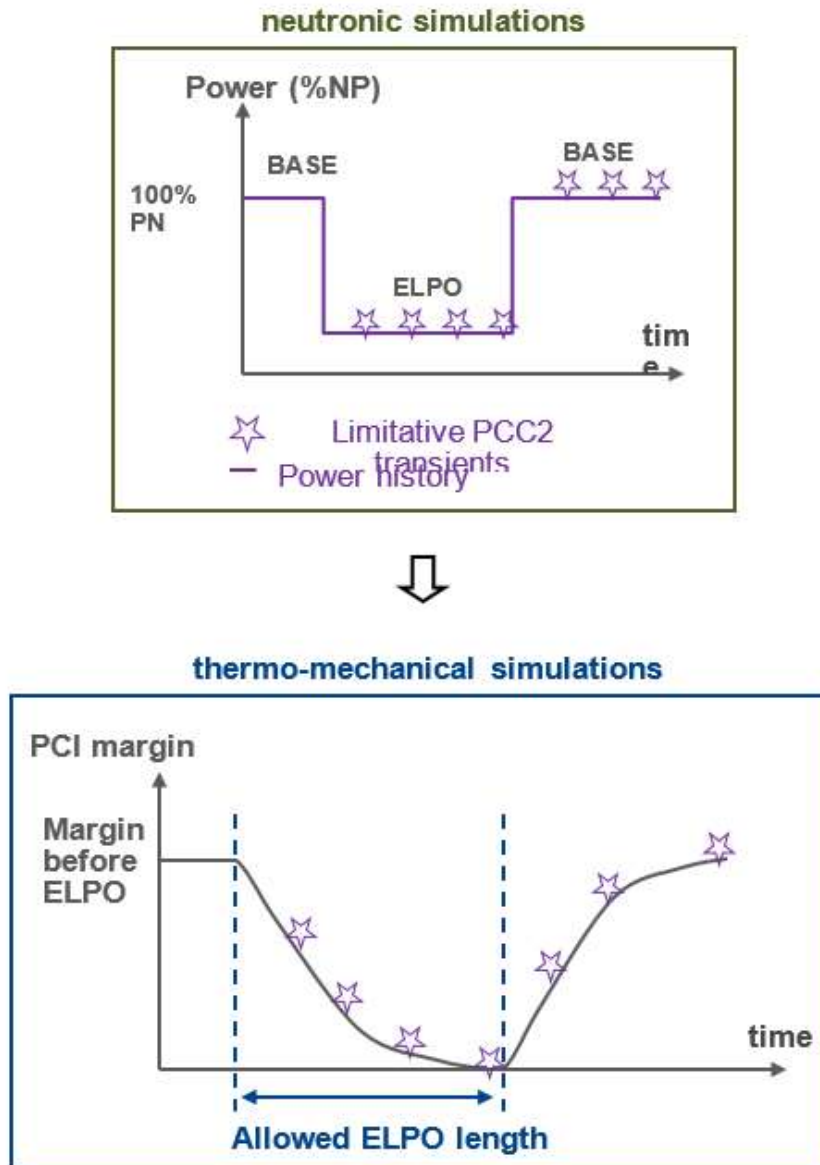


FIG. 2. De-conditioning (ELPO) and re-conditioning (base load operation) simulation.

The effect of the reactivity which appears at the time of the passage at lower power can be ensured by Boron dilution / concentration or by RCCAs. These two strategies of ELPO management, i.e. with extracted or inserted RCCAs, are studied.

3.5.3. Operation in frequency control and load follow

Non-baseload operation like load following and frequency control may lead to ‘deconditioning’ of some fuel rods. Such non-baseload operation is associated to smaller margins than the base-load operation. The comparison of PCI-SCC margins between the baseload and non-baseload operations assesses the PCI margins for load follow and frequency control operations. In the calculation, the fuel performance code is used. Typical power histories for load following and frequency control with respect to the baseload operation are illustrated in Figs 3 and 4.

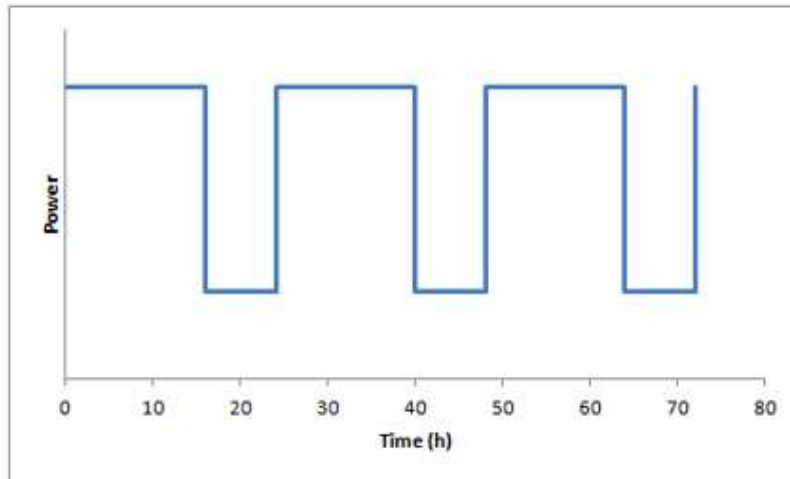


FIG. 3. Load follow simulation.

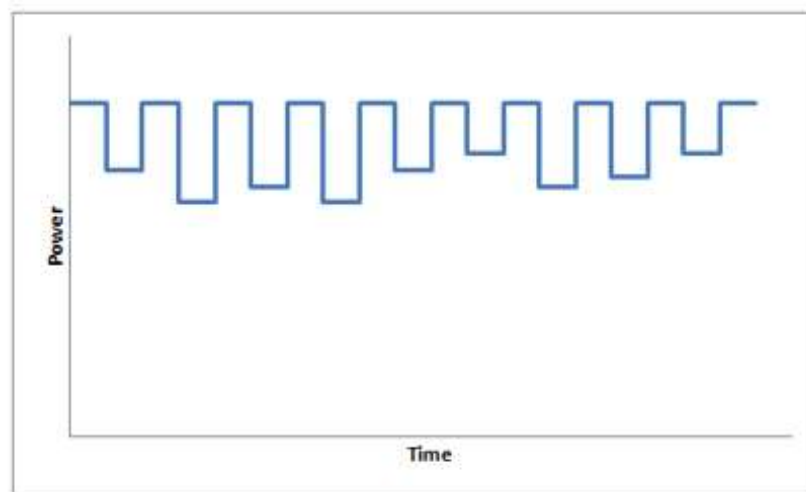


FIG. 4. Frequency control simulation.

4. NEW STATIC APPROACH DEDICATED TO CORE LOADING PATTERNS VARIABILITY

4.1. Description of the static approach

This approach is divided in two steps:

— Step 1 - Evaluation of the PCI margins during PCC-2 transients for one cycle:

- Generate pre-transient operation conditions using neutronic calculations;
- Simulate post-transient operation conditions using neutronic calculations. This stage generates the PCC-2 3D power distributions (PPCC-2);
- Evaluate the thermomechanical SCC-PCI failure risk for various operation conditions:

- ⇒ Reference operations conditions (base load operation, frequency control and load follow operations);
- ⇒ Extended low power operation (ELPO).

This stage generates the 3D maximum allowable power without clad SCC-PCI failure ($P_{\text{allowable}}$) for each conditioning state;

- Calculate the SCC-PCI margins to failure.
- Step 2 - Coverage of the variability of the fuel reload pattern (i.e. deviating from the reference equilibrium cycle):
- Quantify the impact of the variability of the fuel reload patterns with respect to the SCC-PCI margin (comparison between the variable reload patterns and the reference equilibrium cycle) by sizing a specific “variability bias”;
 - Determination of the allowable ELPO durations covering the variability of the fuel loading patterns, through a penalization by the variability bias of the kinetics transients of the MIR study.

4.2. Generation of conditioning power histories

For the thermomechanical analysis, power history should be determined at each point of the core before the beginning of the transient.

The local thermal mechanical conditioning of the rod depends on the power history. The, each fuel rod should be simulated from its loading into the core until the beginning of the transient.

The conditioning power history related to each rod is generated for various operating conditions:

- Base load operation at full power;
- ELPO with inserted RCCA;
- ELPO with extracted RCCA.

4.3. Simulation of the pre-transient operational conditions

The PCC-2 transients are initiated starting from operational situations. They are defined such as they maximize the local power increase during the incidental transient. For each transient, the pre-incidental states are characterized by the burnup, the power level, the axial power distribution, the axial xenon distribution, the position of RCCA, the RCCA control mode and the boron concentration.

4.4. Simulation of the post-transient operational conditions (PCC-2 transients)

The PCC-2 states are simulated using a 3D neutronic code. Conservative decoupling assumptions are made in the static neutronic calculations to cover every PCC-2 situations likely to be reached by the Reactor Pressure Vessel (RPV). These decoupling make it possible not to model explicitly the primary circuit.

The 3D neutronic code provides the fine power distribution on the entire core for each PCC-2 state. These PCC-2 states are simulated starting from a high number of pre-incidental situations.

The restrictive PCC-2 situations are those leading to the strongest and fastest local power increases.

Having taken into account a single failure, the first automatic SCRAM is taken into account.

4.5. Thermal mechanical evaluation of PCI risk

The risk of clad failure by PCI is assessed based on thermal mechanical simulations of a fuel rod under an analytical power transient. An analytical power transient consists in simulating a linear power increase representative of the PCC-2 transients. Also, in consistency with the experimental power transient defining the Technological Limit and with the kinetics of the PCC-2 transients penalizing in terms of PCI risk, the rate of this analytical transient is chosen equal to 100 W/cm/min.

For a given thermomechanical conditioning, the simulation of this analytical transient is done to determine the allowable power $P_{\text{allowable}}$ corresponding to the power level leading to the reaching of the Technological Limit. $P_{\text{allowable}}$ is evaluated with a fuel performance code for each mesh of the core.

$P_{allowable}$ 3D maps of the core are established for various operating conditions:

- Base load operation;
- Extended Low Power Operation (ELPO).

4.5.1. Base load operation

This simulation is based on an irradiation under base load operation followed by an incidental transient.

The conditioning step makes it possible to determine the behaviour of the rod and more particularly of the pellet-clad gap closure before the transient. Conditioning is characterized primarily by the pellet-clad gap which depends on the inwards creeping of the clad and the outward swelling of the fuel pellet.

Each rod and each assembly show specific pre-incidental thermomechanical characteristics evolving with the burnup.

4.5.2. Frequency control and load follow

Operation in frequency control and load follow are taken into account through bounding penalties, such as in the MIR method (see § 2.5.3).

4.5.3. ELPO de-conditioning

In the framework of the PCI studies, the fuel conditioning under ELPO is carried out for several values of low power levels in order to cover all the configurations likely to be met during operation.

The resumption of the reactivity effects which appear during ELPO can be ensured by soluble boron (extracted RCCA) or by the RCCA (inserted RCCA). These two strategies are studied.

In practice, the simulation of an analytical transient after the modelling of a given ELPO duration makes it possible to determine the 3D allowable power associated to this de-conditioning.

4.6. Calculation of PCI margins to failure

Considering a given cycle, for each state of conditioning and each type of incident, the PCC-2 powers are compared with the allowable powers for the whole core.

The margin to failure (in W/cm) is thus obtained by comparison of the distribution of PCC-2 power with the distribution of allowable power.

4.7. Quantification of the variability of the reloads

PCI margins to failure are calculated on a representative range of variability cycles and on the reference equilibrium cycle for the various states of conditioning.

The maximum variation obtained on every situation is retained as the “variability bias”.

4.8. Determination of allowable ELPO durations covering the variability of the cycles

The variability bias is integrated as a penalty into the kinetic transients of the MIR study used to determine the allowable ELPO durations. This penalty is uncoupled with the time, the transient, the power level, the conditioning state or the studied cycle. The allowable ELPO durations are then determined by a new MIR study based on the penalized 3D PCC-2 power histories.

5. COMPARISON OF THE TWO PCI APPROACHES

5.1. Specificities of the new static approach

Some basic principles have been applied to reduce the duration of the study:

- Static neutronic simulation;
- Decoupling of the neutronic and thermomechanical simulations;
- Analytical power transient with a constant speed (100W/cm/min) applied for the thermomechanical study.

There are some counterparts to these simplification principles:

- Penalization of the PCC-2 transients;
- Reduced margins in comparison with the standard MIR method.

A new MIR study, with penalized PCC-2 power histories, can be required after the assessment of the variability bias

5.2. Comparison of the PCI Approaches

Three approaches are compared and examples of allowable durations of ELPO are reported in Table 2:

- Reference MIR study;
- Static new approach, with a direct determination of the allowable durations of ELPO³;
- Static new approach dedicated to the measurement of the impact of the variability, by sizing a with a penalty applied to MIR reference study.

Each approach is characterized as summarized in Table 3. The third approach is the heaviest, but it is the only one which allows taking variability into account. The first one maximizes the PCI margins whereas the second one minimizes the time and size of the study. Each one should then be used according to the main objective of the study (PCI margins, cost of the study, variability).

TABLE 2. EXAMPLE OF MINIMAL ALLOWABLE ELPO DURATION FOR THE MIR APPROACH, THE STATIC APPROACH WITH DIRECT DETERMINATION OF ALLOWABLE ELPO DURATION AND THE MIXED APPROACH WITH DEFINITION OF A VARIABILITY BIAS APPLIED TO MIR CALCULATION

Method	Minimal allowable ELPO duration	Loss compared with MIR duration
MIR	80 days	/
Static approach	54 days	-32%
Mixed approach for variability	42 days	-47%

TABLE 3. COMPARISON BETWEEN THE MIR APPROACH, THE STATIC APPROACH WITH DIRECT DETERMINATION OF ALLOWABLE ELPO DURATION AND THE MIXED APPROACH WITH DEFINITION OF A VARIABILITY BIAS APPLIED TO MIR CALCULATION

Method	PCI margins	Cost of the study	Variability
MIR	Maximized	Expensive	No
Static approach	Reasonable loss / MIR (for one plan)	Optimization of the cost / MIR	Possible (by studying several plans)
Mixed approach for variability	Consequent loss / MIR	Very expensive (MIR study + 1 static approach / variability plan)	Yes

6. CONCLUSIONS

To fulfil the French safety requirements, specific SCC-PCI analyses, presented in this paper, are performed to cover each operational condition of the French Nuclear Power Plants. A SCC-PCI failure criterion, called Technological Limit, has been defined based on the analysis of power ramp tests. The experimental and numerical approaches used to obtain this Technological Limit have been described in this paper.

Two types of approaches are devoted to SCC-PCI studies. First, a specific methodology called MIR (Renovated PCI method) has been developed in co-operation with FRAMATOME. This methodology is based on neutronic (3D kinetics calculations) and thermal mechanical calculations. Since the MIR method is time consuming and focused on a single reference reloading pattern, a new approach has been developed to deal with

³ To obtain the allowable ELPO duration, steps 4.5 and 4.6 are repeated until the predefined ELPO duration lead to minimal PCI margin. Steps 4.7 and 4.8 are not realized in this case.

various core loading patterns and to reduce the calculation time, based on statics neutronic calculations instead of kinetics calculations and decoupled calculations between neutronic and thermal mechanics.

The MIR method and the static approach have been described and compared in this paper. Using MIR method allows maximizing the PCI margins whereas using the static method allows minimizing the cost of the study. The combination of the two approaches allows assessing the impact of core loading patterns variability on PCI margins.

REFERENCES

- [1] LARGENTON, R., THOUVENIN, G. "CYRANO3: the EDF Fuel Performance Code – Global Overview and Recent Developments on Fission Gas Modelling". Paper presented at the LWR Fuel Performance Meeting – Top Fuel 2014 – Sendai, Japan, Sept. 14-17, 2014.
- [2] GARNIER, Ch. et al., "Validation of Advanced Fuel Performance Code on AREVA Global Database up to 100 GWd/tM", Paper presented at the LWR Fuel Performance Meeting – Top Fuel 2009 – Paris, France, Sept. 6-10, 2009.

FLEXIBLE OPERATION FOR FULL SERVICE TO THE GRID FEEDBACK FROM EDF EXPERIENCE

P. PAULIN
EDF,
Lyon, France
Email: philippe.paulin@edf.fr

Abstract

This paper describes the main aspects of pellet-clad interaction assisted by stress corrosion cracking (SCC-PCI) management and feedback from operation experience of EDF nuclear power plants. It also shows examples of industrial needs regarding manoeuvrability and operation at intermediate power. These operational requirements have to be met by fuel rod performances regarding SCC-PCI behaviour.

1. BRIEF RECALL OF PCI RISK ASSESSMENT FOR EDF FLEET

The risk of SCC-PCI failure of the fuel cladding was not assessed in the initial Safety Analysis Reports (SAR) of EDF plants.

The only topic mentioned in the original operation technical specifications (OTS) is related to pellet-clad mechanical interaction (PCMI). Limitations during the power increase after a refuelling outage (with fuel assembly handling) are imposed. The maximal load increase gradient is 3% NP/h above 15% NP, as long as the minimal cumulated time during the last week at a given power level is less than of 72 hours. The purpose of this requirement is mainly to mitigate the effects of pellet surface "sharp edges", which are potentially aggressive towards the clad inner wall.

The SCC-PCI risk in operation has been gradually taken into account by EDF, in two steps:

- first, in the mid-eighties, for normal operation (category 1), especially from the beginning of load follow operation, generating linear power cycles applied to fuel rods;
- then, from the mid-nineties, for abnormal operation occurrences (category 2) involving a local increase of linear power in the fuel rods, likely to induce PCI cladding failure.

2. MAIN PRINCIPLES OF SCC-PCI RISK MANAGEMENT

Presently, the SCC-PCI risk management in operation at EDF is based on three "pillars".

2.1. The surveillance system

The first aim of the surveillance system (alarms) is to monitor the normal operation conditions, considered as the initial state of accidents, while preserving sufficient linear power margins for standard operation.

This surveillance is based on the monitoring of the following parameters:

- normal operation domain ($\Delta I, P$) and/or linear power margins (Fig. 1);
- temperature regulation and power regulation banks positions, especially regarding the insertion limits (Fig. 2).

Apart from surveillance, the second function of the alarms is prevention. This means that the operator should have a sufficient time delay for a corrective intervention before the occurrence of the next steps of automatic actions:

- load reduction or regulation bank extraction blocking;
- reactor trip.

The determination of the surveillance set-points adapted to operation and, at the same time, compatible with PCI constraints is the first major challenge for plant design.

It is a tricky job because the alarms have to be sufficiently far from the normal operation values of parameters to allow manoeuvrability and at the same time not to close to the protection thresholds in order to maintain an acceptable capability for operator corrective action.

900-MW units: example of normal operation domain

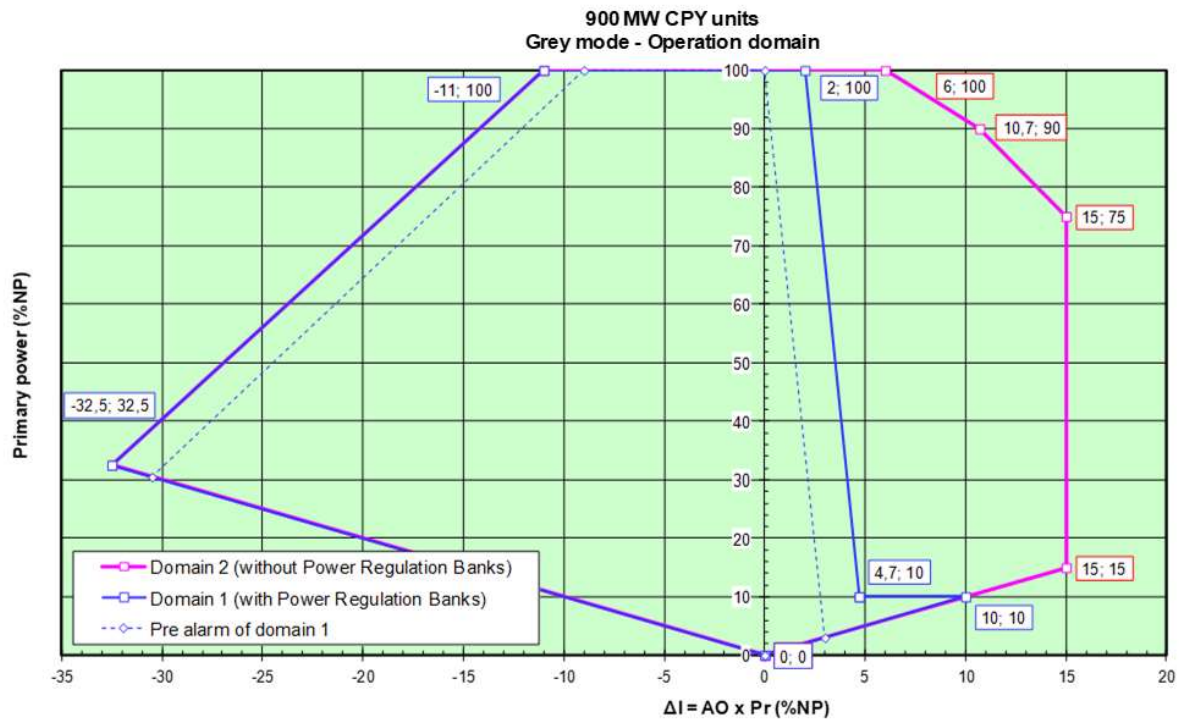


FIG. 1. 900 MW units: example of normal operation domain.

2.2. The protection system

The protection system (scram or reactor trip) is required to stop the transients before PCI cladding failure, in case of abnormal operation occurrences (category 2 events).

The main accidents assessed in the safety analysis are the following:

- Excessive load increase (ELI):

A fast increase of steam flow rate in the Steam Generators (depending on the conventional part of the plant design characteristics) induces an unbalance between primary and secondary power. The subsequent cooling of the core leads to an increase of reactivity and neutronic power, mainly by moderator temperature effect and eventually by banks movements induced by the regulations.

- Uncontrolled regulation bank withdrawal (URBW):

The extraction of a regulation bank leads to an uncontrolled insertion of reactivity. The core power increases rapidly. Until the opening of pressure relief valves on the secondary side, the heat evacuation by the Steam Generators is slower than the core heat generation. The consequences are an increase of primary temperature and pressure.

- Control rod drop (CRD):

Following a rod drop into the core, there is an immediate decrease of reactivity and power. In case of the absence of detection and protection intervention, the unbalance between primary and secondary power induces a decrease of the core inlet temperature via the primary loops.

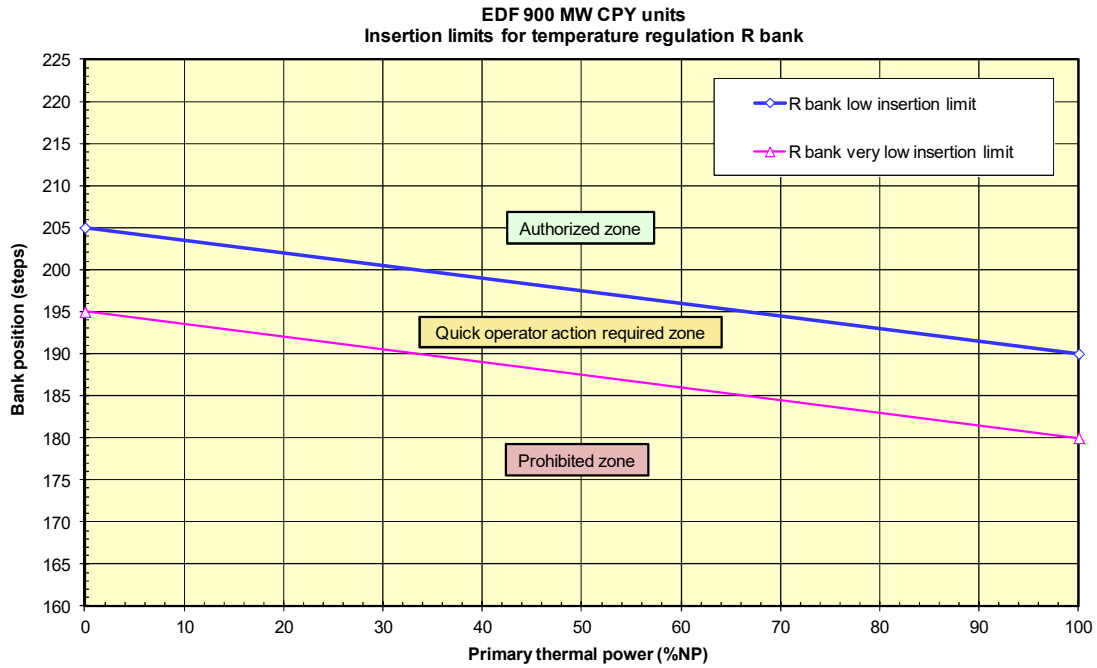


FIG. 2. 900 MW units: example of surveillance system monitoring.

This cooling of the core leads to an increase of reactivity mainly by moderator and Doppler temperature effects and also by temperature regulation banks movements. The core power increases and reaches a new equilibrium, usually close to the initial value.

All these accidents are likely to induce a local linear power increase due both to:

- global core power increase;
- axial and radial power redistribution in the core during the transient.

On EDF PWR plants, the usual protections involved in PCI protection are:

- For 900 MW reactors (Figs 3 and 4 : ΔT_{top} ("OP" for overpower) based on the monitoring of temperature increase ΔT between hot and cold legs of primary loops, with thresholds depending on the average coolant temperature (T_m), the primary pumps rotation speed (Ω_{pp}) and the axial power difference (ΔI);
- For 1300 MW and N4 reactors : high linear power on the digital integrated protection system (SPIN) which makes an on-line evaluation of the axial distribution of maximal linear power based on a reconstruction of the axial power shape $P(z)$ using ex-core power range detectors signals and calculated or measured radial peaking factors $F_{xy}(z)$.

These systems are basically designed to monitor the core peaking factor, which may be sometimes different from the core minimal PCI margin. This "duality" requires some adaptations of the protections.

The determination of the protections thresholds is the second major issue in PCI design studies and for plant operation. The challenge is to provide a robust protection of the core while preserving sufficient margins for power capability and manoeuvrability.

900-MW-units: example of ΔT protections

900 MW CPY units : GARANCE fuel management
 Operation domain and protection ΔT_{OP} et ΔT_{TOT} thresholds

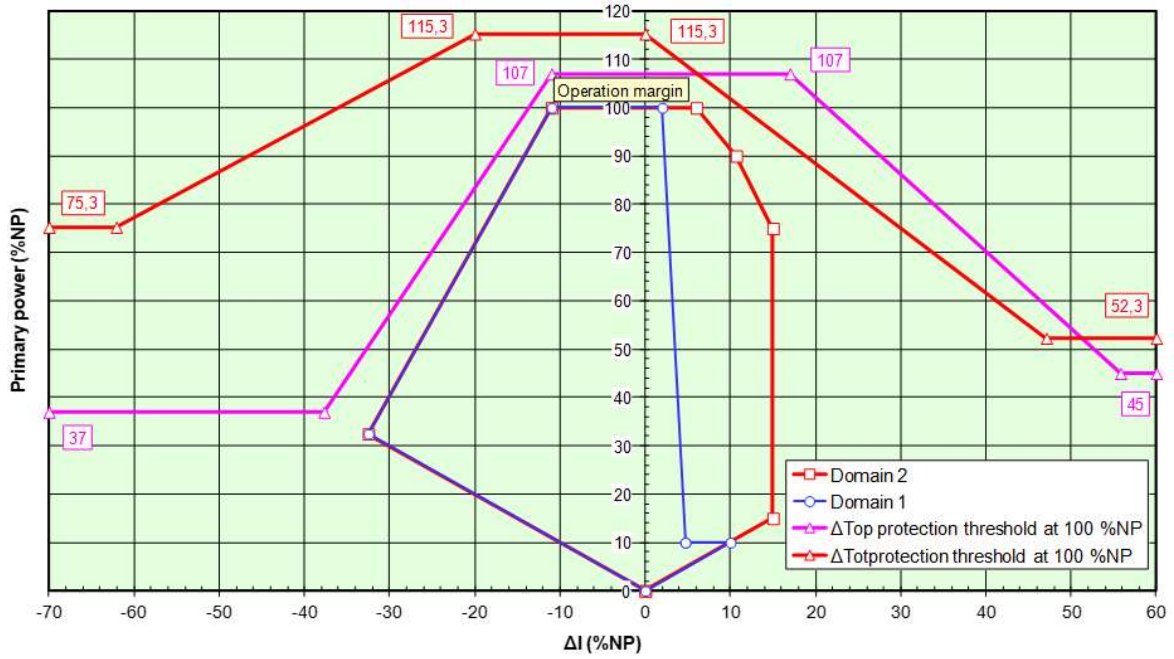


FIG. 3. 900 MW units: example of ΔT protections.

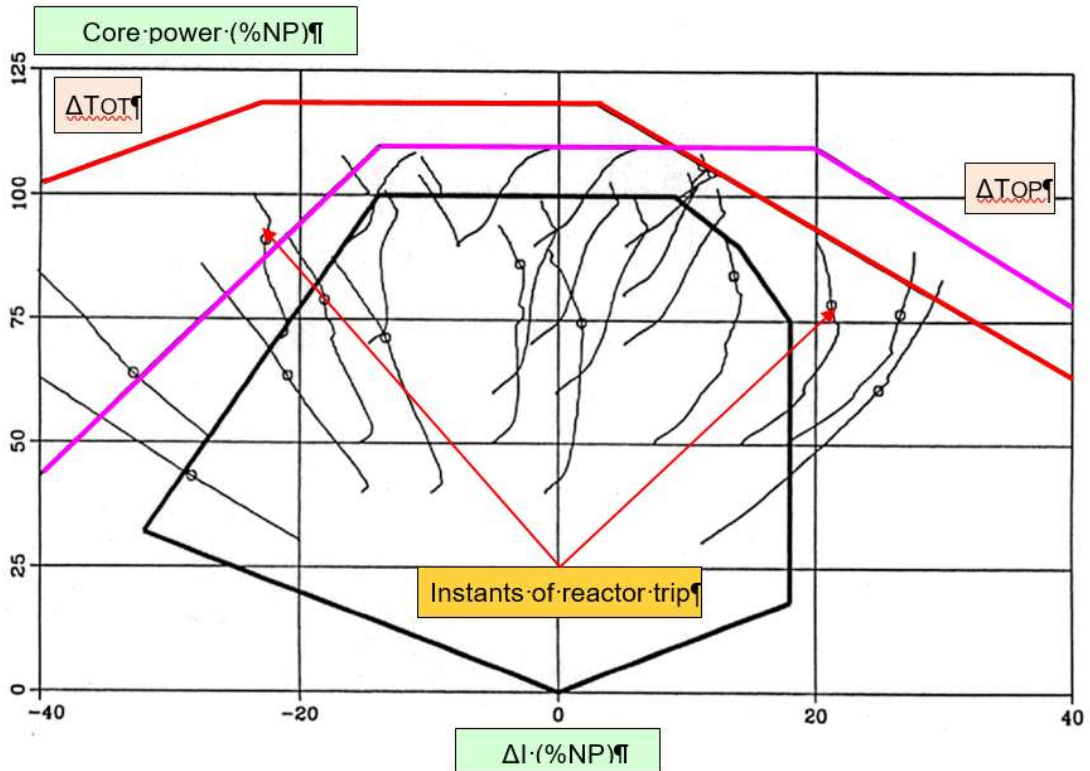


FIG. 4. 900 MW units: example of protection system intervention.

2.3. The operation technical specifications (OTS)

The Operation Technical Specifications purpose is to monitor the fuel "conditioning" (using a PCI "credit"), based on the global core power profile versus time, to ensure that the current thermo-mechanical state of the fuel rods is compatible with safety analysis studies.

The PCI "credit", which is updated every day, depends on operation conditions:

- steady state base load at nominal power (100% NP), most favourable mode for PCI impact (Fig. 5);
- frequency control with limited power "fluctuations" between 92% NP and 100% NP (Figs 6 and 7);
- daily load follow operation, with power "cycles" between 100% NP and 25% NP (Fig. 8);
- Extended Low Power Operation (ELPO), most severe mode for PCI impact, because of fuel rod "deconditioning".

The determination of the minimal allowable ELPO durations is the third major issue in PCI design studies and for plant operation.

2.3.1. Main features of PCI OTS

- The thermo-mechanical state of the fuel is surveyed using a PCI credit (named "K" factor);
- Basically, the K factor decreases at intermediate power (below LPO level 92% NP) and increases or remains stable above 92% NP;
- The load follow operation is "business as usual";
- It is based on a "16/8" daily profile adapted to the European grid needs, with 16 hours above the LPO limit of 92% NP and no more than 8 hours below 92% NP;
- Frequency control and load follow are taken into account through a fixed penalty due to fuel deconditioning caused by daily linear power cycles applied to the fuel and simulating the impact of local alternance between upper and lower levels of the power profile;
- Once this penalty has been applied, the K factor is stable for a given mode : conventionally, the reference value in case of permanent daily load follow operation during the whole cycle is 100;
- Primary frequency control (97.6 +2/-3% NP) and base load operation (≥ 99 %NP) are more favourable than load follow;
- The K factor increases above 100 up to a maximum value (between 110 and 120);
- ELPO is the most deconditioning operation mode;
- The K factor decreases to a minimum authorized value ($K=0 \Leftrightarrow$ zero PCI margin);
- The OTS consider 2 types of ELPO ("rodded" and "unrodded"), at different power levels (10% NP, 30% NP, 50% NP, 70% NP and 85% NP) and at several moments during the cycle (typically beginning, middle, end of cycle and also stretch-out);
- After ELPO, operation above 92% NP allows fuel reconditioning;
- The K factor increases and ultimately reaches a new equilibrium value. There is no specific limit on the power increase rate after the ELPO (≤ 5 % NP/min);
- The OTS depend on the cladding material and its PCI performances;
- At the moment, they are generally based on Zy-4 for the majority of EDF reactors.

The OTS approach is conservative compared to studies results but the main advantage is simplicity.

EDF fleet: example of base load operation

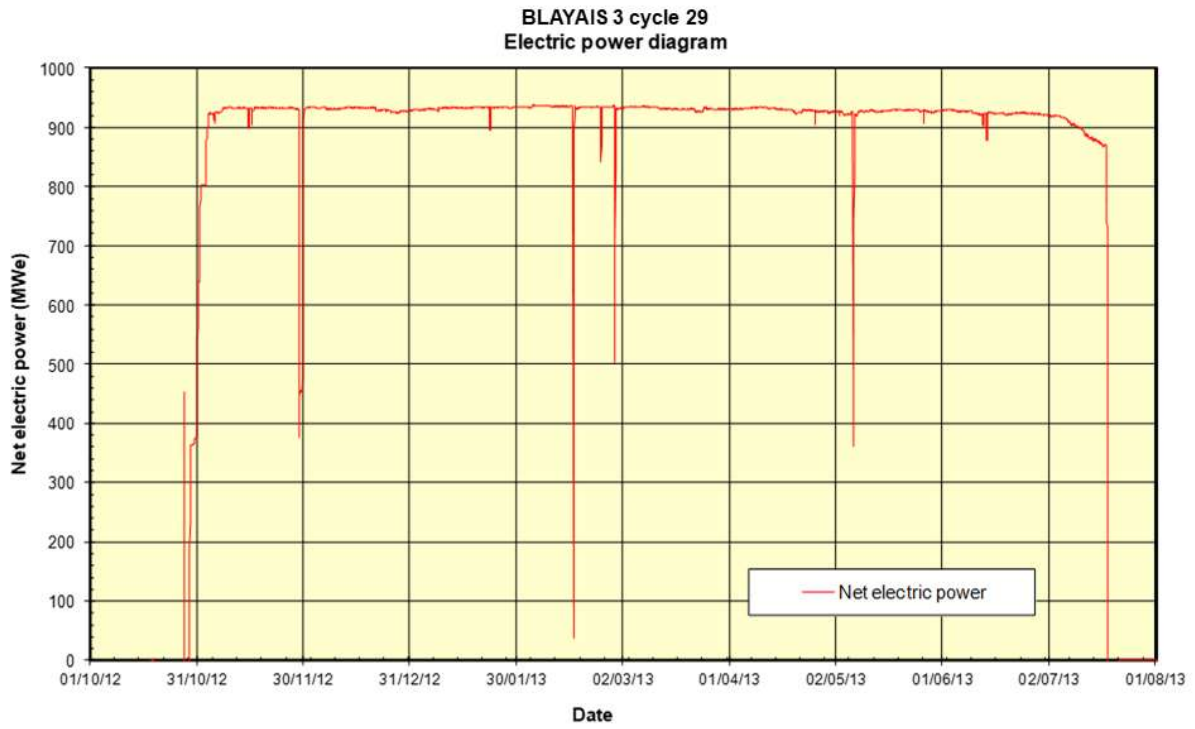


FIG. 5. EDF fleet: example of base load operation.

EDF fleet: example of primary frequency control operation

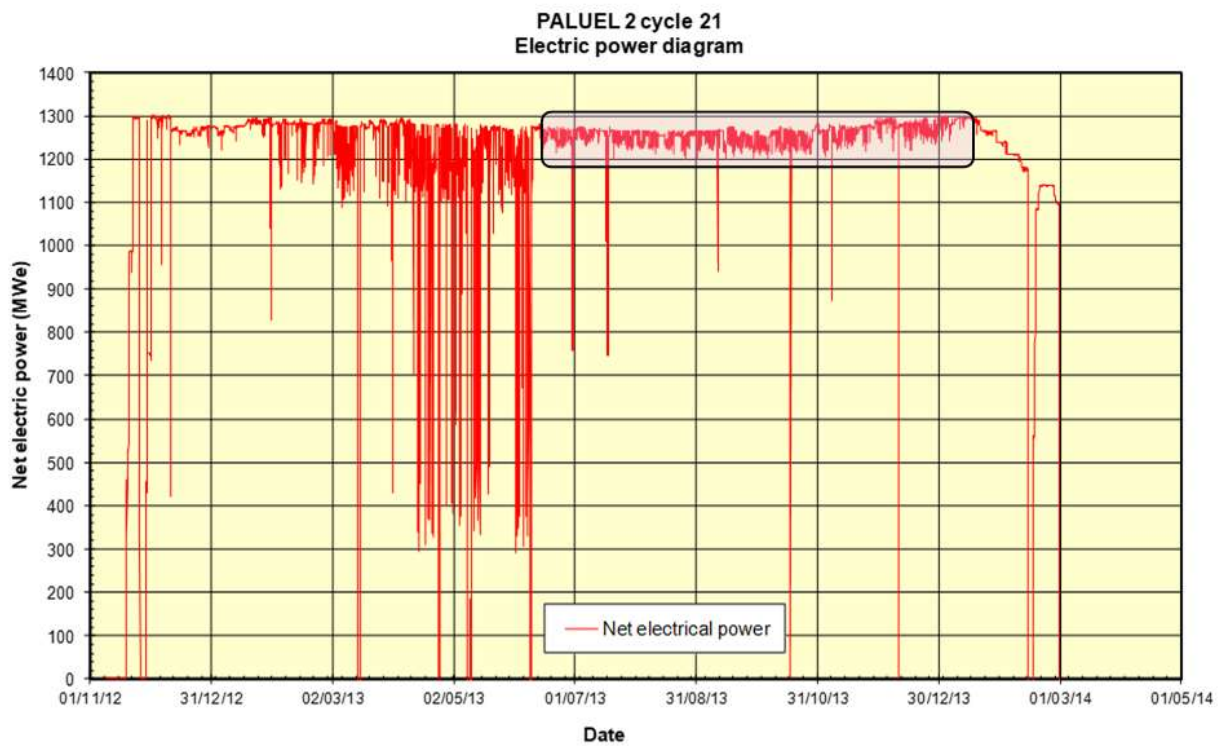


FIG. 6. EDF fleet: example of primary frequency control operation.

EDF fleet: example of primary and secondary frequency control operation

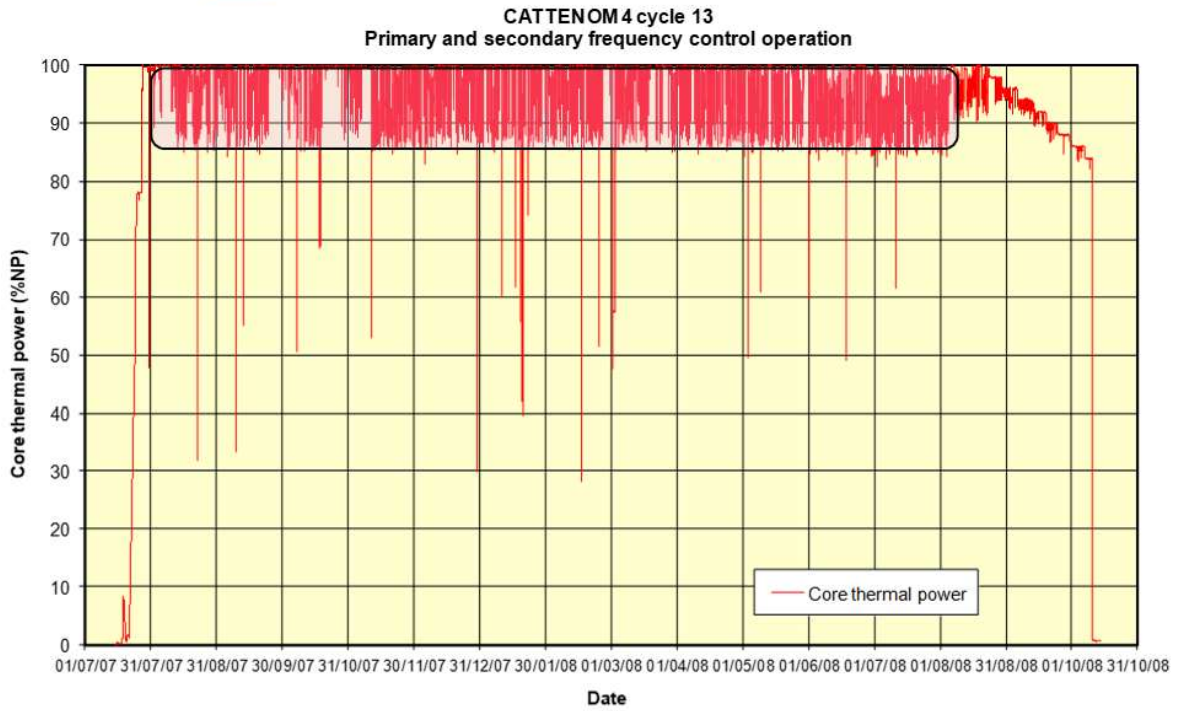


FIG. 7. EDF fleet: example of primary and secondary frequency control operation.

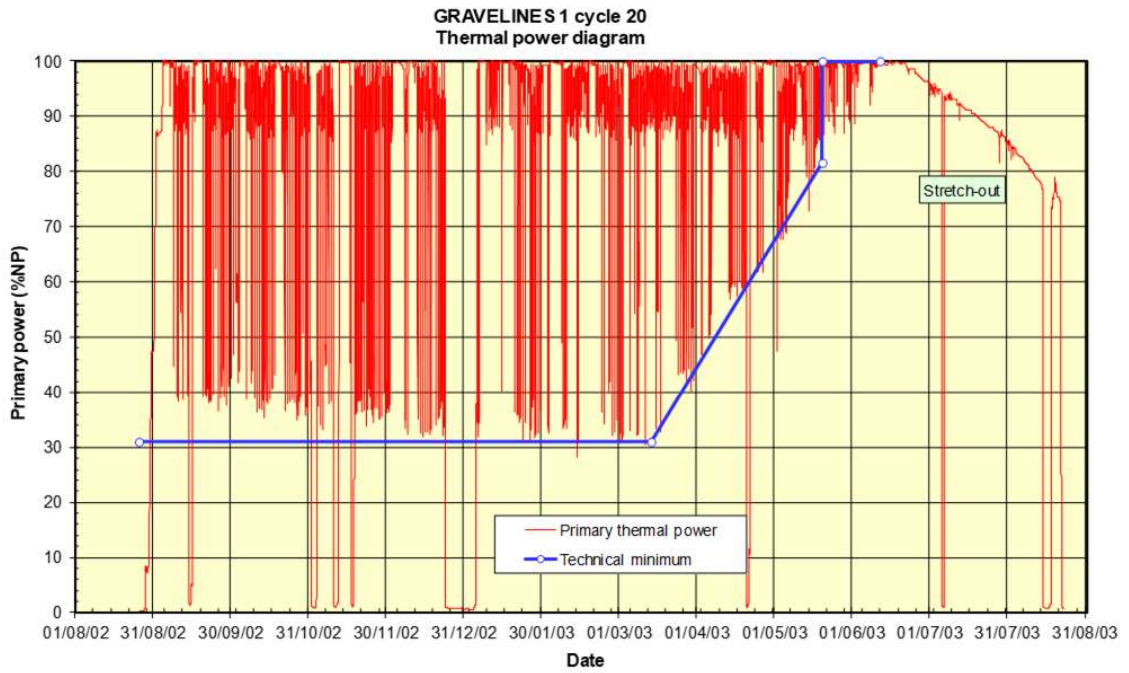


FIG. 8. EDF fleet: example of full grid follow operation.

3. CONSTRAINTS ON MANEUVERABILITY DUE TO SCC-PCI

3.1. Key parameters

The first operational constraint related to SCC-PCI is the potential reduction of manoeuvrability, if the margins between the normal operation conditions (including load follow and frequency control) and the thresholds of the alarms are not sufficient.

This may happen in case of a drastic reduction of thresholds on the protection system or the surveillance system.

At the moment, the most sensitive parameters are:

- the size of the normal operation domain;
- the alarm on the temperature regulation bank insertion.

As illustrated on Figs 9 and 10 based on experience feedback, the operation domain and the regulation bank insertion limits are just sufficient to cover EDF operating needs, and these limits are impacted by PCI safety studies.

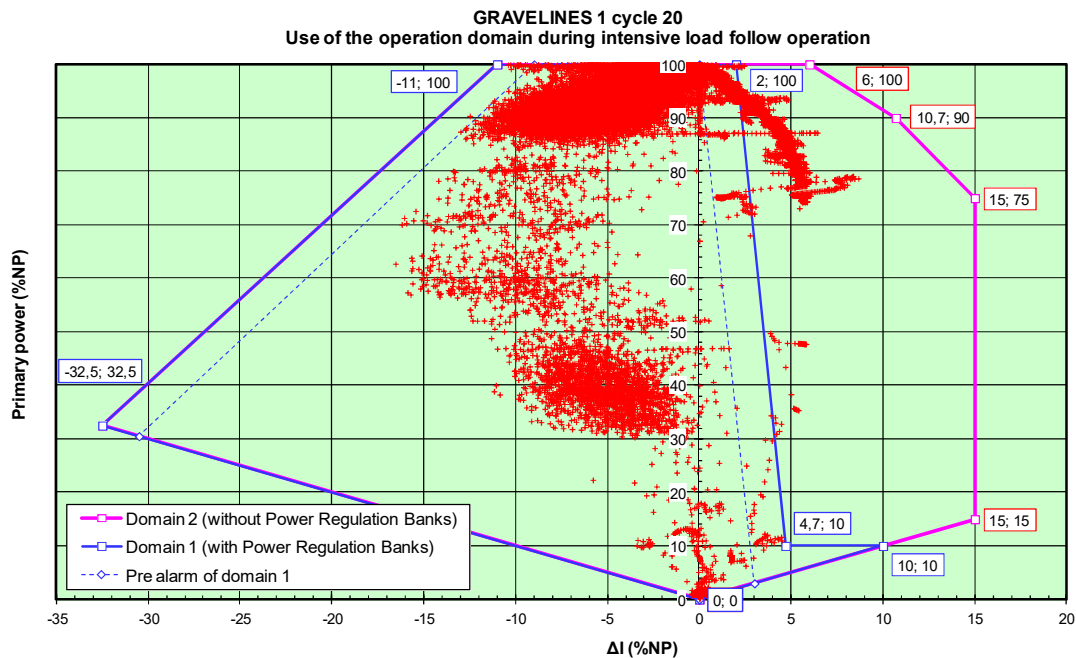


FIG. 9. EDF fleet: example of normal operation domain use.

3.2. Manoeuvring operational needs

They have always been important for EDF fleet since 75% of generation in France is provided by NPPs. It is currently increasing due to renewable energies contribution. It will be probably reinforced in the future with a new energy mix in Europe.

4. CONSTRAINTS ON ELPO DURATIONS DUE TO SCC-PCI

4.1. Definition of extended low power operation (ELPO)

Operation at a power level less than LPO limit (92% Maximum Available Power during the "natural" cycle and the stretch-out) and above 2% NP (Hot Zero Power), during a time interval of more than 8 cumulated hours on a 24-hour "range".

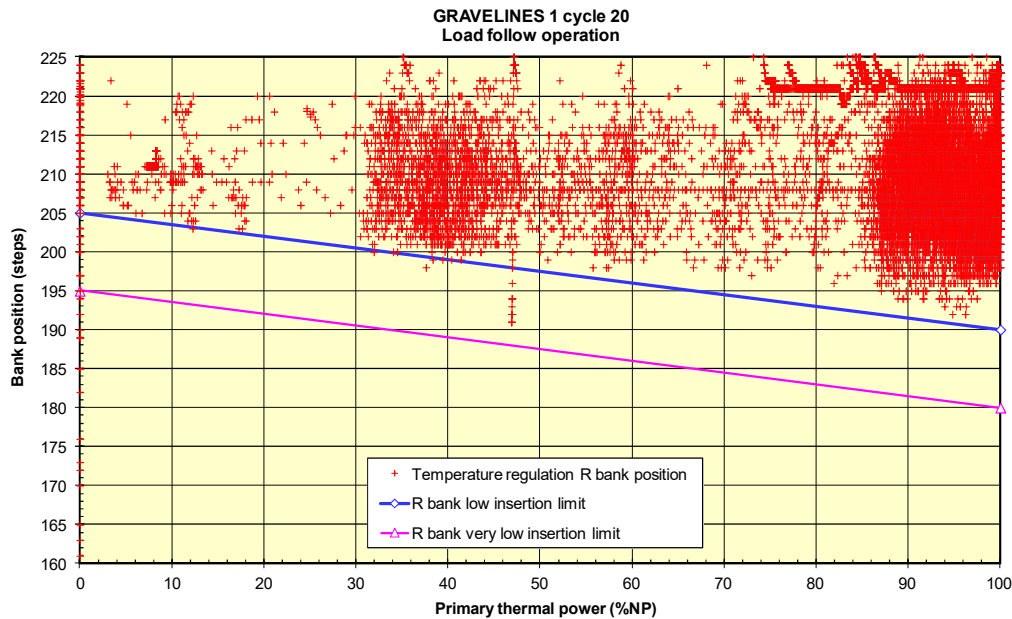


FIG. 10. EDF fleet: EDF fleet: example of regulation bank insertion.

4.2. List of events likely to induce ELPO

ELPO may have various root causes, such as:

- Grid constraints: generation/consumption power balance, renewable energies "abundance" (Fig. 11);
- High voltage power lines maintenance;
- Intended power reduction for plant outage schedule optimization;
- Environment or public health constraints: coolant temperature (Fig. 13), amoeba presence;
- Partial unavailability of secondary system or condenser (Fig. 12): loss of feed water turbo-pump, condenser "raw" water entry, steam leakages;
- Steam generator constraints: primary/secondary leakages (Fig. 16), mud deposit (Fig. 14), clogging, hydraulic stability, high tube plugging ratio;
- Miscellaneous material unexpected events: generators (Fig. 15), transformers.

These events may happen at any moment of the cycle.

4.3. ELPO Operational Needs

4.3.1. Standard ELPOs: minimum requirement for operation 30 days

The main features regarding this kind of events are the following:

- Continuous durations vary typically between 8 and 26 days;
- This type of event may happen at any moment of the cycle;
- The power level varies from the Technical Minimum Power (25-30% NP) up to 85-90% NP; with usually a preferential range between 60 and 90% NP;
- The 30-day "target" is generally met with the OTS (Fig. 17).

EDF R&D has conducted prospective long term studies (up to 2050) illustrating future flexibility needs for EDF PWRs, taking into account the ambitious targets set by the European Commission for Renewable Energy Sources for Electricity (RES-E): up to 60% in 2030 (and 80% in 2050), with 40% of wind and solar generation.

That type of scenario leads to a much more variable demand curve addressed to conventional generation means, with more occurrences of nuclear power plants shut down because of a lack of demand. The 30-day target is considered relevant for long term needs also.

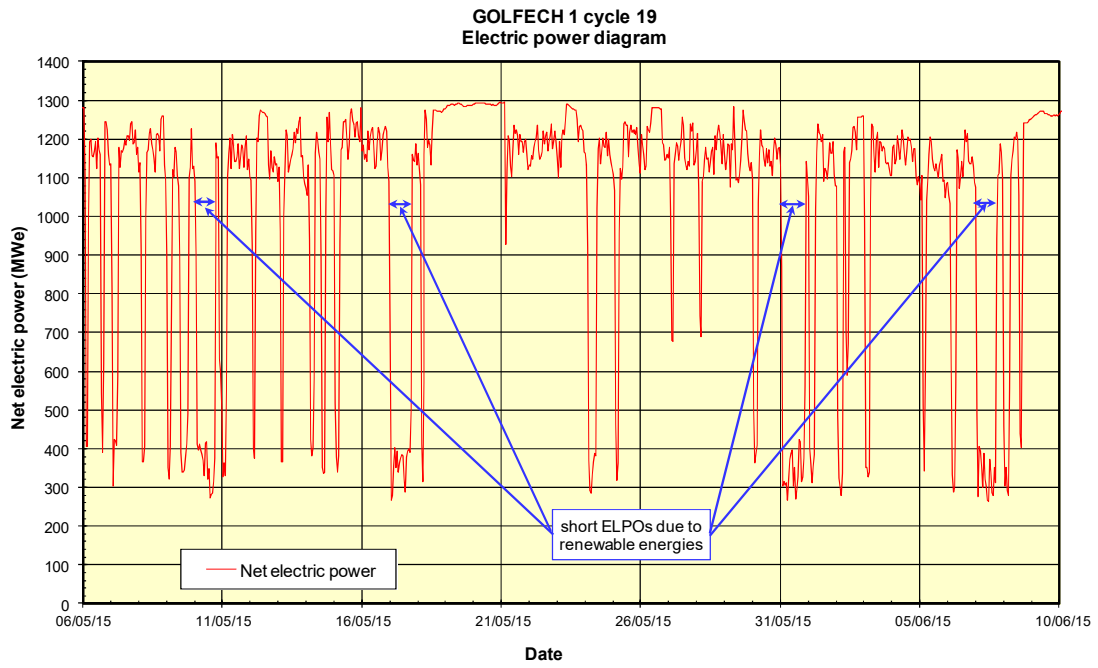


FIG. 11. EDF fleet: example of ELPO because of generation/demand balance.

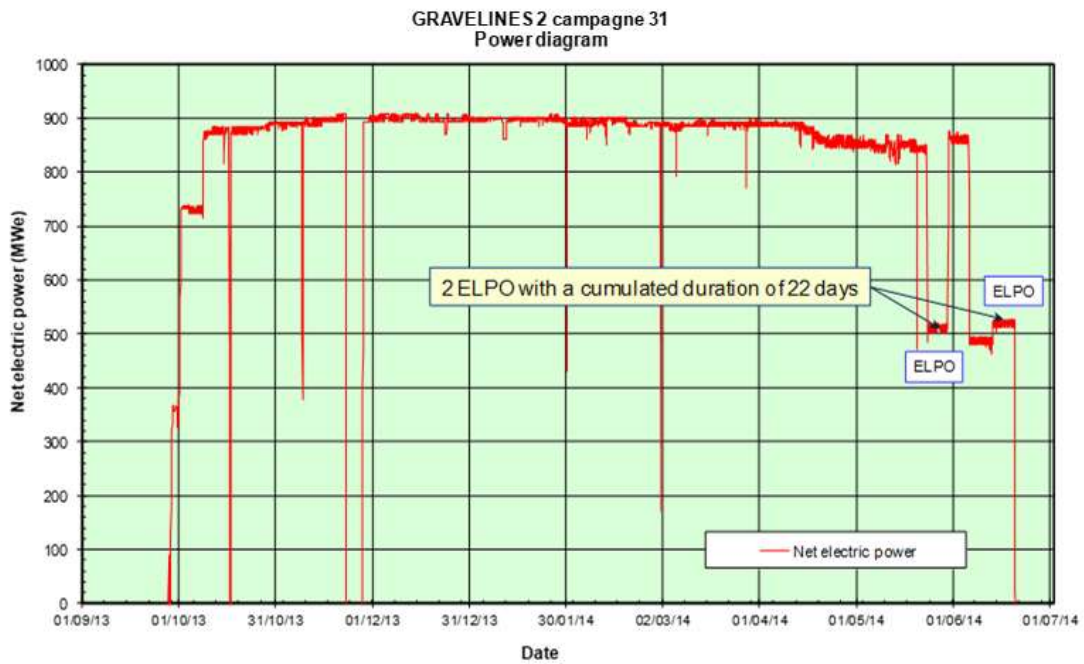


FIG. 12. EDF fleet: example of ELPO for material unexpected events.

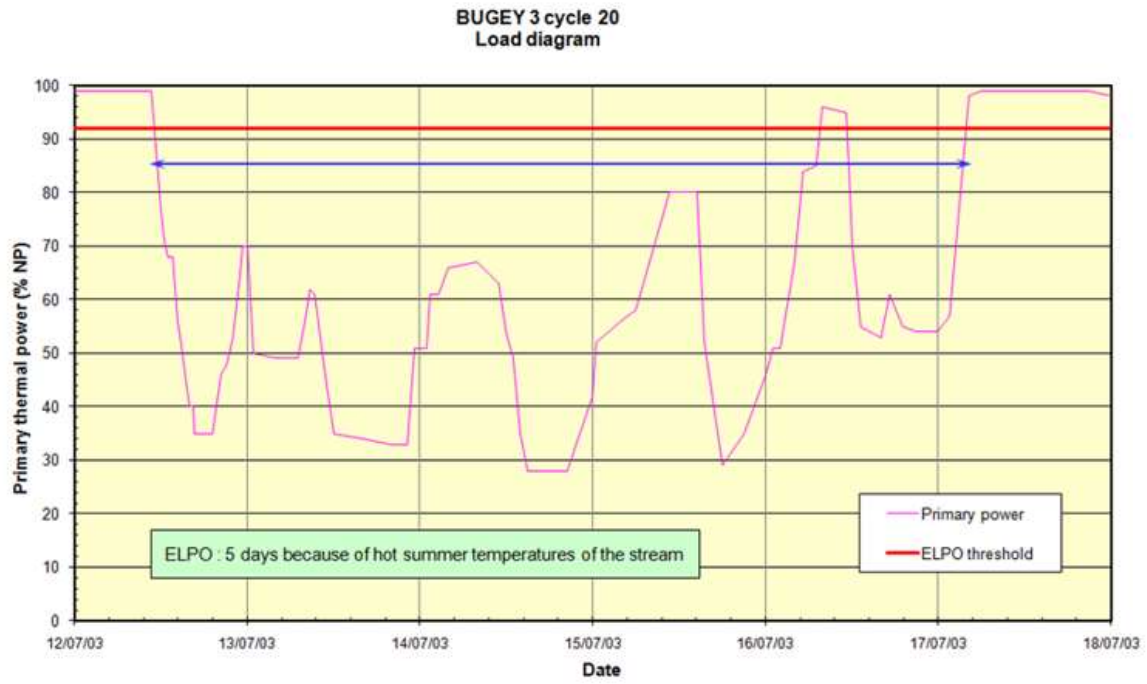


FIG. 13. EDF fleet: example of ELPO because of environment constraints.

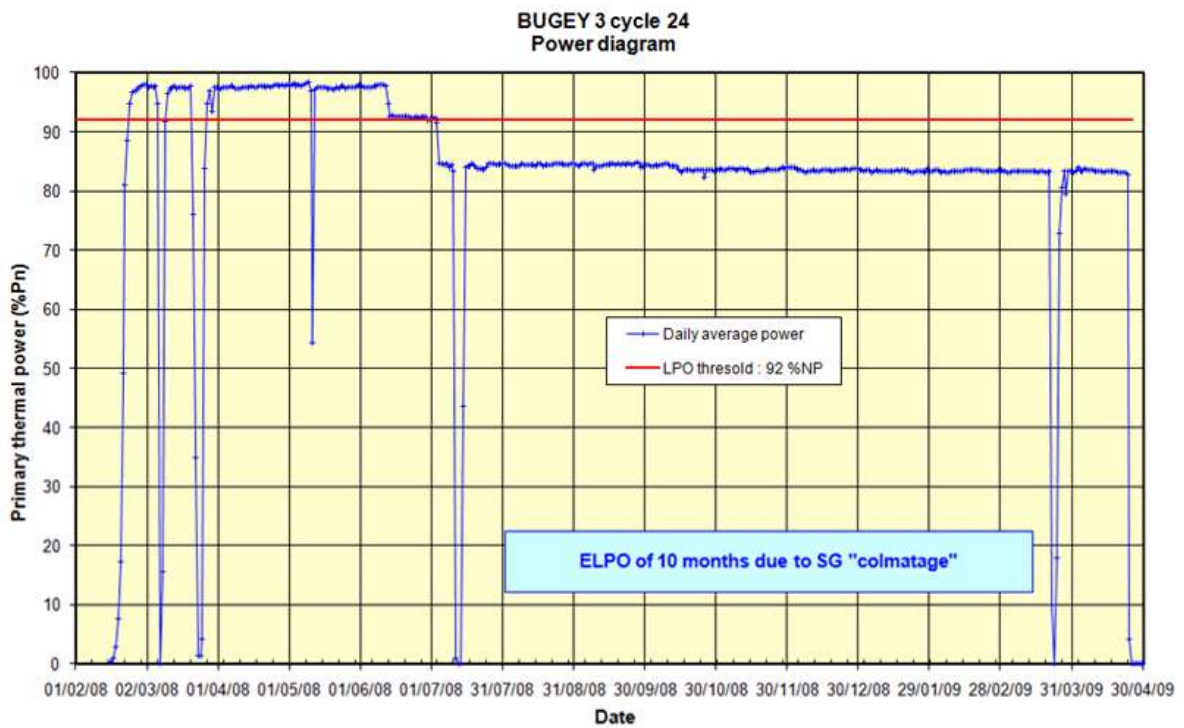


FIG. 14. EDF fleet: example of exceptional ELPO (Steam Generator mud deposit).

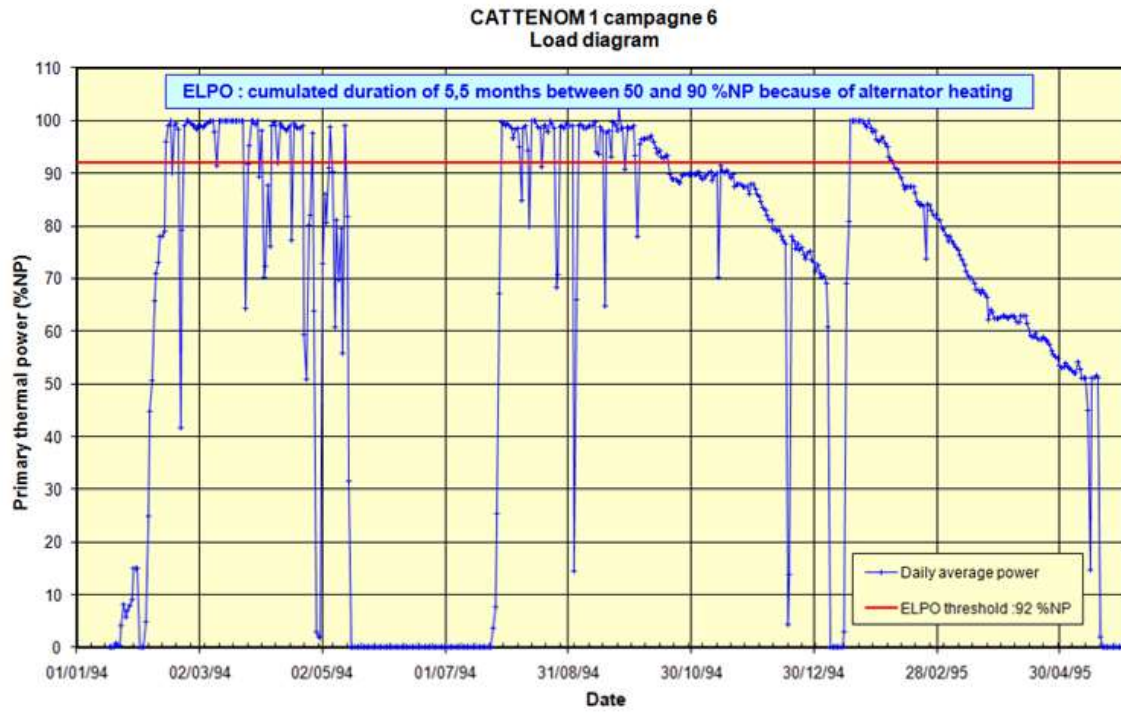


FIG. 15. EDF fleet: example of exceptional ELPO (Electric generator cooling problem).

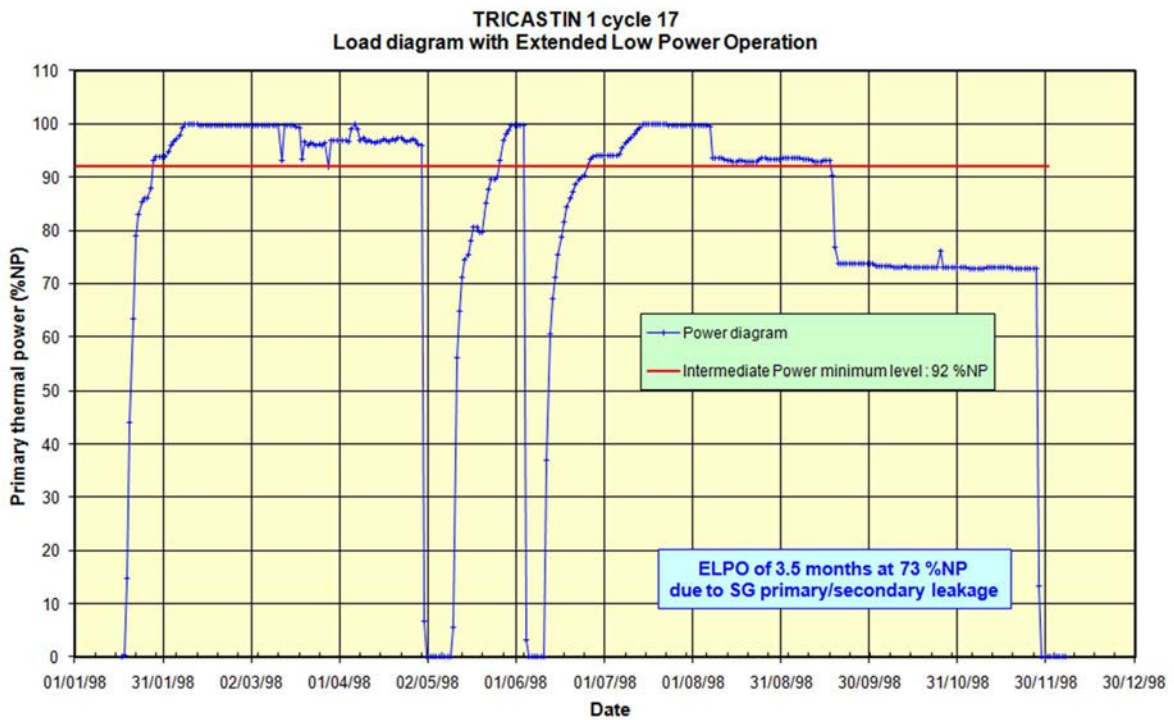


FIG. 16. EDF fleet: example of exceptional ELPO (Electric generator leakage mitigation).

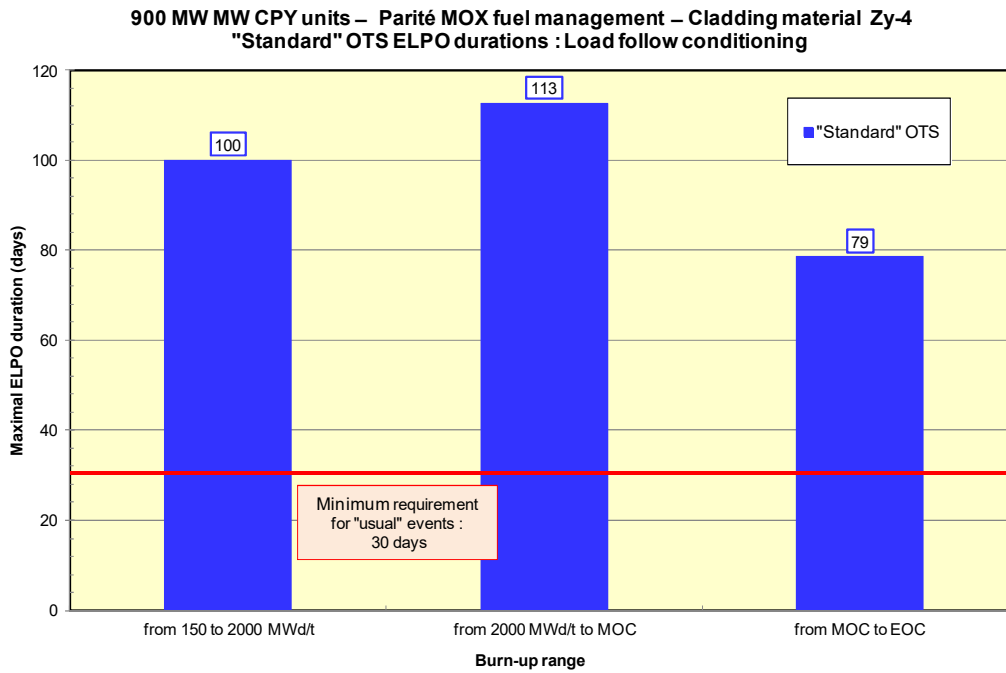


FIG. 17. 900 MW MOX/UOX units: examples of authorized ELPO durations.

4.3.2. Exceptionally long ELPOs in case of major unexpected events: beyond 30 days

The main features regarding this kind of events are the following:

- The ELPO can last from 5 weeks to several months;
- Generic studies are presently licensed to be able to operate at intermediate power ([70% NP, 92% NP]) during a whole cycle with Power Regulation Banks extracted out of the core.

5. CONSTRAINTS ON CORE VARIABILITY DUE TO SCC-PCI

5.1. Definition of core variability

The typical variable core characteristics in EDF fuel management framework are:

- slight variations of the fuel reload: -8, -4, +4 or +4 fresh assemblies, proportion of MOX/UOX fuel during a cycle,
- extension of early shutdown durations (from 25 to 40 EFPD) or stretch-out durations (from 60 to 72 EFPD in some cases).

This variability is necessary for several reasons:

- to cope with the consequences of unexpected events, implying outages schedule modifications,
- to adapt cycle lengths especially in case of strong constraints, such like general plant maintenance and up-date every ten years or Steam Generator replacement,
- to restore a good quality of spare assemblies reserves, which are used in case of loading pattern re-design.

PCI studies are too long and too complex to be performed in the standard industrial Reload Safety Analysis at each refuelling outage.

5.2. PCI variability approach at EDF

A simplified "PCI with variability" approach is being licensed to improve the robustness of PCI studies. EDF has defined "variable" OTS, including a "penalty" on PCI margins (Fig.18) while maintaining a generic design approach.

Meanwhile, the French regulator ASN imposes restrictions. ELPO maximal durations are limited to 8 days with several months of operation above 98% NP for fuel reconditioning.

These restrictions may lead to operation difficulties, as illustrated in Figs 19 and 20. This kind of event has been an incentive to develop the "PCI with variability" approach.

6. CONCLUSIONS

The main operational constraints related to SCC-PCI at EDF are:

- the potential reduction of manoeuvrability, if the margins between the normal operation conditions (including load follow and frequency control) and the thresholds of the alarms are not sufficient;
- the limitation of ELPO durations below the minimal requirements;
- the compatibility with core variability needs.

So far, these constraints have been just compatible with industrial requirements and operation "serenity" for EDF fleet.

In the future, improved designs of fuel rods or enhanced performances of cladding material regarding SCC-PCI are expected to be able to maintain the operational capabilities. Improvements could also be investigated by the plant designers regarding the efficiency of surveillance and protection systems.

This is a crucial challenge, especially for the stability and safety of the European electrical grid, in a context of increased renewable energies generation.

A global review of PCI safety risk status could also be useful. In June 2013, the Advisory Committee on Reactor Safeguards (ACRS) of the US NRC voted not to require specific evaluation of SCC-PCI during abnormal operation occurrences. This position is different from the French regulator approach.

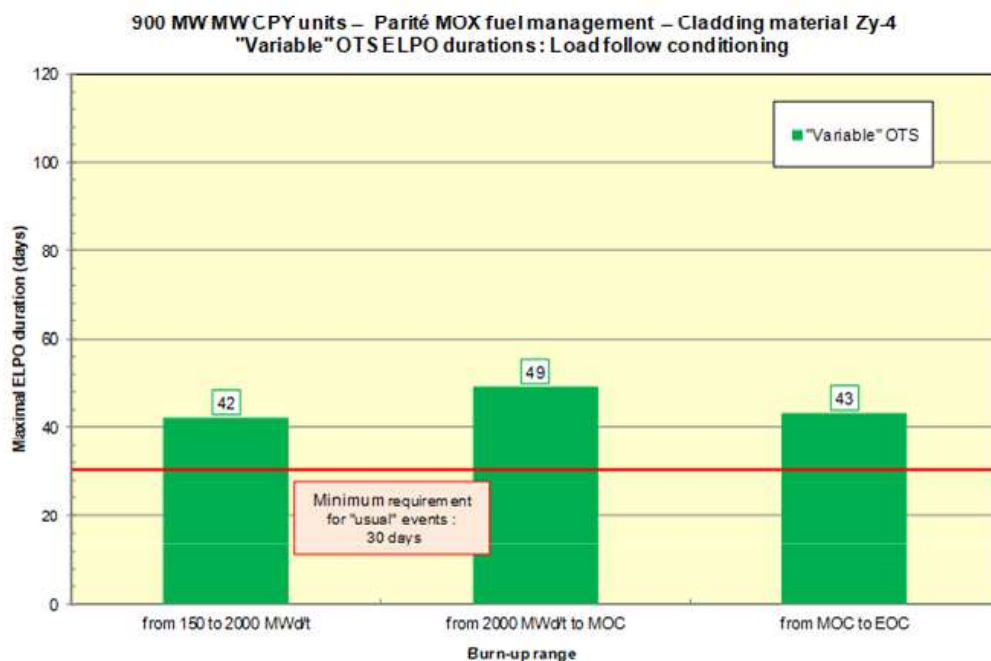


FIG. 18. 900 MW MOX/UOX units: examples of authorized ELPO durations.

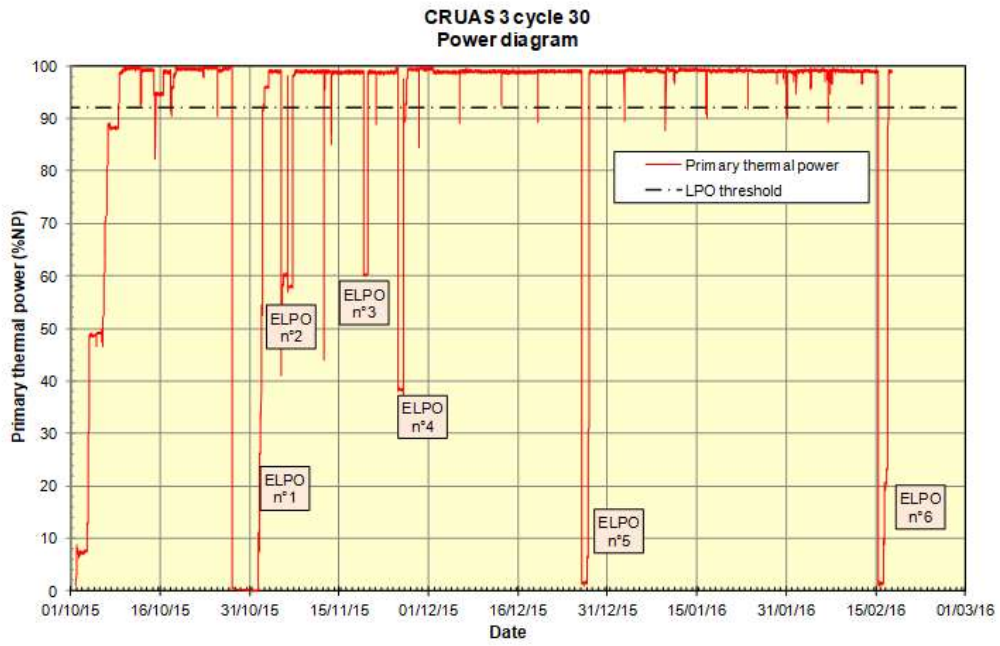


FIG. 19. EDF fleet: example of drastic ELPO restriction to 8 days.

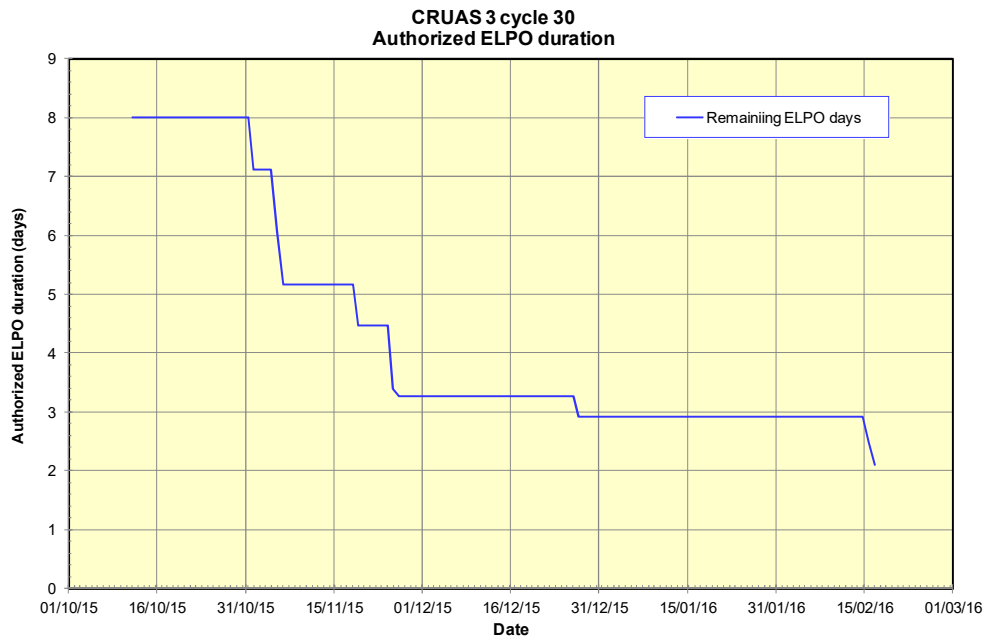


FIG. 20. EDF fleet: example of drastic ELPO restriction to 8 days.

REVIEW OF INTERNATIONAL POWER RAMP PROGRAMS AS A BASIS FOR BWR OPERATING GUIDELINES

V.I. ARIMESCU
Framatome Inc.,
Richland, WA, USA
Email: Ioan.Arimescu@framatome.com

Abstract

The safe operation of fuel assemblies in BWRs is assured by following the operating guidelines that have been developed over time as a set of rules regarding fuel rod power increases that are permissible during BWR manoeuvres, which lead to fuel rod power ramps. The basis for the operating guidelines has evolved, from the theoretical point of view, in accordance with the advances in our knowledge of fuel behaviour. Nevertheless, the formulation of the guidelines strongly relies on the experimental body of information acquired from the international power ramp programmes that have been performed in MTRs, coupled with the experience feedback from fuel operation in power reactors. The paper presents first an outline of the format of the operating guidelines proposed by different organizations and summarizes the different safe operating thresholds and assumptions of the guidelines. Then, the international power ramp programmes are reviewed, and the results are analyzed with respect to fuel rod design vintage, as the fuel design and characteristics have evolved over time. Consideration is given especially to the slow ramp PCI mitigating effect, which is a main component of the operating guidelines. Finally, some remarks are made regarding the advanced fuel types currently in development or in the phase of being introduced in operation, from the point of view of enhancing reliability during operation in BWRs.

1. INTRODUCTION

The occurrence of significant number of fuel failures in the early 1960s, especially in BWR and CANDU power reactors, triggered a flurry of R&D activities [1], that aimed at identifying the causes of those fuel failures and to improve fuel rod resistance to the still to be identified failure mechanism at that time. The goal was to propose mitigating solutions, which would alleviate, if not prevent fuel rod failures.

The analysis of operating conditions showed that the fuel failures in question occurred during power manoeuvres, in which a power ramp was involved. The results of in-reactor and out-of-pile parametric studies led to the hypothesis that cladding cracking was not the result of a mechanical failure by reaching the ductility limit of the material, but rather a chemically-assisted SCC mechanism (sub-critical crack growth process) was involved; this was seen as a generic zirconium alloy failure mode when the fuel rod is subject to a power ramp.

2. BRIEF OVERVIEW OF PCI R&D AND MITIGATING SOLUTIONS

2.1. Early R&D, PCI mechanism hypothesis

The main outcome of the intensive research programmes in the 1970s and early 1980s was the crystallization of the following theory for fuel rod failures that are possible to occur during power ramps:

“Either iodine (I) or cadmium (Cd) are the chemically aggressive fission products that in conjunction with high tensile hoop stress that are developed in the cladding during a power ramp, combine to trigger a SCC process that can result in cladding breach in certain conditions. Because the cladding is mechanically loaded by the pellet-cladding mechanical interaction (PCMI) during a large power increment when the pellet-to-cladding gap is closed, the process was called PCMI-SCC, or simply PCI” [1].

2.2. Mitigating solutions

The complex SCC process that is the basis of the specific duty-related PCI failures was investigated by separate effects tests, which were undertaken to: a) Create stress and chemical environment; b) Attempt to simulate the actual mechanical loading situation e.g. mandrel [2] or fuel swelling simulation test [3] experimental set-ups. It became clear that four conditions were required to be present at the same time, in order for this SCC-PCI failure to occur: high enough stress, the presence of the right chemical environment, sufficient time and a susceptible material.

Therefore, solutions were sought to either prevent or reduce the propensity to PCI, both as new pellet and/or cladding materials that would be less prone to the SCC mechanism, or operating strategies to preclude the critical operational parameters leading to PCI failures.

The proposed mitigating solutions were based on the above-mentioned PCI failure theory and by correlating the experimental data. At the material level, ways to reduce the stress level in the cladding, or prevent simultaneous release of the aggressive fission products, were being investigated and relatively soon two main ideas gained more traction, namely, a cladding inner soft liner (called also barrier) made of pure or very low alloying elements' concentration Zr and a "soft" doped pellet [4].

Eventually the liner concept was adopted in production and it was considered that the PCI issue was resolved from the engineering point of view, by late 1970s, early 1980s. Other measures were taken as well in operation and fabrication. Therefore, the main factors contributing to PCI "resolution" can be summarized as follows:

- Improved understanding and modelling work resulting from laboratory and power ramp tests;
- Adoption of power plant operational measures to prevent PCI failures;
- Better control of fuel fabrication variants e.g. fuel dimensional stability against densification;
- Development of cladding with PCI barriers, notably the sponge-Zr liner, followed by specific liner variants by all vendors.

2.3. Different PCI Variants and Current Understanding

Nevertheless, PCI failures still occurred and operating guidelines were proposed for fuel with either liner or non-liner cladding. These operating recommendations amount to restrictions on power ascension during the power ramp, depending on previous power history and burnup of the ramped fuel rods. This paper's focus is to review the experimental basis and the current status of application in BWRs of these operating guidelines.

The implementation of operating guidelines and/or the liner cladding greatly reduced the number of fuel failures by PCI. However, as mentioned above, spikes of fuel failures still occurred for which all indications were pointing towards a PCI failure type.

Investigation of some of these failures showed a variant of the PCI mechanism, in which the stress is generated by the bending of the unsupported arch of cladding over the missing pellet surface (MPS) due to a circumferential chip at pellet end; this MPS-assisted PCI failure mode has been called "non-classical PCI" or PCI-MPS [5]. The solution to this new failure mode consisted in tightening the operating guidelines as a first response, followed by refining manufacturing with tighter specifications for MPS and enhanced pellet inspection plans in order to prevent to the maximum possible level, MPS chips larger than a critical width. These measures were by and large successful and duty-related PCI-type failures are very sporadic currently.

The research has continued to this day, although at a slower pace, after the engineering solutions mentioned above were implemented in operation. However, full understanding of the process is still lacking, in almost all aspects of the SCC process. Early failures and related research indicated that SCC is the main cause of the PCI failures. However, all the details still not yet clarified: e.g. is the aggressive chemical corrosive agent I or Cd? It was also determined that fuel rod chemistry is a necessary ingredient: e.g. fresh pellets in irradiated cladding did not fail. The other main outcomes of the MTR and laboratory studies are:

- Out-of-pile studies on fresh and irradiated cladding in I and Cd showed similar fractographic features;
- Role of stress very important: time to failure increases as the stress decreases;
- Very little I concentration can still lead to SCC;
- Cladding texture was determined as the most important cladding related parameter (both out-of-the pile and in-pile tests), but also surface finish and residual surface stress;
- Pellet stoichiometry also an important factor with beneficial effects if hyperstoichiometric [6].

3. BASES FOR OPERATING GUIDELINES IN BWRs

3.1. Main operational parameters used in BWR manoeuvring guidelines

The following operational parameters have been ranked as most important factors affecting fuel PCI performance: maximum power at the top of the ramp (RTL), LHGR increment during the ramp, speed of LHGR increase (ramp rate), and dwell time at terminal power level. The distinction between SCC and ductility exhaustion

types of cracking during mechanical loading tests is clearly noticed for conditions of very high strain rates, in which case classical mechanical overload cracking occurs before the SCC process is even initiated.

Therefore, for the SCC to occur first a low to moderate range for the strain rate is required. However, the chemical features of the SCC process are still not fully understood. One of the main unknowns is related to the iodine chemical attack mechanism. One proposed hypothesis was that the iodine adsorbed on zirconium free surfaces weakens the atomic bonds under the surface; an alternative explanation was based on iodine diffusing to the crack tip and corroding the material there. Therefore, more knowledge is needed regarding the times needed for incubation and initiation of the SCC cracks [1].

The maximum (peak) stress in the cladding that is reached after a power increment occurs can be correlated with the power increment and a direct proportionality can be established between the two parameters. However, an additional first-order parameter is the initial LHGR, which in combination with the power history before the power ramp, both determine the status of the pellet-to-cladding gap, which is a crucial parameter influencing the magnitude of the cladding stress after the power ramp. On the other hand, the higher the RTL, the larger the FGR is. Because the release of iodine, which is considered the most likely SCC aggressive chemical agent, is generally accepted to occur at the same time and rate with the release of noble gases, the magnitude of RTL has a direct impact on the chemical part of SCC.

Another finding of the MTR power ramps was the beneficial effect of slow ramps, most of which showed that below a certain ramp rate, the failure threshold is raised above the fast ramp failure threshold. One explanation for this slow ramp benefit was that oxide layer that is present on the cladding inner surface is known to have a passivation effect and consequently prevents SCC as long as it is intact. One of the supporting experimental data in that respect is offered by the SRX rods [7], some of which underwent hot-cell PIE examination. One important finding of that hot-cell PIE was that the cladding inner surface is coated all around by an oxide layer, with a thickness in the 1 to 8 μm range. This is indicative that a significant source of oxygen was present in the rod free volume and available for oxidizing (healing oxide layer cracks) the cladding inner surface during the power ramp. Another case in point is offered by the hot-cell PIE of hyper-stoichiometric UO₂ fuel that was subjected to power ramps [6]. The increased PCI performance hyper-stoichiometric UO₂ fuel was explained in [6] as largely being a consequence of the effect of increased oxygen leading to rapid oxidation of zirconium bare surfaces, which passivates the tip of the crack and thus inhibiting further crack propagation. Therefore, it is clear that fuel chemistry plays an important role in the development of the SCC-PCI process. This is either by affecting the oxygen available for oxidation of cladding inner surface, or by trapping iodine, in whatever chemical combination present in the fuel.

3.2. Brief Description of the Structure of BWR Operating Guidelines

The operating guidelines, PCIOMR, are based on a number of PCI limits, as follows:

- Normally, a safe, "PCI-free" domain is defined, where power changes may occur without restriction;
- Restrictions are posed on the rate of power change outside the "PCI-free" domain;
- Conditioning/ deconditioning effects to be considered after e.g. extended low power operation or outage;
- Thermomechanical limits (fuel centre melting, dryout, internal pressure, 1% hoop strain) apply as an upper power boundary that shall never be exceeded.

The PCIOMRs are incorporated in the core monitoring system of a BWR, providing information on margins and operator alarm if any violation occurs.

The pellet-cladding contact pressure at the ramp terminal level depends not only on LHGR in the pellet stack but also on the conditioning state of the fuel. That is, the gap size and/or the lack thereof as manifested by pellet-cladding contact pressure just prior to the power transient have a major effect on PCMI during a ramp. If the gap is largely open, it will just close without any damaging effect. If significant contact pressure exists before the transient, a severe PCMI can develop with potentially damaging consequences.

Fuel conditioning refers to those thermal-mechanical processes that reduce the negative outcome of a power increment. The relaxation of the contact pressure between cladding and pellet or even re-opening of the gap is the process underlying conditioning. This proceeds by processes in the fuel, namely densification and creep in combination with cladding creep out due to internal gas pressure. On the contrary, fuel deconditioning is the opposite process in which PCMI is enhanced as a consequence of decreasing the gap by solid swelling of the fuel pellets and cladding creep down.

An extended period of time at reduced power contributes to decondition the fuel. A period of time at high power level contributes to condition the fuel; moderate PCMI is actually good for the fuel. The conditioned state of the fuel can be characterized by the power level, called conditioning LHGR, which is characterized by a dynamic equilibrium between conditioning and deconditioning (i.e. where the contact pressure between pellet and cladding does not change with time). Fuel conditioning is a local concept. The conditioning state of the fuel is different in the different axial regions of the rod and from rod to rod.

A risk of cladding failure appears when the fuel, (de)conditioned at low power level, is subjected to a fast power rise up to a high power level. A tangential stress then develops in the cladding which depends on the magnitude of the power increase and the increase rate. Permanent cladding damage can be avoided by limiting either the magnitude of the power changes or the power increase rate.

4. POWER RAMP DATABASE

The effort to develop a fuel resistant to PCI, which at the same time has no negative impact on commercial and licensing requirements, is extensive and complex R&D programmes in MTRs as well as in power reactors are necessary [14]. The MTR power ramp studies are required in order to investigate the entire domain of power levels for power ramps in order to discern fuel failure thresholds, which is not possible in power reactors, where, of course, fuel failures are to be avoided.

The power reactors irradiations are also necessary in order to supply the experience feedback data on fuel performance in actual LWR conditions; also, the fuel rods to be later used for power ramps programmes in MTR are pre-irradiated to various burnups in power reactors.

Therefore, after identifying that power transients are a necessary condition for duty-related fuel failures, several power ramp programmes have been initiated both in MTRs and a few also in power plants. The latter programme aimed at verifying that test-reactor power ramps are representative for fuel behaviour in actual operation in power plants, as some questions have been raised regarding the difference between the smaller rodlets used in MTR programmes and the full-length fuel pins that are irradiated in power plants. The main differences that were brought up were: overall power increase in MTRs, whereas the withdrawal of a control rod in a BWR leads to a sweeping power transient along fuel rod length; trapped stack effects characteristic to full fuel rods are only present in full-length rods in power reactors.

Nevertheless, the outcomes of ramp tests in a MTR e.g. R2 of Studsvik and in a power reactor ([8], [9]) agree to a reasonable degree provided the following features are accounted for: accounting for outlier failures; the difference between ramp rate in a power reactor and in a MTR, the former being much faster; the axial power profile is suddenly distorted at the tip of the moving control rod during a power ramp taking place in a power reactor.

Studsvik started ramp tests in 1969, and since then more than 1000 ramp tests have been performed ([8] and [10]). About 150 of these ramp tests have been part of past internationally funded power ramp projects. The majority of this data is publicly available through OECD/NEA in the IFPE database [11].

In addition to the Studsvik power ramp projects, significant power ramp programmes have been carried out in other MTRs, most notable, Halden, Osiris (CEA), Petten (Netherlands), NRU (AECL), GETR-Vallecitos and others.

In addition to the above discussion of the comparison between power ramps in MTRs and in power reactors, the following elements should also be considered:

- Heterogeneous pellet and cladding design and properties in the fuel rods of the international power ramp database – especially cladding texture;
- Reduced dataset for modern fuel design and materials;
- MPS issue: present from the early days with periods of prominence and mitigating actions in fabrication — Clear MPS effects confirmed from operation and at least one case in the MTR programmes (BG8-1 of Super Ramp programme [12]).

The first item above is of paramount importance, as it has been clearly demonstrated that higher radial texture inhibits the SCC crack propagation. The HCP crystallographic structure of Zr is intrinsically anisotropic and the polycrystalline Zr alloys have a marked degree of anisotropy for all mechanical and physical properties.

One property strongly related to texture is the hydride orientation factor, because the hydrides tend to precipitate parallel to the basal plane. The hydride orientation factor was available for the majority of the power

ramp cases in the Studsvik international programmes and therefore, it was used to investigate the effect of higher radial texture on PCI failure thresholds. The results reported in [13] show indeed a reduction of the failure threshold for less radial texture cases; this result was implemented in production and modern cladding has a high degree of radial texture.

As mentioned above, the operating guidelines are based on the outcomes of the power ramps programmes, both international programmes in combination with proprietary programmes in MTRs and experience feedback (failures in power reactors). Different ways of interpreting the power ramp data have been proposed e.g. [4], [14–16], but in all formats the lowest failure points are used to define the failure thresholds and an additional safety margin is applied to account for experimental and fuel rod characterization uncertainties.

As described above, the international power ramp data are affected by quite large uncertainties because of diverse fuel designs and fabrication processes used in the past. A large weight in setting the failure thresholds is given to the commercial data, i.e. failures in power reactors that have been identified as PCI-related ([17], [18]). Therefore, each vendor has developed proprietary operating guidelines and the utilities use the guidance provided by vendors to develop their own operating procedures for managing BWR manoeuvres (for notch-type BWR plants in the USA), known as control blade exchanges.

Power ramps in MTRs were used for the derivation of power failure thresholds, which are part of the BWR operating guidelines. There are different ways to interpret the power ramp data, as follows:

- There is strong support that the main parameters are ΔP and the initial power, P_i ;
- Both ΔP and P_{max} must be above some thresholds in order to get failure;
- The thresholds show a nonlinear burnup dependence, but piecewise linear relationship is used;
- However, the prevalent way to reduce the data is the P_{max} vs. burnup.

Other formats of failure thresholds derived from MTR power ramps were proposed, as follows:

- One of the analyses [16] used the linear discriminant analysis method in order to rank the determining parameters and to derive best-estimate failure criteria from a database of 713 power ramps, 117 of which have failed;
- The determining parameter in that analysis was found out to be the power increment, which is inversely proportional dependent to the initial power and burnup;
- Other analyses used different statistical procedures: e.g. the CANDU fuel power ramp performance criteria require that both a P_{max} and a ΔP thresholds be exceeded in order for failure to occur. Since P_i is the difference between P_{max} and ΔP , this is equivalent to the inversely linear relationship between P and P_i ;
- On the other hand, GE analysis emphasized the importance of the RTL and interpreted the power ramp data in terms of a maximum power failure threshold depending on burnup. Most of the power ramps of the GE experimental programmes had the same initial power level [4].

Currently, all vendors have continuous quality improvement and surveillance programmes for fuel pellet and cladding manufacturing in order to prevent to the maximum extent possible appearance of pellet flaws (such as MPS) and cladding imperfections, which can impair PCI resistance of the fuel rods. In addition, upgraded and/or improved fuel design and materials are in various stages of development and implementation in production, such as doped pellets: chromia-doped by Framatome [19], chromia-alumina by Westinghouse [20], or Al-Si additive by GNF [21]. In all cases a comprehensive MTR power ramp programme was undertaken to confirm improved PCI performance and allow quantification of updated operating guidelines limits [19].

5. CONCLUSIONS

The international power ramp database is globally, a heterogeneous dataset, but individual datasets of specific power ramp programmes are consistent and show clearer dependencies.

The design and materials characteristics have evolved in time and care must be exercised when using the power ramp data from different programmes with the aim of defining PCI limits. The heterogeneity mentioned above with respect to international power ramp programmes must be taken into account and only the data relevant to current production should be selected.

On the other hand, reactor feedback experience of fuel failures in power reactors must also be considered carefully in two ways: a) determine whether PCI was the actual cause of fuel failure; b) identify whether pellet flaws, such as MPS, played a role.

Currently, there is a need to continue with the power ramp programmes in MTRs, which are necessary in order to support fuel materials modifications, either as evolutionary steps or fundamental changes, such as those contemplated for ATF concepts. Recent shutdowns of a number of MTRs represent a roadblock in performing these needed power ramp programmes and the international community is currently trying to find possible alternative MTRs and expedite the finalization of new MTRs under construction or in various stages of planning. The MTR power ramps will be complemented by power reactor experience feedback that is the final performance confirmation of a particular fuel design or material improvement.

NOMENCLATURES

AECL	Atomic Energy of Canada Limited
ATF	Accident Tolerant Fuel
BWR	Boiling Water Reactor
CANDU	Canada Deuterium Uranium Reactor
CEA	Commissariat a Energie Atomique
FGR	Fission Gas Release
GE	General Electric
GETR	GE Test Reactor
HCP	Hexagonal Compact Packing
ID	Inner Diameter
IFPE	International Fuel Performance Experimental database
LHGR	Linear Heat Generation Rate
MPS	Missing Pellet Surface
MTR	Material Test Reactor
P	Power, same as LHGR
P _i	Initial Power (LHGR) at the beginning of a power ramp
P _{max}	Maximum power (RTL) during a power ramp
ΔP	Power (LHGR) increment during a power ramp
PCI	Pellet-Cladding Interaction
PCMI	Pellet-Cladding Mechanical Interaction
PCOMR	PCI Operating Manoeuvring Recommendations
R&D	Research and Development
RTL	Ramp Terminal Level of LHGR
SCC	Stress Corrosion Cracking
SRX	Super Ramp Extension

REFERENCES

- [1] COX, B., Pellet-Clad Interaction (PCI) Failures of Zirconium Alloy Fuel Cladding – A Review, *Journal of Nuclear Materials* **172** (1989) 249.
- [2] NOBREGA, B.N., KING, J.S., WAS, G.S., WISNER, S.B., Improvements in the Design and Analysis of the Segmented Expanding Mandrel Test, *Journal of Nuclear Materials* **131** (1985) 99-104.
- [3] COLEMAN, C.E., “Simulation of Interaction between Cracked UO₂ Fuel and Zircaloy Cladding”, *Proceedings of International Conference on Physical Metallurgy of Reactor Fuel Elements*, The Metals Society, London, UK (1974) pp. 302-307.
- [4] ROWLAND, T.C., DAVIES, J.H., THOMPSON, J.R., ROSENBAUM, H.S., “Statistical Analysis of Power Ramp PCI Test Data”, Paper presented at the IAEA Meeting on Pellet-Cladding Interaction in Water Reactor Fuel, Seattle, 1983.
- [5] POWERS, C. et al, “Hot Cell Examination Results of Non-Classical PCI Failures at La Salle”, Paper presented at the International LWR Fuel Performance Meeting, Kyoto 2-6 October 2005.
- [6] DAVIES, J.H., HOSHI, E.V., ZIMMERMAN, D.L., Ramp Test Behaviour of High O/U Fuel, *J Nucl. Mater* **270** (1999) 87-95.
- [7] ARIMESCU, I, VALLEJO KARLSSON, I.J., ZHOU, G., GRANDI G, RAYNAUD, P., YUN, Y., DONCEL, N., SERCOMBE. J., PYTEL, M., DOSTAL, M., DUNAVANT, R., YOO, J.S., “Third SCIP Modelling Workshop: Beneficial Impact of Slow Power Ramp on PCI Performance, Paper presented at the WRFPM, Sendai. Japan. September 2014.
- [8] GROUND, M., LYSELL, G., BENGTSSON, S., Fuel R&D at Studsvik II. General Studies of Fuel Behaviour Including Pellet-Cladding Interaction, *Nuclear Engineering and Design* **168** (1997) 151-166.

- [9] VÄRNILD, O., OLSSON, S., "Pellet Cladding Interaction (PCI) Fuel Duty During Normal Operation of ASEA-ATOM BWRs", Proceedings of IAEA Specialists' Meeting on Power Ramping and Cycling Behaviour of Water Reactor Fuel, Petten, Netherlands, 8-9 September 1982.
- [10] KARLSSON, J., CORLEONI, F., "Ramp Testing at the Studsvik R2 Reactor 1969-2005", OECD/NEA/WGFS Workshop on Pellet-Cladding Interaction (PCI) in Water-Cooled Reactors, Lucca, Italy, June 22-24, 2016.
- [11] KILLEEN, J.C., SARTORI, E., TURNBULL, J.A., "Experimental Data on PCI and PCMI within the IFPE Database," Proceedings of a Seminar on Pellet-Clad Interaction in Water Reactor Fuels, Aix-en-Provence, France, 9-11 March 2004, pp. 347-364.
- [12] DJURLE S., The Studsvik SUPER-RAMP Project, Final Report, STUDSVIK-STSR-32, Studsvik, Sweden (1984).
- [13] MOGARD, H., KYAER-PEDERSEN, N., A Review of Studsvik's International Power Ramp Test Projects, STUDSVIK-85/6, Studsvik, Sweden (1985).
- [14] WOOD, J.C., "PCI-OGRAMS: Application of CANDU FUELOGRAM Methodology to PCI Data from Light-Water Reactors," IAEA Specialists' Meeting on Power Ramping and Power Cycling on Water Reactor Fuel and Its Significance to Fuel Behaviour", Arles, France, 14-18 May 1979, IWGFPT/5, IAEA, Vienna (1980).
- [15] ROLSTAD, E., SAUAR, T.O., "Progress with the Probabilistic Fuel Failure Code POSHO," Proceedings of the Specialists' Meeting on Fuel Element Performance Computer Modelling, Blackpool, U.K., 17-21 March 1980, IWGFPT/7, IAEA, Vienna (1981).
- [16] MCDONALD, S.G. et al. "A Statistical Analysis of Pellet-Clad Interaction Failures in Water Reactor Fuel," Specialists' Meeting on Pellet-Clad Interaction in Water Reactors, Denmark, September 1980.
- [17] MANZEL, R., GARTNER, M., SCHLEMMER, F., WOLFF, U., ROTH, E., "Power Ramp Experiments in the Nuclear Power Plant BIBLIS-A", IAEA Specialists' Meeting on Power Ramping and Power Cycling On Water Reactor Fuel and Its Significance To Fuel Behaviour, Arles, France 14-18 May 1979, IWGFPT/5, IAEA, Vienna (1980).
- [18] JUNKRANS S., VESTERLUND, G., VÄRNILD, O., "The Combined Use of MTR Experiments and Power Reactor Tests For The Development of PCI-Resistant Fuel", IAEA Specialists' Meeting on Power Ramping and Power Cycling On Water Reactor Fuel and Its Significance To Fuel Behaviour, Arles, France 14-18 May 1979, IWGFPT/5, IAEA, Vienna (1980).
- [19] DELAFOY, C., ARIMESCU, I., "Developments in Fuel Design and Manufacturing in order to Enhance the PCI Performance of AREVA NP's Fuel," OECD/NEA/WGFS Workshop on Pellet-Cladding Interaction (PCI) in Water-Cooled Reactors, Lucca, Italy, June 22-24, 2016.
- [20] BACKMAN, K., HALLSTADIUS, L., RÖNNBERG, G., "Westinghouse Advanced Doped Pellet Characteristics and Irradiation Behaviour", Proceedings of Advanced Fuel Pellet Materials and Fuel Rod Design for Water Cooled Reactors, Villigen, Switzerland, IAEA-TECDOC-1654, IAEA, Vienna (2009).
- [21] DAVIES, J. H., VAIDYANATHAN, S., RAND, R. A., "Modified UO₂ Fuel for High Burnups", Proceedings of Top Fuel Conference, Avignon, France, 13-15 September 1999, European Nuclear Society (1999).

NUCLEAR FUEL OPERATIONAL EXPERIENCE AT KOZLODUY NPP

D. HRISTOV, K. KAMENOV
Kozloduy NPP,
Kozloduy, Bulgaria
Email: DVHristov77@gmail.com

Abstract

Kozloduy NPP operates two WWER-1000 units. The TVSA type fuel assemblies have been used at Kozloduy NPP, reactors since 2004. Since 2008 the reactor cores of Unit 5 and 6 have been fully loaded with TVSA. The new assembly type TVSA-12 are in operation at Unit 6 from 2016. The new fuel type TVSA-12 contains increased content and enrichment (up to 4.7%) of uranium and also increased grain sized fuel in addition to the increased skeleton robustness. TVSA-12 allows thermal power up-rating up to 104% (3120 MW) using 42 fresh FAs. The paper discuss from practical point of view information about the experience of TVSA and TVSA-12 fuel implementation, fuel assemblies main design characteristics and KNPP reloading schemes, neutron-physics characteristics, relevant measurement data, fuel reliability statistics, I, Xe, Kr concentrations in the moderator and coolant specific activity data, as an indicator for fuel problem during cycle, our methods to prevent fuel failure, controlling the linear power of the fuel rod, burnup and reactor power changes limitations etc.

1. INTRODUCTION

This paper provides some operational experience of Kozloduy NPP with the TVSA and TVSA-12 fuel assembly type. The TVSA operation shows very good results for more than 1200 burned FA (fuel assemblies) so our aim is to present some of the most important reactor operational guidelines, limitations and requirement for the fuel operational conditions. TVSA-12 operation is in the beginning and there is not enough statistics yet, 163 irradiated FA; with this progress KNPP intends to enhance the nuclear safety and economics of the nuclear fuel operation.

2. KOZLODUY NPP FUEL STRATEGY

Kozloduy is the first NPP in south-east Europe and contains 6 units:

- Unit 1 – WWER-440 / B230, commissioned in 1974, shut down since 31 December 2002;
- Unit 2 – WWER-440 / B230, commissioned in 1975, shut down since 31 December 2002;
- Unit 3 – WWER-440 / B230, commissioned in 1980, shut down since 31 December 2006;
- Unit 4 – WWER-440 / B230, commissioned in 1982, shut down since 31 December 2006;
- Unit 5 – WWER-1000/B320, commissioned in 1988, currently in operation with the 26th fuel cycle, power uprated to 104%(3120MW) in 2019;
- Unit 6 – WWER-1000/B320, commissioned in 1991, currently in operation with the 24th fuel cycle, power uprated to 104%(3120MW) in 2017.

Units 5&6 WWER-1000 usually operate in base regime at full uprated power-104%. Since 2008 the reactor cores of Unit 5 and 6 have been fully loaded with TVSA. The last fuel assembly type TVSA-12 is in operation at Unit 6 from 2016. The advanced TVSA-12 assembly contains increased contents of uranium, increased uranium enrichment up to 4.7wt% and increased skeleton stiffness. TVSA-12 allows thermal power up-rating up to 104% (3120MW(th)) using 42 fresh FAs.

During the last ten years the operational strategy at KNPP is as follows:

- Four-year fuel cycle;
- Fuel cycle length ~325 days, 40 days of annual outage;
- Beginning of Unit's 5 outages – the middle of April;
- Beginning of Unit's 6 outages – the middle of September.

Some important design features of TVSA-12 are presented in Table 1. The main improvements in TVSA-12 assembly type are the increased contents of uranium, increased uranium enrichment up to 4.7wt.%, decreased cladding thickness, more robust skeleton and increased fuel ceramic grain size which ensures gases keeping without need of fuel pellet central hole [1, 2].

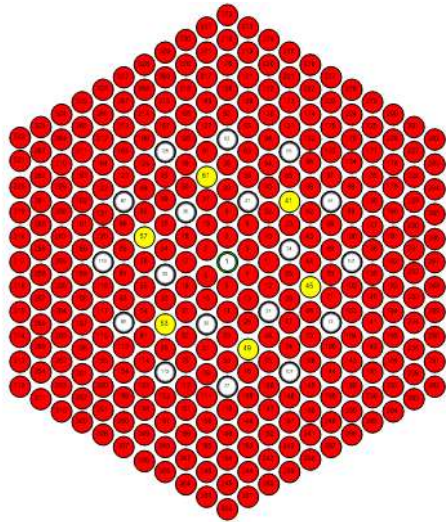
TABLE 1. TVSA AND TVSA-12 FUEL ASSEMBLY FEATURES

	TVSA	TVSA-12
Fuel mass in assembly, UO ₂ , kg	494.5	545.2
Number of fuel assemblies	163	163
Total number of fuel rods and Gd-rods	312	312
Fuel mass in FR/Gd FR, UO ₂ , kg	1.585 / 1.575	1.750 / 1.620
Fuel pellet outer diameter, cm	0.76	0.78 / 0.76
Fuel pellet hole diameter, cm	0.14 / 0.15	0 / 0.12
Cladding outer diameter, cm	0.91	0.91
Cladding inner diameter, cm	0.773	0.793 / 0.773
Average enrichment, wt%	4.30, 3.98	4.62, 4.60, 3.97
Number of Gd rods	6, 6	6, 12, 12
Fuel rods enrichment, wt%	4.4 / 4.0	4.7/ 4.4/ 4.0
Gd-rods enrichment, wt%	3.6 / 3.3	3.6 / 3.3

Configuration of various TVSA models are represented in Figs 1–5. Some of the most significant effects from TVSA-12 implementation are:

- Decreasing the number of fresh fuel assemblies for annual reloading. Before we usually used 42 or 48 fresh FA TVSA, now 42 TVSA-12 are enough;
- Power uprate 3120 MW(104%);
- Minimizing potential debris risk (anti debris filter);
- Decreasing the reactor pressure vessel neutron flux (5 to 8%) using reloading schemes with lower neutron leakage;
- Decreasing the fuel assemblies bending (Increased TVSA-12 skeleton solidity);
- Decreasing the reloading time;
- Decreasing zirconium quantity in the reactor core;
- Decreasing the reactor scram time.

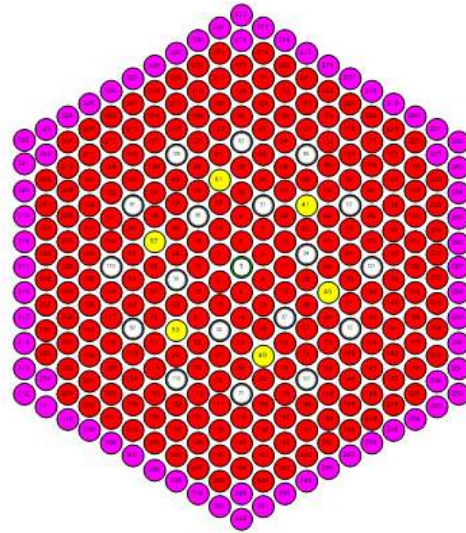
In Figure 6 are presented typical fuel loading schemes with TVSA and TVSA-12. Loadings with TVSA-12 are with bigger power irregularity and higher power peaking factors. Less fresh FAs are in place at the peripheral core so that neutron flux at the reactor vessel is significantly reduced.



306 rods - 4.0wt%
6 Gd rods - 3.3wt%

Central tube
Guide tube

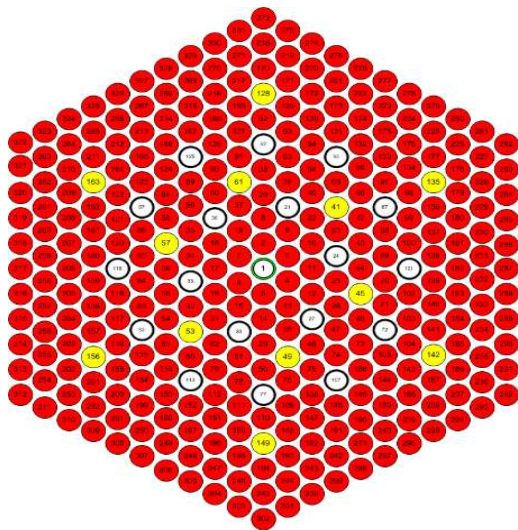
FIG. 1. TVSA layout (3.98 wt.%).



240 rods - 4.4wt%
66 rods - 4.0wt%
6 Gd rods - 3.6wt%

Central tube
Guide tube

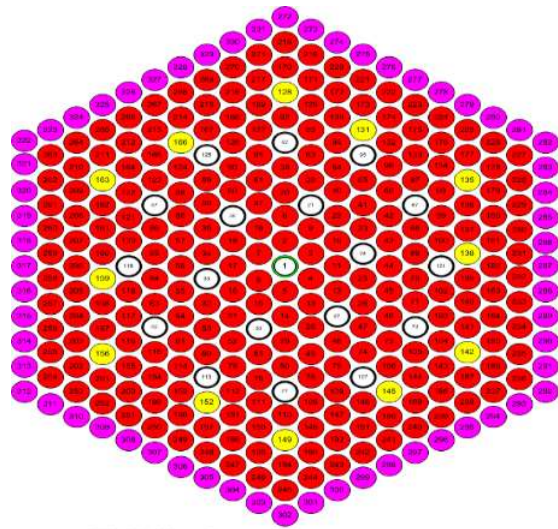
FIG. 2. TVSA layout (4.4 wt.%).



TVSA-12 B40D2 - profiled
300 fuel rods - 4.0wt%
12 Gd rods - 3.3wt%

Central tube
Guide tube

FIG. 3. TVSA-12 layout (3.97wt.%).



TVSA-12 B46G2 - profiled
240 fuel rods - 4.7wt%
60 fuel rods - 4.4wt%
12 Gd rods - 3.6wt%

Central tube
Guide tube

FIG. 4. TVSA-12 layout (4.6wt.%).

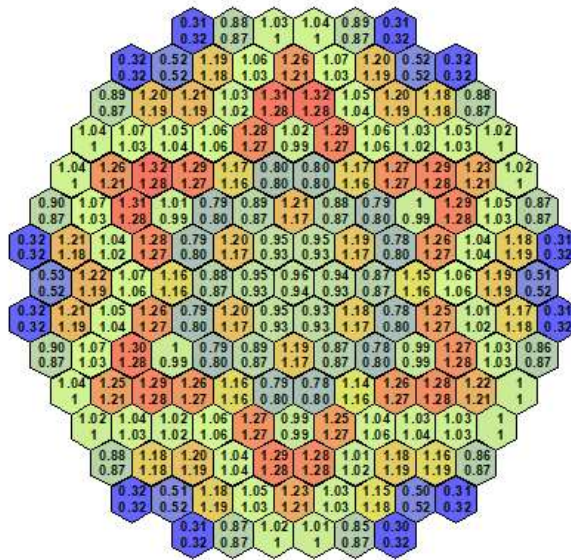


FIG. 7. BIPR-7A code comparison with in-core monitoring system data reconstruction.

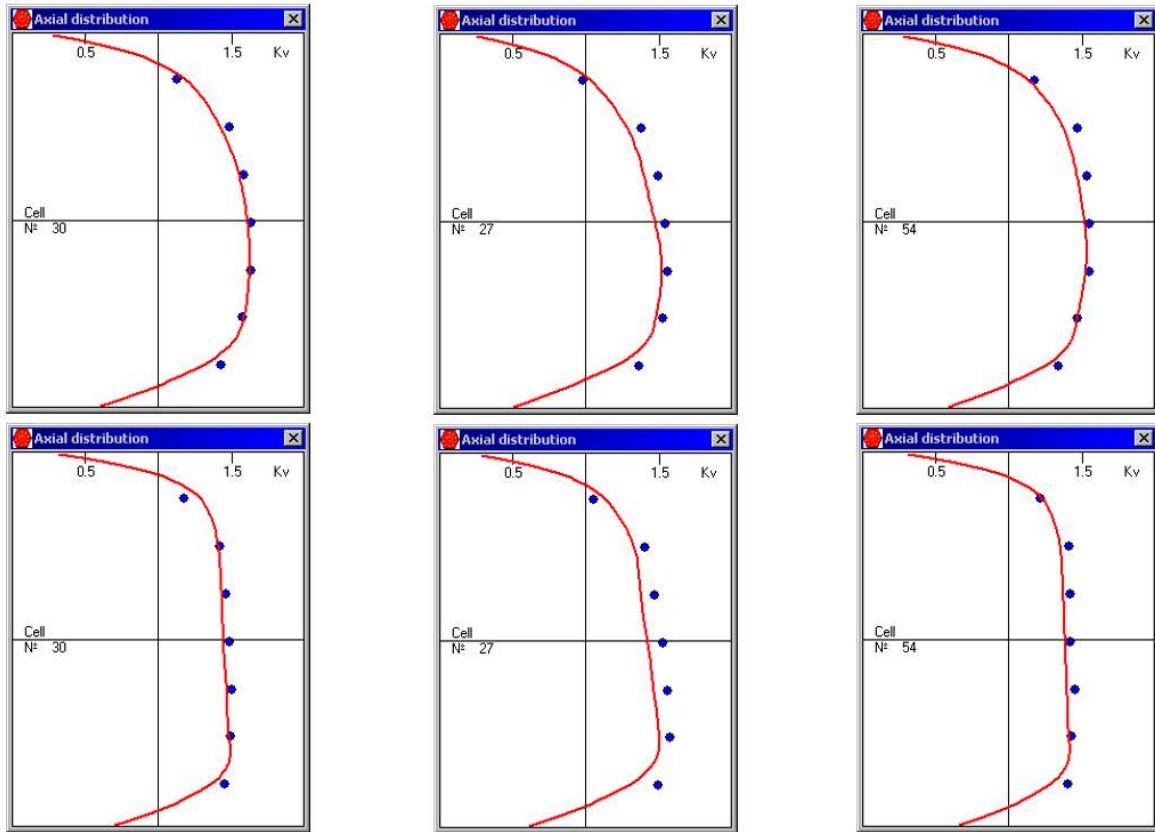


FIG. 8. Assembly axial power distribution-measured and calculated with BIPR-7a code.

4. KOZLODUY NPP OPERATIONAL LIMITATIONS

Reactor power changes speeds limitations for rated power - 3000MW and after power uprate 3120MW are presented in Fig. 9 and Fig. 10 [6].

5. FUEL LINEAR POWER LIMITATIONS

According to the refuelling methodology, the most important parameter is the linear power in the fuel rods $Q_{l_{ijk}}$ [W/cm]:

$$Q_{l_{ijk}} = \overline{Q_l} * K_{o_{ijk}} * K_{eng_{1,2,3}} * K_{power} \quad (1)$$

$$\overline{Q_l} = 172.82 [W/cm]$$

$$K_{eng_1} = 1.153; K_{eng_2} = 1.133; K_{eng_3} = 1.114; K_{power} = 1.04$$

$K_{o_{ijk}}$ – fuel pin relative power; $i = 1 \dots 163$; $j = 1 \dots 30$; $k = 1 \dots 312$.

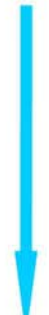
REACTOR POWER CHANGES PERMISSIBLE SPEED			
Planned power decrease	Planned power increase	Power increase after: - main circulation pump start; - long (more than 12 days) reactor operation at decreased power level - after refuelling; - at the end of cycle during reactor coastdown $N < 85\%N_{rated}$	Stepwise increase of reactor power
<p>100%Nrated</p>  <p>Not more than 3% Nrated/min</p> <p>HZP</p>	<p>100%Nrated</p>  <p>Not more than 1% Nrated/min</p> <p>85%Nrated</p> <p>Power level hold for at least 3 hours</p> <p>Not more than 1% Nrated/min</p> <p>45%Nrated</p> <p>Not more than 3% Nrated/min</p> <p>HZP</p>	<p>100%Nrated</p>  <p>Not more than 0.17%Nrated/min</p> <p>80%Nrated</p> <p>Not more than 0.17%Nrated/min</p> <p>50%Nrated</p> <p>Not more than 3% Nrated/min</p> <p>HZP</p>	<p>100%Nrated</p>  <p>Two steps of 10% Nrated and a delay of at least 3 hours between steps</p> <p>50%Nrated</p> <p>Once with 20% Nrated</p> <p>HZP</p>
		The average speed is ensured by a power boost step of 2-4% Nrated at speeds of up to 2% Nnom / min followed by a time delay.	

FIG. 9. Reactor power changes permissible speeds for rated power -3000MW.

REACTOR POWER CHANGES PERMISSIBLE SPEED			
Planned power decrease	Planned power increase	Power increase after: - main circulation pump start; - long (more than 12 days) reactor operation at decreased power level - after refuelling; - at the end of cycle during reactor coastdown $N < 85\%N_{rated}$	Stepwise increase of reactor power
<p>104%Nrated</p>  <p>Not more than 3% Nrated/min</p> <p>HZP</p>	<p>104%Nrated</p>  <p>Not more than 1% Nrated/min</p> <p>80%Nrated</p> <p>Power level hold for at least 3 hours</p> <p>Not more than 1% Nrated/min</p> <p>45%Nrated</p> <p>Not more than 3% Nrated/min</p> <p>HZP</p>	<p>104%Nrated</p>  <p>Not more than 0.17%Nrated/min</p> <p>80%Nrated</p> <p>Not more than 0.17%Nrated/min</p> <p>50%Nrated</p> <p>Not more than 3% Nrated/min</p> <p>HZP</p>	<p>104%Nrated</p>  <p>Two steps of 10% Nrated and a delay of at least 3 hours between steps</p> <p>50%Nrated</p> <p>Once with 20% Nrated</p> <p>HZP</p>
		The average speed is ensured by a power boost step of 2-4% Nrated at speeds of up to 2% Nnom / min followed by a time delay.	

FIG. 10. Reactor power changes permissible speeds after power uprate-3120MW.

On the refuelling stage, the maximum values of the linear power have to satisfy the two limiting curves — Ql vs Bu and Ql vs Hrc. As shown below in Tables 2 and 3 and Figs 11 and 12 the maximum values of the linear power as a function of fuel rod burn-up and reactor core height satisfy the limiting curves with large margins [3].

TABLE 2. LINEAR POWER LIMITS VS NUCLEAR FUEL BURNUP

Fuel element	Burnup, MW·d/kg U	Linear power limit [W/cm]
Fuel rod	0	448
	20	360
	40	310
	70	255
Fuel rod with Gd	0	360
	15	360
	35	310
	65	255

TABLE 3. LINEAR POWER LIMITS VS REACTOR CORE HEIGHT

Fuel element	Reactor core height, [%]	Linear power limit [W/cm]
Fuel rod	0	448
	50	448
	80	360
	100	301
Fuel rod with Gd	0	360
	80	360
	100	301

6. POWER PEAKING FACTORS

List of power peaking factors used at WWER-1000 Kozloduy reactors:

- K_{qi} - relative (normalized to total number of FA in the core) power in the FA with number i ;
- K_q - fuel assemblies power peaking factor in the reactor core, $K_q = \max_i(K_{qi})$;
- K_{vij} - relative (normalized to the total number of volumes in the core) power of volume number j along the height of the FA with number i ;
- K_v - power peaking factor by volumes in the reactor core, $K_v = \max_{ij}(K_{vij})$;
- $K_{v\text{доп}}(i,j)$ - permissible value of the volume power peaking factor at the j -th volume of the i -FA;
- K_{kil} - relative (normalized to the total number of fuel rods in the FA) power of fuel rod number l at volume number j where is $\max K_{vij}$ for FA with number i ;
- K_{ki} - power peaking factor by fuel rods in FA with number i , $K_{ki} = \max_l(K_{kil})$;
- K_r - radial power peaking factor, $K_r = \max_i(K_{qi} \cdot K_{ki})$;
- K_{zi} - power peaking factor along the height of the FA with number i , $K_{zi} = \max_j(K_{vij}) / K_{qi}$;
- K_z - power peaking factor along the height of the FAs in the reactor core, $K_z = \max_i(K_{zi})$;
- K_o - reactor core total power peaking factor, $K_o = \max_{ij}(K_{vij} \cdot K_{ki})$;
- $K_{o\text{доп}}$ - permissible value of the total power peaking factor at the j -th volume of the reactor core;
- K_m - max ratio of calculated to permissible value of the reactor core total power peaking factor.

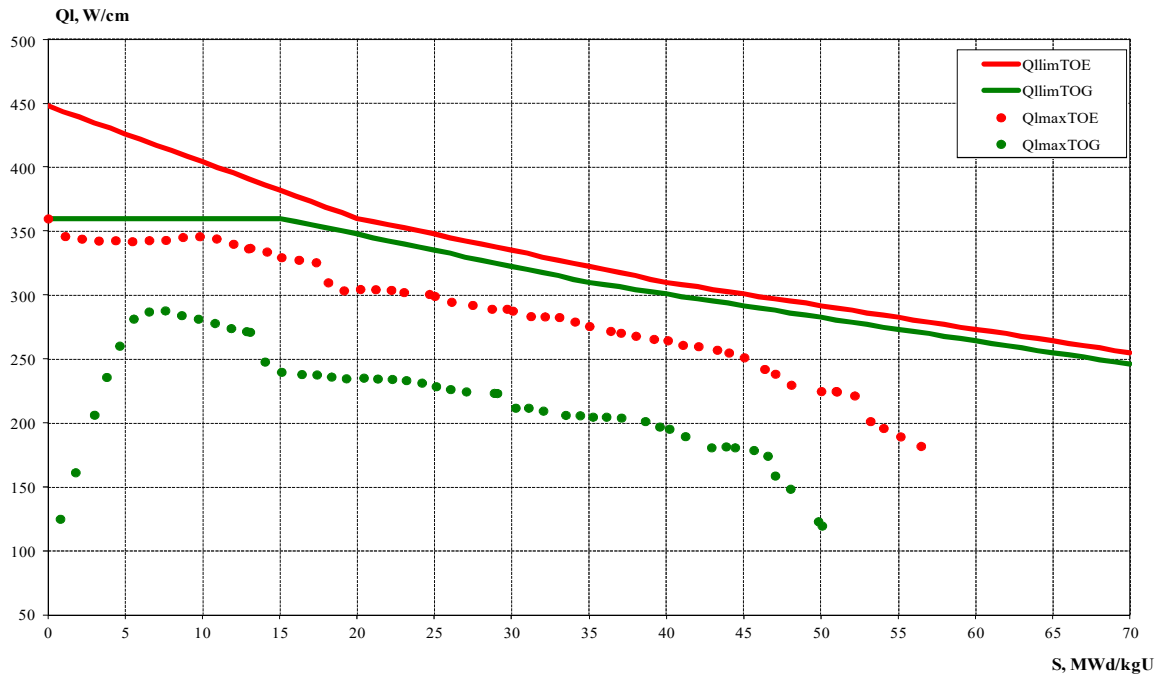


FIG. 11. Linear power limits Maximum values of the linear power vs burnup – U6/C25.

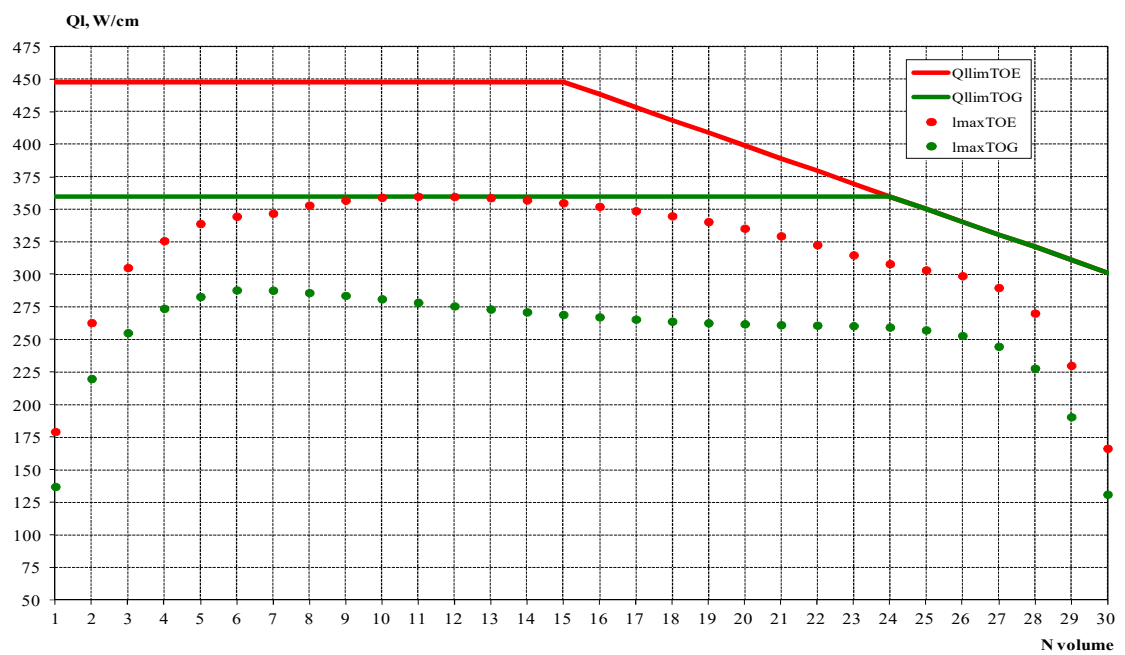


FIG. 12. Linear power limits Maximum values of the linear power vs burnup – U6/C25.

Table 4 represents power peaking factors limitations (*- cycle with assemblies TVSA, **- mixed cycle with assemblies TVSA and TVSA-12, ***- cycle with assemblies TVSA-12)) [3].

TABLE 4. POWER PEAKING FACTORS WITH LIMITING VALUES

Characteristics	Permissible values
Power peaking factors for power 3120 MW	
K _q	≤1.35* ≤1.43** ≤1.50***
K _v	≤2.05* ≤2.05** ≤2.05***
K _r	≤1.50* ≤1.54** ≤1.57***
K _m	≤1.00
K _z	≤1.49* ≤1.40** ≤1.45***
For power peaking factors K _q , K _r , K _m , K _v at N _{current} < N _{rated} - K _{current}	
K _{perm} – permissible factor for 104%N _{rated} ; K _{current} = K _{perm} * f	
When N _{current} / N _{rated} > 0.8	
f = 1/(0.17+0.83* (N _{current} / N _{rated}))	
When 0.3 ≤ N _{current} / N _{rated} ≤ 0.8	
f = 1.019+0.144*(N _{rated} / N _{current})	
When 0.1 < N _{current} / N _{rated} < 0.3	
f = 1/(0.17+0.83 * N _{current} / N _{rated})	
Maximum burnup for FA type TVSA/TVSA-12, MW·d/kgU	
- Average for fuel assembly	≤55.0*, ≤55.0**, ≤62.6***
- Average for fuel rod	≤59.1*, ≤59.9**, ≤65.3***
- In fuel rod pin	≤64.3*, ≤65.5**, ≤71.2***
- Average for Gd fuel rod	≤51.4*, ≤52.4**, ≤57.6***
- In Gd fuel rod pin	≤56.2*, ≤57.5**, ≤63.1***
Maximum operating time of a fuel assembly	≤31500*, ≤31500**, - **

7. MAIN NEUTRON PHYSICS CHARACTERISTICS

Main neutron physics characteristics during Cycle 23 of unit 6, calculated by different codes Bipr-7a/ Permak and HEX3DA/ HEX3DP are presented at Table 5 and Figure 13 [7].

8. FUEL RELIABILITY STATISTICS

At Kozloduy NPP, refuelling is always carried out with full unloading of the fuel assemblies from the reactor. This allows to review the plates and, if necessary, to remove debris. Over the entire Kozloduy NPP TVSA operation period (starting from 2004), more than 1200 assemblies were burned at units 5 and 6, of which only one leaky TVSA was detected for the second year of operation - without achieving a normal operational limit on I-131 in the primary circuit 1.48E+6 Bq/l. Over the Kozloduy NPP TVSA-12 operational period (starting from 2016), 163 assemblies were irradiated only at unit 6, of which two leaky TVSA-12 were detected - without achieving a normal operational limit on I-131 in the primary circuit 1.48E + 6 Bq / l.

TABLE 5. MAIN NEUTRON PHYSICS CHARACTERISTICS DURING CYCLE 23 OF UNIT 6

T	W	tin	C _B	K _q	K _q	K _v	K _v	K _r	K _r	K _o	K _o
fpd	MW	°C	g/kg	Bipr-7a	HEX3DA	Bipr-7a	HEX3DA	Permak	HEX3DP	Permak	HEX3DP
0	3120	286.5	6.54	1.36	1.36	1.63	1.63	1.50	1.52	1.89	1.86
5	3120	286.5	6.62	1.38	1.38	1.65	1.64	1.49	1.51	1.83	1.82
10	3120	286.5	6.46	1.39	1.38	1.65	1.63	1.49	1.50	1.79	1.80
20	3120	286.5	6.17	1.39	1.38	1.64	1.61	1.50	1.50	1.76	1.79
40	3120	286.5	5.71	1.39	1.37	1.60	1.58	1.49	1.51	1.74	1.78
60	3120	286.5	5.27	1.38	1.36	1.56	1.54	1.47	1.51	1.72	1.77
80	3120	286.5	4.84	1.37	1.35	1.53	1.51	1.46	1.51	1.70	1.76
100	3120	286.5	4.41	1.36	1.33	1.52	1.50	1.46	1.51	1.69	1.76
120	3120	286.5	3.99	1.34	1.32	1.53	1.51	1.46	1.51	1.69	1.76
140	3120	286.5	3.59	1.34	1.33	1.55	1.53	1.46	1.51	1.71	1.76
160	3120	286.5	3.21	1.35	1.34	1.58	1.54	1.47	1.52	1.73	1.76
180	3120	286.5	2.84	1.36	1.35	1.59	1.55	1.48	1.52	1.75	1.75
200	3120	286.5	2.46	1.37	1.35	1.59	1.55	1.49	1.52	1.75	1.74
220	3120	286.5	2.06	1.37	1.36	1.57	1.54	1.49	1.52	1.72	1.73
240	3120	286.5	1.64	1.37	1.36	1.55	1.52	1.49	1.51	1.70	1.72
260	3120	286.5	1.22	1.37	1.35	1.53	1.51	1.49	1.51	1.67	1.70
280	3120	286.5	0.79	1.36	1.35	1.52	1.50	1.48	1.50	1.65	1.68
300	3120	286.5	0.35	1.35	1.34	1.50	1.49	1.47	1.49	1.63	1.66
316.3	3120	286.5	0.00	1.35	1.34	1.49	1.48	1.46	1.48	1.62	1.65

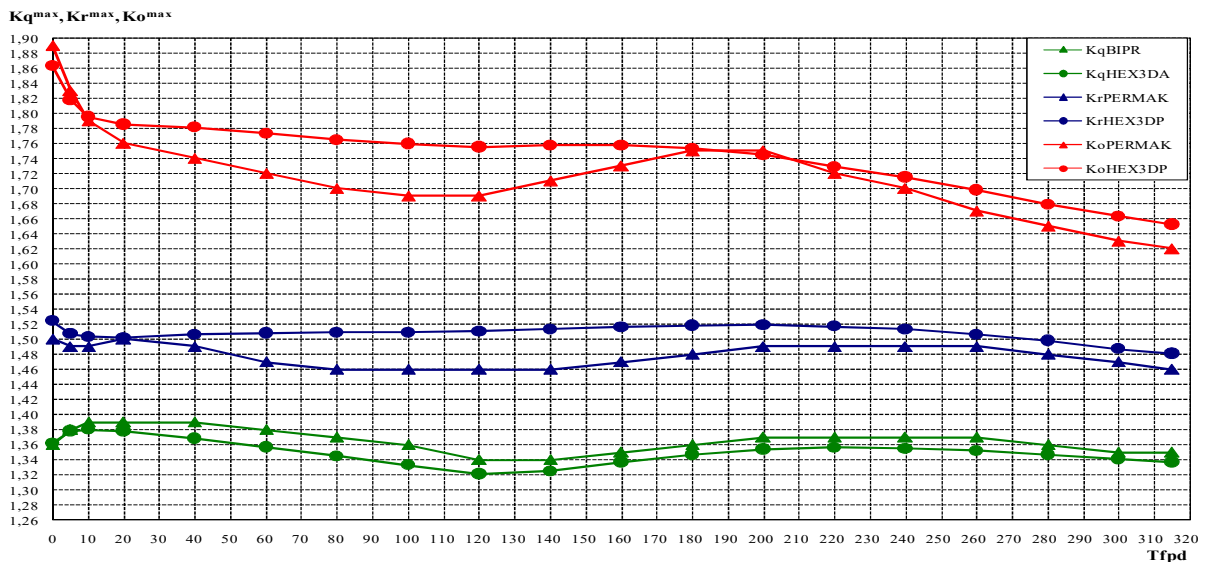


FIG. 13. Assembly, fuel rod and fuel pin power distribution by different codes – U6/C23.

9. SPENT FUEL POOL FUEL COOLING REPORTS

After Fukushima we have taken special measures to prevent fuel damage in the spent fuel pool even when all cooling pumps are seized [7–10]. For every cycle of units 5 and 6 we calculate (using Scale 6.1) report with:

- Decay heat for every Spent Fuel Pool section- B01, B02, B03,
- Time for water heating from $T_1=35^\circ\text{C}$ до $T_2=100^\circ\text{C}$, $\text{Level}_{\text{const}}=35.7\text{ m}$, presented in Fig. 15.
- Time for water evaporation from level 35.7 m to 28.8 m (beginning of dividing to sections B01, B02, B03) at $T=100^\circ\text{C}$, $p=1\text{ atm}$, presented in Fig.16,
- Time for water evaporation from level 28.8 m to 25.8 m (the upper end of the fuel part of the rod) at $T=100^\circ\text{C}$, $p=1\text{ atm}$, for every Spent Fuel Pool section- B01, B02, B03 presented in Fig.17.

Unit 6 total layout of the reactor core and spent fuel pool is presented in Fig. 14 [11].

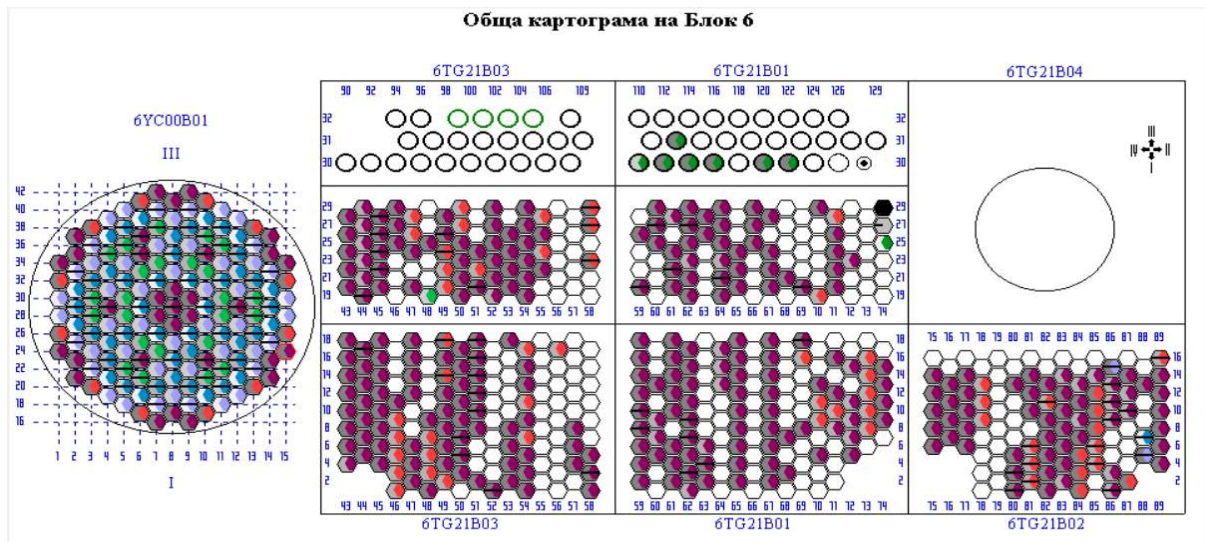


FIG. 14. Total layout of the reactor core and spent fuel pool.

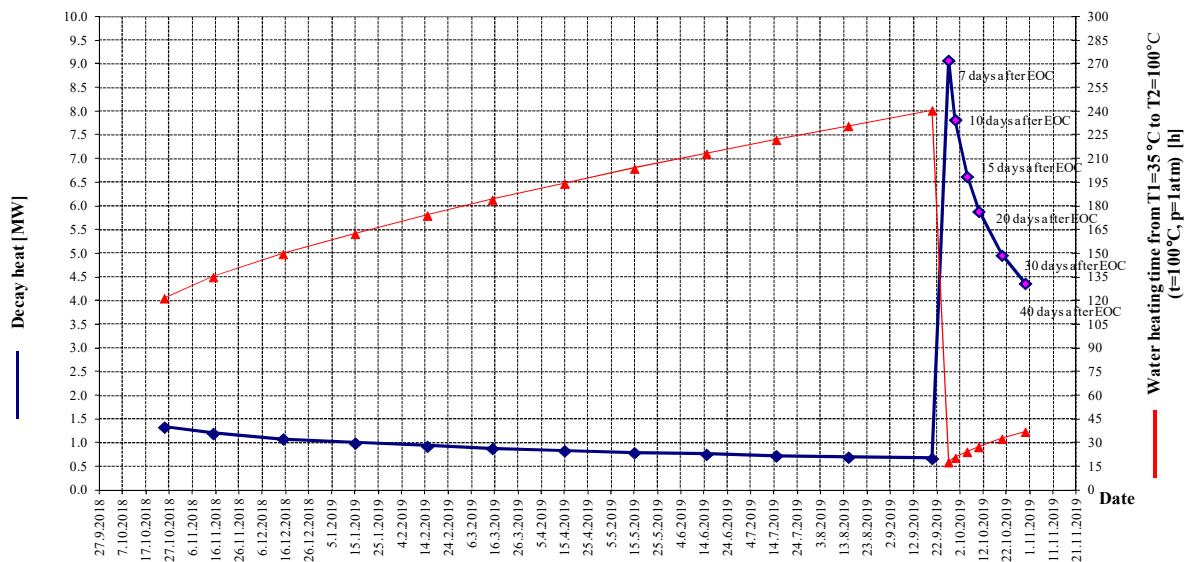


FIG. 15. Decay heat of the fuel assemblies in the unit 6 Spent Fuel Pool and time for water heating from $T_1=35^\circ\text{C}$ to $T_2=100^\circ\text{C}$ for $\text{level}_{\text{const}}=35.7\text{ m}$, for the period of 24-th cycle of unit 6 and outage 2019 (In case of loss of all pumps).

10. CONCLUSION

Over the entire Kozloduy NPP TVSA fuel type operational period (starting from 2004), more than 1200 assemblies were burned at units 5 and 6, of which only one leaky TVSA was detected (for the second year of operation - without achieving a normal operational limit on I-131 in the primary circuit $1.48E + 6$ Bq / l).

Kozloduy NPP reactor operational guidelines, fuel related limitations and good practices ensure reliable nuclear fuel operational conditions.

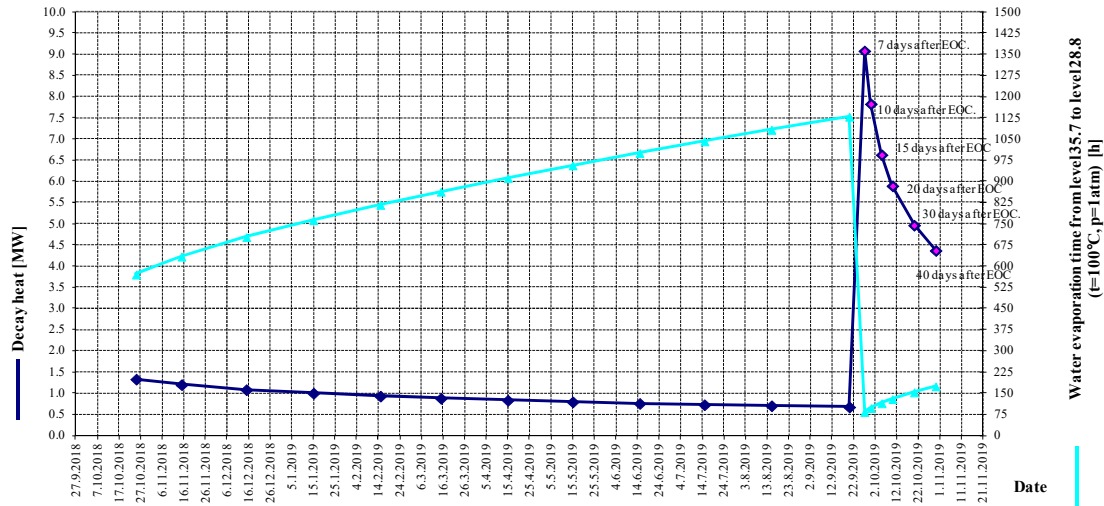


FIG. 16. Decay heat of the fuel assemblies in the unit 6 Spent Fuel Pool and time for water evaporation from level 35.7 m to 28.8 m (beginning of dividing to sections B01, B02, B03) at $T=100^{\circ}\text{C}$, $p=1$ atm for the period of 24-th cycle of unit 6 and outage 2019 (In case of loss of all pumps).

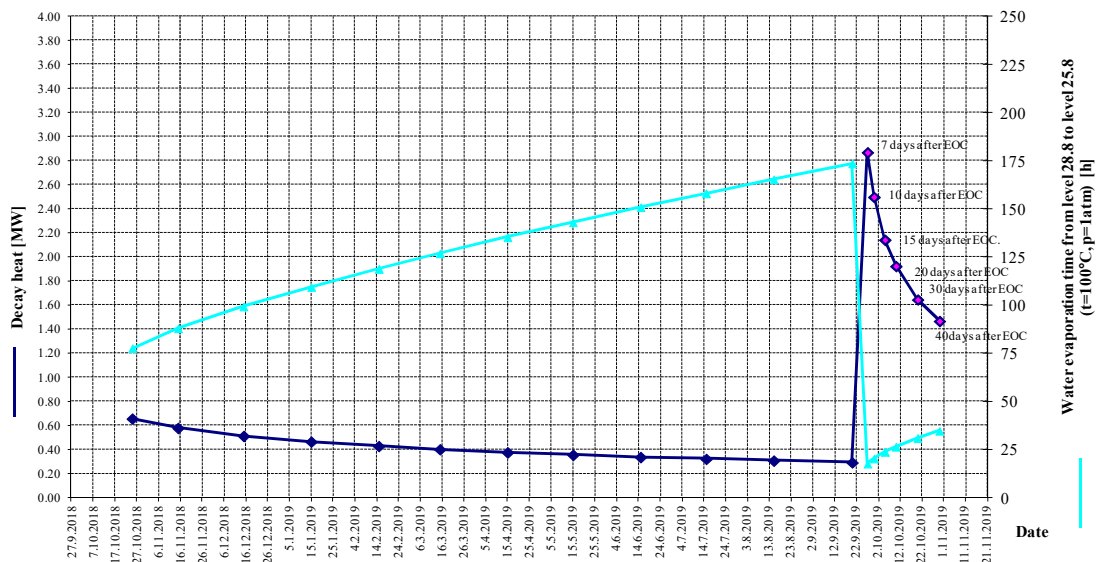


FIG. 17. Decay heat of the fuel assemblies in the section B01 of unit 6 Spent Fuel Pool and time for water evaporation from level 28.8 m to 25.8 m (the upper end of the fuel part of the rod) at $T=100^{\circ}\text{C}$, $p=1$ atm for the period of 24-th cycle of unit 6 and outage 2019 (In case of loss of all pumps).

REFERENCE

- [1] Components of VVER-1000/V320/ reactor core, Catalog description Б 0401.21.00.000 ДКО, 2003.
- [2] TVSA-12 VVER-1000 fuel assemblies set. Catalog description Б 0401.40.00.000 ДКО.
- [3] Administrative Instruction. "Preparation of reports with neutron-physical characteristics of VVER-1000 reactor", №30.ОБ.УС.АД.03/11.
- [4] "Kurchatov Institute", VVER Research Branch. The complex of programs of neutron-physical calculations of RNC KI. PIR_A programme. Description of the algorithm. Application description №32/1-75-401, Moscow, 2001.
- [5] "Kurchatov Institute", VVER Research Branch. The complex of programs of neutron-physical calculations of RNC KI. Complex of "KASKAD" programs. BIPR-7A program. Description of the algorithm. Application description. No. 32 / 1-9-102, Moscow, 2002.
- [6] Technical specifications for safe operation of unit 6 at Kozloduy NPP with reactor VVER-1000/V320/№ 36.06.00.p.01/ 2.
- [7] A. Kamenov, V. Spasova, D. Hristov, Report Neutron physics characteristics for cycle 23 of unit 6 17.36.ОБ.УС.НФХ.23-1/0.
- [8] D. Hristov, Validation report of complex Scale 6.1 for VVER-1000 reactors.
- [9] D. Hristov, Methods for calculation of radiation characteristics of VVER-1000 fuel assemblies Identification No 30. OB.00.00.MT.12 / 2.
- [10] Scale: A Comprehensive Modelling and Simulation Suite for Nuclear Safety Analysis and Design, ORNL/TM-2005/39, Version 6.1, June 2011. Available from Radiation Safety Information Computational Center at Oak Ridge National Laboratory as CCC-785.
- [11] Computer system for the nuclear fuel management, control and reporting "Smart fuel", Datacom, Risk engineering.

THERMO-MECHANICAL ANALYSIS OF TYPICAL FBR FUEL PIN BEHAVIOR

A.K. DEO, A. J. GAIKWAD
AERB,
Mumbai, India
Email: anuj@aerb.gov.in

S. CLEMENT, R. CHANDAR
IGCAR,
Kalpakkam, India

Abstract

In order to realize the target burnup (BU) along with safe operation without any fuel pin failure, it is very important to estimate the evolution of various parameters with BU e.g. fuel clad mechanical interaction Pressure (FCMI), fission gas pressure, centre line temperature, cladding stresses, FCCI (fuel clad chemical interaction) wastage, clad wastage due to corrosion and erosion by coolant, cumulative damage fraction (CDF) in the clad, etc. The modified SATURN-FS1 computer code is used for the thermo-mechanical analysis of a typical FBR fuel pin. With the modified SATURN-FS1 code, it is possible to perform a complete thermo-mechanical analysis of an FBR fuel pin with D9 clad material, taking into account all thermal, mechanical and radiation based effects. The SATURN FS1 code has been modified to account for the effect of axial power profile, updated fuel properties, D9 material properties, FCCI, and calculation of $P_m + P_b$ (primary membrane and bending stresses) in the cladding using numerical integration. The code was also modified to evaluate the creep damage in the cladding.

Together with the above parameters, the analysis is performed to evaluate the fuel performance for a higher BU potential, to identify the parameters that can be optimized for future reactors, to evaluate the available design margins, to identify the areas in which the code needs to be updated and improved. Key findings on the above parameters are discussed in detail in this article.

1. INTRODUCTION

The MOX fuel is selected for Prototype Fast Breeder Reactor (PFBR) with maximum PuO_2 as $\sim 28\%$ and $\sim 20\%$ cold worked austenitic SS called D9 as clad. The target BU is 100 GWd/t with a peak linear power of 450 W/cm. To realize the target burn-up (BU) along with safe operation without any fuel pin failure, it is very important to estimate the evolution of various parameters with BU e.g. FCMI pressure (fuel clad mechanical interaction pressure), fission gas pressure, centreline temperature, stresses in the clad, wastage of clad due to FCCI (fuel clad chemical interaction), wastage of clad due to corrosion & erosion by coolant, incurred cumulative damage fraction (CDF) in the clad etc. SATURN-FS1 [1], a computer code for thermo-mechanical analysis of fuel rod, developed by Kernforschungszentrum (Nuclear Research Centre), Karlsruhe, Germany was modified and used for the analysis of the peak rated fuel pin. With Modified SATURN-FS1 code, it is possible to perform complete thermo-mechanical analysis of an FBR fuel pin having D9 clad material, taking into account all thermal, mechanical and irradiation-based effects. The code was modified to account for the effect of axial power profile, updated fuel properties, D9 material properties, FCCI and calculation of $P_m + P_b$ (Primary membrane & bending stresses) in the clad using numerical integration. Code was also modified to evaluate the creep damage in the clad. In this report, the analysis results obtained from modified SATURN-FS1 code are discussed in detail and the important observations are also discussed. As this exercise is to determine MOX fuel performance, uncertainties involved in the design inputs are not considered and nominal values are taken into account.

2. MODELING OF FUEL PIN

A typical FBR fuel pin is shown in Fig.1 with the geometrical details [2]. It consists of a middle plug over which the pellets are stacked. The active core length is 1000 mm and the two axial blankets are of 300 mm length each. There are two plenum volumes– one at bottom of the pin having 710 mm length and one at the top of the pin having 200 mm length. As the linear power varies along the height of the active core, the generation and release of fission gases also varies along the height which in turn affects the swelling of the fuel as well as the fuel-clad gap conductance. The active core height is divided into smaller elements to account for the effect of axial power profile.

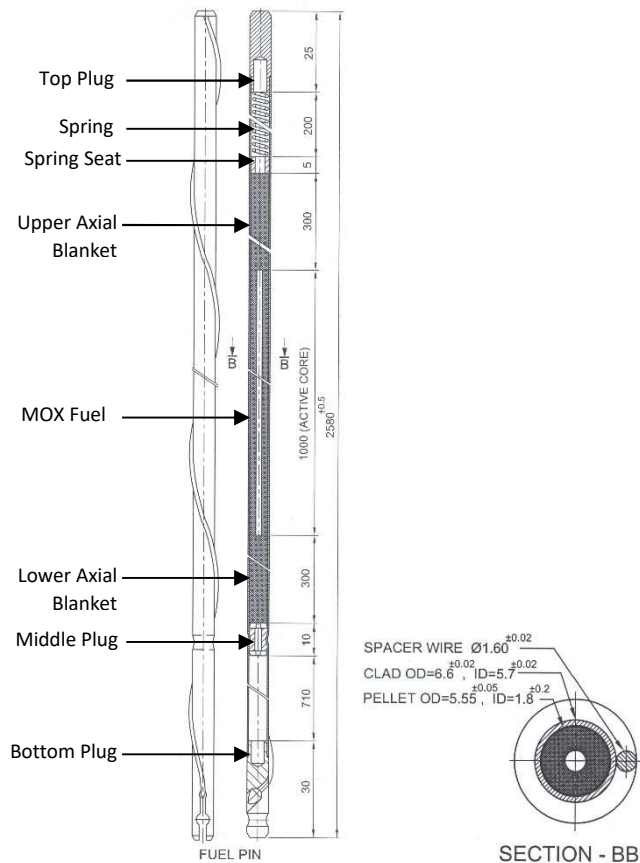


FIG. 1. Typical FBR fuel pin.

Conceptually SATURN-FS1 has a single plenum volume configuration, therefore, the upper plenum volume in the considered FBR pin, is added to lower plenum volume with temperature correction.

3. RESULTS

The code is used for the simulation of the fuel pin behaviour under irradiation equivalent to 555 EFPD (effective full power days) [2, 3] and the various results obtained are discussed in this section. All the results are presented at Active Core Peak Power Location (ACPPL).

3.1. Gap & gap conductance

The radial gap between the fuel and clad has an important role on the fuel temperature as the temperature drop across the gap is of the order of few hundred degrees centigrade. The variation of gas concentration with burnup is shown in Fig.2. It is observed that He concentration decreases to $\approx 12\%$ at the discharge burnup. However, the fission gases Xe & Kr buildup takes place up to $\approx 79.5\%$ & 8% respectively. The fuel-clad gap variation at the burnup is shown in Fig.3. It is observed from the figure that initially the radial gap increases with respect to as fabricated gap of $75 \mu\text{m}$ due to higher thermal expansion of the clad. However, a sudden decrease in the radial gap is observed due to cracking & relocation of the fuel pellets which causes the fuel pellets to fragment and move towards the clad. It is observed that cracking could occur in a fuel pellet at a very low linear power ($< 40 \text{ W/cm}$). The gap closes fully at around 1.2 at % of BU.

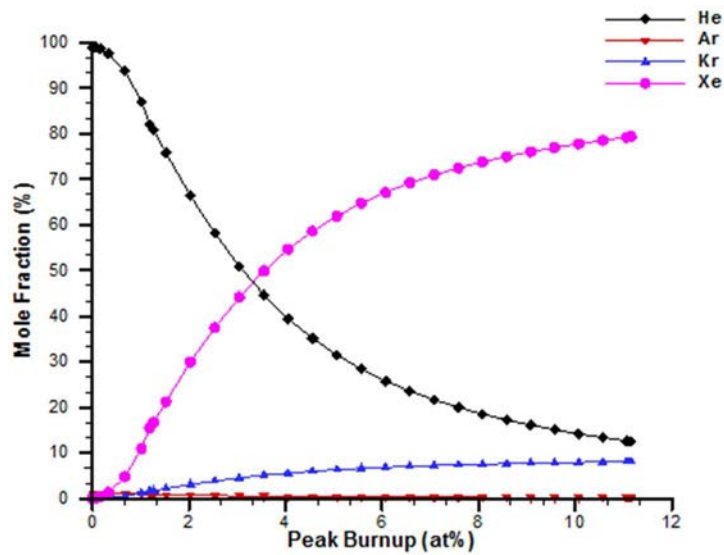


FIG. 2. Concentration of gases in the gap.

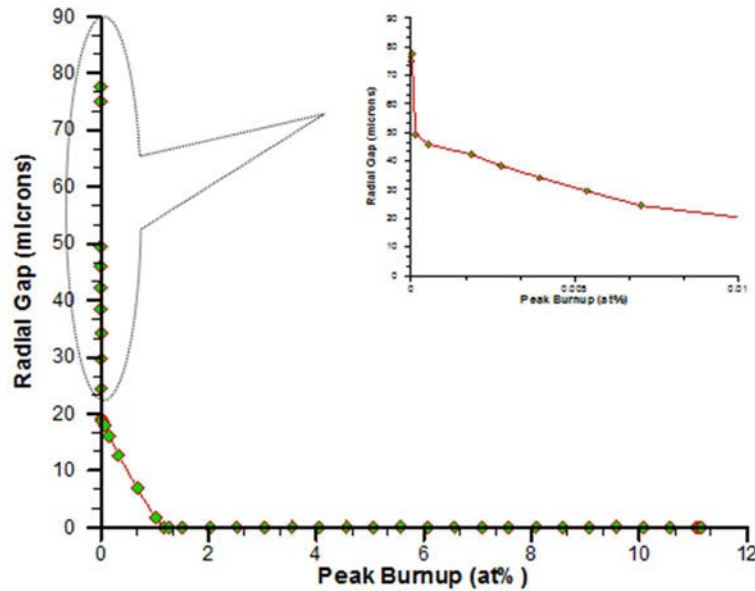


FIG. 3. Variation of radial gap.

The variation of gap conductance is shown in Fig.4. It is observed that till the full power is attained, the gap conductance increases rapidly due to decrease in gap (due to cracking & relocation) and also due to increase in temperatures which cause thermal conductivity of the gases to increase.

After the full power is attained, only swelling of pellets and gap closure due to increase in crack volume contribute to the increase in gap conductance. Therefore, the rate of increase of gap conductance decreases after the full power is attained. It is seen in Fig.4 that the gap conductance increases to $\sim 4.9 \text{ W/cm}^2\text{-K}$ due to gap closure and starts decreasing rapidly thereafter due to dilution of Helium by released fission gases.

It is observed that at room temperature itself the thermal conductivity of fission gases Kr and Xe is around $1/16^{\text{th}}$ and $1/25^{\text{th}}$ respectively with respect to pure He. Although, the dilution of bond gas (He) due to fission gases starts at beginning of life itself, the gap closure effect more profound over dilution effect. Once the gap fully closes, the dilution effect is dominant.

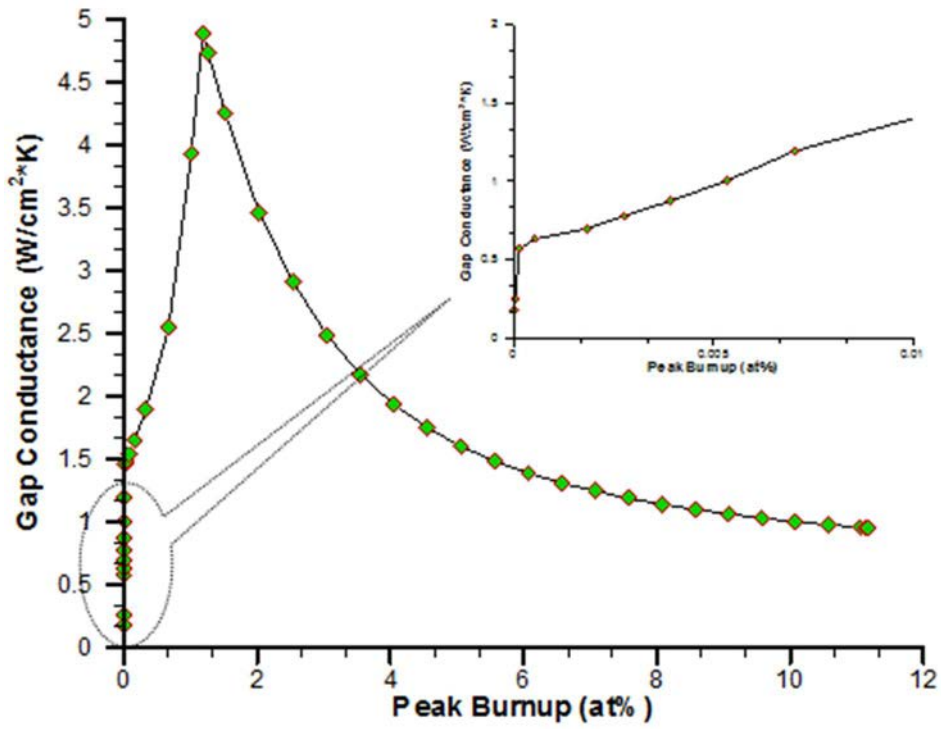


FIG. 4. Variation of gap conductance.

3.2. Fuel centreline temperature

The evolution of fuel centreline temperature is shown in Fig. 5. It is seen that till full power is attained, the centreline temperature increases rapidly as the power increases. Once the full power is attained, the effect of gap conductance gets reflected on the fuel centreline temperature. It is observed that with increase in gap conductance, the centreline temperature decreases, however, it starts increasing again with corresponding decrease in gap conductance. Further, thermal conductivity deterioration of fuel due to buildup of fission products with burnup affects the fuel centreline temperature.

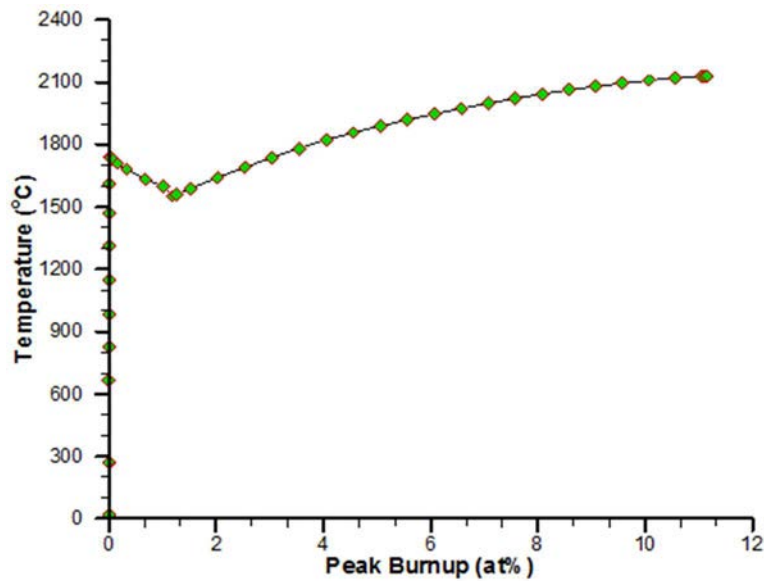


FIG. 5. Variation of centreline temperature.

3.3. Temperature across pin

Temperature contour across the fuel pin are shown in Fig.6(a) & (b) for BOL and EOL respectively. The radial temperature distribution across the fuel pin is depicted in Fig.7.

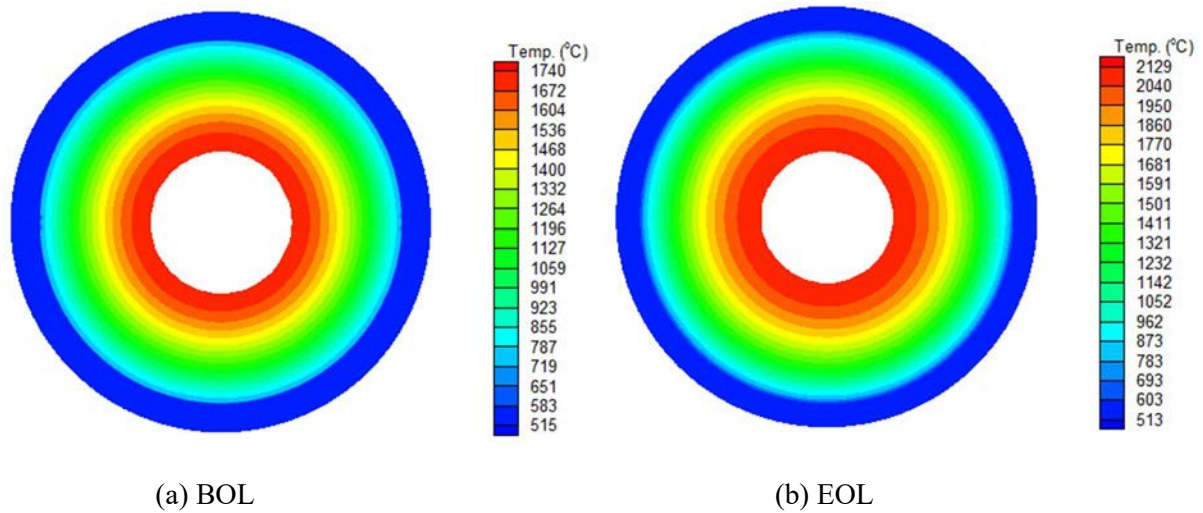


FIG. 6. Contour mapping of temperature across pin.

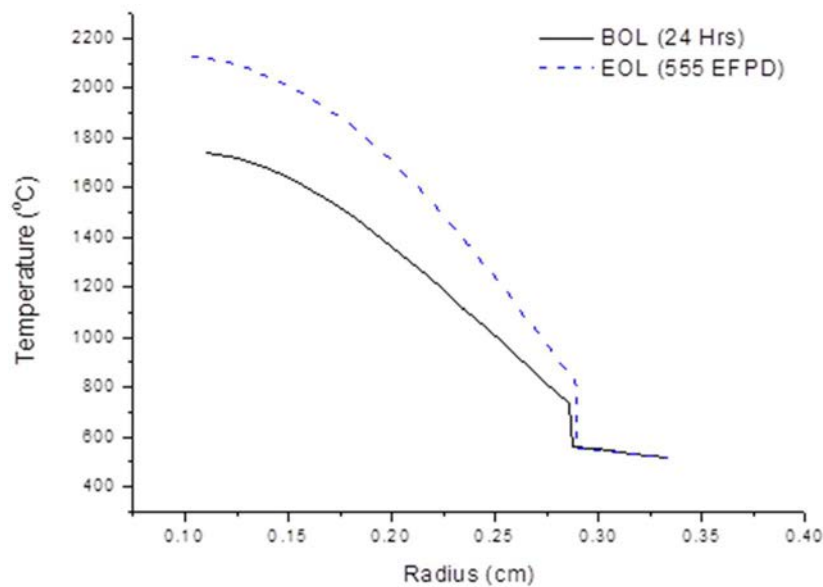


FIG. 7. Temperature distribution across pin.

3.4. Fission gas pressure

The variation of fission gas pressure with burnup is shown in Fig.8. The initial fill pressure is assumed as 0.2 MPa (absolute) at room temperature which further increases to around 0.46 MPa at operating temperature at BOL. It is predicted that at EOL the fission gas pressure increases up to ≈ 3.4 MPa.

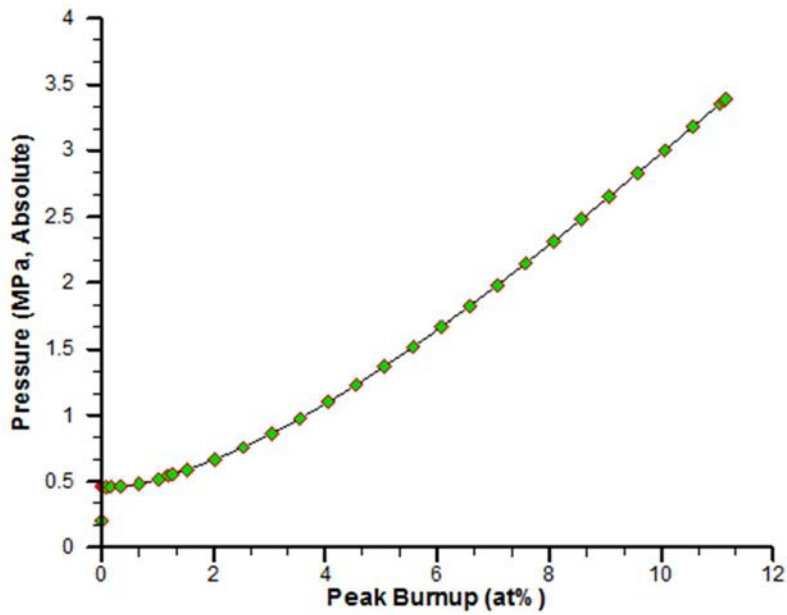


FIG. 8. Variation of fission gas pressure.

3.5. Clad inner radius

The variation in clad inner radius is shown in Fig.9. A substantial increase due to thermal expansion during full power attainment at BOL is observed. After the full power is attained, the increase in clad inner radius is due to swelling. Also, the increase in radius due to swelling follows the trend of volumetric swelling i.e. the rate of increase is higher at higher DPA.

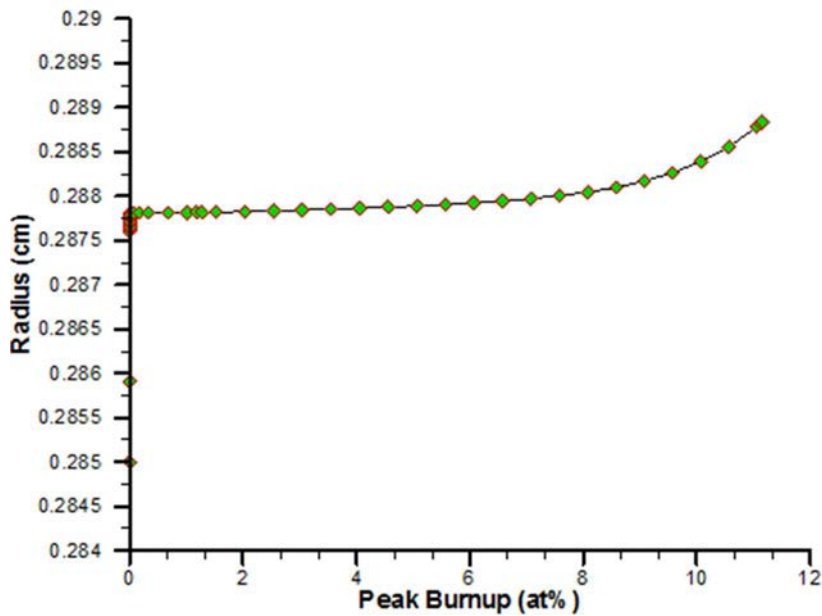


FIG. 9. Variation of clad inner radius.

3.6. Fuel clad mechanical interaction (FCMI)

As it was observed in Fig.3 that the radial gap closes at around 1.2 at % of peak burnup, fuel pellets start exerting pressure on the clad inner wall after that. The FCMI pressure is depicted in Fig.10. The FCMI pressure

reaches a peak value of ≈ 2.2 MPa and starts decreasing thereafter when the clad starts swelling higher than fuel, resulting in rapid increase of clad inner radius as shown in Fig.9.

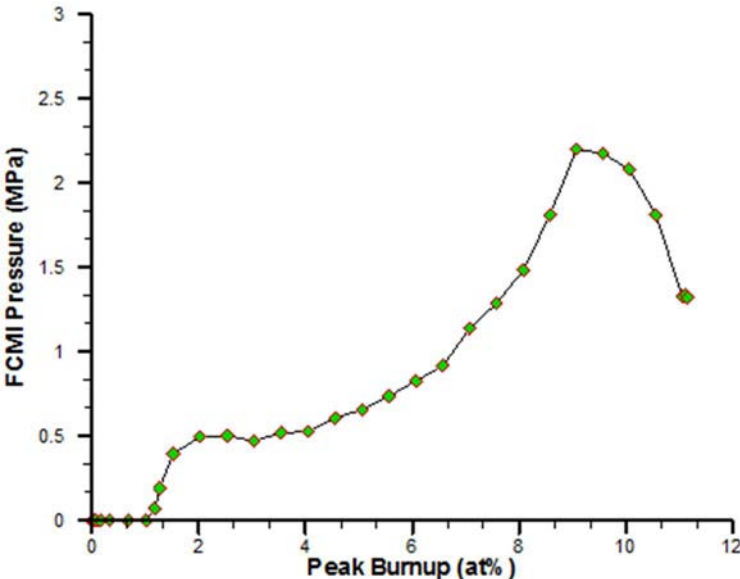


FIG. 10. Variation of FCFMI pressure.

3.7. Stresses in clad

Figure 11 shows the development of the stresses (von Mises, radial, tangential and axial) in the clad inner ring with burnup. Figure 12 shows the development of the stresses in the outer ring of the clad.

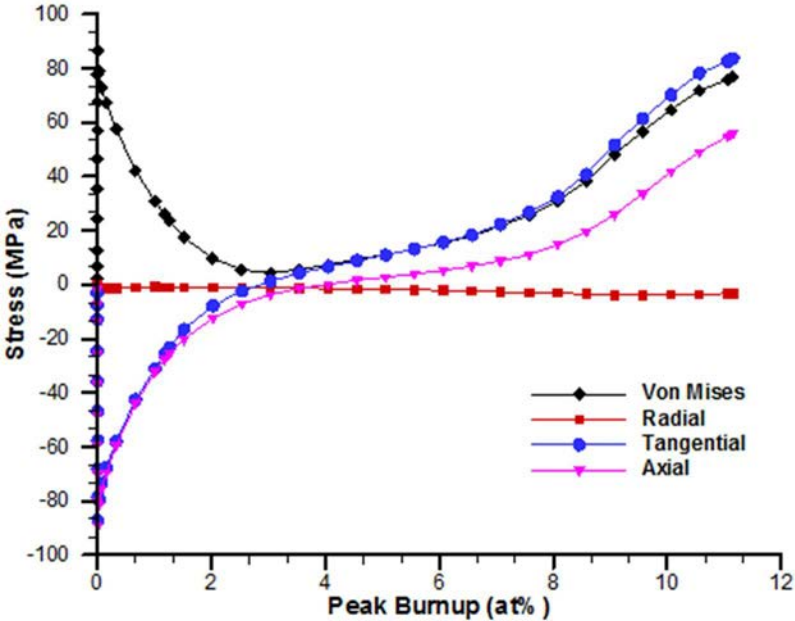


FIG. 11. Stresses in the clad inner ring.

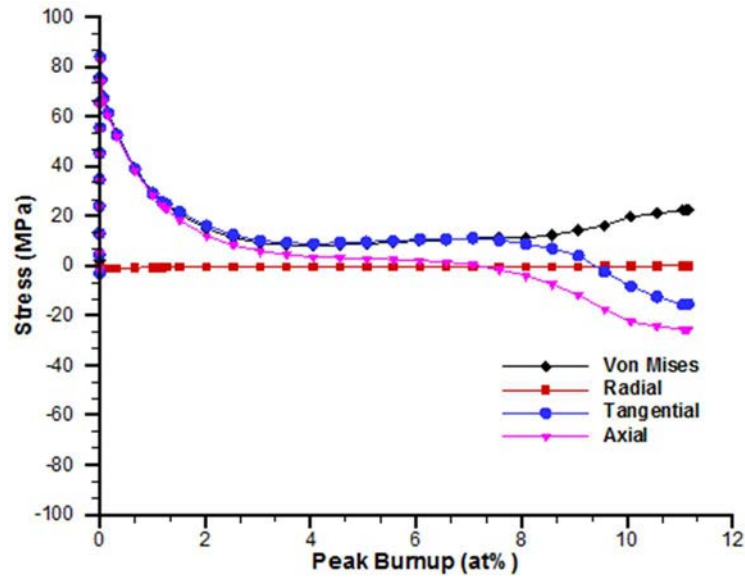


FIG. 12. Stresses in the clad outer ring.

Until full power is reached, the temperature drop in the cladding increases and thermal stresses develop in the cladding. The clad inner wall has a higher temperature and tends to expand more than the clad outer wall, which has a lower temperature. This tendency of higher thermal expansion of the clad inner wall is limited by the clad outer wall, resulting in tangential and axial compressive stresses in the clad inner wall.

However, for the same reason, the clad outer wall experiences tangential and axial tensile stresses.

From Fig. 11 and Fig. 12 it can be seen that after reaching full power, due to radiation creep all the stresses begin to decrease. It is observed that rate of the irradiation creep is much higher (a few orders of magnitude higher) than rate of the thermal creep. Subsequently, the fission gases are released in due course of burnup, which leads to an increase in the internal pressure and causes tensile stresses in the cladding. Later, FCMI (for almost the entire length of the active core) comes into effect, which also causes tensile stresses in the cladding.

Because of these tensile stresses, the already tensile tangential and axial stresses in the clad outer ring further increase, and in the clad inner ring, the tangential and axial stresses which were compressive in nature, first become zero and then tensile. It can also be seen from Fig. 12 that beyond a BU (9 at % BU) where the swelling of the clad becomes significantly high, the clad outer ring transitions into tangential and axial compressive stresses and at the same time the clad inner ring is under tension. This is due to the fact that the clad outer surface has a lower temperature compared to the clad inner surface and therefore swells more. The increased swelling of the clad exterior wall is limited by the clad interior wall, resulting in additional tangential and axial compressive stresses in the clad exterior wall and stresses of the opposite nature (tensile) in the clad interior wall. The compressive stresses being high, nullify the already existing tensile stresses and the clad outer wall goes into compression. Figures 13 and 14 show the variation of the stresses across the clad for BOL and EOL, respectively.

3.7.1. Membrane and bending stresses

The membrane and bending components of the stresses were obtained according to RCC-MR (2007) [4] using numerical integration method.

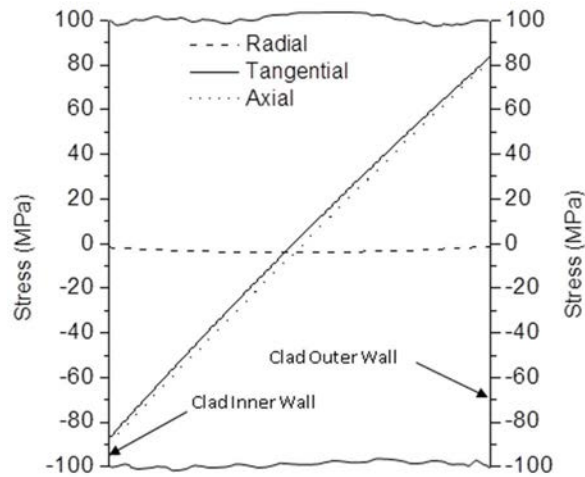


FIG. 13. Stresses across the clad wall (BOL).

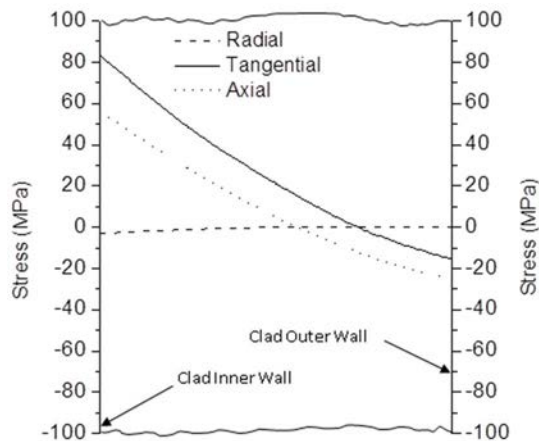


FIG. 14 Stresses across the clad wall (EOL).

Figure 15 shows the development of tangential, axial and radial components of membrane stresses. It should be noted that there is a gradual increase in the tangential component of the membrane stress in Fig.15 at ~ 1.2 at % burnup. This increase is due to the onset of FCMI at this point, as already observed in FIG.10. Again, at a higher burnup due to a decrease in the FCMI, the radial and tangential components of the membrane stresses are seen decreasing as can be seen in Fig.15. Due to stress variations across the clad thickness, bending stresses develop.

The bending components of the stresses were obtained according to RCC-MR (2007). Figures 16 and 17 show the variation of the bending components at the inner and outer walls of the clad, respectively. It is seen that the bending stresses are equal in magnitude but opposite in nature at clad inner and outer wall.

The development of P_m (general primary membrane stress intensity) as well as $P_m + P_b$ (P_b : primary bending stress intensity) is shown in Fig.18. It is seen from Fig.18 that $P_m + P_b$ at clad inner wall is higher than that at the outer wall.

3.8. CDF (cumulative damage fraction) incurred in clad

Since clad is the first boundary for containing the fission products after release from fuel, its integrity for the desired burnup must be ensured. There are two approaches for ensuring the clad integrity:

- Strain limit approach, which limits clad strains to a certain limit for different event categories;
- CDF approach, wherein damage to clad is accumulated throughout the BU and is limited to 0.25 for category 1, 2 and 3 events.

In this analysis, the second approach is adopted. Using the local temperatures and equivalent stresses of the clad elements, CDF is predicted. The variation of CDF with BU is shown in Fig.19.

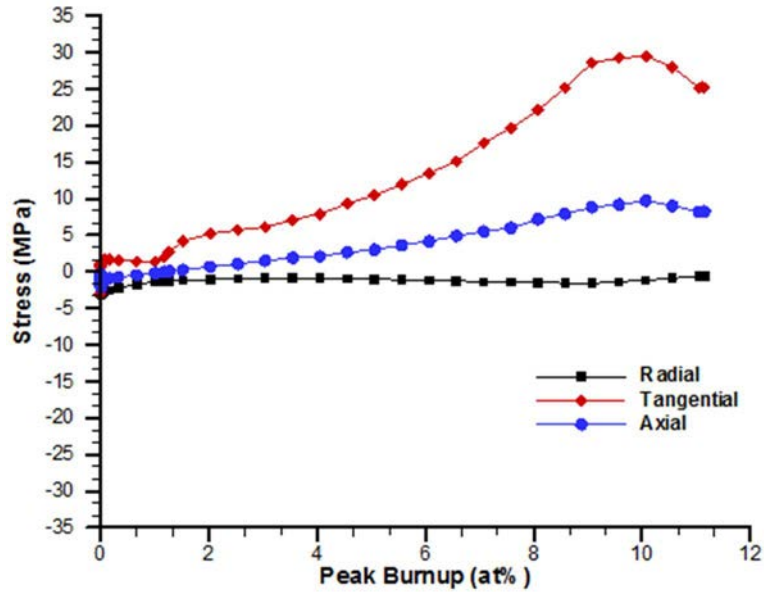


FIG. 15. Membrane stresses.

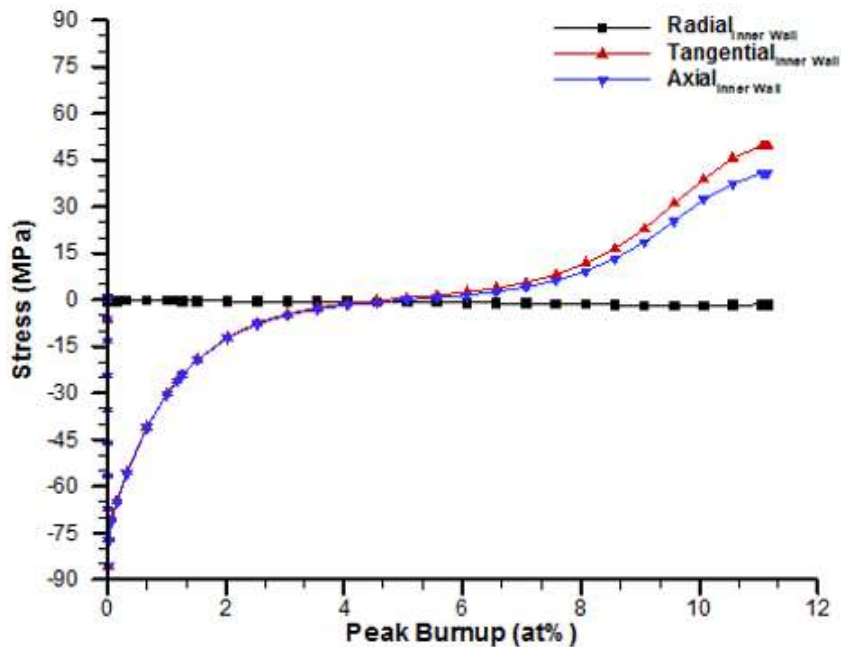


FIG. 16. Bending stresses (Clad Inner Wall).

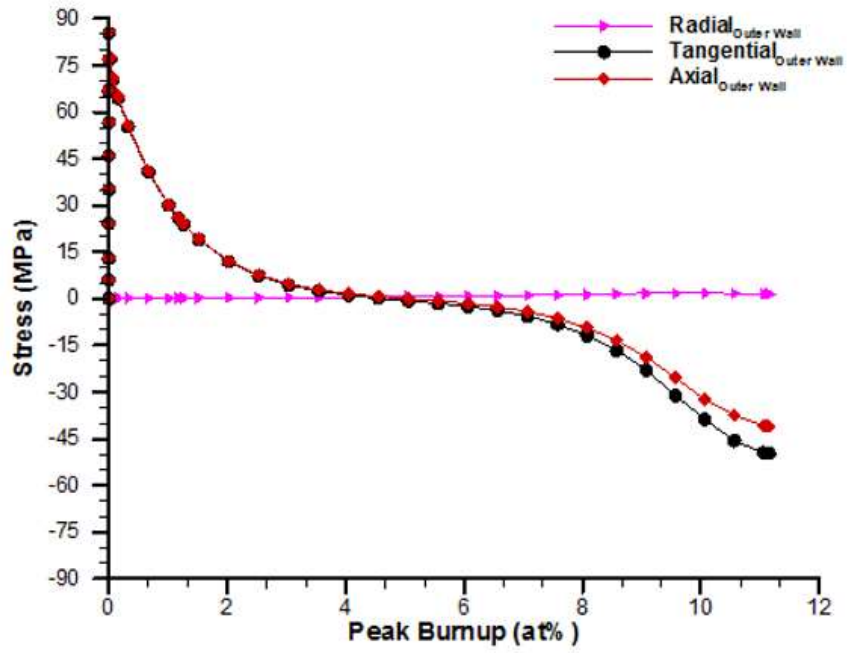


FIG. 17. Bending stresses (Clad Outer Wall).

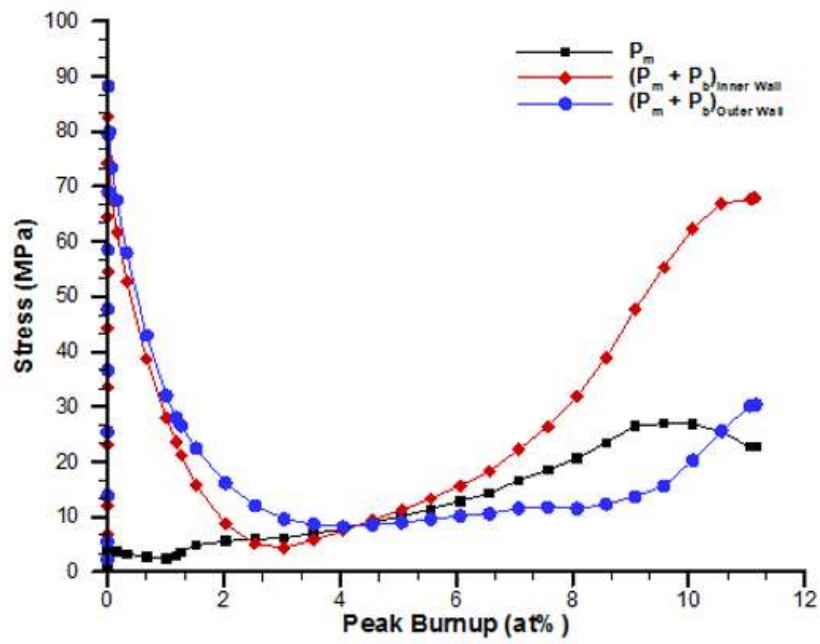


FIG. 18. Variation of P_m and P_m+P_b .

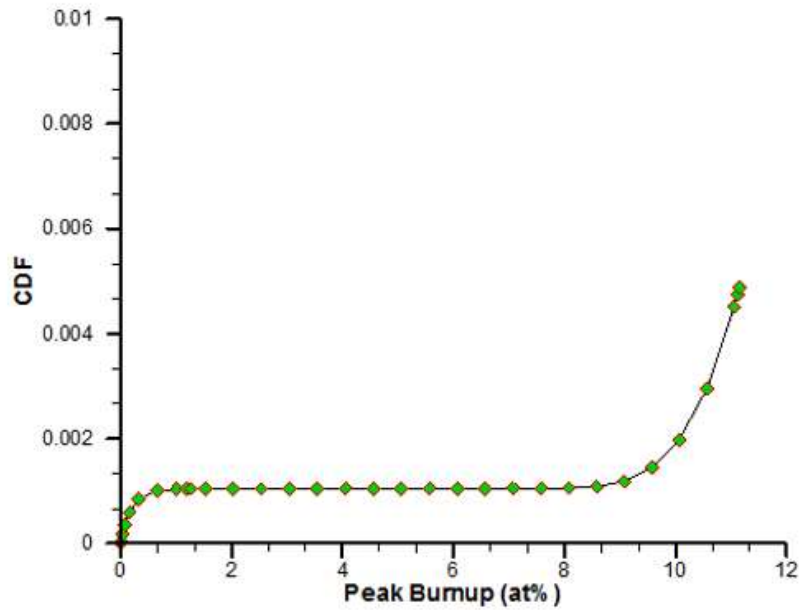


FIG. 19. Variation of CDF.

3.9. Fuel clad chemical interaction (FCCI)

With BU, fission products are generated and attack the cladding from the inside. There is also a wastage of cladding on the outer surface due to sodium erosion and corrosion. Wastage of cladding is the loss of cladding thickness, which leads to an increased stress. For estimating the wastage of cladding at any location, the peak burnup and the peak LHR (Linear Heat Rating) with the local cladding temperature are considered according to the reference document formulation [5].

The axial variation of cladding wastage at EOL is shown in Fig. 20. There is a tolerance of 20 microns for the thickness of the cladding. For a conservative design, this is also considered a wastage and shown in the same figure. The 555 EFPD of operation causes a clad wastage of about 6 microns by Na corrosion and erosion.

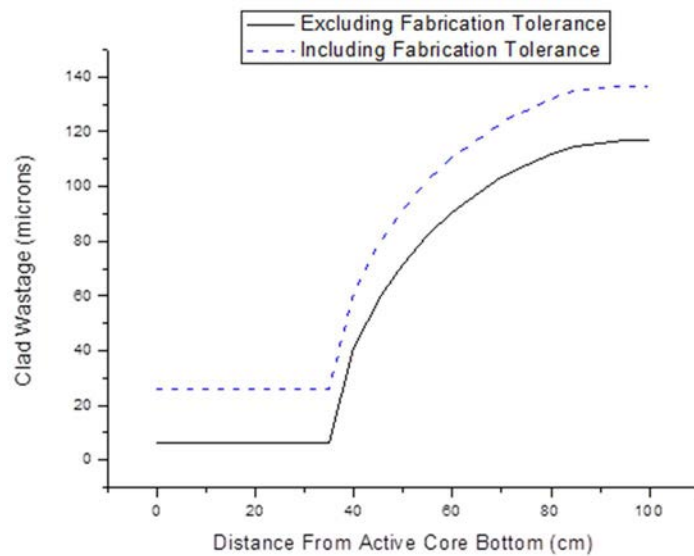


FIG. 20. Axial Variation of Clad wastage at EOL.

From Fig. 20, it is apparent that the wastage is almost identical up to a distance of ~ 35 cm from the active core bottom and is caused only by Na corrosion and erosion or a combination of Na corrosion and erosion and manufacturing tolerance. Up to this location, there is no waste of cladding due to FCCI since the inside temperature of the cladding is less than 800°C .

3.10. Axial variation of CDF taking into account the clad wastage

The variation of CDF along the length of the clad at EOL with reduced clad thickness that occurs due to FCCI, Na corrosion & erosion and manufacturing tolerance is shown in Fig. 21. It is observed that without clad wastage consideration, peak CDF occurs at a distance of about 75 cm from the active core bottom. However, with reduced clad thickness, the CDF value reaches a peak of 0.01367 at a distance of about 57 cm from the active core bottom.

4. CONCLUSIONS

In the present work, a typical FBR fuel pin performance analysis for target peak burnup is performed. This report shows all the results at Active Core Peak Power Location (ACPPL). The following conclusions are based on the thermo-mechanical analysis of the typical FBR fuel pin:

- The FCMI starts at about 1.2 at% of the burnup and increases till 9 at% burnup, where the swelling of the clad increases significantly and the FCMI begins to decrease;
- The increase of the cladding stresses occurs due to differential thermal expansion until full power is achieved, and then a decrease due to the irradiation creep occurs (the thermal creep is much lower compared to the irradiation creep). The stresses in the clad increase again due to the fission gas pressure and the FCMI (at locations where complete closure of the gap is observed);
- FCCI, sodium corrosion and erosion result in wastage of clad. Wastage is about 69 microns at ACPPL, which is equivalent to 15% of the fabricated thickness of 450 microns.

At EOL, the maximum centre line temperature of the fuel is 2132°C , the maximum CDF is 0.014 (considering cladding waste), and the fission gas pressure is 3.4 MPa. There is a wide margin between the maximum centre line temperature and the fuel melting point of 2750°C as well as the accrued and allowed CDF, which ensures safe operation of the fuel pin at 450 W/cm up to 100 GWd/t burnup.

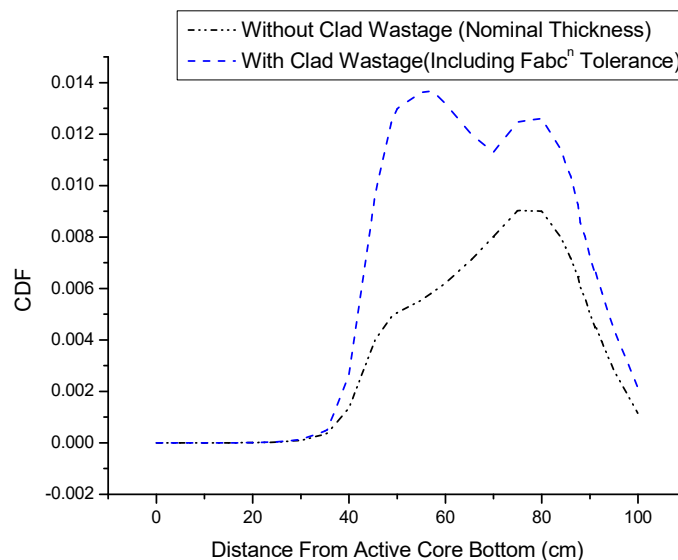


FIG. 21. Axial Variation of CDF at EOL.

REFERENCES

- [1] RITZHAUPT-KLEISSL, H.J., HECK, M., SATURN-FS1, A Computer Code for Thermo-mechanical Fuel Rod Analysis, KfK 5203 (1993).
- [2] PSAR, Chapter 5.2, Core Engineering.
- [3] RPD, Private Communications.
- [4] RCC-MR, 2007 Editio.
- [5] VISVANATHAN, R., "A Report on Clad Wastage Correlation", Task Force on Fuel Modelling, April 2008.

UNDERSTANDING PCI/SCC MECHANISMS

(Session II)

Chairperson

V.I. ARIMESCU
United States of America

FRACTURE MECHANICS I-SCC TESTING AND REVIEW OF OUT-REACTOR PCI BEHAVIOUR

S.M. HANLON

Canadian Nuclear Laboratories,
Chalk River, Canada
Email: sean.hanlon@cnl.ca

M. TOPPING, M.R. DAYMOND, S.M. HANLON

Department of Mechanical and Materials Engineering, Queen's University,
Kingston, Canada

C. GILLEN, P. FRANKEL

School of Materials, University of Manchester,
Manchester, United Kingdom

Abstract

Zirconium alloys are materials used as fuel cladding in the majority of the present global fleet of nuclear power reactors. During service, zirconium fuel cladding is susceptible to pellet-clad interaction (PCI), a degradation mechanism sometimes attributed to iodine stress corrosion cracking (I-SCC). PCI mitigation is achieved through operational restrictions and liner materials; however, these engineering solutions have economic penalties. Although PCI has been studied for many years, the mechanisms and the factors that determine susceptibility are not fully understood. This study includes summaries of several out-reactor PCI testing campaigns in a variety of environments. The tests include: C-ring compression, tube internal pressurization, mandrel testing, uniaxial tension, and fracture mechanics testing. Additionally, new experimental observations of basal plane pseudo-cleavage and twinning near I-SCC cracks are provided in the context of the current literature in an effort to enhance PCI mechanistic understanding. Recommendations for future work include comparisons of different specimen geometries under similar test conditions (i.e. material property tests vs. component tests, including subsequent characterization), direct comparisons of unirradiated, accelerated irradiation (neutrons, protons, and/or heavy ions), and ex-service material, as well as determining the environment and loading conditions most relevant to in-service PCI. The proposed future work could provide a better understanding of PCI mechanisms and could be used to reduce conservative operating restrictions, inform fuel cladding design, and allow for improved predictions of PCI behaviour under new conditions, such as for extended life or new reactor designs.

1. INTRODUCTION

Fuel cladding is fabricated from zirconium alloys for use in water cooled reactors due to the low neutron capture cross section as well as excellent corrosion and mechanical properties under normal operating conditions. During service, the structural integrity of zirconium alloy fuel cladding can become compromised due to a degradation mechanism known as pellet-clad interaction (PCI) often attributed to iodine stress corrosion cracking (I-SCC) [1–4].

As a type of stress corrosion cracking (SCC), PCI requires a susceptible material, tensile stress, and a corrosive environment for cracking to occur. Once a SCC crack initiates it can grow through-wall, allowing coolant to come into direct contact with fuel. PCI mitigation measures include operational restrictions and engineering solutions, such as CANLUB or liner cladding [5–8]. These solutions have economic penalties and limit the load following capabilities of power reactors. PCI has been identified as an important topic with considerable industrial issues. An improved understanding of PCI could increase the flexibility of nuclear power [9] by replacing conservative empirical approaches with mechanistic and physical models that have more predictive power [2].

Using out-reactor testing to simulate in-reactor PCI is highly desirable due to the costs and challenges associated with in-reactor testing, subsequent hot cell processing, and characterization of material with possible fuel contamination. Additionally, secondary damage such as oxidation and hydriding usually occur during an in-service failure once the coolant contacts the fuel, which results in difficulty in the analysis of primary failure features of interest, such as the fracture surface.

A number of previous literature reviews on PCI examine a large breadth of literature and provide a solid base of knowledge for subsequent experiments and modelling [1–4], although there are still several mechanistic questions left unanswered. Examples include the crack initiation mechanism (oxide fracture, pitting, near surface

heavy ion damage), the Van Arkel process and the active zirconium iodide species at the crack tip [4, 14], the iodine and oxygen partial pressure thresholds, the basal pseudo-cleavage mechanism [1], and the effect of radiation damage on crack morphology [13].

The goal of this study is to provide new results from constant-K I-SCC testing, including orientation maps obtained using electron back scatter diffraction (EBSD) taken from near I-SCC crack tips, and discuss these results in the context of the previous literature.

2. REVIEW OF OUT-REACTOR PCI TEST TYPES

The most formidable challenge in performing out-reactor testing is simulating in-reactor PCI in a meaningful way. The high neutron flux (radiation damage and radiolysis), fission product induced damage (i.e. heavy ion irradiation) at the cladding surface, large temperature gradients, transient nature of fuel cracking and crack tip chemistry make it very difficult to simulate in-reactor I-SCC conditions in a lab setting. Choosing the most relevant conditions and isolating the most important variables is critical to successful out-reactor PCI testing.

A list of some critical variables for PCI are as follows: material (composition, orientation, texture, fabrication history, cold work), environment (chemistry, pressure, temperature, irradiation history) and stress (specimen geometry, in-service loading history, residual stresses) [2]. The PCI literature suggests that the choice of variables is not trivial and that Zr degradation in the presence of iodine depends strongly on the test conditions e.g. gaseous iodine or iodized alcohol [10, 11], oxygen control [2] and oxide thickness [12], resulting crack morphology (intergranular, transgranular, pseudo-cleavage) [1], crack tip deformation [2], effect of radiation damage [13], specimen type [11], etc. Many previous out-reactor PCI studies use specimen geometries that can be fabricated directly from fuel cladding; these geometries are referred to as component tests. Examples include C-ring compression, internal pressurization, and mandrel testing. The main benefit of component tests is that the material related variables listed above are the same or similar to in-service conditions. However, the standard fracture mechanics approach to determine general material properties e.g. K_{ISCC} , 'requires that the plastic zone size remains small compared to the wall thickness of the sample considered' [2], which is generally not the case in thin wall cladding specimens. An alternate approach is to use sheet or plate material with a larger thickness. Lessons learned from previous fracture mechanics type PCI studies as well as recommendations listed in an IAEA study [2] were applied during the development of a gaseous iodine testing system at Canadian Nuclear Laboratories [11], which is able to apply constant-K loading to compact tension specimens using a DCPD feedback loop.

This section outlines a variety of PCI specimen types and out-reactor testing systems. In addition to the differences between component and non-component tests described below, significant differences also exist between 'open' and 'closed' test systems. The iodine concentrations in the former are usually lower than the latter; for example, Anghel et al. [15] use an open system with iodine partial pressure of 60 Pa, while Jezequel et al. [16] use a closed system with iodine density of 15 mg/cm³, a maximum iodine partial pressure greater than one atmosphere at 300°C or above (i.e. a change of more than three orders of magnitude).

An IAEA report [2] recommends that open systems use small chamber volumes and frequent air changes to ensure the environment is at a steady state, as well as reducing oxygen partial pressure as much as practical. For closed systems, the iodine partial pressure at a given time is difficult to determine because it is not an independent variable that can be controlled or accurately measured once the test chamber is sealed. However, oxygen pressure in a closed, positive pressure system is likely easier to minimize, given that there are fewer connections susceptible to air leaks, while higher pressures promote inside-out leaks, minimizing oxygen ingress.

The materials used in the PCI test rigs must be selected with care to avoid any unwanted interactions with either iodine or the zirconium alloy specimen [17]. For example, some previous iodine testing systems used stainless steel components in direct contact with the iodine containing environment [2]. It has been shown that the presence of steel affects I-SCC susceptibility [4, 17–19]. An alternate approach is to pre-oxidize stainless steel components (or other metals) to minimize iodine interaction [16]. Decomposition of O-ring grease at elevated temperatures has also been shown to affect test results [11].

2.1. Component tests

Component testing is performed on specimens that can be manufactured directly from fuel cladding. These include, but are not limited to, C-rings, internal pressurization, and mandrel tests. It should be noted that BWR, PWR, and CANDU fuel cladding all have different geometries, composition, etc. such that direct comparisons between 'component test' type studies are not always possible. A split ring, or more commonly C-ring sample can

be constructed quickly and easily from cladding tube. C-ring samples have been frequently used in stress corrosion cracking experiments in a number of industries [20–22]. ASTM provide standards for working with C-ring specimens, for example, the standard suggests an axial length equal to the C-ring diameter [23]. The highest stress location in C-ring samples is located on the opposite side of the opening. When the C-ring is in tension, the highest tensile stress is at the inside surface, meaning the crack will propagate inside-out, which is the same direction as in-reactor SCC. However, the more commonly used C-ring test is compression, which has an outside-in crack direction [23]. During elastic stressing of the ring, the stress may be calculated based upon a change in the slot width using Oding's formula [24], by a change in outer diameter [23], or by finite element or other type of modelling.

Sejnoha and Wood [24] used slotted rings stressed to a fixed deflection to investigate a number of material and experimental factors affecting I-SCC of zircaloy-2 and zircaloy-4. Zircaloy blocks were used to wedge open slotted and notched zircaloy rings, which were then placed into capsules containing iodine. The capsules were sealed, heated to 300 °C, and inspected periodically until failure. Interestingly, these capsules contained air, which was hoped to induce cracking as opposed to pitting alone. The practicality of this test procedure allowed a number of material effects including that of hydrides, stress-relief, and annealing to be quickly investigated. 'Stressed slotted rings' were also found to behave differently in iodine-methanol solution than was the case in iodine vapour. This paper also developed estimates for how the stress of a slotted ring would change as the ring underwent plastic deformation and thermal relaxation [24].

Ferrier et al. [25] used C-ring testing to compare the I-SCC performance of siloxane and graphite coatings on zircaloy-4 cladding. Block wedges were used to stress the C-rings, which were then sealed into an evacuated borosilicate tube with a sealed vial containing iodine, which was broken once the test temperature was reached. Once the samples were removed from the environment the change in ring thickness due to corrosion was determined using a deflection measurement technique.

Gillen et al. compressed C-rings to a fixed load while submerged in an iodised ethanol solution and then applied modern characterisation techniques to the cracked specimens [10,13,26]. The use of C-rings and iodine in solution allowed I-SCC to occur at room temperature. The experimental practicality allowed for many tests to be completed, including cladding tubes of different conditions with enough independent fracture surfaces for quantitative analysis [26]. By maintaining a fixed load upon compressed and submerged C-rings, changes in displacement were found to indicate crack propagation. Removal of load following a change in displacement allowed incipient I-SCC cracks to be produced and then investigated [10,26]. Differences in crack morphology were found in irradiated and unirradiated C-rings [10].

Mattas et al. developed an internal pressurization test system (Figure 1 in [12]) and conducted PCI testing on irradiated cladding with a variety of fluences. They found that the stress threshold for failure in zircaloy cladding irradiated to above 2×10^{21} n/cm² was about 180 MPa when the test time was limited to one day [12]. Jezequel et al. [16] also performed internal pressurization tests, including creep tests, slow strain rate tests, and relaxation tests. (Figure 1 in [16]). They determined that the I-SCC threshold stress was around 240 MPa in unirradiated zircaloy-4 cladding material, regardless of the loading mode, and provided evidence of pits both on the internal surfaces of the cladding and on the I-SCC fracture surfaces [16]. There were several differences between the Jezequel et al. [16] and Mattas et al. [12] studies (e.g. material, specimen gauge length, amount of iodine added) such that the irradiated and unirradiated threshold stress values may not be directly comparable, although the higher threshold stress in unirradiated material general follows the trend observed by Mattas et al. [12].

An expanding mandrel technique for PCI testing was initially developed by researchers at General Electric (Figure 3 in [27]) to determine the PCI resistance of various barrier coatings [27, 28]. Although irradiated material could be tested, it was limited to unfuelled material irradiated in a research reactor or taken from the unfuelled plenum region of an ex-service rod. Anghel et al. [15] developed an expanding mandrel test system that was installed in a hot cell (see Figure 1-5 in [15]), which is capable of testing irradiated cladding material taken from a fuelled section of cladding; this approach is more representative of in-service conditions, although the defueling process could reduce the representativeness (scratches, damage, changes to the surface morphology, etc.). Results show that neutron irradiation increases the PCI susceptibility of zircaloy claddings [15].

2.2. Non-component tests

Non-component tests are selected for one or more of the following reasons: 1) material properties can be extracted when the specimen geometry meets ASTM fracture mechanics criteria, 2) larger specimens allow for

longer crack lengths, more accurate stress intensity measurements, and larger areas for subsequent characterization, 3) flat specimens (e.g. uniaxial tension) are easier to fabricate, notch, apply DCPD techniques, and test compared to curved specimens, 4) constant K loading is more practical, 5) the effect of orientation/texture can be examined without changing other variables, and 6) ion irradiations can be more easily performed on flat samples (temperature control is much easier).

Given that time-dependent corrosion processes are the rate-limiting step for SCC, testing performed at high strain rates will likely fail in a ductile manner since SCC does not have time to occur [29]. The choice of strain rate during an I-SCC test may therefore have a large effect on the results. Additionally, in-service strain following a power ramp is about 0.1% [3] and remains below 1% even after a through-wall PCI crack develops [15], thus higher failure strains are likely not representative of in-service conditions. Selecting a loading programme that allows the applied stress to remain below the flow stress is an improvement compared to a slow strain rate test (SSRT) since there are no competing failure mechanisms (assuming creep is minimal). Under constant-K conditions, plastic deformation is generally limited to the local region around the crack tip and no bulk deformation occurs, while during a SSRT test there is always bulk deformation occurring in the gauge length.

With constant load it should be remembered that the stress intensity rises as the crack grows. The benefits of a notched specimen under constant load perhaps explains the IAEA decision to test uniaxial tension specimens, as outlined in Section 2.2.1 of [2], and the recommendation that notched and pre-fatigued specimens are favoured [2]. A sharp initial flaw (e.g. pre-fatigued) means that only a small volume of the specimen is at the yield stress (plastic zone), thus deformation is localized, perhaps similarly to incipient fuel cladding cracks during in-service PCI.

Compact tension type specimens machined from thick zircaloy plate material have been used to examine the effect of texture on PCI [30, 31]. The results demonstrated that texture has an influence on both I-SCC initiation and propagation. Another testing system was designed with the capability to test both fracture mechanics type compact tension (CT) specimens and C-ring specimens with independent control of iodine partial pressure, test temperature, and load/stress intensity (Figures 1 and 4 in [11]). Additionally, the system is capable of measuring in-situ crack growth rates by means of a direct current potential drop (DCPD) apparatus capable of maintaining constant K loading. Constant K loading is an improvement over constant load tests or strain rate tests, given that the mechanical conditions at the crack tip do not change as the crack grows, assuming the DCPD calibration curve and K calculations are accurate [11, 32]. DCPD with K feedback control has been shown to be critical in developing an understanding of SCC in other nuclear systems [33, 34]. The constant K approach allows for the detection of very slow, subtle cracking and for the effects of real-time changes (such as iodine partial pressure) on crack velocity to be determined. Characterization of constant K cracking tests showed clear fractographic evidence of basal pseudo-cleavage (Figures 10,11 in [11]) and that KISCC was below $2.5 \text{ MPa}\sqrt{\text{m}}$ in the most susceptible orientation [11]. 3D EBSD analysis of the same zircaloy-4 plate material used in this study also shows evidence of transgranular cracking along basal planes [35].

3. EXPERIMENTAL

3.1. Testing

Compact tension specimens with 12 mm thickness (0.5T) and 50 μm root radius were manufactured from a recrystallized zircaloy-4 plate and were tested in a gaseous iodine apparatus. The specimens were instrumented with DCPD to enable on-line crack growth measurements and constant-K loading. The gaseous iodine testing system, material, specimen design, and DCPD system used in this study have been described in more detail in a previous study [11]. Table 1 lists a number of previous tests as well as two new compact tension tests (IDs in bold) presented in this study.

TABLE 1. TEST SUMMARY. BOLDED TEST IDS HAVE NOT BEEN PREVIOUSLY PRESENTED. RESULTS FROM OTHER TESTS CAN BE FOUND IN [11]

Test ID	Test Temp (°C)	Second Bath Temp (°C)	Iodine Pressure (Pa)	Orientation (see Fig. 1)	Characterization
Z9	250	50	293	R-L	Fractography, FIB, TEM
Z10	350	50	293	R-L	Fractography
Z11	350	50	293	R-L	Fractography
Z12	350	45	204	R-L	Fractography
Z13	350	45	204	R-L	Fractography
C-ring	300	47	236	R-L	Fractography
Z14	300	37	112	R-L	Fractography, EBSD
Z2	250	37	112	T-R	Fractography, EBSD

Constant K loading programmes were applied to specimens Z14 and Z2 by using a DCPD feedback loop. As a crack grew (as measured by DCPD), the load was decreased such that the calculated K remained constant. A KISCC loading programme allowed for a starting K, a K decrement, and a crack length threshold to be specified [11].

The previous study using this testing apparatus focused only on the most susceptible orientation for I-SCC [11], the orientation where most of the basal planes are normal to the cracking plane. Given the strong split-basal radial texture of the bulk material, the most susceptible plane is therefore the radial plane; a R-L orientation. However, in-reactor SCC occurs in the transverse plane, where through-wall (radial) cracking causes loss of structural integrity, such that a T-R specimen orientation is most representative of in-reactor cracking. A schematic diagram showing these specimen orientations relative to the zircaloy-4 plate with radial split basal texture is shown in Fig. 1. A pole figure of the plate material can be found in Figure 3 of [11].

Previous work has shown that test failures have occurred due to fluorine contamination from O-ring grease [11] – efforts to minimize this contamination were put in place for test Z2, including a lower test temperature and Krytox grease rated to 350 °C (compared to the previous rating of 299°C).

3.2. Characterization

Specimens were cut with a slow speed diamond saw in a direction normal to the cracking plane such that two symmetric halves were produced, each containing half of the crack area. One half was pulled apart at room temperature to expose the fracture surface while the other half was used for crack cross-section examinations with polarized light metallography and EBSD. The surface being examined was the diamond cut surface, ensuring the crack tip being observed was located in a fully constrained (plane strain) region during the test, rather than near one of the original edges of the specimen (plane stress).

EBSD preparation included grinding with sandpaper up to 1200 grit. This was followed by attack polishing using a solution of 5% HF, 5% H₂O₂, 5% HNO₃, and 85% H₂O with colloidal silica to produce samples with a mirror finish. Finally, the samples were ion milled at room temperature using a PECS II ion mill with 4 keV argon ions with an 8° gun tilt. Care was taken to ensure this process did not cause a widening of the crack through close monitoring using optical microscopy at each preparation stage.

Secondary electron (SE) imaging and EBSD were carried out using a FEI Nova NanoSEM 450 and a Bruker e-Flash EBSD detector. The EBSD analysis was performed using a beam energy of 20 keV and a probe current of 50 nA. Orientation maps were collected with a step size of 200 and 300 nm for samples Z2 and Z14, respectively. All subsequent data analysis of the orientation information was completed using the MTEX toolbox add-on for MATLAB. Grain reconstruction was implemented using an angular threshold of 5°.

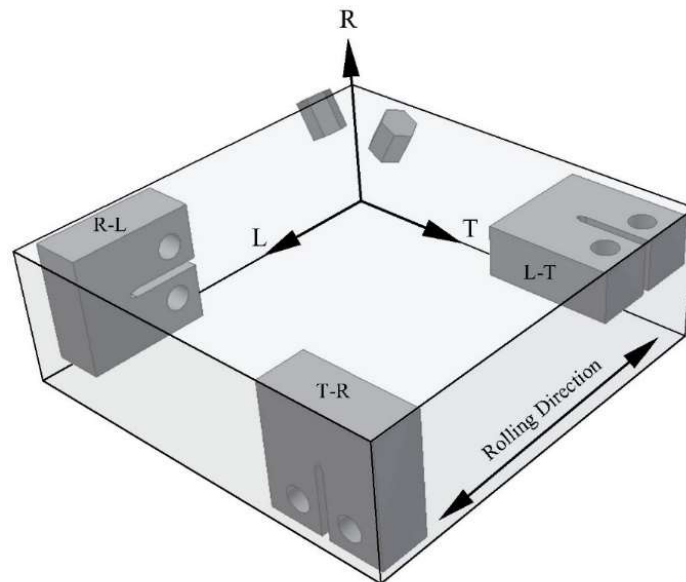


Fig.1. Schematic Diagram of Thick Zircaloy-4 Plate with Split Basal Texture and Compact Tension Specimen Orientation, (reproduced courtesy of Hanlon [11]).

4. RESULTS

The potential drop (PD) plot for Z14 (R-L orientation) is not shown, as it was essentially a repeat of previous testing [11]. The PD plot for specimen Z2 (T-R orientation) is shown in Fig.2.

For specimen Z2 the I-SCC crack initiated from the 50 μm root radius notch with no pre-fatigue. The starting K was 21 $\text{MPa}\sqrt{\text{m}}$ for the first 250 μm of cracking (calculated), then K was dropped in 1 $\text{MPa}\sqrt{\text{m}}$ increments each time that the crack grew an additional 250 μm . At about 47 hours, the K was increased from $K=18 \text{ MPa}\sqrt{\text{m}}$ to $K=22 \text{ MPa}\sqrt{\text{m}}$, then allowed to drop in 1 $\text{MPa}\sqrt{\text{m}}$ increments to the lowest applied K of 17 $\text{MPa}\sqrt{\text{m}}$, where the incubation time was approximately 24 hours. The crack eventually grew to the imposed limit of $V/V_0=1.1$ (equivalent to 3.2 mm of cracking in the notch direction, see Figure 3); this limit was imposed because confidence in the calculated K equation and the DCPD calibration curve decreases with increasing crack growth.

Low and high magnification polarized light images from specimen Z2 are shown in Figures 3 and 4, respectively. Figure 3 shows that the crack propagated at a high angle relative to the notch direction, about 66° , such that the cracking plane was closer to the radial plane than transverse plane (the plane of the notch in a T-R specimen). The higher magnification metallography image of the crack tip in Figure 4 shows that locally, the crack follows a tortuous path that sometimes includes propagation in the transverse direction, which is normal to the notch plane. The image also shows twins, which are mostly found within a distance of a few grain diameters from the crack. Figure 5 shows an orientation map of the same crack tip region shown in Figure 4. Orientation maps taken from specimen Z14 crack tip and taken 800 μm away from the Z14 crack are shown in Figures 6 and 7, respectively. The Figure 5 inverse pole figure (IPF) colouring is oriented in the y direction (c-axis in y direction is 'red'), while in Figures 6 and 7 the IPF is oriented in the x direction (c-axis in x direction is 'red'). These different orientations were chosen so that a red grain tends to have its c-axis normal to the cracking plane, regardless of specimen orientation, such that red grains are well-aligned for cracking along a basal plane. The prisms overlaid onto the EBSD images provide an improved means of determining the direction of crack growth relative to the crystal orientation of each grain, since at a grain scale the crack angle can vary significantly from the average. The grain colour provides a guide to the eye, but the prisms provide a better indication of whether the crack locally follows basal planes.

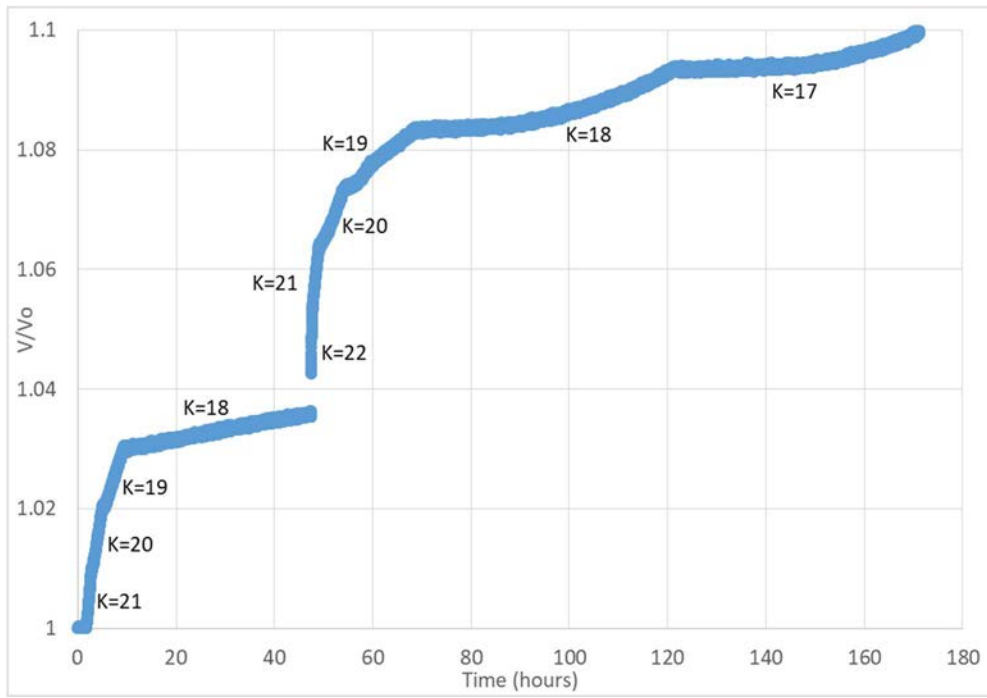


FIG.2. PD Plot for Specimen Z2 as function of time. *K* values are indicated.

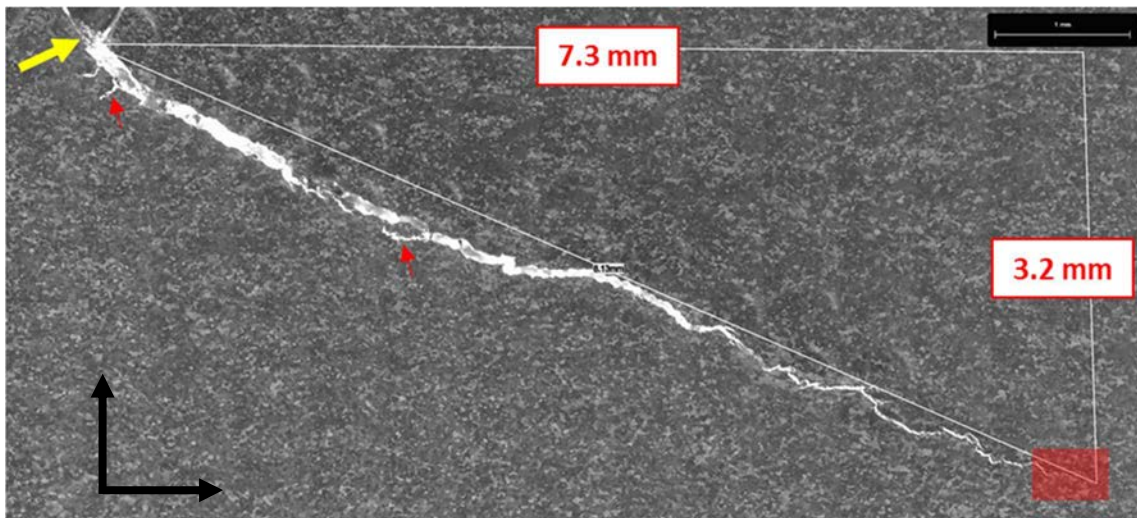


FIG.3. Low magnification polarized image of Specimen Z2. Large yellow arrow indicates the notch, small red arrows show examples of secondary cracking, and red transparent box represents the area shown in Figure 3.

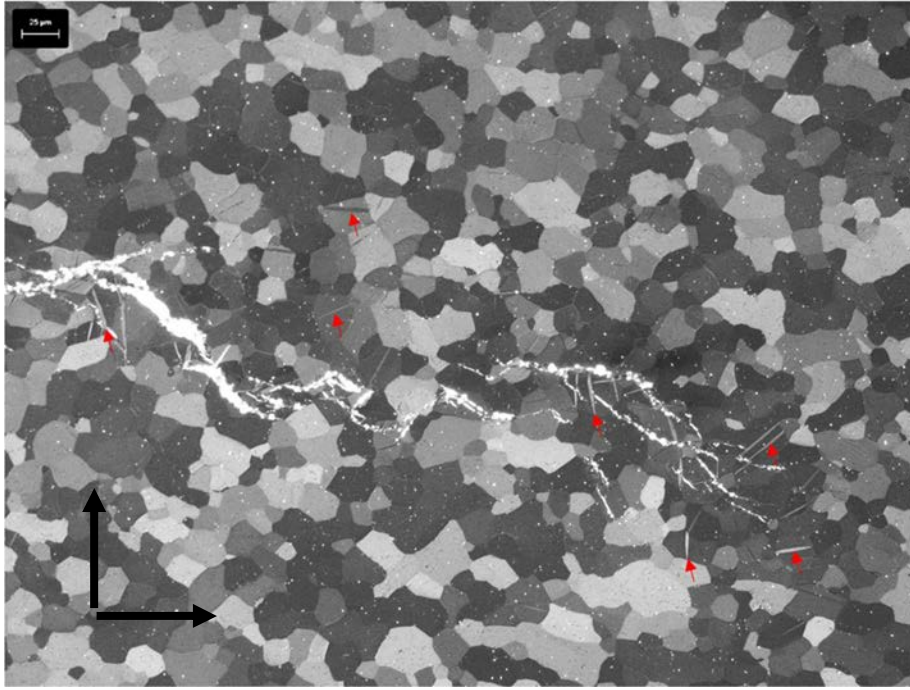


FIG.4. High magnification polarized image of the Z2 crack tip. Arrows indicate examples of twinning.

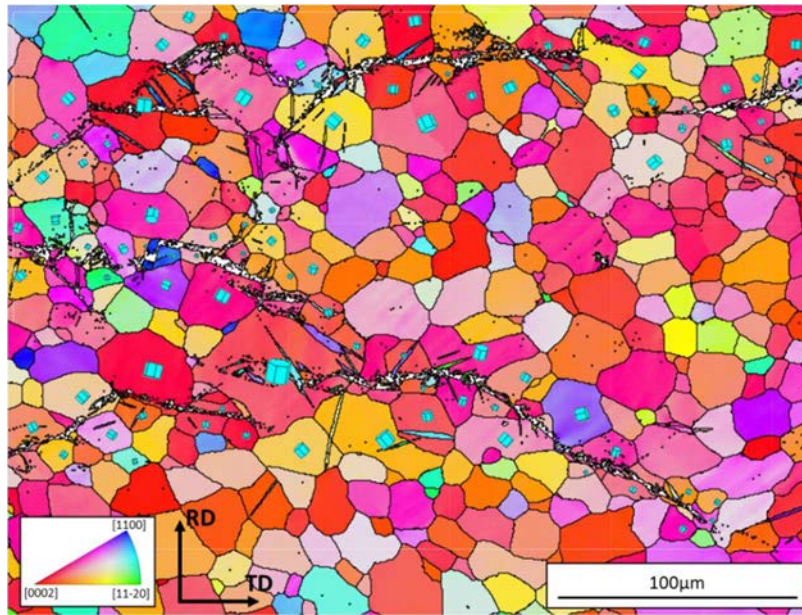


FIG.5. Orientation map of the Z2 crack tip. Inverse pole figure legend (y -direction – nearly normal to the cracking plane) shown in bottom left. Hexagonal crystals overlaid on grains near the I-SCC crack.

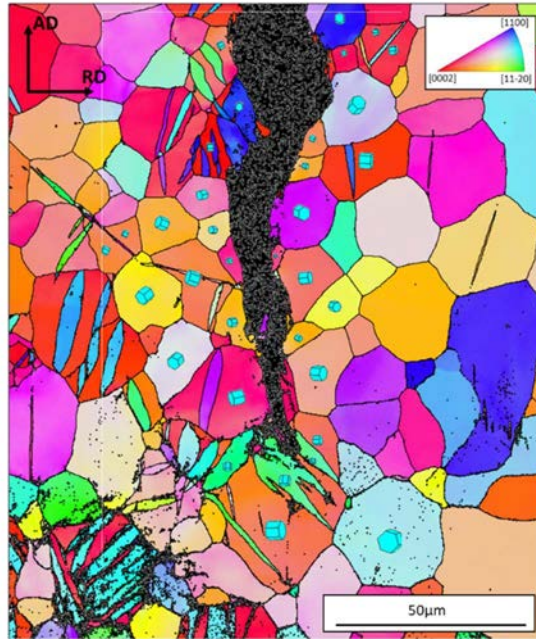


FIG.6. Orientation map of the Z14 crack tip. Inverse pole figure legend (x -direction – normal to the cracking plane) shown in top right. Hexagonal crystals overlaid on grains near the I-SCC crack.

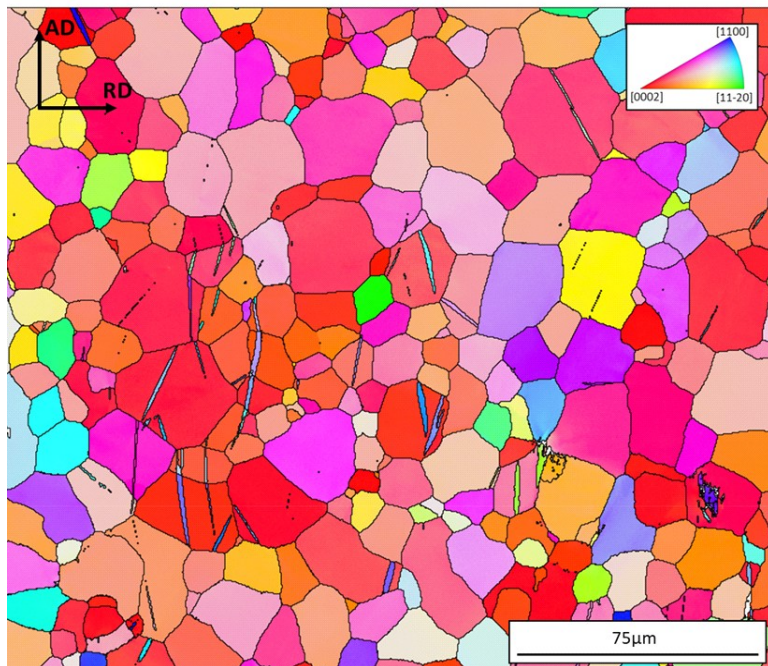


FIG.7. Orientation map of the Z14 specimen 800 μm away from the I-SCC crack. Inverse pole figure legend (x -direction) shown in top right.

5. DISCUSSION

Observations of ‘tangential cracking’, similar to that shown in Figure 3, have been made previously (see Figure 5 in [10]), where the average angle was about 40° towards the tangential plane. Interestingly, the cold-worked (CW) ZIRLO material cracked in room temperature iodized ethanol by Gillen et al. had a more tangential crack path than similar recrystallized (RX) material tested in the same environment [10]. Given that the textures of the two materials were similar, but the grain size and morphology were different (see Figure 1 in [10]), the tendency to crack tangentially was attributed to grain morphology. It is also possible that a higher yield strength

in the cold worked material had an effect. The specimens used in this study were all made from the same equiaxed RX zircaloy-4 plate, such that the only difference between specimen Z14 and Z2 was the texture relative to the cracking plane. Each ‘most susceptible’ oriented specimen (see Table 1) had a radial crack direction; no ‘tangential cracking’ was observed on a mm scale. Figure 6 shows the radial crack propagating along basal planes, which has also been observed previously in the same material using 3D EBSD [35]. The 3D EBSD work provides far greater statistical significance by analyzing a cracked volume containing nearly 1000 grains. Figure 3 shows evidence of tangential cracking in a T-R oriented specimen, while Figure 5 demonstrates that this cracking is again predominantly along the basal planes; the overlaid prisms show that cracking in nearly every grain is along the basal plane. These observations provide conclusive evidence that texture affects the crack direction and morphology.

Based on previous work by Peehs et al. [36], Cox et al. [1] postulated that intergranular cracking occurs on or close to the basal plane (within 15°), but that basal pseudo-cleavage does not occur when the basal plane is greater than 45° from the stress direction. The results in the current study show that basal pseudo-cleavage is possible when the basal plane is at higher angles, at least 90° from the stressing direction. This type of ‘high angle’ basal pseudo-cleavage was perhaps not observed by Peehs et al. (see Figure 6 in [36]) because KISCC is relatively high and I-SCC growth rates are relatively low when basal planes are at a high angle relative to the stress direction [30, 31]. Perhaps with more time some radial cracks would have formed, unless the conditions were such that KISCC could not be exceeded, as with the unnotched C-rings in [11]. A future study will include several more T-R specimens as well as L-T specimens, as it is of interest to confirm the extent of tangential cracking in the ‘most representative’ orientation and also determine the crack morphology in the ‘least susceptible’ orientation. Performing 3D EBSD on all three orientations would allow for more quantitative comparisons to be made.

The RX material in the Gillen et al. study [10] and the L-T oriented RX material in this study have markedly different crack directions, yet their textures are similar. This could be due to differences in average grain size, since the grains in this study are about a factor of five times larger in average diameter than those reported by Gillen et al. [10]. However, the differences in crack direction could also be due to differences in the environment, crack tip stress state, or material (ZIRLO vs. zircaloy-4); a more systematic study is required before a definitive conclusion can be made.

One of the benefits of using large grain material, low stress intensities, and low iodine partial pressures is that the crack width is far less than the average grain diameter, allowing for high confidence that cracking through most grains is intragranular rather than intergranular. A larger grain size may not only allow easier detection of intragranular cracks, but it may skew the crack propagation mode from intergranular towards transgranular, since cracks can propagate greater average distances down favourable transgranular orientations (i.e. basal planes) prior to reaching a new grain boundary where intergranular cracking may temporarily be favourable. However, a large unfavourably oriented grain may favour a long intergranular crack. Previous 3D EBSD results [35] suggest that I-SCC cracks can avoid unfavourable grains by cracking through more favourably oriented neighbouring grains (since the crack front is not simply a 2D plane), such that the overall tendency is likely for larger grains to favour intragranular cracking because fewer grain boundaries are crossed. High iodine partial pressures can cause pitting [16] while high notch tip stress can cause crack tip blunting, both of which could widen the crack such that the crack plane cannot be confidently determined. Future industry wide efforts to use similar I-SCC test parameters, such as temperature, iodine partial pressure, strain rate, or notch tip stress, would allow for more direct comparison to be made between various out-reactor PCI studies.

The ‘tangential cracking’ observed in specimen Z2 is a concern for the DCPD system and ASTM K calculation used in this study. Future work, including FEM, is required to confirm the accuracy of the PD calibration curve and ASTM K equation when the crack is substantially out of plane, given that both equations are based on in-plane cracking. An additional concern is related to calculating incubation times at each K threshold. As the crack grows (several mm), both K and applied load are dropped (see Figure 1), potentially causing the crack tip region to close or narrow, such that it may become increasingly difficult for the active species to reach the crack tip, especially at the centre of a 12 mm thick specimen.

In-reactor PCI crack initiation is not fully understood; the contributions of fission fragment hardening and chemistry changes [see Figure 17 in [3] and Figures 27-30 in [37]], oxide cracking [12], intergranular attack and pitting [16] are difficult to separate. Without a stress riser, cracking of unirradiated ZIRLO C-rings under the conditions listed in Table 1 was not observed [11], however, with a $50\ \mu\text{m}$ deep nanoindenter scratch I-SCC could occur. Ohara et al. observed $10\ \mu\text{m}$ deep cracks in power ramped BWR fuel [37], about the same depth as fission fragment deposition and a layer of higher hardness, referred to as a brittle surface layer [2]. Applying heavy ion

and/or other types of accelerated irradiation types to a plane surface, or to a broad root radius notch [38], could provide a more representative crack initiation condition, especially if the surface oxide is similar to those during service. Care should be taken in interpreting crack initiation results using a specimen with a machined notch, such as used in this study; the cold work from machining may cause a larger hardness increase than the subsequent irradiation [38]. The role of pitting on in-service PCI initiation is unclear; at high iodine partial pressures pitting occurs regardless of stress, strain, or temperature [16], while PCI is also possible at low concentrations without a pre-machined stress riser where no pitting was observed [15]. In this study there was no evidence of pitting. Without a strong understanding of in-service crack initiation mechanisms, it is difficult to design out-of-reactor experiments where meaningful time-to-failure or stress thresholds can be determined, especially if irradiation history affects the crack initiation mechanism. For example, it would be difficult to use out-of-reactor results to make predictions of in-reactor crack initiation behaviour if the mechanism is different (e.g. pitting vs. microcracks in a brittle surface layer).

The results in Figures 4-7 show that there is more twinning within a few grains of the crack than away from the crack. Similar observations have been made previously via 3D EBSD misorientation analysis [35]. Figure 6 shows that twinning can lead to crack arrest in a grain that is otherwise well oriented for basal plane cracking, and it appears that more twinning is observed near the I-SCC crack in the R-L specimen (Figure 4) than the T-R specimen (Figure 5), likely due to more c-axes being parallel to the stress direction in the R-L specimen orientation (since twinning in Zr alloys is favoured by tension along c-axes). Additional work is required to better quantify deformation near I-SCC cracks and interpret the significance.

Future efforts to select the most relevant environmental conditions for I-SCC testing are encouraged, as are efforts to directly compare results from the various out-reactor test types under similar conditions, perhaps using material exposed to accelerated irradiation(s), to in-reactor PCI failures.

6. CONCLUSIONS

Based on the review of out-reactor PCI testing, as well as the compact tension specimen results presented in this study, the following conclusions are provided:

- Basal pseudo-cleavage is the dominant I-SCC mechanism for both the R-L and T-R specimen orientations under the constant-K conditions used in this study.
- Texture has a dramatic effect on the extent of out of plane cracking, also referred to as ‘tangential cracking’.
 - Basal pseudo-cleavage was observed in grains with basal planes oriented up to 90 degrees away from the stress direction.
- No pitting was observed.
- Large grains, low iodine partial pressures and low stress intensities allow for high confidence in determining the I-SCC crack path.
- A higher twin density is observed near the I-SCC crack in the R-L specimen than the T-R specimen, likely because more c-axes were aligned with the stress direction in the R-L orientation. Much less twinning was observed away from the crack.
- A need exists to better understand crack initiation, the basal pseudo cleavage growth mechanism, I-SCC crack tip deformation, and the effects of radiation damage on PCI morphology and mechanisms.

ACKNOWLEDGMENTS

Thanks to Andrew Phillion for the continual improvement of the CNL I-SCC rig design and operation, and for running the I-SCC tests. Thanks to Ioan Arimescu, Heidi Nordin, and Mitch Mattucci for valuable discussions. Thanks to Ken Kidd for specimen preparation and to Mark Seguin for metallography.

This study was funded by Atomic Energy of Canada Limited, under the auspices of the Federal Nuclear Science and Technology Program. C. Gillen and P. Frankel acknowledge financial support provided by EPSRC [EP/L018616/1 & EP/L015390/1] and invaluable discussions carried out as part of the PACE consortium on Pellet Cladding Interaction.

REFERENCES

- [1] COX, B., Pellet-Clad Interaction (PCI) Failures of Zirconium Alloy Fuel Cladding—a Review, *Journal of Nuclear Materials* **172** (1990) 249-292.
- [2] INTERNATIONAL ATOMIC ENERGY AGENCY, Iodine Induced Stress Corrosion Cracking of Zircaloy Fuel Cladding Materials, IAEA-TECDOC-1185, IAEA, Vienna (2000).
- [3] PIRO, MARKUS, H.A., SUNDERLAND, D., LIVINGSTONE, S., SERCOMBE, J., REVIE, W., QUASTEL, A., TERRANI, K., JUDGE, C., “A Review of Pellet–Clad Interaction Behaviour in Zirconium Alloy Fuel Cladding”, *Ref. Modul. Mater. Sci. Mater. Eng.*, Elsevier (2017).
- [4] SIDKY, P.S., Iodine Stress Corrosion Cracking of Zircaloy Reactor Cladding: Iodine Chemistry (a Review), *Journal of Nuclear Materials* **256** (1998) 1-17.
- [5] ADAMSON, R., COX, B., DAVIES, J., GARZAROLLI, F., RUDLING, P., VAIDYANATHAN, S., Pellet-Cladding Interaction (PCI and PCMI), *Advanced Nuclear Technology International, ZIRAT-11 Special Topic Report* (2006).
- [6] WOOD, J.C., BAIN, A.S., HARDY, D.G., Power Ramping Performance of Water Reactor Fuel. Chalk River Nuclear Laboratories, Fuel Engineering Branch (1979).
- [7] WOOD, J.C., SURETTE, B.A., AITCHISON, I., CLENDENING, W.R., Pellet Cladding Interaction—Evaluation of Lubrication by Graphite, *Journal of Nuclear Materials* **88** (1980) 81-94.
- [8] SHIMADA, S., NAGAI, M., Evaluation of the Resistance of Irradiated Zirconium-Liner Cladding to Iodine-Induced Stress Corrosion Cracking, *Journal of Nuclear Materials* **114** (1983) 305-311.
- [9] BÉGUIN, S., “PCI-Related Constraints on EDF PWRs and Associated Challenges”, *Seminar Proceedings on Pellet-clad Interaction in Water Reactor Fuels, Aix-en-Provence, France, 9-11 March 2004* (p. 53).
- [10] GILLEN, C., GARNER, A., PLOWMAN, A., RACE, C.P., LOWE, T., JONES, C., MOORE, K.L., FRANKEL, P., Advanced 3D Characterisation of Iodine Induced Stress Corrosion Cracks in Zirconium Alloys, *Materials Characterization* **141** (2018) 348-361.
- [11] HANLON, S. M., PHILLION, A., GILLEN, C., DAYMOND, M.R., “Development of a Gaseous Iodine Testing System to Determine the I-SCC Properties of Zirconium Alloys”, *Proceedings of the 19th International Conference on Environmental Degradation of Materials in Nuclear Power Systems—Water Reactors* (2019).
- [12] MATTAS, R.F., YAGGEE, F.L., NEIMARK, L.A., Iodine Stress-Corrosion Cracking in Irradiated Zircaloy cladding [PWR; BWR], CONF-790441-7, Argonne National Lab., IL (1979).
- [13] GILLEN, CONOR, GARNER, A. TEJLAND, P., FRANKEL, P., High Resolution Crystallographic and Chemical Characterisation of Iodine Induced Stress Corrosion Crack Tips Formed in Irradiated and Non-irradiated Zirconium Alloys, *Journal of Nuclear Materials* **519** (2019) 166-172.
- [14] WOOD, J.C., Factors Affecting Stress Corrosion Cracking of Zircaloy in Iodine Vapour, *Journal of Nuclear Materials* **45** (1972) 105–122.
- [15] ANGHEL, C., ALVAREZ, H., LYSELL, G., KARLSSON, S., JAKOBSSON, R., SUND, E., SHEIKH, M.T., An Out-of-Pile Method to Investigate Iodine-induced SCC of Irradiated Cladding (2009).
- [16] TRISTAN, J., AUZOUX, Q., LE BOULCH, D., BONO, M., ANDRIEU, E., BLANC, C., CHABRETOU, V., MOZZANI, N., RAUTENBERG, M., Stress Corrosion Crack Initiation of Zircaloy-4 Cladding Tubes in an Iodine Vapor Environment During Creep, Relaxation and Constant Strain Rate Tests, *Journal of Nuclear Materials* **499** (2018) 641-651.
- [17] LIDE, D.R., KEHIAIAN, H.V., *CRC Handbook of Thermophysical and Thermochemical Data*, CRC Press. (1994).
- [18] WOOD, J.C., Interactions Between Stressed Zirconium Alloys and Iodine at 300° C, *Nuclear Technology* **23** (1974) 63-79.
- [19] COX, B. “Stress Corrosion Cracking of Zircaloys in Iodine Containing Environments”, *Zirconium in Nuclear Applications*, ASTM International (1974).
- [20] PRAWOTO, Y., DJUANSJAH, J.R.P., NIK, W.B.W., ENEMUOH, E., Critical View on the Usage of C-Ring Specimen for Stress Corrosion Crack (SCC) Test on Orthopedic Implant: Experimental, Numerical and Analytical Approaches, *Mater. Sci. Eng. C* **32** (2012) 1271–1279.
- [21] DYMEK, S., DOLLAR, M., TEM Investigation of Age-Hardenable Al 2519 Alloy Subjected to Stress Corrosion Cracking Tests, *Mater. Chem. Phys.* **81** (2003) 286–288. doi:10.1016/S0254-0584(02)00603-X.
- [22] ELIAZ, N., SHACHAR, A., TAL, B., ELIEZER, D., Characteristics of Hydrogen Embrittlement, Stress Corrosion Cracking and Tempered Martensite Embrittlement in High-Strength Steels, *Eng. Fail. Anal.* **9** (2002) 167–184.
- [23] AMERICAN SOCIETY FOR TESTING AND MATERIALS, Standard Practice for Making and Using C-Ring Stress-Corrosion Test Specimens, ASTM G38 - 01(2013). doi:10.1520/G0038-01R13.
- [24] SEJNOHA, Y R., WOOD, J.C., Iodine-Induced Stress Corrosion Cracking of Fixed Deflection Stressed Slotted Rings of Zircaloy Fuel Cladding, *Zircon. Nucl. Ind. Fourth Int. Symp.* (1979) 244.
- [25] FERRIER, G.A., FARAHANI, M., CHAN, P.K., CORCORAN, E.C., “Mitigating the Iodine-Induced Stress Corrosion Cracking Of Zircaloy-4 Fuel Sheathing Using Siloxane Coatings”, *Iodine-Induced Stress Corros. Crack. Work.*, 2015.

- [26] GILLEN, C., GARNER, A., FRANKEL, P., "Investigating Iodine-Induced Stress Corrosion Cracking of Zirconium Alloys Using Quantitative Fractography", Private communication.
- [27] TOMALIN, D. S., ADAMSON, R. B., GANGLOFF, R. P., "Performance of Irradiated Copper and Zirconium Barrier-Modified Zircaloy Cladding under Simulated Pellet-Cladding Interaction Conditions", Zirconium in the Nuclear Industry, ASTM International (1979).
- [28] WILLIAMS, C. D. et. al, "Zircaloy-2 Lined Zirconium Barrier Fuel Cladding", Proc. of Zirconium in the Nuclear Industry: Eleventh International Symposium, ASTM STP 1295, E. R. Bradley and G. P. Sabol (Eds.), American Society for Testing and Materials, p. 676 (1996).
- [29] UNE, K., Deformation and Fracture Behaviour of Zircaloy-2 Deformed at Constant Strain Rate in Iodine Environment (I): Uniaxial Tension Test", Journal of Nuclear Science and Technology **16**[8] (1979) 577-587.
- [30] KNORR, D. B., PELLOUX, R. M., Effects of Texture and Microstructure on The Propagation of Iodine Stress Corrosion Cracks in Zircaloy, Metallurgical Transactions A, **13**[1] (1982) 73-83.
- [31] KNORR, D.B., PELTIER, J.M., PELLOUX, R.M., "Influence of Crystallographic Texture and Test Temperature on Initiation and Propagation of Iodine Stress-Corrosion Cracks in Zircaloy", Zirconium in the Nuclear Industry, ASTM International (1984).
- [32] AMERICAN SOCIETY FOR TESTING AND MATERIALS, Standard Test Method for Determining a Threshold Stress Intensity Factor for Environment-Assisted Cracking of Metallic Materials, ASTM E1681-08 (2008).
- [33] ANDRESEN, P.L., MORRA, M.M., IGSCC of Non-Sensitized Stainless Steels in High Temperature Water, Journal of Nuclear Materials **383** (2008) 97-111.
- [34] ANDRESEN, P.L., MORRA, M.M., Effect of Rising and Falling K Profiles on SCC Growth Rates in High Temperature Water, ASME 2005 Pressure Vessels and Piping Conference, American Society of Mechanical Engineers Digital Collection (2008) pp. 693-708.
- [35] FRANKEL, P., GARNER, A., PLOWMAN, A., HANLON, S., GILLEN, C., PHILLION, A., RACE, C., DONOGUE, J., ANGHEL, C., AMBARDE, A., DAYMOND, M., "Towards a Mechanistic Understanding of Pellet Cladding Interaction using advanced 3D Characterisation and Atomistic Simulation", Zirconium in the Nuclear Industry, Nineteenth International Symposium, 2019.
- [36] PEEHS, M., STEHLE, H., STEINBERG, E., "Out-of-Pile Testing of Iodine Stress Corrosion Cracking in Zircaloy Tubing in Relation to the Pellet-Cladding Interaction Phenomenon", Zirconium in the Nuclear Industry. ASTM International (1979).
- [37] OHARA, H., IRUBE, M., FUTAKUCHI, M., NOMATA, T., IWATA, S., "Fuel Behaviour During Power Ramp Tests", Proceedings, 1994 International Topical Meeting on Light Water Reactor Fuel Performance, American Nuclear Society, West Palm Beach, FL
- [38] MATTUCCI, M.A., WANG, Q., SKIPPON, T., DAYMOND, M.R., WAS, G.S., SMITH, J., JUDGE, C.D., "Nano-Mechanical Testing of Proton Irradiated 304L SS at 100°C and 360°C to Support IASCC", 19th International Conference on Environmental Degradation of Materials in Nuclear Power Systems – Water Reactors August 18-22, 2019, Boston, Massachusetts, USA.

EXPERIMENTAL CHARACTERIZATION AND MODELING OF I-SCC OF ZIRCONIUM ALLOY IN AN IODINE VAPOR ENVIRONMENT

D. LE BOULCH, M. BONO
CEA,
Saclay, France
Email: david.leboulch@cea.fr

E. FEDERICI
CEA,
Cadarache, France

N. MOZZANI
EDF/R&D,
Moret-Sur-Loing, France

L. BARBIE, B. BAURENS
EDF/DT,
Villeurbanne, France

V. CHABRETOU
FRAMATOME,
Lyon, France

Abstract

The I-SCC behaviour of cold-worked stress-relieved (CWSR) zircaloy-4 was investigated with internal pressure tests in inert and vapor iodine environments. I-SCC susceptibility was established from tests on un-irradiated and neutron-irradiated cladding tubes. I-SCC crack propagation rates were evaluated from tests on pre-cracked tubes. The internal pressure tests conducted on un-irradiated CWSR zircaloy-4 cladding tubes in a gaseous iodine environment were used to investigate the influence of test temperature (320°C, 350°C, or 380°C) on the I-SCC process. The experimental results exhibited an apparent threshold hoop stress, below which I-SCC does not occur. The tests were simulated by finite element models using a specific viscoplastic constitutive equation. The I-SCC initiation and time-to-failure predictions were modelled by a Kachanov's damage law written with a hoop stress threshold. In the simulations, the Kachanov's law can be used in post-treatment of calculations or coupled with the viscoplastic constitutive equation for the cladding in order to simulate both the initiation and the propagation of the I-SCC crack. The coupling was implemented in the CAST3M finite element code [1] using either massive elements or Cohesive Elements.

1. INTRODUCTION

The pressurized water reactor (PWR) core is made of fuel assemblies. The fuel cladding is the first barrier for confining the fusion products. During an increase of the reactor power, the expansion of the pellets leads to the pellet-cladding interaction (PCI) that results in a thermomechanical loading on the cladding. In conjunction with corrosive iodine released by the pellet, it can lead to the hypothetical failure of the cladding by iodine induced stress corrosion cracking (I-SCC).

The objective of this paper is to describe the experimental and the modelling approaches used at CEA to describe I-SCC of zircaloy-4 tube claddings. The I-SCC initiation and time-to-failure predictions are modelled by a Kachanov's damage law written with a hoop stress threshold. The Kachanov's model can be used in post-treatment of calculations or coupled with the viscoplastic constitutive equation for the cladding.

The experimental procedure with some I-SCC results are first presented. Based on these results, the different features of the model are described. Finally, simulation vs. experiment comparisons are presented.

2. EXPERIMENTAL PROCEDURE AND RESULTS

I-SCC susceptibility of different batches of CWSR Zy-4 PWR cladding was investigated by means of internal pressure tests. To determine the influence of irradiation on I-SCC susceptibility, the tests were performed on un-irradiated and neutron-irradiated cladding.

To create the iodine vapor environment, approximately 75 mg of iodine was introduced inside a crucible which was introduced inside each specimen. Then, the specimen is heated and pressurized. The iodine surface concentration obtained is about 3 mg.cm^{-2} . This value is in the range of concentrations above which the effect of the iodine content on I-SCC susceptibility of zircaloy-4 is saturated [2]. The iodine partial pressure at the beginning of the tests was evaluated to 3.10^5 Pa [3]. It was found in [4] that a critical iodine partial pressure is needed for the I-SCC to occur. This critical range is between 0 and 60 Pa, and above 60 Pa, the iodine partial pressure leads to saturated effect of the iodine content on the I-SCC behaviour.

The diametrical strain of the cladding is measured by a laser throughout the tests. The inner pressure can be regulated based on the measured diameter in order to pilot the diametrical strain. In this paper, all the inner pressure tests presented were conducted at constant pressure.

The mean hoop stress applied to the cladding is expressed in Eq. (1) as a function of the pressure 'P' applied inside the cladding, the outer radius ' R_{out} ', the inner radius ' R_{in} ' and the thickness 'e' of the cladding.

$$\sigma_{\theta\theta} = P \frac{(R_{out}+R_{in})}{2e} \quad (1)$$

In the tests presented in this paper, the pressure P is applied at 2 bar/s until a target value is reached, then the pressure is maintained at a constant value. The pressure rate of 2 bar/s is fast enough that the time required to load the specimen to the target value is small compared to the expected times-to-failure (a few minutes versus a few hours, respectively). It is also slow enough to avoid significant adiabatic heating of the gas inside the specimen.

I-SCC susceptibility was studied on unirradiated CWSR Zy-4, at temperatures ranged from 320°C to 380°C [3] (see the results in Fig.1). The irradiated CWSR Zy-4 was studied at a temperature of 350°C [5] (see Fig.2).

I-SCC susceptibility (as defined as the difference between the time-to-failure obtained under the iodine vapor environment and the time-to-failure obtained under the inert environment) decreases with temperature. In contrast, the more the temperature increases the more the I-SCC times-to-failure decrease (together with the times-to-failure obtained under the inert environment). The kinetic of the I-SCC fracture is accelerated by the temperature. The irradiation increases the I-SCC susceptibility of the CWSR Zy-4. On unirradiated material, there is an apparent stress threshold of about 240 MPa that seems to be independent of the temperature between 320°C and 380°C.

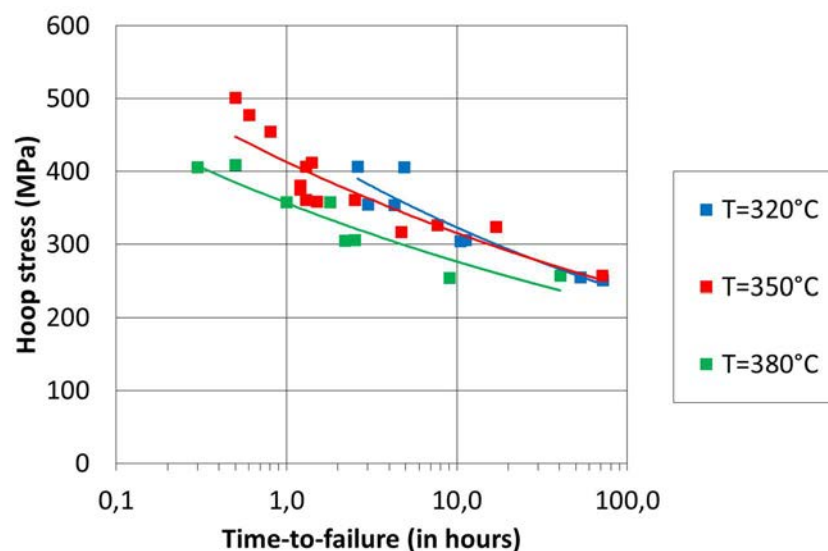


FIG. 1. Inner pressure tests at a constant pressure under iodine vapor environment: Effect of the temperature on I-SCC susceptibility of un-irradiated CWSR Zy-4 cladding.

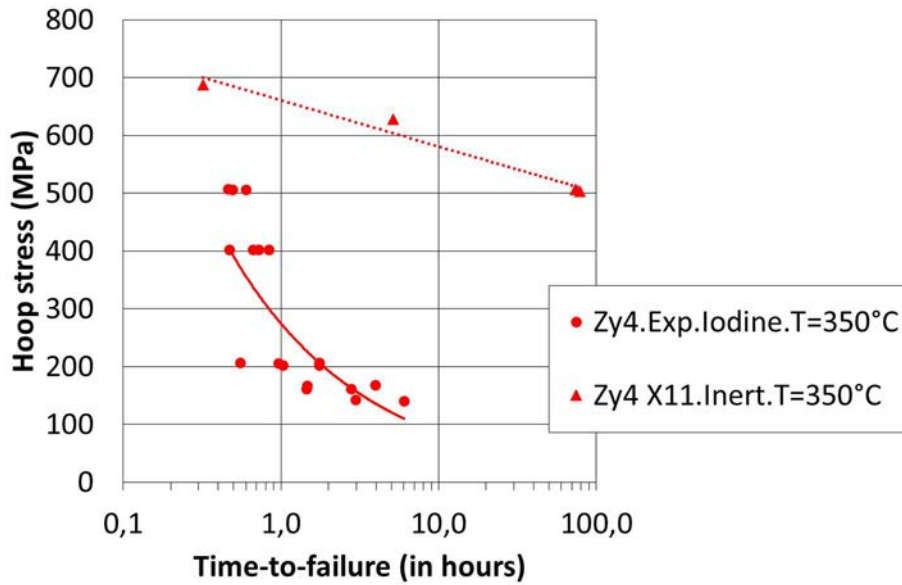


FIG. 2. Inner pressure tests at constant pressure. I-SCC susceptibility of irradiated CWSR Zy-4 cladding: Comparison of the results obtained under iodine vapor environment with results obtained under inert environment,

In order to evaluate the rate of I-SCC crack growth and I-SCC tenacity ' K_{SCC} ', internal pressure tests have also been carried out on pre-cracked specimens. Results were obtained at temperatures ranged from 350°C to 420°C on unirradiated CWSR Zy-4 [6] (see the results in Fig.3). The pre-cracking procedure is a fatigue-corrosion process and is described in [6]. Results were also obtained for irradiated CWSR Zy-4 at 350°C [7] with a fatigue procedure described in [8]. These results are plotted on Fig.4 together with the results obtained on unirradiated CWSR Zy-4 (previously presented on Fig.3).

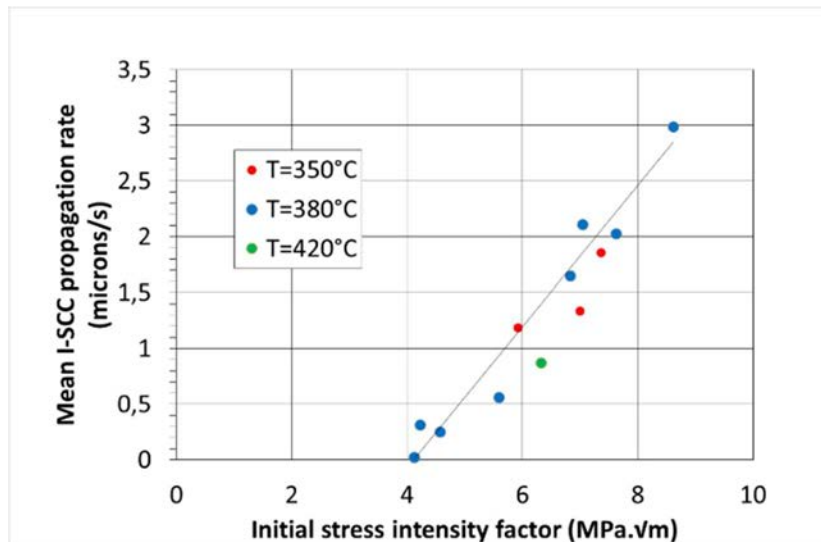


FIG. 3. Inner pressure tests at constant pressure on pre-cracked specimens of unirradiated CWSR Zy-4: Effect of temperature on I-SCC tenacity ($K_{SCC}=4 \text{ MPa}\cdot\sqrt{\text{m}}$) and on the I-SCC propagation rate.

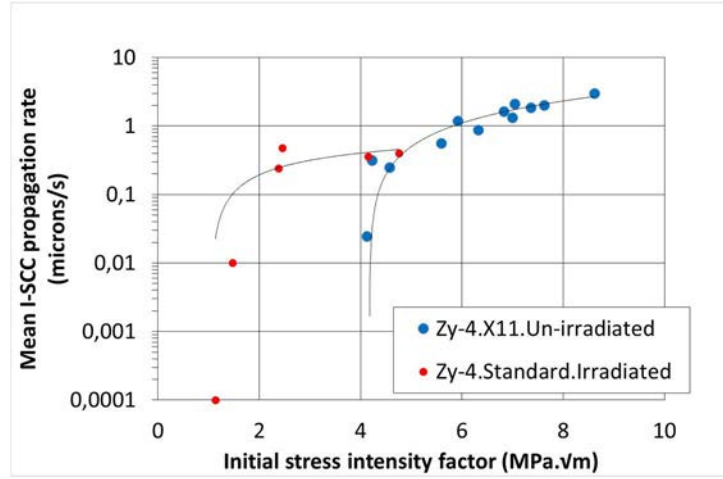


FIG. 4. Inner pressure tests at constant pressure on pre-cracked specimen: Effect of the irradiation on I-SCC tenacity ($K_{SCC}=1$ MPa.√m on irradiated CWSR Zy-4.

The results give mean propagation rates ‘V’ in terms of the initial stress intensity factor ‘ K_0 ’ applied to each specimen (Eq. (2)). The mean propagation rate V is expressed as a function of the time-to-failure ‘ t_F ’, and the difference between the final I-SCC crack depth ‘ a_f ’ and the pre-crack depth ‘ a_0 ’ both measured post-mortem.

$$V = \frac{a_f - a_0}{t_F} \quad (2)$$

‘ K_0 ’ is expressed in Eq. (3) as a function of the mean hoop stress ‘ $\sigma_{\theta\theta}$ ’, as defined in Eq. (1) and the pre-crack depth ‘ a_0 ’.

$$K_0 = \sigma_{\theta\theta} \cdot \sqrt{\pi \cdot a_0} \quad (3)$$

The I-SCC tenacity and the propagation rate seem independent of temperature. The irradiation decreases the I-SCC tenacity of the CWSR Zy-4.

The I-SCC propagation time appears to be short compared to typical initiation times (a few minutes versus a few hours respectively). As a consequence, the experimental time-to-failure can be assimilated to the time to initiate an I-SCC crack on the non-precracked specimen.

3. RESULTS AND MODELING

3.1. Simulation of the inner pressure experiments

To simulate the inner pressure tests, finite-element simulations were performed with CAST3M [1] in the 2D radial-tangential plane of the cladding. The viscoplastic behaviour of the cladding was simulated with an orthotropic viscoplastic model [9] for irradiated or un-irradiated Zy-4 cladding. This model is implemented in CAST3M through the MISTRAL module [10].

The internal pressure consist in radial nodal forces applied at the inner wall of the cladding. The internal pressure results in an axial force F that acts on the end caps of the specimen. The value of F is written as a function of the internal pressure P and the inner radius R_{in} of the cladding (Eq. (4)):

$$F = P \pi R_{in}^2 \quad (4)$$

In order to take into account F, the simulations were made with the assumption of generalized plane strain. Within this assumption, the resultant axial load F is applied to the mesh at the centre of the generalized plane strain centre, which is situated at the centre of the cladding (Eq. (5)). In the example presented on the left side of Fig.5, the simulated angle is $\theta = 22.5^\circ$. As a consequence, the force that is applied in the simulations ($F_{applied}$) is equal to $F/16$.

$$F_{applied} = \frac{F \cdot \theta_{rad}}{2\pi} \quad (5)$$

The geometry of the mesh was updated with the calculated displacements after each step of the calculation. The radial nodal forces that are applied at the inner wall of the cladding and the axial force F were recomputed with the updated geometry, after each step too. As a consequence, the value of the hoop stress defined in Eq. (1) is its initial value.

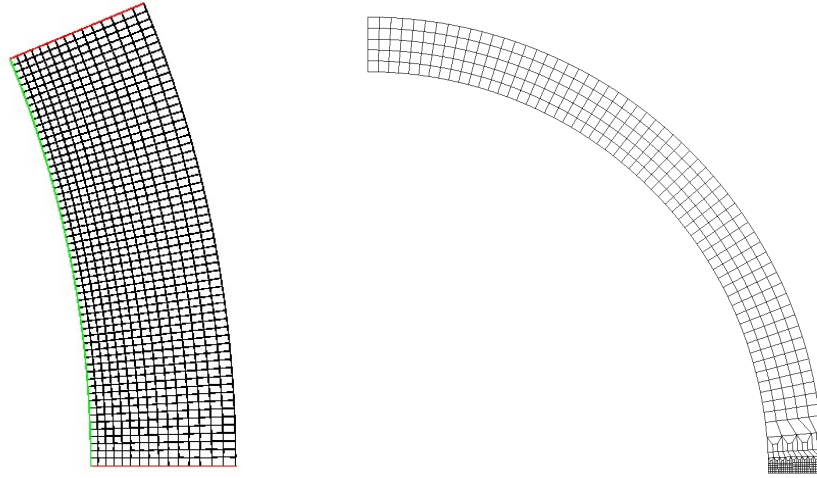


FIG. 5. On the left, 2D finite element mesh used in the simulations with the symmetrical boundary conditions (red lines) and the pressure applied at the inner wall of the cladding (green line). On the right, an example of the mesh used for the calculations with the Kachanov-Miller's model.

3.2. I-SCC modelling with the Kachanov's model

I-SCC is described using Kachanov's damage model [11] as written in Eq. (6).

$$\frac{dD}{dt} = A \left\langle \frac{\sigma_{\theta\theta}}{1-D} - \sigma_0 \right\rangle^n \text{ with } \langle X \rangle = \begin{cases} X & \text{if } X > 0 \\ 0 & \text{if } X < 0 \end{cases} \quad (6)$$

This model describes the evolution of a damage variable D in terms of an effective hoop stress ($\sigma_{\theta\theta}/(1-D)$) and a threshold stress σ_0 . The scalar 'A' and the exponent 'n' are parameters of the model. The damage variable D is a scalar that ranges from 0 to close to 1. Before any damage occurs, D is equal to 0. Then, with the effective hoop stress higher than the threshold stress σ_0 , D increases with time.

3.3. Kachanov's Model used in post-treatment of FE simulations

The Kachanov's model can be used in post-treatment of the FE simulations. The effective $\sigma_{\theta\theta}$ used in Eq. (6) is the hoop stress calculated at the inner surface of the cladding. The value D=1 represents the initiation of an I-SCC crack at the inner wall of the cladding, in the calculations. Because the I-SCC propagation time is short compared to the initiation time, the crack initiation time calculated with Kachanov's model (D=1) can be considered to be the same as the experimental time-to-failure.

A set of parameters was identified for the un-irradiated CWSR Zy-4 in [3], on the results presented in Fig.1. The effect of the temperature on I-SCC is taken into account with an activation energy Q as written in Eq. (7). The stress threshold $\sigma_{iodine}=240$ MPa appeared independent of temperature.

$$\frac{dD}{dt} = A_{Iodine} e^{-\frac{Q}{T}} \left\langle \frac{\sigma_{\theta\theta}}{1-D} - \sigma_{Iodine} \right\rangle^{n_{Iodine}} \quad (7)$$

The times-to-failure calculated with the Kachanov's model are compared with experimental results in Fig.6. As an illustration, the times at which the calculated Diametrical Strain "DS" is larger than 40% are plotted on the figure under the name 'Inert-DS>40%' curves. These curves illustrate the times-to-failure that could be obtained in an inert environment due to mechanical failure. In that figure (and the following figures), it is assumed that the times-to-failure calculated with the Kachanov's model cannot be longer than the times-to-failure evaluated with

the ‘Inert-DS>40%’ curves. The parameters of Eq. (7) were identified for the irradiated CWSR Zy-4. Only the activation energy ‘Q’ was fixed to its value identified on un-irradiated CWSR Zy-4 [3]. The Kachanov’s model for irradiated CWSR Zy-4 is compared to the experimental results in Fig.7. As an illustration, the times at which the calculated Diametrical Strain ‘DS’ is larger than 20% are plotted in the figure.

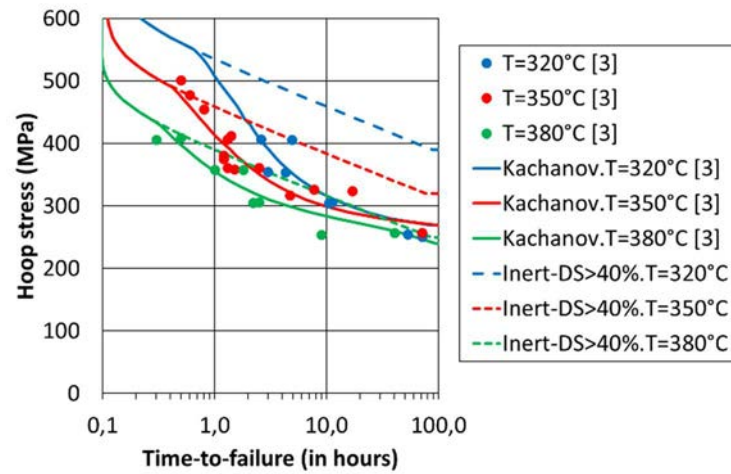


FIG. 6. Inner pressure tests at constant pressure: Comparison of the Kachanov’s model with the experimental results obtained on the un-irradiated CWSR Zy-4.

3.4. Coupled Kachanov’s model in CAST3M

For a simulation of the initiation and the propagation of a crack, the Kachanov’s model can be coupled to the viscoplastic models of the cladding. For that purpose, it has been implemented in the MISTRAL module and coupled to the viscoplastic models available in that module [12].

To simulate the crack opening, a crack strain tensor ‘ ε^f ’, as described in the Ottosen’s model [13], has been added to the other type of strains in the MISTRAL module. It’s a method to make the coupled damage model independent of the size of the mesh used in the calculation [13]. For an application to the tangential direction of the cladding, the tangential component is the only non-null value of the tensor. The tangential component is written in Eq. (8) as a function of the length L_θ of the elements in the tangential direction and of the critical opening of the crack ‘ u_c ’.

$$\frac{d\varepsilon_\theta^f}{dt} = \frac{dD}{dt} \cdot \frac{u_c}{L_\theta} \text{ with } G_0 = \frac{1}{2} \cdot \sigma_0 \cdot u_c \quad (8)$$

The critical crack opening ‘ u_c ’ and the stress threshold σ_0 , as defined in Eq. (6) in the Kachanov’s model, allow the minimal fracture energy ‘ G_0 ’ of the model to be defined.

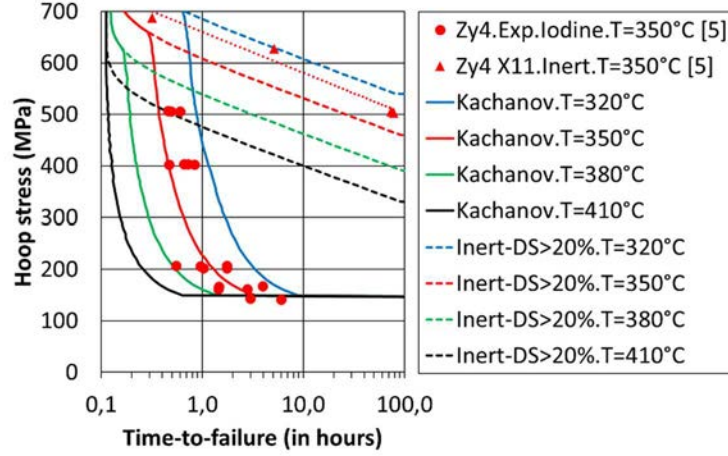


FIG. 7. Inner pressure tests at constant pressure. Comparison of the Kachanov's model with the experimental results obtained on irradiated CWSR Zy-4. (The effects of the temperature are extrapolated with the Kachanov's model.).

Figure 8 illustrates the response of the coupled Kachanov's model under a uni-directional loading that consists in applying a constant strain rate V , on one element, with the properties of the cladding in its tangential direction (with the viscoplastic model for the CWSR Zy-4 [9]). The fracture energy G , which is defined as the area under the curve in this figure, tends to ' G_0 ' as the applied strain rate V decreases. It can be noticed that the displacement-to-failure is equal to the critical crack opening u_c plus a viscoplastic elongation of the material. For the lowest strain rates V , the viscoplastic elongation is negligible and the displacement-to-failure is equal to the critical crack opening u_c .

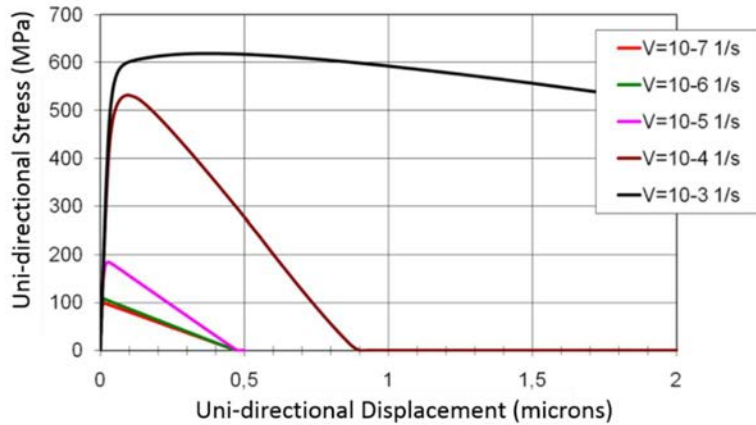


FIG. 8. Uni-directional response of the Kachanov's model coupled with a viscoplastic model in CAST3M, at different uni-directional constant strain rate V . The calculation was made on one element, with $\sigma_0=100$ MPa and $u_c=0.5$ microns. The curves obtained with $V=10^{-7} s^{-1}$ and $V=10^{-6} s^{-1}$ are superposed and define the minimal fracture energy G_0 .

In order to account for the embrittlement of the cladding due to the local iodine content I in the material, the Kachanov's model (Eq. (7)) is re-written as a function of embrittlement functions $A(I)$ and $\sigma_0(I)$ in Eq. (9):

$$\frac{dD}{dt} = A(I) \cdot e^{-\frac{Q}{T}} \left(\frac{\sigma_{\theta\theta}}{1-D} - \sigma_0(I) \right)^n \quad (9)$$

The critical crack opening u_c is a function of the embrittlement function $G_0(I)$ deduced from Eq. (10):

$$G_0(I) = \frac{1}{2} \cdot \sigma_0(I) \cdot u_c(I) \quad (10)$$

Figure 9 presents the embrittlement functions according to the local iodine content I . When I is lower than a threshold value $IC1$, there is no embrittlement of the material. The Kachanov's model is supposed to model the damage of the material under an inert environment. When I is higher than a saturation iodine content $IC2$, the I-SCC susceptibility of the material does not change. The local iodine content I and the parameters $IC1$ and $IC2$ are dimensionless quantities.

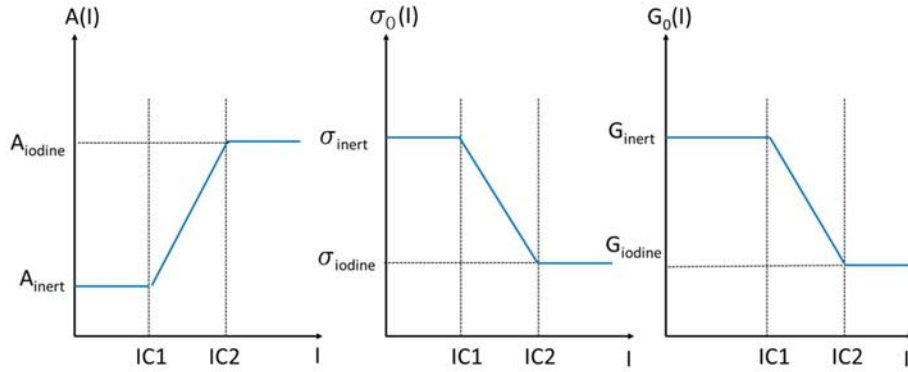


FIG. 9. Embrittlement functions according to the iodine content « I ».

The local iodine content I is assumed to follow I-SCC Miller's model [14]. This model is based on Fick's law of diffusion. Assuming that iodine does not diffuse in the zirconium, except in the I-SCC crack or at the tip of a crack, Fick's law can be written as in Eq. (11) in [14].

$$\frac{dI}{dt} = \frac{1}{\tau} (I_{EXT} - I) \quad (11)$$

This equation is suitable for a 2D Radial-Tangential FE application. In Eq. (11), I_{EXT} is the 'external iodine load'. In this paper, it is a dimensionless quantity. Both, the iodine load I_{EXT} and the local iodine content I are fields of values defined on all the elements of the mesh in the FE simulations. The parameter τ in Eq. (11) is a period of time that is characteristic of the diffusion of iodine, limited to the crack and the tip of a crack, in the zirconium. This parameter could depend on the local mechanical fields as in Miller's model [14] but was not taken into account in this paper.

The coupled Kachanov's model used with the Miller's model described above is called Kachanov-Miller's model in the following.

Before any I-SCC crack is initiated in the calculation, the value of I_{EXT} is set to 0 everywhere except in one element of the inner wall of the cladding chosen arbitrarily. In that element, the local iodine content I evolves from 0 to the local non null value of I_{EXT} . The evolution of the local iodine content I can lead to local embrittlement of the cladding and to subsequent local damage. The external iodine load I_{EXT} is updated after each step of calculation in CAST3M according to the updated position of the I-SCC crack, so that, the values of I_{EXT} are 0 everywhere in the mesh except in an I-SCC crack and at the tip of an I-SCC crack, as illustrated in Fig.10.

The 'external iodine load' can be updated according to the position of the damaged zone. The damaged zone is defined as the zone where $D > D_{min}$. It includes the I-SCC crack. In the following, the external iodine load was updated according to the "damaged zone" with $D_{min}=0.01$.

The Kachanov-Miller's model has been applied to the simulation of the inner pressure tests on irradiated CWSR Zy-4. Both the tests realized on smooth (see Fig.2) and pre-cracked specimens (see Fig.4) have been simulated.

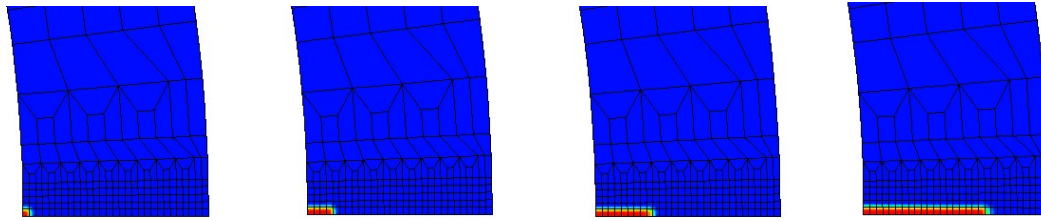


FIG. 10. Simulation of the I-SCC crack with the Kachanov-Miller's model. The iso-values of the external iodine load « I_{EXT} » that range from 0 (blue) to 1 (red) are depicted. The external iodine load starts at the inner wall of the cladding and follows the I-SCC crack that runs along the radius of the cladding, at different time steps (from the left to the right).

Figure 11 presents the results obtained with the Kachanov-Miller's model applied to simulations of inner pressure tests at constant pressure on irradiated CWSR Zy-4 smooth specimens. The parameters under iodine of the embrittlement functions (see Fig.9) were those identified with the Kachanov's model used in post-treatment, as described in Eq. (7) and Fig.7. The parameters of the embrittlement functions for an inert environment were arbitrarily chosen to avoid any damage without iodine. The parameters IC1 and IC2 are arbitrarily set to 0.2 and 0.5 respectively in order to saturate the iodine embrittlement. I-SCC initiation and failure of the smooth specimens are properly simulated by the Kachanov-Miller's model. I-SCC cracks evolve fast enough in the calculations to conclude that the times-to-failure and the times-to-initiate an I-SCC crack are close in the calculations as in the experimental tests.

Figures 12 and 13 present the results obtained with the Kachanov-Miller's model applied to simulations of inner pressure tests at constant pressure on pre-cracked specimens, with 2 different pre-cracks 'C' in the calculations and 2 different sizes of the mesh 'L', respectively. The pre-crack is simulated in affecting $D=1$ to a row of elements as initial values in the calculations. The calculations are post-treated like the experiments using Equations (1)–(3). As expected, the result of the model is the same for a given initial stress intensity factor, regardless of the depth of the pre-crack C in the calculation. The result is independent of the size of the elements of the mesh L where a crack strain tensor ' ϵ^f ' is defined as in Eq. (8) of [13].

The calculated I-SCC tenacity ' K_{SCC} ' is close to the experimental value ($K_{SCC}=1 \text{ MPa}\cdot\sqrt{\text{m}}$). In the calculation, the I-SCC propagates when the local tangential σ_θ stress is larger than the I-SCC stress threshold σ_{iodine} . In the coupled modelling, the I-SCC tenacity K_{SCC} and the I-SCC stress threshold have the same mechanical meaning: the coupled Kachanov's model leads to a crack propagation when the local hoop stress is locally bigger than the I-SCC stress threshold. K_{SCC} and the I-SCC stress threshold are both independent of the temperature in the range 320°C to 380°C ([3, 6]).

In this paper, the initiation and the propagation of an I-SCC crack are supposed to be led by the same mechanism (modelled with the Kachanov's model). The I-SCC propagation rate is under-estimated with the set of parameters that predicts correctly the I-SCC initiation. The set of parameters had to be modified to properly evaluate the I-SCC propagation rate (see Fig.14). The Aiodine parameter, as defined in Fig.9, was multiplied by 10. This result suggests that a specific mechanism could govern the propagation of an I-SCC crack.

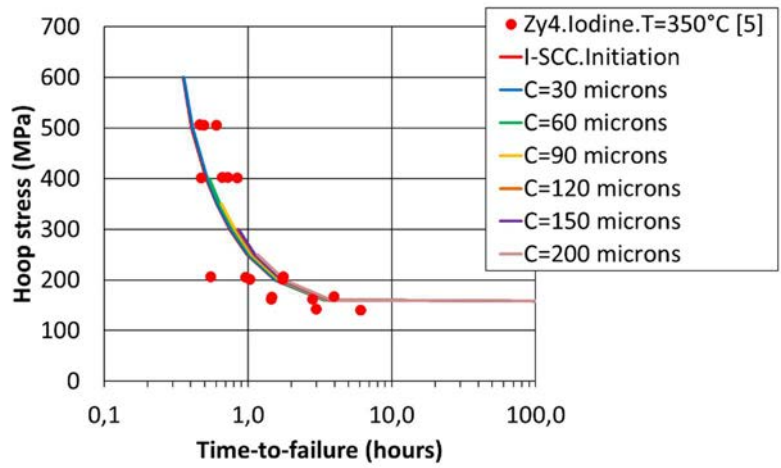


FIG. 11. Inner pressure tests at constant pressure on smooth specimen: Comparison of the Kachanov-Miller's model with the experimental results obtained on irradiated CWSR Zy-4, Each curve represents the time required to initiate a crack or to develop a crack of depth C in the calculations.

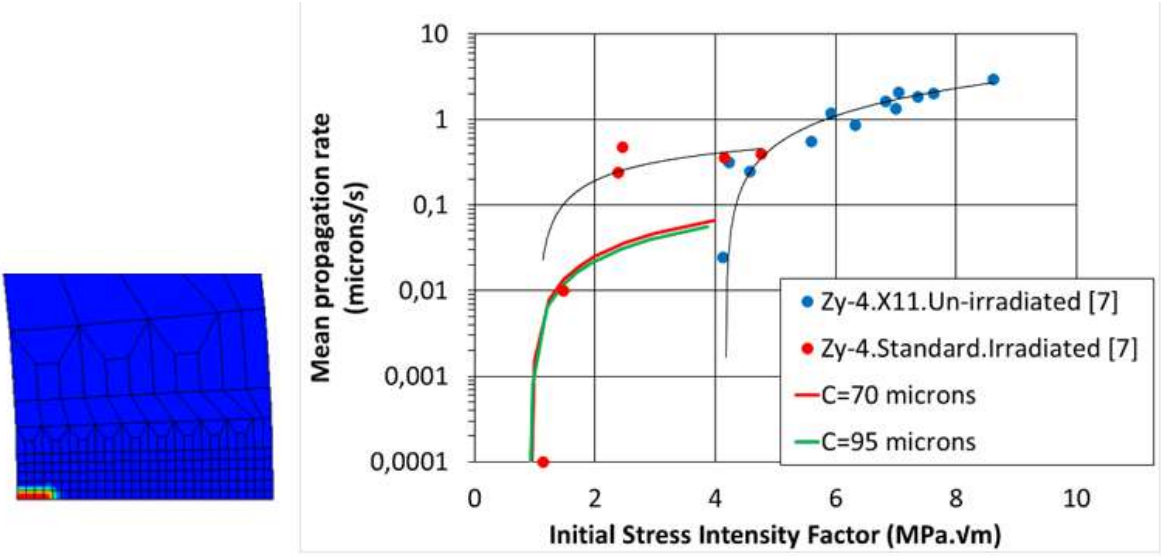


FIG. 12. Inner pressure tests at constant pressure on pre-cracked specimens: Comparison of the Kachanov-Miller's model with the experimental results obtained on irradiated CWSR Zy-4, for 2 values of the depth of the pre-crack C in the calculations. On the left, the pre-crack is represented by the elements where $D=1$ (red) with $D=0$ (blue) anywhere else. Only a portion of the mesh used in the calculations is represented.

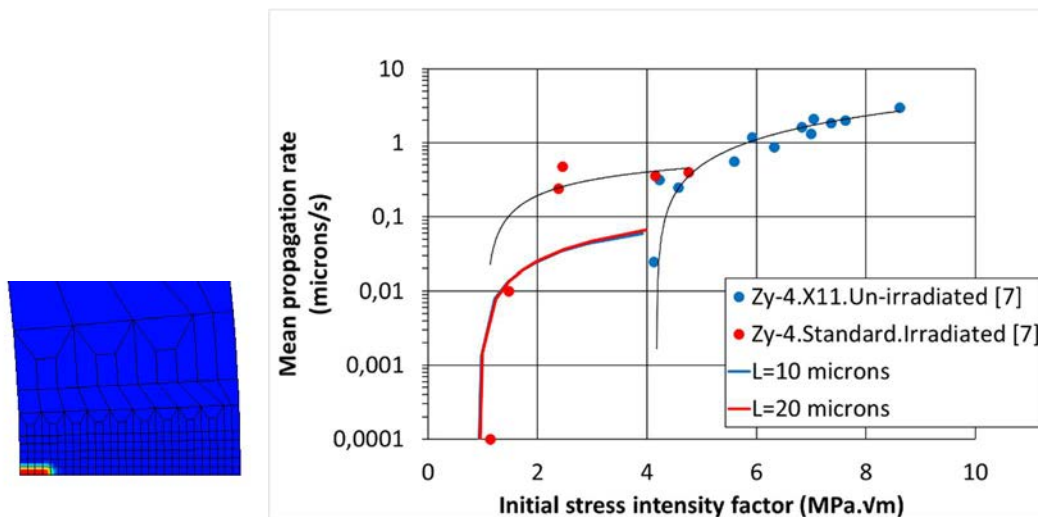


FIG. 13 Inner pressure tests at constant pressure on pre-cracked specimen. Comparison of the Kachanov-Miller's model with the experimental results obtained on irradiated CWSR Zy-4, for 2 values of the size of the mesh L in the calculations.

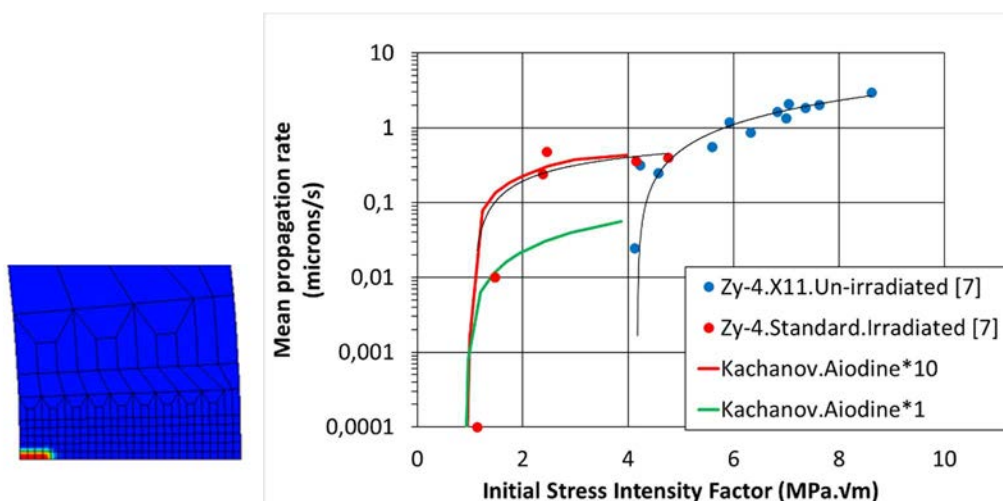


FIG. 14 Inner pressure tests at constant pressure on pre-cracked specimen. Comparison of the Kachanov-Miller's model with the experimental results obtained on irradiated CWSR Zy-4. Effect of the modified set of parameters on the I-SCC propagation rate.

4. FUTURE WORK

The Kachanov-Miller's model was implemented in Alcyone in 2D-R \square and will be implemented in Alcyone 3D [15]. The goal of this implementation is to enable a good discrimination of failed and non-failed cladding samples during ramp tests. In Fig.15, an I-SCC crack initiated and developed from the inner wall to the outer wall of the cladding, assuming that the 'external iodine load' conducted to saturated iodine embrittlement in the calculation.

Following the advances in the characterization of the chemical environment involved in the PWR rods [17–19], a new experimental device allowing studies of I-SCC in a controlled chemical environment was developed [20] (see Fig.16). The goal of this experimental device is to allow studies of the chemical aspects of I-SCC, such as the effect of iodine partial pressure, the effect of oxygen partial pressure, the role of ZrI_x compounds, and the incubation time. The study of other factors, such as applied stress and surface conditions, is possible as well. Due

to the fact that iodine can react quickly with many materials, including most metals, the experimental device was built using inert materials. The portions of the experimental device that are in direct contact with iodine vapor are made of either glass or PTFE.

First results show that the time to rupture of the specimen is inversely related to the iodine partial pressure. The lowest tested iodine partial pressure, 150 Pa, resulted in an I-SCC crack. Post-Mortem microstructural observations provide evidence of iodine corrosion of zircaloy-4. These results are consistent with earlier studies [4,21,22].

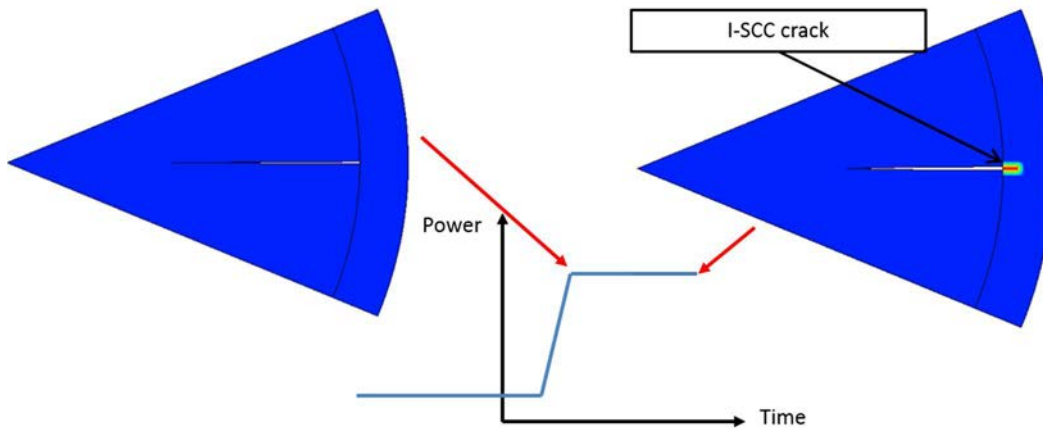


FIG. 15. Example of a ramp test simulated with Alcyone and the Kachanov-Miller's model in the cladding. The I-SCC crack initiates and propagates in front of a crack in the pellet during the upper level of the ramp test.

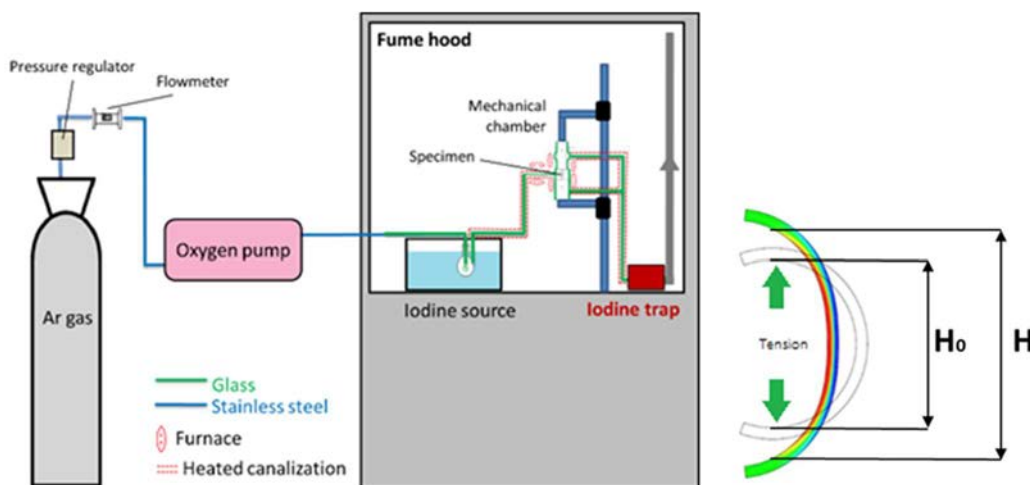


FIG. 16. Experimental setup used to study I-SCC in a controlled chemical environment: A C-Ring specimen is tested in tension in a mechanical chamber made of glass (reproduced courtesy of WILCZYNSKA [20]).

5. CONCLUSIONS

The inner pressure tests carried out at constant pressure, under iodine vapor environment, on smooth CWSR Zy-4 specimens, tend to reveal a hoop stress threshold for I-SCC. This stress threshold does not seem to depend on the temperature in the range 320°C to 380°C.

This result is consistent with the fact that the I-SCC tenacity 'KSCC' also seems to be independent of the temperature.

The experimentally determined stress threshold is about 240 MPa on un-irradiated CWSR Zy-4. This value is close to the stress threshold of 300 MPa exhibited in [16] on un-irradiated CWSR Zy-4. The stress threshold is about 150 MPa on irradiated CWSR Zy-4.

The Kachanov's model, used in post-treatment of finite-element calculations, was used to model the initiation of I-SCC. A set of parameters was identified, from inner pressure tests under iodine vapor, for both un-irradiated and irradiated CWSR Zy-4.

This set of parameters was used in the Kachanov-Miller's model presented in this paper. The model properly simulated both I-SCC initiation and I-SCC tenacity "KSCC" for irradiated CWSR Zy-4. It tends to give the same physical meaning to the I-SCC stress threshold and to the I-SCC tenacity KSCC in the calculations. The I-SCC propagation rates were under-estimated with that set of parameters. In order to better evaluate the I-SCC propagation rates, some parameters have to be re-evaluated, or a specific mechanism have to be added to the modelling of the propagation of I-SCC cracks.

REFERENCES

- [1] <http://www-cast3m.cea.fr/>
- [2] FANDEUR O., Etude expérimentale et modélisation de la corrosion sous contrainte du Zircaloy-4, Ph.D. thésis, Ecole Centrale de Paris (2001).
- [3] JÉZÉQUEL, T., Stress Corrosion Crack Initiation of Zircaloy-4 Cladding Tubes in an Iodine Vapor Environment During Creep, Relaxation and Constant Strain Rate Tests, *Journal of Nuclear Materials* 499 (2018) 641-651.
- [4] ANGHEL, C., ALVAREZ HOLSTON, A-M., LYSELL, G., KARLSSON, S., JAKOBSSON, R., FLYGARE, J., MAHMOOD, S-T., LE BOULCH, D., ARIMESCU, I., "Experimental and Finite Element Modeling Parametric Study for Iodine-Induced Stress Corrosion Cracking of Irradiated Cladding", *Proceedings of Top Fuel 2010*, Orlando, Florida, USA, September 26-29, 2010, paper 111.
- [5] FOURNIER L., ROUILLON L., Comportement en CSC par l'iode du Zy-4 irradié 1 cycle REP, Note technique CEA-Saclay, DMN/SEMI/LCMI/ NT/00-045/A.
- [6] FOUCHET, J., DELETTE, G., ROUILLON, L., Caractérisation de la phase transgranulaire lors de la fissuration par CSC du Zy-4 détendu en milieu iodé, Note technique CEA-Grenoble DTP/SECC 98/062A.
- [7] SCHUSTER, I., LEMAIGNAN, C., JOSEPH, J., Testing and Modelling the Influence of Irradiation on Iodine-Induced Stress Corrosion Cracking of Zircaloy-4, *Nucl. Eng. Design* 156 (1995) p. 343.
- [8] LEMAIGNAN, C., Controlled Cracking of Tubes, *International Journal of Pressure Vessels & Piping* 15 (1984) 241-249.
- [9] SONIAK, A., L'HULLIER, N., MARDON, J.P., REBEYROLLE, V., BOUFFIOUX, P., BERNAUDAT, C., "Irradiation Creep Behaviour of Zr-Base Alloys", *Proceedings of 13th ASTM. International Symposium on Zirconium in the Nuclear Industry*, Annecy, 2001, STP 1423, pp. 837-862.
- [10] LIMON, R., LEHMANN, S., A Creep Rupture Criterion for Zircaloy-4 Fuel Cladding under Internal Pressure, *Journal of Nuclear Materials* 335 (2004) 322-334.
- [11] KACHANOV L. M., Rupture Time Under Creep Conditions. *Int. J. Fract.* 97 (1999) 11-18.
- [12] LE BOULCH, D., STRUB, C., HOURDEQUIN, N., Modélisation de la Corrosion Sous Contrainte par l'Iode. Présentation d'un modèle d'endommagement couplé au comportement des alliages de Zirconium dans MISTRAL, Note technique CEA-Saclay DMN/SEMI/LCMI NT/2008-013/A.
- [13] OTTOSEN, N.S., Constitutive Model for Short Time Loading of Concrete, *Journal of Engineering Mechanics* 105 (1979) 127-141.
- [14] MILLER, A.-K., OCKEN, H., TASOOJI, A., Iodine Stress Corrosion Cracking of Zircaloy, Laboratory Data: a Phenomenological Model and Predictions of In-Reactor Behaviour, *Journal of Nuclear Materials* 99 (1981) 254-268.
- [15] FÉDÉRICI, E. et al, Recent Advances in the Understanding of the Physical Mechanisms Involved in PCI I-SCC and Their Modelling with ALCYONE Application, NEA/CSNI/R(2018)9.
- [16] MAGNUSSON, P., LE BOULCH, D., PURANEN, A., JÄDERNÄS, D., LYSELL, G., "An Experimental and Finite Element Modelling Study of Cladding Strain and Localized Stresses under Simulated Iodine-Induced Stress Corrosion Cracking", *proc. WRFPM 2014*, Sendai, Japan, 2014.
- [17] SERCOMBE, J., RIGLET-MARTIAL, C., BAURENS, B., Simulations of Power Ramps with ALCYONE Including Fission Products Chemistry and Oxygen Thermo-Diffusion, NEA/CSNI/R(2018)9.
- [18] BAURENS, B., SERCOMBE, J., RIGLET-MARTIAL, C., DESGRANGES, L., TROTIGNON, L., MAUGIS, P., 3D Thermo-Chemical-Mechanical Simulation of Power Ramps with ALCYONE Fuel Code", *Journal of Nuclear Materials* 452 (2014) 578-594.
- [19] KONARSKI, P., SERCOMBE, J., RIGLET-MARTIAL, C., NOIROT, L., ZACHARIE-AUBRUN, I., HANIFI, K., FREGONESE, M., CHANTRENNE, P., 3D Simulation of a Power Ramp Including Fuel Thermochemistry and Oxygen Thermo-diffusion, *Journal of Nuclear Materials* 519 (2019) 104-120.

- [20] WILCZYNSKA, K., BONO, M., LE BOULCH, D., FREGONESE, M., CHABRETOU, V., MOZZANI, N., BARBIE, L., BAURENS, B., "Development and Validation of a New Experimental Device for Studies of Iodine Stress Corrosion Cracking of Zirconium Alloys", The 19th International Conference on Environmental Degradation of Materials in Nuclear Power Systems- Water Reactor, August 18-22 2019, Boston USA.
- [21] PEEHS, M., STEHLE, H., STEINBERG, E., "Out of Pile Testing of Iodine Stress Corrosion Cracking in Zircaloy Tubing in relation to the Pellet-Cladding Interaction Phenomenon", Zirconium in the Nuclear Industry, Philadelphia, USA, ASTM International (1979).
- [22] CHEN, H., YAN, M., LONG, C., WANG, H., WEI, T., WANG, P., "Effect of Iodine Partial Pressure on the Iodine Stress Corrosion Cracking Behaviours of Zr-Sn-Nb Alloy Using the Ring Tensile Test, Journal of Nuclear Science and Technology **55** (2018) 496-502.

RAMP TESTING AND MICROSTRUCTURAL/CHEMICAL EVOLUTION OF ADVANCED PELLET NUCLEAR FUEL RELATED TO PCI

D. JÄDERNÄS, A. PURANEN, J. KARLSSON, J. PAKARINEN
STUDSVIK,
Sweden
Email: Daniel.Jadernas@studsvik.com

Extended Abstract

In modern UO_2 nuclear fuel pellets, additives and dopants are used to improve the in-reactor performance, such as pellet cladding interaction (PCI) and failure performance during power transients. However, it is not completely understood if and why advanced pellets with different additives/dopants display a better PCI behaviour. Proposed mechanisms include increased compliance, resulting in higher creep rates and the trapping of aggressive fission product species involved in PCI initiation and crack propagation. Additive fuel typically has a larger grain size compared to standard fuel, which affects the migration of fission products.

To see if the additive pellets display a better performance during power transients, all the historical ramp tests conducted in the Studsvik R2 reactor were analyzed and evaluated. Figure 1 shows that for Gd fuel none of the tested rods failed but they were above the failure limit. The failure limit was established by using the data from all similar ramp tests in the Studsvik R2 database. A similar trend can be seen for other additive fuel where all but one fuel rod did not fail during the ramp test.

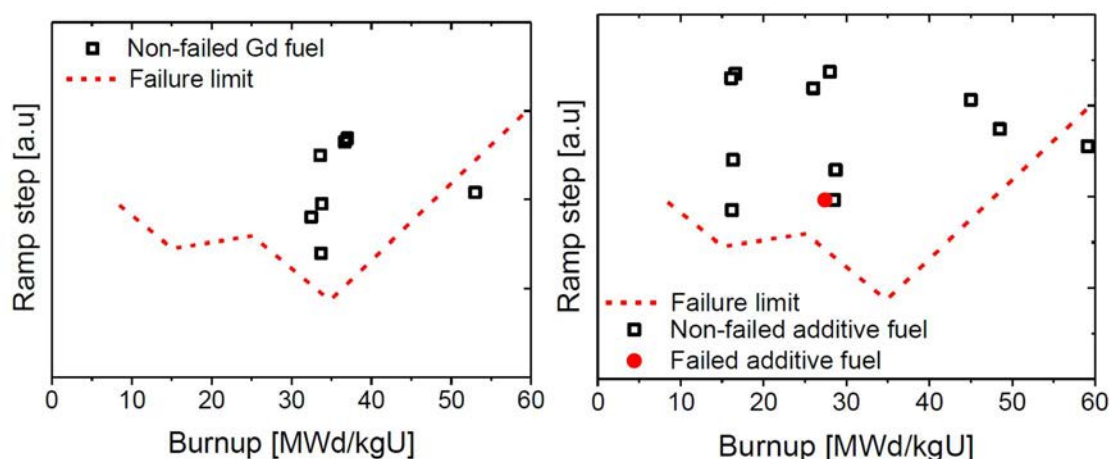


FIG.1. Ramp step as a function of burnup for the Gd fuel (left) and other additive/doped fuel (right) (reproduced courtesy of Studsvik [1]).

To understand why the good behaviour of these pellets was observed, a task of the Studsvik Cladding Integrity Project II (SCIP II) was implemented focusing on the PCI failure mechanisms. One important objective was to map the chemical and microstructural differences between different pellet types, which may be of importance for the PCI behaviour. The different pellet types included in this study have Al/Si and Al/Cr as well as Gd oxide additives and have been subjected to power ramp tests in the Halden research reactor. Standard UO_2 fuel was also included in the test matrix as reference materials. The pre-ramp conditions of the different fuels have also been characterized. Table 1 summarizes the samples that were characterized in this work. As can be observed, the ramp terminal levels are between 31-48 kW/m which is potentially a little lower than what could be expected during a PCI event resulting in relatively low fuel centreline temperatures, see Figure 2. This results in that some high temperature effects may not be observed in these tests e.g. high temperature enhanced creep rates of certain additive fuel types.

The ramp tested additive/dopant fuels have been characterized using Field emission Gun Scanning Electron Microscope (FEG-SEM) equipped with a Focused Ion Beam (FIB) source. The analytical equipment consists of a wavelength dispersive spectroscopy (WDS/EPMA) and Electron Backscattered Diffraction (EBSD). In order to measure the volatile fission products in the pellet such as I and Cs, Laser Ablation (LA) combined with Inductively

Coupled Plasma Mass Spectrometry (ICP-MS) measurements have been performed. Transmission electron microscopy was also employed.

TABLE 1. RAMP STEP AS A FUNCTION OF BURNUP FOR THE GD FUEL (LEFT) AND OTHER ADDITIVE/DOPED FUEL (RIGHT) (REPRODUCED COURTESY OF STUDSVIK [1]).

Pellet type	Average burnup (local) [MW·d/kgU]	Ramp power (local) [kW/m]
Std. pellet	57 (50)	31 (30)
Al-Si pellet	44 (48)	48 (40)
Al-Cr pellet	58 (56)	38 (30)
Gd pellet	53 (53)	42 (41)

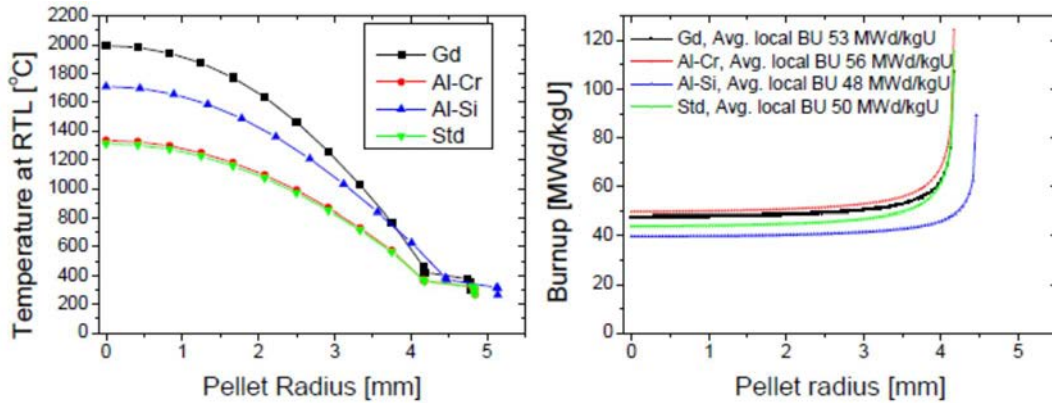


FIG.2. Radial burnup and temperature profiles during the ramp test for the different tested fuel rodlets) (reproduced courtesy of Studsvik [1]).

The results of the analyses showed different characteristics from the standard pellets in the aspects of the microstructure and distribution of fission products in the modern pellets after base irradiation and power ramps. The observed behaviour depends on the type of additive/dopants added at the time of manufacturing.

The observations that were made for Gd fuel was that no trapping of fission products could be detected. The volatile, and potentially aggressive, species (Cs, I, Te and Cd) were all present on the cladding inside as measured using SEM, TEM and LA. Figure 3 shown an example where Cs and Cd are detected in a small crack through the inner oxide of the cladding.

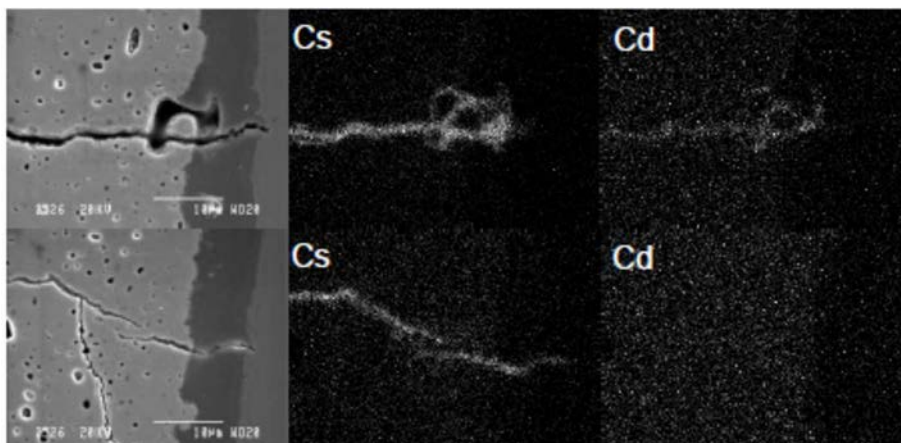


FIG.3. WDS mapping in the fuel-cladding interface region of the Gd fuel sample (reproduced courtesy of Studsvik [1]).

A relative decrease in the oxygen concentration in the hot centre parts comparing before and after ramp testing could also be observed for the Gd fuel rodlet, see Figure 4. A Gd homogenization was observed in the same region suggesting that oxygen might be released from this region during the high temperature transient due to the formation of oxygen vacancies in the UO_2 lattice. If the oxygen partial pressure in the free volume of the fuel is higher it may compete with the aggressive species in the crack tip and halt the propagation of the PCI cracks.

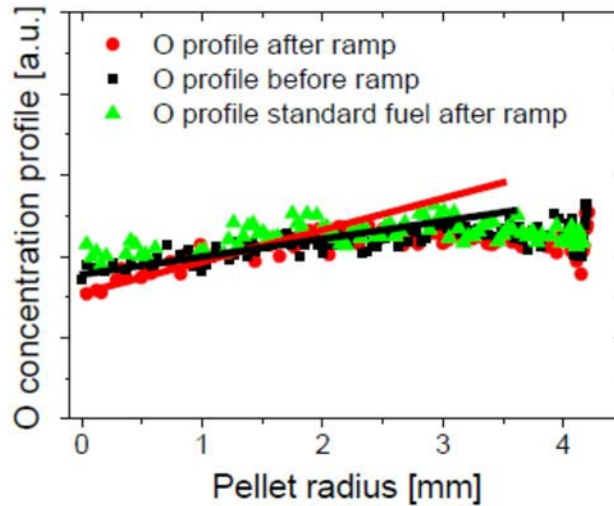


FIG. 4. SEM/WDS maps of the oxygen profiles for Gd fuel before and after ramp testing (reproduced courtesy of Studsvik [1]).

For the Al-Cr fuel rod migration of Cr could be observed towards the centre part of the pellet, see Figure 5. Together with the observation of Ba-Cr-Cr rich particles in this region by TEM could indicate that a similar mechanism might be active also in this type of fuel since similar oxides are known to dissociate at temperatures above 1200°C .

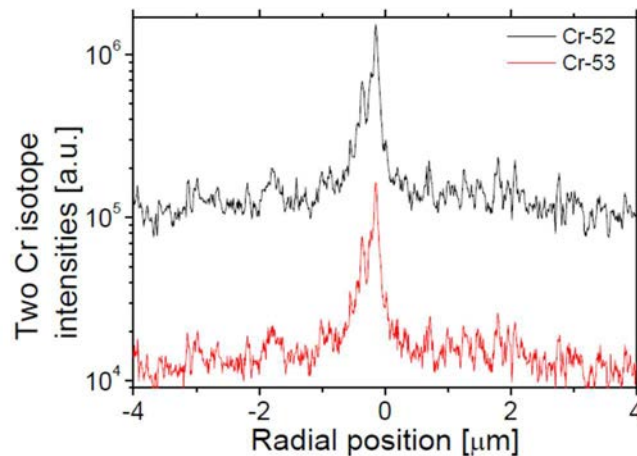


FIG. 5. Cr migration towards the hot pellet center after the transient measured by LA-ICP-MS (reproduced courtesy of Studsvik [1]).

The Al-Si fuel rod showed evidence of trapping of fission product in the Al-Si additive grain boundary phase. However, calculation show that only a fraction of the available aggressive fission products needs to be available for PCI to occur. It is thus unlikely that the trapping effects is efficient enough to stop crack propagation. It can also be hypothesized that the Al-Si glassy phases in the fuel can be unstable at higher temperatures. This may

release oxygen during the transient that could compete with the aggressive species in the PCI crack tip decreasing the risk for PCI.

It should be noted that reports showing an increased high temperature creep rate for the Al-Si and Al-Cr additive fuel samples tested in this program have been published. However, this could not be observed in this program possibly due to the relatively low centreline temperatures during the ramp tests.

In summary, a number of potential effects occurring during the ramp test impacting the PCI resistance could be observed. Trapping of aggressive fission products, oxygen release during the high temperature transient and Gd homogenization.

REFERENCE

- [1] JADERNAS, D., CORLEONI, F., PURANEN, A., TEJLAND, P., GRANFORS, M., MATSUNAGA, J., Conference Proceedings TopFuel Conference, Zurich, Switzerland, 2015

HOT CELL SETUP FOR PELLET CLADDING INTERFACE INVESTIGATION

F. NINDIYASARI, M. KOLLURI, S. VAN TIL, R. HANIA, T. BAKKER, A. DE JONG
Nuclear Research & consultancy Group (NRG),
Petten, Netherlands
Email: nindiyasari@nrg.eu

Abstract

Thermo-mechanical loads transmitted via the pellet-cladding interface play a crucial role in inducing the local stress concentrations which can lead to PCMI failures in claddings. Shear stress at the pellet-cladding interface being proportional to hoop stress aggravates the risk of cladding failure/rupture. Furthermore, an interface bonding co-determines the stress state in the cladding. Hence, experimentally determined interface properties (interface shear stress) are needed as an input to models the hoop stresses in the cladding during PCMI failures. In this regard, a test fixture was developed for the characterization of pellet-cladding interface properties using the miniature tensile test machine in NRG's hot cell laboratory. The test setup was used to characterize pellet-cladding interface properties of the fast reactor fuel pin experiment TRABANT-2/3 sample irradiated in HFR, Petten that was cut into some sections. The results showed that the load needed to push the fuel out of the cladding was 7.8N - 190.4N. Some tested sections were further cut into four segments and some SEM images were taken to investigate the surface of the inner side of the fuel segments after the push-out test. The restructuring of the fuel due to irradiation condition was found to be strongly affecting the closure and opening of the fuel-cladding gap, making it more difficult to actually assess the PCI. More investigation is needed to assess all parameters affecting PCI of the TRABANT-2/3.

1. INTRODUCTION

Pellet swelling during power transients can cause Pellet Cladding Mechanical Interaction (PCMI). This further can cause to the rupture of the cladding during a Reactivity Initiated Accident (RIA). It was identified that thermo-mechanical load transmitted via the pellet-cladding interface plays a crucial role in inducing the local stress concentrations which can lead to PCMI cladding failure [1,2]. Shear stress at the pellet-cladding interface aggravates the risk of cladding failure/rupture. Interface bonding co-determines the stress state in the cladding. Experimentally determined interface properties (interface shear stress) are needed as an input of the models used to estimate resulting hoop stresses in the cladding during PCMI failures.

At NRG, a technique was developed to be able to measure Mechanical Interaction (PCMI). This further can cause to the rupture of the cladding. An irradiated fast reactor MOX-fuel pin, TRABANT-2/3, was investigated using this push-out mechanical test setup in the alpha tight hot cell line at the Hot Cell Laboratory in Petten.

2. EXPERIMENTAL

2.1. Fuel pins

TRABANT-2/3 fuel pin was irradiated in 2001 until 2005 (3 cycles). It contained annular FR- MOX pellets, UO_2 and PuO_2 of 55% and 45%, respectively. The cladding used was an austenitic steel clad 15-15Ti (ID =5.65mm and OD=6.55mm) used in the Phénix and Super Phénix reactors. The initial fuel-cladding gap was 0.11mm. The pin was submersed in a sodium-filled capsule and the experiment was designed to produce an LHR of 450-480 W/cm in the HFR and the central fuel and cladding temperatures of 2500 °C and 600 °C, respectively. However, at the end of the irradiation, the LHR decreased to 336 – 430 W/cm with a central fuel temperature of 1500 – 1750 °C for the fuel upper and lower sections.

Due to an axial variation in the neutron flux variation, the LHR over the length of the pin varied, with a maximum of ~300W/cm in the axial outer regions, up to 430 W/cm in the highest LHR region / max flux plane. The maximum central fuel temperature was calculated to be 1500 °C in the axial outer region and went up to ~2700 °C at the max flux plane.

Neutron radiography, profilometry and light microscopy were performed at the end of irradiation to get better understanding of the fuel pin.

2.2. Push-out mechanical test

The TRABANT-2/3 fuel pin was cut at the HCL and some sections of 3mm in height were prepared. A special fixture that was fitted in the miniature tabletop tensile machine at the HCL was fabricated (Fig.1). The tensile machine was equipped with a LVDT that measured the cross-head movement (displacement). A debris container was attached to the setup in order to collect the fuel debris after the push-out test.

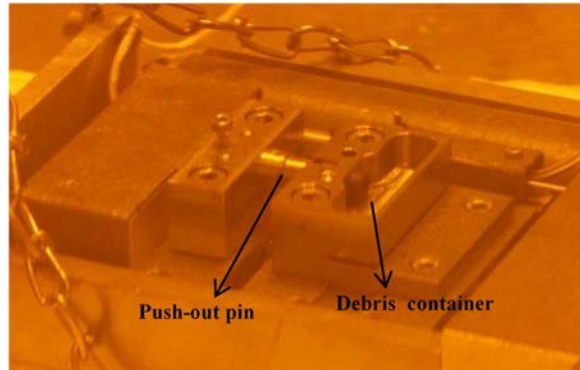


FIG. 1. The push-out setup designed for the hot cell.

2.3. Scanning electron microscope (SEM)

The sections were also investigated with the SEM to see the surface structure after the push-out test. The sections were cut into four segments. The investigated area was the area where the fuel was pushed out of the cladding. A shielded scanning electron microscope (JEOL 6490 LV SEM) located at the HCL, was used in this study.

3. RESULT

3.1. Irradiation history

TRABANT-2/3 fuel pin consisted of annular MOX fuel with fuel external diameter of 5.4 mm and internal diameter of 2.32mm (Fig.2). The height of each fuel pellet was 8.0 – 8.2 mm. The initial porosity of this fuel pellet is ~86%TD (theoretical density). This high initial porosity, generally, causes a high temperature (lower conductivity) and, additionally, results to a large effect upon restructuring.

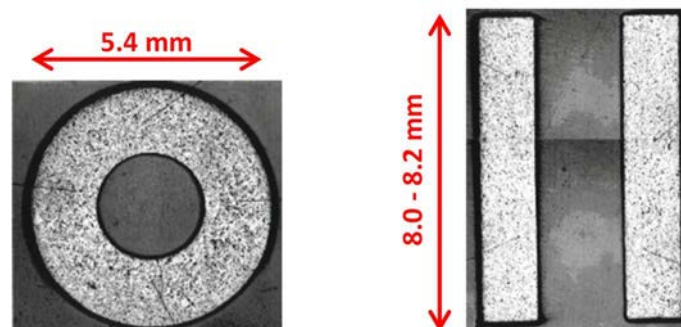


FIG. 2. Overview of the TRABANT MOX fuel.

The irradiation was stopped after 3 cycles due to some appearance of central hole relocation. Some light microscope images were taken as representatives of different zones having varied LHR, BU and central hole temperature (Fig.3).

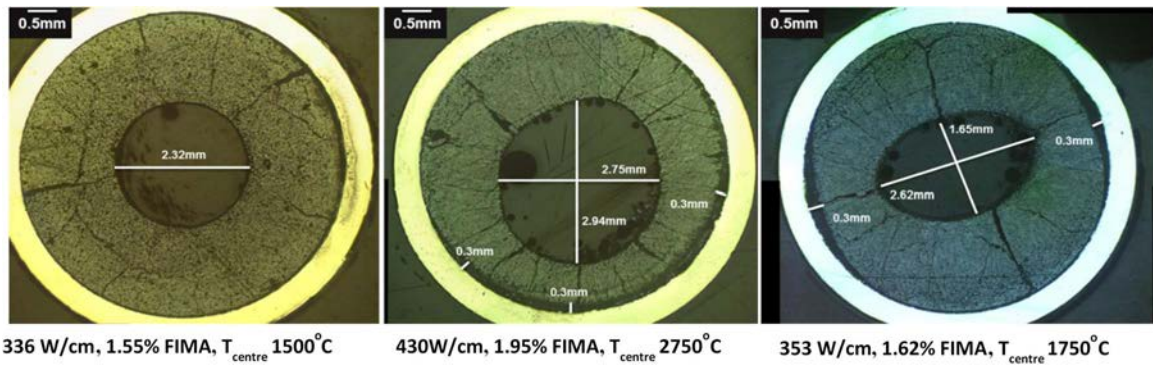


FIG.3. Some light microscope images showing the restructuring of the central hole with the respective linear heat rate, BU and central hole temperature.

The restructuring of the central hole, as seen from the light microscopes images depended on the central hole temperature that further influenced the BU and linear heat rate (Fig.3). The central hole temperature of 1500°C resulted in the least fuel pellet central hole restructuring among other investigated sections. This structure was recognised as an as-received state of the fuel pin before irradiation. However, some small expansion of the fuel touching the cladding was seen at some of fuel corners. A slightly higher temperature of 1750°C resulted to a more visible restructuring of the fuel. The central hole of the fuel restructured into an oval-liked shape where some thinning of the fuel area appeared resulting to a formation of a bigger gap between fuel-cladding (~0.3mm). Note that the initial gap was 0.11 mm. On the contrary, the other area of the fuel thickened and touched the cladding. In the case of the highest central temperature, 2750°C, the restructuring of the fuel became even more visible. The central hole enlarged, and the formation of the gap was more apparent. It was also expected that the fuel area that touched the cladding would have stronger interaction to the cladding.

3.2. Profilometry

Profilometry was performed over 600 mm of the Trabant-2/3 fuel pin with 0.5 mm increments. The uncertainty limits of the setup is ~ 3µm. The scan moved from the filler toward the steel then the fuel (Fig.4). The first raise of the peak up to ~30µm located slightly before the filler could be attributed as an increased of the cladding tube thickness due to end-cap welding result. The next raise of the peak (up to ~40 µm) located at the filler was believed to be some deposit, e. g. oxide product. Another peak appeared at the fuel area up to ~30µm. As there was no other peak appeared along the fuel area, this raise of the peak could be attributed as some dirt or unknown anomaly.

From the profilometry, the expansion of the cladding due to PCI as a result of the central hole relocation could not be seen. The cladding expansion did not occur as the irradiation was stopped before it could happen.

3.3. Push-out mechanical test

There were nine sections from the TRABANT-2/3 fuel pin that were collected for the push-out mechanical tests (Fig.5). It was expected that the selected areas represented some variation in the Burn-up (BU) value as well as LHR and temperature. The neutron radiography image (Fig.5) clearly showed some fuel movement along the pin.

The load versus displacement curves can be seen in Figure 6 together with some photographs taken before the push-out mechanical tests. Central hole relocation could clearly be observed. Some photographs of a section after the push-out test and its debris were also presented in Fig.6. The fuel after the push-out test appeared as dust-like debris instead of pellet. It indicated that the fuel pellet after irradiation became brittle due the appearance of some macroscopic cracks.

Fuel pin diameter of TRABANT pin 291-6

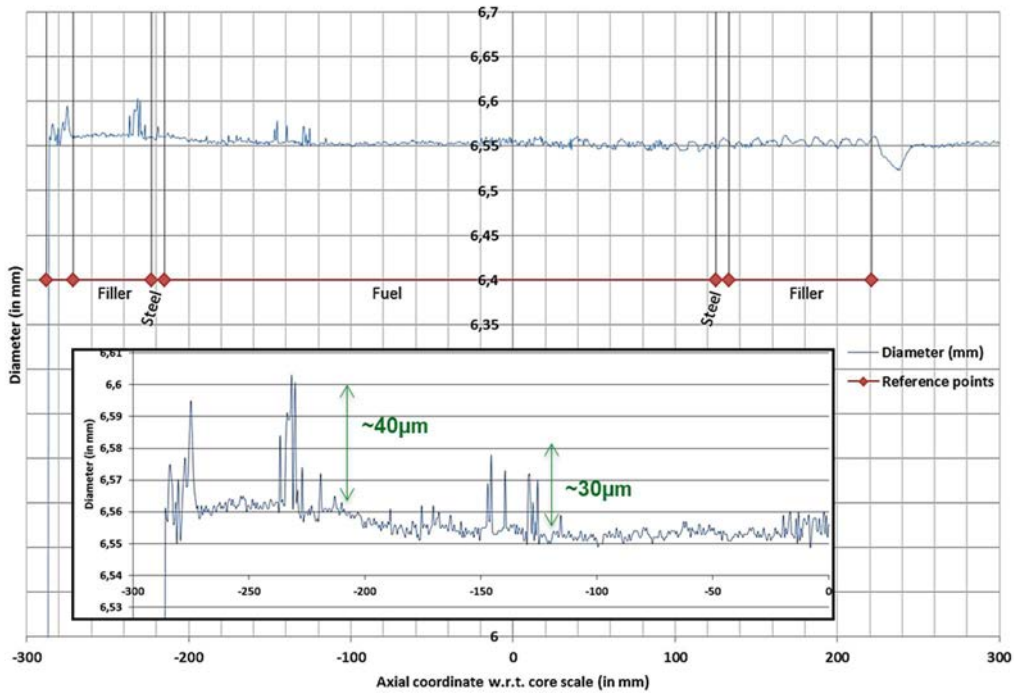


FIG. 4. Profilometry of the Trabant-2/3 pin after 3 cycles of irradiation.

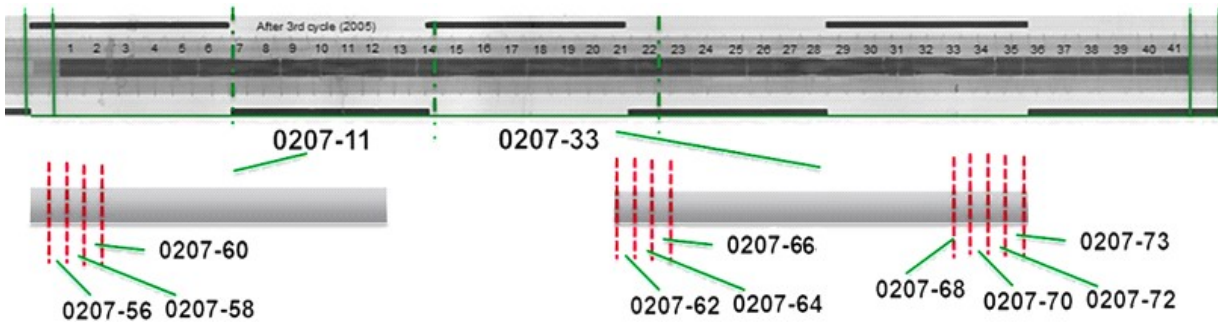


FIG. 5. Neutron radiography of TRABANT-2/3 pin after 3 cycles showing the respective cutting position for the mechanical push-out tests.

From the load versus displacement curves, it was clear that section 207-58 has the least strong fuel-clad interaction among the tested sections as the force needed to push the fuel out was less than 10N. On the contrary, the section 207-66 has the strongest fuel-clad interaction among the tested sections having the force reached up to 190.4N. More detailed results of the total nine sections could be seen in Table 1.

The load was further converted to obtain the shear stress. This simple conversion took into account 100% contact between the pellet and the cladding. Note that a simple assumption of 100% contact is almost impossible to have in an actual fuel-pellet. Hence, the correction to find proper shear strength value needs to be added, such as by adding some SEM visual investigation of the pellet-cladding contact.

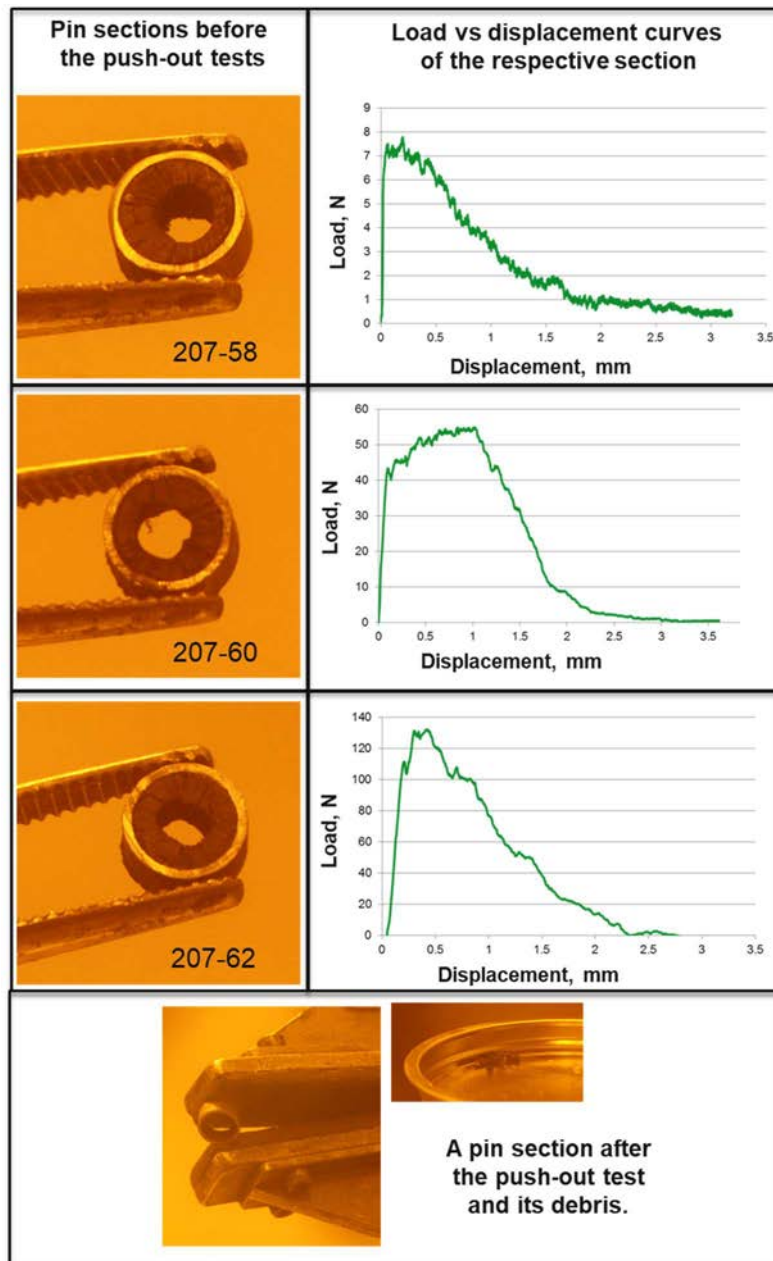


FIG.6. Photographs of some sections before push-out mechanical test completed with its respective load versus displacement curves. The inserts showed a section after the push-out test and its debris.

3.4. Surface investigation

Surface investigation using SEM showed no appearance of the scratch marks on some sections of TRABANT-2/3 fuel pin (Fig.7). This result could be correlated to a weak interaction between fuel and cladding as the force needed to push out the fuel was relatively low.

The visual investigation using SEM was additionally used to estimate the pellet-cladding contact. The estimation was performed on several SEM images and some scratches indicating some pellet-cladding contact was searched. The estimation of the pellet-cladding contact could be seen in Table 1. The estimation was further used to correct the shear stress calculation from the load versus displacement curves (Fig.6).

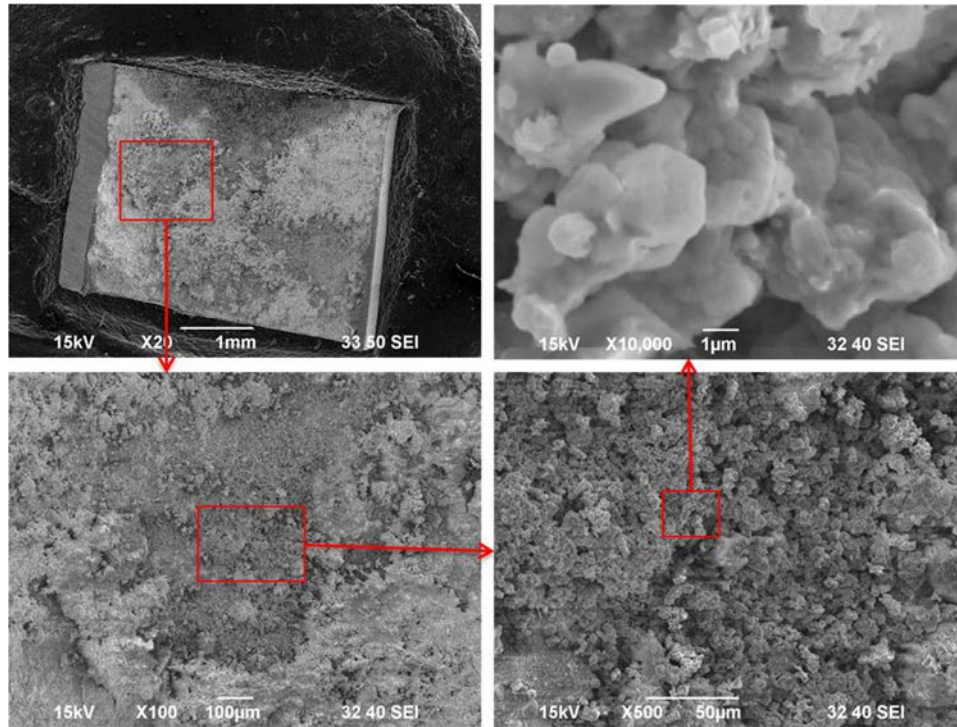


FIG. 7. Some SEM images of the surface of the specimens after the push-out test.

TABLE 1. SUMMARY OF THE PUSH-OUT MECHANICAL TEST OF THE TRABANT-2/3

Specimen-ID	Max. force (N)	Shear stress* (MPa)	Shear stress – SEM** (MPa)	BU (%FIMA)	T _{central} (°C)	LHR (W/cm)	Comment
207-56	14.5	0.26	—	1.87	~1500	411	No-interaction, only friction
207-58	7.8	0.14	0.56 (~25% contact)	1.87	~1500	411	No-interaction, only friction
207-60	55.0	1.00	—	1.87	~2750	413	Relative weak interaction
207-62	132.4	2.41	—	1.88	~2750	415	Strong interaction
207-64	69.7	1.23	1.64 (~75% contact)	1.95	~2750	431	Relative weak interaction
207-66	190.4	3.53	—	1.95	~2750	430	Strong interaction
207-68	11.6	0.21	—	1.95	~1750	430	No-interaction, only friction
207-70	15.4	0.28	1.11 (~25% contact)	1.75	~1750	382	No-interaction, only friction
207-72	17.1	0.30	—	1.73	~1750	379	No-interaction, only friction

*Assumption of 100% contact.

**SEM visual investigation.

4. DISCUSSION

During irradiation of the fuel pins, it is well known that there will be fuel thermal expansion depending on the characteristics of the fuel as well as the irradiation condition. Some relevant characteristics of the fuel are the chemical composition, porosity, fabrication, shape, dimension, the smoothness of the fuel, etc., while the irradiation conditions can be appointed as central hole temperature, linear heat rate, Burn-Up (BU), produced crack patterns, etc. Another important point is the cladding material, such as its properties (physically, chemically and mechanically), its fuel-cladding initial gap, etc.

The TRABANT-2/3 fuel pin contained annular MOX pellets. In general, oxide pellets will undergo restructuring during irradiation at temperatures $>1800^{\circ}\text{C}$. After only 3 cycles of irradiation of TRABANT-2/3 in the HFR, Petten, the Netherlands, it was found that the relocation of the central hole of the fuel pellets was visible. This restructuring occurred in an off-normal way which made it more difficult to assess. Due to its shape as an annular fuel, the densification or swelling had the opportunity to relax not only outwards towards the cladding, but also inwards toward the annulus (fuel free volume).

The complexity of the fuel characteristic after irradiation clearly affected the PCI. The initial fuel-cladding gap was 0.11 mm. As we have seen in the previous chapters, for some segments depending on the irradiation condition, the fuel-cladding gap enclosed and enlarged (up to ~ 0.3 mm) at the same time. This condition is an indication that PCI is a complex mechanism. However, as seen from the profilometry, the PCI did not result to a cladding expansion and failure of cladding tube.

Table 1 and Fig.8 give a summary of the push-out mechanical test for nine segments of the TRABANT-2/3 fuel pin with their respective irradiation condition after 3 cycles. The measured load needed to push the fuel pin out of the cladding varied from 7.8N up to 190.4N depending on the irradiation condition. The force could be correlated to the presence of pellet-cladding mechanical interaction. The high load, as seen in some sections, was due to a strong fuel-cladding interaction while the small load could be attributed to the presence of weak interaction or no- interaction at all (only friction).

Further investigation is needed to understand and correlate the irradiation condition to the closure and opening of the fuel-cladding gap and its influence on the fuel-cladding interaction. It is also important to investigate the fuel initial condition to be really able to see its influence on the closure and opening of the fuel-cladding gap.

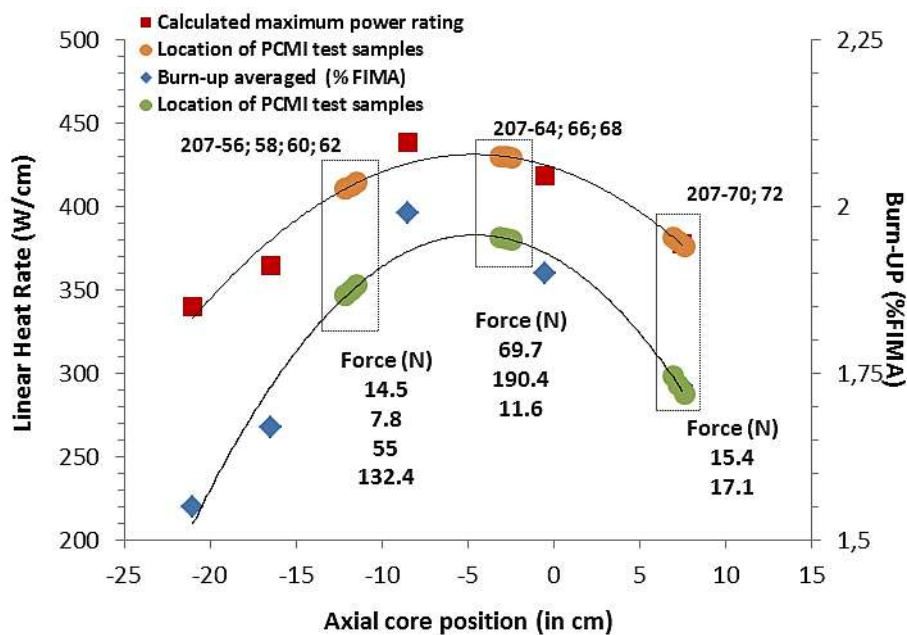


FIG. 8. Curves of the summary of the LHR, BU and force from the mechanical push-out tests along the axial core position for nine different investigated sections.

5. CONCLUSIONS

A new test setup for characterization of pellet-cladding interface properties was developed and installed at the NRG's hot cell laboratory. The test setup was used to investigate the sections taken from the TRABANT-2/3 fuel pin irradiated in High Flux Reactor in Petten.

Among the investigated sections, it was found that the load to push-out the TRABANT-2/3 was the highest for the section that was located close to the central core as it had a respective high temperature, BU and linear heat rate. The restructuring of the fuel pellet due to irradiation condition made it more difficult to assess the actual PCI as the closure and opening of the gap was not uniform in any of the sections.

More thorough investigation is needed to correlate the initial fuel condition, either chemically or mechanically, to the closure and opening of fuel-cladding gap during irradiation that further influences the fuel-cladding interaction. Furthermore, some modelling will be valuable to assess the whole irradiation process.

ACKNOWLEDGEMENT

This research is supported by the Dutch ministry of economic affairs (EZ). The fuel pin sections were obtained from work carried out earlier in projects, supported by the European Commission through the FP7 ESNII+ project and EZ. EU DuC= 0E001.⁴

REFERENCES

- [1] ROBERTS, G., The Concentration of Stress in Cladding Produced by the Expansion of Cracked Fuel Pellets, Nucl. Eng. Des. **47** (1978) 257 – 266.
- [2] MICHEL, B., SERCOMBE, J., THOUVENIN G., A New Phenomenological Criterion for Pellet–Cladding Interaction Rupture, Nucl. Eng. Des. **238** (2008) 1612 – 1628.

⁴ Goods labeled with an EU DuC (European Dual-use Codification) not equal to ‘N’ are subject to European and national export authorization when exported from the EU and may be subject to national export authorization when exported to another EU country as well. Even without an EU DuC, or with EU DuC ‘N’, authorization may be required due to the destination and purpose for which the goods are to be used. No rights may be derived from the specified EU DuC or absence of an EU DuC.

DAMAGE TO THE CLADDING OF THE FUEL ELEMENTS IN THE WATER-WATER POWER REACTOR UNDER PCI/ SCC

V.V. NOVIKOV

Stock Company "A.A. Bochvar High-technology Research Institute of Inorganic Materials" (SC "VNIINM"),

Russian Federation

Email: VVNovikov@bochvar.ru

The cracking mechanism was determined (based on laboratory studies) to explain the destruction of the cladding of fuel elements during a power ramp. The basis of the mechanism is the effect of iodine and tensile stresses on the zirconium cladding resulting from the interaction between the expanding fuel and the cladding. Iodine was realized as a result of exposure to cesium iodide [1-4].

Obviously, iodine must overcome the oxide film (ZrO_2) in order to interact with the cladding metal. The following possible mechanisms can be proposed for the implementation of this phase of SCC:

- Diffusion of iodine through zirconium oxide;
- Chemical interaction of fission products (including iodine and cesium iodide) with ZrO_2 [7];
- Mechanical cracking of zirconium oxide and diffusion of iodine along the formed cracks.

Studies conducted for iodine implanted in ZrO_2 have showed that iodine diffusion in ZrO_2 is limited below 1373 K, indicating a significantly lower mobility at operating temperatures (in other words, iodine cannot penetrate through ZrO_2 as a result of diffusion. [6])

Fission products released in the fuel-cladding gap may affect the degree of degradation of the oxide film.

Through the result of the BWR fuel rod claddings irradiated to a burnup of $\sim 8 \text{ MW}\cdot\text{d}/\text{kgU}$ study, it can be indirectly confirmed that the concentration of fission products influences the permeability. The cladding of fuel elements with low gaseous fission products output $\sim 0.2\%$ in comparison with the cladding of the fuel rod that had a yield 14.3% showed in tests for SCC (temperature 325°C and concentration $c = 0.6 \text{ m}^2/\text{cm}^2$) higher strength (280 MPa) compared with 200 MPa for the cladding of a fuel rod with a high yield efficiency [8].

If the formed compounds differ markedly in volume from the initial oxide, then the induced stresses can potentially lead to cracking of zirconium oxide or reduce the stresses necessary for the loss of its protective properties.

Based on the foregoing, it can be concluded that factors that can affect the degree of degradation of the oxide film during its interaction with cesium iodide are:

- Fission gas release rate level (and, consequently, aggressive fission products);
- Temperature (responsible for the reaction rate of ZrO_2 with CsI).

To some extent, increased fission gas release at power ramp shall also affect the state of the oxide film - of course; the effect of tensile stresses cannot be excluded. The results of reactor experiments on power ramp conducted on high burned WWER fuel rods have showed in subsequent metallurgical studies the presence of a 'chemical' damage to the cladding in places coinciding with radial cracks in the fuel pellets (Fig. 1).

The data obtained shows that because of internal fuel processes, chemical interaction of fission products and the cladding inner surface is possible. However, the "chemical" development of cladding destruction under the conditions of the PCI/SCC did not occur in the future.

Mechanical cracking of an oxide film, as a necessary stage in achieving iodine metal cladding.

Experiments on the corrosion cracking of unirradiated fuel claddings showed that iodine penetrated the metal after the destruction of ZrO_2 along the grain boundaries of the metal as a result of the implementation of grain boundary shear deformation [12]. Irradiation of claddings without fuel (in particular, up to a fluency of $\sim 10^{22} \text{ n}/\text{cm}^2$) and further tests for long term strength showed an increase in stresses and time for the implementation of the SCC process (Fig.2).

In any case (for irradiated without fuel and an unirradiated cladding), a local rupture of the oxide film was required to start iodine cracking, which occurred when some microplastic shear deformation along the grain boundaries of the zirconium alloy was achieved [5,7,12,14].

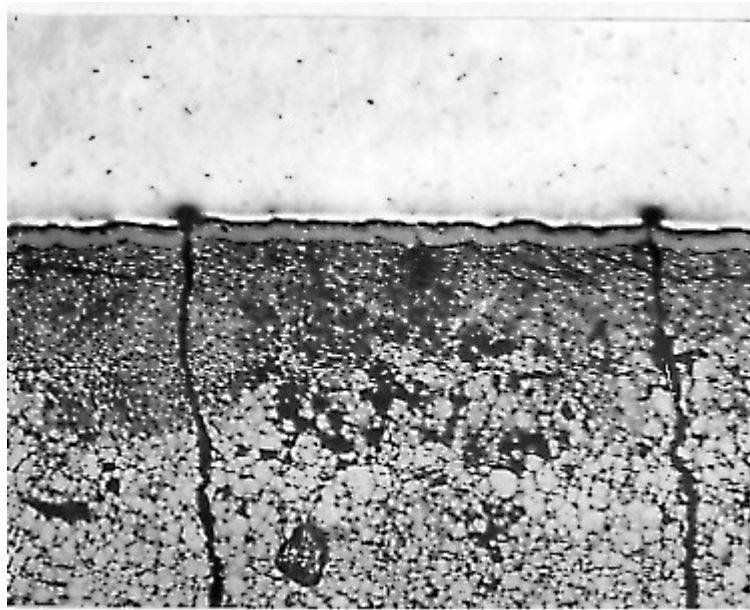


FIG. 1. State of the inner surface of the cladding in the cross section of a fuel rod after a power ramps of 190 W/cm - 430 W/cm in ~ 12 minutes, burnup 60 MW·d/kgU.

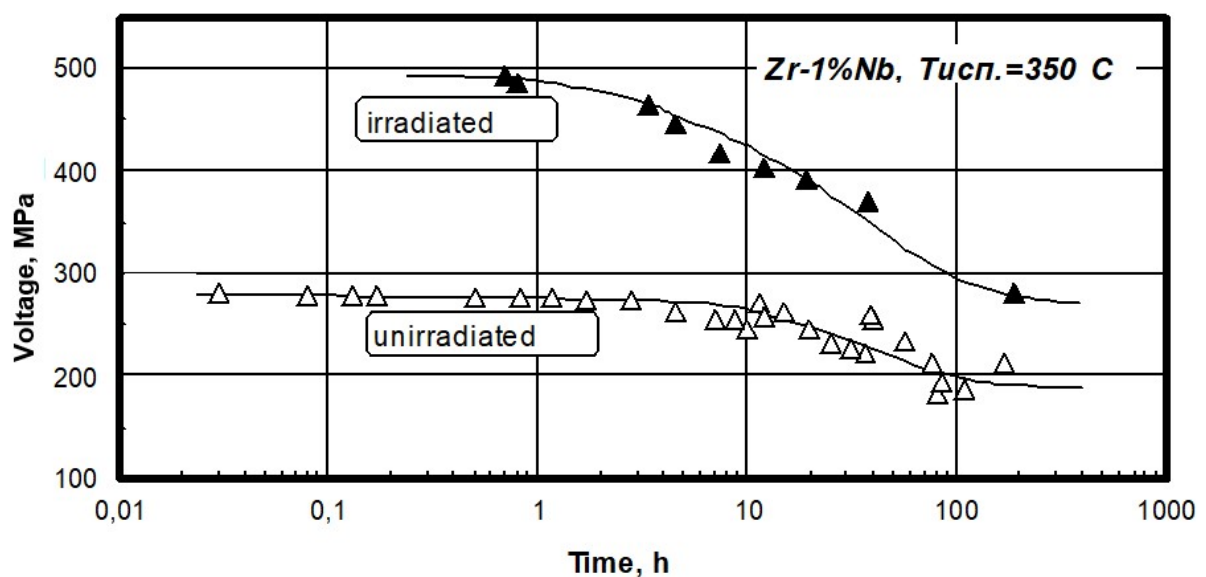


FIG. 2. Long term strength of E-110 alloy claddings based on tests up to 200 hours. Fluence $0.9 \times 10^{22} \text{ n/cm}^2$.

These results also show that cladding irradiation in a research reactor does not affect the mechanism of fracture onset formation: the deformation of the metal and, accordingly, of the oxide film reaches a certain critical value, after which rupture of zirconium oxide and the penetration of iodine to the metal occur [15–17]. Stresses for the SCC process of the irradiated cladding increase.

The different picture takes place when testing the claddings of fuel rods irradiated as part of fuel assemblies in power reactors. Tests have shown that for the cladding of a fuel rods (previously the fuel was removed from the fuel rod in a hot cell), it takes significantly less time to fracture than for a cladding irradiated in a research reactor that has received the same. Moreover, failure occurs at lower voltages compared to even unirradiated claddings. This was shown in our experiments on WWER fuel rods with Zr-1% Nb alloy claddings, as well as in experiments

with BWR fuel rods (Zry-2 claddings) and with PWR fuel (Zry-4 claddings). [8, 14, 15, 17]. In fact, it should be recognized that the study of SCC on the claddings of non-irradiated or irradiated in a research reactor does not allow simulating the initial stage of the SCC of the cladding irradiated in the fuel element, and therefore, the entire SCC process.

What is the difference between the claddings irradiated in a research reactor and the claddings of irradiated fuel elements? First of all, in the state of oxide on the inner surface. The difference between oxide films formed on the cladding inner surface from irradiations in a research reactor and irradiations in an energy reactor as a part of fuel rods is as follows:

- The inner surfaces of the cladding of the fuel rods are affected not only by neutron and γ -radiation, but also by the action of fission products, as high energy particles;
- The excess oxygen released from UO_2 diffuses to the cladding inner surface and oxidizes it (for the claddings irradiated without fuel, this process is absent).

Figure 3 shows the thickness of the corrosion layer in terms of burnup. As a rule, the thickness of the layer is uneven along the perimeter of the cladding. The minimum thickness is ~ 2 microns. With increasing burnup, the layer thickness slowly increases (Fig. 3) and reaches $12 \mu\text{m}$ [10, 11]. In addition, as a result of fuel swelling, growth of ZrO_2 on the inner surface, as well as creep of the casing under the coolant pressure, the fuel-cladding gap decreases, and a $(\text{U,Zr})\text{O}_2$ interaction layer forms with high burnup.

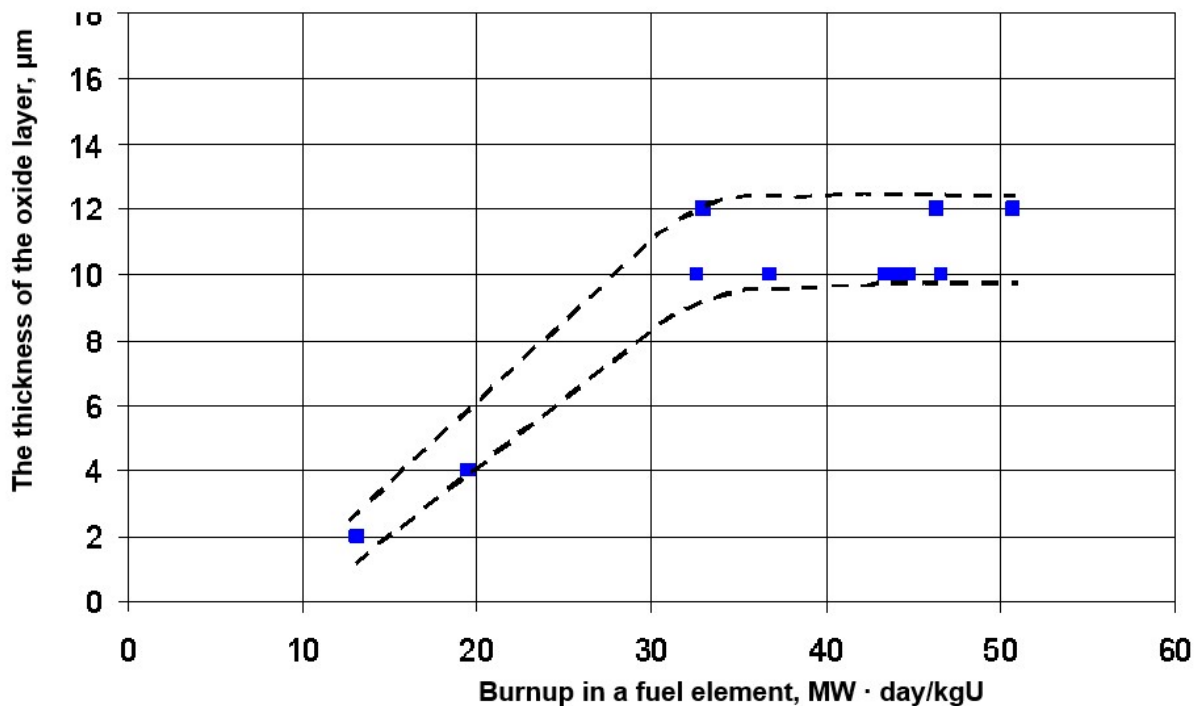


FIG. 3. Dependence of the maximum thickness of the oxide layer on the cladding inner surface on fuel burnup.

A feature of the formation of an oxide film on the cladding inner surface is the effect of fission products on it.

The oxide structure varies depending on the film thickness, passing from tetragonal to monoclinic. These transformations, when exposed to irradiation, lead to porosity of the film and the appearance of cracks in columnar ZrO_2 grains [16].

Therefore, micro cracks in ZrO_2 can arise during the operation of fuel rods. Mechanical loading of the cladding as a result of expansion of the fuel with such an oxide layer can cause additional advancement of cracks to the zirconium-metal barrier and overcome it. Tests were carried out with claddings made of Zr-1% Nb alloy to assess the effect of the oxide layer thickness on the inner surface of the cladding of a fuel rod.

Tests of Zr-1% Nb alloy claddings with various oxide layer thicknesses.

Researches were performed on tubular samples of Zr-1% Nb alloy loaded with internal pressure. On the inner surface, the samples had a pre-created ZrO₂ film with a thickness of 0.5, 1.0, 2.0; 5.0, 10.0 μm.

The sequence of sample preparation was as follows:

- Pipes 150 mm long with the outer diameter of 9.15 mm and a wall thickness of 0.7 mm cut from the unirradiated cladding of WWER-1000 fuel rod were oxidized in air in a resistance furnace at a temperature of 773 K;
- The oxidized claddings were machined from the outside in the middle part at a length of 40 mm to create a section of increased stress. The average cladding thickness after thinning was 350±15 μm;
- After preliminary vacuum drying, the samples were filled with inert gas (argon) and iodine in an amount of 0.2 mg/cm². Sealing of the samples was carried out by contact spot welding. The argon pressure under the cladding at room temperature was 6.5 MPa and was controlled by a manometer, as well as by weighing the samples before and after filling;
- The oxidation temperature of 773 K was chosen based on the exposure time of the samples necessary to obtain a maximum oxide layer thickness of 10 μm. Some of the images were oxidized at a temperature of 673 K. The difference in oxidation temperatures did not affect the test results of claddings on SCC.

In appearance, the oxide layer can be divided into types:

- Black, tight-fitting film with a thickness of up to 2 - 2.5 μm;
- A grey, friable film with a thickness > 2 to 10 μm;
- A spotty film with a thickness exceeding 10 μm, with bright spots of 1-3 μm in size against a grey oxide background.

Tests of samples with the internal oxide layer for long term strength were carried out at a temperature of 653 K. The iodine concentration was 0.2 mg/cm²; control samples without iodine were also used. The tangential tensile stresses were 165 MPa, i.e. they were close to the conditional yield strength $\sigma_{0.2}$ of Zr-1% Nb alloy claddings at the test temperature.

The experimental results are presented in Figure 4. The claddings in the delivery state, which did not have the oxide film on the inner surface and tested at an iodine concentration of 0.2 mg/cm², had an average time to failure of t_f of 29 hours. The oxide layer 0.5 μm thick increases the average fracture time under conditions of iodine corrosion up to 56 hours. Smooth decrease in the durability of the claddings was observed from 13 to 4-5 hours with a further increase in the thickness of the ZrO₂ layer from 1 to 10 μm. For samples without iodine, the character of the dependence of durability on the thickness of the ZrO₂ layer was approximately the same. The time to destruction of samples with iodine was on average 3-4 times less than the time of destruction of samples without iodine, both for claddings with the initial state of the inner surface and for oxidized claddings with a ZrO₂ layer thickness of 10 μm.

Previous studies of unoxidized claddings has showed that under conditions of cladding loading by internal pressure, the crack initiation time is up to 90% of the total fracture time. Obviously, the formation of the oxide film makes significant changes to the first stage of iodine corrosion. These changes include:

- Cracking of oxide films and the associated increasing permeability to iodine of oxide films;
- The presence of tensile stresses in the cladding as a result of oxide growth.

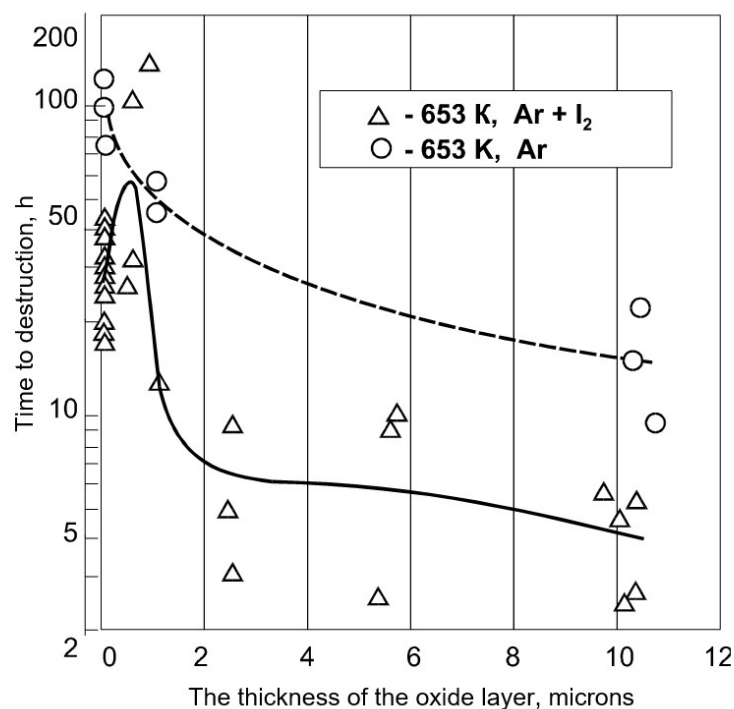


FIG. 4. Effect of ZrO_2 layer thickness on the inner surface claddings for their long term strength in the presence of iodine and in an inert environment.

1. CONCLUSIONS

For the beginning of the PCI-SCC, it is necessary to overcome the barrier - zirconium dioxide on the inner surface of the cladding.

The process of SCC begins with the cracking of the oxide layer as an integral result of structural changes in zirconium oxide during its growth during burning and the action of high energy particles of fission products and stresses. The loss of the protective properties of the oxide layer on the cladding inner surface is the main factor in the implementation of the stress corrosion mechanism, leading to a drop in SCC threshold stresses with an increase in fuel burnup.

REFERENCES

- [1] CUBICCIOTTI, D., DAVIES, J., The Release of Iodine from Iodine Salts by Gamma Radiolysis, Nuclear Science and Engineering **60** (1976) 314-319.
- [2] KONASHI, K., YATO, T., KONEKO, H., Radiation Effect on Partial Pressure of Fission Product Iodine, Journal of Nuclear Materials **116** (1983) 86-93.
- [3] BIBILASHVILI, Yu. K., VLADIMIROVA, M.V., GOLOVNI, I.S., KULIKOV, I.A., NOVIKOV, V.V., SOTNIKOV, A.S., "Studies of Radiation-Thermal Decomposition of Caesium Iodide and Stress Corrosion Cracking of VVER Fuel Clads on Gamma-Irradiation", Technical Committee on Fuel Rod Internal Chemistry and Fission Products Behaviour, Karlsruhe, 11-15 November 1985, IWGFPT / 25, IAEA, Vienna (1986) pp.167-172.
- [4] BALL, R.G.J, BURNS, W.G., HENSHAW, J., MIGNANELLI, M.A., POTTER, P.E., The Chemical Constitution of the Fuel-Clad Gap in Oxide Fuel Pins for Nuclear Reactors, Journal of Nuclear Materials **167** (1989) 191-204.
- [5] NOVIKOV, V.V., SOKURSKYI, Yu.N., BIBILASHVILI, Yu.K., VLADIMIROVA M.V., SOTNIKOV A.S., BOBKOV Yu.V., KULIKOV I. A., "Study of Crack Initiation and Propagation Mechanism on SCC of Zr-1% Nb VVER fuels", Proceedings of Int. Conf. on Radiation Materials Science, Alushta, USSR, 22-25 May 1990, pp. 158-164.
- [6] FREGONESE, M., LEFEBVRE, F., LEMAIGNAN, C., MAGNIN, T., Influence of Recoil-Implanted and Thermally Released Iodine on I-SCC of Zircaloy-4 in PCI-Conditions: Chemical Aspects, Journal of Nuclear Materials **265** (1999) 245-254.

- [7] CHEN, T.M., KAUZLARICH, S.M., CORBETT, I.D. Reactions and Products in the Cs-Zr-IO System Relevant to Fission Product Chemistry - A Review, *Journal of Nuclear Materials* **151** (1988) 225-237.
- [8] MATTAS, R.F., YAGGEE, F.L., NEIMARK, L.A., "Effect of Zirconium Oxide on the Stress-Corrosion Susceptibility of Irradiated Zircaloy Cladding", *Proceedings of the Fifth International Conference on Zirconium in Nuclear Industry*, Boston, USA, 4 - 7 August 1980, ASTM-STP **754** (1980) P.158.
- [9] LUNDE, L., OLSHAUSEN, K.D., "Stress Corrosion Testing of Irradiated Cladding Tubes", *Specialists Meeting on Power Ramping And Power Cycling of Water Reactor Fuel and Its Significance To Fuel Behaviour*, Arles, France, May 14-18, 1979, IWGFPT/5, IAEA, Vienna (1980) pp. 83-90.
- [10] SMIRNOV, A., KANASHOV, B., KUZMIN, V., MARKOV, D., POLENOK, V., SMIRNOV, V., TZYKANOV, V., PANJUSHKIN, A., BEK, E., ROZHKOVA, V., YENIN, A., BIBILASHVILI, YU., MEDVEDEV, A., "Results of Post-Irradiation Examinations to Validate WWER-440 and WWER-1000 Fuel Efficiency at High Burnups", *Fourth International Conference on WWER Fuel Performance, Modelling and Experimental Support*, Albena-Varna, Bulgaria, October 1-5, 2001.
- [11] BIBILASHVILI, YU.K., MEDVEDEV, A.V., NOVIKOV, V.V., TSYKANOV, V.A., GOLOVANOV, V.N., SMIRNOV, V.P., OVCHINNIKOV, V.A., "Studies into WWER Fuel Rod Behaviour at High Burnup in Power Ramps", *OECD Halden Reactor Project*, Lillehammer, Norway, 1998, Report HRP-349/44.
- [12] FREGONESE, M., REGNARD, C., ROUILLON, L., MAGNIN, T., LEFEBVRE, F., LEMAIGNAN, C., "Failure Mechanisms of Irradiated Zr Alloys Related to PCI: Activated Slip Systems, Localized Strains, and Iodine-Induced Stress Corrosion Cracking", *Twelfth International Symposium Zirconium in Nuclear Industry*, Toronto, Canada, June 15 - 18, 1998, ASTM-STP **1354** (1998) P.377.
- [13] SCHUSTER, I., LEMAIGNAN, C., JOSEPH, J., Testing and Modelling the Influence of Irradiation on Iodine-Induced Stress Corrosion Cracking of Zircaloy-4, *Nuclear Engineering and Design* **156** (1995) 343-349.
- [14] VIDEM, K., LUNDE, L., HOLLOWELL, T., VILPPONEN, K., VITANZA, C. Cracking of Cladding Tubes Caused by Power Ramping and by Laboratory Stress Corrosion Experiments, *Journal of Nuclear Materials* **87** (1979) 259-267.
- [15] MILLER, A.K., OCKEN, H., TASOOJI, A., Iodine Stress Corrosion Cracking of Zircaloy: Laboratory Data, A Phenomenological Model, and Predictions of In-Reactor Behaviour, *Journal of Nuclear Materials* **99** (1981) 254-268.
- [16] BOSSIS, P., THOMAZET, J., LEFEBVRE, F., "Study of the Mechanisms Controlling the Oxide Growth Under Irradiation: Characterization of Irradiated Zircaloy-4 and Zr-1Nb-O Oxide Scales", *Thirteenth International Symposium Zirconium in Nuclear Industry*, Annecy, France, June 10 - 14, 2001, ASTM-STP **1423** (2001) 190-221.
- [17] FANDEUR, O., ROUILLON, L., PILVIN, P., JACQUES, P., REBEYROLLE, V., "Modelling of Stress Corrosion Cracking in Zirconium Alloys", *IAEA TCM*, Windermere (UK), 19-23 June 2000.
- [18] BIBILASHVILI, YU. K., DOLGOV, YU. N., NOVIKOV, V.V., GLAZKOV, A.G., Crack Initiation in Zr-1% Nb Alloy Shells under Stress Corrosion Cracking, *Atomic Energy* **80** (1996) 258-263.

IMPROVING PCI/SCC MODELLING AND SIMULATION
(Session III)

Chairperson

T. FORGERON
France

3D MODELING OF PCI-SCC IN ALCYONE FUEL PERFORMANCE CODE

J. SERCOMBE, P. KONARSKI, C. RIGLET-MARTIAL, J. JULIEN, C. INTROÏNI
CEA, Cadarache, France,
Email: jerome.sercombe@cea.fr

D. LE BOULCH
CEA, Saclay, France

Abstract

The paper presents the latest developments in ALCYONE fuel performance code concerning the modelling of pellet-cladding interaction (PCI) and clad failure caused by iodine-induced stress corrosion cracking (I-SCC). ALCYONE includes a 3D finite element model to describe the thermo-mechanical behaviour of a fuel pellet fragment and its frictional contact with the surrounding cladding. ALCYONE provides a precise evaluation of the temperature and stress state across the clad wall during power transients that can lead to clad failure by I-SCC. The application of an I-SCC crack propagation model in the 3D simulations of PCI with ALCYONE is of primary interest in the paper. A series of power ramps performed in the OSIRIS materials test reactor are analyzed. The calculated times to failure by PCI induced I-SCC are compared to in-reactor measurements, which shows a good agreement each other. Advanced simulations of non-failed rods during power ramps are then proposed to analyze the potential reasons for the clad resistance to I-SCC in relation to the build-up of a suitable chemical environment at the clad inner wall. The simulations include thermodynamic equilibrium calculations of the uranium dioxide matrix with the fission products (FP) of interest for I-SCC (I, Cs, Te) that are coupled to the fission gas release model (MARGARET) of ALCYONE. They illustrate the importance of a correct assessment of the chemical conditions at the triple point with respect to I-SCC crack propagation modelling.

1. INTRODUCTION

ALCYONE is a multi-dimensional fuel performance code jointly developed by the CEA, EDF and FRAMATOME within the PLEIADES computational environment [1]. ALCYONE includes a 3D model of pellet-clad interaction (PCI) that is dedicated to the evaluation of the stresses across the clad wall during power ramps [2]. In the last years, the 3D PCI model of ALCYONE has been improved by the consideration of irradiated fuel thermochemistry in order to provide some estimation of FP release during power transients [3,4]. In consequence, the chemical aspects of iodine-induced stress corrosion cracking (I-SCC), i.e. iodine chemical form and quantity at the clad inner surface, can now be analyzed.

With a sufficient quantity of iodine, clad failure by I-SCC is known to be primarily controlled by the stress level and the temperature. I-SCC models that describe the crack propagation mechanisms in relation to the thermo-mechanical fields have been formulated based on laboratory experiments [5,6]. In this paper that an I-SCC crack propagation model in the 3D simulations of PCI with ALCYONE is applied. After a brief presentation of ALCYONE 3D model and of the I-SCC crack propagation model, simulations of power ramps performed in the OSIRIS reactor that have led to clad failure are detailed. The calculated I-SCC crack depths and times to failure are compared to available experimental data.

2. ALCYONE 3D MODEL

ALCYONE is able to perform simulations of the fuel rod behaviour in the operational states and accidental conditions [7]. The fuel performance code ALCYONE includes a number of modules that can be used independently or called at each node of the mesh. A typical coupled calculation requires the following successive steps, which are run iteratively until convergence of the four main fields (temperature, displacements, stresses and fission gas-induced swelling strains) is achieved:

- A neutronics calculation to estimate the power deposition at each node of the finite element (FE) mesh,
- A thermo-mechanical calculation of the fuel-gap-clad system to estimate the temperature, displacements and stresses at each node of the FE mesh,
- A fission gas calculation, which concerns only the bulk of fission gases in the fuel pellet, i.e. the fission products or noble gases Xe and Kr (chemically inert), and gives estimates of fission gas release (FGR) and fission gas swelling at each node of the FE mesh,

- A thermochemical calculation to estimate the chemical speciation of FPs other than noble gases and their release at each node of the mesh. Iodine, cesium and tellurium are of particular interest for I-SCC.

The thermo-mechanical calculation is rather standard for fuel performance codes and has already been detailed elsewhere [8]. In brief, ALCYONE relies on the finite element code Cast3M [9] for the thermo-mechanical calculations. Many non-linearities, either related to material behaviour (e.g. fuel and clad creep, clad plasticity, fuel smeared cracking) or structural behaviour (e.g. pellet-clad unilateral contact with friction, axial locking of the pellet and the cladding) are taken into account. The 3D scheme of ALCYONE is specific for PCI analyses since it can model local stresses and strains at the triple point [10] (in front of a pellet radial crack and of a pellet end, on the clad inner wall, see Figure 1) where PCI failures in PWRs typically occur during class 2 power transients [11].

To date, PCI failure/non-failure assessment in 3D simulations of power ramped fuel rods relies on the calculations of the average hoop and shear stresses at the clad inner surface [12]. The shear stress criterion was introduced to better classify fuel pellets with marked differences in radial cracking during power transients. This paper is intended to present the recent developments in ALCYONE where PCI failure propensity is assessed from crack propagation modelling based on I-SCC laboratory tests.

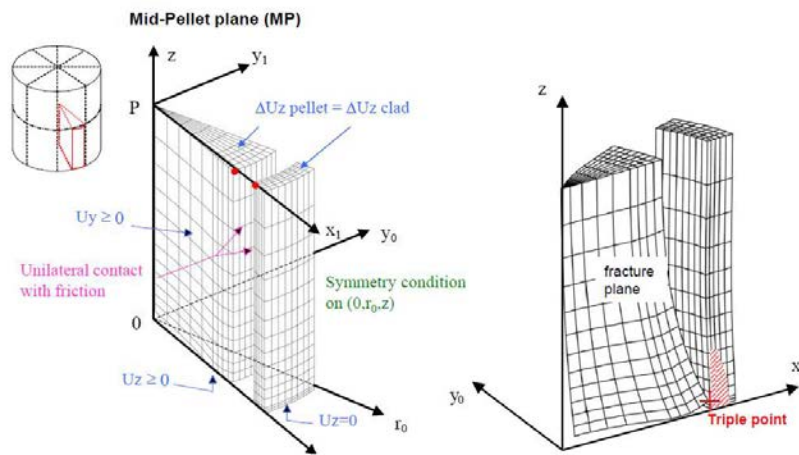


FIG. 1. Mesh and boundary conditions in the 3D scheme of ALCYONE. A fuel pellet is divided in 8 identical fragments in order to account for the crack network that forms during nominal irradiation. Position of the triple point where I-SCC failure occurs.

3. I-SCC CRACK PROPAGATION MODEL

I-SCC mechanisms have been extensively studied at CEA [5, 6]. A series of internal pressurization tests were performed to characterize and model different stages of I-SCC: 1) crack initiation phase, 2) incubation phase (also called subcritical propagation phase or intergranular phase), 3) crack propagation phase (also called critical propagation phase or transgranular phase). The authors have studied both irradiated and non-irradiated stress-relieved (SR) zircaloy-4 cladding (raw) samples to investigate the impact of irradiation on I-SCC susceptibility. The pressurization tests have been performed in inert and iodine environments. The iodine concentration in the tests was around 1.5 mg/cm² of clad internal surface. The temperatures in the experiments were 350°C, 420°C and 480°C but most of the tests on irradiated materials were made at 350°C. The internal pressure was changed in the tests to investigate the impact of the applied stress on the time to failure. Internal pressurization tests have also been performed on non-irradiated pre-cracked samples. Pre-cracks of the clad inner surface were generated by means of corrosion-fatigue in an iodine-methanol solution at room temperature [13]. Crack propagation rates have been estimated from these experiments. Experimental results suggested that a stress intensity factor threshold for intragranular crack propagation may exist K_I^{I-SCC} . According to these experiments, the crack propagation rate and K_I^{I-SCC} are independent of temperature. These test results have been used to model the three phases of I-SCC [5]. The crack propagation phase can be expressed as follows:

$$\dot{a} = C (1 + D(K_I - K_I^{I-SCC})) \quad (1)$$

where a is the crack depth, K_I is the stress intensity factor, and C and D are constant parameters. The K_I factor is given by the relation:

$$K_I = \alpha \sigma_{\theta\theta} \sqrt{\pi \alpha} \quad (2)$$

where α is the crack shape coefficient and K_I is the applied hoop stress. For unirradiated zircaloy-4, the following parameters have been identified from the tests on pre-cracked samples ($K_I^{I-SCC} = 4.2 \text{ MPa}\cdot\text{m}^{1/2}$, $C = 10^{-10} \text{ m/s}$ and $D = 5500 \text{ MPa}^{-1}\cdot\text{m}^{-1/2}$). The same parameters are used to model I-SCC propagation in irradiated cladding.

The incubation phase takes place between the crack initiation and crack propagation phases. It is considered the most important phase in I-SCC, even if the crack depth due to this phase does not exceed 10 to 30 μm . It is a slow process that gives its overall kinetics to I-SCC failure during pressurized tube tests at 350°C. This phase ends when the threshold stress intensity factor K_I^{I-SCC} is reached. The duration of the incubation phase t_{sub} is estimated as follows:

$$t_{sub} = t_f - t_z - t_{propa} \quad (3)$$

where t_f is the time to failure measured in the pressurization tests with raw samples, t_z is the time needed to break the internal zirconia layer, and t_{propa} is the duration of the crack propagation phase. Based on the tests performed with unirradiated samples, the incubation phase appears to be dependent on temperature and has been described mathematically as follows:

$$t_{sub} = A e^{\frac{Q}{RT}} \sigma^B \quad (4)$$

where A, B and Q are constant coefficients. Also, the threshold stress intensity factor K_I^{I-SCC} defines the critical crack depth a_{SCC} where the incubation phase ends:

$$\alpha_{SCC} = \frac{1}{\pi} \left(\frac{K_I^{I-SCC}}{\alpha \sigma} \right)^2 \quad (5)$$

By assuming that the crack propagation rate during the incubation phase is equal to the mean crack growth rate, the following relation can be written:

$$\dot{\alpha} = \frac{\alpha_{SCC}}{t_{sub}} \quad (6)$$

The experimental data obtained on raw and pre-cracked samples have been used to fit the parameters for irradiated Zy-4 materials: $\alpha = 1, Q = 20240 \text{ K}, A = 97.6 \text{ s}\cdot\text{MPa}^{-B}, B = -1.5$. Recently, Jezequel et al. studied the I-SCC susceptibility of non-irradiated SR Zy4 with internal pressurization tests performed at temperatures ranging from 350°C to 380°C [14]. The recorded times to failure and temperature dependency are qualitatively and quantitatively consistent with those given by the I-SCC model of this paper. In particular, the results exhibited a hoop stress threshold for I-SCC crack propagation that is independent of temperature, consistent with the constant stress intensity factor threshold K_I^{I-SCC} in equation (5).

In the crack propagation model given by equations (1) – (6), it is assumed that concentration of iodine is always high for I-SCC to proceed. In irradiated samples, two additional conditions are necessary for I-SCC crack initiation: 1) the existence of incipient cracks in the protective zirconia layer and 2) a minimum tensile hoop stress. The first condition is usually met when the cladding hoop strain is high enough to break the zirconia layer. To find the critical strain value, the internal pressurization tests have been simulated with the finite element code Cast3M [5]. The authors concluded that for irradiated samples, the critical hoop strain is very low and can be neglected. From the pressurized tube tests results on irradiated samples, a minimum tensile hoop stress of around 150 MPa was found necessary to initiate I-SCC. On non-irradiated samples, the stress threshold appears to be closer to 300 MPa [14, 15].

Validation of the model against the experimental measurements on irradiated Zy-4 samples is shown in Figure 2. The comparison shows that the model predicts the time to failure dependency on the stress level properly. At 350°C, it can be seen that the duration of the propagation phase (difference between the dotted and solid blue lines) is negligible compared to that of the incubation phase.

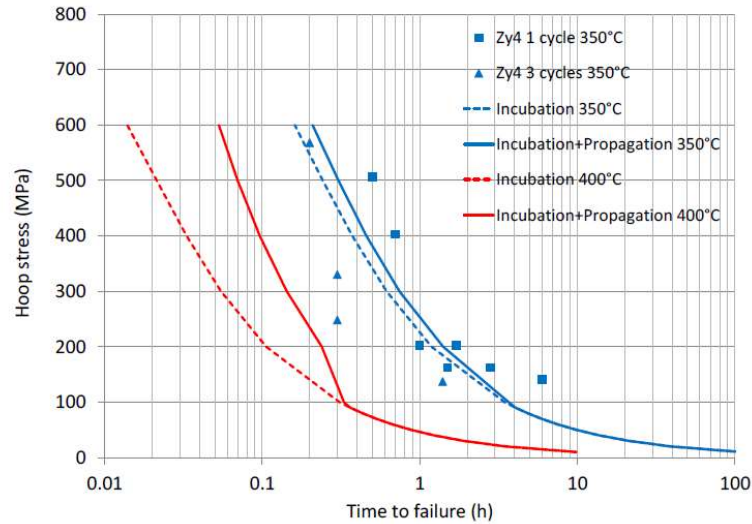


FIG. 2. Time to failure in I-SCC pressurized tube tests performed on irradiated Zy-4 cladding samples as a function of the applied hoop stress. Experimental results (symbols) and models (lines).

4. SIMULATION OF FUEL ROD FAILURE BY PCI-SCC

To test the I-SCC model, 12 power ramps from the OSIRIS material test reactor (MTR) have been selected and simulated with ALCYONE 3D model. All the selected fuel rods have a burnup within the critical range for PCI failure (20 – 45 GWd/tU). They are clad with Zy-4 or M5. The experimental protocol was identical in all the power ramps with a conditioning plateau at a nominal linear heat rate (LHR) within 150 – 250 W/cm followed by an LHR increase of 100 W/cm/min till the ramp terminal level (RTL), the latter maintained during 12h or till failure detection. When failure occurred (during 6 of the 12 power ramps), the time to failure has been estimated from the FP release in the pressurized loop of the device used for ramp testing in the OSIRIS reactor [11]. The recorded times to failure are plotted in Figure 3 in function of the power increase during the ramp test. Figure 3 shows some interesting features. First, all the times to failure recorded are within 1 to 10 minutes, notably smaller than those measured in I-SCC laboratory tests at 350°C, see Figure 2. Second, irrespective of the cladding, the time to failure decreases with power increase till 250 W/cm and are then independent of the power increase. Third, there is a marked difference between Zy-4 and M5, equivalent times to failure being obtained at higher power increase with M5.

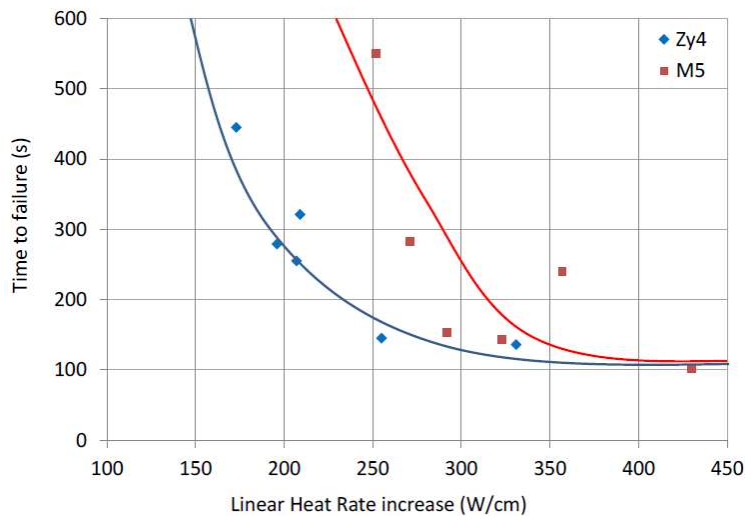


FIG. 3. Time to failure during power ramps in the OSIRIS reactor ($t=0$ when the LHR equals 400 W/cm) as a function of the LHR increase.

The simulation of crack propagation due to I-SCC in the cladding during ALCYONE 3D simulations was implemented as follows:

- ALCYONE 3D simulations provide the clad hoop stress and temperature evolutions at the triple point;
- These quantities are used in equations (1)–(6) to estimate the crack depth evolution in the cladding thickness during the incubation and crack propagation phases, when the calculated crack depth reaches 50% of the clad thickness, instantaneous ductile shear failure is assumed to take place [16];
- The crack propagation is not explicitly simulated, meaning that there is no impact on the 3D simulation. This assumption is reasonable for the incubation phase where the crack depth is negligibly small compared to the clad wall thickness but questionable for the crack propagation phase.

Initiation of I-SCC is related to plastic strains (instantaneous) that develop in the cladding inner surface in consequence of PCI. Laboratory I-SCC experiments on unirradiated Zy-4 samples have shown that a minimum stress level (between 150 and 300 MPa [14]) consistent with the onset of plasticity is necessary to initiate SCC. The underlying mechanism is a weakening of clad grain boundaries that ease the diffusion of iodine in consequence of the locally excessive deformations [16]. Considering a plastic strain threshold is furthermore consistent with the I-SCC sensitivity on strain rate (no failure when LHR increase is slow [17]).

The calculated distributions of hoop stresses and equivalent plastic strains on the Zy-4 clad inner surface of a rodlet that failed in a few minutes after reaching RTL are presented in Figure 4.

A remarkable characteristic that is caught by the 3D model is the development of high stresses and strains at the triple point, consistent with the position of I-SCC through-wall cracks. The stress and strain localizations occur furthermore early, even before RTL is reached, meaning that the onset of I-SCC is possible during the power increase phase of the ramp. Let us emphasize that the clad material model in ALCYONE 3D combines anisotropic plasticity and viscoplasticity, the latter to reproduce the time-dependent strains that are generated at high temperatures and stresses. The clad model parameters have been determined from an extensive database of pressurized tube tests, axial tensile tests and hoop tensile tests performed on irradiated cladding specimens in temperature and stress conditions representative of those expected during power ramps [18].

The calculated evolutions of the hoop stress, equivalent plastic strain and temperature at the triple point during six power ramps on UO₂-Zy-4 rodlets are plotted in Figure 5, together with the resulting I-SCC crack depths.

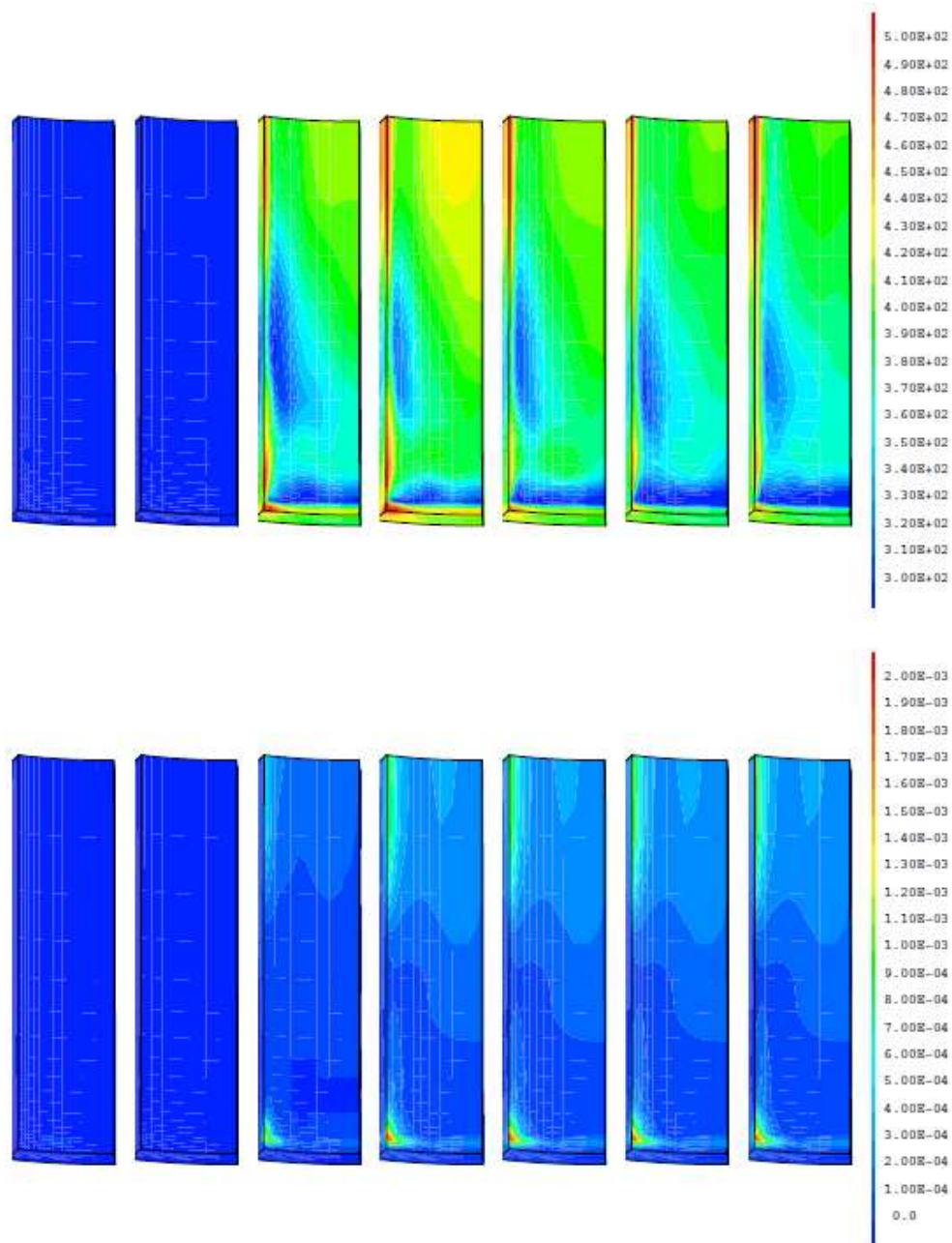


FIG. 4. Spatial distribution of the hoop stress (top, in MPa) and of the equivalent plastic strain (bottom) on the clad inner wall, from ALCYONE 3D simulations. From left to right are given the stress/strain distributions at -100 s, -50 s, -10 s, 0 s, +10 s, +50 s and +100 s (0 s is the time at which RTL is reached).

The large differences in RTL and LHR increase during the power ramps explain the obtained differences in crack depth evolution. The resulting times to failure are plotted in Figure 6 in function of the LHR increase. The main features of Figure 3 are recovered in the 3D simulations. A decrease of the failure time with power increase is obtained till 200-250 W/cm followed by a stabilization of the time to failure around 2 minutes. 3D simulations indicate that this stabilization is due to fuel and clad creep which level the stresses at 400-500 MPa once RTL is reached. It must be emphasized that the strong localization at the triple point in consequence of the pellet-clad contact discontinuity in both the circumferential and axial directions remains after RTL is reached. The stress relaxation is thus limited in magnitude.

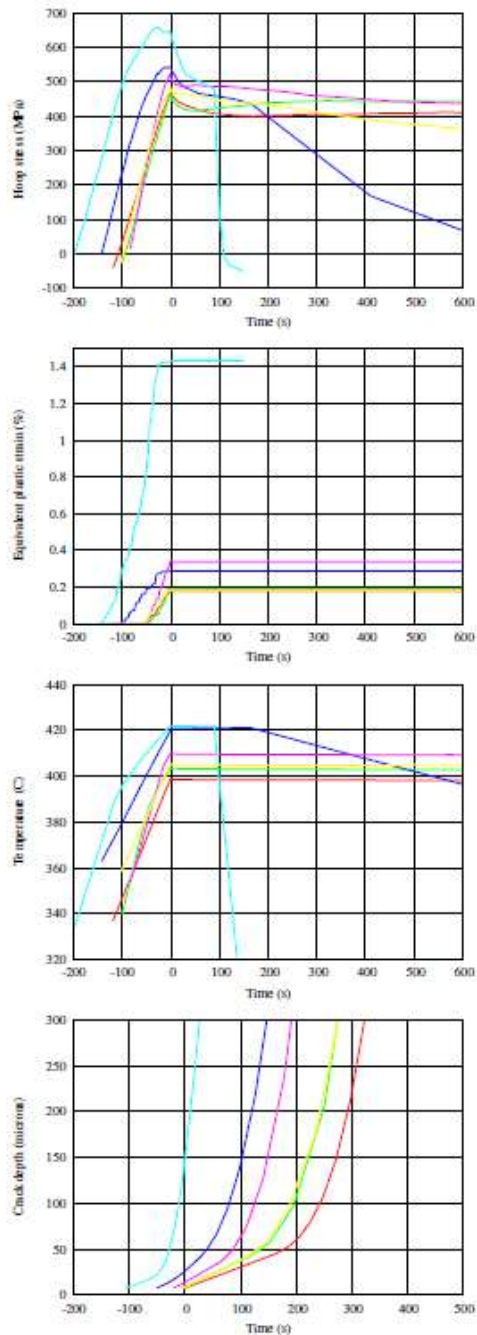


FIG. 5. Evolution of the hoop stress, of the equivalent plastic strain, of the temperature at the triple point and of the resulting I-SCC crack depth, from ALCYONE 3D simulations (0 s is the time at which RTL is reached).

Figure 6 also presents the durations of the incubation phase that are notably smaller than those of the crack propagation phase. This surprising result is a consequence of the higher temperatures experienced by the clad inner wall (generally over 400_C) compared to the 350_C considered in the I-SCC laboratory tests. Figure 2 presents an extrapolation of the I-SCC models to a temperature of 400_C (red lines), confirming that the times to failure at high stresses (400-500 MPa) in pressurized tube tests performed at this temperature are expected to be less than 10 minutes and mostly due to the propagation phase. Finally, the calculated times to failure are compared in Figure 7 to the experimentally assessed values.

A reasonable agreement is obtained in spite of the shortcomings of the I-SCC model, i.e. the calculated crack propagation has no impact on the stress state in the cladding. A more severe limitation in the systematic use of the I-SCC model derived from laboratory tests in ALCYONE 3D simulations is the fact that all the simulated power

ramps led to the failure of the cladding (6 out of 12 actually failed in the OSIRIS reactor). Considering that the times to failure are correctly predicted from the calculated stresses and temperatures, it obviously means that the conditions leading to the initiation and ending of I-SCC are not properly caught. In our opinion, there are two main reasons that could explain the overprediction of clad failure with the I-SCC model. First, the chemical conditions (oxygen and iodine partial pressures mainly) in the laboratory tests (quasi-infinite supply of gaseous iodine) are probably far from the chemical conditions seen by the cladding during a power transient. Second, the strong and spatially extended pellet clad contact that takes place during power transients could limit the access of gaseous iodine to the clad inner wall. In contrast, gaseous iodine can easily reach the clad inner wall during laboratory pressurized tube tests which could also lead to faster failure by I-SCC.

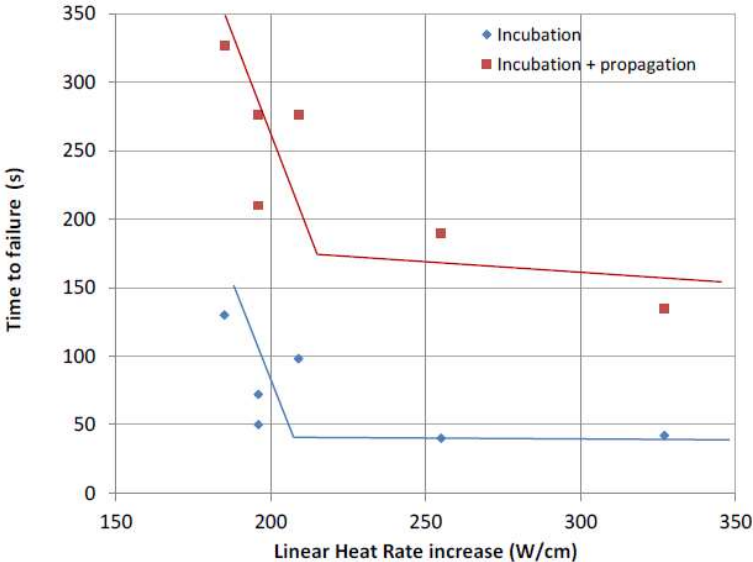


FIG. 6. Calculated times to failure versus LHR increase during a selection of power ramps from ALCYONE 3D simulations.

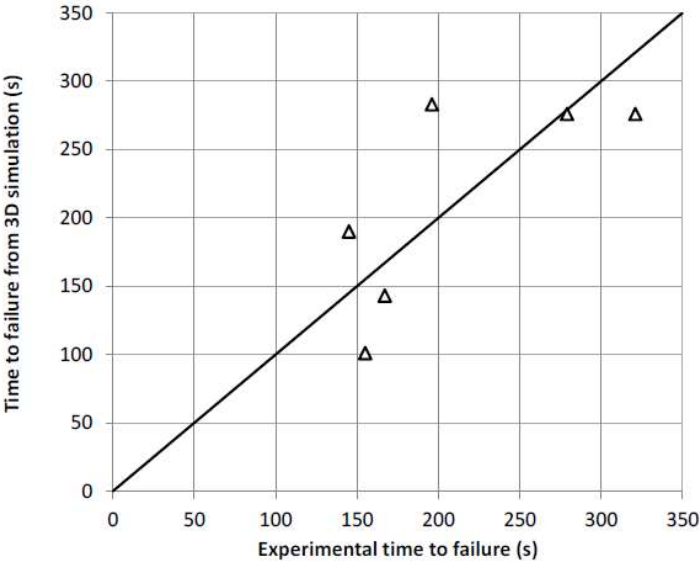


FIG. 7. Calculated times to failure versus measurements during a selection of power ramps from ALCYONE 3D simulations.

5. IMPACT OF IODINE RELEASE AND ACCESSIBILITY TO THE CLAD INNER SURFACE

The traditional approach to crack propagation modelling is to consider that iodine is always available at the pellet-clad interface in sufficient quantity for I-SCC to occur, a consequence of the van Arkel process presumed to be at the origin of the phenomenon, where a cyclic transport process within the crack depth leads to the regeneration of gaseous iodine. Therefore, a very small quantity of iodine is thought necessary to initiate the process. According to Sidky, if gaseous iodine is postulated as the main cause for I-SCC, thresholds should be expressed in g/cm^3 of free volume in contact with the cladding [19]. Alternatively, the iodine partial pressure of the atmosphere in contact with the clad inner wall might be used. There are very few laboratory I-SCC tests where partial iodine and oxygen pressures are thoroughly controlled to match in-reactor conditions. In the mandrel tests performed within the SCIP international project, a threshold of 120 Pa iodine partial pressure in anoxic conditions was identified as the necessary condition for a Zy-2 clad failure by I-SCC at 320°C [20].

To assess the chemical conditions seen by the cladding inner surface during a power transient, a thermochemical solver (ANGE) coupled to the fission gas release model (MARGARET) has been implemented in ALCYONE [3, 4, 21]. Thermochemical equilibrium calculations of the uranium dioxide fuel with the FPs were found necessary to correctly predict the release of iodine, tellurium and cesium during a power transient, a great part of the cesium being immobilized in the fuel in liquid or solid compounds (cesium molybdates and cesium iodides), even at the high temperatures of the pellet centre. In consequence, the fractional release of cesium can be notably lower than those of iodine and tellurium [3]. To illustrate this point, results from the 3D simulation of a challenging power ramp (RTL 520 W/cm) with a short holding period at RTL (90 s) that has led to the development of a $100\ \mu\text{m}$ deep I-SCC crack but not to the rod failure, are detailed hereafter [22]. Figure 8 gives the remaining fractions of Xe, Cs, Te and I along the fuel pellet radius after the completion of the power ramp.

As can be seen, while $\sim 80\%$ of Cs and Xe are still present at the pellet centre, only $\sim 40\%$ of Te and I remain.

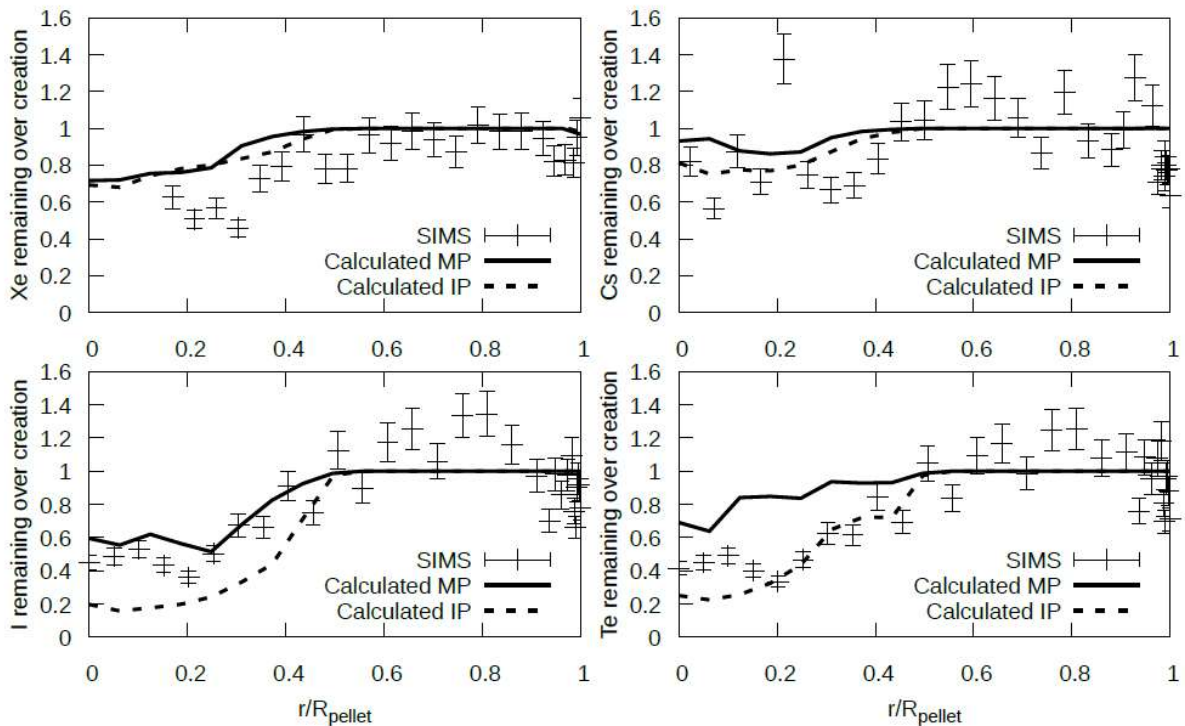


FIG. 8. Comparison of the calculated radial profiles of Xe, Cs, I and Te with SIMS measurements along the mid-pellet and inter-pellet planes at the end of the power ramp, from ALCYONE 3D simulations (reproduced courtesy of P. Konarski [22]). The experimental error is estimated to be 10%.

These differences in FP release can only be captured if the chemical speciation of the compounds formed within the fuel is considered in the calculations. In fact, solid and liquid compounds are assumed immobile in the fuel, only the gaseous compounds (CsI(g) , $\text{I}_2\text{(g)}$, $\text{Te}_2\text{(g)}$...) can be released.

The correct assessment of iodine concentrations released made possible the estimation of the chemical conditions at the clad inner surface, represented by the iodine partial pressure in the free volume at the pellet-pellet interface, calculated by the ideal gas law. As proposed by Baurens et al. [3], only the iodine gas species released from the pellet core and reactive with the Zr from the cladding (I(g) , $\text{I}_2\text{(g)}$ and $\text{TeI}_2\text{(g)}$) have been considered in the calculation of the iodine partial pressure (referred as reactive iodine further on in the paper). The free volume at the pellet-pellet interface accounts for the chamfer, the dish and the radial cracks which all evolve during the power ramp, as illustrated in Figure 9.

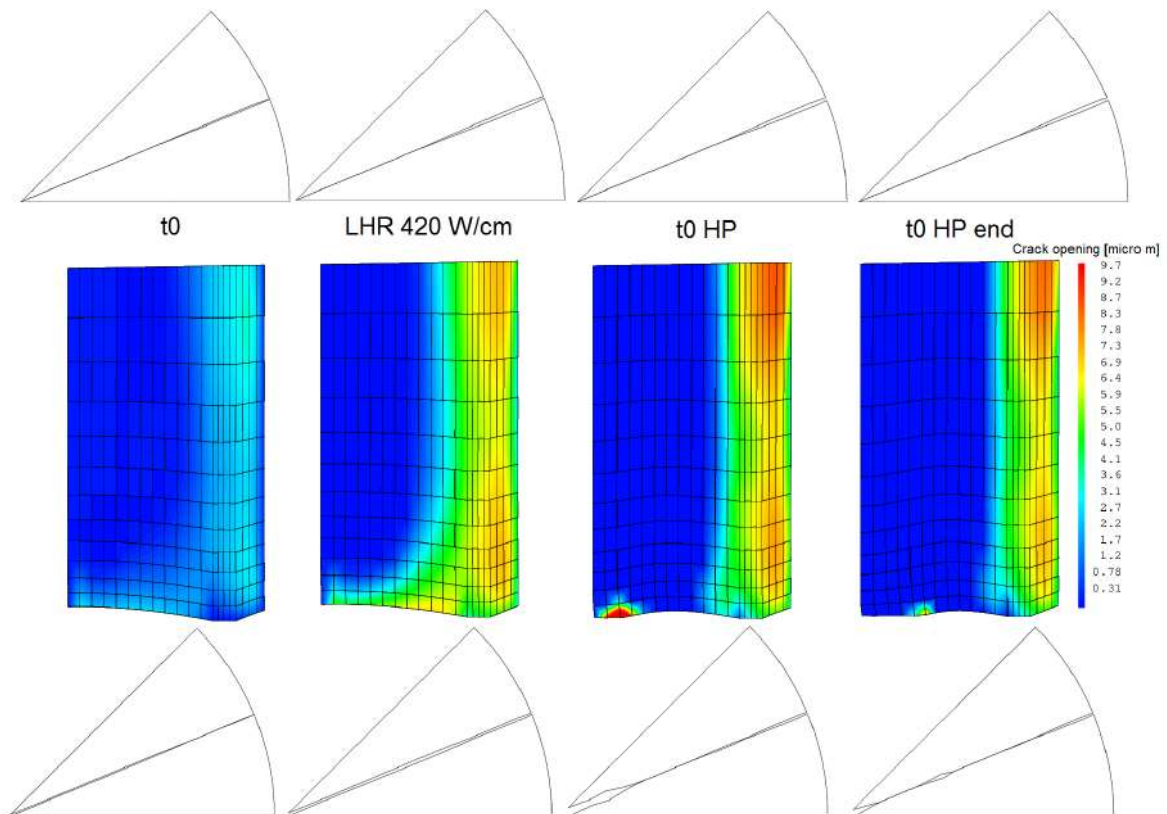


FIG. 9. Calculated pellet radial crack opening at different times during the power ramp, from ALCYONE 3D simulations (reproduced courtesy of P. Konarski [22]). Upper graphs give the mid-pellet plane. Lower graphs the inter-pellet plane. Iso-values give the distribution of crack opening on the fracture surface.

Note that the radial cracks are the only path where the gaseous compounds released from the pellet centre can reach the cladding when strong pellet-clad contact takes place. A salient result of the 3D simulation is that the radial crack remains opened to the pellet centre only at inter-pellet level. At mid-pellet level, it is closed on about half of the pellet radius. The impact of this crack opening distribution on fission gases transport to the clad inner wall is certainly important and at least consistent with the location of I-SCC failures. The maximum crack tip opening reaches 10 μm at RTL, meaning that there might be a non-negligible part of fission gases that will interact (condensation, adsorption) with the crack lips.

In the previous section, the hoop stress, the equivalent plastic strain, the temperature at the triple point from the thermo-mechanical 3D simulation and the crack propagation from the I-SCC model during this challenging power ramp are presented in Figure 5 (light blue lines). The very early development of plastic strains at the triple point (at -150 s before RTL), the mechanical condition considered to initiate I-SCC, leads to the clad failure in less than 20 s after RTL. This 3D simulation with I-SCC crack propagation has been improved by the consideration of reactive iodine release from the fuel pellet and of its transport to the clad inner surface. Figure 10 gives the

calculated evolution of the hoop stress at the triple point and of the reactive iodine partial pressure in the free volume at the pellet-pellet interface. The hoop stress evolution follows the one already given in Figure 5 with a maximum of 600 MPa and a decrease to 500 MPa after RTL is reached, owing to clad and fuel creep. Considering now that I-SCC initiation depends also on chemical conditions, for instance, on a reactive iodine partial pressure threshold, leads to a non-negligible delay in I-SCC initiation when compared to the mechanical based criterion. With a reactive iodine pressure threshold of 120 Pa, I-SCC starts -50 s before RTL, to be compared with the -150 s initiation time with the plastic strain criterion. The calculated crack depth evolution is given in Figure 11.

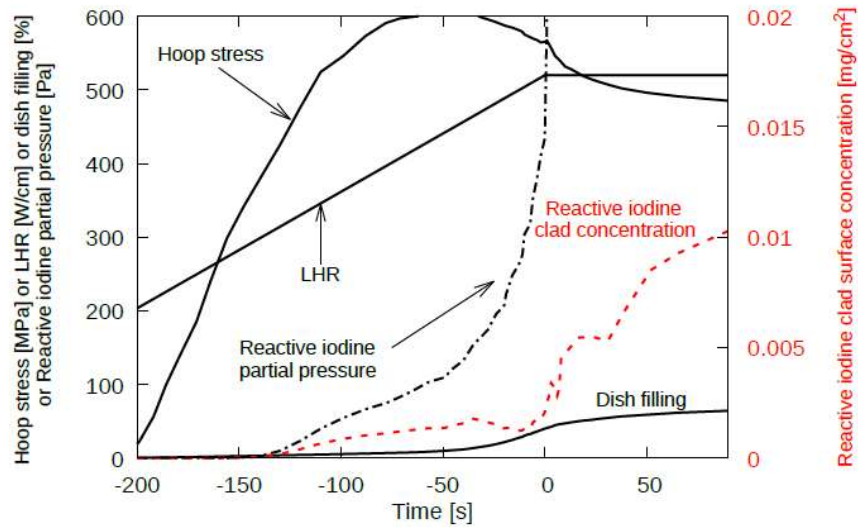


FIG. 10. Calculated evolutions of the hoop stress at the triple point and of the reactive iodine partial pressure in the free volume at the pellet-pellet interface during a power ramp, from ALCYONE 3D simulations (reproduced courtesy of P. Konarski [22]).

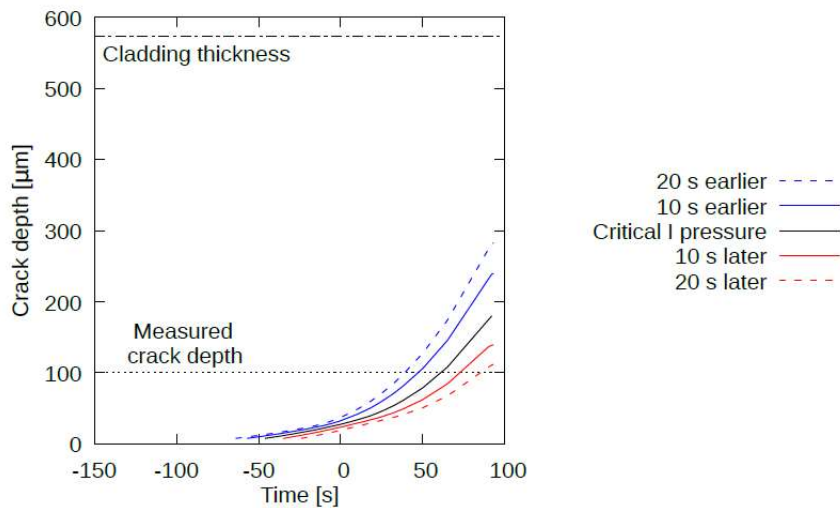


FIG. 11. Calculated crack depth during the power ramp as a function of the reactive iodine partial pressure threshold (the times in the legend refer to an I-SCC initiation delayed or ahead of the time at which the critical 120 Pa iodine pressure threshold is reached), from ALCYONE 3D simulations (reproduced courtesy of P. Konarski [22]).

Sensitivity studies on the reactive iodine pressure threshold (80 to 200 Pa) indicate a non-negligible variation in the calculated crack depth at the end of the power ramp (100 to 300 μ m), as shown in Figure 11. These results

illustrate the potential importance of a correct assessment of the chemical conditions at the triple point with respect to I-SCC crack propagation modelling, a fast phenomenon leading to clad failure in less than 10 minutes.

6. CONCLUSIONS

In this paper, 3D PCI simulations during power ramps that have led to the cladding failure by I-SCC have been presented. The 3D simulations include an I-SCC crack propagation model with parameters determined from laboratory tests with irradiated Zy-4 cladding. The clad mechanical model combines anisotropic instantaneous plasticity and viscoplasticity (creep). From the calculated evolution of the hoop stress, of the equivalent plastic strain and of the temperature at the triple point in the 3D simulation, the I-SCC crack propagation kinetics is estimated. The failure times obtained from this modelling approach are in reasonable agreement with those recorded during the power ramps (between 1 and 10 minutes). More complex 3D simulations with thermodynamic equilibrium calculations aiming at the evaluation of the chemical environment at the triple point (iodine partial pressure) have then been presented. They have led to a better assessment of I-SCC initiation and consequently of the I-SCC crack depth within a rod that did not fail during a power transient at 520 W/cm.

ACKNOWLEDGEMENTS

The authors would like to thank EDF and FRAMATOME for the technical and financial support to this work.

REFERENCES

- [1] MICHEL, B., NONON, C., SERCOMBE, J., MICHEL, F., MARELLE, V., Nuclear Technology **182** (2013) 124.
- [2] SERCOMBE, J., MICHEL, B., RIGLET-MARTIAL, C., FANDEUR, O., “Modelling of Pellet Cladding Interaction”, Comprehensive Nuclear Materials, edited by Könings, R., Elsevier (2019).
- [3] BAURENS, B., SERCOMBE, J., RIGLET-MARTIAL, C., TROTIGNON, L., MAUGIS, P., Journal of Nuclear Materials **452** (2014) 518.
- [4] KONARSKI, P. et al., Journal of Nuclear Materials **519** (2019) 104.
- [5] LE BOULCH, D., FOURNIER, L., SAINTE-CATHERINE, C., “Testing and Modelling Iodine Induced Stress Corrosion Cracking in Stress Relieved Zircaloy”, Workshop on Pellet-clad Interaction in Water Reactor Fuels, Aix-en-Provence, France, 2004, OECD NEA/6004.
- [6] LE BOULCH, D. et al., “Testing and Modelling Iodine-Induced Stress Corrosion Cracking in Zircaloy Alloys”, Workshop on Pellet-Clad Interaction (PCI) In Water-Cooled Reactors, Lucca, Italy, 2016, NEA/CSNI/R(2018)9.
- [7] GUÉNOT-DELAHAIE, I. et al., Nuclear Engineering and Technology **50** (2018) 268.
- [8] SERCOMBE, J., AUBRUN, I., AND NONON, C., Nuclear Engineering and Design **242** (2012) 164.
- [9] Cast3M, <http://www-cast3m.cea.fr/>.
- [10] SERCOMBE, J., JULIEN, J., MICHEL, F., MICHEL, B., AND FÉDÉRICI, E., “3D Modelling of Strain Concentration due to PCI within the Fuel Code ALCYONE”, TopFuel conference proceedings, Charlotte, USA, 2013.
- [11] MOUGEL, C. et al., “Power Ramping in the OSIRIS Reactor: Database Analysis for Standard UO₂ Fuel with Zy-4 Cladding”, Workshop on Pellet-clad Interaction in Water Reactor Fuels, Aix-en-Provence, France, 2004, OECD NEA/6004.
- [12] MICHEL, B., SERCOMBE, J., THOUVENIN, G., Nuclear Engineering and Design **238** (2008) 1612.
- [13] FOUCHET, J., DELETTE, G., ROUILLON, L., Characterization of the Transgranular Crack Propagation Phase during I-SCC of Zy-4, Internal Report, CEA Grenoble, France (1998).
- [14] JEZEQUEL, T. et al., Journal of Nuclear Materials **499** (2018) 641.
- [15] Magnusson, P., Puranen, A., Jädernäs, D., Lysell, G., and Boulch, D., An experimental and finite element modelling study of cladding strain and localized stresses under simulated iodine-induced stress corrosion cracking, in WRFPM conference proceedings, Sendai, Japan, 2014.
- [16] MILLER, A., OCKEN, H., TASOOJI, A., Journal of Nuclear Materials **99** (1981) 254.
- [17] ARIMESCU, I., KARLSSON, J., Journal of Nuclear Science and Technology **52** (2015) 1274.
- [18] SONIAK, A. et al., “Irradiation Creep Behaviour of Zr-Based Alloys”, 13th Int. Symp. on Zirconium in the Nuclear Industry, Annecy, France, 2002, ASTM International.
- [19] SIDKY, P., Journal of Nuclear Materials **256** (1998) 1.
- [20] ANGHEL, C. et al., “Experimental and Finite Element Modelling Parametric Study for Iodine-Induced Stress Corrosion Cracking of Irradiated Cladding”, TopFuel conference proceedings, Orlando, USA, 2010.
- [21] SERCOMBE, J., RIGLET-MARTIAL, C., BAURENS, B., “Simulations of Power Ramps with Alcyone Including Fission Products Chemistry and Oxygen Thermo-Diffusion, Workshop on Pellet-Clad Interaction (PCI) in Water-Cooled Reactors, Lucca, Italy, 2016, OECD NEA/CSNI/R(2018)9.

- [22] KONARSKI, P., Thermo-Chemical-Mechanical Modelling of Nuclear Fuel Behaviour. Impact of Oxygen Transport in the Fuel on Pellet Cladding Interaction, PhD thesis, INSA Lyon, France (2019).

MULTI-DIMENSIONAL CREEP ANALYSIS USING THE NOVEL OFFBEAT FUEL PERFORMANCE CODE

A. SCOLARO, C. FIORINA
École Polytechnique Fédérale de Lausanne (EPFL),
Lausanne, Switzerland,
Email: alessandro.scolaro@epfl.ch

I. CLIFFORD, A. PAUTZ
Paul Scherrer Institut (PSI),
Villigen, Switzerland

Abstract

The EPFL and the PSI are currently working to enhance the knowledge of complex phenomena relevant for reactor safety, by developing advanced methodologies based on physics-based and high- simulations. In this framework, a new multi-dimensional fuel behaviour solver is under collaborative development at the two institutes. The new tool, OFFBEAT, which has been developed based on the C++ library OpenFOAM, is envisioned as a complement to traditional fuel performance codes for the investigation of complex phenomena affecting fuel integrity, such as a PCMI with a missing pellet surface defect or an asymmetric heat exchange. In this regard, efforts are underway to devise an optimal coupling strategy with the TRANSURANUS code. Additionally, OFFBEAT can be used to perform more traditional axisymmetric analyses of the nuclear fuel rod, using semi-empirical correlations for swelling, densification and relocation strains, and for the temperature and burnup dependence of the material properties. Recently, models that capture the non-elastic behaviour of the zircaloy cladding, both in terms of instantaneous plasticity and thermal and irradiation creep, have been introduced. This paper focuses on the methodological development associated with creep modelling in OFFBEAT and presents a preliminary multi-dimensional creep analysis for a test-case rodlet.

1. INTRODUCTION

Traditional fuel performance codes are extensively used by fuel vendors, regulators and research institutes. These codes offer excellent performances, a wide validation base, and are equipped with a large set of behavioural and material models introduced during the course of their long development. However, a trade-off for their effectiveness is a considerable simplification of the fuel rod analysis, which includes employing the quasi-2D approximation (or at least modelling the fuel as a single smeared column) and using approximated models for several important aspects of the fuel behaviour, for instance: the rod neutronics and depletion, the thermal exchange with the coolant and the cladding chemistry. Thus, the reproduction of local multi-physics and multi-dimensional features of complex phenomena as in the pellet-cladding-interaction (PCI) or in a loss-of-coolant accident (LOCA), escapes the realm of possibilities of most traditional fuel performance codes.

In the last decade there has been a growing interest in the fuel performance community toward the use of higher-fidelity and physics-based methodologies for enhancing the knowledge on some of the most complex phenomena affecting fuel integrity. This is demonstrated by publications such as [1] and by the development of the BISON [2], MARMOT [3], ALCYONE [4] and DYONISIO [5] codes. The computational burden of these modern tools is certainly higher than that of traditional codes, but it is justified by the increasingly growing computational power availability and by their mostly research-oriented applications.

The Laboratory for Reactor Physics and Systems Behaviour (LRS) of the École Polytechnique Fédérale de Lausanne (EPFL) and the Paul Scherrer Institute (PSI) have recently joined these international efforts, establishing a collaboration for the development of a new multi-dimensional fuel performance code, called OpenFOAM fuel behaviour analysis tool or OFFBEAT. Based on the OpenFOAM C++ platform, the new code can be directly coupled to CFD, neutronics or chemical solvers developed by the OpenFOAM community [6]. Additionally, the coupling with the Monte Carlo neutron transport code Serpent is simplified thanks to Serpent multi-physics interface, as already demonstrated in [7]. The development of OFFBEAT aims also at exploring the possibilities deriving from complementing a traditional 1.5D fuel performance code such as TRANSURANUS [8] with a higher-fidelity tool, and from using a multi-dimensional code to help designing and interpreting new fuel rod experiments, often featuring unconventional design and multi-dimensional behaviour.

OFFBEAT has been used to perform a first 3-D analysis for the asymmetric heat exchange during a partial burnout [9], and it has undergone a preliminary validation for the thermal response of axisymmetric light water

reactor (LWR) rods [10]. These first applications, however, were limited to a linear-elastic framework with the inclusion of the phenomena of fuel densification, swelling and relocation, while the behaviour of the fuel rod is strongly affected by plastic phenomena both during normal operation and during more complex scenarios. Especially relevant is the accumulation of creep deformations in the zircaloy cladding.

Since the coolant pressure is higher than the filling gas pressure (at least for a low burnup rod), the cladding gradually creeps down toward the pellets. This reduces the initial gap width and gas free volume, having a large impact on the gap conductance and on the thermal response of the rod. Once the gap is closed or small, a sudden power excursion might cause strong PCI, with the concentration of high tangential stresses in the vicinity of pellet ends or crack tips. Stress-relaxation due to creep in the cladding might influence the transient dynamics and the rod rupture. Outward creep deformation might be caused also by the over-pressurization of the rod at high burnup, following the release of a large fraction of fission gases. If the clad creep rate exceeds the pellet swelling rate, the gap might re-open leading to the so-called cladding lift-off and to the potential failure of the rod.

Recent efforts have been carried out to include the non-elastic behaviour of zircaloy in OFFBEAT models . After the introduction of an instantaneous plasticity model based on von Mises theory [11], the main development efforts have focused on the implementation of the Limbäck and Anderson creep model, following the work of Liu [12] for the Peregrine code. In the Limbäck and Anderson model, also used in FALCON and BISON, the zircaloy creep is described as the combined effect of three mechanisms, i.e. a secondary thermal creep with a strain rate hardening caused by irradiation, a fast primary creep that quickly reaches saturation and an irradiation-assisted creep caused by defect clustering. For each of the three mechanisms a correlation is derived as a function of stress, time, temperature, metallurgic properties and (fast) neutron flux or fluence.

This work describes the numerical implementation of the Limbäck model in OFFBEAT and presents a first test application to an LWR rodlet. The paper is structured in the following manner. Following a brief summary of the main characteristics of the code in Section 2, Section 3 presents the Limbäck model main equations, the numerical implementation in OFFBEAT and the results of a simple benchmark test. Finally, Section 4 focuses on a more realistic test-case scenario where the creep model is used to analyze the formation and evolution of cladding ridges in the presence of strong pellet-to-cladding contact.

2. OFFBEAT

OFFBEAT has been developed based on the open-source C++ library OpenFOAM [13]. OFFBEAT uses advanced finite volume techniques in solving the heat conduction and the momentum balance equations on unstructured meshes with an arbitrary geometry. Geometrical domain decomposition and the MPI communication protocol are employed to achieve a potentially massive parallelization. A more complete description of the equations, structure and models in OFFBEAT can be found in previous works [9]. Additional details on the original solution scheme on which the code is based can be found in seminal paper from Jasak and Weller [13, 14].

The system of coupled governing equations is solved in a segregated manner, relying on a fixed-point segregated scheme. Thus, the equations are iteratively solved until the temperature and displacement residuals fall below a user defined threshold. A block-coupled solver might be explored in the future, although this might be proven useful only for strongly coupled problems with significant bending and it is not very memory efficient (which might be a serious issue for large problems).

OFFBEAT takes into account thermal expansion, densification, swelling, relocation and irradiation growth strains. An instantaneous plasticity model for the zircaloy cladding has been recently introduced and benchmarked [11], and an explicit penalty method model is used to handle fuel cladding contact, which at the moment is assumed to be frictionless. A custom boundary condition is developed to handle the thermal feedbacks and the evolution of the gap conductance with a variation of gap width and temperature. Semi-empirical correlations derived from MATPRO [15] and IAEA [16] are used to take into account the dependence of the material properties on temperature and burnup. The evolution of the gap composition and pressure is tracked with a gap and fission gas release models, both derived from FRAPCON [17].

3. CREEP MODEL

3.1. Limbäck model

The Limbäck and Anderson model is described in detail in [18] and in [12]. Nevertheless, the main equations are reproduced here for clarity. The Limbäck model calculates the total effective creep strain of zircaloy, $\epsilon_{c,eff}$, as the combination of two main components, i.e. the primary creep and the secondary creep, which in turn is composed of thermal and irradiation-induced creep.

The irradiation induced creep rate $\dot{\epsilon}_i$ (hr^{-1}) is given as:

$$\dot{\epsilon}_i = C_0 \phi^{C_1} \sigma_{eff}^{C_2} \quad (1)$$

where σ_{eff} is the effective or von Mises stress (MPa), ϕ is the fast neutron flux (n/m^2 -sec), $C_0 = 3.557 \times 10^{-24}$ ($(n/m^2$ -sec)- C_1 (MPa)- C_2 /hr), $C_1 = 0.85$ and $C_2 = 1.0$.

The secondary thermal creep rate $\dot{\epsilon}_{th}$ (hr^{-1}) is given as:

$$\dot{\epsilon}_{th} = A \frac{E}{T} \left(\sinh \frac{a_i \sigma_{eff}}{E} \right)^n \exp \left(-\frac{Q}{RT} \right) \quad (2)$$

where T is the temperature (K), E is the Young's modulus (MPa):

$$E = 1.148 \times 10^5 - 59.9T \quad (3)$$

a_i is an irradiation hardening parameter calculated as:

$$a_i = a [1 - A_1 (1 - \exp(-A_2 \Phi^{A_3}))] \quad (4)$$

and Φ is the fast neutron fluence (n/cm^2). The following values are used for the remaining parameters: $Q = 201$ (kJ/mol), $a = 650$, $n = 2.0$, $A = 1.08 \times 10^9$ (K/MPa-hr), $A_1 = 0.56$, $A_2 = 1.4 \times 10^{-27}$ (n/cm^2)- A_3 and $A_3 = 1.3$.

The primary creep strain is derived from Matsuo correlation for saturated primary creep [19]:

$$\epsilon_p = \epsilon_p^s [1 - \exp(-C \sqrt{\dot{\epsilon}_s t})] \quad (5)$$

where t is the time in hr, $C = 52$ is a fitting parameter, $\dot{\epsilon}_s$ is the secondary creep rate, $\dot{\epsilon}_s = \dot{\epsilon}_i + \dot{\epsilon}_{th}$, and ϵ_p^s is the saturated primary creep strain given by:

$$\epsilon_p^s = B \dot{\epsilon}_s^b [2 - \tanh(D \dot{\epsilon}_s)]^d \quad (6)$$

where $B = 0.0216$ (hrb), $b = 0.109$, $D = 35500$ (hr) and $d = -2.05$.

Finally, the total effective creep strain at time t is given as:

$$\epsilon_{c,eff} = \epsilon_p^s [1 - \exp(-C \sqrt{\dot{\epsilon}_s t})] + \dot{\epsilon}_s t \quad (7)$$

3.2. Limbäck model numerical implementation

The Limbäck model obtains the creep strain components as a function of the stress state. In OFFBEAT, the stress tensor σ (Pa) is calculated employing Hooke's law:

$$\boldsymbol{\sigma} = 2\mu \boldsymbol{\epsilon}_{el} + \lambda \text{tr}(\boldsymbol{\epsilon}_{el}) \mathbf{I} \quad (8)$$

where μ (Pa) and λ (Pa) are the first and second Lamé parameters. Thus, the current stress state is proportional to the elastic strain tensor, ϵ_{el} , which is just one component of the total strain tensor, ϵ_{tot} . In particular, for the cladding the total strain tensor is:

$$\boldsymbol{\epsilon}_{tot} = \boldsymbol{\epsilon}_{el} + \boldsymbol{\epsilon}_{th} + \boldsymbol{\epsilon}_{irr} + \boldsymbol{\epsilon}_c + \boldsymbol{\epsilon}_{plast} \quad (9)$$

where ϵ_{th} is the strain component due to thermal expansion, ϵ_{irr} is the strain component due to irradiation growth, ϵ_c is the creep strain component and ϵ_{plast} is the instantaneous plasticity strain component. Given the incremental nature of plastic phenomena, it is more suitable to decompose the plastic strain terms into old time (o) and incremental component (Δ), obtaining:

$$\boldsymbol{\epsilon}_{tot} = \boldsymbol{\epsilon}_{el} + \boldsymbol{\epsilon}_{th} + \boldsymbol{\epsilon}_{irr} + \boldsymbol{\epsilon}_c^o + \Delta \boldsymbol{\epsilon}_c + \boldsymbol{\epsilon}_{plast}^o + \Delta \boldsymbol{\epsilon}_{plast} \quad (10)$$

For a small strain, the total strain tensor is calculated as

$$\boldsymbol{\varepsilon}_{\text{tot}} = \frac{1}{2}(\nabla\bar{\mathbf{D}} + (\nabla\bar{\mathbf{D}})^T) \quad (11)$$

using the latest available solution of the displacement field $\bar{\mathbf{D}}$ (m), obtained by solving the system of three coupled momentum balance equations (one for each Cartesian direction) given by

$$\frac{\partial^2(\rho\bar{\mathbf{D}})}{\partial t^2} = \nabla \cdot \boldsymbol{\sigma} \quad (12)$$

where ρ is the density (kg/m³). In order to solve this system of equations a closure relation is needed for $\boldsymbol{\sigma}$.

Extracting ε_{el} from Eq.(10), using Eq.(11) for the total strain, and inserting it into Eq.(8), the closure relation, Eq.(13), is obtained with $\boldsymbol{\sigma}$ expressed as a function of the displacement field and of the strain increment:

$$\begin{aligned} \boldsymbol{\sigma} = & \mu \left(\nabla\bar{\mathbf{D}} + (\nabla\bar{\mathbf{D}})^T \right) + \lambda \text{tr}(\nabla\bar{\mathbf{D}})\mathbf{I} - 2\mu(\boldsymbol{\varepsilon}_{\text{th}} + \boldsymbol{\varepsilon}_{\text{irr}}) - \lambda \text{tr}(\boldsymbol{\varepsilon}_{\text{th}} + \boldsymbol{\varepsilon}_{\text{irr}})\mathbf{I} \\ & - 2\mu\boldsymbol{\varepsilon}_{\text{c}}^0 - 2\mu\Delta\boldsymbol{\varepsilon}_{\text{c}} - 2\mu\boldsymbol{\varepsilon}_{\text{plast}}^0 - 2\mu\Delta\boldsymbol{\varepsilon}_{\text{plast}} \end{aligned} \quad (13)$$

As previously mentioned, OFFBEAT solves the governing equations in a segregated manner (operator splitting), i.e. the code solves iteratively and separately each physics until convergence of the respective residuals. When solving for the displacement field, the thermal and irradiation growth strains in Eq.(13) are fixed, because they are solely determined by the temperature and neutron fluence, and thus they are not influenced by the solution of the system in Eq.(12). The creep strain increment, instead, is a function of the stress state, which in turn is a function of the creep increment. Therefore, at iteration $n+1$, the value of the stress is calculated using the strain increment obtained at the end of iteration n . In order to calculate the creep strain increment, an algorithm similar to the one already used for determining the plastic strain and derived from the one proposed in the work of Liu is followed:

- At time $t+\Delta T$, the latest available displacement solution $\bar{\mathbf{D}}^n$ is used to calculate the total strain increment $\Delta\boldsymbol{\varepsilon}_{\text{tot}}^n$ with Eq.(11);
- Using Eq.(13), a trial stress tensor $\boldsymbol{\sigma}^{\text{tr},n}$ and a trial effective stress $\sigma_{\text{eff}}^{\text{tr},n}$ are calculated assuming that all the additional strain $\Delta\boldsymbol{\varepsilon}_{\text{tot}}^n$ is due to elastic and thermal deformation, with the addition of irradiation growth strains;
- The effective stress σ_{eff}^n as a function of the trial stress and of the equivalent creep increment is given by

$$\sigma_{\text{eff}}^n = \sigma_{\text{eff}}^{\text{tr},n} - 3\mu \Delta\varepsilon_{\text{c,eff}}^{n-1} \quad (14)$$

- The effective strain increment is given by:

$$\Delta\varepsilon_{\text{c,eff}}^n = f(\sigma_{\text{eff}}^n)\Delta t \quad (15)$$

where f is:

$$f(\sigma_{\text{eff}}^n) = \dot{\varepsilon}_{\text{i}}^n + \dot{\varepsilon}_{\text{th}}^n + \frac{\varepsilon_{\text{p}}^{s,n} [1 - \exp(-C\sqrt{\varepsilon_{\text{s}}^n(\tau^n + \Delta t)))] - \varepsilon_{\text{p}}^0}{\Delta t} \quad (16)$$

and τ^n is:

$$\tau^n = C^{-2}(\dot{\varepsilon}_{\text{i}}^n + \dot{\varepsilon}_{\text{th}}^n)^{-1} \left[\ln \left(1 - \frac{\varepsilon_{\text{p}}^0}{\varepsilon_{\text{p}}^{s,n}} \right) \right]^2 \quad (17)$$

- The multi-axial creep strain increment is obtained with the Prandtl-Reuss flow rule:

$$\Delta\boldsymbol{\varepsilon}_{\text{c,i}}^n = \frac{3\sigma_{\text{dev}}^{n-1}}{2\sigma_{\text{eff}}^n} \Delta\varepsilon_{\text{c,eff}}^n \quad (18)$$

where $\boldsymbol{\sigma}_{\text{dev}}$ is the deviatoric component of the stress tensor.

The updated creep strain increment is introduced in Eq.(13) to determine the stress tensor $\boldsymbol{\sigma}^n$, eventually after the additional calculation of the instantaneous plastic strain. If the displacement residuals are still above the user defined threshold, $\boldsymbol{\sigma}^n$ is introduced in Eq.(12) to solve for $\bar{\mathbf{D}}^{n+1}$ and the presented algorithm is repeated.

3.3. Creep model verification test

The implementation of the Limbäck creep model in OFFBEAT was verified against the numerical benchmark proposed always in the work of Liu. The case consists of a cladding segment irradiated for 1E+5 seconds under uniform temperature and constant neutron flux. The pressure is higher on the outer side and the case is in plain stress, i.e. the axial stress is zero, and due to the operation time span considered the neutron fluence is assumed to be zero. The case specifics are shown in Table 1.

TABLE 1. DIMENSIONS AND SPECIFICS FOR THE NUMERICAL VERIFICATION TEST

Parameter	Value
Inner Radius	5.0 mm
Outer radius	5.5 mm
Inner pressure	1.0 Pa
Outer pressure	15.5 Pa
Temperature	650 K
Neutron flux	$1014 \frac{n}{\text{cm}^2\text{s}}$

The cladding segment is reproduced as a single wedge cell, made of 8 nodes or vertices. On the sides or wedge surfaces, a specific OpenFOAM boundary condition was applied to ensure azimuthal symmetry. A constant time step of 1E+4 seconds was used, for a total of 10 time steps.

The main results obtained with OFFBEAT are summarized in Table 2 where they are compared to the corresponding analytical solution. As seen, the code is able to accurately replicate the analytical values with relative errors lower than 0.1%.

TABLE 2. MAIN RESULTS OF THE NUMERICAL VERIFICATION CASE. THE RESULTS OBTAINED WITH OFFBEAT ARE COMPARED TO THE ANALYTICAL SOLUTION

Parameter	Analytical Solution	OFFBEAT
$\dot{\epsilon}_i$ [s^{-1}]	3.08 E-10	3.08 E-10
$\dot{\epsilon}_{th}$ [s^{-1}]	77.82 E-10	77.86 E-10
ϵ_p	3.527 E-3	3.529 E-3
$\epsilon_{c,eff}$	4.336 E-3	4.339 E-3
$\epsilon_{c,radial}$	1.987 E-3	1.990 E-3
$\epsilon_{c,azimuth}$	4.331 E-3	4.334 E-3
$\epsilon_{c,axial}$	2.344 E-3	2.344 E-3

4. TEST CASE

A more realistic scenario is conceived to test the creep model and to show how multi-dimensional features of fuel rod behaviour might be captured using OFFBEAT. The test case consists of a UO₂ rodlet made of 10 pellets with the dimensions and specifics shown in Table 3. The zircaloy cladding extends a few millimetres above the top end of the fuel column, so that the expanding pellets are always facing the cladding. The rod is fresh, and it is filled with helium pressurized at 0.1 MPa at room temperature, while the coolant is at 15 MPa and 573 K. After a linear rise in power in the first 60 seconds, the rod is irradiated at 30 kW/m for approximately 180 days (see Fig.1 for the power history), reaching a burnup of approximately 10 MW·d/kg. At the end of irradiation, the power descends back to zero in 60 seconds and the rod is allowed to cool for further 100s in order to reach equilibrium with the coolant temperature.

Due to the symmetrical nature of the case, the rodlet is reproduced with the axisymmetric model shown in Fig.2. A 5×1200 cells mesh is used for the cladding, while a 20×100 cell mesh is used for each pellet, for a total of 26000 cells. As shown also in the detail on the right side of Fig.2, the pellet mesh is radially more refined in the land and chamfer region. This mesh is significantly denser along the axial direction than those typically used in traditional fuel performance codes. This level of refinement, however, is necessary to accurately capture multi-dimensional local phenomena such as the formation of the cladding ridges.

TABLE 3. DIMENSION AND SPECIFICS FOR THE TEST-CASE RODLET

Parameter	Value
N. of UO ₂ pellets	10
Outer pellet radius	4 mm
Pellet height	13.8 mm
Dish radius/height	3/0.3 mm
Chamfer width/height	0.6/0.2 mm
Cladding inner radius	4.1 mm
Cladding outer radius	4.7 mm
Cladding Height	150 mm
Helium pressure	0.1 MPa
Neutron flux	1014 $\frac{n}{cm^2s}$
Coolant temperature	573 K
Coolant pressure	15 MPa
Linear heat rate	30 kW/m

Although the pellet chamfers and dishes are included in the model, the fuel forms a continuous column through the land, that is the flat region surrounding the dish (as it seems to be a common approach in similar works [20]). Certainly, this modelling choice influences the local stress distribution in the pellet in the vicinity of the land, but it greatly simplifies the numerical problem by avoiding the solution of the pellet-to-pellet contact mechanics while still capturing most of the hourglass-shape thermal expansion. Efforts are underway to develop appropriate inter-pellets boundary conditions to provide a more accurate solution to this problem. The bottom surfaces of fuel and cladding are connected to the ground while a fixed pressure is imposed on the top surfaces. In particular, the filling gas pressure is imposed on the top fuel surface and the coolant pressure is imposed on the top cladding surface (adjusted for the annular geometry given that the top cap is not modelled). An important simplification comes from considering the fuel as a purely thermo-elastic body, with the addition of swelling and densification strains. The absence of a smeared cracking and creep model will affect the magnitude of the pushing force that the pellets are able to exert on the cladding. Also, the fission gas release model is not activated, although this should not influence significantly the contact mechanics given the initial small gap, the final low burnup of the rod and the relatively large plenum.

Two cases are considered, one where also the cladding behaves as a thermo-elastic body and one where the models for zircaloy creep and plasticity are activated. An adaptive time-step size is used so that the change in power during the initial ramp and during the final power descent are well captured. The adaptive scheme allows either a maximum power increase of 25% or a maximum burnup increase of 0.1 MW·d/kg. This corresponds to a time step of approximately 1.4E5 seconds during the long phase at constant power. However, toward the end of the holding period the time step decreases gradually so that it is in the order of 10s during the final power descent.

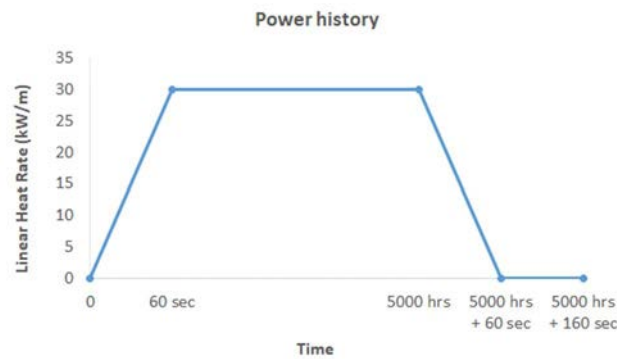


FIG. 1. Power history for the test-case rodlet. The time axis is not to scale.

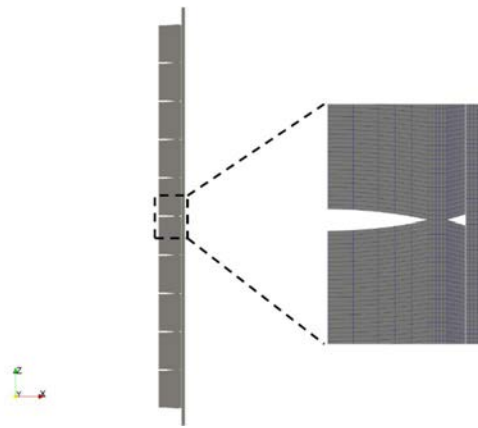


FIG. 2. Axisymmetric model used for the test-case rodlet simulations. The pellets are attached through the land region. A detail of the computational mesh is visible on the right.

At the beginning of irradiation, the rod response is purely thermo-elastic for both simulations and, because the initial gap is small, the pellets enter in contact with the cladding already during the power ramp. Figure 3 shows the outward displacement of the cladding outer and inner surfaces at 100s, when the rod temperature has almost reached its steady state (for fresh rod conditions). The graph shows the formation of cladding ridges with an amplitude of 40 micrometres, caused by the hourglass deformation of the pellets. This characteristic structure can be clearly seen also on the right of Fig.3. The colour map shows the concentration of equivalent stresses in the ridges.

Following this initial expansion, the rod starts to shrink due to the fuel densification, until this effect saturates between 1 and 2 MW·d/kg. When the fuel reaches a burnup of approximately 5 MW·d/kg, the swelling fuel starts to push the cladding outward and, from this point on, the behaviour of the cladding differs greatly between the two considered cases. The expansion of the fuel causes the stresses to increase significantly in the elastic cladding and, particularly at the location of the ridges, the von Mises stress gradually approaches values close to the yield point. When using the creep model, instead, the cladding accommodates the fuel expansion by deforming permanently and stress relaxation due to creep keeps the von Mises stress at considerably smaller values. This different behaviour can be seen on the graph in Fig.4. Here the cladding von Mises stress is shown for both cases at the end of the constant power phase. On the inner side of the elastic cladding, the equivalent stress in the ridges reach values larger than $2.5E+8$ Pa, while they remain below $7E+7$ Pa when the creep model is used.

Finally, once the power generation stops and the rod cools down to the coolant temperature, the gap opens once again due to the contraction of the pellets. Figure 5 shows the displacement of the cladding inner and outer surfaces at the end of the simulation. The elastic cladding has no permanent deformation (only the uniform expansion for being at a high temperature), while creep deformations following the ridge structure might be observed for the second rod.

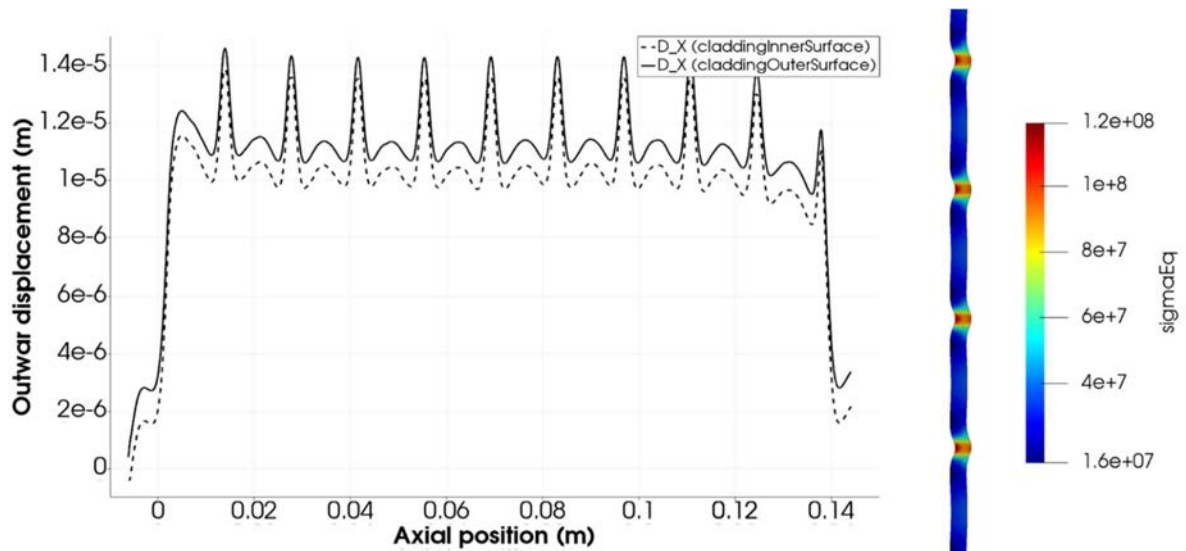


FIG. 3. Outward displacement of inner and outer cladding (left). Colour plot of the von Mises or equivalent stress (Pa) for a segment section of the cladding (right). The geometry is warped using the displacement field multiplied 50 times.

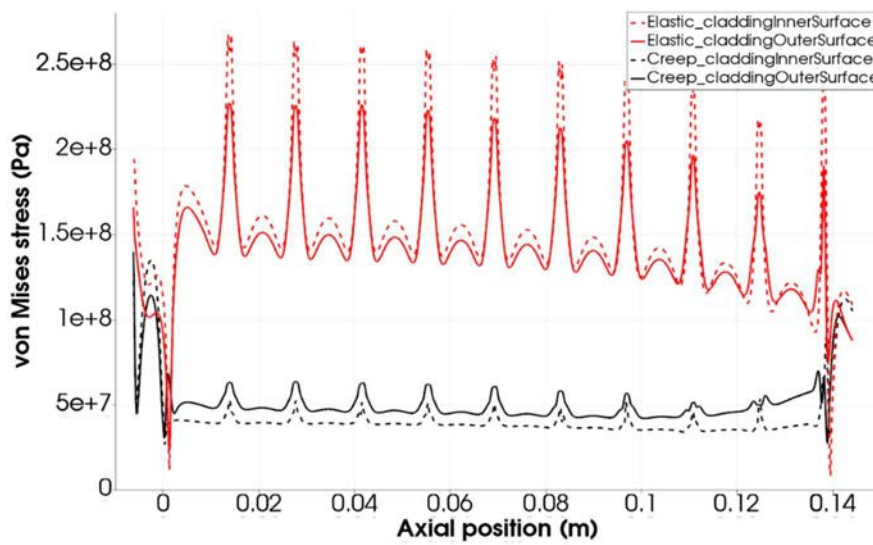


FIG. 4. Von Mises or equivalent stress on the inner and outer surface of the cladding. The results for both elastic and non-elastic cladding are shown.

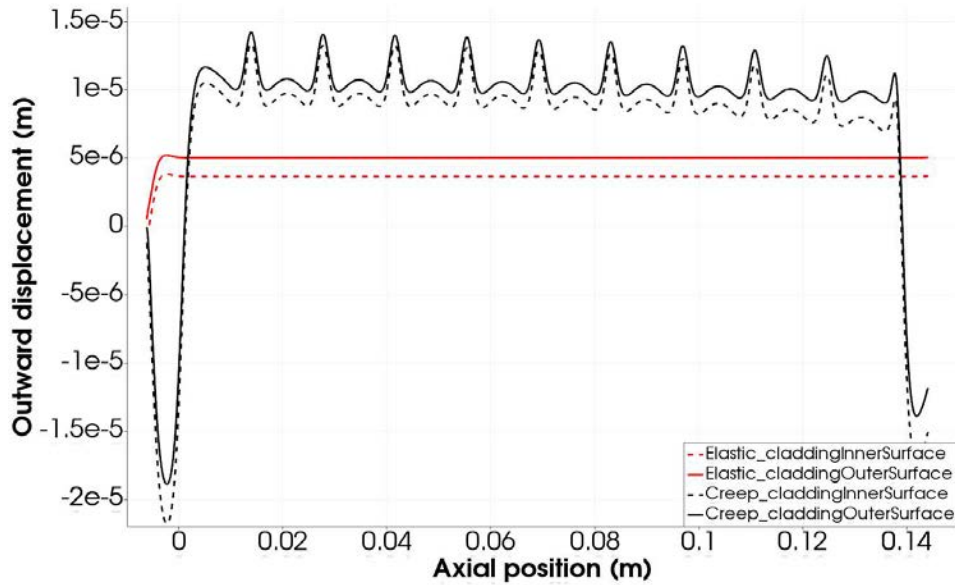


FIG. 5. Outward displacement of inner and outer cladding surfaces at the end of the simulation (with the rod in thermal equilibrium with the coolant). Permanent deformations due to creep following the ridges structure are visible for the second case.

4.1. Penalty Factor and Performance

The results presented in this section are obtained using a penalty factor equal to 1 for the contact boundary condition. Indeed, the contact model used in OFFBEAT [11] allows cladding and pellets to overlap and it applies to the two bodies a pressure proportional to the penetration. The penalty factor governs the relative amount of penetration allowed in a particular simulation. A penalty factor as high as one for the mesh size considered in this paper results in only a minor penetration (approximately $1\text{E-}8$ m). While being more accurate, this makes the problem numerically more cumbersome and, in order to reach convergence, the linear system has to be under relaxed, slowing down the simulation. A smaller penalty factor might be used to improve the code performances, but it is important to be aware that a very low penalty factor might have a significant impact on the results of the simulation. It is always better to strive for a compromise between accuracy and performance and, if possible, use the highest penalty factor allowed by the size of the problem, its convergence properties and the numerical power available. Nevertheless, even a small penalty factor (down to $1\text{E-}3$) might still give some insights on the physics of the problem (e.g. the formation of ridges and the relative height of the ridge) provided that results are correctly interpreted and used. For the cases presented in this paper, the total time needed to complete the simulation was approximately 5 hours using one single core from a desktop unit equipped with an Intel® Xeon® CPU E5-1660 v4 processor with 8 GHz cores. Although not comparable with traditional fuel performance codes, this performance might be considered acceptable given the elevated detailed with which the contact and the ridging are captured, the high number of time steps simulated and the possibility in OpenFOAM to effectively parallelize the simulation [21]. Considerable boost in performance might come in the future thanks to the current developing efforts focusing on improved contact boundary conditions and the use of acceleration techniques.

5. OUTLOOK AND CONCLUSIONS

This work focused on the numerical implementation, verification and testing of the Limbäck and Anderson creep model for the zircaloy cladding within the novel OFFBEAT code. With this addition, OFFBEAT allows the preliminary analysis of localized detailed phenomena such as the formation and evolution of cladding ridges in cases of strong contact between pellet and cladding. Certainly, further testing is needed as well as validation against experimental measurements of the cladding external diameter and axial elongation. For more accurate results, the near future development efforts will focus on the implementation of a model for fuel cracking and creep, and on the addition of a frictional component to the contact model.

REFERENCES

- [1] RASHID, Y.R., YAGNIK, S.K., MONTGOMERY, R.O., Light Water Reactor Fuel Performance Modelling and Multi-Dimensional Simulation, *JOM* (2011).
- [2] NEWMAN, C., HANSEN, G., GASTON, D., Three-Dimensional Coupled Simulation of Thermomechanics, Heat and Oxygen Diffusion in UO₂ Nuclear Fuel Rods, *J. Nucl. Mater.* **392** (2009) 6–15.
- [3] TONKS, M.R., GASTON, D., MILLETT, P.C., ANDRS, D., TALBOT, P., An Object-Oriented Finite Element Framework for Multiphysics Phase Field Simulations, *Comput. Mater. Sci.* (2012).
- [4] MARELLE, V. et al., “New Developments in ALCYONE 2.0 Fuel Performance Code”, *Top Fuel 2016* (2016).
- [5] SOBA, A., DENIS, A., DIONISIO 2.0: New Version of the Code for Simulating a Whole Nuclear Fuel Rod Under Extended Irradiation, *Nucl. Eng. Des.* (2015)
- [6] FIORINA, C., CLIFFORD, I., AUFIERO, M., MIKITYUK, K., *Nucl. Eng. Des.*, 294 (2015) 24–37.
- [7] SCOLARO, A., ROBERT, Y., FIORINA, C., CLIFFORD, I., PAUTZ, A., “Coupling Methodology for the Multidimensional Fuel Performance Code OFFBEAT and the Monte Carlo Neutron Transport Code Serpent”, *TopFuel 2019* (2019).
- [8] LASSMANN, K., TRANSURANUS: A Fuel Rod Analysis Code Ready for Use, *J. Nucl. Mater.* (1992).
- [9] CLIFFORD, I., PECCHIA, M., MUKIN, R., COZZO, C., FERROUKHI, H., GORZEL, A., Studies on the Effects of Local Power Peaking on Heat Transfer under Dryout Conditions in BWRs, *Ann. Nucl. Energy* **130** (2019) 440–451.
- [10] SCOLARO, A., CLIFFORD, I., FIORINA, C., PAUTZ, A., “First Steps Towards the Development of A 3D Nuclear Fuel Behaviour Solver with OpenFOAM”, *ICONE 2018*, London, 2018.
- [11] SCOLARO, A., CLIFFORD, I., FIORINA, C., PAUTZ, A., “Cladding Plasticity Modelling with the Multidimensional Fuel Performance Code OFFBEAT”, *TopFuel 2019*, 2019.
- [12] LIU, W. et al., “Numerical Method of Modelling Creep of Zirconium-Alloy Cladding in a Multi-Physics Fuel Performance Code”, *LWR Fuel Performance Meeting*, *Top Fuel 2013*, 2013.
- [13] WELLER, H. G., TABOR, G., JASAK, H., FUREBY, C., A Tensorial Approach to Computational Continuum Mechanics Using Object-Oriented Techniques, *Comput. Phys.* (1998).
- [14] JASAK, H., WELLER, H.G., Application of The Finite Volume Method and Unstructured Meshes to Linear Elasticity, *Int. J. Numer. Methods Eng.* (2000).
- [15] HAGRMAN, D.L., REYMANN, G.A., MATPRO-Version 11: A Handbook of Materials Properties for Use in The Analysis of Light Water Reactor Fuel Rod Behaviour, 1979.
- [16] KIM, Y., PARK, J., CLEVELAND, J., “Thermophysical Properties Database of Materials for Light Water Reactors and Heavy Water Reactors,” 2006.
- [17] BERNA, G.A., BEYER, G.A., DAVIS, K.L., LANNING, D.D., “FRAPCON-3: A Computer Code for the Calculation of Steady-State, Thermal-Mechanical Behaviour of Oxide Fuel Rods for High burnup, 1997.
- [18] LIMBÄCK, M., ANDERSSON, T., “A Model for Analysis of the Effect of Final Annealing on the In- and Out-of-Reactor Creep Behaviour of Zircaloy Cladding”, *Zirconium in the Nuclear Industry: Eleventh International Symposium*, 2009.
- [19] MATSUO, Y., Thermal Creep of Zircaloy-4 Cladding under Internal Pressure, *J. Nucl. Sci. Technol.* (1987).
- [20] SPENCER, B.W., WILLIAMSON, R.L., STAFFORD, D.S., NOVASCONE, S.R., HALES, J.D., PASTORE, G., 3D Modelling of Missing Pellet Surface Defects in BWR Fuel, *Nucl. Eng. Des.* **307** (2016) 155–171.
- [21] FIORINA, C., AMATI, G., RUGGIERO, V., SPISSO, I., “SHAPE Project Milano Multiphysics: Evaluation of the Intel Xeon Phi performances for high fidelity nuclear applications,” Sep. 2018.

THREE-DIMENSIONAL PCI MODELLING IN DIONISIO 3.0

E. GOLDBERG, A. SOBA
Comisión Nacional de Energía Atómica,
Provincia de Buenos Aires, Argentina
Email: ezequielgoldberg@cnea.gov.ar

Abstract

A recently developed three-dimensional finite element model for pellet-cladding interaction (PCI) based in the Cohesive Zone Method, originally developed to treat discontinuities that progress in the continuum, in the 3.0 version of the DIONISIO code is presented. Given that the numerical technique used in DIONISIO is based on the finite element method to solve differential equations over defined domains, the development of a cohesive zone method provides a very robust formulation to manage the gap between pellet and cladding treated as a discontinuity. The approach resulted in a natural mode to tackle PCI considering specifically the cylindrical geometry of pellet and cladding, being innocuous when contact surfaces are apart, and presenting the expected behaviour through the entirety of contact and in the case that the surfaces were to disjoin any number of times during the simulation. Selected results of the model compared to special experiments designed to simulate the pellet-cladding thermomechanical interaction and under irradiation experiments taken from the IAEA database as well as a deep discussion about the advantages and shortcomings of this methodology are presented. Additionally, allowing the use of three-dimensional geometries, this model offers the possibility of performing simulations of asymmetric scenarios such as certain oblations or eccentricity of the pellet or the cladding, heating conditions regarding the position of the rod in a reactor core, pellet superficial defects as a result of fuel element assembly and ballooning of the cladding in LOCA cases, among others.

1. INTRODUCTION

The DIONISIO nuclear fuel code simulates many of the phenomena that occur to a fuel rod while being irradiated, both under typical operation and accident conditions of a nuclear reactor. The models included predict the thermo-chemical and thermo-mechanical behaviour of the rod, the thermo-hydraulic performance of the coolant, thermal variations in the plenum, the release of different species generated in the pellet, amongst the vast amount of processes that can come to pass in a nuclear fuel element such as pellet-cladding interaction (PCI) and fracture. The system involving the pellet, gap, and cladding is solved using the finite element method (FEM). The current version of the code allows the user to choose an axisymmetric [1, 2] or three-dimensional domain [3]. The user can select a given number of sectors to divide the rod, to subject them to diverse linear power histories, with the objective of better representing the nonuniform neutron flux distribution and to vary boundary conditions along the rod length. Differential equations are solved for strain, stress, and heat considering a representative pellet and the cladding part for each of these sectors, which contain a number of pellets. Thermal expansion, creep, elastoplastic deformation, swelling, and densification of the pellet and growth under irradiation of the cladding are all taken into account over the material system [4–7].

The interaction with the pellet makes a considerable contribution to the mechanical demand to which the cladding is subjected, induced by the pellet's swelling and thermal expansion, and the accompanying significant external pressure applied to the cladding, in addition to the challenge that it represents from a computational point of view. The phenomenon must be considered in different scenarios and under several operating environments, such as low burnup, in CANDU [8] and PWR/BWR [9,10] type reactors, and also in high burnup (HB) circumstances [11]. In the case of accident conditions, especially in RIA [12], PCI must be taken into account given that it may allow short power pulses to cause severe damage.

In addition to theoretical, analytical, and experimental research of these events in the past [13–19], there is an ongoing high volume of relevant work being done on said topic, as well as new simulations and experiments providing different solutions and alternative points of view. Examples of this are tests being carried out on systems that emulate PCI conditions, acquiring strain, and stress data in idealized, highly controlled environments with ease of measurement. This kind of study without irradiation, emulates high power ramps [12, 20], or subjects sheathings of Zry or new ATF materials, to typical fields of stress in PCI [21–23], gathering valuable data which enables the validation of numerical models. On the other hand, tests under irradiation, which prove to be of higher difficulty regarding the acquisition of data, are continuously performed in an assortment of facilities [16–18, 24–27]. Accident tolerant fuel claddings need the consideration of the requirements to which they will be subjected to, including an analysis of PCI during operation conditions by carrying out numerical simulations and experiments of their behaviour [28, 29].

Several nuclear fuel codes contain models devoted to simulating PCI applying axial symmetry for the domain containing the pellet, gap, and cladding, considering different axial positions of the rod to evaluate points of thermo-mechanical interaction (1.5D [30–34] and 2D axisymmetric [35–38]). Coupled code systems are quite frequent as well, making use of FEM packages to perform simulations of the thermo-mechanical interaction and linking the results with fuel codes, of which many examples can be found in the literature [9,33,35,38,39].

In recent years, a few codes have attempted to approach PCI with three-dimensional domains instead of considering certain symmetries. A 3D module dedicated to PCI simulation was developed in FRAPCON-3.4 [40]; the BISON code also treats the interaction explicitly in three dimensions [41], to name a few. One of the latest published versions of DIONISIO (3.0) [3] includes a new contact algorithm based on cohesive elements developed for three-dimensional domains for the interfaces between pellet and cladding and between pellets, with a contact law that does not modify the resolution matrix of the system, simplifying the solution and making it easier to parallelize. We will discuss the advantages and drawbacks of this choice in the next section.

2. COHESIVE ZONE PCI MODEL

The concept of a Cohesive Zone was conceived by Barenblatt (1962) [42], Dugdale (1960) [43], Rice (1968) [44] to treat discontinuities within the continuum such as cracks. The fracture was considered as a gradual phenomenon of separation of two virtual surfaces that are adjacent and are considered a prolongation of the tip of the fissure. The separation is resisted by forces of cohesion expressed through laws of stress-separation that relate the microstructural failure mechanism to the field of deformation of the continuum. Whereas there is no stress transmitted between surfaces for a conventional crack, the “virtual fissure” that the cohesive zone describes is a dynamic field of reciprocal stress. The process of fracture is represented as the decline of the material strength on the aforementioned virtual surfaces. The atomic structure of the material changes when external pressure is exerted, which reflects as variations in the cohesive traction. This force increases up to a critical separation distance, where it decreases towards zero, determining the creation of a macroscopic crack.

Similarly, two real surfaces could be simulated as if they were a virtual separation. The law governing the stress as a function of the distance has no effect when surfaces are not in contact and defines the behaviour of the force when contact is experienced [45]. Considering all components of stress (normal and tangential) as behaving linearly with distance, they are calculated as follows:

$$T_n = \Phi \delta_n \quad T_t = \Phi \delta_t \mu \quad (1)$$

where Φ is derived from the materials’ Young Modulus, δ_n is the normal distance, δ_t the distance of sliding (when in contact) and μ represents the coefficient of friction between surfaces. The model of the continuous parts remains in the usual manner, by classical constitutive equations, such as Von Mises plasticity considering large deformations [44–46].

We can express the general equations for two contacting bodies as:

$$\begin{aligned} \nabla \cdot \sigma + f^\Omega &= \frac{d^2 u}{dt^2} && \text{for } \Omega \\ n \cdot \sigma &= t && \text{for } \Gamma_t \\ u &= u_0 && \text{for } \Gamma_u \\ n_d^+ \cdot \sigma &= t_c^+ ; n_d^- \cdot \sigma = t_c^- && \text{for } \Gamma_d \end{aligned} \quad (2)$$

with f^Ω representing volumetric forces, t fixed stresses over the domain or the discontinuity (c), u being the displacement field and σ the stress tensor. As for the domains, Γ stands for the surface of the volume and Ω for the volume itself. The equation is assembled in the weak form as follows:

$$\int_{\Omega} (\rho_0 \ddot{u} + \bar{\sigma} : \nabla u) d\Omega + \int_{\partial\Omega_c} \|u\| T_c d\Gamma_c = \int_{\Omega} f^\Omega \bar{u} d\Omega + \int_{\Gamma} t \bar{u} d\Gamma + R \quad (3)$$

where $\|u\|$ represents the jump in discontinuity $d\Gamma_c = \Gamma_{c+} - \Gamma_{c-}$ and T_c is the cohesive element’s stress function.

The formulation conveys an equation of dynamic equilibrium, in which the first integral on the left side of the equation contains the displacement vector’s double derivative in time multiplied by the mass. Additionally, the

second integral of the left side is only considered for the cohesive elements and accounts for the role of the disjointedness. The right side of the equation does not differ from that used in the continuum. It is important to highlight that the value of the analytical T_c function depends on the physical model, whether a material that is brittle [47] or ductile [48] or large displacements are being considered [46] among other examples. A wide assortment of models is available in the literature [44, 45, 47, 48, 51–54].

As per the above explanation, the CZM within the FEM presents several advantages in contact problems over other methods. Nodes that already exist on the gap boundaries are used to construct the cohesive elements. Since no new nodes are needed, no equations are appended to the system, keeping the properties that the matrices have for the continuum. Furthermore, all coding is introduced where each cohesive element's local contribution is calculated. Finally, given that the method offers a natural response when surfaces are distanced after contact, the cycle involving contact and separation can be fulfilled any number of required times.

We applied the method in cases with a relative tangential (axial) displacement between contact surfaces (see next section) and added an axial force in one of the contactors, in order to analyze a scenario that could be lived in any PCI situation in real experiments. In all cases, the cohesive elements show a good performance. The CZM might cause the contact surfaces to undergo some non-physical interpenetration during the iterative process. We reduce the impact of this problem using a dynamic explicit solver with a sufficiently small fictitious critical time step (different from the actual time step of the power history) that allows us to calculate the displacements with small increments, which at the same time limits the overlapping to a minimum (typically no more than 3% of the thickness of the cladding) while ensuring convergence and without losing stability [48–50]. Several examples of the algorithm in use are presented in the next section.

3. RESULTS

3.1. Comparison with a controlled experiment

Reference [22] studies a composite of nuclear grade silicon carbide fibre and matrix, subjected to a high temperature gradient, given that it is a material to be considered for fuel cladding of accident tolerant type. In their work, experimental results are compared to those obtained using commercial software COMSOL (Stockholm, Sweden) to create a FEM model. The SiC sample has an inlaid solid alumina substitute (bonded with an adhesive), which is electrically heated, producing thermal expansion which results in pressure exerted on the sample. In our model, we do not simulate the ceramic adhesive because it provides a buffer for strain and stress and we intend to study the surfaces' mechanical interaction. Figure 1 displays the geometry and its temperature on the first and last steps of the simulation. Displacements in the radial direction were increased by a factor of 25, causing an unreal interpenetration of the surfaces that appears bigger than it is; real values are below ten microns (0.5% of the thickness of the cladding). Modifications of this case have been simulated with an initial axial displacement of the alumina surrogate to have the cohesive element faces not perfectly match, as well as applying an axial force to the alumina surrogate to test the tangential (specifically, axial) behaviour of the CZM. Results for strain and stress of the continuous material remain as in the original case; the only noteworthy difference is the expected increase in axial tangential force by the cohesive elements.

Figure 2 presents a good correlation of radial and hoop components of mechanical and total (mechanical plus thermal) strain between Dionisio and the commercial software model [22], with the exception of the adhesive (0.9 mm from the centre up to 1.2 mm), which takes in a considerable amount of the strain in the radial direction. Results of stress along both the length and the thickness of the sample show very similar values for both models (Fig.3), excluding the step caused by the bond layer.

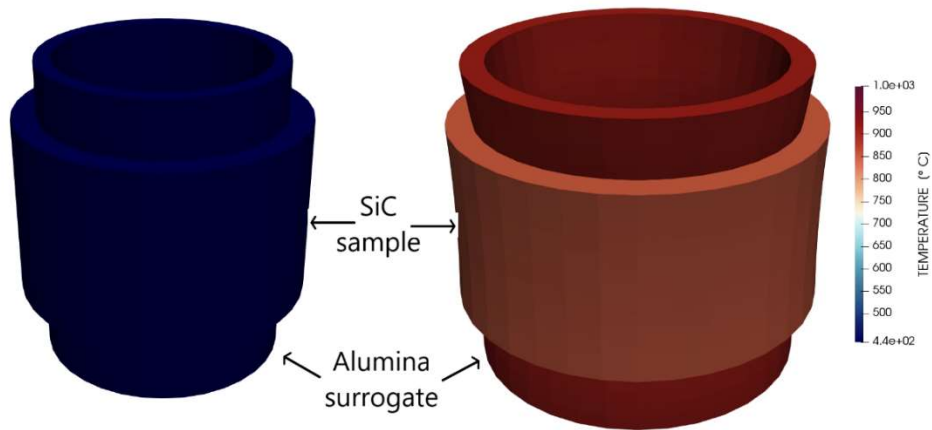


FIG. 1. Initial (left) and final (right) status of the domain (radial displacements $\times 25$).

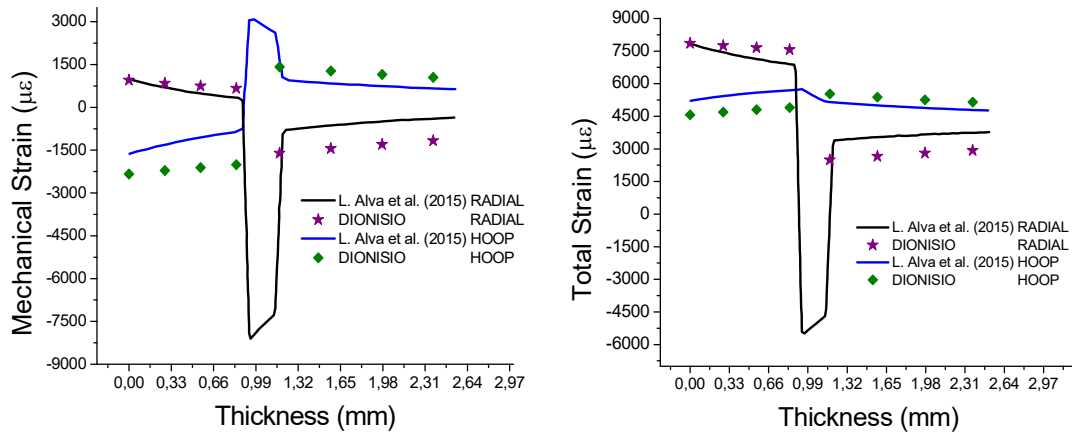


FIG. 2. Hoop and radial strain through the thickness of the sample compared to numerical results.

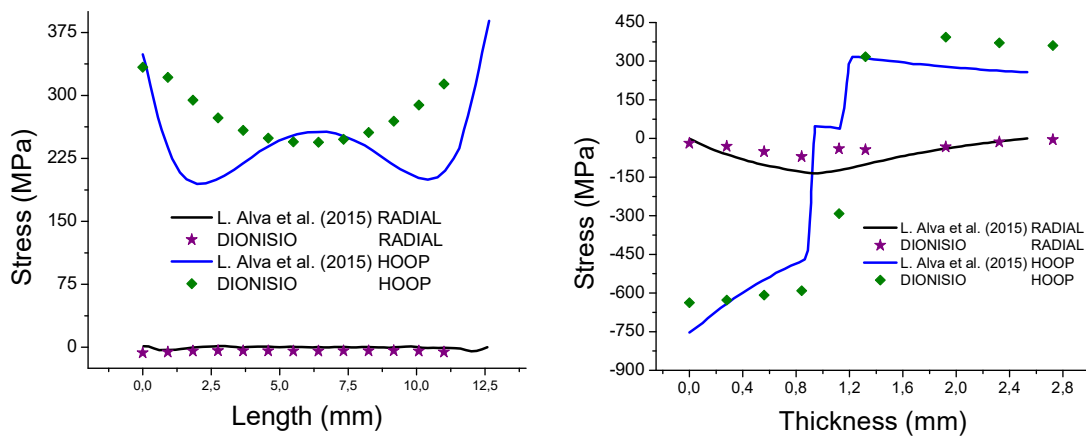


FIG. 3. Hoop and radial stress along the length (left) and thickness (right) of the sample, compared to numerical results.

3.2. DIONISIO 3D results

3.2.1. Experimental fuel element no. 51 – INR Pitesti Romania

The Romanian irradiation test programme had the main objective of providing information about the behaviour of fuel elements of CANDU type with the design parameters' limits. Two tests were conducted on elements coded 89 and 51, of which we chose to compare results to the latter [55]. Experimental measurements of the ridge along the length of the rod were made for different angles of the circumference.

In Fig.4, we present a comparison of the diameter of the cladding at two different angles for the entire length of the stack, after irradiation. Numerical results obtained with DIONISIO correlate very well with experimental measurements made in situ, showing varying ridges at different angles of the rod.

Figure 5 presents the progress of the radii of the contact surfaces (i.e. the radius of the pellet and inner radius of the cladding) with the hoop component of the stress tensor of the cladding, plotted as they vary with the burnup, to exhibit the stress increase when contact takes place and the decrease when the bodies separate.

3.2.2. The MOX experiment [56]

The earliest prototypes of MOX fuels designed in Argentina for PHWR reactors, constructed in CNEA at the Alpha facility, were irradiated at Petten, Holland in the high flux reactor. Examinations after irradiation took place at Forschungszentrum, Karlsruhe, Germany. We have focused on the rod labelled A.1.3 to evaluate the ridges on the cladding accompanying the distribution of the pellets.

In Fig.6 colormap distributions of the domain at a peak of linear power can be observed for a representative pellet of the MOX experiment. The image on the left shows Von Mises stress with the highest values at the centre of the pellet, decreasing in both axial and radial directions. Values reached in the centre of the pellet are fairly high because the model has yet to consider creep or microcracks in the pellet. Nevertheless, it contains a term of viscoplasticity that causes relaxation of stresses with time. On the right of the image, a thermal profile is displayed with values decreasing in the radial direction from the centre outwards. Displacements in the radial direction were augmented 25 times to enable the visualization of the “bamboo effect” on the cladding.

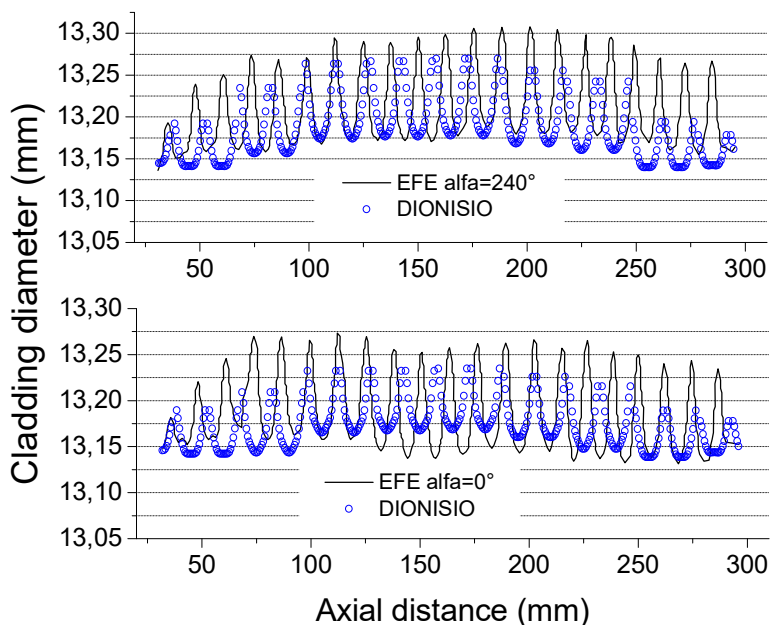


FIG. 4. Cladding diameter for the entire rod at different angles. Numerical results with DIONISIO over post-irradiation experimental measurements.

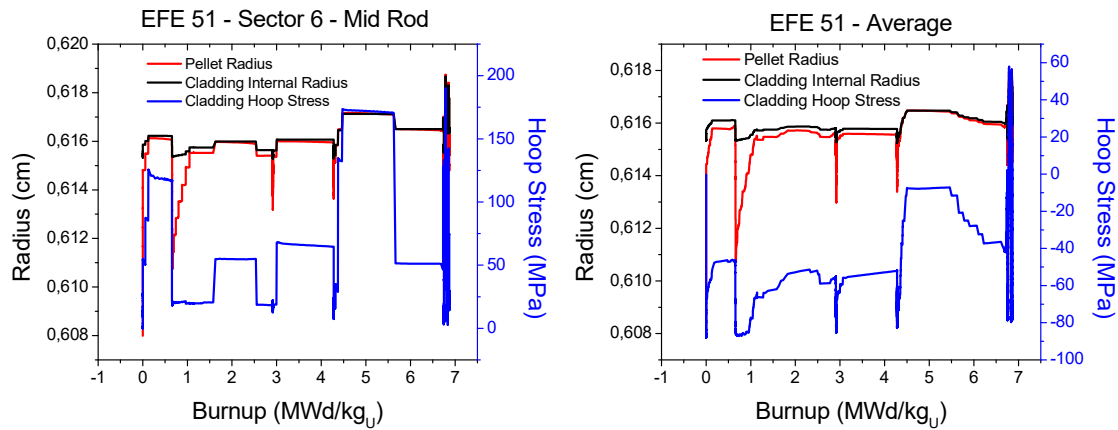


FIG. 5. Evolution of pellet and cladding inner radius (contact surfaces) and hoop stress. Left: sector 6 (mid rod, highest burnup). Right: rod average.

4. CONCLUSIONS

A new contact algorithm for the DIONISIO code was developed based on the Cohesive Zone Method, a framework encompassed in the concepts of the FEM, conceived to work with discontinuities in fracture mechanics. Despite some restrictions previously discussed, the new algorithm displays a very good performance when compared to experimental tests that emulate PCI conditions. When including the phenomenon of irradiation and the interconnection with the rest of the modules of the DIONISIO code, the new model provides a satisfactory prediction of radial cladding deformation, including “bamboo effects”. We exhibit in this work the results of certain experiments such as the INR N° 51 rod experiment and the MOX experiment. Results of asymmetric experiments were analyzed to show the array of possibilities that a three-dimensional code provides, with special emphasis in cases where the asymmetry plays a very important part in the resulting behaviour of the fuel elements. Even though the cases selected for comparison are comprised of Zircalloy or SiC, any material can be simulated adjusting the corresponding properties, including other candidate materials for Accident Tolerant Fuels.

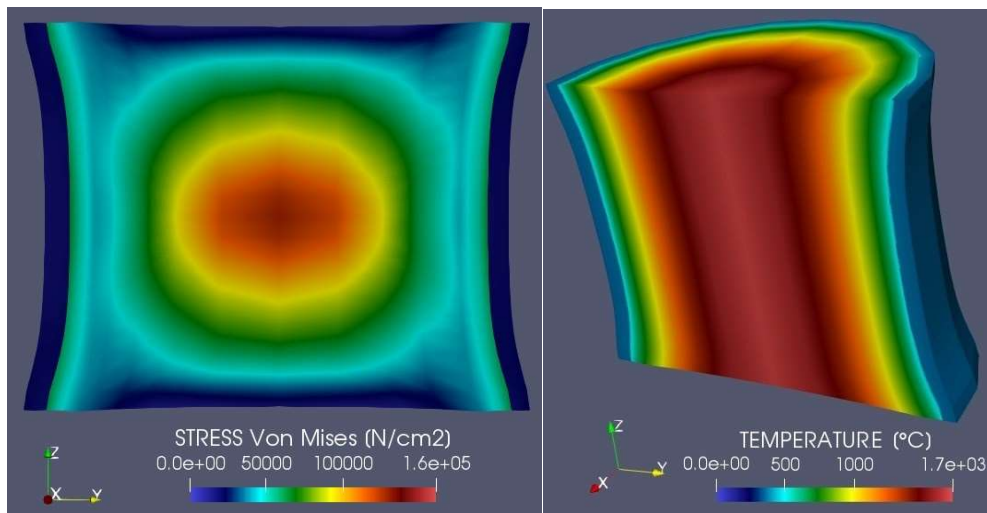


FIG. 6. Von Mises stress (left) and temperature (right) colormaps of a representative pellet of the MOX experiment (radial displacements $\times 25$).

ACKNOWLEDGMENTS

We thank IAEA for the grant which made possible the presentation of this work at the Technical Meeting. E. Goldberg has a scholarship from Comisión Nacional de Energía Atómica. A. Soba is a researcher at the CONICET.

REFERENCES

- [1] SOBA, A., Simulación Del Comportamiento Termomecánico De Una Barra Combustible En Operación, Doctoral thesis, FCEyN, UBA (2007).
- [2] SOBA A., DENIS, A., Simulation with Dionisio 1.0 of Thermal and Mechanical Pellet-Cladding Interaction in Nuclear Fuel Rods, *J. Nucl. Mater.* **374** (2008).
- [3] GOLDBERG, E., LOZA PERALTA, M. E., SOBA, A. DIONISIO 3.0: Comprehensive 3D Nuclear Fuel Simulation Through PCMI Cohesive and PLENUM Models, *J. Nuclear Materials* (2019).
- [4] SOBA, A., DENIS, A., DIONISIO 2.0: New Version of the Code for Simulating a Whole Nuclear Fuel Rod under Extended Irradiation, *Nuclear Engineering and Design* **292** (2015).
- [5] SOBA, A., DENIS, A., ROMERO, L., VILLARINO, E., SARDELLA, F., A High Burnup Model Developed for the DIONISIO Code, *Journal of Nuclear Materials* **433** (2013).
- [6] SOBA, A., LEMES, M., DENIS, A., An Empirical Formulation to Describe the Evolution of the High Burnup Structure, *Journal of Nuclear Materials* **456** (2015).
- [7] SOBA, A., LEMES, M., GONZÁLEZ, M. E., DENIS, A., ROMERO, L., Simulation of the Behaviour of Nuclear Fuel under High Burnup Conditions, *Annals of Nuclear Energy* **70** (2014).
- [8] LEWIS, B.J., IGLESIAS, F.C., DICKSON, R.S., WILLIAMS, A., Overview of High-Temperature Fuel Behaviour with Relevance to CANDU Fuel, *Journal of Nuclear Materials* **394** (2009).
- [9] STIMPSON, S., POWERS, J., CLARNO, K., PAWLOWSKI, R., GARDNER, R., NOVASCONE, S., GAMBLE, K., WILLIAMSON, R., Pellet-Clad Mechanical Interaction Screening Using VERA Applied to Watts Bar Unit 1 Cycles 1–3, *Nuclear Engineering and Design* **327** (2018).
- [10] Herranz, L.E., Vallejo, Khvostov, I., G., Sercombe, J., Zhou, G., Assessment of Fuel Rod Performance Codes under Ramp Scenarios Investigated within the SCIP Project, *Nuclear Engineering and Design* **241** (2011).
- [11] SUZUKI, M., UETSUKA, H., SAITOU, H., Analysis of Mechanical Load on Cladding Induced by Fuel Swelling during Power Ramp in High Burnup Rod by Fuel Performance Code FEMAXI-6, *Nuclear Engineering and Design* **229** (2004).
- [12] YUEH, K., KARLSSON, J., STJARNASATER, J., SCHRIRE, D., LEDERGERBER, G., MUNOZ-REJA, C., HALLSTADIUS L., Fuel Cladding Behaviour under Rapid Loading Conditions, *Journal of Nuclear Materials* **469** (2016).
- [13] MATHEWS, J., The Quantitative Description of Deformation and Stress in Cylindrical Fast Reactor Fuel Pins, *Advances in Nuclear Science and Technology* **6** (1972).
- [14] CAILLOT, L., LINET, B., LEMAIGNAN, C., “Pellet Clad Interaction in PWR Fuel. Analytical Irradiation Experiment and Finite Element Modelling”, Proc. SMIRT 12, Stuttgart, Germany, 1993.
- [15] DENIS, A., SOBA, A., Simulation of Pellet-Cladding Thermomechanical Interaction and Fission Gas Release, *Nuclear Engineering and Design* **223** (2003).
- [16] TURNBULL, J.A., “IFPE/Contact Rev.1, Database for Contact Experiments Irradiated at CEA Grenoble”, Revision 1, January 2003.
- [17] BRUET, M., DODALIER, J., MELIN, P., POINTUD, M.L.: "CONTACT 1 and 2 Experiments: Behaviour of PWR Fuel Rods up to 15000 MW·d/t", IAEA Specialists' Meeting on Water Reactor Fuel Elements Performance Computer Modelling, Blackpool, UK, 17-21 March 1980.
- [18] CHARLES, M., LEMAIGNAN, C., Fuel Performance under Normal PWR Conditions: A Review of Relevant Experimental Results and Models, *J. Nucl. Mater.* **188** (1992).
- [19] KINOSHITA, ICHIKAWA. Analysis of fuel rod deformation, *Nucl. Eng. and Des.* **56** (1980).
- [20] DESQUINES, J., KOSS, D.A., MOTTA, A.T., CAZALIS, B., PETIT, M., The Issue of Stress State during Mechanical Tests to Assess Cladding Performance during a Reactivity-Initiated Accident (RIA), *Journal Of Nuclear Materials* **412** (2011).
- [21] CAZALIS, B., DESQUINES, J., CARASSOU, S., LE JOLU, T., BERNAUDAT, C., The Plane Strain Tests in the PROMETRA Program, *Journal of Nuclear Materials* **472** (2016).
- [22] ALVA, L., SHAPOVALOV, K., JACOBSEN, G.M., BACK, C.A., HUANG, X., Experimental Study of Thermo-Mechanical Behaviour of SiC Composite Tubing under High Temperature Gradient Using Solid Surrogate, *Journal of Nuclear Materials* **466** (2015).
- [23] KIM, S-K, BANG, J-G., KIM, D-H., LIM, I-S., YANG, Y-S, SONG, K-W, KIM, D-S., Hoop Strength and Ductility Evaluation of Irradiated Fuel Cladding, *Nuclear Engineering and Design* **239** (2009).

- [24] SAGRADO, I. C., HERRANZ, L.E., Modelling RIA Benchmark Cases with FRAPTRAN and SCANAIR: A Comparative Exercise, *Nuclear Engineering and Design* **278** (2014).
- [25] ALAM, T., KHAN, M.K. PATHAKA, M., RAVIB, K., SINGHB, R., GUPTAB, S.K., A Review on the Clad Failure Studies, *Nuclear Engineering and Design* **241** (2011).
- [26] LUXAT, J.C., NOVOG, D.R., A Generalized Failure Map for Fuel Elements Subject to a Power Pulse, *Nuclear Engineering and Design* **241** (2011).
- [27] DE MENIBUS, A.H., SERCOMBE, J., AUZOUX, Q., POUSSARD, C., Thermomechanical Loading Applied on the Cladding Tube during the Pellet Cladding Mechanical Interaction Phase of a Rapid Reactivity Initiated Accident, *Journal of Nuclear Materials* **453** (2014).
- [28] Kurt A. Terrani. Accident tolerant fuel cladding development: Promise, status, and challenges. *Journal of Nuclear Materials* **501** (2018).
- [29] BEN-BELGACEM, M., RICHET, V., TERRANI, K.A., KATOH, Y., SNEAD, L.L., Thermo-Mechanical Analysis of LWR SiC/SiC Composite Cladding, *Journal of Nuclear Materials* **447** (2014).
- [30] LASSMANN, K., TRANSURANUS: A Fuel Rod Analysis Code Ready for Use, *J. Nucl. Mater.* 188 (1992).
- [31] MARINO, A.C., SAVINO, E.J., HARRIAGUE, S., BACO (Barra Combustible) Code Version 2.20: A Thermo-Mechanical Description of a Nuclear Fuel Rod, *J. Nucl. Mater.* **229** (1996) 155-168.
- [32] PALMER, I., ROSSITER, G., WHITE, R., “Development and Validation of The ENIGMA Code for MOX Fuel Performance Modelling”, IAEA/OECD Symposium on MOX Fuel Cycle Technologies for Medium and Long Term Deployment, Vienna, 2000.
- [33] GEELHOOD, K., LUSCHER, W., BEYER, C., FLANAGAN, M., FRAPCON-3.4: A Computer Code for the Calculation of Steady-State, Thermal-Mechanical Behaviour of Oxide Fuel Rods for High Burnup, NUREG/CR-7022 (1) (2011).
- [34] MOAL, A., GEORGENTHUM, V., MARCHAND, O., SCANAIR: A Transient Fuel Performance Code, Part One: General Modelling Description, *Nuclear Engineering and Design* **280** (2014).
- [35] CHEON, J-S., LEE, B-H., KOO, Y-H., OH, J-Y., SOHN, D-S., Evaluation of a Pellet-Clad Mechanical Interaction in Mixed Oxide Fuels during Power Transients by Using Axisymmetric Finite Element Modelling, *Nuclear Engineering and Design* **231** (2004).
- [36] SUZUKI, M., SAITOU, H., UDAGAWA, Y., NAGASE, F., Light Water Reactor Fuel Analysis Code FEMAXI-7; Model and Structure, JAEA-Data/Code 2013-005 (2013).
- [37] ZANGARI, A., MONTGOMERY, R., Fuel Analysis and Licensing Code: FALCON MOD01, Volume 2: User's Manual, Technical Report 1011308, EPRI (2004).
- [38] LINET, B., SUO, X., “The METEOR/TOUTATIS Code: A 2D/3D Code for Fuel Behaviour Simulation”, Canadian Nuclear Society/American Nuclear Society 4th International Conference on Simulation Methods in Nuclear Engineering, Canada, 1993.
- [39] BAURENS, B., SERCOMBE, J., RIGLET-MARTIAL, C., DESGRANGES, L., TROTIGNON, L., MAUGIS, P., 3D Thermo-Chemical–Mechanical Simulation of Power Ramps with ALCYONE Fuel Code, *J. Nucl. Mater.* **452** (2014) 578–594.
- [40] KIM, H., SEO, S.K., LEE, S.U., YANG, Y.S., Development of NUFORM3D Module with FRAPCON3.4 for Simulation of Pellet-Cladding Mechanical Interaction, *Nuclear Engineering and Design* **318** (2017).
- [41] CAPPS, N., KENNARD, M., LIU, W., WIRTH, B.D., RASHID, J., PCI Analysis of a Commercial PWR Using BISON Fuel Performance Code, *Nuclear Engineering and Design* **324** (2017).
- [42] BARENBLATT, G. I., The Mathematical Theory of Equilibrium Cracks in Brittle Fracture, *Advances in applied mechanics* **7** (1962).
- [43] DUGDALE, D.S., Yielding of Steel Sheets Containing Slits, *Journal of the Mechanics and Physics of Solids* **8** (1960).
- [44] RICE, J.R., Mathematical Analysis in the Mechanics of Fracture, *Fracture: An Advanced Treatise* **2** (1968).
- [45] XU, X.P., NEEDLEMAN, A., Numerical Simulations of Fast Crack Growth in Brittle Solids, *Journal of the Mechanics and Physics of Solids* **42**[9] (1994).
- [46] BATHE, K-J., *Finite Element Procedures*, Prentice Hall (1996).
- [47] TVERGAARD, V., NEEDLEMAN, A., Effects of Nonlocal Damage in Porous Plastic Solids, *Int. J. Solids Struct.*, **32** [8/9] (1995).
- [48] NOELS, L., RADOVITZKY, R., A General Discontinuous Galerkin Method for Finite Hyperelasticity. Formulation and Numerical Applications, *Int. J. Numer. Meth. Engng* **68** (2006) 64–97.
- [49] RADOVITZKY, R., SEAGRAVES, A., TUPEK, M., NOELS, L., A Scalable 3D Fracture and Fragmentation Algorithm Based on a Hybrid, Discontinuous Galerkin, Cohesive Element Method, *Comput. Methods Appl. Mech. Engrg.* **200** (2011).
- [50] NOELS, L., RADOVITZKY, R., An Explicit Discontinuous Galerkin Method for Non-Linear Solid Dynamics: Formulation, Parallel Implementation and Scalability Properties. *Int. J. Numer. Meth. Engng;* **74** (2008) 1393–1420.
- [51] PLANAS, J., ELICES, M., GUINEA, G.V., GÓMEZ, F.J., CENDON, D.A., ARBILLA, I., Generalizations and Specializations of Cohesive Crack Models, *Engineering Fracture Mechanics* **70** (2003).

- [52] RADOVITZKY, R., SEAGRAVES, A., TUPEK, M., NOELS, L., A Scalable 3D Fracture and Fragmentation Algorithm Based on a Hybrid, Discontinuous Galerkin, Cohesive Element Method, *Comput. Methods Appl. Mech. Engrg.* **200** (2011).
- [53] Seif, T., Ductile Fracture Analysis in a Steel Plate by Cohesive Zone Modelling, Master thesis (2014).
- [54] CIRAK, F., ORTIZ, M., PANDOLFI, A., A Cohesive Approach to Thin-Shell Fracture and Fragmentation, *Computer Methods Applied Mechanics and Engineering Comput.* **194** (2005).
- [55] PARASCHIV, M. C., The Romanian Irradiation Tests Prepared for IAEA/OECD Database, Private communication.
- [56] MARINO, A., PÉREZ, E., ADELFIANG, P., Irradiation of Argentine (U,Pu)O₂ MOX Fuels: Post Irradiation Results and Experimental Analysis with the BACO Code, *J. Nucl. Mater.* **229** (1996) 169-186.

DEVELOPMENT AND ASSESSMENT OF THE BISON FUEL PERFORMANCE CODE FOR PCMI AND PCI ANALYSIS

G. PASTORE, R.L. WILLIAMSON, B.W. SPENCER, A. CASAGRANDA, J.D. HALES
Idaho National Laboratory,
Idaho Falls, United States
Email: Giovanni.Pastore@inl.gov

Y.R. RASHID, W. LIU
Structural Integrity Associates, Inc.,
San Diego, United States

Abstract

BISON is a finite-element based, multidimensional nuclear fuel performance code developed at Idaho National Laboratory (INL). This contribution focuses on the application of BISON to the analysis of Pellet-Cladding Mechanical Interaction (PCMI) and Pellet-Cladding Interaction (PCI) in light water reactor fuel rods. First, we present BISON simulations of several PCMI fuel rod problems and comparisons of results to experimental data of cladding outer diameter and cladding elongation. Second, we present a demonstration of PCMI analysis in presence of a Missing Pellet Surface (MPS) defect using BISON's 3D capability. Third, we give an account of PCI cladding failure models that were developed recently at Structural Integrity Associates and can be applied in PCI screening analyses using BISON.

1. INTRODUCTION

The US Department of Energy (DOE) has been developing state-of-the-art capabilities to simulate nuclear fuel behaviour within the Consortium for Advanced Simulation of Light Water Reactors (CASL) and Nuclear Energy Advanced Modelling and Simulation (NEAMS) programmes. The result of this effort is the BISON code [1], a modern finite-element based, multidimensional fuel performance code which was developed at Idaho National Laboratory (INL).

BISON is built using the Multiphysics Object-Oriented Simulation Environment (MOOSE) framework of INL [2]. BISON can apply 1D, 2D or 3D geometric representations to analyse the integral fuel element behaviour including local, multidimensional effects. The ability to use massively parallel computing for BISON simulations allows for analysing full-length fuel rods in 2D during complex irradiation histories as well as 3D problems. BISON has been applied to modelling various fuel forms including light water reactor (LWR) fuel rods, TRISO fuel particles, and metallic fuel in both rod and plate geometries. The code can be used for both steady-state and transient analysis and has been applied to the simulation of fuel behaviour during normal reactor operation, design-basis accidents and storage conditions.

One important area of BISON application is the analysis of Pellet-Cladding Mechanical Interaction (PCMI) and the related failure mechanism of Pellet-Cladding Interaction – Stress Corrosion Cracking (PCI-SCC) in LWR fuel. In this paper, we provide an overview of BISON development and assessment work performed to date for PCMI and PCI analysis. First, we present BISON simulations of several PCMI fuel rod problems and comparisons of results to experimental data of cladding outer diameter and cladding elongation. Among the considered cases, the Halden test IFA-629.4 is related to participation of INL in the recent PCMI benchmark organized by the OECD/NEA [3]. Second, we present a demonstration of a BISON 3D PCMI analysis in presence of a Missing Pellet Surface (MPS) defect. The simulated case is a BWR fuel rod including a pellet with an MPS defect and undergoing various power transient events. Third, we give an account of PCI-SCC cladding failure models coupled to BISON that were developed at Structural Integrity Associates and can be used for PCI screening analyses.

The structure of the paper is as follows. Section 2 presents BISON analyses of PCMI experiments and comparisons of results to experimental data. Section 3 deals with the application of BISON to a 3D fuel rod analysis in presence of MPS defects under PCMI. Section 4 gives an account of recent developments of PCI failure models for BISON. A summary is provided in Section 5.

2. SIMULATION OF PCMI EXPERIMENTS AND COMPARISONS TO DATA

2.1. Initial assessment to fuel rod experiments from the IFPE database

As part of the BISON validation study presented in [4], comparisons of simulations to rod diameter measurements for several fuel rod irradiation experiments from the International Fuel Performance Experiments (IFPE) database [5] were performed. Because most of the considered experiments involved PCMI, the study represents a first assessment of BISON for PCMI analysis. The experiments simulated with BISON in [4] that included rod diameter measurements are listed in Table 1. For all considered cases, the fuel stack was represented as a smeared fuel column. While this approach was chosen for simplicity, BISON's capabilities include discrete pellet analysis.

TABLE 1. FUEL ROD EXPERIMENTS WITH ROD DIAMETER MEASUREMENTS SIMULATED WITH BISON IN [4]. (DETAILS OF THE EXPERIMENTS CAN BE FOUND IN [5].)

Experiment	Rod	Burnup (MW·d/kgU)	Cladding type	Ramp	Rod diameter comparisons*
Risø-2	GE-m	15.8	Zircaloy-2	Y	Axial average (B, R)
Risø-3	AN2	40.7	Zircaloy-4	Y	Axial average (B), axial peak (R)
Risø-3	GE7	40.9	Zircaloy-2	Y	Axial average (B), axial peak (R)
Risø-3	II3	17.6	Zircaloy-2	Y	Axial average (B, R)
Risø-3	II5	47.6	Zircaloy-2	Y	Axial midplane (B, R)
OSIRIS	H09	46.1	Zircaloy-4	N	Axial average (B)
OSIRIS	J12	26.7	Zircaloy-4	Y	Axial average (B), axial peak (R)
REGATE		47	Zircaloy-4	Y	Axial average (B), axial peak (R)
USPWR	TSQ002	53.2	Zircaloy-4	N	Axial average (B)
USPWR	TSQ022	58.1	Zircaloy-4	N	Axial average (B)
R.E. Ginna	2	51.2	Zircaloy-4	N	Axial average (B)
R.E. Ginna	4	57.0	Zircaloy-4	N	Axial average (B)
Tribulation	BN1/3	50.7	Zircaloy-4	Y	Axial midplane (20.2 MW·d/kgU, B, R)
Tribulation	BN1/4	50.6	Zircaloy-4	N	Axial midplane (19.7 MW·d/kgU, B)
Tribulation	BN3/15	51.1	Zircaloy-4	N	Axial midplane (37.7 MW·d/kgU, B)

* B = after base irradiation, R = after ramp

The comparisons between simulation results and experimental data in terms of rod (i.e. cladding outer) diameter are shown in Fig. 1. Data are shown as measured minus predicted diameter vs. burnup. Results after both base irradiation and power ramps are included. In general, the calculation results after base irradiation (Fig.1-left) point to a tendency to overpredict the reduction in rod diameter early in life (low burnup cases) due to cladding creep-down, and overpredict the increase in diameter occurring late in life (higher burnup) during PCMI, when cladding deformation is controlled by fuel expansion. The fact that the predicted cladding diameter for the higher burnup cases is significantly higher than the measured diameter points to a tendency to overpredict the radial growth of the fuel. This may be partially associated with the lack of a model for pellet-fragment relocation recovery in BISON in [4]. Uncertainty in the calculation of fuel swelling and consideration of fuel creep (neglected in [4]) provide further explanation for the discrepancies. It is worthwhile noting that in general, cladding diametral strain prediction is an open issue for fuel performance codes, as was demonstrated in multiple international benchmark exercises of the International Atomic Energy Agency (IAEA) [6,7].

Eight experiments from Table 1 involved power ramp testing after base irradiation. Post-ramp diameter comparisons for these cases are plotted in Fig. 1-right. To isolate cladding deformation during the ramp test, the differences between diameter at the end of the base irradiation and at the end of the ramp test are shown.

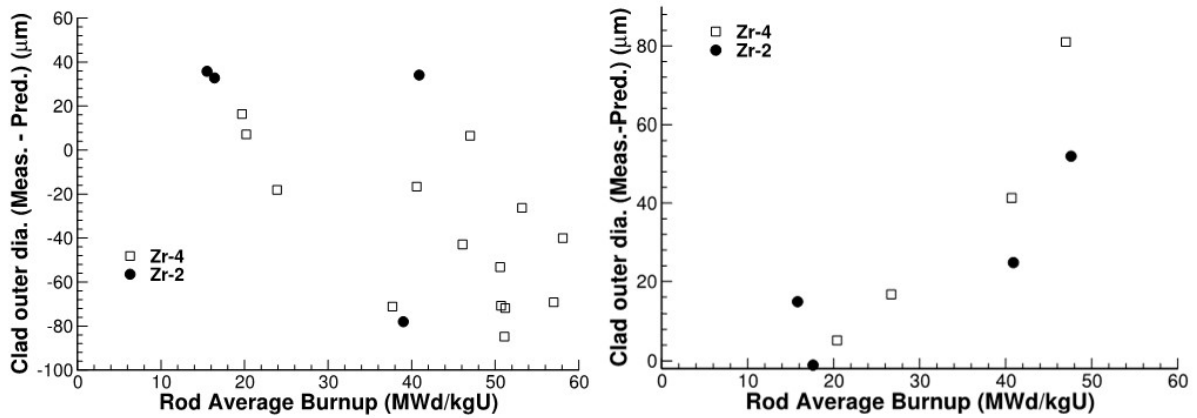


FIG. 1. Difference between measured and predicted rod diameter as a function of burnup during base irradiation (left) and ramp testing (right) (reproduced courtesy of Elsevier [4]).

Comparisons appear reasonable at low burnup; however, they grow worse with increasing burnup. Note that, as opposed to the behaviour during base irradiation, for power ramps the rod diameter increase due to fuel radial growth during PCMI is generally underpredicted. During power ramps, fuel radial growth is mainly due to thermal expansion and gaseous swelling. A recently performed sensitivity study indicated that uncertainties in modelling gaseous fuel swelling significantly impact cladding strain predictions during power ramps [8]. Work is ongoing to improve BISON's gaseous swelling calculation by including in the fission gas model the complexities associated with the transient behaviour of intra-granular bubbles.

Figure 2 illustrates the comparison between calculated and measured cladding outer diameter as a function of axial position, both after the base irradiation and after the power ramp test, for the Risø-3 GE7 case. BISON overpredicts cladding creep-down during base irradiation. The comparison between calculated and measured change in rod diameter during the ramp test indicates that BISON predicts the trend of transient mechanical behaviour during PCMI with reasonable accuracy; however, the differences in magnitude are attributed to the same factors that are at play for Fig. 1. In addition, as mentioned above, modelling of transient fuel gaseous swelling may partly explain the observed discrepancies.

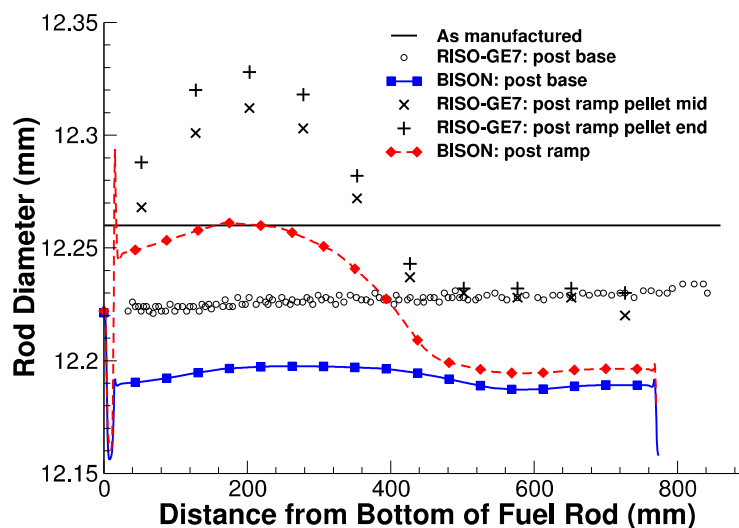


FIG. 2. Comparison of computed and measured rod diameter for the Risø-3 GE7 case (reproduced courtesy of Elsevier [4]).

2.2. Addition of a Relocation Recovery Model to Bison

Following the initial validation study [4] discussed above, a model for pellet-fragment relocation recovery during PCMI was implemented in BISON [9]. The model is activated once the fuel and cladding come into contact and progressively recovers the fuel relocation strain as the cladding pushes the expanding fractured fuel inwards. The default value for the maximum fraction of relocation strain recovered in a given fuel element is 0.5, which is taken from FRAPCON-4.0 [10]. Details of the model are given in [9]. The updated version of BISON with the relocation recovery model was applied to the same set of cases simulated in [4] and listed in Table 1.

By way of example, Fig. 3 shows the comparison between the rod diameter predictions from BISON and the experimental measurement as a function of axial position for the OSIRIS J-12 case (Table 1). The relocation recovery model leads to a significantly more accurate diameter predictions compared to the reference simulation. In addition, the “bamboo” effect on the cladding can be clearly seen. This is related to the use of a discrete-pellet mesh and demonstrates the ability of BISON to capture local PCMI behaviour. Predictions for the whole set of cases (Table 1) are illustrated in Fig. 4. Comparisons are limited to base irradiation in this case. It can be observed that the relocation recovery model generally improves the BISON predictions.

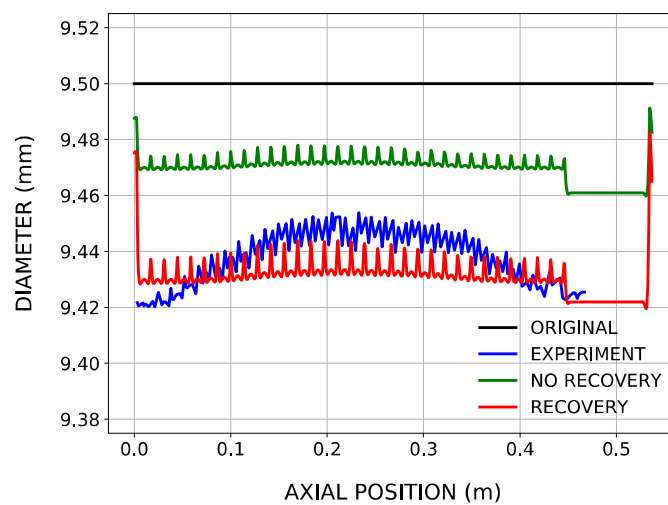


FIG. 3. Comparison of computed and measured rod diameter for the OSIRIS J-12 case (reproduced courtesy of Elsevier [9]).

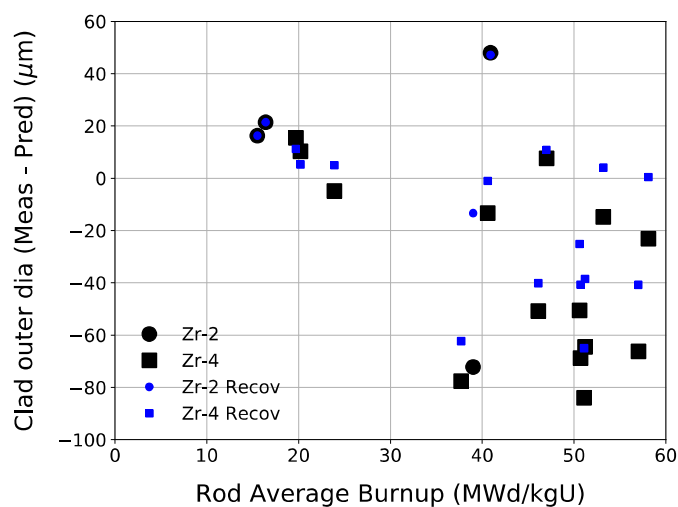


FIG. 4. Difference between measured and predicted rod diameter as a function of burnup during base irradiation, with and without relocation recovery, for the cases listed in Table 1.

2.3. Simulation of the Halden IFA-629.4 ramp test

In the context of INL's participation in the OECD/NEA benchmark on PCMI [3], BISON simulations of the Halden IFA-629.4 test [11] were originally performed. Here, we present updated, most recent BISON simulations of rod 7 in IFA-629.4. The main focus is comparison of calculated cladding elongation to experimental data. As the IFA-629.4 test involved power ramps and PCMI, this study represents an additional assessment of BISON for PCMI modelling. The study also exercises an orthotropic smeared fuel cracking model that had not been applied in previous simulations and a frictional fuel-cladding contact capability that has been recently added to BISON (prior models assumed frictionless contact).

Rod 7 in IFA-629.4 is a UO₂/zircaloy-4 PWR rod base-irradiated to 54.7 MW·d/kgUO₂ before re-fabrication and ramp testing in the Halden HBWR [11]. Using the geometric parameters from [11], a 2D axisymmetric finite-element mesh was developed to represent the rod, including individual fuel pellets. The time-dependent boundary conditions (linear heat rate, coolant temperature) were developed in conjunction with the PCMI benchmark of the OECD/NEA [3]. Various BISON simulations were run to enable parametric analysis. In particular, calculations were performed assuming either elastic fuel without cracking, or creeping fuel with either an orthotropic smeared cracking model [12] and an isotropic softening model for cracking [13].

The IFA-629.4 rod 7 power history for the first 10 days of the Halden irradiation, displayed in Fig. 5, shows that the rod average power is increased in a series of ramps and holds (identified as Phases). Comparisons reported here focus on the Phase 2 ramp. The predicted and measured cladding elongations as a function of rod average linear heat rate are shown in Fig. 6. An estimate of the fuel thermal expansion slope, taken from [11], is also included. A fuel-cladding friction coefficient of 0.3 was assumed for these simulations. However, additional simulations with values varying between 0.1 and 1000 did not indicate a strong sensitivity to this parameter.

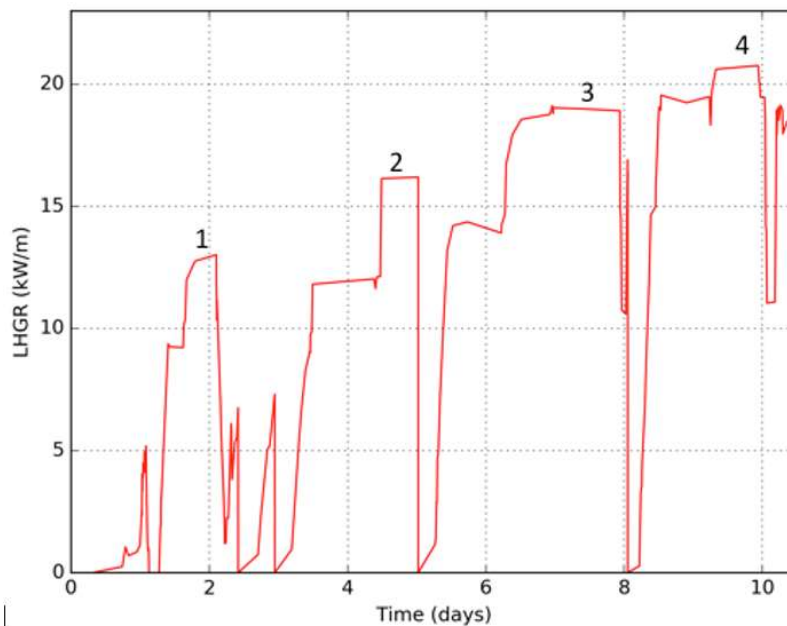


FIG. 5. IFA-629.4 rod 7 power history for the first 10 days of Halden irradiation.

Both the experimental data and simulations with the elastic fuel approximation suggest three different elongation slopes, which are likely correlated to different contact conditions between the fuel and cladding (namely non-contact, intermediate-contact, and hard-contact). During non-contact, the rod elongation simply follows the thermal expansion of the cladding. During intermediate-contact, there appears to still be slip between the fuel and cladding, however, the cladding diameter increases slightly as driven by radial fuel thermal expansion, resulting in a flattening of the axial elongation slope due to the Poisson effect. Following the onset of hard-contact at approximately 12 kW/m, the cladding is locked (or partially locked) to the fuel and thus the predicted rod elongation reflects the fuel thermal expansion. This explanation generally follows that given in [11], where the IFA-629.4 experimental results were analyzed in detail.

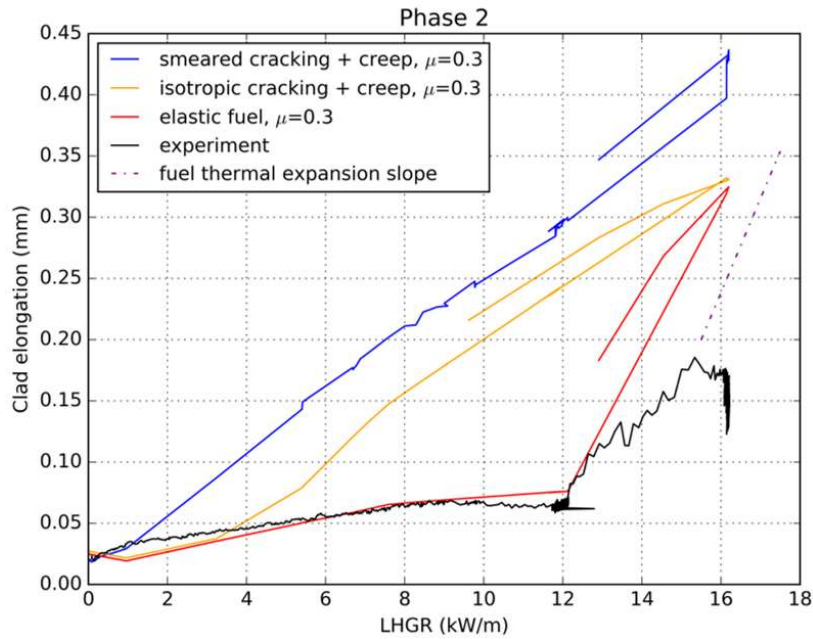


FIG. 6. Predicted and measured rod elongation, as a function of rod average power, during the Phase 2 power ramp for IFA-629.4 Rod 7. Predictions are shown assuming elastic fuel and creeping fuel with either isotropic or smeared cracking material models.

For the Phase 2 ramp simulation with the elastic fuel approximation, the computed and measured rod elongation evolutions correlate very well during both the non- and intermediate-contact phases, and the onset of hard-contact is predicted accurately. There are, however, discrepancies in both the elongation slope and magnitude during the hard-contact period. BISON tends to follow the fuel thermal expansion slope, as expected, while the measurement indicates a lesser slope, suggesting that other physics must be in play. The oscillations in the measured elongation suggest there could be periodic slip occurring between the fuel and cladding. Another possibility is axial fuel compaction, possibly by the closure of axial cracks, resulting from the force imposed by the cladding.

It is clear in Fig. 6 that the simulations which included fuel creep and cracking predict the onset of hard contact much too early in the power ramp. However, once contact is established, the rate at which the elongation increases with power is similar to that measured. These results confirm that including fuel creep and cracking is needed to appropriately model PCMI. This aspect will be further investigated, as will be the discrepancies in the predicted onset of hard contact when the fuel cracking models are applied. Also, additional comparisons to cladding elongation measurements, also covering different irradiation conditions, will be considered in the future. Finally, it is interesting to note the similar behaviour of the two fuel cracking models, which attempt to represent the cracking effect based on markedly different approaches [12,13].

The computed cladding outer diameter over the active fuel length, at different stages in the calculation, is shown in Fig. 7. Ridges in the cladding at each pellet-pellet interface result from the hourglass shape of the fuel pellets, as reproduced in this discrete-pellet BISON simulation. Although PIE cladding diameter measurements are not available for this experiment, computed end-of-life ridge heights of 7-10 μm are reasonable based on similar experiments. Finally, note that including fuel creep results in a secondary ridge at the waist of each fuel pellet, a phenomenon that has been observed in earlier studies.

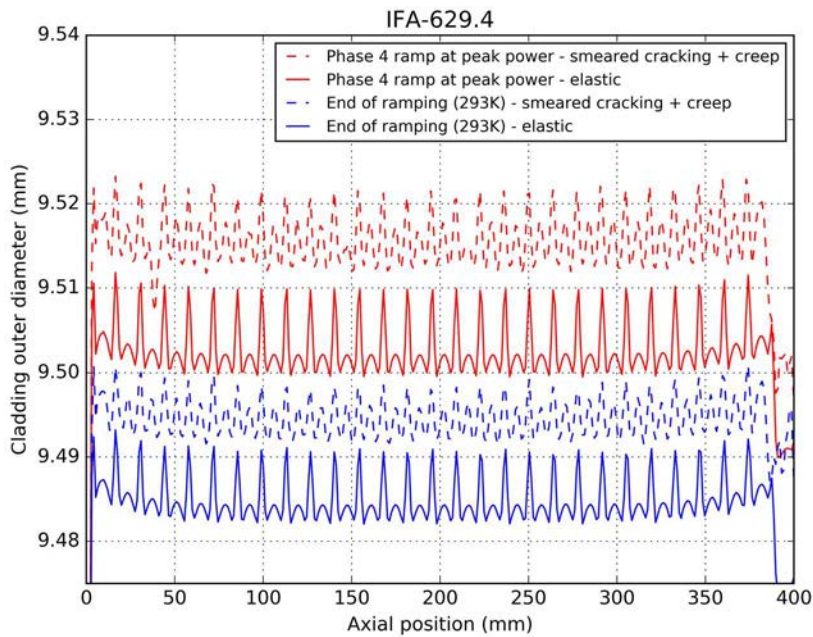


FIG. 7. Computed cladding outer diameter vs axial position, at different times in the calculation.

3. ANALYSIS OF MISSING PELLET SURFACE DEFECTS IN 3D

Geometric irregularities in the fuel pellets associated with fabrication defects can lead to local concentration of stress in the cladding during PCMI and increase significantly the likelihood of PCI failure. In particular, missing pellet surface (MPS) manufacturing defects have been identified as a cause of PCI cladding failure [14]. Such failures have been observed to occur during power ramps. Accurate modelling of MPS defects (which is an inherently 3D problem) using fuel performance codes can bring a better understanding of the PCI-MPS failure mechanism.

A modelling approach was presented in [15] that involved coupling a 2D model of a full-length fuel rod (for the calculation of integral quantities, such as the plenum pressure and gap conductance) to a 3D model of the defective (MPS) pellet region. The BISON code was used to run both of these models. The simulated case was a BWR fuel rod containing an MPS and undergoing various transient events, including the withdrawal of a control blade and a ramp to high power. Fig. 8 shows the considered pellet geometry and the 3D finite element mesh used to model the MPS region.

As an example of results, contours of calculated hoop stress in the cladding are shown in Fig. 9. The results demonstrate the effects of the MPS during PCMI as reproduced by the BISON 3D analysis. Such effects include plate bending behaviour of the cladding in the region across from the MPS, as well as stress reversal around the defect boundaries, with high tensile stresses on the exterior and high compressive stresses on the interior of the cladding. More results and details on the calculations are given in [15].

4. DEVELOPMENT OF PCI FAILURE MODELS FOR BISON

In the multi-physics application domain, BISON as part of CASL's VERA-CS coupled system of codes, is used for core-wide PCI screening analysis. The development of PCI cladding failure models for BISON is described in [16], where a procedure for PCI-screening failure-analysis is also outlined. In particular, two PCI failure models for BISON are developed:

- A time-to-failure based cumulative damage index (CDI) model, where the CDI is computed as a linear accumulation of fractions of damage over each time step, as:

$$CDI = \sum_i D_i, \quad D_i = \frac{\Delta t_i}{t_f}, \quad (t - t_{max}) \leq \tau \quad (1)$$

where D_i is the damage computed at time step i , Δt_i the time step duration, t_f the time to failure under the average peak cladding hoop stress over the time step, t_{max} the time at which the maximum cladding hoop stress is reached during the simulation, and $\tau = 1000\text{s}$. The model for the time to failure is based on [17].

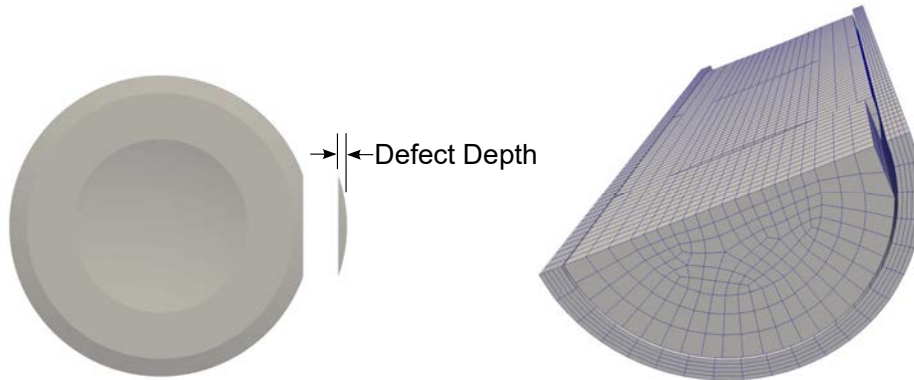


FIG. 8. Left: Geometry of defective pellet modelled in current study, with view from one end. Right: 3D finite element mesh of region of defective pellet showing fuel and cladding (reproduced courtesy of Elsevier [15]).

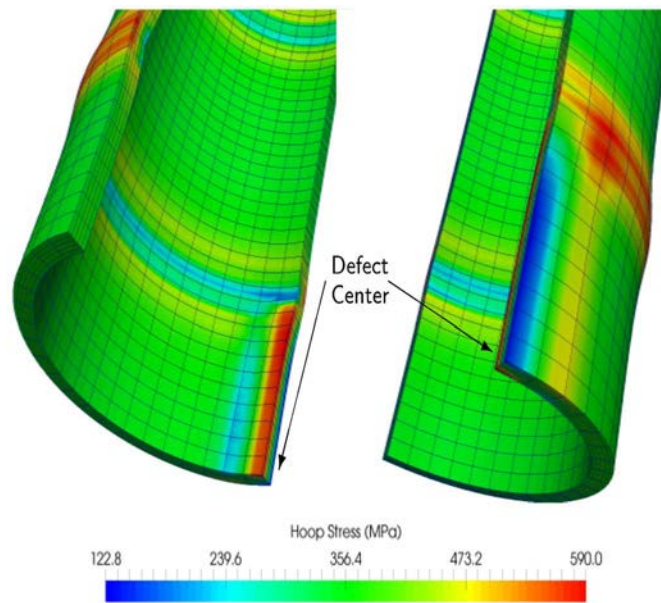


FIG. 9. Contours of hoop stress in the cladding around the MPS region for the BISON 3D analysis (reproduced courtesy of Elsevier [15]).

— A fracture-mechanics based fracture toughness model, based on adaptation of Rice’s path-independent J-Integral methodology [18] to the treatment of a surface flaw in a closed surface. The derivation procedure described in [16] leads to the following expression:

$$\text{CSED} = 0.0166 K_{JSCC}^2 \quad (2)$$

where CSED is the critical strain energy density, which is the failure metric for the SCC-driven PCI failure, and K_{JSCC} is the fracture toughness. The best-estimate value for K_{JSCC} to use with the above equation, estimated from [16], is $10 \text{ MPa m}^{1/2}$.

These models are applicable to both the PCI-SCC and PCI-MPS cladding failure modes. The reader is referred to [16] for a detailed description of the models and validation studies. Below, we only present the CDI model as an illustration of the methodology.

Fig. 10 shows a comparison of model calculations for the time to cladding failure due to PCI-SCC to experimental data from tube tests in iodine environment. Input conditions represent the metallurgical conditions of cladding specimens and average iodine concentrations in the testing environments. This application showcases the time to failure calculation in the CDI model.

The CDI model has been implemented in BISON at Structural Integrity Associates and can be used in conjunction with the BISON cladding stress calculation to predict PCI rod failure. To this end, BISON was applied to the analysis of several fuel rod power ramp experiments from the IFPE Database for calibration of the model using a probabilistic approach [16]. Selected results from this work are presented in Fig. 11, while a more complete discussion is found in [16]. Fig. 11-left illustrates the calculated maximum hoop stress at the peak power axial location for the performed BISON simulations. Based on the BISON CDI calculations for these cases and the experimental data for rod failure, the probability of PCI failure as a function of the calculated CDI was derived in [16]. Fig. 11-right shows the cumulative distribution of failure probability that was developed based on the same set of analyses in Fig 11-left. Using this distribution and the CDI model, the PCI failure probability for a given fuel design and operation conditions can be estimated and applied to PCI screening analyses. It should be emphasized that the above probabilistic approach provides a metric for the failure potential, while the selection of a failure probability threshold for PCI screening would be at the user's discretion.

Importance of accurately modelling fuel cracking and creep in order to perform realistic PCMI simulations was pointed out. Then, we presented a 3D analysis for a BWR fuel rod containing an MPS defect and subject to PCMI using BISON. This capability can be used to calculate the inherently 3D stress/strain/temperature distributions in the cladding in presence of an MPS and ultimately, as a basis for PCI-MPS failure analyses. Finally, we gave an account of recently developed PCI failure models coupled to BISON. Models are based on either a cumulative damage index or a fracture toughness approach and can be applied to PCI screening analyses using BISON.

5. SUMMARY

In this contribution, an overview was given of BISON development and assessment work performed to date for PCMI and PCI analysis. First, BISON simulations of several fuel rod experiments from the IFPE Database involving PCMI, and comparisons of results to experimental data were presented. Predictions of cladding diameter change during PCMI were generally reasonable, although the need to further improve BISON's fuel mechanics (cracking, creep, swelling) and cladding creep models was identified. The recent incorporation into BISON of a model for fuel relocation recovery under PCMI was shown to bring a first noticeable improvement in the predictions. For the IFA-629.4 power ramp experiment simulation, related to participation of INL in the recent PCMI benchmark of the OECD/NEA, comparisons for cladding elongation before and during PCMI demonstrated proper qualitative behaviour, but also highlighted areas where model refinements are needed. In particular, the importance of accurately modelling fuel cracking and creep in order to perform realistic PCMI simulations was pointed out. Then, we presented a 3D analysis for a BWR fuel rod containing an MPS defect and subject to PCMI using BISON. This capability can be used to calculate the inherently 3D stress/strain/temperature distributions in the cladding in presence of an MPS and ultimately, as a basis for PCI-MPS failure analyses. Finally, we gave an account of recently developed PCI failure models coupled to BISON. Models are based on either a cumulative damage index or a fracture toughness approach and can be applied to PCI screening analyses using BISON.

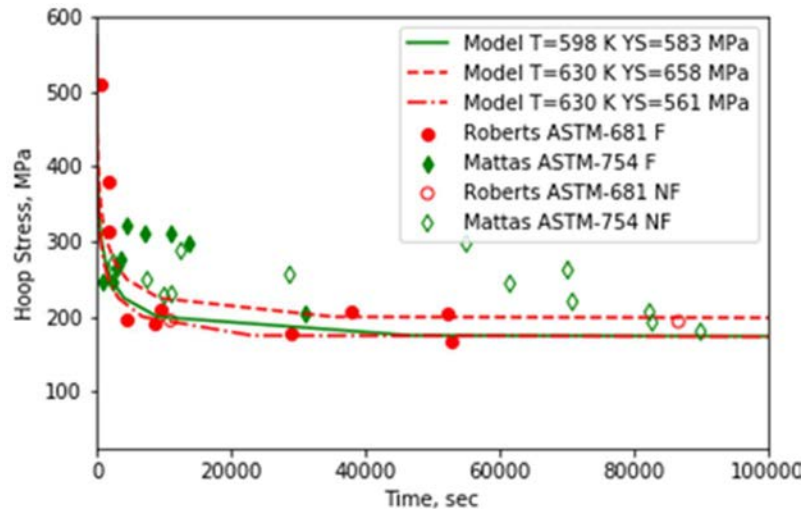


FIG. 10. Comparisons of calculated PCI-SCC cladding failure time to experimental data from tube tests in iodine environment (reproduced courtesy of J.Y.R. Rashid, et al [16]).

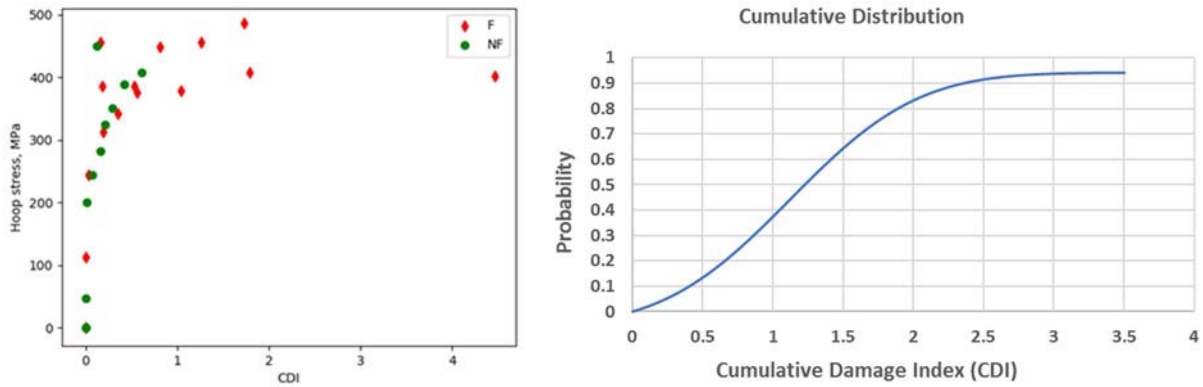


FIG. 11. Left: BISON predictions of hoop stress vs CDI for analyses of power ramp cases. F/NF indicate cases for which PCI cladding failure occurred/did not occur experimentally. Right: Cumulative distribution function for failure probability vs CDI.

NOMENCLATURE

BWR	Boiling Water Reactor
CASL	Consortium for Advanced Simulation of Light Water Reactors
CDI	Cumulative Damage Index
CSED	Critical Strain Energy Density
HBWR	Heavy Boiling Water Reactor
IAEA	International Atomic Energy Agency
IFPE	International Fuel Performance Experiments
INL	Idaho National Laboratory
LWR	Light Water Reactor
MPS	Missing Pellet Surface
NEA	Nuclear Energy Agency
NEAMS	Nuclear Energy Advanced Modeling and Simulation
OECD	Organisation for Economic Co-operation and Development
PCI	Pellet-Cladding Interaction
PCMI	Pellet-Cladding Mechanical Interaction
PWR	Pressurized Water Reactor
SCC	Stress Corrosion Cracking
VERA-CS	Virtual Environment for Reactor Applications Core Simulator

ACKNOWLEDGMENTS

The UK National Nuclear Laboratory and JRC-Karlsruhe are acknowledged for the work in defining model input parameters and boundary conditions for the IFA-629.4 experiment in the OECD/NEA PCMI benchmark. This work was funded by the U.S. DOE's Nuclear Energy Advanced Modelling and Simulation (NEAMS) and Consortium for Advanced Simulation of Light Water Reactors (CASL) programmes. The manuscript has been authored by a contractor of the U.S. Government under Contract DE-AC07-05ID14517. Accordingly, the U.S. Government retains a non-exclusive, royalty free license to publish or reproduce the published form of this contribution, or allow others to do so, for U.S. Government purposes.

REFERENCES

- [1] WILLIAMSON, R.L., HALES, J.D., NOVASCONE, S. R., TONKS, M.R., GASTON, D.R., PERMANN, C.J., ANDRS, D., MARTINEAU, R.C., Multidimensional Multiphysics Simulation of Nuclear Fuel Behaviour, *Journal of Nuclear Materials* **423** (2012) 149.
- [2] GASTON, D., NEWMAN, C., HANSEN, G., LEBRUN-GRANDIÉ, D., MOOSE, A Parallel Computational Framework for Coupled Systems of Nonlinear Equations, *Nuclear Engineering and Design* **239** (2009) 1768.
- [3] ROSSITER, G. et. al., "OECD/NEA Benchmark on Pellet-Clad Mechanical Interaction Modelling with Fuel Performance Codes", OECD/NEA Workshop on Pellet-Cladding Interaction (PCI) in Water-Cooled Reactors, Lucca, Italy, 22-24 June 2016.
- [4] WILLIAMSON, R.L., GAMBLE, K.A., PEREZ, D.M., NOVASCONE, S.R., PASTORE, G., GARDNER, R.J., HALES, J.D., LIU, W., MAI, A., Validating the BISON Fuel Performance Code to Integral LWR Experiments, *Nuclear Engineering and Design* **301** (2016) 232.
- [5] SARTORI, E., KILLEEN, J., TURNBULL, J.A., International Fuel Performance Experiments (IFPE) Database, OECD/NEA, 2010, available at <http://www.oecd-nea.org/science/fuel/ifpelst.html>.
- [6] INTERNATIONAL ATYOMIC ENERGY AGENCY, Fuel Modelling at Extended Burnup (FUMEX-II): Report of a Coordinated Research Project 2002–2007, IAEA-TECDOC-1687, IAEA, Vienna (2012).
- [7] INTERNATIONAL ATYOMIC ENERGY AGENCY, Improvement of Computer Codes Used for Fuel Behaviour Simulation (FUMEX-III): Report of a Coordinated Research Project 2008–2012, IAEA-TECDOC-1697, IAEA, Vienna (2013).
- [8] PASTORE, G., SWILER, L.P., HALES, J.D., NOVASCONE, S.R., PEREZ, D.M., SPENCER, B.W., LUZZI, L., VAN UFFELEN, P., WILLIAMSON, R.L., Uncertainty and Sensitivity Analysis of Fission Gas Behaviour in Engineering-Scale Fuel Modelling, *Journal of Nuclear Materials* **465** (2015) 398.
- [9] ZAHOOR, M., CASAGRANDA, A., Fuel Relocation Recovery Implementation in Bison, *Journal of Nuclear Materials* **511** (2018) 473.
- [10] GEELHOOD, K.J., LUSCHER, W.G., RAYNAUD, P.A., PORTER, I.E., FRAPCON-4.0: A Computer Code for the Calculation of Steady-State, Thermal-Mechanical Behaviour of Oxide Fuel Rods for High Burnup, PNNL-19418 Vol.1 Rev. 2, Pacific Northwest National Laboratory (2015).
- [11] KOIKE, H., MURAKAMI, N., KOLSTAD, E., TVERBERG, T., Ramp Tests with Two High Burnup UO₂ Fuel Rods in IFA-629.4, HWR-769, OECD Halden Reactor Project (2004).
- [12] RASHID, Y.R., Mathematical Modelling and Analysis of Fuel Rods, *Nuclear Engineering and Design* **29** (1974) 22.
- [13] BARANI, T., PIZZOCRI, D., PASTORE, G., LUZZI, L., HALES, J.D., Isotropic Softening Model for Fuel Cracking in BISON, *Nuclear Engineering and Design* **342** (2019) 257.
- [14] POTTS, G.A., "Recent GE BWR fuel experience", Proceedings of the 1997 International Topical Meeting on LWR Fuel Performance, Portland, USA, March 2-6, 1997.
- [15] SPENCER, B.W., WILLIAMSON, R.L., STAFFORD, D.S., NOVASCONE, S.R., HALES, J.D., PASTORE, G., 3D Modelling of Missing Pellet Surface Defects in BWR Fuel, *Nuclear Engineering and Design* **307** (2016) 155.
- [16] RASHID, J.Y.R., LIU, W., WILLIAMSON, R.L., "Bison as a PCI screening tool – PCI failure model development", Top Fuel 2019, Seattle, USA, September 22-26, 2019.
- [17] ROBERTS, J.T.A. et. al., "A Stress Corrosion Cracking Model for Pellet-Cladding Interaction Failures in Light-Water Reactor Fuel Rods," Zirconium in the Nuclear Industry, Fourth Conference, ASTM STP **681** (1979) pp. 285-305.
- [18] RICE, J.R., "A Path Independent Integral and the Approximate Analysis of Strain Concentration by Notches and Cracks," *Journal of Applied Mechanics* **35** (1968) 379.

SIMULATING OF THE FUEL ROD BEHAVIOUR UNDER FAST POWER RAMP CONDITIONS IN THE START-3A CODE

E.A. AVDONINA, A.V. KRUPKIN, V.I. KUZNETSOV, B.I. NESTEROV, V.V. NOVIKOV
Stock Company "A.A. Bochvar High-technology Research Institute of Inorganic Materials"
(SC "VNIINM"),
Russian Federation
Email: avkrupkin@bochvar.ru

A.I. DOLGOV, A.G. ESHCHERKIN, A.L. IZHUTOV, V.A. OVCHINNIKOV
Joint Stock Company "State Scientific Center — Research Institute of Atomic Reactors" (JSC "SSC RIAR"),
Russian Federation

Abstract

The paper presents an analysis of the behaviour of fuel rods subject to in the NGV1 power ramp test. In the NGV1 ramp test included seven WWER-1000 fuel rods (six full-scaled fuel rods and one refabricated fuel rod).

A special feature of the test was the use of special irradiation devices with a rotary hafnium screen. Using this screen allows you to achieve fast power ramp speed, which is realized in some AOO transients. The test was performed according to the following scenario: (1) Conditioning fuel rods at base irradiation level during ~ 48 h; (2) The first power ramp, made by reactor power raise, at ~ 15 min; (3) Exposure during ~ 17 h; (4) The second power ramp, made by rotating Hf screen, at ~ 1 min; (5) Exposure during ~ 12 h. This formed two groups of fuel rods: (1) On the fuel rods of the first group a "slow" power ramp was realized with long conditioning time after power rise; (2) The fuel rods of the second group experienced two ramps: first 'slow', then 'fast' with a short conditioning time. After the test, on the all of the fuel rods were fixed increase in outer diameter caused by fuel composition gas swelling. Maximum achieved residual strain was 1.13%. The paper presents an analysis of the behaviour of the tested fuel rods using the START-3A code.

1. INTRODUCTION

The power ramp test NGV1 is continuation of the NG test series (NG1[1, 2], NG4, NG5, NG6K).

The NG test series were intended to investigate the behaviour of a fuel with a thin wall cladding and the fuel with a large grain (~ 25µm) without central hole under transient operation modes.

NG1, NG4, NG5, NG6K tests were carried out according to the same scenario (while the fuel rods had a different base irradiation history), which included 3 stages: preconditioning, power ramp and exposure.

The NGV1 test was intended to investigate the behaviour of the fuel during fast power ramp.

Table 1 shows the comparison of the achieved power ramp rates in the NG test series. As can be seen from Table 1, the rate of power increase in NGV1 test was significantly higher. Therefore, the main task of this work is to show how the increase in the rate of power raise affected on the process of gas swelling of the fuel.

TABLE 1. RATES OF POWER INCREASE IN THE NG TEST SERIES

Test name	Maximum ramp rate, kW/(m·min)
NG1	0.96
NG4	0.91
NG5	0.79
NG6K	1.22
NGV1	25.4

2. TEST RODS BASE IRRADIATION HISTORY

For the NGV1 ramp, there were selected seven full scaled fuel rods (№№35, 49, 63, 77, 78, 94, 95) from the fuel assembly № ID02293. One of these fuel rods (№ 49) was re-fabricated, the rest were tested without re-fabrication. The fuel rod 49 was shortened and equipped with temperature and elongation sensors.

The fuel rods had an advanced design with a thinned cladding (9.1×7.93 mm) and fuel pellets without a central hole and with large grain ($\sim 25\mu\text{m}$).

Fuel assembly № ID02293 was operated on the first unit Kalinin NPP for three fuel cycles.

Maximum burnup of selected fuel rods is $\sim 44 \text{ MW}\cdot\text{d/kgU}$.

3. TEST DEVICE DESIGN

To conduct the NGV1 test, a special irradiation device was developed, the scheme of which is shown in Figure 1.

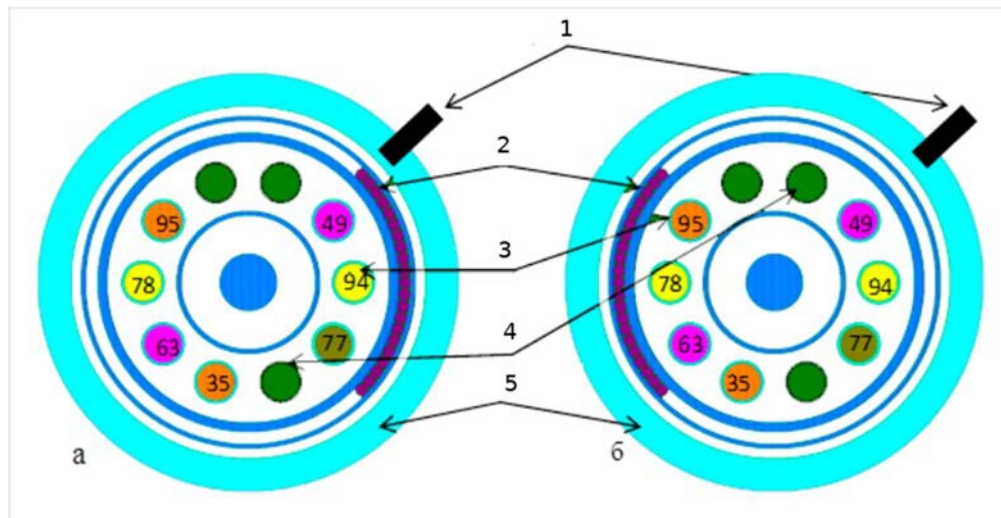


FIG. 1. Irradiation device for the NGV1 test: 1 — loop channel head; 2 — hafnium screen; 3 — fuel rod; 4 — displacers; 5 — loop channel shell.

In the active part of the irradiation device, in one row around the circumference are six full scaled fuel rods, one re-fabricated rodlet with a thermal couple and an elongation sensor for additional control of the kinetics of changes in the power of the fuel rods at “ramp” and axial deformation, two tubes – displacers, cable neutron detector with a hafnium emitter.

In addition to the fuel rods, the irradiation device contains the following main nodes: a moving absorbing screen, central bearing inner tube with spacing elements, sealing head, sensors and metal hose for cable outlets from sensors.

The absorbing screen was made of 21 shafts of $\varnothing 2.45$ mm, located close to each other on a cover movable pipe. Hafnium screen driven by a shaft located in the central pipe. Shaft connected with a drive to the central hall of the reactor.

Rotating the screen allows for quick power rises that are impossible when raising the power with the reactor.

4. NGV1 RAMP SCENARIO

The NGV1 test was conducted as follows:

- Exposure at the level of basic irradiation for ~ 50 h;
- Reactor power raise at 10 - 15 min;
- Exposure at this level for ~ 20 h;
- Rotate the absorbing screen at ~ 1 min;
- Exposure for ~ 12 h.

With that, the tested fuel rods were divided into two groups:

- On the fuel rods of the first group (№№ 49, 94, 77) two power ramps were realized (first ‘slow’, then ‘fast’);
- On the fuel rods of the second group (№№ 35, 63, 78, 94) one ‘slow’ power ramp were realized.

Figure 2 shows the change in the linear heat rate of the fuel rods in the NGV1 test.

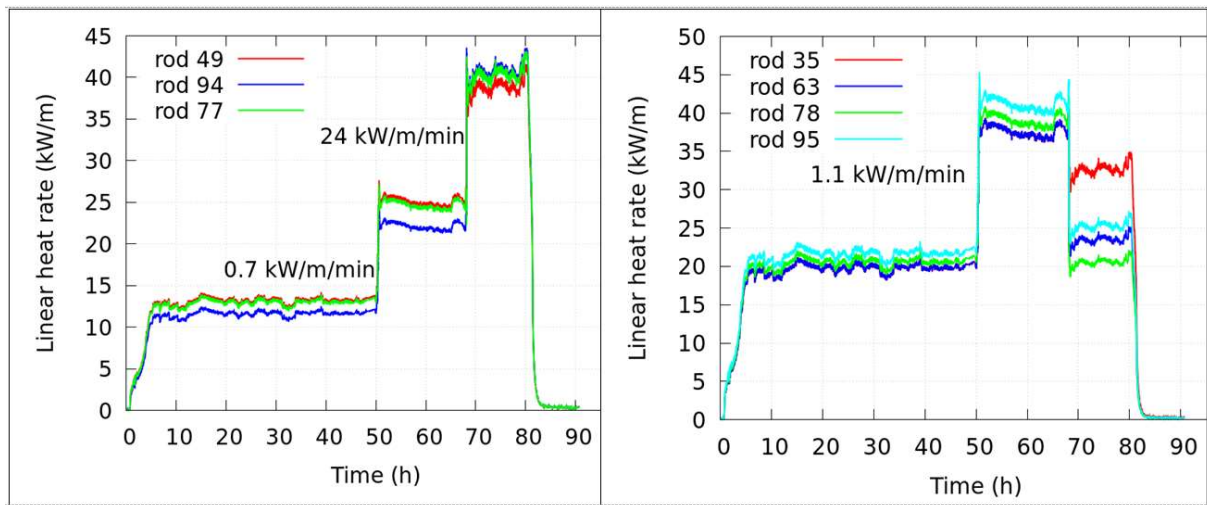


FIG. 2. Linear heat rate change in the NGV1 test.

5. FUEL CENTER TEMPERATURE AND GAS RELEASE

The temperature field in the studied fuel rods was estimated by calculation in the START-3A code.

The fuel rod 49 was not modelled, because at the moment the START-3A code cannot simulate the re-fabrication.

Figure 3 shows the change of the fuel centre temperature for the full scaled fuel rods.

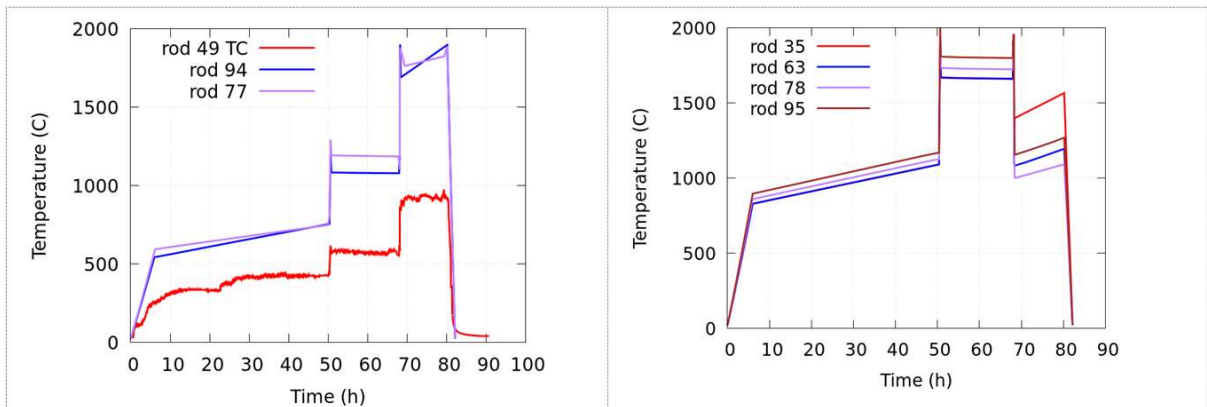


FIG. 3. The results of code START-3A simulating fuel centre temperature for the full scaled fuel rods in the NGV1 test. Output of the fuel rod 49 thermocouple.

For fuel rod 49, the thermocouple outputs are shown in the same figure. It is necessary take into account that the thermocouple was not in the most heat stressed section. The temperatures for full scaled fuel rods are given for the centre of the core (the coordinate is ~ 500 mm, and the thermocouple was located approximately at the coordinate of ~ 230 mm from the top of the reactor core [total length of the reactor MIR core is 1000 mm]).

In Figure 3, the central temperature of the fuel pellet for all rods was quite high (~ 2000 °C), which caused large gas release.

Figure 4 shows the measured value of fission gas release for full scaled fuel rods after power ramp. For re-fabricated fuel rod, 49 measurements were carried out before the ramp.

In Figure 4, the power ramp resulted in a significant release of a fission gases from the fuel matrix. Moreover, the level of gas release was higher for the slow ramp more than for the fast ramp. This is due to the fact that the slow fuel rods stayed longer in the high temperature zone (see Figure 3).

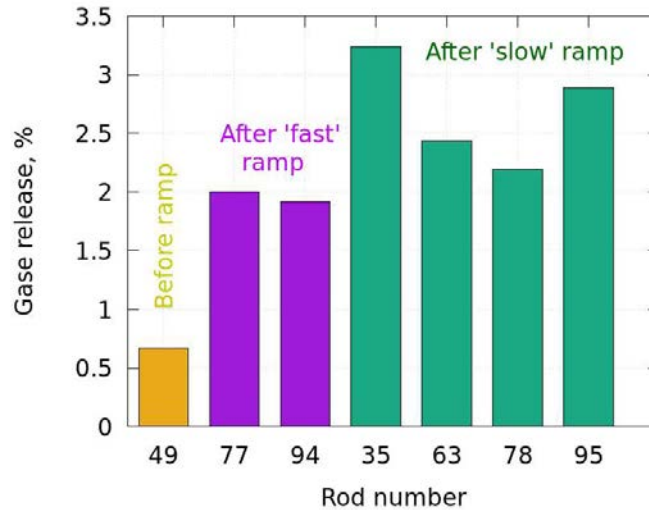


FIG. 4. The results of fission gas release measurements after the NGV1 test.

6. POST IRRADIATION EXAMINATION

Figure 5 compares post irradiation examination results of the fuel structure between the rod 35 (slow ramp) and 77 (fast ramp).

For each fuel rod, structures were investigated at the section with maximum linear heat rate (structure after a power ramp) and in the unloaded part of the rod (structure before a power ramp).

Figure 5 shows that the structure in the central part of the fuel for both rods has undergone characteristic changes.

After basic irradiation a finely porous structure with gas bubbles distributed uniformly in the grain body was formed (the dark area in the top left part of Figure 5).

After the test, this structure was preserved only in a small part of the fuel cross section (dark ring at the at the top right part of Figure 5).

In the central part, small bubbles disappeared, and large pores formed. It says that in the test there was a process of the fuel gas swelling.

7. OUTER DIAMETER CHANGE

Figure 6 shows the diameter change through the fuel rods length (profilograms) before and after NGV1 test.

Analysis of the data on the change in diameter after basic exposure shows a significant scatter of experimental data (all studied fuel rods were in neighbouring positions in the fuel assemblies at the stage of base irradiation and gained the same burnup from gamma scan investigations). This indicates a significant range of volumetric swelling properties of the fuel.

As can be seen from Figure 6, the START-3A code shows approximately the same diameter change for all fuel rods.

A comparison of the pattern of diameter changes before and after a power ramp shows that the diameter for all fuel elements increased by about the same amount. What says that the rate of increase in power did not have a significant effect on process of gas swelling of fuel.

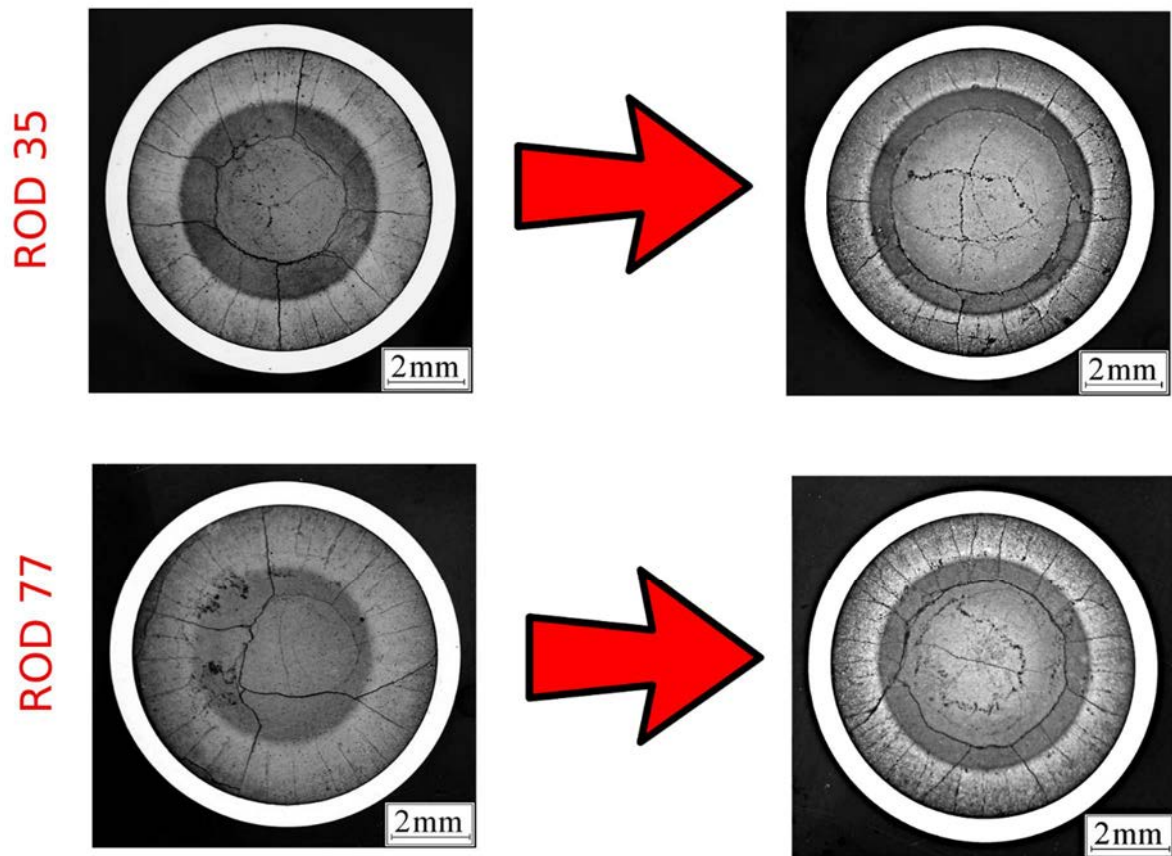


FIG. 5. The results of post irradiation examination of fuel structure before and after ramp for fuel rods 35 (slow ramp) and 77 (fast ramp) of the NGV1 test.

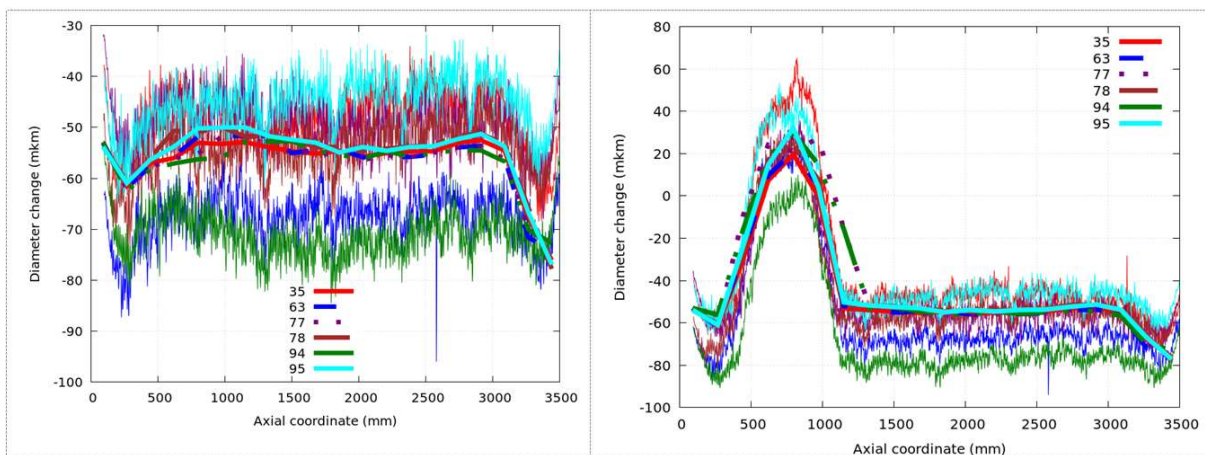


FIG. 6. Diameter change through rods length before and after NGV1 test. Bold lines show code START-3A simulation results.

8. CONCLUSIONS

This paper presents the behaviour of fuel rods with improved design features (e.g. a thinned E110opt alloy cladding and fuel pellets with large grain $\sim 25\mu\text{m}$ without central hole) under conditions of a fast power ramp at $\sim 24 \text{ kW/m/min}$.

Analysis of the test results indicated that for all the fuel rods an increase in diameter and a characteristic change in the structure of the fuel were caused by gas swelling of the fuel composition. For all the fuel rods, scored approximately the same residual strain $\sim 1.3\%$. So, you can conclude that the rate of increase in power does not affect the kinetics gas swelling.

It should be noted that the process of gas swelling is accompanied by intense the release of fission gas products. Moreover, from the fuel of a group of the fuel rods experienced a slow ramp under the cladding of a fuel rod released more gas. It's related, apparently with the fact that this group of fuel rods was at a higher level of power for longer time.

REFERENCES

- [1] KRUPKIN, A.V., KUZNETSOV, A.V., KUZNETSOV, V.I., NOVIKOV, V.V., "Numerical-Experimental Study of Influence of Chip in the Fuel Pellet on the Fuel Rod Cladding Strength", Proc. of WRFPM 2017, Jeju Island, Korea, 2017.
- [2] KRUPKIN, A., KUZNETSOV, V., NESTEROV, B., NOVIKOV, V., "Simulation of Ramp Tests on WWER-1000 Fuel Rod without a Central Hole in ANSYS Software", Proc. of 11th International Conference on WWER Fuel Performance, Modelling and Experimental Support, Varna, Bulgaria, 2015.

RECENT DEVELOPMENT OF PCI MODELING AT VTT

J. PELTONEN, H. LOUKUSA, V. TULKKI
VTT Technical Research Centre of Finland Ltd.,
Finland
Email: jussi.peltonen@vtt.fi

Abstract

PCI related phenomena have been investigated at VTT and novel models have been developed for their study. As standard creep models do not accurately model stress reversals and reductions, new transient creep model with the anelastic creep component has been developed. The model accurately predicts creep behaviour during stress reversals. Accurate modelling of creep is required for the determination of cladding stresses during pellet-cladding interaction.

The chemical behaviour of the fuel pellet-cladding gap has also been investigated with a new thermochemical model including radiolysis. As caesium iodide is unreactive towards the cladding, its radiolysis may contribute to the amount of corrosive iodine on the cladding inner surface, and cause stress-corrosion cracking.

In addition, missing pellet surface defects have been investigated with the BISON fuel performance code with a simplified model, and capacity to model such phenomena at VTT has increased.

1. INTRODUCTION

Pellet-cladding interaction (PCI) results from the dimensional changes experienced by the pellet and cladding during in-reactor operation and is considered a chronic performance issue. It can negatively impact the integrity of a fuel rod during normal operating conditions, resulting in stress corrosion cracking (SCC) that can lead to failure of the fuel rods. This issue is further augmented by irradiation. Modelling mechanisms that lead to PCI and SCC is vital in the future development of efficient nuclear reactors. Recently VTT has conducted computational studies of both PCI and SCC, of which studies on three topics are briefly described in this paper [1–3]. Two of the studies focus on the mechanical evolution of the fuel rod, thus being related to PCI, whereas the third study investigates chemical equilibrium that are known to cause SCC.

The first study consists of three papers [7–9] that approach the issue of cladding tube creep response to transient stresses. Traditional models based on strain hardening law have severe limitations in regard to load reductions and reversals, due to these models only considering the elastic and viscoplastic components of deformation. The articles derive a cladding mechanical model that can consistently solve the creep and stress relaxation behaviour in a fuel rod, while being appropriately limited in complexity in order to be utilized in a fuel performance code.

The second study presents the first attempt on modelling missing pellet surfaces with the BISON fuel performance code [2]. This work examined missing pellet surfaces and their impact on the pellet-cladding interface of the reference 2D-RZ-geometry in a BISON simulation. The generation method of an intricately modified pellet surface mesh was also studied in the work and documented thoroughly. The radial-axial 2D model of this work had considerable limitations in modelling the reference case due to the relative simplicity of the model.

The third study investigates how caesium iodide vaporization and radiolysis occur in a radiation field that is constrained by Gibbs energy minimization. The kinetic model of caesium iodide radiolysis is solved with a MATLAB programme to determine a steady state, which can be used to constrain the equilibrium of a nuclear fuel pellet surface. These calculations indicate that when taking into account radiolysis of caesium iodide, hydrogen iodide is the thermodynamically favoured form of iodine at low fuel temperatures in a fuel rod, which might have an impact on stress-corrosion cracking.

2. DEVELOPMENT OF CLADDING CREEP MODELS AT VTT

Conventionally, fuel cladding deformation consists of elastic and viscoplastic component, latter of which is described by the primary stage, the secondary steady-state stage and the tertiary stage which leads to failure. The correlations are fitted to experimental data with a single stress increase, while the change of stress for Zirconium alloys is handled by the strain hardening law in usual operation conditions [4]. In the transient situation, the strain hardening law acts as a simplification that is not universally applicable. Therefore, an ideal model of pellet-cladding interaction contains a mechanical model that accounts the transient phenomena.

Stress reversal and stress reduction are exceptions in which the hardening law fails, and additional assumptions are required to model the observed behaviour [4,5,6]. Complex models have been developed to describe these phenomena, but their usage in fuel behaviour modelling remains limited due to their computational limitations. Three articles by Tulkki and Ikonen [7,8,9] present the development of a cladding mechanical model for the consistent description of creep and stress relaxation behaviour. These papers start off by using mechanical analogue of Standard Linear Solid (SLS) model for the description of creep and relaxation behaviour. The total strain caused by external stress can be formulated as:

$$\varepsilon = \varepsilon_{el} + \varepsilon_p + \varepsilon_s \tag{1}$$

where ε_{el} is the elastic response, ε_p is the primary creep and ε_s is the secondary creep. In a mechanical analog this is presented as seen in Fig. 1:

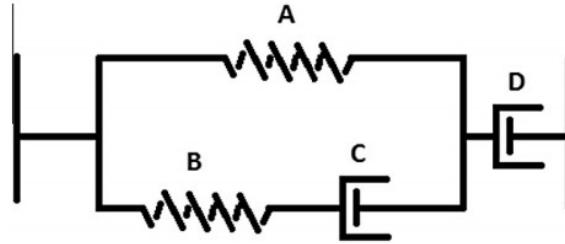


FIG. 1. Mechanical analog of the Standard Linear Solid model created using one Maxwell unit.

where A and B represent elastic components and the dashpots C and D represent viscous components. Of these the nodes A, B and C form the SLS model, whereas the dashpot D stands for the secondary creep consisting of irradiation and thermal steady state creep.

The first version of the model by Tulkki and Ikonen [7] presents a simple formulation for primary creep ε_p to describe the evolution of cladding creep under transient conditions. This formulation was tested against stress data from Halden in-pile experiment IFA-585 [10]. A creep model based on this formulation could accurately simulate the behaviour observed during stress reversal and drop load situations as seen from Fig. 2, while performing similarly to strain hardening rules in scenarios where the latter are known to work. A formulation by Matsuo [11,12] based on out-of-pile tests was investigated, which indicated that primary creep re-initiation behaves differently in in-pile and out-of-pile experiments.

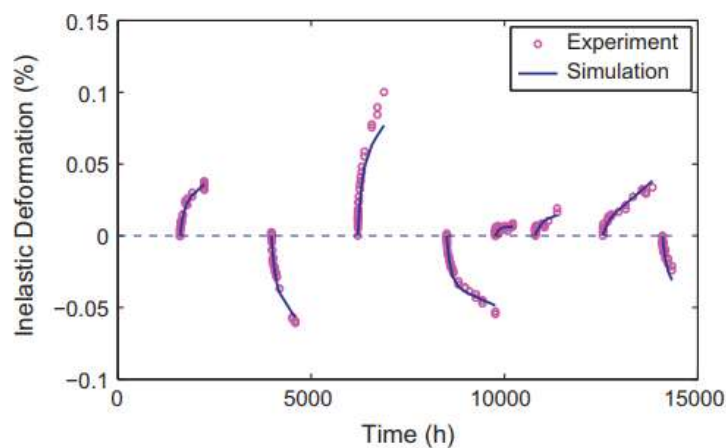


FIG. 2. The model behaviour compared to measurements at the beginning of each stress step. Each pressure step starts from $\varepsilon = 0$.

The second development of the model [8] approaches the issue by developing the primary creep model further and comparing its results to experimental data from Halden experiments IFA-699 and IFA-696 [13, 14]. In this paper a creep model based on viscoelasticity was derived and used to model experimentally observed macroscopic transient creep phenomena and to interpret the experimentally observed creep strain recovery phenomenon.

The results of IFA-699 simulation are compared to experimental data in Fig. 3. The experimental results trend towards positive direction in comparison to the computational predictions of the viscoelastic model. This difference is speculated to originate from either the model of driving force or cladding oxidation, latter of which was accounted in the results of Fig. 3. In the experiment IFA-696 a sample contracted during a period of very low stress at the operational temperature and flux of the reactor. Whereas the models based on the traditional strain hardening rule cannot predict such behaviour, the viscoelastic model predicts such contraction.

The final version of the model [9] implements anelastic contribution to the mechanical model of the cladding. This enables the consistent modelling of both cladding creep, as well as stress relaxation. The model offers an explanation to several experimental observations in transient situations and is compared to a published set of creep and stress relaxation experiments that used comparable samples.

The model is built using Kelvin units which are analogs with parallel springs and dashpots. These are depicted in Fig. 4. In this study, $n = 1,2$ Kelvin units are used in series with a spring and a dashpot. The individual Kelvin units model the evolution of various relaxation processes at different time scales. By increasing their number in the analog, a more accurate representation of a system with several relaxation modes can be produced. However, this increases the complexity of the model and results in higher computational requirements.

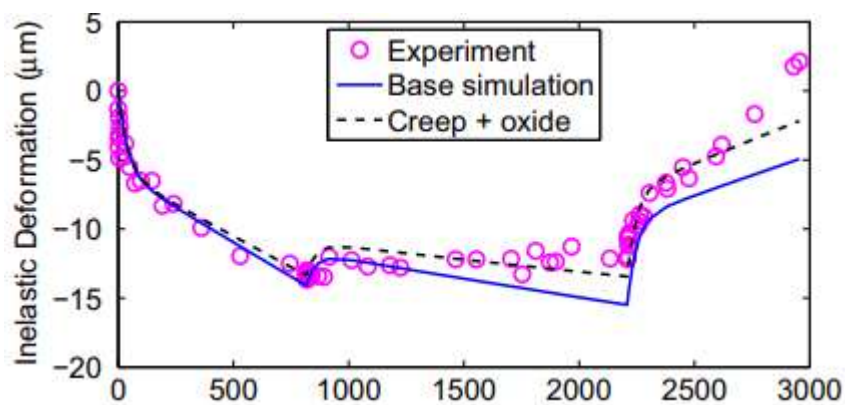


FIG. 3. Creep and oxidation in a Zircaloy-4 segment sample of IFA-699 experiment.

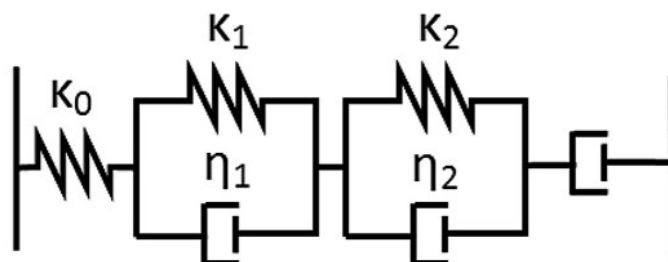


FIG. 4. Mechanical analog consisting of two Kelvin units and a dashpot.

To demonstrate that the model is capable of describing creep and stress relaxation behaviour, experimental data from a cold worked stress relieved zircaloy-4 sample was used [15]. Material dependent coefficients were obtained from the data of the creep experiment, which were used with the improved model to simulate the stress relaxation experiment. The fit of the former dataset is visualized in Fig. 5 and the simulation results of the stress

relaxation experiment in Fig. 6. The simulation of the stress relaxation and its accuracy improves as the number of Kelvin pairs is increased from none to $n = 1, 2$, especially in the early stages of the simulation.

Based on these results and further analysis in the third article, accounting the anelastic contribution in cladding mechanical models improves the simulation results. However, the correspondence of in-pile and out-of-pile cladding behaviour alongside the changes in temperature, as well as the validity of the assumptions offer further challenges in the development of the cladding mechanical models.

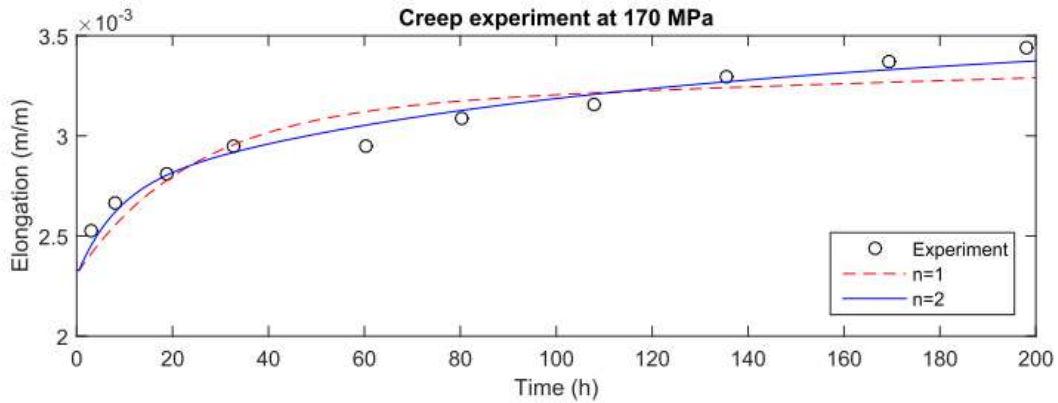


FIG. 5. Creep of cold worked stress relieved samples modelled with varying numbers of Kelvin units and compared to the experimental data (circles). $n = 0$ represents the pure elastic and plastic deformation, $n = 1$ represents the Standard Linear Solid and plastic deformation, $n = 2$ represents the model with anelastic contribution.

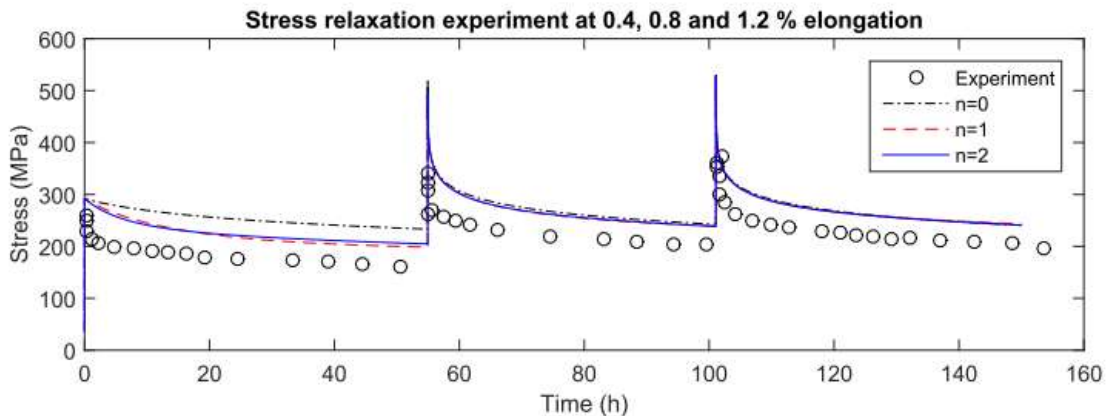


FIG. 6. Relaxation of cold worked stress relieved samples with $n = 0, 1, 2$ Kelvin units.

3. MODELLING MISSING PELLET SURFACE DEFECTS WITH BISON FUEL PERFORMANCE CODE

Missing pellet surface defects have been analyzed with BISON by Spencer et al. [16,17], and similar simplified simulations with BISON were performed by Loukusa [2]. The work analyzed the evolution of pellet and cladding temperatures and von Mises stresses in two steady-state test scenarios with three and eleven pellets. These test scenarios were produced by utilizing an example scenario provided with BISON and a mesh generated automatically with the BISON mesh script. The 2D-RZ-geometries (2D radial-axial geometry) of these test scenarios were modified slightly by introducing the missing pellet surface defect in the Trellis software, after which the results of the modified scenario were compared to the original scenario.

Fuel performance code BISON [18] is based on the MOOSE (Multiphysics Object-Oriented Simulation Environment) framework and has been developed at the Idaho National Laboratory (INL) in the USA since 2008. By solving the coupled nonlinear partial differential equations that govern nuclear fuel performance, it is capable

of 2- and 3-dimensional finite element analysis of nuclear fuel behaviour. The BISON code has been initially taken into use at VTT by Arkoma [19].

In the usual 1.5-dimensional approach used in fuel behaviour modelling, the pellet is assumed to be tangentially uniform, so the temperature distribution and mechanical behaviour in a single axial location is only solved in the radial direction. However, due to the axial and tangential non-uniformity of a missing pellet surface defect these assumptions are not valid. Therefore, a greater number of dimensions is required for modelling these phenomena, as shown also in this work. A missing pellet surface defect is typically a missing section of the cylindrical pellet, as seen in the Fig.7.

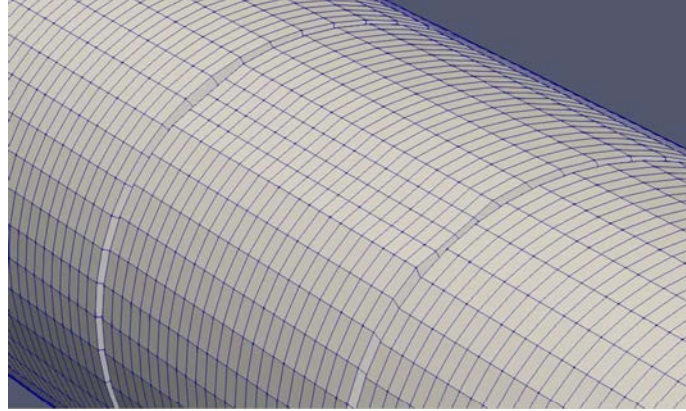


FIG. 7. A type of missing pellet surface defect. Mesh generated with BISON mesh script and modified with the meshing tool Trelis.

In the cladding at the location of the missing pellet surface defect, the cladding experiences different stresses compared to a typical pellet due to the pellet-cladding gap remaining at the location of the defect. As the neighbouring areas push the cladding outwards, only the balance between internal pressure and coolant pressure acts on the cladding at the defect, pushing inwards. Especially on the edges of the defect higher stresses on the cladding would be expected to occur. These stresses can be described using von Mises stress σ_e which provides a convenient way of determining whether the material yields or not under a multiaxial loading.

$$\sigma_e = \sqrt{\frac{1}{2}[(\sigma_{rr} - \sigma_{\theta\theta})^2 + (\sigma_{\theta\theta} - \sigma_{zz})^2 + (\sigma_{zz} - \sigma_{rr})^2]}, \quad (2)$$

where stress components are defined in the cylindrical coordinates with the Cauchy stress tensor σ as:

$$\sigma = \begin{bmatrix} \sigma_{rr} & \sigma_{r\theta} & \sigma_{rz} \\ \sigma_{\theta r} & \sigma_{\theta\theta} & \sigma_{\theta z} \\ \sigma_{zr} & \sigma_{z\theta} & \sigma_{zz} \end{bmatrix} \quad (3)$$

Von Mises stresses of the 11-pellet reference scenario with and without the surface defect can be seen in Fig. 8 below. In the latter case, the stresses are notably increased at the pellet-pellet and pellet-cladding interfaces. Also, a small gap can be seen between the edges of the central pellet and the opposing cladding wall in the modified scenario, whereas in the reference scenario gap closes uniformly.

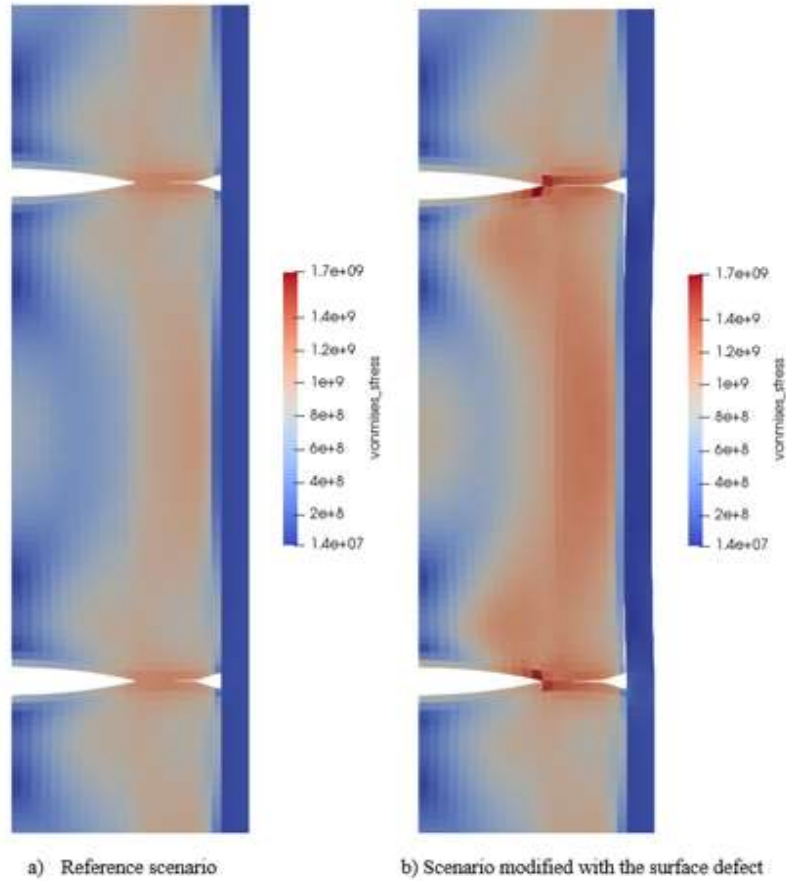
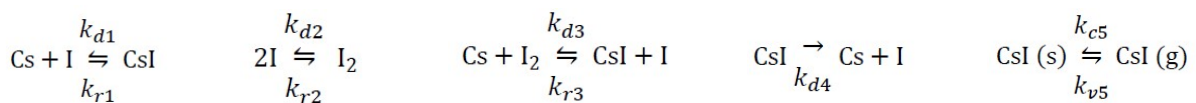


FIG. 8. Overall von Mises stresses in the 11-pellet reference case and the respective missing pellet surface case at 787 days. Only the pellet stress distribution is visible, as the magnitude of the cladding stresses (see Fig. 9) is much lower. The scales are the same in both figures. Units are in Pascals.

4. ANALYZING THE RADIOLYSIS OF CESIUM IODIDE WITH GIBBS ENERGY MINIMIZATION

Gibbs energy minimization is an effective method for the prediction of the chemical composition of nuclear fuel. However, this method is limited to the thermochemical (local) equilibrium state, in which pressure and temperature remain constant and all components are perfectly mixed. Due to the low diffusion of solid nuclear fuel, the system is not ideally mixed, and all reactions may not proceed to equilibrium. Especially in a radiation field there may be a non-equilibrium state present in the fuel. It is possible to overcome these limitations with constrained Gibbs energy minimization in which kinetic constraints are used alongside material constraints. Radiolysis of caesium iodide was analyzed in this way by Loukusa and Valtavirta [3], calculating the dissociation of caesium iodide. While caesium iodide doesn't react towards fuel cladding, atomic and molecular iodine do, and are capable of causing stress-corrosion cracking [20].

Several caesium iodide radiolysis models are available from the literature, of which the model by Konashi et al. [21,22] was chosen due to its basis on experimental data and simplicity. The Konashi model considers radiation from both the fission fragments, as well as from the collision cascade particles. The model features the species Cs, I, I₂ and CsI. These concentrations are calculated with three equilibria, and two decomposition reactions that are treated as a single effective decomposition reaction. In addition, a vaporization-condensation reaction with solid and gaseous caesium iodide was considered, which was not present in the original model. These equations can be seen below.



The kinetic model was solved with a MATLAB script. Gibbs energy minimization was performed with a previously developed routine [23], whereas the mole amounts of PWR fuel rod were calculated with Serpent. The initial values of the gas phase kinetic model were compared to the work of Konashi et al, and the results of Fig.10 were found to be roughly in agreement. However, the equilibrium concentrations of atomic and molecular iodine calculated by Konashi et al may be underpredicted, according to a thermochemical equilibrium calculation performed on the fuel. This alongside the oxidation of caesium would cause the effects of radiolysis to be negligible. Regardless, the caesium iodide radiolysis might have a significant effect at a fuel rod temperature in which caesium iodide is either solid or a liquid.

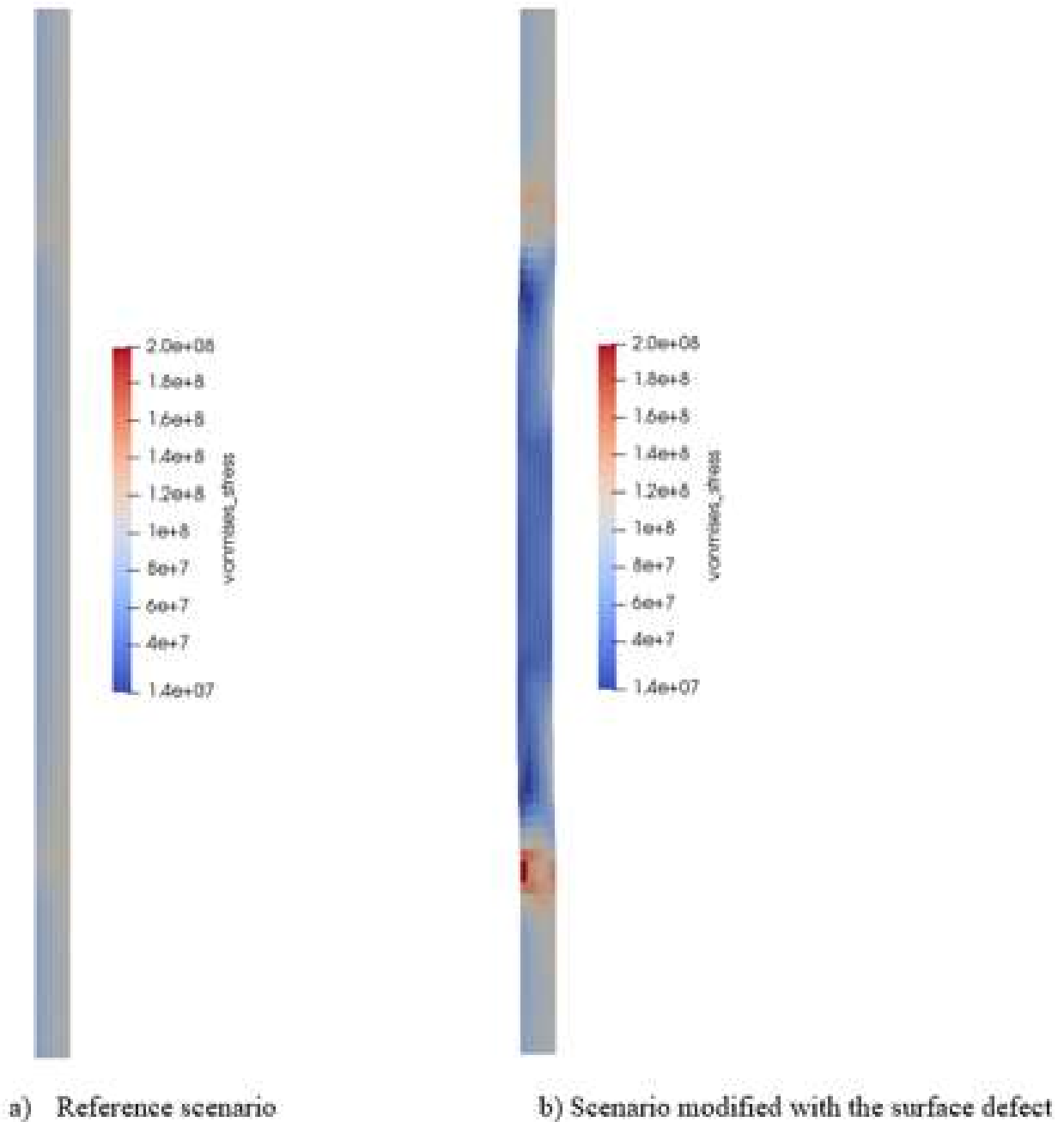


FIG. 9. Von Mises stresses in the cladding in the 11-pellet reference case and the respective missing pellet surface case at 787 days. The scales are the same in both figures. Units are in Pascals.

The condensation and vaporization reactions stabilize quickly when the kinetic model with radiation is applied to solid cesium iodide. The formation of hydrogen iodide seems more favoured at the fuel rod temperature, as seen in the top part of Fig.10. Formation of hydrogen iodide is however limited by the available hydrogen in the system. Hydrogen is present as a minor product from nuclear reactions, but also as an impurity. Only the amount from nuclear reactions was considered in this study. Even though this amount was small, it was the same order of magnitude as other iodine species and even the most dominant.

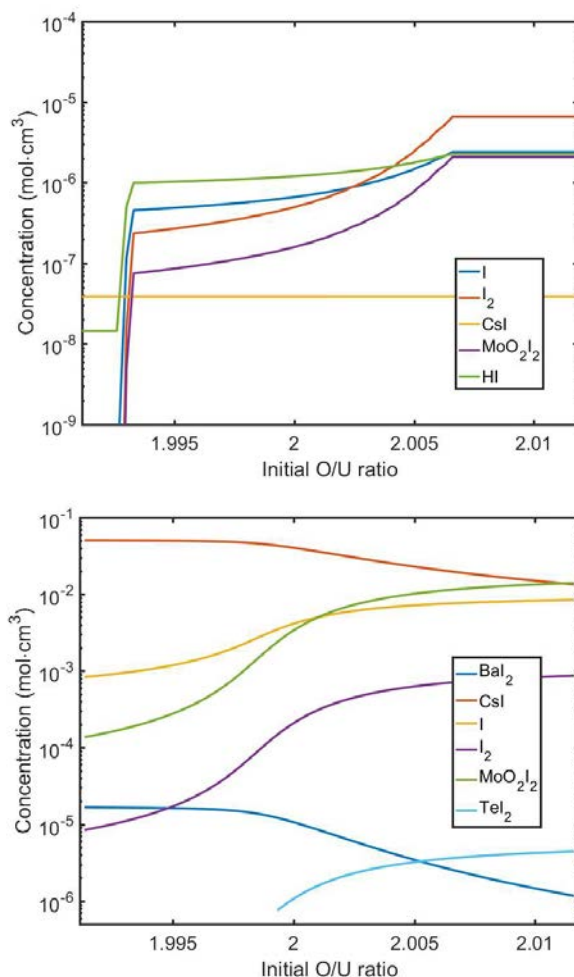


FIG. 10 The highest concentrations of the gas phase species containing iodine at a temperature of and 773 K (top) and 1473 K (bottom).

5. CONCLUSIONS

At VTT, the topic of PCI including SCC has been approached by modelling the mechanical and chemical behaviour of a fuel rod. These studies have focused on the phenomena that have an impact on PCI either directly or secondarily. The work on cladding creep by Tulkki and Ikonen presented the development of transient cladding creep models with varying levels of complexity. This study is connected to PCI secondarily, as it describes the mechanical states of the fuel rod that precede PCI and the stress state during pellet-cladding contact.

Two studies by Loukusa were also summarized, with one of them directly investigating the mechanical evolution of the pellet-cladding interface for a fuel rod with a missing pellet surface defect. The impact of the defect was simulated using BISON fuel performance code. This research will facilitate the further usage of BISON at VTT, when the topic will be revisited with more complex computational tools. The second study by Loukusa utilized the Gibbs energy minimization method to investigate the chemical evolution of the pellet surface. The

conclusion was that hydrogen iodide is the thermodynamically favoured form of iodine at low fuel temperatures in a fuel rod, which might have an impact on stress-corrosion cracking.

REFERENCES

- [1] TULKKI, V., Modelling Nuclear Fuel Behaviour and Cladding Viscoelastic Response (2015).
- [2] LOUKUSA, H., Modelling Missing Pellet Surface Defects with BISON, Technical report VTT-R-00067-19, VTT Technical Research Centre of Finland Ltd (2019).
- [3] LOUKUSA, H., VALTAVIRTA, V., “Application of Constrained Gibbs Energy Minimization to Nuclear Fuel Thermochemistry”, Proceedings of TopFuel, 2018. Paper A0127.
- [4] LUCAS, G., PELLOUX, R., Nucl. Technol. **53** (1981) 46–57.
- [5] MURTY, K., YOON, K., Transactions of the 5th International Conference on Structural Mechanics in Reactor Technology (SMiRT-5) C3/6, 1979.
- [6] MATSUO, Y., ASTM STP **1023** (1989) pp.678–691.
- [7] TULKKI, V., IKONEN, T., Modelling of Zircaloy Cladding Primary Creep during Load Drop and Reversal, Journal of Nuclear Materials **445** (2014) 98-103.
- [8] TULKKI, V., IKONEN, T., Viscoelastic Modelling of Zircaloy Cladding In-Pile Transient Creep, Journal of Nuclear Materials **457** (2015) 324-329.
- [9] TULKKI, V., IKONEN, T., Modelling Anelastic Contribution to Nuclear Fuel Cladding Creep and Stress Relaxation, Journal of Nuclear Materials **465** (2015) 34-41.
- [10] MCGRATH, M., HWR-471 (1996).
- [11] MATSUO, Y., ASTM STP **1023** (1989) pp.678–691.
- [12] MATSUO, Y., Journal of Nuclear Science and Technology **24** (1987) 111–119.
- [13] KOZAR, R., JAWORSKI, A., WEBB, T., SMITH, R., Journal of Nuclear Materials **444** (2014) 14–22.
- [14] HANAWA, S., HWR-882 (2008).
- [15] DELOBELLE, P., ROBINET, P., GEYER, P., BOUFFIOUX, P., Journal of Nuclear Materials **238** (1996) 135-162.
- [16] SPENCER, B. W., HALES, J. D., NOVASCONE, S. R., WILLIAMSON, R. L., “3D Simulation of Missing Pellet Surface Defects in Light Water Reactor Fuel Rods”, TopFuel (2012).
- [17] SPENCER, B. W., WILLIAMSON, R. L., STAFFORD, D. S., NOVASCONE, S. R., HALES, J. D., PASTORE, G., 3D Modelling of Missing Pellet Surface Defects in BWR Fuel, Nuclear Engineering and Design **307** (2016) 155–171.
- [18] HALES, J. D., GAMBLE, K. A., SPENCER, B. W., NOVASCONE, S. R., PASTORE, G., LIU, W., STAFFORD, D. S., WILLIAMSON, R. L., PEREZ, D. M., GARDNER, R. J., BISON User’s Manual - BISON Release 1.1. Technical Report INL/MIS-13-30307 Rev. 2, Idaho National Laboratory, Idaho Falls, IA, USA (2014).
- [19] [ARKOMA, A., BISON Fuel Performance Code: Initial Investigations at VTT, Technical Report VTT-R-02258-18, VTT Technical Research Centre of Finland Ltd., Espoo, Finland (2018).
- [20] COX, B., Pellet-Clad Interaction (PCI) Failures of Zirconium Alloy Fuel Cladding - A Review, Journal of Nuclear Materials **172** (1990) 249–292.
- [21] KONASHI, K., YATO, T., KANEKO, H., Radiation Effect on Partial Pressure of Fission Product Iodine, Journal of Nuclear Materials **116** (1983) 86–93.
- [22] KONASHI, K., YAMAWAKI, M., YONEOKA, T., CsI Decomposition Due to Collision Cascade Initiated by Fission Fragments, Journal of Nuclear Materials **160** (1988) 75–80.
- [23] LOUKUSA, H., IKONEN, T., VALTAVIRTA, V., TULKKI, V., Thermochemical Modelling of Nuclear Fuel and the Effects of Oxygen Potential Buffers, Journal of Nuclear Materials **481** (2016) 101–110.

PCMI BENCHMARKS AND THE NEA FRAMEWORK FOR IN-PILE FUEL AND MATERIAL TESTING

D. COSTA, J.-F. MARTIN, M. FLEMING, I. HILL, T. IVANOVA
Nuclear Energy Agency,
Paris, France
Email: davide.costa@oecd-nea.org

Abstract

Member countries of the OECD/NEA have increasingly engaged in joint scientific studies aimed at investigating fuel behaviour in normal operation and accident conditions. Pellet Clad Mechanical Interaction (PCMI) is a particular topic of high importance within the Nuclear Science Committees (NSCs) programme of work. Notably, two ongoing benchmarks are examining different aspects of PCMI; the Expert Group on Reactor Fuel Performance (EGRFP) PCMI benchmark, and the Expert Group on Multi-Physics Experimental data, Benchmarks, and Validation (EGMPEBV) Multi-physics benchmark.

Launched in 2015, the EGRFP PCMI benchmark is aimed at improving both the understanding and modelling of this phenomenon amongst NEA member organisations. By comparing PCMI predictions of different fuel performance codes for a number of cases, the source of differences and sensitivity to different modelling assumptions and material properties are analysed. The EGRFP benchmark is focused on single physics, while the EGMPEBV benchmark seeks to answer questions regarding the consequences of coupling methods of fuel performance simulations with other physics such as neutronics and thermal-hydraulics. Within this context, the EGMPEBV has engaged in a benchmark exercise dedicated to quantifying the uncertainties associated with multi-physics modelling using R2 reactor ramp data, provided by Studsvik. This activity will provide expert recommendations to enhance multi-physics modelling and simulation.

On the experimental side, the NEA and IAEA have collected a large number of benchmarks within the International Fuel Performance Experiments (IFPE) database that are suitable for testing code predictions of PCMI. However, it is clear that a gap in experimental data still exists. To address member countries concerns about the experimental data for fuel performance, the NEA is launching a multilateral initiative to strengthen the global fuel- and material-related experimental capabilities for the benefit of a broad community of users. This effort was elicited by the recent closure of the Osiris, Halden and NRU reactors that potentially threaten the continuity of the fuel performance tests and qualification in support of the safe, reliable and efficient long-term operation of Nuclear Power Plants. In response, the NEA member countries have initiated the development of a framework to conduct multinational joint experimental campaigns for in-pile fuel and material testing. The framework will allow the NEA membership to access irradiation facilities and materials in a way that compliments their domestic needs and capabilities

1. INTRODUCTION

The Nuclear Energy Agency (NEA) Division of Nuclear Science promotes and coordinates cooperation among member countries in the domain of the research and development for peaceful application of nuclear technology.

Under the direction of the Nuclear Science Committee (NSC), representing the NEA member countries, the different activities coordinated by the Division of Nuclear Science have been organized into working parties that are mandated by the NSC to address various technical topics:

- Working party on the scientific issues of reactor systems (WPRS);
- Working party on the scientific issues of the fuel cycle (WPFC);
- Working party on multi-scale modelling of fuels and structural materials for nuclear systems (WPMM);
- Working party on international nuclear data evaluation co-operation (WPEC);
- Working party on nuclear criticality safety (WPNCSS).

Under the guidance of these working parties, expert groups are formed in which subject matter specialists, nominated by working party members, collaborate to deliver outputs consistent with the programme of work. Typical deliverables of the NSC working parties are joint data evaluations, benchmark exercises, state-of-the-art reports, and experimental data. The role of the Division of Nuclear Science is to coordinate the efforts of the different working parties, to preserve their outputs, and to foster the use of the collected information to challenge and strengthen the scientific basis of the nuclear technology. In this respect, one of the main missions of the Division of Nuclear Science is to establish appropriate links between the different activities and enhance the communication and information exchange among different scientific communities (e.g. modelers and experimentalist).

The various NSC activities related to fuel are carried out within different working parties and expert groups (Figure 1). In particular, the pellet cladding mechanical interaction (PCMI) related studies mainly pertain to the Expert Group on Reactor Fuel Performance (EGRFP) within the WPRS and the Expert Group on Multi-Physics Experiments Benchmarking (MPCMIV). Benchmark exercises, with different scopes and purposes, are being conducted or planned within these two expert groups. These activities will be described in section II.

On the data preservation side, the NSC, through the EGRFP, is supporting the improvement of the accessibility and usability of the data collected in the International Fuel Performance Experiments described in section III. A relational database was built to enforce a robust and efficient storage of the data; an associated graphical user interface (GUI) was also developed that allows browsing and plotting the data, thus enabling preliminary data analysis.

Finally, on the experimental side the NSC, in collaboration with the Committee on the Safety of Nuclear Installations (CSNI), is pursuing the establishment of a multilateral initiative to strengthen fuel- and material-related worldwide in-pile testing capabilities for the benefit of a broad international community of users. This initiative - whose goal is to facilitate the collection of experimental evidence in support of the safe, reliable and efficient operation of nuclear power plants - has become even more relevant since the closure of the Halden test reactor. A core objective of this endeavour is the development of a multinational framework enabling a coordinated, efficient, and cost-effective strategy for the performance of key experiments using the available facilities around the world.

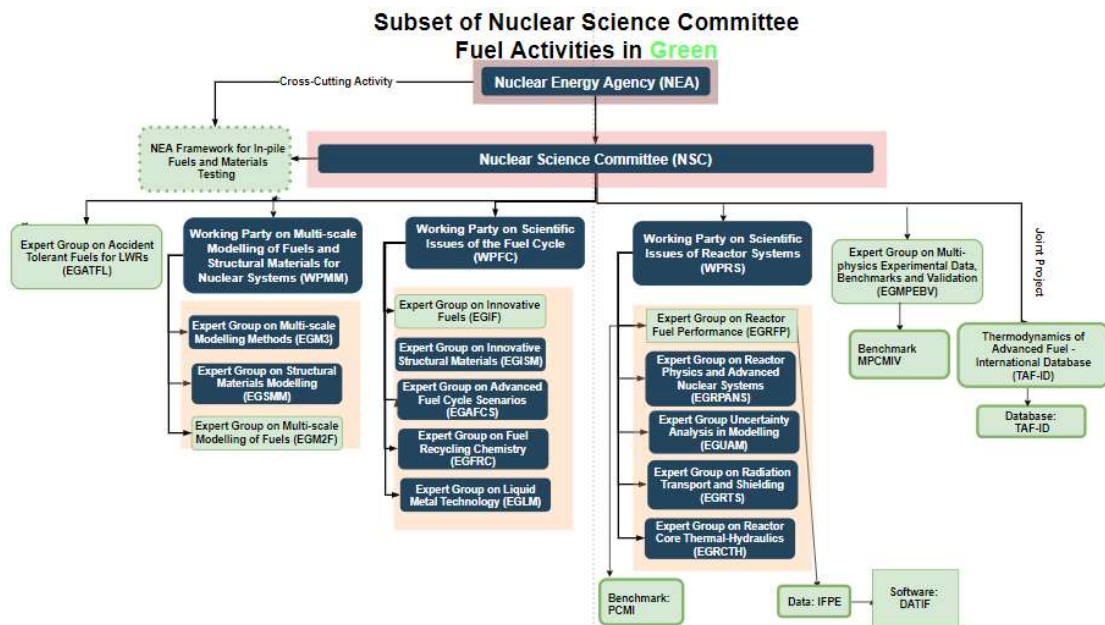


FIG. 1. Subset of NSC Activities linked to fuel for existing and advanced reactors.

2. NEA PCMI BENCHMARKS

Two PCMI benchmarks are currently ongoing or being planned within the NEA Division of Nuclear Science activity. The first is being conducted within the EGRFP, The second is being organized within the Expert Group on Multi-Physics Experiments, Benchmarks and Validation (EGMPEBV) [3].

Additional details on these benchmark studies on PCMI will be given in the next two subsections.

2.1. EGRFP PCMI benchmark

Launched in 2015 the EGRFP PCMI benchmark is aimed at improving both the understanding and modelling of this phenomenon amongst NEA member organizations. By comparing PCMI predictions for a number of cases, the source of differences and sensitivity to different modelling assumptions and material properties can be analyzed. Cases 1, 1a, 2, 2a are numerical verification cases intended to investigate the effects of code-to-code

differences. While cases 3, 4, are actual irradiations for use in comparison of code predictions with experimental measurements.

A description of cases is as follows:

- Case 1: modelling of hypothetical BOL ramp of PWR rodlet [1];
- Case 1a: model case 1 with a fixed number of cracks and friction coefficient [2];
- Case 2: modelling of hypothetical BOL ramp of commercial PWR rod;
- Case 2a: model case 2 with a fixed number of cracks and friction coefficient [2];
- Cases 3 and 4: modelling and comparison with experimental data provided by Halden Reactor Project (HRP):
- Case 3: BOL ramp of experimental rods with different pellet designs, IFA-118 rig (irradiated in the Halden Boiling Water Reactor (HBWR) from 1969 to 1970);
- Case 4: EOL ramp of PWR rodlet IFA-629.4 rod 7.

2.2. EGMPEBV: Multiphysics pellet-clad mechanical interaction validation (MPCMIV)

The EGMPEBV has engaged in a benchmark exercise dedicated to Multiphysics Pellet-Clad Mechanical Interaction Validation (MPCMIV) relying on R2 reactor ramp data, provided by Studsvik and compiled by N.I.N.E under the approval and guidance of the EGMPEBV and support from US DoE. Reactor physics, thermal-hydraulics and fuel performance tools need to be coupled to achieve a high fidelity simulation, although participants relying on either fuel performance tools, traditional and/or novel coupled tools are invited to contribute. To this day, 24 participants from 16 organizations and 8 countries have registered to be part of the exercise.

3. DATABASE FOR IFPE (DATIF)

One of the key missions of the NEA is knowledge preservation. The EGRFP is committed to the preservation and dissemination of fuel performance experimental data and, particularly, the international fuel performance experiments (IFPE) database. In the subsections below we will present some background information on the IFPE and the efforts that are being pursued within the EGRFP to improve the accessibility of the IFPE data.

3.1. Background: International fuel performance experiments database (IFPE)

The IFPE (International Fuel Performance Experiments) collection, developed jointly by the OECD/NEA and IAEA for over 20 years [4], contains measurements characterising approximately 1500 fuel rods having undergone both in-pile and out-of-pile testing. Data primarily consist of LWR (PWR, BWR, WWER) fuel, but also contains other types of fuels (PHWR, demonstrator reactor fuels ...). The relative proportion of rods, categorized by associated reactor-fuel-clad types, are displayed in Figure 2.



FIG. 2. Indicative proportion of rod types in the IFPE collection as of 2019.

This accumulated data is an authoritative resource for the validation of fuel performance codes predictions, spanning a wide range of phenomena, such as fission product release [5,6], thermal performance [7] and fuel swelling with various irradiation and power histories. The IFPE data has been at the centre of many international programmes/activities benchmarking fuel performance codes, for example FUMEX, FUMAC [8-11] at the IAEA, the Expert Group on Reactor Fuel Performance (EGRFP) and Working Group on Fuel Safety (WGFS) at the OECD/NEA. It is widely distributed via the OECD/NEA Databank Computer Program Services, with approximately sixteen thousand single experiment packages distributed over the period 1995-2018.

The collection is actively maintained, and new additions can be integrated routinely – a guide is available that provides the list of necessary information for inclusion of an experimental data set into IFPE [12]. In particular, foreseen additions to the collection include, for the near future, cases covered in the recent IAEA FUMAC exercise, with data from the Halden Reactor Project. In a longer-term future, activities initiated within the IAEA about fuel performance dedicated to fast reactor fuels may feed the IFPE collection with a new type of data, namely fast reactor fuel data.

3.2. Need for an Updated Interface for IFPE

As IFPE has grown, its further expansion has created challenges. The structure of IFPE has remained unchanged from its inception, namely, a collection of reports. Having accumulated a considerable amount of data has made identifying key data for validating specific phenomena a cumbersome process. Furthermore, identifying trends in the data is a labour-intensive process requiring hundreds of hours of manual extraction, done across hundreds of packages; clearly each organization performing this work in isolation is counterproductive. In order to maximise the utility of the data set, the OECD/NEA has launched an initiative aimed at building a Relational database and associated GUI that can accommodate fuel performance experiments, such as those contained in IFPE, in line with recommendations provided by the EGRFP.

Relying on the in-house know-how for building relational databases and associated graphical user interface (GUI) [13, 14], the NEA has developed in 2018-2019 a piece of software named DATIF for DATAbase for IFpe. DATIF shall enhance the accessibility of collected experimental data and allow the user to dedicate his time to analyzing the data rather than extracting it.

3.3. Data available in the relational database

The data embedded in the relational database consists of (1) fabrication data for the fuel, pellets, clad, assembly as applicable, (2) irradiation data in terms of thermal-hydraulics coolant conditions, thermal power, burn up and neutron fluxes, as well as in-pile measurements if applicable, and (3) post-irradiation experiments.

In order to accommodate data for all these “steps” of the life of a tested rod, the database can concatenate a variety of data types, ranging from a single values (‘metadata’, either numerical or non-numerical) such as average grain size, fuel enrichment etc. to full time-dependent datasets reaching a few hundred points for the description of the irradiation history, to again key values for the PIE, but also images obtained from PIE analysis of the fuel and/or clad samples.

3.4. Interface: Searching

Once the data is formatted and loaded into the relational database, the GUI allows to navigate the data in an intuitive manner. A screenshot of DATIF’s homepage is provided in Figure 3.

One can distinguish on the latter figure the “search panel” which allows to define sorting criteria to select experiments/rods of interest. The left panel provides the “categories” of data which can be used for defining the search criteria, while the criteria themselves are in the central panel. The bottom panel provides a reminder of the search parameters, and at the very bottom, one can see the number of experiments/rods that fulfil the criteria – this information being dynamically updated, prior launching the “search” (note that the IFPE data has not yet been fully implemented in the database, therefore one can only access a subset of the data for now). Special care has been dedicated to defining identifiers for the datasets, which allow organization of experiments and rods in a self-consistent manner while providing a glimpse of the experiment topic. The identifier contains the fuel, clad and reactor type of the investigated rod. Reactor type refers to the design of the rod rather than the irradiation reactor: for example, a rod prototypical of BWR designs, tested in a research reactor, will be categorized as BWR rods.

The screenshot is representative of queries built upon the identifier, but it is also possible to search by fabrication properties (initial enrichment, fuel-clad gap, geometry of pellets, ...), by irradiation histories (ramp testing, fast flux values, ...) and/or by availability of specific measurement results (in-pile elongation, PIE fission gas release measurement, ...) so as to construct a query that specifically fits the user's needs and interests.

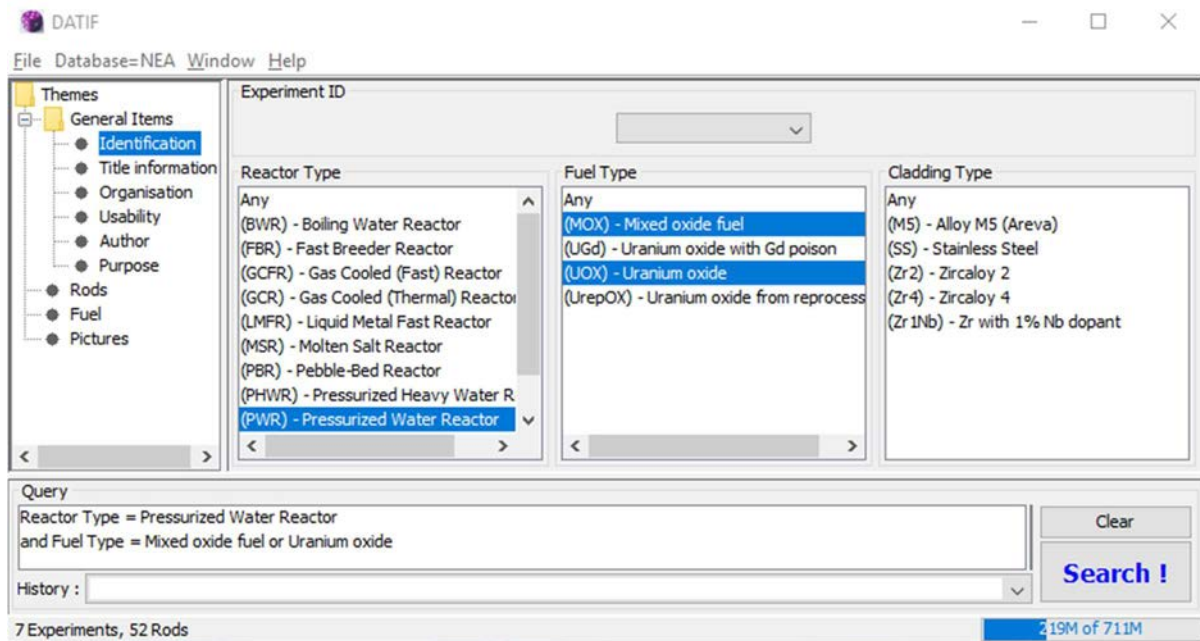


FIG. 3. Screenshot of DATIF homepage.

3.5. Progress Status and Future Plans

Currently, about 20% of the rods contained in IFPE is accessible via DATIF, and progress on filling-in the database is continuous; however one should note that DATIF does not aim to replace IFPE and it will always be necessary for the end user to refer to the original experimental report provided in the IFPE collection.

Incentives to implement automatic generation of code inputs from the data contained in DATIF, and to run sensitivity calculations, are currently being investigated and will be an added future feature of DATIF. This topic is covered in [15].

After internal testing in 2018, DATIF will be made available in 2019 to the EGRFP members for external testing. Public release is foreseen to take place in 2020. Interested parties can contact datif@oecd-nea.org.

4. NEW FRAMEWORK FOR FUELS AND MATERIALS TESTING

During the last two years, the NEA organized a series of workshops with the aim of gathering relevant representatives from the international community to address the worldwide progressive decrease of in-pile material and fuel testing facilities. The shutdown of the Halden reactor in Norway, the OSIRIS in France, the JMTR in Japan, the NRU in Canada, among others, captures this trend. This situation threatens the capability of the nuclear community to guarantee the minimum level of R&D effort which is key to maintain the safe, reliable, and efficient long term operation of the current nuclear reactors fleet. Furthermore, these circumstances hinder the effectiveness of the nuclear industry to absorb innovations arising in various scientific area and to integrate them into commercial power plants.

In particular, the safe, reliable and efficient operation of nuclear power plants may not benefit from the evolving nuclear fuel and materials (F&M) technology because of the incapability of testing new products' performances and to pursue their optimization beyond the laboratory scale. To achieve this, experimental evidences have to be sought through thorough experimental campaigns, which can only be run in test facilities with the ability to perform neutron irradiation under representative steady state or transient conditions. F&M test facilities are essential for:

- Validating safety margins, simulation tools, and demonstrating operational performance;
- Assessing material behaviour in the context of the long term operation programmes;
- Developing advanced F&M.

In particular, the availability of test facilities for loss-of-coolant accidents, reactivity-initiated accidents and power ramps, is crucial.

The above-mentioned series of workshop was organized by the NEA Nuclear Science Committee (NSC) and the Committee on the Safety of Nuclear Installation (CSNI) to share the views of regulators, technical support organizations, research organizations, and the industry from the NEA member countries. All these entities agreed on the need for fuel and material testing capacities on an ongoing basis and agreed on the fact that nuclear safety and innovation in the nuclear technology are global challenges that require to be faced through a joint international effort. Consequently, a strong consensus arose on the need of creating a common framework to address current and future experimental needs, and the international community is now coming together under the aegis of an NEA initiative to form a new multinational framework for in-pile fuels and material testing as a new NEA joint research undertaking: the Framework for Irradiation ExperimentS (FIDES).

The main missions of FIDES are the following:

- identifying and prioritizing the needs of the nuclear energy community, including regulators and their technical support organizations, the industry and the research organizations;
- identify and assure access to research facilities around the world in the most efficient way and facilitate high priority experiments at those facilities;
- define and implement a co-ordinated multilateral programme that meets short- and long term experimental needs;
- promote and sustain relevant state-of-the-art capacities: infrastructure, technology and skills;
- establish the conditions necessary for conducting experiments on a bi-lateral contract basis.

By consolidating the needs and resources from the involved parties, FIDES will provide the framework for the implementation of Joint Experimental Programmes (JEEPs) (Figure 4).

The objective being to supervise the JEEPs to ensure they efficiently address the needs of the FIDES participating organizations and to help them completing domestic researches with ad hoc international programmes.

The expectation is that the FIDES framework will create a co-operative dynamic for sustained investment in the worldwide experimental capacity. These investments will include new experimental devices in existing facilities or new research reactors by:

- Providing continuity and sustainability in the strategic field;
- Building a collective awareness of needs and capabilities Identifying gaps that require investments and facilitating related implementations;
- Optimizing the value of experimental campaigns through cross-cutting activities;
- Development of state-of-the-art instrumentation and modelling & simulation;
- Preservation and quality management of experimental data;
- Professional development and educational activities;
- Addressing practical issues (nuclear fuel transport and waste management and others).

At the moment, the following six JEEPs with different level of maturity have been proposed to be implemented within the FIDES:

- Programme for quantifying thermomechanical clad load mechanisms during LWR slow transient (P2M) at the BR2 reactor in Belgium and at the CEA hot cells in France;
- Programme for studying fuel rod behaviour under LOCA conditions at the MIR.M1 reactor in Russia;
- In-pile Creep Studies of ATF Claddings (INCA) at the LVR-15 material test reactor in Czech Republic;
- Programme for studying PWR fuel rods behaviour under LOCA conditions at the CABRI reactor in France;
- International NSRR Test Programme for LWR fuels (INSTEP) which considers possible RIA tests on additive fuels at the newly restarted NSRR facility in Japan;
- Missing Pellet Surface (MPS) experimental programme using conventional LWR fuel to support 3D modelling and simulation.

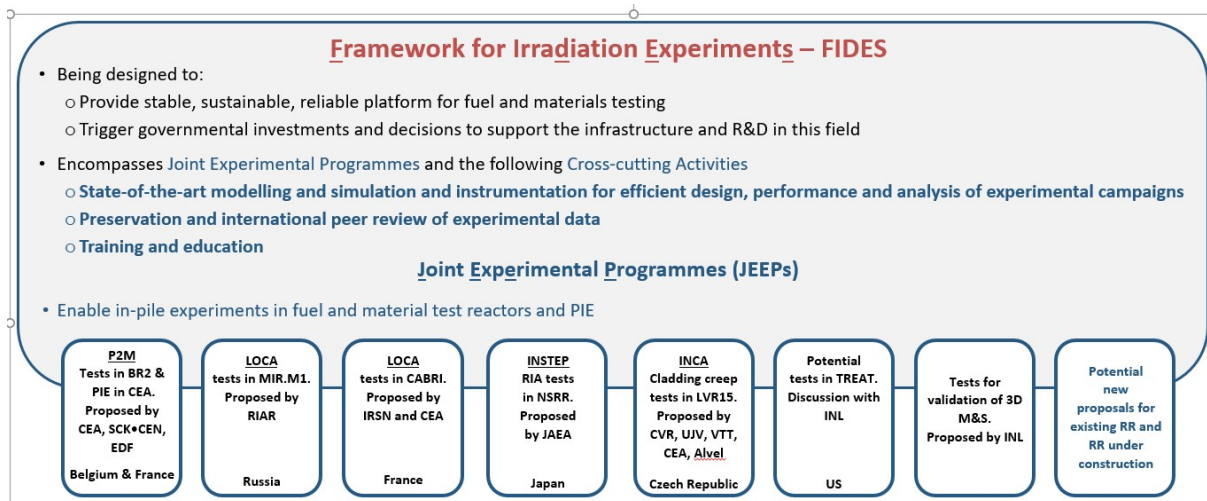


FIG. 4. Framework for Irradiation Experiments (FIDES) and its Joint Experimental Programmes (JEEPs).

Of the JEEP proposals made so far, the most mature are due to start by the end of 2020. To avoid discontinuities in fuel and materials testing while maintaining the momentum for the prompt conclusion of the framework, both JEEP proposals and the framework agreement are being developed in parallel. In addition, discussions with research organizations that operate F&M testing facilities continue to identify research priorities and to look for further research opportunities to address them.

5. CONCLUSIONS

The study of nuclear fuel is central to many activities ongoing in the NEAs nuclear science committee. As fuel modelling advances and moves towards more mechanistic models, which are informed by lower scale physics, the need for both verification activities such as code to code comparisons, and validation activities underpinned by transparent databases such as the IFPE will be of increased importance.

Previously, countries were able to domestically embark on large scale experimental campaigns to test and down select nuclear fuels and materials. This capacity is being progressively degraded by the closure of some key facilities and the reduction of country's investments on R&D related to nuclear energy production. This situation threatens the capability of the NEA member countries to safely and efficiently deliver low carbon power in the long term. International cooperation can be part of the strategies to overcome this situation. The NEA, under the guidance of its member countries is developing the FIDES framework with the objective of centralizing the coordination of the worldwide existing in-pile testing facilities to efficiently match the demand in terms of data.

ACKNOWLEDGMENTS

The work presented in this paper is based on the contributions of participants in the NEA activities, and in particular the chairs of the relevant groups, Glyn Rossiter (EGRFP), Tim Valentine (EGMPEBV) mentioned in the paper. The authors wish to acknowledge the NEA IT development team Manuel Bossant and Nicolas Soppera for the development of the DATIF software.

REFERENCES

- [1] ROSSITER, G. et al., "OECD/NEA Benchmark on Pellet-Clad Mechanical Interaction Modelling with Fuel Performance Codes", OECD/NEA Workshop on Pellet-Cladding Interaction (PCI) in Water Cooled Reactors, 22-24 June 2016, Lucca, Italy.
- [2] DOSTAL, M. et al., "OECD/NEA Benchmark on Pellet-Clad Mechanical Interaction Modelling with Fuel Performance Codes: Impact of Number of Radial Pellet Cracks and Pellet Clad Friction Coefficient", TopFuel 2018, Prague, Czech Republic.

- [3] VALENTINE T, IVANOV K, AVRAMOVA M, et al. "OECD-NEA Expert Group on Multi-Physics Experimental Data, Benchmarks and Validation", ASME International Conference on Nuclear Engineering, Volume 4 Nuclear Safety, Security, and Cyber Security; Computer Code Verification and Validation ():V004T15A009. doi:10.1115/ICONE26-81571
- [4] MENUT, P., SARTORI, E., TURNBULL, J. A., "The Public Domain Database on Nuclear Fuel Performance Experiments (IFPE) for the Purpose of Code Development and Validation", ANS International Topical Meeting on Light Water Reactor Fuel Performance, Park City, Utah, USA, April 2000, pp. 10-13.
- [5] SCHUBERT, A, LASSMANN, K, VAN UFFELEN, P, VAN DE LAAR, J, ELENKOV, D, ASENOV, S, BONEVA, S, DJOURELOV, N, GEORGIEVA, M. "Analysis of Fuel Centre Temperatures and Fission Gas Release Data From the IFPE Database", Bulgaria, 2003.
- [6] TURNBULL, J. A., MENUT, P., SARTORI, E., "A Review of Fission Gas Release Data within the NEA/IAEA IFPE Database", Fission Gas Behaviour In Water Reactor Fuels (2002) p117.
- [7] KILLEEN, J. C., SARTORI, E., TURNBULL, J. A.. "Experimental Data on PCI and PCMI within the IFPE Database", Seminar Proceedings on Pellet-clad Interaction in Water Reactor Fuels, Aix-en-Provence, France, 9-11 March 2004, p. 347. OECD Publishing, 2005.
- [8] INTERNATIONAL ATOMIC ENERGY AGENCY, FUMEX, IAEA-TECDOC-998, IAEA, Vienna (1998).
- [9] INTERNATIONAL ATOMIC ENERGY AGENCY, Fuel Modelling at Extended Burnup (FUMEX-II). IAEA-TECDOC-1687, IAEA, Vienna (2012).
- [10] INTERNATIONAL ATOMIC ENERGY AGENCY, Improvement of Computer Codes Used for Fuel Behaviour Simulation (FUMEX-III), IAEA-TECDOC-1697, IAEA, Vienna (2013).
- [11] VESHCHUNOV, M., STUCKERT, J., VAN UFFELEN, P., WIESENACK, W., ZHANG, J., "FUMAC: IAEA's Coordinated Research Project on Fuel Modelling in Accident Conditions", Trans. TopFuel (2018).
- [12] Requirements for including data in the IFPE Database, NEA document, available at <https://www.oecd-nea.org/science/wprs/fuel/>
- [13] Hill, I., Gulliford, J., Soppera, N., Bossant, M., DICE 2013. New capabilities and data. No. JAEA-CONF--2014-003. 2015.
- [14] HILL, I., SOPPERA, N., BOSSANT, M., IDAT: The International Handbook of Evaluated Reactor Physics Benchmark Experiments Database and Analysis Tool, Nuclear Science and Engineering 178 [3] (2014) 280-294.
- [15] O'GRADY, D, PRICE, D, KOZLOWSKI, T., MARTIN, J.-F., HILL, I., "A Framework for Consistent Fuel Performance Calculations", paper presented at TopFuel 2019.

OPTIMIZING PCI/SCC DESIGN METHODOLOGY AND LICENSING

(Session IV)

Chairperson

N. WAECKEL

France

REGULATORY APPROACHES TO JUSTIFY THE STRENGTH AND OPERABILITY OF WWER REACTORS FUEL ELEMENTS

V.S. RUBTSOV

Scientific and Engineering Centre for Nuclear and Radiation Safety,

Moscow, Russian Federation

Email: vrubtsov@secnrs.ru

1. INTRODUCTION

In the Russian Federation a lot of attention is paid to the structural integrity and tightness of fuel elements of WWER reactors under operation. According to the normative document «General Provisions for Ensuring the Safety of Nuclear Power Plants» NP-001-15 [1], the cladding of the fuel rods is identified as one of physical barriers to prevent the spread of radionuclides in the environment. Specifically for the fuel cladding integrity, the normative document «Nuclear Safety Rules for Reactor Plants of Nuclear Power Plants» NP-082-07 [2] states that “the design and implementation of the core and its components (including fuel rods and fuel assemblies) should be such that during normal operation and operational events, including design basis accidents, fuel damage limits would not be exceeded taken account of:

- design operational modes of reactor, their number and design course;
- mechanical, thermal and radiation impact on the nuclear core components;
- physical and chemical interaction of the core structural materials and coolant;
- limiting deviations from design, process characteristics and process parameters;
- shock and vibration impacts, thermal cycling, radiation and thermal creep and material ageing;
- influence of the radionuclides and admixtures of coolant on strength and corrosion resistance of the fuel rods;
- other factors which lead to the mechanical properties of the core structural materials degradation and may lead to the loss of fuel rods cladding integrity.”

For normal operating conditions of WWER reactors, the following limits for the defective fuels are established [2]:

- “Defects leading to gas leaks - not more than 0.2% of the number of fuel elements in the core;
- Defects leading to direct contact of nuclear fuel with the coolant - not more than 0.02% of the number of fuel elements in the core.”

The main requirements for justifying the strength and operability of the fuel elements of WWER reactors are established in the normative document «The main requirements for justifying the strength and thermomechanical behaviour of the fuel assemblies and fuel elements in the core of water cooled power reactors» NP-094-15 [3], which has been valid since 2016 and has the status of federal norms and rules in the field of nuclear energy, the requirements of which are mandatory for nuclear plants in the territory of the Russian Federation.

Rules NP-094-15 [3] define:

- “Requirements for the physical and mechanical characteristics of structural materials of fuel elements and fuel assemblies, taking into account the effect of irradiation and chemical composition of the coolant. For the materials of the cladding of the fuel elements, the physical and mechanical characteristics must be determined taking into account the influence of the gas chemical composition under the cladding;
- The criteria for the strength and operability of the fuel elements and fuel assemblies during operation;
- Requirements for the analysis of strength and operability of fuel elements and fuel assemblies, including safety factors, types of loads and phenomena that should be taken into account in calculations;
- The list of mandatory calculations of fuel assemblies for strength and requirements for these calculations;
- Requirements for the experimental justification of strength and operability of fuel elements and fuel assemblies.”

2. FIELD OF APPLICATION OF THE NORMATIVE DOCUMENT NP-094-15

Federal norms and rules in the field of nuclear energy «The main requirements for justifying the strength and thermomechanical behaviour of the fuel assemblies and fuel elements in the core of water-cooled power reactors» NP-094-15 [3] establishes the requirements for strength and operability justifications of fuel assemblies and fuel elements for operating WWER-440, WWER-1000 and WWER-1200 reactors in all plant states including normal operation, deviations from normal operation and design basis accidents.

The action of NP-094-15 does not apply to the following cases:

- In the presence of extrinsic objects in the coolant of the primary circuit;
- In case of violations of the standards for conducting the water-chemical regime of the reactor primary circuit;
- During accident conditions, including reactivity-initiated accidents, loss of coolant and other accidents with drastic violations of heat removal from fuel elements as well as in accidents with the fall of fuel assemblies during transportation and technological operations.

3. THE MAIN PROVISIONS OF NORMATIVE DOCUMENT NP-094-15

The strength and operability of fuel elements and fuel assemblies shall be justified in the reactor design, and the results of the justification shall be presented in the NPP safety analysis reports (SAR). The impact of the introduced changes on the following items shall be justified: the use of new structural materials, changes in the chemical composition of the fuel, changes in the manufacturing technology of fuel elements, fuel or fuel element cladding (if these changes may affect their strength characteristics), changes in the standards of water chemistry regime of the primary coolant, changes in the design conditions of operation, the strength and operability of fuel elements and fuel assemblies.

According to NP-094-15 [3], the justification on the strength and operability of fuel elements and fuel assemblies shall be based on the results of calculations and (or) experiments which shall demonstrate that the limit states of fuel elements and fuel assemblies will not be achieved throughout their designed life for all regimes, provided by the reactor design basis.

The safety factor values for the limiting states of the fuel elements and fuel assemblies shall be set so that throughout the design life of the fuel elements and fuel assemblies, their strength and operability are ensured with due regard to all operational loads for all regimes in accordance with design basis.

The methods used to calculate the stress-strain state of fuel elements and fuel assemblies and to predict their thermo-mechanical behaviour during operation shall take into account all the loads acting on fuel elements and fuel assemblies in the all modes and determine the numerical values of the parameters characterizing the achievement or non-achievement of the limit states during operation.

4. REQUIREMENTS FOR PHYSICAL AND MECHANICAL CHARACTERISTICS OF THE STRUCTURAL MATERIALS OF FUEL ELEMENTS AND FUEL ASSEMBLIES

The structural materials used for the manufacture of fuel elements and fuel assemblies shall have radiation and chemical resistance in the coolant of WWER reactors throughout the entire service life.

Physical and mechanical characteristics of materials of fuel elements and fuel assemblies shall be defined in the temperature range covering all design modes with due regard to anisotropy of properties of materials (if available) and influence of exposure to radiation. The range of radiation doses at which the physical and mechanical properties of the materials are determined shall be sufficient to justify the strength and operability of the fuel elements and fuel assemblies throughout the service life of the fuel assemblies to the design fuel burn-up values.

Determination of physical and mechanical characteristics of materials required for justification of strength and operability of fuel elements and fuel assemblies (modulus of elasticity of the first and second type, tensile strength, yield strength, Poisson's ratio, elongation, relative contraction, tensile strength, deformation diagram of fuel assemblies materials at different rates of deformation, long term strength curves, thermal and radiation creep rate, anisotropy coefficient of plasticity and creep, fracture toughness characteristics, fatigue curves, isochronous creep curves, constants that determine the rate of incremental growth of cracks during operation) is provided by material research centre. Numerical values of the specified physical and mechanical characteristics shall be available in the standardization documents.

The material research centre should provide keeping the confirmatory documents which laid down in the basis of standardization documents containing physical and mechanical characteristics of materials of fuel elements and fuel assemblies.

Fatigue curves, crack resistance characteristics and constants which determine the rate of crack growth during operation should be defined taking into account the influence of exposure to radiation and chemical composition of coolant. For the material of cladding of fuel elements, these parameters should also take into account the influence of the chemical composition of the gases under the fuel element cladding.

5. CRITERIA OF THE STRENGTH AND OPERABILITY OF FUEL ELEMENTS

Numerical characteristics of the following limit states shall be used as the criteria for strength and operability of fuel elements:

- The threshold value of the first principal stress in the fuel cladding, the non-exceedance of which excludes the unstable growth of the postulated initial crack, the dimensions of which are set by the designer of the fuel element;
- Loss of stability of cladding of the fuel element (both instantaneous and long term one, with the progression of the initial out-of-roundness due to creep) under the influence of coolant pressure;
- Maximum value of fatigue damage of the fuel element cladding due to cyclic loads;
- Limit value of damage of the fuel element cladding due to thermal and radiation creep;
- Limit value of total bending stresses (or strains) in claddings of fuel elements under seismic or other dynamic impacts;
- Limit value of effective plastic deformation of the fuel element cladding;
- Limit value of the change in the cladding diameter of the fuel element;
- Limit value of elongation of the fuel element;
- Fuel melting point (for chemical composition, burn-up and manufacturing technology defined by the design of the fuel element);
- Limit value of pressure of the gases inside of the fuel element;
- Maximum thickness of the oxide film on the outer surface of the fuel element;
- The limit content of hydrogen in the cladding of the fuel element, an excess of which would result in unacceptable embrittlement of the cladding.

Numerical values of the strength and operability criteria of fuel elements for the above mentioned limit states should be determined and justified by the designer of the fuel element and fuel assemblies on the basis of experiments and (or) calculations. The specified values should be justified in the design basis of reactor and given in the SAR.

6. CRITERIA OF THE STRENGTH AND OPERABILITY OF FUEL ASSEMBLIES

The following limit states should be used as the criteria for fuel assembly strength and operability:

- Coverage of the entire section of the most loaded component of the fuel assembly with plastic deformations (loss of bearing capacity), with no defects;
- Unstable growth of a crack (brittle fracture);
- Loss of stability of the fuel assembly as a whole, or its component;
- Maximum value of fatigue damage of the fuel assembly due to cyclic loads;
- The limiting value of plastic deformation at which the destruction of a component may occur;
- Crack initiation by the mechanism of corrosion cracking.

For structural components made of zirconium-based alloys, in addition to above mentioned limit states, the following limit states shall be used additionally:

- Values of accumulated creep deformations which may result in the destruction of a component;
- Values of the thickness of the oxide film on the surface of thin-walled components of fuel assembly which may result in unacceptable embrittlement of the metal;
- Values of the hydrogen content in the metal which, once reached, results in its unacceptable embrittlement.

For fuel assembly as a whole, as the limit state shall be the values of the maximum permissible changes in the geometric dimensions and shape, including deflections.

For those limit states which are characterized by numerical values of the criteria of strength and operability, the values of these criteria shall be established by a specialized material science organization and the fuel assembly designer and justified in the design basis of reactor and presented in the SAR. With changes in the design of fuel assembly, the use of new materials, changes in the design of fuel elements, changes in the standards of the water chemical regime of the coolant of the primary circuit, changes in the manufacturing technology of fuel assembly, the numerical values of the strength and operability criteria shall be justified, or their previous values shall be confirmed.

7. SAFETY FACTORS FOR THE CRITERIA OF STRENGTH AND OPERABILITY OF FUEL ELEMENTS AND FUEL ASSEMBLIES

In justifications of the strength and operability of fuel elements and fuel assemblies, safety factors shall be provided for all plant states. The numerical values of the safety factors shall ensure that the limit states will not be reached during operation and should be justified experimentally and confirmed by the experience of operation of prototypes. For justification of the numerical values of safety factors, the following shall be taken into account:

- Experience of operation of fuel elements and fuel assemblies of similar design (if any);
- Results of experiments on test beds and in research reactors;
- Calculation error of stress-strain state and thermo-mechanical behaviour of fuel elements and fuel assemblies;
- Error which caused by a spread of values of physical and mechanical characteristics of materials of fuel elements and fuel assemblies.

Numerical values of safety factors should be justified in the design basis of reactor and presented in the SAR.

8. REQUIREMENTS FOR CALCULATED JUSTIFICATIONS OF FUEL ELEMENTS STRENGTH AND OPERABILITY

In calculated justification of the strength and operability of fuel elements, the following should be accounted for:

- Mechanical interaction between the fuel and cladding during operation, including disappearance and reappearance of a gas gap between them;
- Influence of exposure to radiation, temperature and hydrogen on physical, thermal mechanical properties of materials of fuel and cladding;
- Change of pressure and composition of the gases in the fuel element, including gas release from fuel;
- Anisotropic mechanical properties of the fuel and cladding materials;
- Creep, swelling, shrinkage, radiation growth of fuel and claddings;
- The effect of the gas gap between the fuel and cladding of the fuel element, pressure and composition of the gases on its thermal resistance.

During the operation of fuel elements, reaching of the above mentioned limit states with taking into account the safety factors provided in justifications of strength and operability of fuel elements shall not be allowed.

Justification of the strength of fuel elements in case of seismic and other dynamic impacts shall be carried out within the design basis of fuel assembly, taking into account the accumulated geometric changes of fuel elements.

9. REQUIREMENTS FOR CALCULATED JUSTIFICATIONS OF FUEL ASSEMBLIES STRENGTH AND OPERABILITY

Justification of the strength and operability of fuel assemblies shall be based on the calculated stress-strain states of either fuel assemblies as a whole or its individual components, as well as on the calculated thermo-mechanical behaviour of the core as a whole. The justification of non-achievement of all above mentioned limit states during operation of fuel assemblies shall be subject to calculated justification, except for those limit states, non-achievement of which is justified experimentally.

When performing calculations, it is necessary to consider:

- Effects of exposure to radiation and temperature on the physical, mechanical and thermal properties of the fuel assembly's materials;
- Anisotropy of physical and mechanical properties of the metal components of the fuel assemblies (if any);
- Creep, radiation growth (if any) of the metal parts of fuel assemblies made of zirconium-based alloys, during operation;
- Slippage (or non-slippage, in case of jamming) and rotations of fuel elements in spacer grids;
- Slippage of the guide channels (or the absence of slippage in the case of jamming) in spacer grids;
- Neutron flux and temperature distribution both along the fuel assembly's height and in the horizontal plane;
- Change of interaction forces between the fuel elements and spacer grids in the course of operation;
- Changes in the geometric characteristics of fuel elements and fuel assemblies in the course of operation;
- Transverse forces of interaction between the fuel assemblies (in case of mechanical interaction);
- Axial loads on fuel assemblies (mechanical, weight and hydraulic ones).

The strength and operability of the fuel assemblies shall be justified based on the following calculations:

- For static strength;
- For long term static strength (only for components made of zirconium-based alloys);
- For loss buckling;
- For fatigue;
- For long term cyclic fatigue (only for components made of zirconium-based alloys);
- for resistance to brittle fracture (unstable development of a postulated crack);
- For progressive deformation;
- For vibration strength;
- For seismic and other dynamic impacts;
- For the time of crack initiation by the mechanism of corrosion cracking (only for materials prone to corrosion cracking);
- For determination of the growth of cracks in the thin plate components (if cracks are found).

The geometric dimensions of the structural components shall be determined by the designer on the basis of the required physical and thermal hydraulic characteristics of the core, as well as the experience of operation of the fuel assembly prototypes.

The designer of fuel assembly should specify all operating modes, their number over the time of operation, as well as the sequence of alternation of these modes during operation.

The stress state of fuel assembly (or structural component) should be determined according to the sequence of operating modes established in the design basis of reactor taking into account mechanical and temperature loads, changes in physical and mechanical characteristics of structural materials, resizing and reshaping due creep and radiation induced growth.

The document NP-094-15 also provides requirements for each of above-mentioned types of strength and operability analysis.

10. REQUIREMENTS FOR EXPERIMENTAL JUSTIFICATION OF STRENGTH AND OPERABILITY OF FUEL ELEMENTS AND FUEL ASSEMBLIES

Experimental justification of the strength and operability of fuel elements and fuel assemblies shall be performed in research reactors and (or) on experimental test beds (including equipment for post irradiation examinations) under similar operating conditions of fuel elements and fuel assemblies in WWER reactors.

Experimental justification of the strength and operability of fuel elements and fuel assemblies shall be preceded by the development of a programme of experiments which shall specify the goals and objectives of the experiments, a list of characteristics to be measured, and methods of their control.

11. CONCLUSIONS

- In the Russian Federation much attention is given to the structural integrity and tightness of fuel elements of operating WWER reactors. The requirements for fuel elements are stated in the main regulatory documents containing the requirements for substantiating the safety of nuclear power plants in general - «General Provisions for Ensuring the Safety of Nuclear Power Plants» NP-001-15 [1], requirements for ensuring nuclear safety of reactor plants «Nuclear Safety Rules for Reactor Plants of Nuclear Power Plants» NP-082-07 [2], and in the specialized regulatory document «The main requirements for justifying the strength and thermomechanical behaviour of the fuel assemblies and fuel elements in the core of water-cooled power reactors» NP-094-15 [3];
- Normative document NP-094-15 [3] contains:
 - “Requirements for the physical and mechanical characteristics of structural materials of fuel elements and fuel assemblies, taking into account the effect of irradiation and chemical composition of the coolant.
 - The criteria for the strength and operability of the fuel elements and fuel assemblies during operation.
 - Requirements for the analysis of strength and operability of fuel elements and fuel assemblies, including safety factors, types of loads and phenomena that should be taken into account when performing calculations.
 - The list of mandatory calculations of fuel assemblies for strength and requirements for these calculations.
 - Requirements for the experimental justification of strength and operability of fuel elements and fuel assemblies”;
- The combination of the above mentioned requirements, together with the requirements for the manufacturing and operation, allows to ensure the tightness of the cladding of the WWER reactor fuel rods during operation at a sufficient level.

REFERENCES

- [1] NP -001-15, General Provisions for Ensuring the Safety of Nuclear Power Plants.
- [2] NP-082-07, Nuclear Safety Rules for Reactor Plants of Nuclear Power Plants.
- [3] NP-094-15, The main requirements for justifying the strength and thermomechanical behaviour of the fuel assemblies and fuel elements in the core of water-cooled power reactors.

LESSONS LEARNED FROM SAFETY ANALYSES INCLUDING A DESIGN CRITERION FOR CLADDING HOOP STRESS

K. KULACSY

Hungarian Academy of Sciences Centre for Energy Research (MTA EK),

Budapest, Hungary

Email: kulacsy.katalin@energia.mta.hu

Abstract

Fuel design criteria may cover PCI, and one of the main parameters to be investigated in PCI analysis is cladding hoop stress. However, this is a calculated quantity that cannot be measured, calculations can therefore not be validated directly. Indeed, code to code comparison of calculated hoop stresses show enormous differences even for the simplest setups. Russian design criteria include a maximum value for cladding hoop stress to avoid stress corrosion cracking. The independent verification of Russian fuel licensing analyses has to cover this criterion, which gives rise to several questions: How to interpret the results, especially when limit violation is found? What are the most critical moments in the power histories? How to deal with restart analyses, i.e. when fast AOO transients are simulated with a transient fuel behaviour code initialised by a steady-state code? Lessons learned are presented based on results obtained with the steady-state fuel behaviour code FUROM developed at MTA EK and the transient code FRAPTRAN.

1. INTRODUCTION

Hungary has four units of WWER-440 V213 at the Paks site, providing about 40% of the electrical energy consumed in the country in base load operation. Unit 1 was started up in 1982, Unit 4 in 1987. The units have undergone power uprating to 108% and lifetime extension by 20 years. Two new WWER-1200 units are planned at the same site and are undergoing preliminary safety assessment. These units are required to have a load-follow capability.

All four existing units have always run on Russian fuel, with several fuel modifications implemented over time, the last ones being the introduction of radially profiled assemblies with three and later six gadolinium-containing rods. Very few leakers have been found, and they were typically in their 1st cycle of operation. Licensing of a new fuel type, with an optimised water to uranium ratio (the so-called slim fuel), is in progress.

Fuel licensing in Hungary is based on Russian safety analyses, verified by analyses made at the Centre for Energy Research (MTA EK). The transients analysed from the PCMI point of view, agreed upon by Hungarian and Russian experts, are in normal operation:

- Fast start-up at the beginning of the cycle, where the rated reactor power increases at a rate of 48%/h until it reaches 20% of the nominal value and at 30%/h afterwards;
- 100%-0%-100%, where the reactor is shut down for two days and starts up again at a rate of 48%/h;
- 100%-50%-100%, where the reactor power is reduced to 50% of the nominal value for 6 h and then increased back to $\approx 95\%$ at a rate of 48%/h and more slowly to 100%;
- 100%-90%-100%, where the reactor power is reduced to 90% of the nominal value for 6 h and then increased back to 100% at a rate of 48%/h;
- Restart of closed, cold loop, which in practice is excluded by the operating instructions

and as an anticipated operational occurrence:

- Inadvertent control assembly group withdrawal until the reactor reaches 110% of its nominal power, when the transient is terminated by a scram.

All these analyses are performed using reactor physics and thermal hydraulics inputs provided to both the Russian and the Hungarian parties by MTA EK. The design criteria to be met are provided by the Russian vendor.

One of the design criteria aims at limiting true cladding hoop stress in order to avoid stress corrosion cracking (SCC). However, this is a calculated quantity that cannot be measured, calculations can therefore not be validated directly. Indeed, code to code comparison of calculated hoop stresses show enormous differences even for the simplest setups [1]. As the independent verification of Russian fuel licensing analyses has to cover this criterion, several questions arise:

- How to interpret the results, especially when limit violation is found?
- What are the most critical moments in the power histories?

- How to deal with restart analyses, i.e. when fast AOO transients are simulated with a transient fuel behaviour code initialised by a steady-state code?

Lessons learned are presented based on results obtained with the steady-state fuel behaviour code FUROM [2] developed at MTA EK and the transient code FRAPTRAN [3] adapted to Russian fuel by MTA EK.

2. INTERPRETATION OF THE RESULTS OF THE ANALYSES

The hoop stress criterion originates from tests performed on gas- and iodine-filled, pressurised cladding samples, thus the numerical value of the limit is well established. However, stresses calculated by the codes in a PCMI situation have a very high uncertainty, the comparison of the calculated values to the limit or to each other is therefore not trivial. In order to gain deeper understanding on the technical basis for the possible differences between the codes, a large number of ramp tests should be simulated by both codes to perform code-to-code comparisons. However, this would require experimental data available to both parties.

Until this is done, the actual numerical values of the maximum hoop stresses arising in the core during different transients cannot be directly compared to the limit value. What can be done is

- To compare the locations and moments of the highest stresses found in the Russian and the Hungarian analyses to make sure nothing has been overlooked,
- To compare the effective stresses to the yield stress and the ultimate tensile strength of the cladding,
- To compare the maximum hoop stresses to maxima calculated with the same code for past core loads with the same fuel, where there were no leakers.

3. CRITICAL MOMENTS IN THE POWER HISTORIES

The locations and moments of the maximum values of the hoop stress are by all means indicative of possible issues with the reload core design or the control strategy. In WWER-440 reactors power control over the cycle is performed by injecting or diluting boric acid in the primary coolant. Short-term power variations, however, are performed by inserting or withdrawing control assemblies that are above the core, power changes therefore affect primarily the top part of fuel assemblies close to the control assemblies used for this purpose. Too high stress values obtained for power change transients indicate a possible need to limit the speed at which control assemblies are withdrawn, i.e. the rate at which the reactor can be brought back to power.

As an example, Figure 1 shows a fuel rod undergoing a 100%–50%–100% transient in the reactor, representing a turbine trip, calculated by the code FUROM. The gap in the top axial node almost closes towards the end of the second cycle. At the end of the cycle where the boron concentration diminishes, control rods are withdrawn to maintain reactor power, which leads to gap closure and a sharp increase of the cladding hoop stress up to moderate values, followed by reactor shut down. During the third cycle, the gap closes definitively and at the end of the cycle, during the transient, when the reactor rises back to power, the stress increases beyond the SCC limit due to the fast local linear heat generation rate (LHR) increase caused by the control assembly movement.

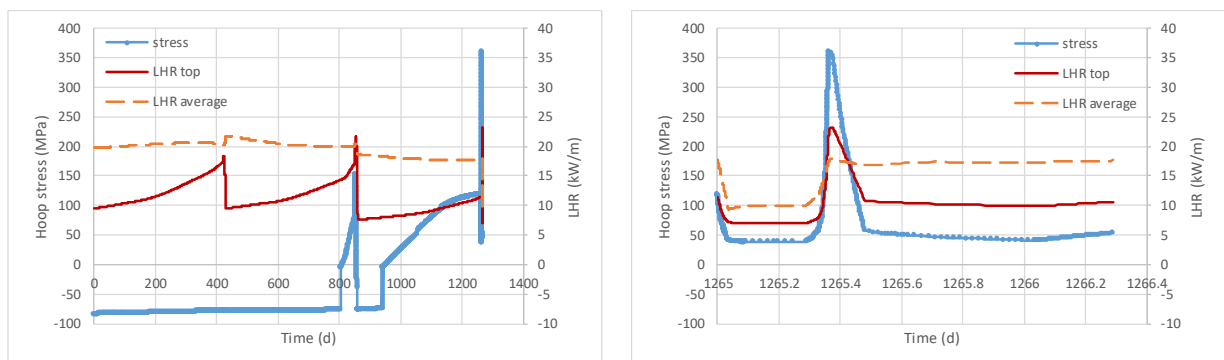


FIG. 1. LHR (average and top axial node) and cladding hoop stress in the top axial node, calculated with the code FUROM for a 100%–50%–100% transient (left: whole irradiation, right: transient).

4. FAST TRANSIENT ANALYSES OF IRRADIATED FUEL RODS

In Hungarian licensing practice non-steady-state analyses are done with the transient fuel behaviour code FRAPTRAN initialised by the steady-state code FUROM, which is called a restart. This makes it possible to take into account the burnup-dependent state of each fuel rod at the beginning of the transient. However, differences in the models implemented in the two codes may result in difficulties starting the code FRAPTRAN from a state prescribed by the code FUROM. A short period of numerical conditioning may be necessary to reconcile the transient code with the initial condition of the fuel rod, in which case a fictive first-time step at zero power followed by a slow ramp back to the real initial power is introduced before the transient. This prevents excessive stresses to appear in the simulation due to the change from one set of models to the other. However, the state of the fuel rod at the moment of the restart can show remarkable differences between the two codes, as illustrated in Fig. 2, which leads to significant differences in the calculated stresses.

5. FURTHER ISSUES

In reload core designs where a low power second cycle is followed by a high power third one for certain assemblies, the hoop stress limit may result in limit violation in these assemblies. This entails a limitation of the rate at which the reactor can be brought to power at the beginning of the cycle. Technically this can be done by limiting the increase rate of the electrical power output of the reactor. However, there are several issues with this method:

- The calculation of the increase rate involves numerical differentiation, which is in itself a source of large uncertainties;
- The determination of the power output has its own uncertainty;
- Control assemblies are not withdrawn at a constant speed and the power output is not a linear function of the control assembly position, therefore calculated increase rates show abrupt changes that do not necessarily reflect linear heat generation rate (LHR) changes experienced by individual fuel rods.

For the above reasons the calculation of the increase rate involves some sort of averaging (see Fig. 3), which implies a certain degree of arbitrariness, and it becomes increasingly difficult to establish a relationship between calculated and real stresses. Thus, it is difficult to prove that the original purpose of the limitation (exclusion of SCC) is achieved.

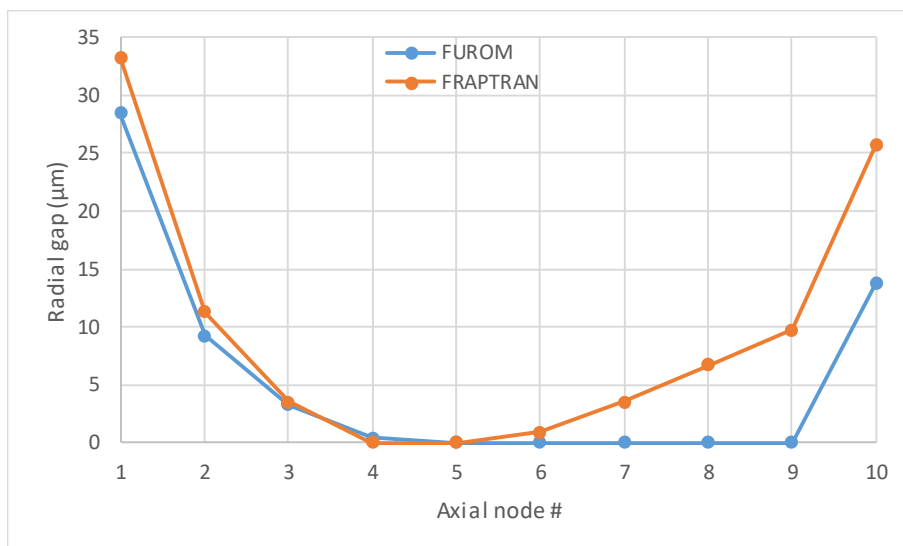


FIG. 2. Radial gap along the fuel rod as calculated by the codes FUROM and RAPTRAN for the same conditions (rod average burnup: 38 MW-d/kgU).

6. SOLUTION

Parallel to the cladding hoop stress limit, there exists a burnup-dependent LHR jump limit that also has to be met. As pointed out in [4], the purpose of the two limitations is identical and an LHR jump limitation can easily be implemented during both reload core design and operation. For operational purposes the LHR jump limitation is therefore the suitable means to prevent SCC failures. However, a detailed reassessment of the LHR jumps, the corresponding calculated stresses and the dependence of the latter on other factors such as initial LHR, burnup, contact pressure, time elapsed since gap closure etc. is planned for the reload design of the slim fuel to identify possible further operational limitations. An evaluation of real commercial power histories is also considered to be established the maximum calculated stresses that did not lead to cladding failure. Moreover, ramp tests with WWER fuel could also be simulated to be established the failure limit with the code FUROM, but this requires access to such test data, which at the moment is limited.

7. CONCLUSIONS

Due to large uncertainties in calculated hoop stresses and the lack of means to validate these calculations, the justification of the fulfilment of a direct cladding hoop stress limit in the design criteria is very difficult and would require the simulation of a large number of ramp tests, which are not available to MTA EK. Calculated hoop stresses are useful and indicative of the most critical moments in a reload core design or to analyse the effects of e.g. an inadvertent control assembly withdrawal, but they are less suitable as a design criterion. A well-established LHR jump limit is much better suited to prevent SCC failures in the context of Russian-Hungarian dual fuel licensing.

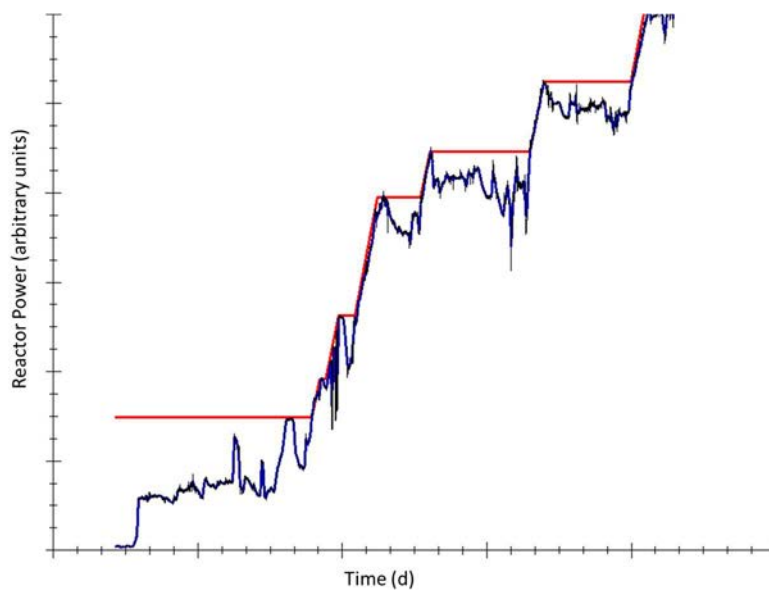


FIG. 3. Measured and averaged reactor power.

REFERENCES

- [1] Report on the PCMI benchmark organised by the OECD NEA WPRS EGRFP (in preparation).
- [2] GADÓ, J., GRIGER, Á., KULACSY, K., The Fuel Behaviour Code FUROM and Its High Burn-Up Simulation Capabilities, *Nuclear Engineering and Design* **327** (2018) 274-285.
- [3] GEELHOOD, K.J., LUSCHER, W.G., CUTA, J.M., PORTER, I.A., FRAPTRAN-2.0: A Computer Code for the Transient Analysis of Oxide Fuel Rods, PNNL-19400, Vol.1 Rev2 (2016).
- [4] INTERNATIONAL ATOMIC ENERGY AGENCY, Analysis of Differences in Fuel Safety Criteria for WWER and Western PWR Nuclear Power Plants, IAEA-TECDOC-1381, IASEA, Vienna (2003).

A PCI MARGIN ANALYSIS FRAMEWORK BASED ON COMBINED 1-D AND 3-D FUEL ROD MODELLING METHOD

Y. DING, X. WEI, L. ZHU

Shanghai Nuclear Engineering Research & Design Institute Co. Ltd. (SNERDI),

Shanghai, China

Email: dingyang@snerdi.com.cn

Abstract

Pellet cladding interaction (PCI) has been a confusing phenomenon for a long period of time in nuclear power industry. It was believed that pellet cladding contact force and corrosive ambience are major causes of PCI. Pellet cladding contact force was strong related to the pellet cladding gap condition, which was strong related to power history and power ramp rate. Traditional 1-D (or sometimes called 1.5-D) fuel rod performance codes can analyse such phenomenon. Further study showed that local stress concentration, local temperature distribution, and sometimes local hydride distribution may also have effect on PCI. 3-D modelling method is required to describe such phenomenon considering local geometry and local physical parameters' distribution. SNERDI developed a 1-D fuel rod performance code RoPE, which can be used to analysis the gap condition under different power histories, the uniform cladding stress response under different ramp rates. Technical limit for PCI using RoPE code was generated by comparing to RAMP test results. At the same time, 3-D finite element methods (FEM) using commercial FEA software was used to analyse local thermal-mechanic distribution of pellet and cladding. Results from 3-D FEM can be used to adjust 1-D fuel rod performance analysis outputs. Thus, PCI margin can be analyzed. Then sensitivity calculations were carried out to study the effect of burnup, initial power, time of low power operation, etc. on PCI margin. In this way, a PCI margin analysis framework which can combined 1-D and 3-D fuel rod modelling methods was set up by SNERDI. Currently only 3-D thermal and mechanical analysis was carried out and used for the margin analysis. Furthermore, 3-D hydride distribution could be modelled with the local thermal distribution results, so that local cladding degradation phenomenon could be described using this framework.

U-GD FUEL SIZE CHANGE MODELLING IN START-3A FUEL PERFORMANCE CODE

P.G. DEMYANOV, V.V. NOVIKOV, V.I. KUZNETSOV, A.S. EREMENKO
SC "VNIINM",
Russian Federation
Email: PGDemyanov@bochvar.ru

E.A. ZVIR, V.A. ZHITELEV
SC "RCC RIIAR",
Russian Federation

T. TVERBERG
IFE,
Norway

Abstract

1. INTRODUCTION

Experience in operating UO_2 WWER-1000 fuel using a built-in burnable absorber in the form of Gd_2O_3 (hereinafter U-Gd fuel) showed that the elongation of some U-Gd fuel rods in the first exploitation period has bigger value than UO_2 fuel rods, and to the end of operation elongation of U-Gd rods and common fuel rods becomes almost equal. This effect happens as for WWER as for PWR fuel rods [1].

Different ways of size-changing behaviour of UO_2 and U-Gd fuel rods are influenced by such factors as the difference in fuel and cladding temperatures, different energy release and neutron characteristics at the start of irradiation. When varying the structural parameters within the tolerances and different kinds of irradiation histories, it is possible to obtain as U-Gd fuel rod lengths excess over UO_2 rods as reverse situation.

The analysis of experimental data of Russian type WWER-1000 assemblies after earlier stages of irradiation in case of U-Gd fuel rod lengths excess over UO_2 rods was carried out as well as data analysis for middle and later stages of irradiation [2,3]. Fuel rods size change behaviour data were obtained by specialists of SC "SCC RIIAR" during post-irradiation investigations. In-pile data of the IFA-676 and IFA-681 experiments [4,5] (Halden, Norway) was also analyzed.

Based on the analysis results of experimental data, the reasons for the increased growth of U-Gd fuel rods in the initial period of operation were determined. U-Gd fuel rods fuel size change behaviour model was proposed with densification, cracking and repositioning processes taken into account. The model is implemented in the START-3A fuel performance code [6].

Multi-parameter validation of the model against the results of operation and post-irradiation investigations of 10 UO_2 and 10 U-Gd rods of Russian WWER-1000 assemblies of different construction was carried out.

2. EXPERIMENTAL DATA ANALYSIS

The WWER-1000 assemblies that underwent post-irradiation investigations were selected to cover burnups ranging from ~ 10 to ~ 60 MW·d/kgU and cover 6 fuel cycles. While the assemblies' data of IFA-676 and IFA-681 helped to illuminate the in-pile process of UO_2 and U-Gd fuel rods size changes from the qualitative point of view.

Figure 1 shows the elongation of the cladding of UO_2 and U-Gd fuel rods loaded in the IFA-676 assembly. Figure 2 shows on the elongation of the fuel stack of UO_2 and U-Gd fuel rods of the same assembly for the first 400 operational days.

The lower envelope curves in Figures 1 and 2 indicate the readings of the elongation detectors during power downs; using these data it is possible to compare elongation of UO_2 and U-Gd rods at the same temperature and thus eliminate the effect of thermal expansion of materials.

From Figure 1 one can see that up to 200 operational days of the claddings of UO_2 and U-Gd fuel rods are about the same length, then the U-Gd cladding starts to elongate with higher rate than UO_2 one. And by the time 320 operational days U-Gd cladding has received a significant increase. It can also be seen that the growth rate of

UO₂ cladding decreases with time, this may be due to radiation hardening of the cladding material and, as a result, a decrease in the cladding creep rate.

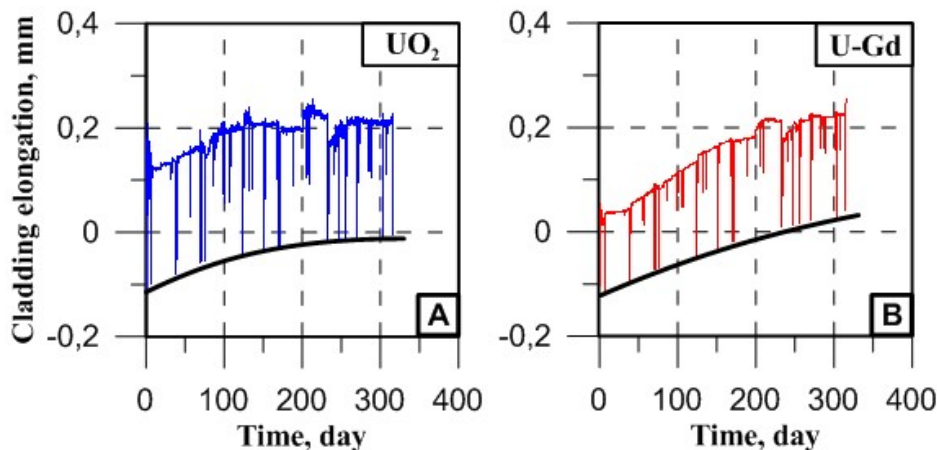


FIG. 1. Cladding elongation detector data for UO₂ and U-Gd fuel rods of the IFA-676 for the first 400 operational days.

In Figure 2A, a characteristic behaviour is observed for uranium dioxide — fuel densification in the initial period of irradiation, followed by fuel solid swelling. While the fuel stack of the U-Gd fuel rod (Figure 2B) increases due to the cracking and repositioning of the fuel with no densification observed, the reason could be the density of the fuel that is close to theoretical density.

Currently authors don't have direct experimental confirmation of the greater cracking of U-Gd fuel in the initial stages of irradiation but Figure 2B is an indirect evidence of this process.

Fuel stack behaviour (i.e, fast growth of fuel stack from 0 to 25 days) on the Figure 2B can be explained by fuel repositioning and this is not observed on UO₂ fuel (Figure 2A). Second assumption that leads us to the repositioning idea is that the presence of gadolinium oxide in the crystal lattice of uranium dioxide leads to the formation of a heterogeneous structure, which is prone to cracking. There is also double effect of high fuel temperature. On one hand higher temperature leads to a higher tensile stresses on the other hand high temperature leads to raised plasticity of the fuel and higher crack resistance in UO₂ fuel.

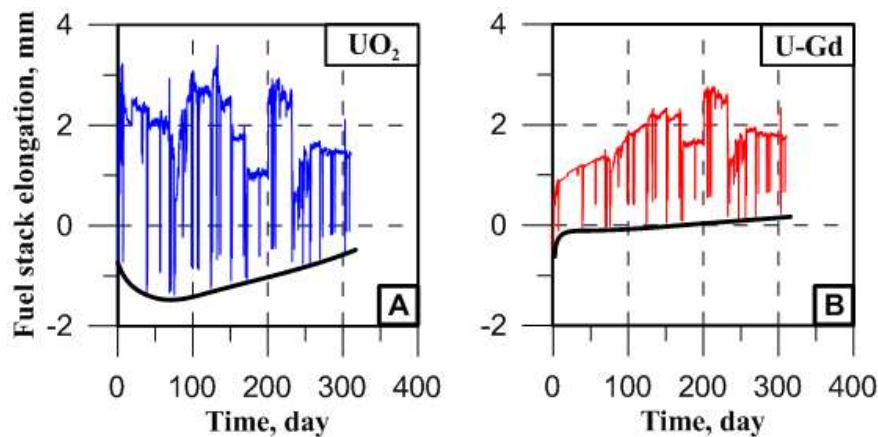


FIG. 2. Fuel stack elongation detector data for UO₂ and U-Gd fuel rods of the IFA-676 for the first 400 operational days.

Figure 3 shows fuel stack elongation detector data for UO₂ and U-Gd fuel rods of the IFA-676 assembly, depending on fuel burnup.

The solid straight lines in Figure 3 characterize the irreversible dimensional changes in the fuel column associated with the swelling of the fuel. The lines are built from the point of non-zero burnup in order to eliminate the influence of fuel densification process in UO₂ rod and fuel repositioning in U-Gd rod. The dashed line is constructed to highlight the slope of the envelope lines in Figure 3A and 3B. By estimating the slope angle of the

envelope curves for UO_2 and U-Gd fuel rods it can be concluded that the solid swelling rates (per burnup unit) are the same for both types of fuel.

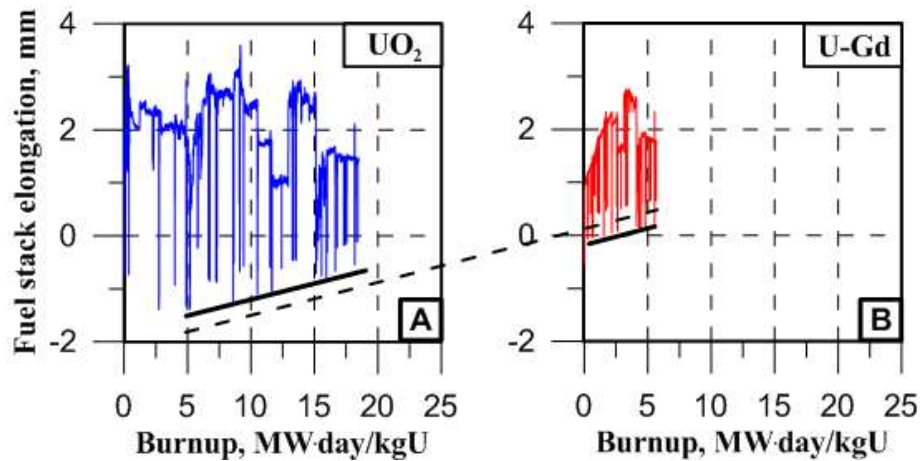


FIG. 3. Fuel stack elongation detector data for UO_2 and U-Gd fuel rods of the IFA-676 versus fuel burnup.

Figure 4 shows relative fuel volume change data at hot-stand-by conditions (HSB; zero power, 235°C) for UO_2 and U-Gd fuel rods of the IFA-681 assembly with different Gd contents, depending on fuel burnup per kilogram of oxide.

On the Figure 4 the same fuel behaviour as for IFA-676 is observed, namely fuel densification for UO_2 rods (Figure 4A) and cracking for U-Gd rods (Figure 4B and 4C), all followed by solid swelling.

An assumption can be done that gadolinium content can affect the cracking rate which can be seen from the comparison of Figures 4B (2 wt. % Gd), 2B (5 wt. % Gd) and 4C (8 wt. % Gd). There is a trend towards an increase in cracking rate depending on the gadolinium oxide content in the fuel.

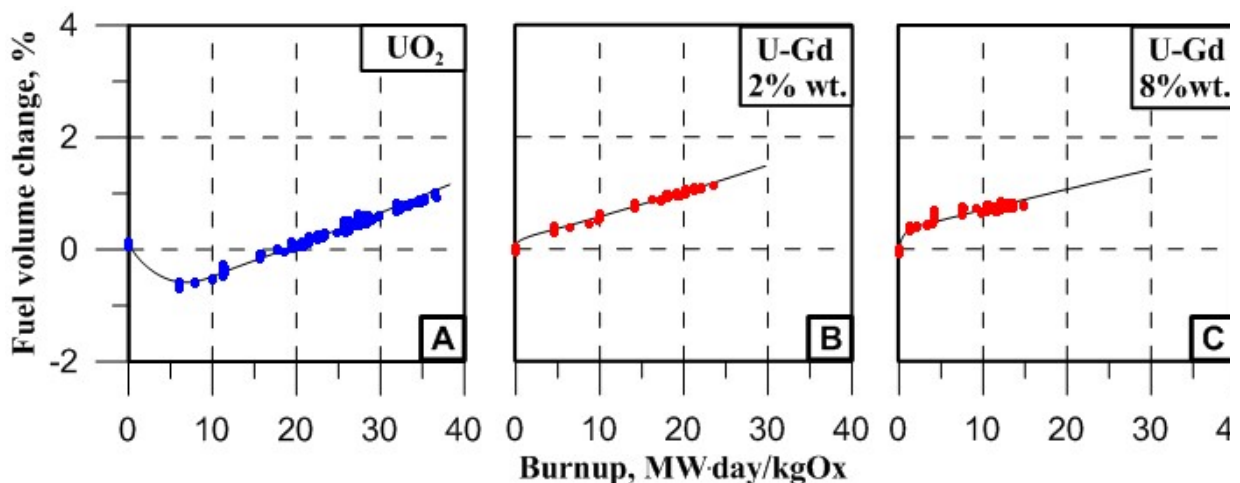


FIG. 4. relative fuel volume change data at hot-stand-by conditions for UO_2 and U-Gd fuel rods of the IFA-681 versus fuel burnup.

The results of the IFA-676 and IFA-681 tests in this work are used for the qualitative analysis of the dimensional behaviour of UO_2 and U-Gd fuel rods; the data were not used for quantitative analysis.

A quantitative analysis of the dimensional behaviour of UO_2 and U-Gd fuel rods was carried out based on the results of operation and post irradiation investigations of full-scale fuel rods of WWER-1000 operated for 1-6 fuel cycles on Russian commercial nuclear power plants.

UO_2 and U-Gd fuel rods profilometry results comparison of WWER-1000 assemblies after 1 fuel cycle (Figure 5) and after 6 fuel cycles (Figure 6) was carried out.

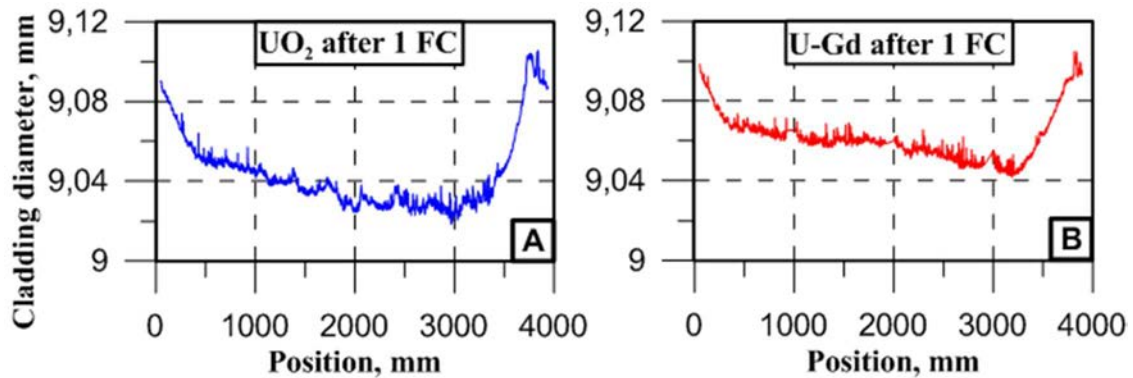


FIG. 5. UO_2 and U-Gd fuel rods profilometry results comparison of WWER-1000 assemblies after 1 fuel cycle.

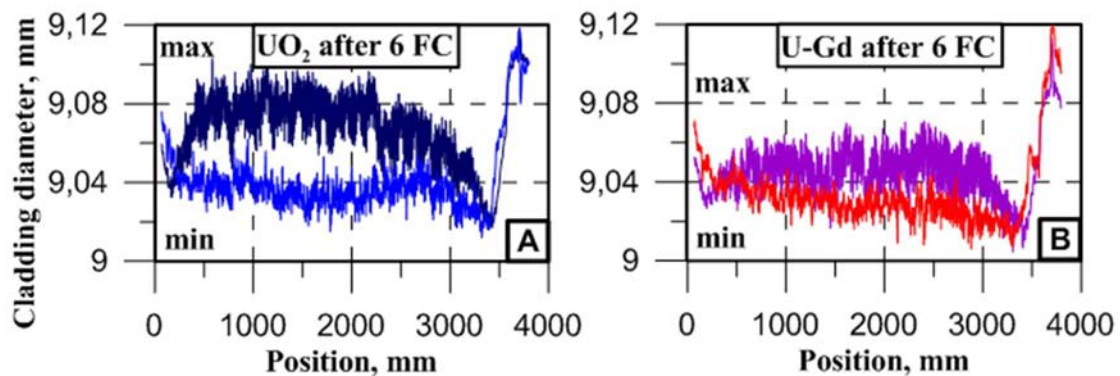


FIG. 6. UO_2 and U-Gd fuel rods profilometry results comparison of WWER-1000 assemblies after 6 fuel cycles. Rods with maximal and minimal by assembly diameter are given.

The results of profilometry of UO_2 fuel rod (Figure 5A) and a U-Gd fuel rod (Figure 5B) after 1 fuel cycle show the formation of ridging on the U-Gd rod that was not found on the UO_2 rod. Which indicates an earlier pellet-cladding interaction (hereinafter PCI) in U-Gd rod.

In Figure 6 UO_2 fuel rods and U-Gd fuel rods with maximal and minimal by assembly mean diameters are shown. The results of profilometry of fuel rods after 6 fuel cycles show the formation of ridging on both UO_2 fuel rods (Figure 6A) and U-Gd fuel rods (Figure 6B). That indicates that on later stages of irradiation PCI takes place for both types of the fuel.

Figure 7 presents the results of radiography of UO_2 fuel rods and U-Gd fuel rods after 4 fuel cycles. The deviation from the average value of the fuel stack length was measured and is shown in Figure 7B.

Radiography results indicate no significant difference in the elongation of the fuel stack between UO_2 fuel rods and U-Gd fuel rods after 4 fuel cycles.

Experimental data on the elongation of full-scale rods of WWER-1000 assemblies of various designs (a total of 8 assemblies) that were operated from 1 to 6 fuel cycles were systematized. Figure 8 shows the absolute values of cladding elongation, averaged over fuel rods and over each of the fuel cycles, depending on the number of fuel cycles.

The solid lines in Figure 8 are not an approximation of the experimental data; they illustrate the key nature in the elongation behaviour of UO₂ and U-Gd cladding, i.e. the intersection of the curves at the end of first fuel cycle — beginning of the second fuel cycle.

Non-monotonous increase in elongation during the 3-6 cycle can be explained by the different design of assemblies used in the by-cycle analysis.

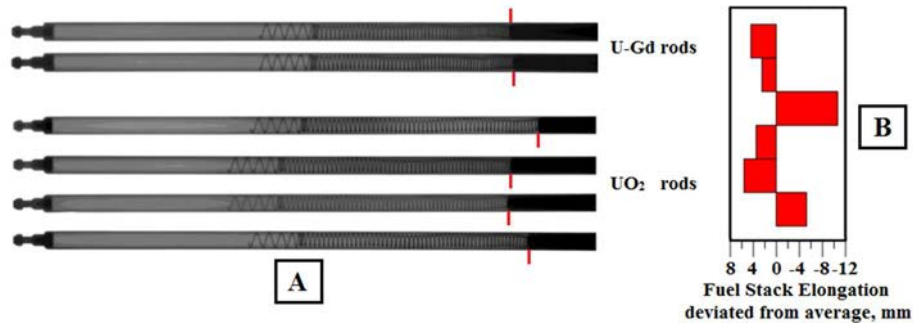


FIG. 7. UO₂ and U-Gd fuel rods of WWER-1000 assembly radiography results after 4 fuel cycles.

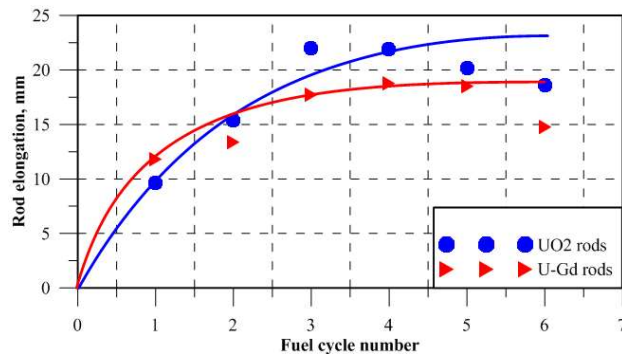


FIG. 8. Averaged (by rod and by fuel cycle) values of elongation of UO₂ and U-Gd fuel rods of Russian type WWER-1000 assemblies' dependence on the fuel cycle number.

According to the analysis of experimental data, the following features of size change process of UO₂ and U-Gd fuel rods were identified:

- At the initial stage of irradiation, there is a reduction in UO₂ fuel stack length due to densification process and an increase in U-Gd fuel stack length due to cracking and repositioning of the fuel. Due to compressive or tensile stresses in these processes, the rod diameter behaves the same way as fuel stack length. After initial densification and repositioning processes, the fuel swells at the same rate per burnup unit as for UO₂ as for U-Gd fuel;
- Different behaviour of UO₂ and U-Gd fuel at the initial stage of irradiation leads to an earlier closure of the gap in U-Gd;
- The PCI for U-Gd rod occurs earlier (about the end of 1 fuel cycle) than for UO₂ rods (about 2-3 fuel cycle). After that, the swelling fuel of U-Gd rods begins to pull the cladding increasing its length;
- Faster PCI for U-Gd fuel rods leads to greater length compared to the length of the UO₂ rods at the initial stages of irradiation. After that PCI begins in UO₂ rods the swelling fuel also starts to pull the cladding increasing its length;
- During whole operation time UO₂ rods gain a greater burnup value than U-Gd rods, which with time leads to diminishing of the delta occurred between UO₂ and U-Gd fuel stack lengths due to fuel densification and repositioning processes. Over time it leads to alignment of the cladding length fuel rods and possibly further exceeding of the elongation of UO₂ rods compared to U-Gd rods due to PCI.

3. U-GD SIZE CHANGE MODEL TEST CALCULATIONS

Based on the behaviour of U-Gd, the “bilinear swelling model” was developed [2]. The model was designed to check the general assumptions of UO₂ and U-Gd rods size change behaviour.

The model was incorporated in the START-3A code [6], a test calculation was carried out. Irradiation of neighbouring UO₂ and U-Gd rods was simulated, the history of linear heat rate is presented for 3 fuel cycle shown in Figure 9.

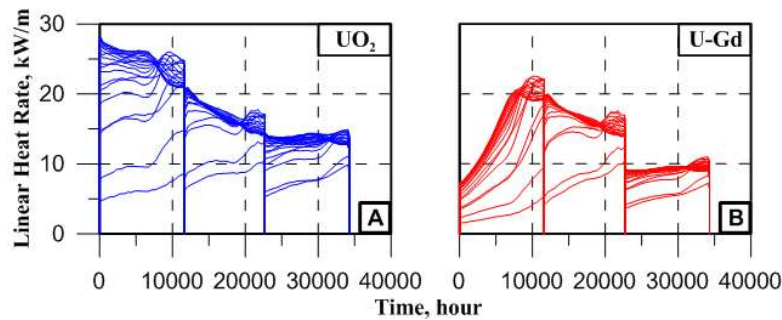


FIG. 9. Irradiation history of UO₂ and U-Gd rods during test calculation.

Experimental data points to verify test calculations were obtained from two WWER-1000 assemblies of the same design that were irradiated for 1 and 3 fuel cycles and were chosen for better comparison of experimental and calculation results.

Test calculations were in good agreement with experimental datapoints, qualitatively and quantitatively, on WWER assemblies and set the way for further improvement of UO₂ and U-Gd rods size change behaviour modelling.

A comparison between the calculation results and experimental data points is presented in Figure 10.

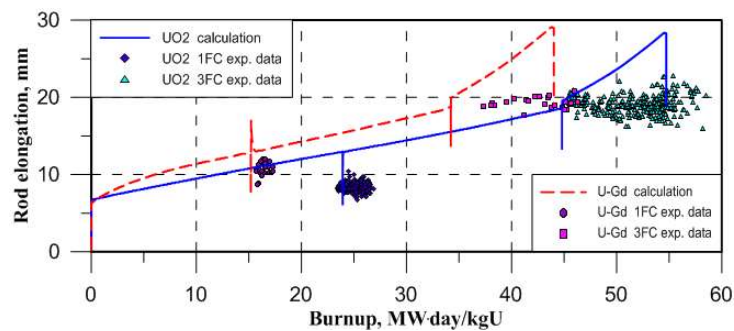


FIG. 10. Comparison of the calculation results and experimental data of the test calculation for bilinear model of fuel swelling.

Qualitative and quantitative coincidence with the experimental data were obtained, that can be seen from Figure 10.

4. VALIDATION OF U-GD SIZE CHANGE MODEL

As continuation and development of the bilinear swelling model, taking into account the peculiarities of the behaviour of uranium-gadolinium fuel and the analysis of a wide range of experimental data, a model of the size change behaviour of uranium-gadolinium fuel was developed taking into account the densification, cracking and repositioning of the fuel.

The model is implemented in the START-3A fuel performance code, validation calculations of UO₂ and U-Gd rods irradiated held at Russian nuclear power plants for 1-6 fuel cycles were carried out. 10 UO₂ rods and 10 U-Gd rods of various design WWER-1000 assemblies were selected as validation sets.

The validation sets' assemblies were differed by following factors:

- Different cladding width (0.59-0.69 mm);
- Different rod length (3836 – 3988 mm);
- Different cladding material (E110, E110opt.);
- Different gadolinium oxide content (5-8 wt. %);
- With and without fuel central hole (0-1.2 mm).

Irradiation of UO₂ and U-Gd rods with the most detailed post-irradiation investigations data in a wide range of burnup was modelled. The validation was carried out according to the following parameters:

- Average rod burnup;
- Oxide film width;
- Cladding elongation;
- Fuel stack elongation;
- Cladding diameter change;
- Rod free volume;
- Rod gas volume;
- Rod gas pressure.

Validation of U-Gd size change model results are presented in Figures 11–13.

The experimental data are plotted along the abscissa, and the calculated data are plotted along the ordinate. Such a system for presenting validation results is widely used. The best match is the location of the points on the line $y = x$. If the points are located above the line $y = x$, this means that the code over-predicts the experimental data and vice versa.

The burnup validation (Figure 11A) is given mainly in order to show that irradiation history for the fuel rods was set correctly and also to show the burnup validation range.

Oxide film with validation is given on Figure 11B. Under operating conditions of WWER reactors, oxide film width usually does not exceed 10 microns. Oxide film is taken into account when calculating the cladding diameter change.

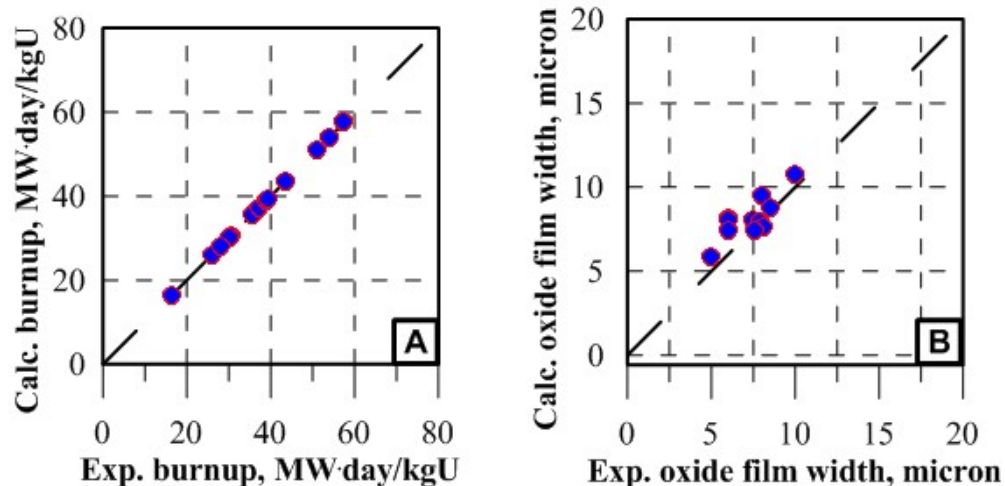


FIG. 11. Validation results for burnup and oxide film width values.

Validation results of cladding and fuel stack size change are presented in Figure 12.

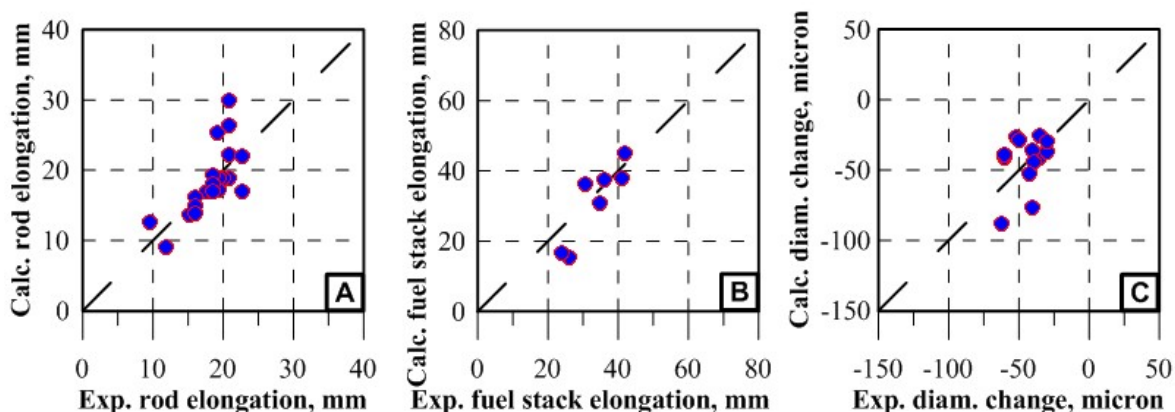


FIG. 12. Validation results for size changes of the rods.

Validation results for rod free volume, gas volume and gas pressure are presented in Figure 13.

The validation shows that code START-3A calculation satisfactorily describes the dimensional behaviour of uranium-gadolinium fuel qualitatively and quantitatively.

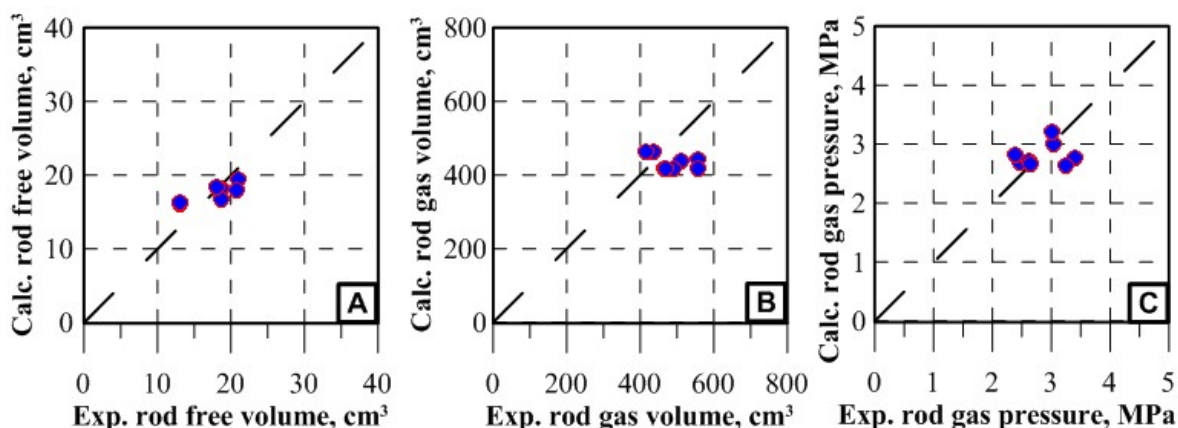


FIG. 13. Validation results for rod free volume, gas volume and gas pressure.

5. CONCLUSIONS

In the scope of this work the analysis of post irradiation investigations of UO₂ and U-Gd fuel rods of WWER-1000 assemblies as well as in-core measurements of the IFA-676 and IFA-681 assemblies data analysis was carried out.

According to the results of the analysis of experimental data and computational studies, the reasons for the increased growth of U-Gd rods in the initial period of operation were identified.

The main reason for the increased growth of U-Gd rods is the difference in the size change behaviour of the fuel stack of UO₂ and U-Gd fuel rods in the initial period of irradiation, namely, the absence of or lower rate of densification for U-Gd fuel and the presence of cracking and repositioning in a higher rate than for UO₂ fuel. Presumably this is due to the high density of the U-Gd fuel which within the limits of tolerances to the nominal value according to the technical specification, turned out to be close to the theoretical density. That leads to a complicated process including PCI that has been described in detail above in this paper and it comes as a result as exceeding length of U-Gd rods over UO₂ rods on the initial stages of operation.

A model is developed to describe UO_2 and U-Gd fuel rods size change behaviour with taking into account fuel densification, cracking and repositioning. The model is incorporated in the START-3A fuel performance code [5].

The model underwent multi-parameter validation against the results of operation and PIE of 10 UO_2 and 10 U-Gd rods of Russian WWER-1000 assemblies of different construction. The calculation results are in good agreement with the experimental results.

From the comparative data analysis of IFA-676 and IFA-681 fuel stack size changes (rods with 0, 2, 5, and 8 wt. % Gd content) one can conclude that gadolinium content can affect the cracking rate. There is a trend towards an increase in cracking rate depending on the gadolinium oxide content in the fuel.

Additional experimental investigations of the crack resistance of a fuel, depending on the theoretical density and content of gadolinium oxide, is required for further model development and understanding of complicated behaviour of nuclear fuel rods.

REFERENCES

- [1] YOO, J., KIM, J., JANG, Y., JEON, K., "Examination of the Irradiation Growth Behavior of $\text{Gd}_2\text{O}_3\text{-UO}_2$ Fuel Rod in PWR", Proceedings of Top Fuel 2009, Paris, September 6-10, 2009.
- [2] NOVIKOV, V.V., KUZNETSOV, V.I., DEMYANOV, P.G. et al., "Calculation and Experimental Investigation", International Conference: «Operation of Russian Fuel in VVER NPPs: Experience, Analyses, Perspectives, Prague, September 10-14, 2018.
- [3] NOVIKOV, V.V., KUZNETSOV, V.I., DEMYANOV, P.G. et al., "Modelling of the Elongation of $\text{UO}_2\text{-Gd}_2\text{O}_3$ Fuel Rods of VVER-1000", XI Conference on Reactor Material Science, Dimitrovgrad, 2019.
- [4] HRP Test Fuel Data Base IFA-676.1, Halden.
- [5] HRP Test Fuel Data Base IFA-681.1, Halden.
- [6] «Software tool START-3A», FBE «SEC NRS» Rostechndzor, registration number 328 of passport of attestation of software tool, 18.04.2013.

ABBREVIATIONS

AOO	Anticipated operational occurrence
BWR	Boiling water reactor
CANDU	Canada Deuterium Uranium.
CWSR	Cold worked stress relieved
ELPO	Extended low power operation, also known as ERPO
ERPO	Extended reduced power operation
IFPE	International fuel performance experiments
I-SCC	Iodine induced stress corrosion cracking
LHGR	Linear heat generation rate
LPPRA	Loading pattern PCI/PCMI risk assessment
MPS	Missing pellet surface
PCI	Pellet-cladding interaction
PCMI	Pellet-cladding mechanical interaction
PIE	Post-irradiation examination
PWR	Pressurized water reactor
RP	Rated power
RSST	Power range, step, speed and time
RTL	Ramp terminal level
R-L	Radial-longitudinal
SCC	Stress corrosion cracking
T-R	Transverse-radial
US NRC	United States Nuclear Regulatory Commission

CONTRIBUTORS TO DRAFTING AND REVIEW

Arimescu, I.	Framatome, United States of America
Federici, E.	Commissariat à l'énergie atomique (CEA)-Cadarache, France
Forgeron, T.	CEA-Cadarache, France
Ryu, W-S.	Korea Atomic Energy Research Institute (KAERI), Korea, Republic of
Scolaro, A.	École polytechnique fédérale de Lausanne, Switzerland
Sim, K.	International Atomic Energy Agency
Waeckel, N.	Electricité de France (EDF), France
Zhang, J.	Tratebel, Belgium
Vinze, P.	International Atomic Energy Agency

Technical Meeting

Aix-en-Provence, France, 8–11 October 2019

Consultancy Meeting

Vienna, Austria, 3–5 December 2019



IAEA

International Atomic Energy Agency

No. 26

ORDERING LOCALLY

IAEA priced publications may be purchased from the sources listed below or from major local booksellers.

Orders for unpriced publications should be made directly to the IAEA. The contact details are given at the end of this list.

NORTH AMERICA

Bernan / Rowman & Littlefield

15250 NBN Way, Blue Ridge Summit, PA 17214, USA

Telephone: +1 800 462 6420 • Fax: +1 800 338 4550

Email: orders@rowman.com • Web site: www.rowman.com/bernan

REST OF WORLD

Please contact your preferred local supplier, or our lead distributor:

Eurospan Group

Gray's Inn House
127 Clerkenwell Road
London EC1R 5DB
United Kingdom

Trade orders and enquiries:

Telephone: +44 (0)176 760 4972 • Fax: +44 (0)176 760 1640

Email: eurospan@turpin-distribution.com

Individual orders:

www.eurospanbookstore.com/iaea

For further information:

Telephone: +44 (0)207 240 0856 • Fax: +44 (0)207 379 0609

Email: info@eurospangroup.com • Web site: www.eurospangroup.com

Orders for both priced and unpriced publications may be addressed directly to:

Marketing and Sales Unit

International Atomic Energy Agency

Vienna International Centre, PO Box 100, 1400 Vienna, Austria

Telephone: +43 1 2600 22529 or 22530 • Fax: +43 1 26007 22529

Email: sales.publications@iaea.org • Web site: www.iaea.org/publications

**International Atomic Energy Agency
Vienna**